# Investigation of particle number measurement and combustion and emissions from alternative fuels in diesel engines

**Yanlong Wu**

**Submitted in accordance with the requirements for the degree of Doctor of Philosophy**

**The University of Leeds**

**School of Chemical and Process Engineering**

**July 2019**

The candidate confirms that the work submitted is his/her/their own, except where work which has formed part of jointly authored publications has been included. The contribution of the candidate and the other authors to this work has been explicitly indicated below. The candidate confirms that appropriate credit has been given within the thesis where reference has been made to the work of others.

The pure HVO fuel results in Chapter 7 and Chapter 8 are based on the work from a jointly authored publication: **Investigation of Combustion and Emission Performance of Hydrotreated Vegetable Oil (HVO) Diesel.** Authors: Yanlong Wu, Jason Ferns, Hu Li, and Gordon Andrews. The experiment and data processing was conducted by the candidate. Other authors contributed to the publication by verifying the data, revising the draft, and proof-reading the paper.



*Assertion of moral rights*

## Acknowledgement

I would first express my appreciation to my supervisors Dr Hu Li, and Professor Gordon, E, Andrews for their guidance and advices. Without Their guidelines and assistance in each step of the research, it's impossible for me to conduct the research.

I would also like to thank technicians, Scott Prichard and Jonathan Stephenson for all their assistance and contribution in the engine lab. It's their professional knowledge and patience that helped the research project to be carried out.

I want also to show my gratitude to Royal Dutch Shell Plc, Neste Oyj for providing GTL diesel fuel and HVO diesel fuel to support this research. Special thanks to the Caterpillar Inc, for inviting me to join their global PN research programme, which formed a chapter of my thesis.

And finally, I want to say special thanks to my wife and parents, it's your encouragements and supports helped me to overcome all the difficulties during the study.

## Abstract

The popular usage of diesel engine and diesel fuels in recent decades leads to enormous reliance on fossil derived fuels and environment pollution. Alternative fuels for diesel engine can be a solution. However, considering the production limitation of those alternative fuels, finding an effective and environmental way to apply alternative fuels to diesel engines is an important research topic. The hydrotreated vegetable oil (HVO) and gas to liquid (GTL) fuels can be directly used on diesel engines with any desirable blending ratio to diesel fuel. In addition, the HVO and GTL fuels consist of straight chains and no aromatics compounds, indicating the potential to reduce total hydrocarbon (THC) and particle number (PN) emissions.

The PN emissions from a diesel engine is always critical and the accurate PN measurement is very challenging. Because the PN is very sensitive to sampling conditions and types of PN measurement instruments. This research presents the comparison of PN (Particle Number) measurement results from five PN instruments (two HORIBA SPCSs, one DMS 500, one SMPS, and one AVL 438) with different sampling frequency and various dilution settings. The correlation factors among the tested instruments were obtained and the lower detection limit of the DMS 500 was found to be $2\times10^4$ (#/$cm^3$).

In addition to by the PN research, HVO and GTL fuels were blended with diesel fuels at 30%, 50%, 70%, and 100%. Their combustion and emission performances were tested on a IVECO made 3-litre direct injection diesel engine equipped with EGR and intercooler. The engine is EURO 5 compliant. The combustion performance was measured with a pressure transducer installed at the top dead centre (TDC) of one combustion cylinder. The particle number size distribution and gaseous emissions were measured using DMS 500 and HORIBA MEXA 7100. The results showed that HVO, GTL, and their blends can significantly reduce the particle number (PN) and THC emissions, and the reduction increased with the increasing of blend ratio. At the engine outlet, the peak values of accumulation mode particles reduced with the increasing of blending ratio. The PN emissions measured at the downstream of the aftertreatment system was below the DMS lower detection limits. The pure GTL and HVO fuels did

show similar $NO_x$ emissions with diesel fuel, however, the blended fuels all showed $NO_x$ reduction from 20% to 35%. The combustion performances of all fuels were similar in general, especially when the engine power reached 27 KW. The ignition delay became shorter with the increasing of blending ratio.

# Contents

# List of figures

## List of tables

## Nomenclature

AFR: Air to Fuel Ratio

BDC: Bottom Dead Centre

BMEP: Brake Mean Effective Pressure

CI engine: Compression Ignition Engine

CLD: Chemi-luminescence Detector

$CO_2$: Carbon Dioxide

CPC: Condensation Particle Counter

DI: Direct Injection

DMS: Particle Differential Mobility Sizer

DOC: Diesel Oxidation Catalyst

DPF: Diesel Particle Filter

EEA: European Environment Agency

EGR: Exhaust gas recirculation

FAME: Fatty Acid Methyl Ester

FID: Flame Ionization Detector

FTIR: Fourier Transform Infra-Red

GCMS: Gas Chromatography-Mass Spectrometry

GTL: Gas to Liquid

HC: Hydrocarbons

HDPE: High-Density Polyethylene

HVO: Hydrotreated Vegetable Oil

ICE: Internal Combustion Engine

ID: Ignition Delay

IDI: Indirect Injection

IMEP: Indicated Mean Effective Pressure

Mini-CAST: Miniature Combustion Aerosol Standard

MPD: Magneto-Pneumatic Detection

NAC: $NO_X$ Absorber Catalysts

NDIR: Non-Dispersive Infrared

NMVOC: Non-methane Volatile Organic Compounds

PM: Particulate Matter

PN: Particle Number

SCR: Selective Catalytic Reduction

SI engine: Spark Ignition engine

SMPS: Scanning Mobility Particle Sizer

TCIC: The Turbocharged and Intercooled

TDC: Top Dead Centre

TGA: Thermogravimetric Analysis

THC: Total Hydrocarbon

VOCs: Volatile Organic Compounds

# Chapter 1. Introduction

## 1.1 Background

The diesel engine has been widely used for many decades in varies of fields since Rudolf Diesel invented the diesel engine in the 1890s. The higher power output and thermal efficiency, robustness and fuel flexibility made diesel engines a good candidate for medium to heavy vehicle, off road mobile and non-mobile machines, electricity generators, marine and agricultural applications etc.

However, after years of society development, the concern about effective and environmental application of diesel engines is currently becoming a focus issue. This is due to two reasons: the heavy reliance on fossil derived fuel and the pollutants' emission. Considering the limited fossil fuel resources stored on this planet and the protection of the natural environment, it's necessary to find solutions for better usage of diesel engine. Admittedly, new forms of hybrid or electricity light duty vehicles are continuously introduced to the public. However, if considering the emissions produced from the generation of electricity, the application of electric cars is transferring air pollution from urban areas to electricity power plants rather than really eliminate the pollution generated from transportation. According to the world coal association, the coal-fuelled power plants provide 37% of global electricity and is the higher than any other forms of electricity generation, for instance renewable, natural gas or nuclear. [World Coal Association, 2015] The renewable power plants are environmentally friendly. However, they do require high costs and maintenance. In addition, the installation of electricity power chargers at parking areas can also raise the costs and maintenance of application of electric vehicles. In addition, the heavy-duty diesel engines cannot be replaced by electric drives as the high engine power required by heavy duty sectors, for example off road machineries, marine diesel engines, heavy duty vehicles etc. Therefore, all these mentioned above hindered electric vehicles to be a total substitute for diesel engine, and the diesel engine technology is still crucial to modern society.

One of the solutions for reducing adverse impacts of conventional diesel fuels is the application of alternative fuels for instance fuels generated from forms other than crude oil, for instance vegetable oil and natural gas. Those fuels, on one side, can reduce the heavy reliance on limited natural resources as fossil derived fuels. On the other side, can reduce the carbon related emissions as soot, smoke, hydrocarbons due to their advantages in chemical structure. Admittedly, some advanced biofuels can be directly used for instance the hydrotreated vegetable oil and gas to liquid oil, but the production can be limited due to complicated processing procedure. Therefore, finding best blending ratios of certain type of alternative fuels with diesel can have great benefits for its application in diesel engines.

This research used two types of alternatives fuels: Hydro- treated vegetable oil (HVO) and Gas to liquid fuel (GTL) on an IVECO Euro 5 emission compliance diesel engine. Each type of fuel was blended with diesel fuel at 0%, 30%, 50%, 70%, and 100% in volume. The engine was three-litter, four-cylinder with maximum power output of 96 kw equipped with EGR and intercooler. The engine was equipped with an integrated Diesel oxidation catalyst (DOC) and Diesel particle filter (DPF) aftertreatment system. Emission performances were both measured at the upstream and downstream of the exhaust aftertreatment system. A DMS500 particle size measurement instrument was used for measuring particles between 5 nm and 1000nm. Gaseous emissions were measured using a HORIBA 7100 series gas analyser. The combustion performances were measured using an AVL system including AVL pressure transducer, AVL crank angle encoder, and AVL Indicom software. The engine was instrumented with several thermocouples so that the engine temperature conditions were closely monitored. The tests were conducted at nine selected RPM and loads steady state conditions.

Particle number emissions from diesel engine are always critical to academic research. Those combustion-oriented particles are comprised of carbonaceous materials, liquid droplet and ashes. However, the determination of particle concentrations is affected by many parameters such as sampling flow rate, temperature and instruments used. Different instruments may give different readings. There is no consensus on which instrument can be used as a gold standard or benchmarking. This has raised a question

on the comparison of results measured by different instruments. There is a knowledge gap in determination of the particle measurement devices' performance under the impact of sampling dilution system, sampling frequency and the concentration of sampling gas. In this project, a research was conducted comparing five particle number measure instruments sampling from soot emission generated from a miniature combustion aerosol standard (Mini-CAST) soot generator using propane as a fuel. The five particle number instruments were set at different sampling dilution ratios and sampling frequency in order to find out the differences among them.

## 1.2 Research aim and objectives

The overall aim of this research is to investigate the performances of the combustion and emission performances of two alternative fuels (HVO and GTL). Both pure and blends of HVO and GTL fuels with standard fossil diesel were studied. The fuel blending ratios applied for GTL fuel and HVO fuel were respectively 0%, 30%, 50%, 70%, and 100% by volume. The emission research focused on the $NO_x$ and particle number emissions.

The specific objectives are:

1. Determine the differences in particle number measurement methods and how their operating conditions impact the measurement.
2. Find out the particle number concentration detection limits of DMS500.
3. Estimate the particle density.
4. Evaluate the performance of HVO, GTL fuels and their blends on engine power, engine torque, IMEP, and BMEP.
5. Analyse the combustion behaviour of HVO, GTL fuels and their blends in terms of ignition delay, in-cylinder pressure change and combustion stability.
6. Investigate the particle number concentrations and size distributions of HVO, GTL and their blends at different power conditions.
7. Quantify the efficiency of the exhaust aftertreatment system, particularly the impact on particle size distributions
8. Quantify the impact of alternative fuels on NO, $NO_2$ and total $NO_x$ emission.
9. Quantify the impact of alternative fuels on THC and CO emissions.

10. Suggest the optimum way of using HVO and GTL blends in light duty diesel engine.

## 1.3 Thesis outline

This thesis is comprised with nine chapters, and the brief outline of each chapter is given below:

- **Chapter 1: introduction**

This chapter introduces the background and motivation of this research, addresses the research aims, research objectives, and thesis outline.

- **Chapter 2: literature review**

This Chapter presents the literature review related to this research project. It starts from the basic working principles of internal combustion engine, diesel engine, and then explains the emission generation principles of diesel engine. The review also includes the emission legislation, emission impacts on environment, emission measurement, particle number measurement, and alternative fuels.

- **Chapter 3: Experiment and methodologies**

This chapter contains two parts. The first part presents the experiment equipment introduction and experiment methology for particle number measurement research, including the five kinds of different particle number measurement devices used, experiment procedure, and data analysing process. The second part gives the description of equipment, experiment procedure and data processing for diesel engine test. This includes the experiment engine, gases analyser, particle number measurement, combustion performance detection devices, blended fuel test procedure, and data analysing process.

- **Chapter 4: Investigation of particle number measurement-influence of instrument and sampling conditions, and the determination of the detection limit**

This section contains the results of particle number instruments comparison research. From the research, presents the correlation factors among five particle number instruments, the impact of dilution ratio, the impact of sampling frequency, the instrument detection limits determination, and the estimation of particle density.

- **Chapter 5: Fuel property and combustion analysis of GTL and its blends**

This chapter provides the fuel property analysis of pure diesel fuel and pure GTL fuel, including their distillation characteristics, elemental components, and carbon chain distribution. The analysis of combustion performance involves: pressure to crank angle diagram near top dead centre, ignition delays, peak combustion pressure, average combustion pressure, P-V diagrams and engine power.

- **Chapter 6: Emission analysis of GTL and its blends**

This chapter presents the emission comparison among pure diesel, pure GTL fuel and GTL blended fuel with diesel at 30%, 50%, and 70%. The results include major emissions ($NO_X$, THC, CO, $CO_2$), particle number distributions, the efficiency of aftertreatment system, From the results analyses, give the conclusion of how GTL blended fuel can contribute to emission control.

- **Chapter 7: Fuel property and combustion analysis of HVO and its blends**

This chapter first gives the fuel property analysis of pure diesel fuel and pure HVO fuel, including their distillation characteristics, elemental components, and carbon chain distribution. Then the analysis of combustion performance is conducted involves: pressure to crank angle diagram near top dead centre, ignition delays, peak combustion pressure, average combustion pressure, P-V diagrams and engine power.

- **Chapter 8: Emission analysis of HVO and its blends**

This chapter presents the emission comparison among pure diesel, pure HVO fuel and HVO blended fuel with diesel at 30%, 50%, and 70%. The results include major emissions ($NO_X$, THC, CO, $CO_2$), particle number distributions, the efficiency of aftertreatment system, From the results analyses, give the conclusion of how HVO blended fuel can contribute to emission control.

- **Chapter 9: Conclusion and future work**

This final chapter summarize the core findings of this research, including how GTL and HVO blending fuel can contribute to emission control, and how particle number measurement can be improved based on current measurement technology. The recommendation for future research is given in this chapter as well.

# Chapter 2. Literature review

This chapter provides the critical literature review relating to the research, including the basics of diesel engine, emission formation and generation, emission legislation, emission control methods, and the current application of biofuel and fuel additives.

## 2.1 Internal combustion engine and diesel engines

This section introduces the development of internal combustion engines, then focus on the four-stroke compressed ignition engine (CI engine) or named as diesel engine, presenting the working principles of diesel engine as well as its thermal working cycles and the combustion condition. And finally, the modern turbocharge technology will be introduced.

### 2.1.1 Introduction to internal combustion engine

The internal combustion engine (IC engine) is an engine that converts the thermal energy generated from the combustion of fuels (typically fossil derived fuels) with oxidizer (typically air) to mechanical power, and thus utilizes the mechanical power to drive the mechanical equipment.  Before the year 1900, several kinds of internal combustion engines designs were already created by human beings, included the invention of spark ignition engine and compressed ignition engine; however, only till the early of 20$^{th}$ century, the public and commercial application of the internal combustion engines became widespread. This was due to the drilling and production of petroleum was commercialized until around 1850s. [Dickey, 1959]. Then after more than one hundred years of development, the internal combustion engine technology has been well established and utilized in transport, machinery, agriculture and electricity generation industry, etc. The IC engine are a heat engine that converts the chemical energy in the fuel to thermal via fuel combustion and achieving mechanical energy, suggesting that the operating of IC engines would inevitably create emissions. Therefore, one of the key challenges to achieve environmental application of CI engine is to minimise the emissions from combustion.

Broadly speaking, ICE includes reciprocating, rotating and gas turbine engines. However, it is typically referring to the internal combustion engines to reciprocating

piston engines. Piston engines can be classified based on either their working cycles or ignition systems. This is shown in the figure 2-1. However, the most common type of the IC engines applied today are the four stroke IC engine, especially in the transportation sector, including the railway and on-road vehicles.

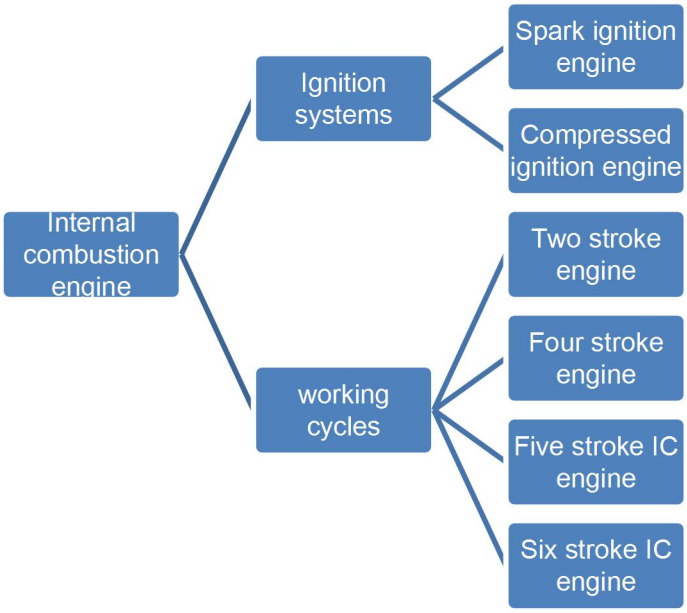


**Figure 2-1** The classification of internal combustion engines.

The key component of a four-stroke engine is the combustion chamber and cylinder. It's the place where the fuel air mixture is combusted for achieving the thermal power and later converts it to the mechanical power. The figure 2-2 shows the basic geometry internal combustion engine [Pulkrabek, 1997]. The combustion of the fuel air mixture generates large amount of heat, and thus creates pressure which can push the piston in the cylinder to move. Since the piston is connected with the crankshaft with rod, the come-back moving of the piston therefore helps to convert the thermal power to mechanical power.

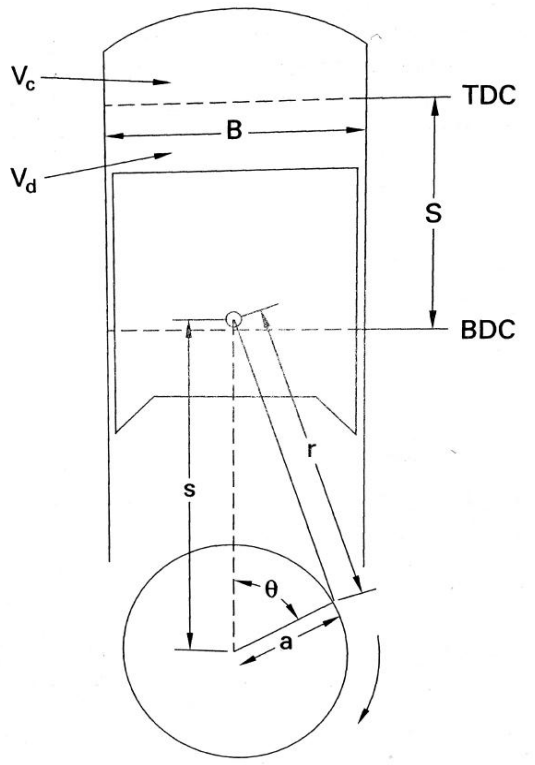


**Figure 2-2** The piston and cylinder geometry of internal combustion engine

B= bore, S= stroke, r= connected rod length, a= crank offset, s= piston position, θ= crank angle, VC =clearance volume, Vd = displacement volume

The four-stroke internal combustion engine has air intake stroke, compression stroke, expansion or also named as power stroke, the exhaust stroke. During the air intake stroke, the piston shown in the figure 2-3 [3M. 2013]. moves from the Top Dead Centre (TDC) to the Bottom Dead Centre (BDC) and allows air to be taken into the combustion cylinder; the at the compression stroke, the piston moves back to the TDC and thus compressed the gas inside the cylinder; then after this, the power stroke occurs as the high pressure generated by the combustion of fuel mixture pushes the piston to the BDC; finally, in the exhaust stroke where the piston moves back to the TDC and pushes the residual of combustion out of the cylinder.

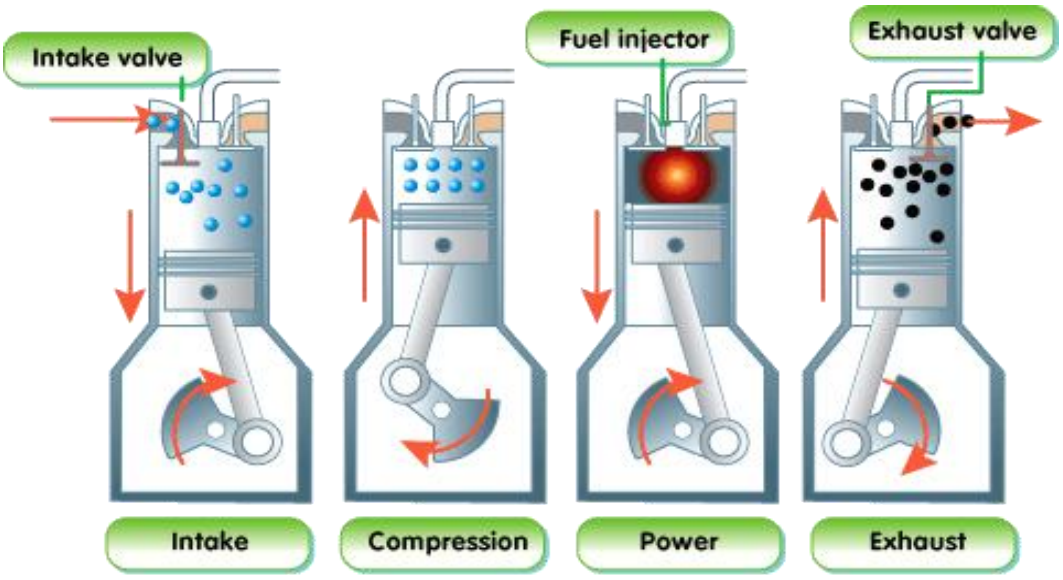


**Figure 2-3** The working of four stroke engine.

However, the real working cycle of internal combustion engine is very complex. The main reason is the air flow in the engine will mixed with the slight amount of residual from the previous combustion's exhaust. This is decided by the mechanical principle of the engine as the engine couldn't totally discharge all the exhaust in the cylinder after combustion. Since the exhaust is open to the surrounding environment, the components of the gas in the combustion cylinder each time can be slightly different, indicating the working cycle of engine is an open cycle in link with its working environment, and it is quite difficult to analyze. [Pulkrabek, 1997]. In addition, some modern diesel engine is equipped with exhaust gas recirculation (EGR), which intends to bring exhaust gas to join the next combustion cycle so as to reduce the NOx emission. Besides, the turbulence and swirl existed in the gas flow inside the cylinder will lead to the combustion process in cylinder to be little varied among each other. Therefore, in order to understand the engine working cycle in a much more manageable way, the idealized cycle is applied to replace the real cycle in a very much approximate manner.

### 2.1.2 The working cycle of CI engine

The Compressed ignition (CI) engine or known as diesel engine enables its combustion via the compression of air. The fuel is directly injected to the combustion chamber in Direct Injection (DI) diesel engine which is much more popular applied now than Indirect Injection (IDI) engine. The engine power is controlled by the fuel injection. This feature helps the diesel engine to achieve higher thermal efficiency as there is absence of pumping losses which is inevitable in spark ignition (SI) engine due to the application of air throttle. Once the flame is generated by the combustion process, the burning in the combustion chamber will create high pressure which drives the piston to move and thus convert the thermal power to mechanical power.

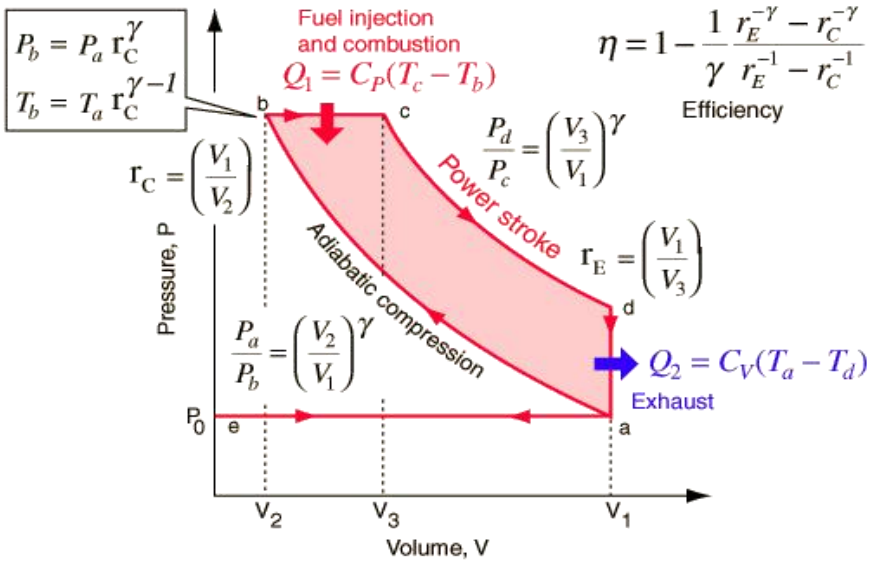


**Figure 2-4** The ideal pressure-volume diagram of diesel cycle.

Figure 2-4 [Nave, 2014] presents the ideal P-V diagram of the diesel working cycle for CI engines. Similar to Otto cycle of SI engine, it has four strokes: Intake, compression, power or expansion, and exhaust. Fuel injection and combustion occur at around the TDC. The diesel cycle's efficiency can be derived according to the following theoretical calculation:

If, as shown in the figure 2-4, at point A, pressure = $P_a$, volume = $V_1$, and temperature = $T_a$;

At point B, pressure = $P_b$, volume = $V_2$, and temperature = $T_b$;

At point C, pressure = $P_c$, volume = $V_3$, and temperature = $T_c$;

At point D, pressure = $P_d$, volume = $V_1$, and temperature = $T_d$;

$C_v$ is the heat capacity at constant volume;

$C_p$ is the heat capacity at constant pressure;

And $\gamma=C_p/C_v$.

Then the four strokes could be expressed as following:

Firstly, the compression stroke is from point A to point B, during which the gas inside the combustion chamber is seen as ideal gas and this process is treated as an adiabatic process. Thus, according to the thermodynamics, the pressure and volume parameters should match with the formula:

Equation 1……. $\frac{\mathrm{Pa}}{\mathrm{Pb}} = (\frac{\mathrm{V2}}{\mathrm{V1}})^{\gamma}$;

Second, the fuel injection and combustion are from point B to point C, which in theory is considered as isobaric combustion. This is impossible in the actual situation as the combustion takes time, and during this period of time, the pressure couldn't remain unchanged. Theoretically, the energy achieved by constant pressure expansion of gas should meet the formula:

Equation 2…… $\mathrm{Q1} = \mathrm{Cp} \times (\mathrm{Tc} - \mathrm{Tb})$;

Third, the expansion stroke is from point C to point D, which is considered as adiabatic process as the compression stroke, therefore, similarly, the pressure and volume parameters in this process should meet the thermodynamic formula:

Equation 3……$\frac{\mathrm{Pd}}{\mathrm{Pc}} = (\frac{\mathrm{V3}}{\mathrm{V1}})^{\gamma}$;

Finally, the heat rejection is from point D to point A, this process is seen as an isometric process, therefore the heat rejected out of the cylinder should meet the formula:

Equation 4……$Q2 = Cv \times (Ta - Td)$.

This symbolizes the end of one diesel cycle and the ready for another new cycle. Then because the engine's thermal efficiency should equal to (Energy in – Energy rejected)/ Energy in, and Energy in=Q1 while Energy rejected = Q2. Thus, the engine efficiency could be written as:

Equation 5……$\eta = \frac{Q1-Q2}{Q1} = 1 - \frac{1}{\gamma} \times \frac{Ta-Tb}{Tc-Tb}$

This formula can be rewritten to different forms when consider the ideal gas law PV=nRT, for instance if: $r_c = \frac{v1}{v2}$, and $r_e = \frac{v1}{v3}$, then the final efficiency expression can be:

Equation 6…… $\eta = 1 - \frac{1}{\gamma} \times \frac{r_e^{-\gamma} - r_c^{-\gamma}}{r_e^{-1} - r_c^{-1}}$ .

However, this ideal efficiency could not be acquired in the actual situation. One reason is the fuel injection timing and the other is fuel mixing. The former needs the injection to start before the piston reaches the TDC in the compression stroke due to the ignition delay. Thus, the compression process could never be perfectly matched with the combustion stroke as treated in an ideal condition where the combustion occurs instantly after compression. In fact, the flame is generated at the end of compression stroke and the highest pressure is acquired at the beginning of power stroke. The reason for the latter is that the mixing of fuel and air in the cylinder requires time. Any inappropriate mixture due to gas swirls or lubricate oil can also cause insufficient burning, thus reducing the efficiency and raising PM emission as well.

### 2.1.3 Combustion in CI engines

Combustion in diesel engines (CI engines) is quite different from SI engine. Essentially, it's a movement of a flame front throughout the combustion cylinder filled up with fuel air mixture. It differs from the SI engine by utilizing the injection of fuel to control the engine power instead of applying the air throttle. This is also the reason the CI engine generally obtains better thermal efficiency as there is no pumping losses.

The combustion of CI engine includes five stages:

1. Spray and atomization

The fuels injected into combustion chamber break into small droplets in this process as to undergo efficient burning.

2. Vaporization

The fuel droplets evaporate into vapor under the high pressure and high temperature condition created by CI engine. The higher the compression ratio is, the faster the fuel evaporation will be.

3. Mixing

After the vaporization, the fuel vapor will be mixed with the compressed air in the cylinder. This is under the assistance of high fuel injection velocity and the turbulence of air created at the compression stroke. The equivalence ratio (ø) of fuel-air mixture has be within the combustible range, from 1.8 to 0.8, where ø =1.8 indicates rich combustion and ø =0.8 indicates lean combustion. The figure 2-5 [Pulkrabek, 1997]. shows the air-fuel zones around the injector.

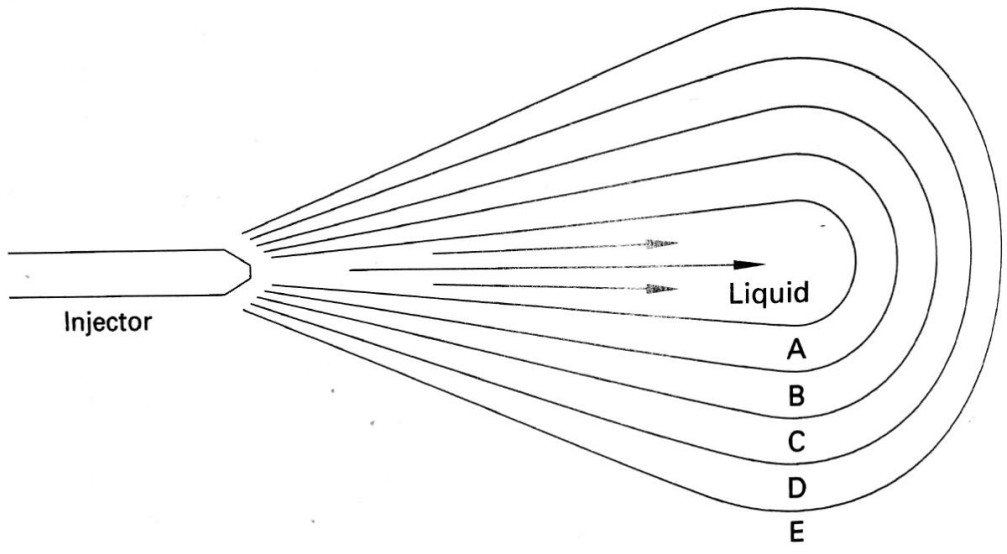


**Figure 2-5** Diesel fuel injector showing its surrounding vapor zone.

In the middle it's liquid form of diesel fuel. Then the fuel spreads to around, atomizing, evaporating, and mixing. The mixture in area A is too rich to burn; B is rich burning; C is stoichiometric burning; D is lean burning; and E is too lean to burn. The unburned mixture from zone A will generate smoke and soot and thus be the source for PM emission, while the self-ignition occurs in zone B and C.

4. Self-ignition

When the pressure and temperature in the cylinder is high enough, the air-fuel mixture will ignite automatically. This is called self-ignition.

5. Combustion

   The figure 2-6 [Austen and Lyn, 1960]. helps to understand the combustion process of the diesel engine. From the point A, the fuel injection starts. The point B is a turning point, after which the pressure in the cylinder increased rapidly, indicating from the point B, the self-ignition occurs. The combustion process starts from those many sites of self-ignition and flame is spreading very quickly. The beginning of the combustion is called uncontrolled combustion, during which, the cylinder is still filled up with combustible fuel-air mixture and the pressure is high, thus allow the flame to spread at high speed. From point B To nearly TDC, which the rapid increasing of pressure in Figure 2-6 represents the uncontrolled combustion. After this, it's the controlled combustion, which is the moderate rising of pressure after the initial quick rise shown in Figure 2-6. During this period, the fuel injection is still continuing. The rate and amount of fuel injection take control the engine power. The point C in the figure presents the end of fuel injection. After that, the fuel burning would continue and end in the exhaust stroke and finally the cylinder is prepared for another cycle.

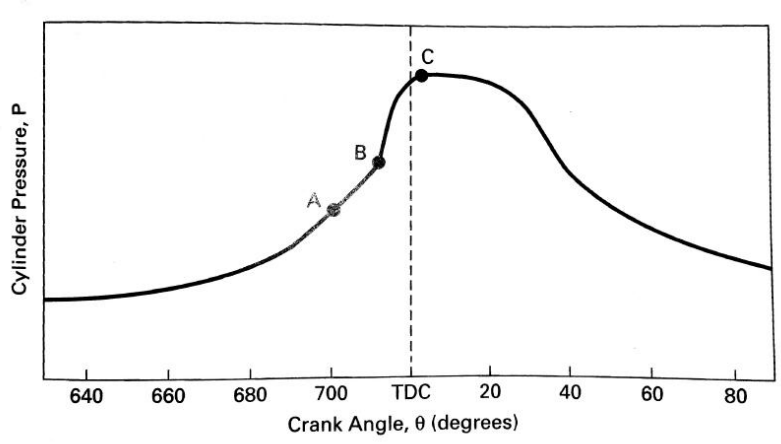


**Figure 2-6** Cylinder pressure as a function of crank angle θ of diesel (CI) engine.

### 2.1.4 Turbocharger technology

In order to achieve higher fuel efficiency and generate more power from the engine, turbocharging technology is applied in the majority of modern internal combustion engines. Since the basics of the internal combustion engine is to convert thermal energy into mechanical power, and the thermal power generated is decided by the amount of fuel and air available in the combustion, thus increasing the amount of air enables the engine generates more power. Turbocharger achieves this purpose via increasing the pressure of the inlet air sending to the combustion cylinder. Similarly, to the supercharger, which utilizes the mechanical power to increase the pressure of inlet air, the turbocharger uses the exhaust gas flow to drive its compressor and thus raising the air pressure.

For instance, if a four-stroke internal combustion engine has following parameters:

Combustion chamber volume 1 L = 0.001 $m^3$,

Air to fuel ratio (AFR) = 20:1,

Engine speed = 2000 rpm,

Taken the ideal gas and the diesel fuel with $C_v$ = 43 MJ/kg as the gas and fuel joined the combustion.

If the ambient air pressure at the ground surface of earth is 101 KPa, then in the condition without turbocharger:

The air density in the combustion chamber should meet the ideal gas law:

Equation 7…….$PVT = nR$

Equation 8…….$\rho = \frac{P}{RT} = \frac{101\times1000P}{287J/kg.K\times(20+273)K} = 1.2kg/m^3$ , ($R_{air}$ is 287J/kg.K);

Thus, the air mass is = 1.2kg/$m^3$ × 0.001 $m^3$ = $1.2\times10^{-3}$ kg;

If the four-stroke engine runs at 2000 rpm, then there would be (2000 ÷ 60 × 2) thermodynamic cycles per second, and the air flow rate = $1.2\times10^{-3}$ kg × (2000 ÷ 60 × 2) =0.08 kg/s;

Consider the air to fuel ration, then the fuel flow = 0.08 kg/s ÷ 20 = 0.004 kg/s;

Consequently, the power generated per second = 0.004 kg/s × 43 MJ/kg =172 KW.

If the engine is equipped with turbocharger which helps it to double the air pressure, then the new air density should be doubled, thus the new air mass should be double as well and equals to $2.4\times10^{-3}$ kg;

Similar to former calculation the power generated per second = $2.4\times10^{-3}$ kg × (2000 ÷ 60 × 2) ÷ 20 × 43 MJ/kg = 344 KW, which doubled the power generated without the application of turbocharger.

Besides the advantage of generating more power, the turbocharger also improves the emission from the engine. As the turbocharger can increase the engine power by increasing the air pressure, it can help the engine to achieve specific power with less fuel consumption vice versa. In addition, the power to drive the turbocharger is from the waste energy of engine's exhaust gas. Therefore, to recover the waste energy and saving of fuel could enable the turbocharger to reduce the pollutants emissions, mainly $NO_X$ from diesel fuel.

The figure 2-7 indicates the working cycle of turbocharger of a diesel engine. [Ricky, 2015] First the hot exhaust gas produced in the combustion flows out through the exhaust manifold and part of that exhaust flows into the turbocharger housing. Then the exhaust gas hits the turbine wheel and drives the turbine wheel to move rapidly, physically transferring the kinetic energy of the exhaust gas to the wheel. After the exhaust gas hits the wheel, the coupled compressor drawn in the ambient air, compressing it and sending the it to the cooling system. The compressor is cooled typically by a fan as if the temperature in the compressor is too high, very probably there will occur self-ignition as there exist compressed oxygen from the air and the lubricate oil in the machine. The hot compressed air also undergoes the cooling system (when applied on engine, the turbocharger is always equipped with intercooled system, which assists to reduce the temperature of the compressor to raise the density of air as physically the density of matter decreases with the increasing of temperature, and increases with the decreasing of temperature) and enters the combustion chamber though the intake manifold, following by the injection of diesel fuel to generate fire flame and pushing the piston down (power stroke).

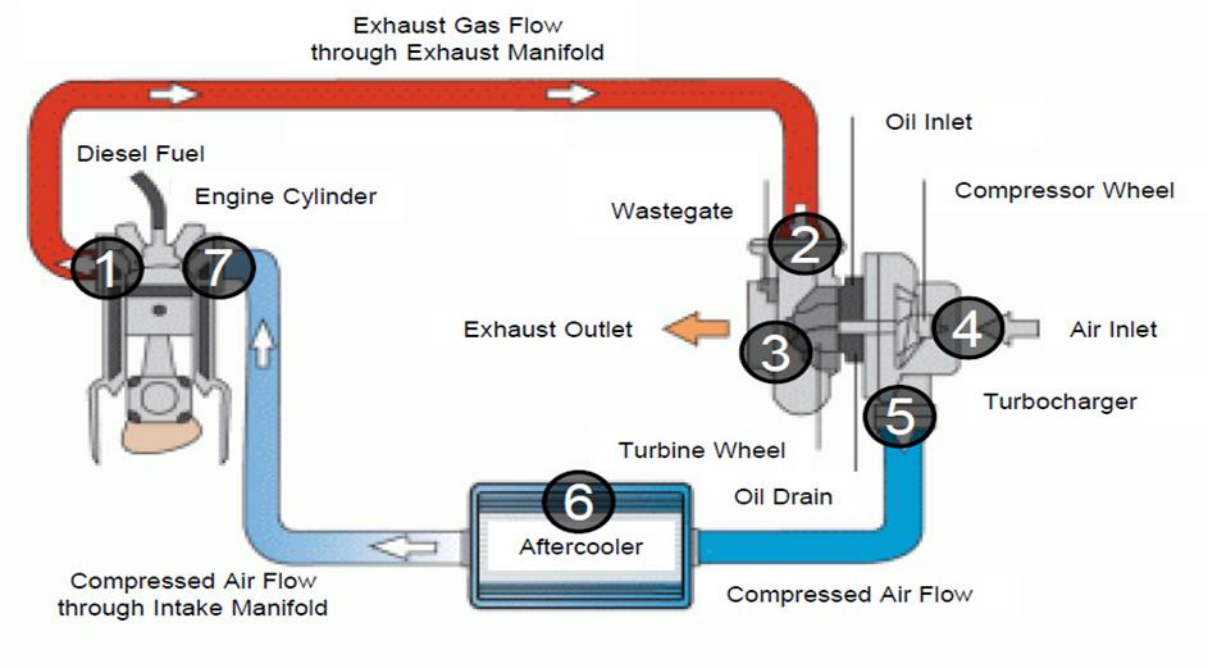


**Figure 2-7** The working cycle of a turbocharger.

The IVECO made diesel engine used in this research is equipped with a turbocharger and intercooler. The turbocharger of the engine is shown in figure 2-8. The air at atmospheric temperature enters the turbocharger through the black line shown at right down side in the figure 2-8. The black air inlet line is connected with an air filter. Then the turbocharger pressurizes the inlet air and sends the compressed air to the intercooler through the orange line shown in figure 2-8. The intercooler comprises an engine coolant radiator and is designed to lower the temperature of compressed air before it been sent to the combustion cylinders.

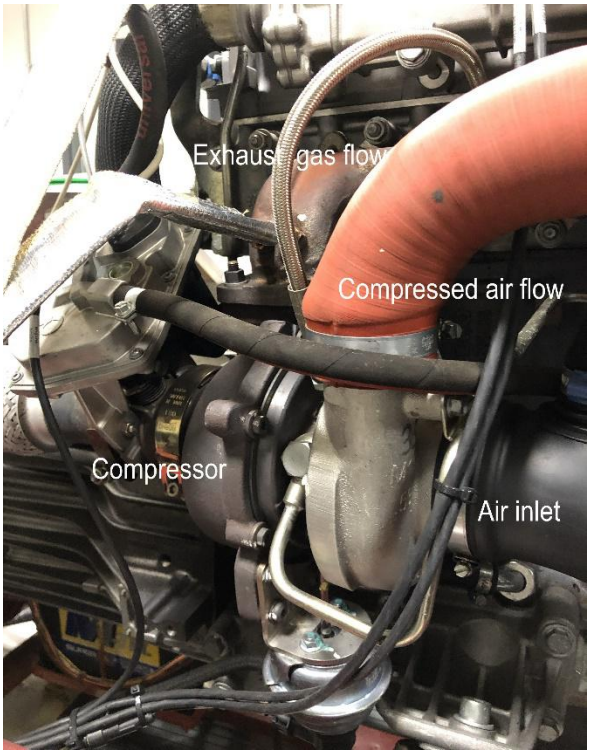


**Figure 2-8** The turbocharger of experiment engine.

## 2.2 Emissions from diesel engines

Figure 2-9 shows a typical composition of diesel exhaust gases [Majewski, 2012]. The dominant component is nitrogen from air. Carbon dioxide, water vapor and unreached oxygen make up the major fractions. The fraction of pollutants due to incomplete combustion of fuels in diesel engine such as CO, HC, $NO_X$ and PM is small in general,

but they are both harmful to human health and the ecosystem. This section provides the knowledge of emission formation, related emission legislation and control methods.

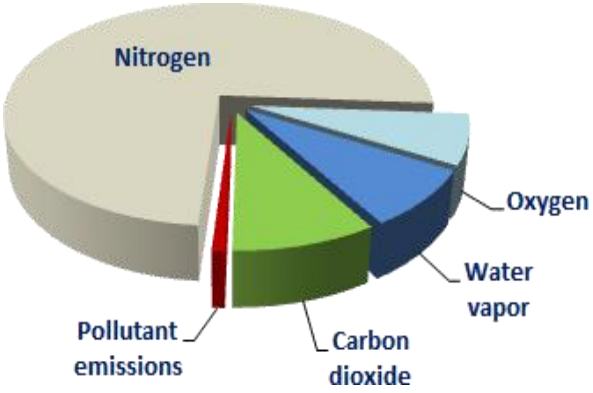


**Figure 2-9** The typical composition of diesel exhaust gas.

### 2.2.1 CO and HC emissions from diesel engines

Diesel engines emit the CO, HC, NOx and PM in respective ways. Among them the CO emission is not significant as it does in SI engines, since CO is generated due to the incomplete oxidation of fuel carbon and diesel engines operate in lean combustion condition instead of stoichiometric combustion [Wu et al, 2004]. This can be explained by the following example:

CH4 is the major component of the fuel, then if it is burning in the lean condition where enough oxygen is provided, then the chemical equation can be written as: $CH_4 + 2O_2 \rightarrow CO_2 + 2H_2O$, indicting only water and $CO_2$ will be generated after the combustion. In this case, there is no CO production. But if some fuel failed to be mixed with enough oxygen, indicating inadequate amount of oxygen joined the combustion, for instance only 80% of stoichiometric oxygen is provided, then the chemical equation can be rewritten as: $CH4 + 1.6O_2 \rightarrow 0.8CO + 0.2CO_2 + 2H_20$, proving the formation of CO emission. Thus, CO emission is an issue mostly decided by fuel air mixing in diesel engine. This can be proved in figure 2-10 [Zervas et al, 2001]. The CO emission from CI engine dropped reduces when the fuel to air equivalence ratio increased, because the fuel consumption increased in this research enable the engine to achieve shorter ignition delay, which indicated the better fuel-air mixing. [Heywood, 1988], [Stone, 1999].

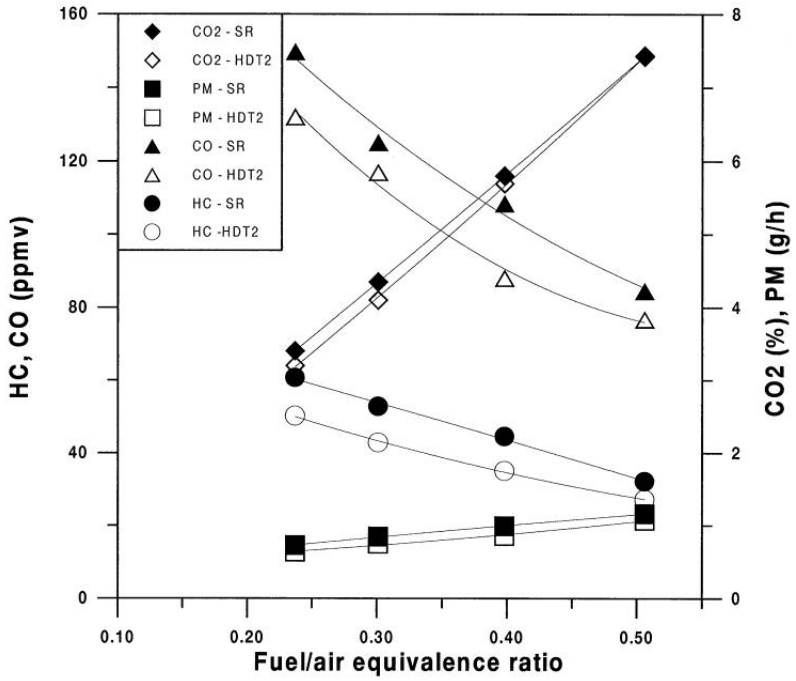


**Figure 2-10** The CO emission against equivalence ratio.

The hydrocarbons in diesel engine exhaust are the products of engine combustion and can be generated during the process of fuel evaporation, fuel mixing, and combustion. The fuel mixing is a major reason leads to the HC production: the fuel could be mixed leaner than the ideal lean combustion limit during the ignition delay, which is the time between fuel injection and auto- ignition occur, or the fuel could be mixed richer when the fuel injection is at low velocity, for instance at the end of combustion process [Chehroudi, 2015]. Both these two conditions contribute the formation of HC in diesel engine. However, as the majority of fuel is burned in lean combustion condition, therefore the HC emission from the diesel engine is not significant. This can also be addressed from figure 2-10, that the HC emission reduces with the fuel-air mixing improvement acquired by increasing fuel injection.

### 2.2.2 $NO_X$ emissions from diesel engines

The lean combustion in diesel engines provides effective oxidation of fuels during which HC and CO emissions are not significant. However, the rich oxygen combustion leads

to a large amount of air joining the combustion. As the air consists of 78% of nitrogen, the nitrogen exposed to high temperature in the cylinder would undergo endothermic reaction and thus generating $NO_X$ emissions. In addition, the combustion in diesel engine also occurs much faster than SI engine, thus the turbulence in the fuel injection could cause the HC in the fuel failed to undertake the sufficient burning at anticipated mix condition, indicating some part of HC becomes the particulate matter (PM) residual after the inappropriate combustion. According to the Union of Concerned Scientists, [Ucsusa. 2015]. the $NO_X$ and PM created by diesel engine vehicles or other diesel facilities contribute respectively almost 50% of the all the NOx emission and more than 66% of PM emission for the overall US transportation emission.

Three categories of NOx are formed in the CI engine: the prompt NOx, the fuel bound nitrogen NOx, and the thermal NOx. During the combustion process, the prompt NOx forms very quickly at the reaction zone with HC intermediaries, and its concentration is higher if the combustion mixture is richer and otherwise lower if the combustion mixture if leaner. Even in the lean combustion condition, the prompt NOx can still be a few ppm, which indicates the combustion generated NOx can always exist. Besides this, the fuel bound nitrogen NOx requires the fuel used consist with organically bound nitrogen components, which consequently forms NOx in the engine. The thermal NOx is produced via the reaction between nitrogen and oxygen in the air at high temperature above 1800k, and it is the dominant NOx emission from the CI engine. [Andrews, 2015]. The formation of $NO_x$ from diesel engine can be expressed in below based on Zeldovich mechanism [Mellor, et al, 1998]:

$O+N_2 = NO + N$

$N+O_2 = NO + O$

$OH + N = NO + H$

$N_2O + O = 2NO$

$N_2 +O+M=N_2O + M$

$O_2 + M = 2O + M$

The $NO_X$ formation rate against in-cylinder temperature is shown in figure 2-11.

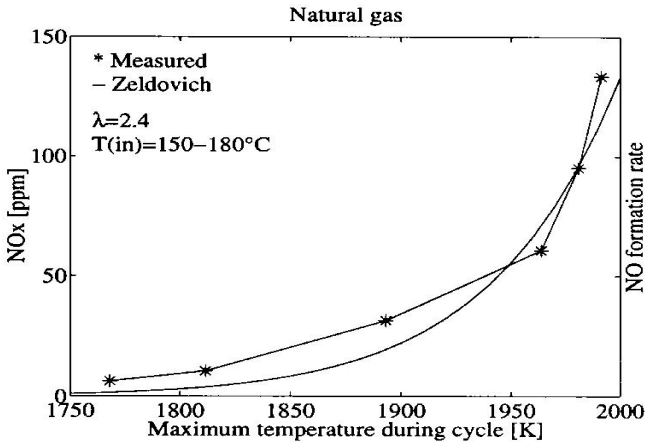


**Figure 2- 11** NOx formation as function of maximum temperature (evaluated from the cylinder pressure) during cycle for natural gas. [Chistensen and Johansson, 1999].

The fuel used in diesel engines is a complex mixture of hydrocarbons. In the case of complete combustion, hydrocarbons will be converted to $CO_2$ and $H_2O$. However, even in the complete combustion, $NO_x$ formation is inevitable since the engine works in the environment of the atmosphere, where 78% of air is nitrogen by mole. [BBC. 2014]. and the unit is percentage by mole.

The composition of air indicates each mole of $O_2$ (oxygen) provided to the engine combustion will inevitably bring another (78/21) 3.71 mole of $N_2$ (nitrogen) into the combustion together with some other elements in the air. Therefore, it can be expressed as the following balanced chemical equations:

The formula for a ultra-low sulphur hydrocarbon fuel can be written as $C_xH_y$, where, the sulphur, nitrogen, and oxygen contents are negligible.

If it's the combustion in pure oxygen, the emissions will only be water and $CO_2$, which two behave harmless to the environment.

Equation 9…… $C_xH_y + (x+y/4)\ O_2 \rightarrow xCO_2 + y/2\ H_2O$

If considering the real case for instance combustion in the air (nitrogen joined the reaction), the equation should be rewritten as following:

Equation 10..... $C_xH_y + (1+e)(x+y/4)(O_2 + 3.71N_2) \rightarrow x\,CO_2 + y/2\,H_2O + (x+y/4)\,e\,O_2 + 3.71e\,(x+y/4)\,N_2$

Here, e represents the level of excess air, e.g. if there is 10% excess air, e will be 0.1. In the case of stoichiometric combustion, e=0.

The $N_2$ formed at high temperature will undergo endothermic reaction with surrounding oxygen in the air, creating $NO_X$ (NO nitric oxide and $NO_2$ nitrogen dioxide). [Iaccsea. 2015]. In addition, considering the large amount of nitrogen exists in air, the amount of nitrogen achieved at high temperature is enormous as well.

Generally, the combustion in the engine cylinder cannot be perfect, even the excess oxygen is available in diesel engines. This is related to fuel air mixing at local scales. There will be fuel rich zones around fuel injection areas where the complete oxidation of hydrocarbons in the very short time scale cannot be completed.

### 2.2.3 Particle emissions from diesel engines

The diesel particulate matter (PM) is defined as material captured on the particulate filter paper where exhaust gas passes after been cooled by dilution to 50 ℃ and below, including carbonaceous components, soot, unburnt fuel, lubricating oil, sulphates, and ash etc. The diesel engine's PM emission can be 100 times as the SI engines, and this fact led the regulation of PM emissions for CI engine. [Andrews. 2015]. Typical composition of diesel PM is shown in the figure 2-13.

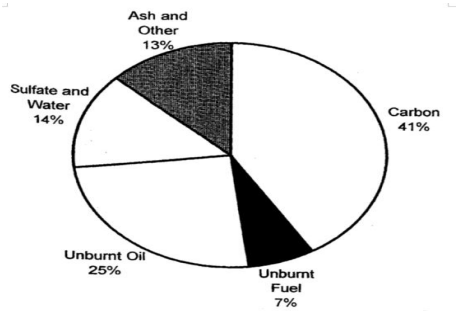


**Figure 2-12** The composition of diesel PM. [Liu, et al. 2003].

As shown in the above figure 2-12, the majority composition in the diesel PM is the carbon. This is generated from the diffusion burning of fuel mixture and the rich

combustion process. The unburnt oil and unburnt fuel in the PM are both produced as the consequent of cooling process, because the low temperature caused the insufficient combustion. The lubricating oil in the engine can be burned in the combustion process and those organo-metallic additives within will produce ash as contribution to the PM emission. The sulphur in the fuel can also forms sulphates which each gram absorbs 1.3g of water at 50℃. [Andrews, 2015]. The particulates from the CI engine exhaust vary from sizes, this is shown in the following table 2-1 and their distribution is shown in the following figure 2-14 [Kittelson, 1998].

**Table 2-1** The size and mode of PM.

| Name | Maximum diameter (nm) | Minimum diameter (nm) | Mode |
|---|---|---|---|
| PM 10 | 10,000 | 2,500 | Coarse |
| Fine particles | 2,500 | 100 | Accumulation and agglomeration |
| Ultrafine particles | 100 | 50 | Accumulation |
| Nanoparticles | 50 | 0 | Nuclei |

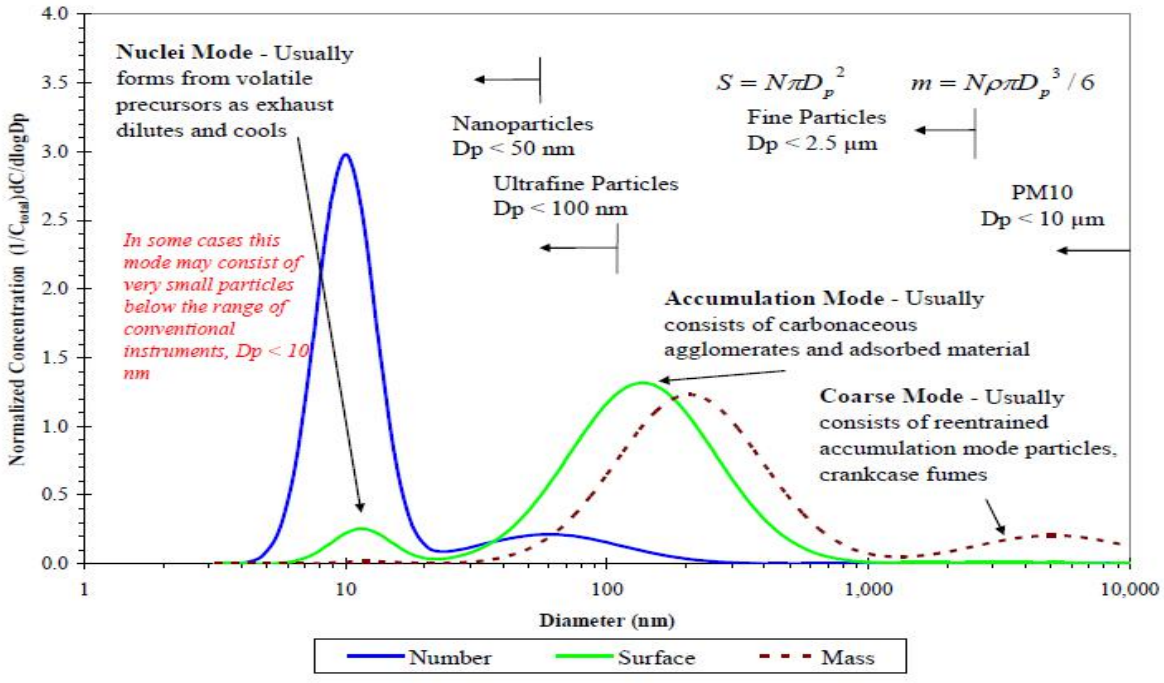


**Figure 2-13** Typical engine exhaust particle size distribution by mass, number and surface area.

As shown in figure 2-13, the particle emissions generated from a diesel engine can be classified into three kinds: the coarse mode particles, the accumulation mode particles and nuclei mode particles. The coarse mode particles are produced from deposition of particulate of combustion chamber and exhaust gas system and have the largest particle size. The accumulation mode particles are formed due to agglomeration in condensation and consisted of solids and adsorbed material, for instance heavy hydrocarbon fractions. Their size typically ranged from 50 nm to 500 nm. The nuclei mode particles are the smallest particles produced from diesel engine, with particle diameter smaller than 50 nm, and are generated due to the nucleation of volatile materials. [Alam, et al., 2016].

## 2.3 Emission impacts and European emission legislation

The emissions form transportation, including on road vehicles, shipping and aviation, can all contribute to the air pollution and be harmful to either human health or ecosystem. This is the reason for the born of emission legislations, which limit the emission level to certain level and below and thus to protect the environment. This section introduces the effects of major pollutants from the vehicles and the development of EU emission legislation relating to vehicles.

### 2.3.1 Impacts of emissions on air quality

Transportation emissions pollute the air inevitably. One research conducted by the EEA (European Environment Agency) over 32 of its member countries provided the detail of transportation's contribution to the entire air pollution. [EEA, 2018].

As shown in figure 2-14 provided by EEA, the transportation emissions contributed to overall air pollution via the emission of $NO_X$, NMVOC (Non-methane volatile organic compounds), $SO_X$, CO, for $PM_{2.5}$, and for $PM_{10}$. Among all of these pollutants, the on-road vehicles contributed to the majority pollutants except for $SO_X$, which the dominant part came from the international shipping transportation. Therefore, it can be concluded that for the on-road vehicles, four major pollutants are respectively the NOx, NMVOC, CO and PM, and all of them can bring damage either to human health or our ecosystem.

$NO_X$ will react with moisture and oxygen in air to generate the acid precipitation or generally known as acid rain, which can bring harm to the land-use, public facilities and human health. As the acid rain contains acid components, it acidizes the agriculture soil when the land is rained and thus reduces the usability of land for agriculture since the crops failed to grow normally with such extra amount of acid. The acidity in the acid rain hurts the human skin as well. The corrosive chemical property of the acid precipitation allows it to bring damage to the public facilities as well, particular to those metal facilities. For instance, the rail way or metal suspend bridge, after frequent contact with acid rain for a long period, the corroded parts will bring awfully potential danger to the public. The smog can also be formed when $NO_X$ reacts with volatile organic compounds (VOCs) under heat and sunlight. This hurts the respiratory tract especially for children and those suffering from lung diseases like asthma and those who work or exercise outside, damaging the lung tissues and reducing their lung functions. [Extraordinaryroadtrip, 2015].

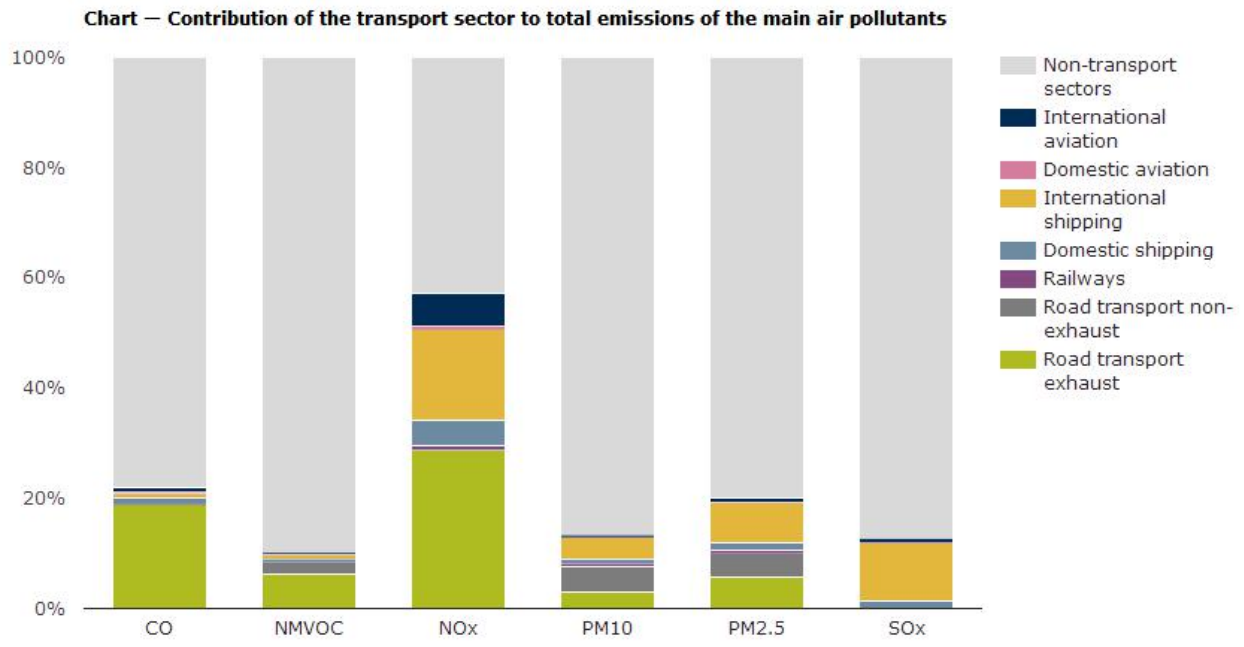


**Figure 2-14** The contribution of the transport sector to total emissions of the main air pollutants in 32 of its member states of EEA (European Environment Agency) in 2016.

NMVOC generally infers to a wide range of hydrocarbons (HC) for instance benzene, ethanol, etc. Those VOCs generated with the using of petroleum, can be directly toxic to both the environment and the human health. They damage the organ system in the human body, for instance the nervous system, respiratory system, circulatory system, immune system, reproductive system, sensory system, endocrine system, liver, kidney, etc and consequently can cause a wide range of diseases and disorders [Costello, 1979]. The NMVOC also assists the formation of ozone at the ground level via the photochemical reaction. The high concentration of ozone can bring damage to the human health despite the fact of absorbing ultraviolet rays to protect people from skin diseases. A research conducted by Laurent, A and Hauschild, MZ using sector-specific substance profiles to study the impacts of NMVOC emissions on human health in European countries for 2000-2010 shows that NMVOC hurts people's health mainly by its directly toxic effects. The toxic impacts to human health are mainly caused by the substances of formaldehyde, acrolein and furan, which are found in NMVOC. And effective air pollution abatement strategies are needed. [Laurent and Hauschild, 2014].

CO emitted to the air can be inhaled by people and thus enters human bloodstream through respiratory system. The carbon monoxide being taken into human body has strong affinity to bind with hemoglobin in blood and will form carboxyl-hemoglobin, which reduces oxygen carrying capacity of the blood itself. Therefore, the CO pollution could lead to lack of oxygen delivered to the organs and tissues in human body, and this will bring symptom as headache, nausea, asphyxiation and fainting. [Tutorvista, 2013]. Although the relevant low concentration of carbon monoxide is only a threat to those who suffered from cardiovascular diseases, evidence has shown that even at some concentrations in the low level, CO can affect healthy people as well, resulting the reduction of working ability or suffering from visual impairment. [Cleanairtrust, 1999].

PM in the atmosphere can affect people's lungs and hearts. Since those small particles are small enough to be inhaled by people, the microscopic solids or liquid droplets carried by PM can have access to the lungs or enter the blood circulation system especially for those ultrafine particles. This could cause serious health problems such as nonfatal heart attacks, irregular heartbeat, aggravated asthma, or decreased lung

function or even premature death in people especially who suffered from cardiopulmonary diseases. [EPA[b], 2014]. The PM emission in the atmosphere can reduce the visuality as well.

### 2.3.2 EU emission legislation

As the on-road transportation emissions are either harmful to people's health or the natural environment, the emission legislation has been enacted. The EU emission legislation was firstly started from Euro 1 in 1992 for light duty vehicles and from Euro 0 in 1988 for heavy duty vehicles. Every 3 to 5 years, the new generation emission standard has been created. Table 2-2 provides the development scale of European emission legislation from beginning to now; and table 2-3 provides the European emission standards for light commercial vehicles ≤1305 kg (Category N1-I), g/km. [Europa[a], 2011].

**Table 2-2** The European emission standard development time scale.

| Light Duty Vehicle standards | Heavy Duty Vehicles standards | Year |
|---|---|---|
| Euro 1 | Euro I | 1993 |
| Euro 2 | Euro II | 1996 |
| Euro 3 | Euro III | 2000 |
| Euro 4 | Euro IV | 2005 |
| Euro 5 | Euro V | 2008/2009 |
| Euro 6 | Euro VI | 2015 |

As the diesel engine emits more PM and NOx while the petrol engine generates more CO and HC based on their working principles, the emission standards are more focussed on restricting $NO_X$ and PM emission for diesel engines and simultaneously limit the CO and HC emissions from gasoline engines. This also can be noticed from the table 2-3.

**Table 2-3** European emission standards for light commercial vehicles ≤1305 kg (Category N1-I).

| Tier | Date | CO | THC | NMHC | NOx | HC+NOx | PM |
|---|---|---|---|---|---|---|---|
| Diesel | | | | | | | |
| Euro 1 | Oct-94 | 2.72 | - | - | - | 0.97 | 0.14 |
| Euro 2 | Jan-98 | 1 | - | - | - | 0.7 | 0.08 |
| Euro 3 | Jan-00 | 0.64 | - | - | 0.5 | 0.56 | 0.05 |
| Euro 4 | Jan-05 | 0.5 | - | - | 0.25 | 0.3 | 0.025 |
| Euro 5a | Sep-09 | 0.5 | - | - | 0.18 | 0.23 | 0.005 |
| Euro 5b | Sep-11 | 0.5 | - | - | 0.18 | 0.23 | 0.005 |
| Euro 6 | Sep-14 | 0.5 | - | - | 0.08 | 0.17 | 0.005 |
| Petrol (Gasoline) | | | | | | | |
| Euro 1 | Oct-94 | 2.72 | - | - | - | 0.97 | - |
| Euro 2 | Jan-98 | 2.2 | - | - | - | 0.5 | - |
| Euro 3 | Jan-00 | 2.3 | 0.2 | - | 0.15 | - | - |
| Euro 4 | Jan-05 | 1 | 0.1 | - | 0.08 | - | - |
| Euro 5 | Sep-09 | 1 | 0.1 | 0.068 | 0.06 | - | 0.005* |
| Euro 6 | Sep-14 | 1 | 0.1 | 0.068 | 0.06 | - | 0.005* |
| * Applies only to vehicles with direct injection engines | | | | | | | |

## 2.4 Emission control

The methods for emission control can either be improving the engine combustion or cleaning the exhaust gases via exhaust aftertreatment devices. This can be seen from the figure 2-15. For instance, applying Exhaust gas recirculation (EGR) can reduce the peak temperature of the combustion and reduce the $NO_X$ emissions, and utilizing the PM filter in the exhaust gas pipe can effectively reduce the PM emission. Typically, the methods applied in the after treatment are Diesel Oxidation Catalyst (DOC), which intends to reduce HC and CO emissions, Diesel Particle Filter (DPF), which is designed to remove the PM and soot from exhaust gas, and DeNOx equipment, which aims to reduce NOx emissions. Currently, integrated emission control systems combing

different after treatments together are also applied in order to control the emission more effectively.

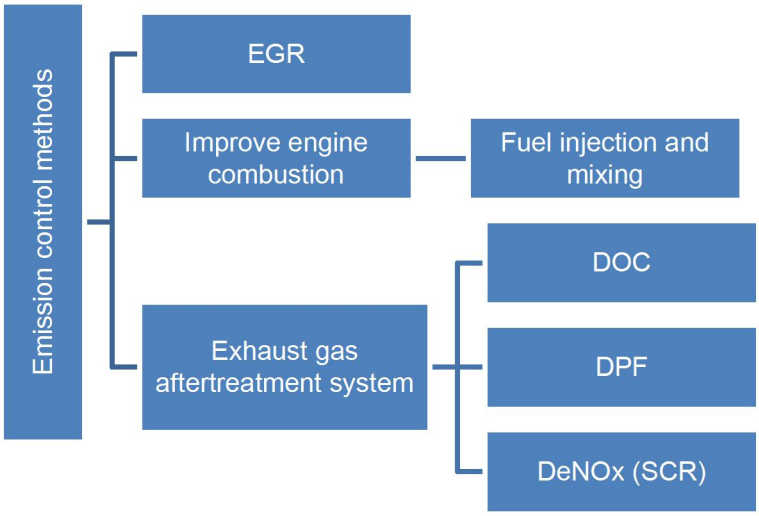


**Figure 2-15** The emission control methods diagram.

### 2.4.1 EGR

The EGR system is a method to reduce $NO_X$ emissions from source-combustion chamber. It recirculates a part of exhaust gas back to the engine combustion cylinder. The exhaust gas dilutes the oxygen in the combustion chamber acting as inert components to combustion, therefore the peak combustion temperature decreases, resulting less $NO_X$ formed during the combustion process. Other methods such as modifying the fuel injection timing or control the ignition delay can also improve the engine combustion so as to reduce PM and NOx emissions.

### 2.4.2 Fuel injection and fuel mixing

In order to improve the fuel mixing and fuel combustion, engine manufactures utilize different piston design and fuel injection technology and strategy. The figure 2-16 shows the piston design of the IVECO diesel engine used in this research. The physical concave-convex design of the piston could create swirl of fuel after the fuel injection, and thus enhance the fuel mixing before the fuel combustion occurs. As the fuel mixing

is improved by this design, the emissions generally produced from unburnt fuel can be reduced, typically the hydrocarbon emissions.

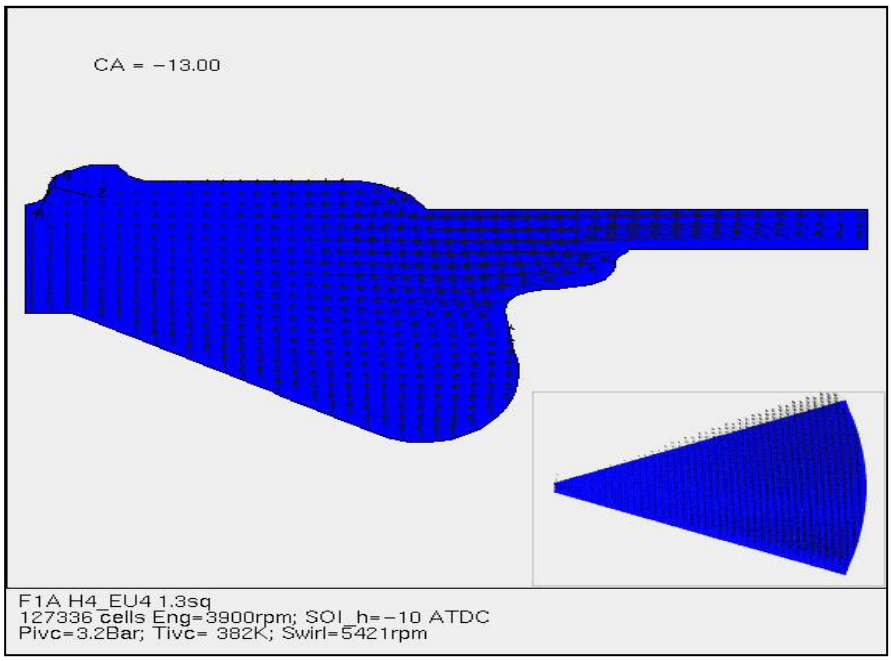


**Figure 2-16** The IVECO diesel engine piston design. [Schmidt, 2014].

Besides the piston design, the fuel properties and fuel injection pressure could also lay impact on the fuel spray and fuel mixing. One of the important fuel injection characteristics is the fuel droplet size. According to the study of Dernotte, the Sauter mean diameter is defined as the mean diameter of fuel droplets generated under high injection pressure, and can be expressed using formulation shown in below [Dernotte, et al., 2011]:

Equation 11…….$SMD = 9.59 \times Vact^{-0.37} \times \rho_{gas}^{0.21} \times \rho_{fuel}^{0.28} \times e^{0.03Vfuel}$

Where:

Vact is the actual fuel jet velocity in m/s; $\rho_{gas}$ is the gas density; $\rho_{fuel}$ is the fuel density; and Vfuel is the fuel kinematic viscosity.

The Vact is determined by multiplying the coefficient of discharge for nozzle opening by the theoretical fuel velocity issuing from nozzle opening. These two parameters are

calculated using the pressure drop across the nozzle opening, nozzle outlet diameter and fuel kinematic viscosity.

Thus, it can be found that the fuel droplet size is determined both by the fuel properties and the fuel injection parameters. Other parameters like temperature can also affect the fuel droplet size. From the study of Dizayi, B, et al, increasing the fuel injection temperature from 40°C to 90°C can improve the fuel mixing and reduce the fuel droplet size. [Dizayi, et al, 2014]. In this research, different types of fuels were tested under same engine power conditions to acquire comparisons, therefore, only the fuel property should contribute to the fuel droplet size difference. The viscosity between HVO, GTL and diesel fuels are similar, however the HVO and GTL fuels have lower density, which caused the fuel droplet size of HVO, GTL and their blends be smaller.

### 2.4.3 DOC

The DOC is widely used in diesel engines to control the HC and CO emissions. The DOC catalysts are usually using platinum and palladium, to oxidize the HC and CO. The chemical oxidation reactions for CO and HC can be expressed as below (Under the reaction with catalyst) [Brandt et al, 2000]:

Equation 12……$2CO + O_2 \rightarrow 2CO_2$

Equation 13.....$C_XH_{2X+2} + (1.5X + 0.5)\ O_2 \rightarrow X\ CO_2 + (X+1)\ H_2O$

According to research of Andy Walker and Claus Görsmann, both the age of catalyst and the engine speed can impact the DOC performance. As show in figure 2-17 [Walker and Görsmann, 2015], the fresher catalyst will convert the HC more effectively while the higher engine speed helps the DOC to achieve better efficiency at temperature 200℃ and below. Although in low temperature around 150℃ and below the DOC behaves ineffectively to oxidize the HC and CO, Walker and Görsmann pointed out the utilization of Zeolites can solve this problem. Because the zeolite can absorb HC at low temperature and release them at high temperature, thus solving the problem of low oxidation.

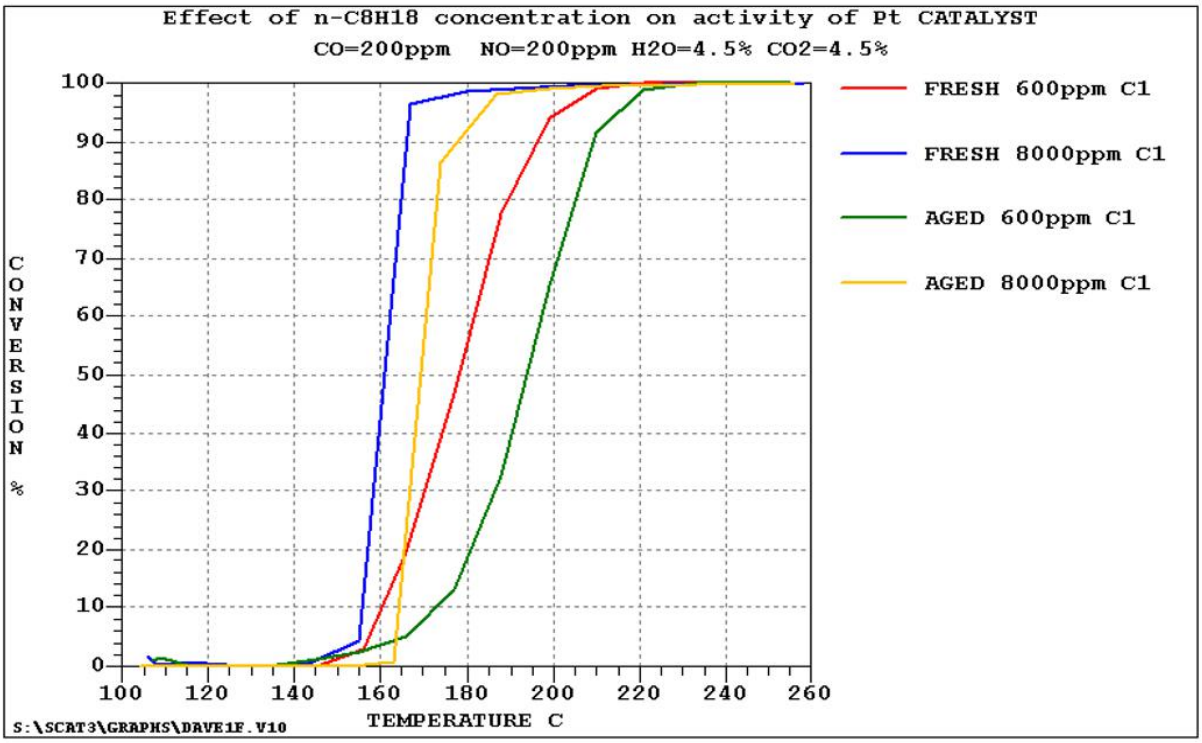


**Figure 2-17** $C_8H_{18}$ Concentration Effect on Fresh and Aged Pt Catalyst.

The DOC also contributes to lower PM emission as it removes the HC part which could form to particle matter later. However, DOC could not remove the elemental carbon in the exhaust gas since the residence time of elemental carbon in the DOC is generally too short for the DOC to break it down. Therefore, further treatment to reduce PM emission is necessary.

### 2.4.4 DPF

The DPF is designed as a filter to reduce the diesel particle matter or soot from the diesel engine, and it's classified based on the materials used in the filter. Typically, there are Cordierite wall flow filters (Also known as Ceramic Wall-Flow filters), Silicon carbide wall flow filters, Ceramic Fiber Filters, Metal fiber flow-through filters. Those filters have high filtration efficiency while low pressure drop, thus maximizing the PM reduction efficiency. Their chemical stability and thermal resistance are also important for safety concern and economic perspective. The following figure 2-18 provides an example of Cordierite wall flow filter, which the most widely used DPF type currently.


**Figure 2-18** Ceramic Wall-Flow DPF Materials.

Composition detail: Cordierite ($2MgO2Al_2O_35SiO_2$); Silicon Carbide (α-SiC); AT ($Al_2TiO_5$) [ Murtagh, 2015]

The DPF regeneration can be competed in either active method or passive method. For the active DPF regeneration, the vehicle would detect the backpressure on DPF and thus adjusting the engine fuel injection so as to increase the exhaust temperature and burn off the soot on DPF. For the passive DPF regeneration, the cleaning process would occur when the vehicle is running with high exhaust temperature condition. This is very likely to happen when the vehicle is running on motor ways. The high exhaust temperature would burn off the soot on the DPF, thus completing the regeneration process. [Wei, et al, 2011].

### 2.4.5 SCR

Besides the DOC and DPF, the DeNOx devices are designed to reduce NOx emissions from diesel engine. Typically, the Selective Catalytic Reduction (SCR) or NOx Absorber Catalysts (NAC) is used.

The SCR technology chemically converts NOx, including NO and $NO_2$ to nitrogen and water using urea which contained ammonia. The chemical reactions can be expressed as followings [Long and Yang, 2002]:

Equation 14.....$4NO + 4NH_3 + O_2 \rightarrow 4N_2 + 6H_2O$

Equation 15.....$2NO_2 + 4\ NH_3 + O2 \rightarrow 3\ N_2 + 6\ H_2O$

Equation 16.....$NO + NO_2 + 2\ NH_3 \rightarrow 2\ N_2 + 3\ H_2O$

The type of catalyst and exhaust temperature can impact the SCR efficiency. Typically, the SCR efficiencies are above 70%, and can achieve as high as > 95%. According to the research of Tao, the utilization of Wash coated, SCR Catalysts reduces more than 95% of NOx emission from the exhaust gas of a diesel engine. [Tao, et al. 2004]

### 2.4.6 Integrated emission control

Currently, as the DOC intends to reduce CO and HC while DPF and SCR are designed to remove PM and NOx, the integrated after treatment system combing those methods together is applied for controlling emissions more effectively. For instance, the compact SCTR system, which combines the DOC, DPF, SCR technologies all together, successfully achieved effective performance in emission control of diesel engines. Its configuration and performance are shown in the figure 2-19 and figure 2-20 below.

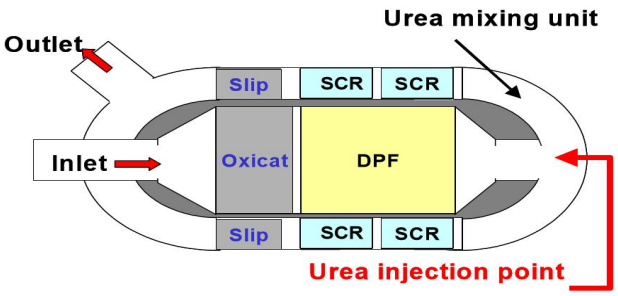


**Figure 2-19** The working diagram of compact SCTR system.

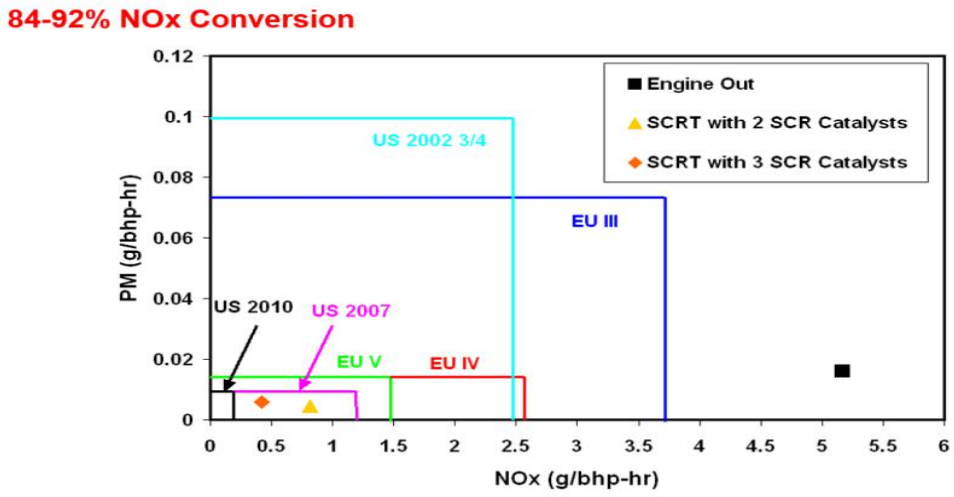


**Figure 2-20** The performance of compact SCRT system.

The SCRT system combines different types of SCR catalysts as well, and as shown in the figure 2-21, the SCRT with 3 SCR catalysts achieved better performance than with 2 SCR catalysts.

## 2.5 Gas emission measurement

Different kinds of gas measuring principles are applied for different types of gases. The following table presents the general measuring principle corresponding to particular gas types.

**Table 2-4** Gas measurement principles.

| **Exhaust gas type** | **Measuring principle** |
|---|---|
| CO and $CO_2$ | Non-Dispersive Infrared (NDIR) |
| NO and NOx | Chemi-luminescence detector (CLD) |
| THC | Flame ionization detector (FID) |
| $O_2$ | Magneto-pneumatic detection (MPD) |
| THC specification | FTIR technology |

### 2.5.1 Non-Dispersive Infrared (NDIR)

The Non-Dispersive Infrared (NDIR) utilizes the physical principle that CO and $CO_2$ can absorb certain wavelength's lights. The test chamber is emitted by a beam of infrared, containing of a wide range spectrum, and be known in concentration for each wavelength. Then the sample gas passes the chamber, and the CO and $CO_2$ existed in the sample gas will absorb a specific wavelength of light. After this, the remaining light will be collected on the end of the chamber, and the system will compare the concentration of the specific wavelength's infrared (the infrared can be absorbed by CO and $CO_2$). Thus, according to the difference in concentration of specific wavelength infrared, the amount of infrared has been absorbed can be acquired, and via further calculation, the concentration of CO and $CO_2$ in sample gas can be achieved as well. [Wang, et al, 2015].

### 2.5.2 Chemi-luminescence detector (CLD)

The Chemi-luminescence detector utilizes the photons generated when NO reacts with ozone. This can be expressed as below:

Equation 17.....$O_3 + NO \rightarrow NO_2^{*} + O_2$

The excited $NO_2$ would be formed first and then the excited $NO_2$ emits photons. Since the photons created will generate electricity voltage, and this voltage is proportional to the NO (or NOx) concentration, thus the concentration of NO and NOx can be acquired. [Planchet and Kaiser, 2006] For $NO_X$ measurement, $NO_2$ will be converted to NO via a conversion catalyst first and then the same procedure applies.

### 2.5.3 Flame ionization detector (FID)

The Flame Ionization Detector (FID) is based on measuring the ions produced as the HC compounds are combusted in hydrogen flame environment. Because the total ions generated during the combustion are proportional to the organic species concentration of sample gas participated in the test. Therefore, the THC concentration can be obtained via converting data from ions production to organic concentration. Generally, the ions generated are detected by the ammeter equipped in the FID. [Black and High, 1977]

### 2.5.4 Magneto-pneumatic detection (MPD)

The magneto-pneumatic detection is based on the Oxygen modules' physical paramagnetic properties, which directs them to the strongest magnetic field they are placed in. First, before the measurement, the reference gas containing oxygen enters the test chamber where non-homogenous magnetic field is created by electricity. Due to the oxygen's paramagnetic property, the oxygen modules placed in the chamber will then move to the strongest magnetic field produced by electricity, and therefore generating pressure flow which can be detected by miniature flow sensor. Then, during the measurement, the sample exhaust gas with oxygen needs to be determined is mixed with reference gas and enters the test chamber where the non-homogenous magnetic field remains same, generating pressure flow which later be recorded as well. After this, by comparison the difference in pressure flow, the oxygen difference between

the sample exhaust gas and reference gas can be acquired. Finally, the system can achieve the oxygen concentration of the sample gas via systematic calculation, because the sample gas' properties (Oxygen concentration) are already known. [Spirometryworks, 2011].

## 2.6 Particle number measurement

The measurement of particles can be treated as two steps: first the sample particles are classified into different size categories in order to analyze for their size distribution; second the sample particles are counted in number in order to acquire their concentration level.

### 2.6.1 Particle size classifier

The size classification of particles is realized based on the physical mobility of particles. The mobility of particles can be divided into electrical and aerodynamic mobility based on their different size. Thus, two classification methods commonly used are electrical mobility classifier and aerodynamic classifier. The electrical mobility classifier first adds particles with prescribed charges which are proportional to the surface area of them. Then those charged particles enter in a strong electrical field produced by high voltage electrode. Finally, they can be classified by the electrometer detectors equipped in the column, because the differences of mobility of particles decided by their sizes. One very commonly used electrical mobility PN analyser is DMS 500. [Cambustion, 2015]. The aerodynamic classifier consists with multiple cascaded collection stages. Each stage has penetration holes in particular size. Therefore, when the particles passed through the cascaded stages, they can be classified based on their aerodynamic diameter. One very commonly used aerodynamic mobility instrument is ELPI®+ (Electrical Low-Pressure Impactor). [Dekati, 2017].

### 2.6.2 Particle number counter

The particle counting methods generally used is CPC (Condensation particle counter) and electricity charger counter. Since the particles generated from engine combustion is too small to be detected by conventional optical particle counter, the CPC is designed to

enlarge the particle to a detectable level via a condensation process in supersaturated gas. This is due to during the heterogenous nucleation of particles in supersaturated vapor, the particles will grow up to form droplets. After the particles are enlarged, optical particle counter can be used to measure the particle number. [Cheng, 2011]. The CPC is applied in SMPS (Scanning Mobility Particle Sizer Spectrometer). The electricity charger counter detects the particles which have been charged already. As the total electricity received by the electrometer should be proportional to the total particle number, therefore, the current signal generated by the detected electricity can be converted to the particle number concentration. The Cambustion DMS500 is using electricity counter to acquire particle number concentration. [Cambustion, 2015].

### 2.6.3 SMPS and DMS 500

Two commonly used PN analyzing in current academic are: The scanning mobility particle sizer (SMPS) and the differential mobility sizer (DMS 500). Both of those two systems utilize the electric field force to either generates mobility to the particles or classify the particles.

The SMPS is designed to detect the size distribution and concentration of particles in a range from 2 nm to 1 μm. Its working principle can be explained in the figure 2-21. [Tsi, 2015]. Since the particles will receive electric field force in an electric field and generate movement depending on their sizes, the high voltage rod in the figure 2-21 creates electric field, and thus achieves mobile particles, allowing the system to calculate the particle size and mobility distribution.

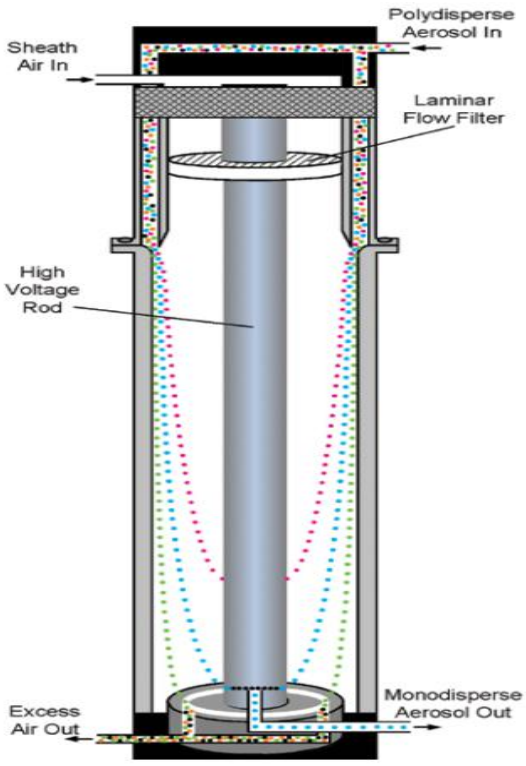


**Figure 2-21** The working principle of SMPS spectrometer.

Compared to SMPS, the DMS 500 is capable of measuring fast aerosol size in real time, minimizing the particle loss due to diffusion. Its operating principle is expressed in the figure 2-22. First, the particles are added with prescribed charges, which are proportional to the surface area of them, via a unipolar corona polar. Then those charged particles enter in a strong electrical field produced by high voltage electrode as shown in the figure 2-22 and be classified by the electrometer detectors equipped in the column, because the differences of mobility of particles decided by their sizes. Finally, the output signals from those 22 electrometers are processed in real time to provide the concentration and distribution data. The system operates under fixed pressure so as to avoid sample fluctuation. And the short residence time for classification and surface tension effects prevent the evaporation of those volatile particles. Its sizing range is from 5 nm to 1 μm, with fastest response time at 200 ms. [Cambustion, 2015].

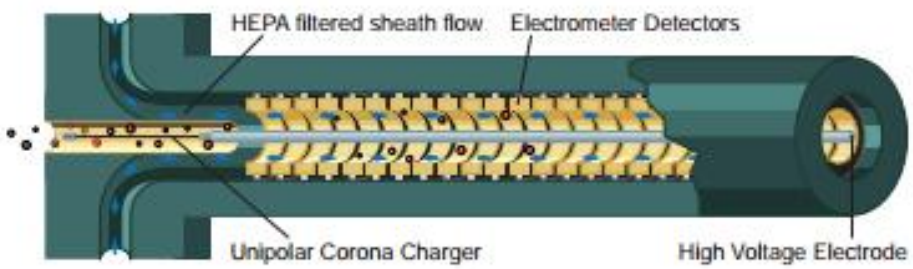


**Figure 2-22** The operating principle of DMS 500.

## 2.7 Alternative fuels

Because of the rising development of transportation, industry, and human activities, the application of diesel engines spreads widely, leading the consumption in petroleum derived fuels to have kept increasing in the past decades. However, as the petroleum derived fuels are fossil derived energy resources, indicating they're limited natural resources. Therefore, alternative fuel technology is currently becoming more and more necessary as to reduce the heavy reliance on fossil derived fuels and to control the pollutants' emissions. In this research, HVO fuel and GTL fuel were used to determine how these two alternative fuels can improve engine combustion and emission performances.

### 2.7.1 HVO fuel

Hydrogenated vegetable oil (HVO) can either be derived from waste cooking oil or animal fats and thus can be deemed as renewable energy resources. The chemical scheme of HVO production is explained in figure 2-23. [Neste, 2018]. In the hydro-treated process of HVO production, the oxygen in triglycerides from vegetable oil is removed by hydrogen, and the original triglycerides are be split into three saturated paraffinic hydrocarbon chains. Thus, the HVO consists of only straight chains and branched paraffins, indicating that HVO fuel can be blended with conventional diesel fuel at any desirable bending ratio when applied on diesel engine and HVO fuel can be burned off more completely. In other words, in the process of refining HVO, oxygen is

removed by the hydrogen added at the isomerization stage, leaving the HVO free of aromatics, which contributes to polycyclic aromatic hydrocarbons emissions [Correa and Arbilla, 2006]. Previous study by Sugiyama, et al, [2011]. also showed the HVO with zero aromatics produced lower hydrocarbon and PM emissions than petroleum diesel

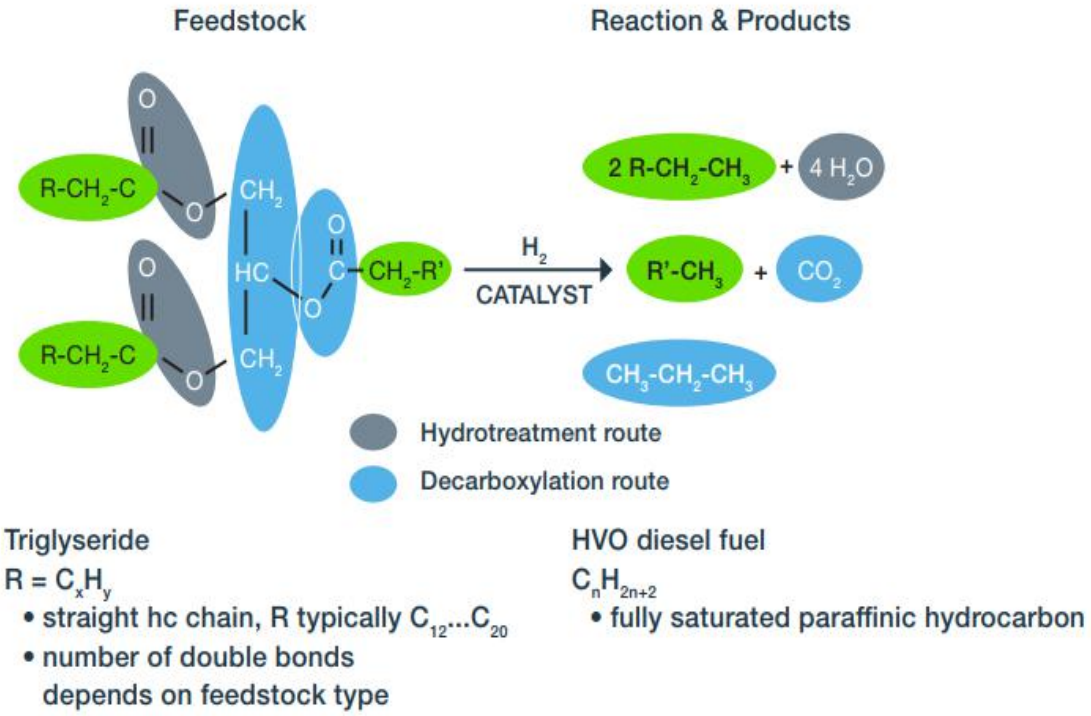


**Figure 2-23** The chemical reactions for HVO fuel production.

The hydrotreated vegetable oil can assist the engine to emit less particulate matter because in absence of aromatic compounds and less $NO_X$ as the adiabatic flame temperature decreased [Pflaum, et al, 2010]. It can be used either as blended or neat HVO, and different types of injection timing can be modified so as to achieve the best emission standards and fuel consumption. The following table 2-5 and figure 2-24 provide the different injection timing example, and the respectively 30% HVO blended, HVO neat, and diesel performance in $NO_x$ emission and fuel consumption. [Aatola, et al, 2008].

**Table 2-5** Effect of HVO on emissions and fuel consumption by using different injection timing settings in a heavy-duty engine without EGR and after treatment (Reference is EN 590 diesel fuel)

| Injection timing -> | Default | Advanced | Remarkably advanced | Retarted |
|---|---|---|---|---|
| $NO_x$ | -6 % | 0 % | +4 % | -16 % |
| Smoke | -35 % | -37 % | -32 % | -32 % |
| Fuel cons (mass) | -3 % | -6 % | -8 % | 0 % |
| Fuel cons (volume) | +5 % | +2 % | 0 % | +8 % |

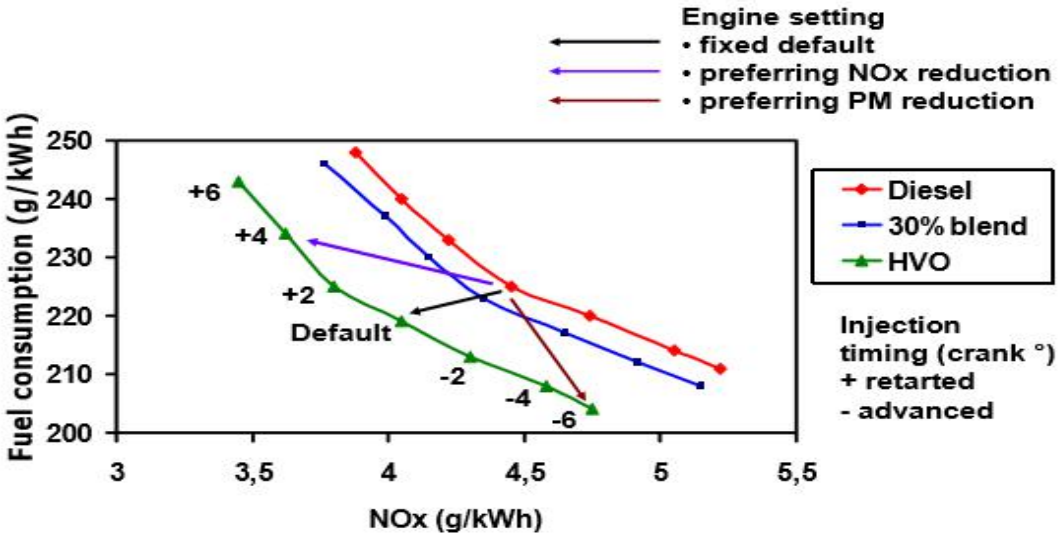


**Figure 2-24** NOx to fuel consumption trade-off curves of diesel fuel, diesel fuel with 30 % HVO and neat HVO.

But unfortunately, this research only provided with the 30% blending ratio. There might exist another blend solution which can bring better emission performance than the 30% blending condition.

According to the manufacture of HVO [Neste, 2014], the difference between HVO and diesel is HVO fuel obtains higher cetane number and contains much less sulfur and

aromatics components. This indicates HVO fuel should have lower PM and THC emissions than EN 590 diesel. The figure 2-25 shows the effect of HVO blending ratio on emissions of a Euro 4 truck engine with EGR [Kuronen et al, 2007].

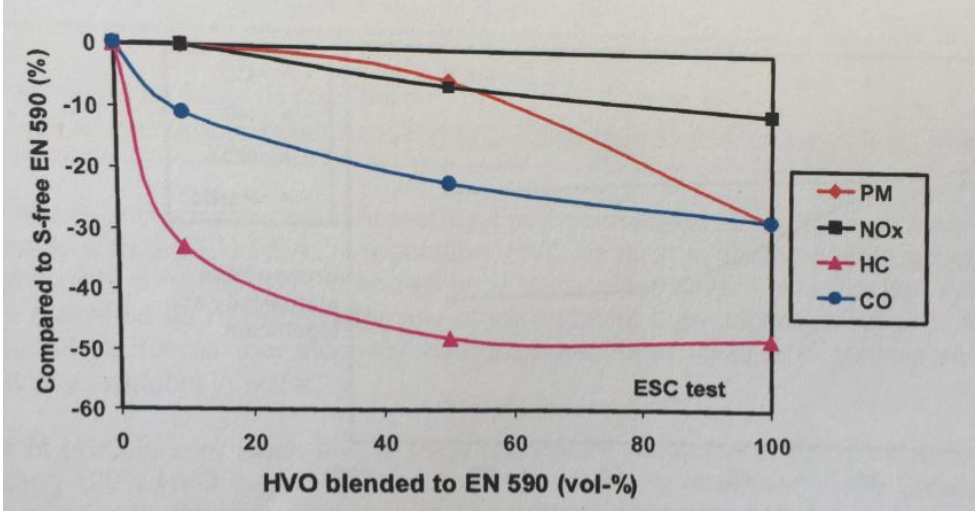


**Figure 2-25** The effect of HVO blending ratio on emissions of a Euro 4 truck engine with EGR.

Therefore, via increasing the blending ratio, it will enable us to reduce the PM and THC emissions, and via decreasing the blending ratio, it will enable us to acquire better economics.

### 2.7.2 GTL fuel

The gas to liquid (GTL) fuel is a type of alternative fuel to conventional diesel produced from natural gas. The chemical composition of GTL fuel is nearly all paraffinic. Compared with diesel, the GTL fuel has hardly any levels of unsaturated molecules and aromatics, and just normal and iso paraffinic. This gives GTL fuel higher cetane number. These properties allow the GTL fuel to burn faster and cleaner than conventional diesel fuels.

The gas to liquid (GTL) fuel can be one possible solution to reduce the diesel engine emissions. Though GTL fuels are still produced from fossil resources, the reservation of

natural gas is huge. According to PR newswire the global market for natural gas will expanded to $763.60 Billion by the year of 2019. [PR, 2014] This is boosted with the development of shale gas technology. So, GTL fuels can be as an alternative fuel for diesel engines.

The production of GTL fuel is based on the technology developed in the 1920s, named as Fischer-Tropsch process which allowing the carbon monoxide and hydrogen gas to be converted to liquid hydrocarbons. [Hensman, 2005], [Schanke, 2001]. First, the synthesis gas was produced from natural gas by partial oxidation. Then, CO and $H_2$ acquired will be converted to liquid hydrocarbons using Fischer-Tropsch process. Finally, the liquid generated would be treated with hydrocracking processed so as to fractionate its chemical bonds and to achieve high quality paraffinic liquid fuel which can be used in diesel engine. Figure 2-26 provides the production process of GTL fuel. [Shell, 2018]

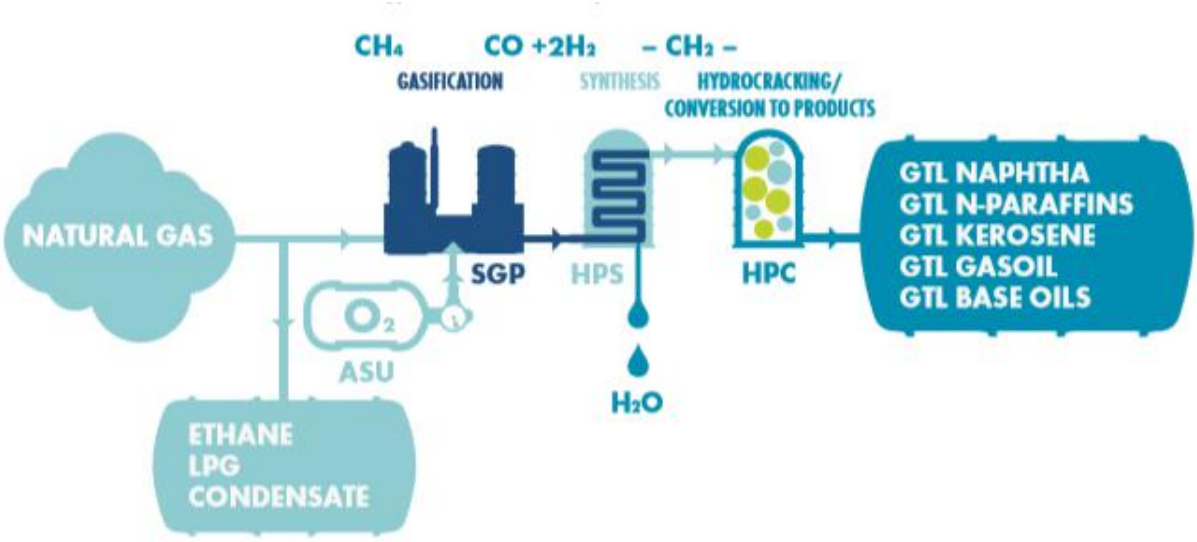


**Figure 2-26** The production process of GTL fuel.

The GTL fuel on the one hand is considered as clean fuel, because it is nearly aromatic free of unsaturated molecules and obtains with high cetane number, indicating it can be combusted fast and sufficiently. [Kitano, et al, 2005]. According to Kitano's research, the GTL fuel is capable of reduce particle emission significantly when compared to diesel on the application of direct injection diesel engine albeit the NOx emission wasn't

improved obviously. Similar results were found by Myburgh [2003]. that the GTL fuel could reduce all regulated emissions except no clear improvement on $NO_X$ emission was observed. The result is shown in figure 2-27. Therefore, the possible solution for NOx reduction of GTL application might be engine system alternations. According to AbuJrai's [2009]. research the NOx emission can be reduced to 40% using reformed exhaust gas recirculation (EGR) system. On the other hand, the GTL fuel is produced from natural gas instead of crude oil, indicating the application of GTL fuel can relieve the reliance on conventional crude oil derived from limited fossil resources.

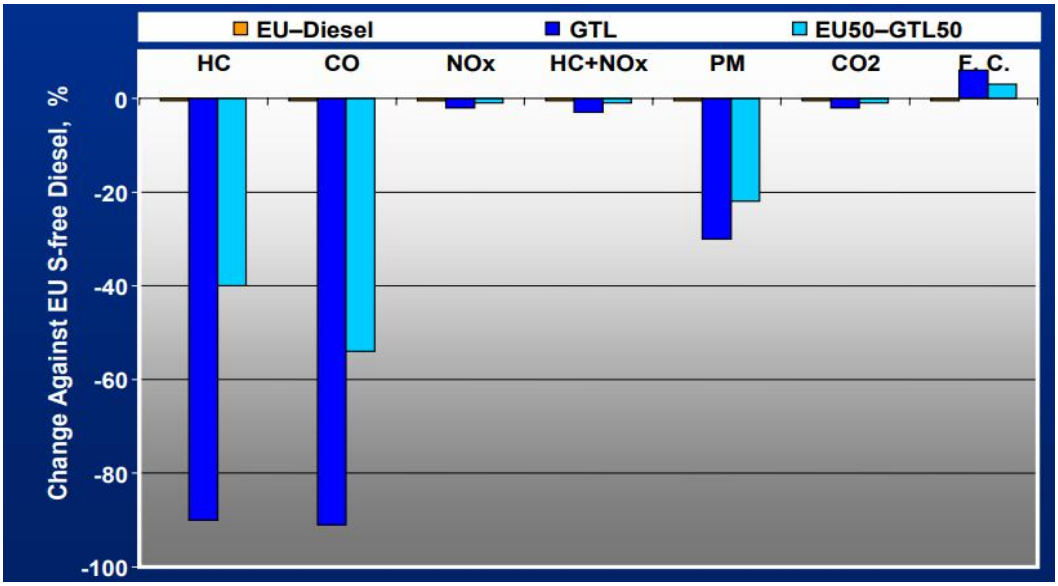


**Figure 2-27** The emission reduction of pure GTL and 50% GTL fuels against to diesel.

### 2.7.3 The impact of aromatic component on combustion and emission

The pure HVO and GTL fuels discussed in the previous section were used as alternative fuels and blended with diesel fuel in this research. A very important difference between HVO/GTL fuels and diesel fuel is that diesel fuel contains aromatics. (Both HVO and GTL fuels are aromatic free.) Therefore, it's necessary to study the combustion and emission characteristics of aromatics in diesel engine combustion.

Aromatics are a type of hydrocarbons consisted of at least one benzene ring which six carbon atoms are connected with double bonds (sigma bond). Because they have

sweet and pleasant odours, they are named as aromatics. [Meinschein, 1969]. Their chemical formula can be written as $C_nH_{(2n-6)}$. [Woltermann, et al, 1993]. Aromatics are different from straight hydrocarbon chains which in absence of double bonds and can be written as $C_nH_{(2n+2)}$. [Knothe, et al, 2003]. [Allison, 2019]. Since the double bond existed in aromatics is a strong chemical bond and require high energy to breakup, the aromatic component can be more difficult to be decomposed and oxidised in diesel engine combustion. Therefore, aromatics contribute to particulate emissions. [Kee, et al, 2005] As shown in figure 2-28, it can be fund that the particulate emission increased when the aromatic concentration was increased. This eventually caused the diffusion combustion and ignition delay to take longer time period. In contrast to aromatic containing fuel, the aromatic free fuels can be combusted more completely and rapidly because the single bond can break up easier than aromatic double bond. Therefore, the fuel containing no aromatics would have a faster combustion phase, leaving less time allowed for the formation of $NO_x$. [Kidoguchi, et al, 2000]. This can also be supported by figure 2-28. The NO emission decreased when the aromatic concentration was reduced. The total hydrocarbon and particulate emissions from aromatic fuels are also higher than from aromatic free fuels, since aromatic fuels are difficult to be combusted completely.

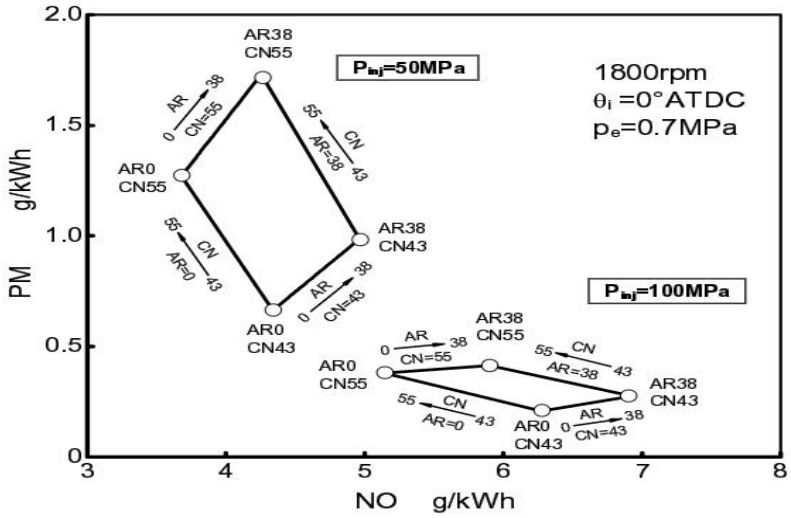


**Figure 2-28** Relationship between NO and particulate emissions at different cetane number and aromatic containing fuels. [Kee, et al, 2005].

### 2.7.4 Other alternative fuels

Generally, the alternative fuels for diesel engine can be biofuels which have three categories: first generation, second generation, and third generation. The first generation of biofuels indicating fuels derived from edible biomass, while the second-generation biofuel is mainly converting non-edible lignocelluloses feedstock to cellulosic ethanol. And the third-generation biofuel refers to biofuels generated from microalgae, however the difficulties in finding economic and environmental solution for sustainable cultivation of the sources hinders its development. Nowadays, the biofuels can be typically processed into two kinds: bioethanol and biodiesel.

The traditional production of bioethanol is based on chemical fermentation of hexose: the enzymes and microorganisms added to the chemical reaction assist the fermentation of hexose, which is produced after the raw sources are heated and crushed controlled temperature, moisture, and pressure. As a result, the hydrous ethanol and carbon dioxide are created as products, then after distillation, which filters out the co-products and refines the original hydrous ethanol, the bioethanol is achieved. Usually, the raw sources can either be sugars or starches, both of which have high hexose storage. The following figure 2-29 expresses the process procedure of generating bioethanol from sugar and starch. [Sims , 2008].

As the bioethanol chemically is a form of alcohol, indicating it is ignitable and therefore can be applied directly in adapted engine. According to Balat, the bioethanol although has lower energy density when compared to petroleum gasoline (66% of the gasoline's), it achieves high thermo efficiency due to the higher-octane number it obtains. [Balat, et al, 2008]. Or the bioethanol can be blended with proper amount of petroleum diesel and in-directly used in diesel engine. According to Magín, utilizing anhydrous bioethanol blended with petroleum diesel, with 10% volume of bioethanol and no fuel additives, then the engine was tested under five selected steady stages from European Emission Directive 70/220 on a stationary engine test bed. The results showed the PM and soot emissions were reduced significantly, thus providing a solution for emission control and fulfilling the governmental policy (required to use more than 5.75% of biofuel in 2010). [Lapuerta, 2008].

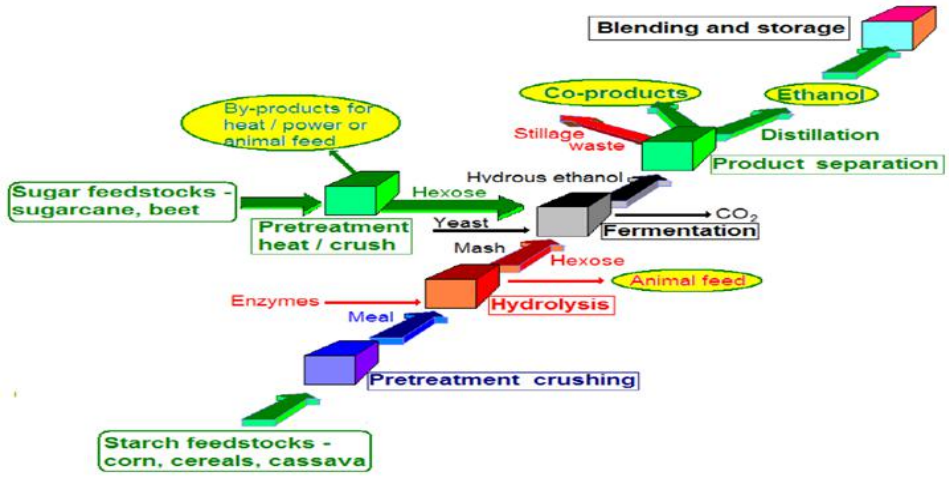


. **Figure 2-29** Process procedure of generating bioethanol from sugar and starch.

Biodiesel is Fatty Acid Methyl Esters (FAME) produced by adding alcohol to vegetable oils through the transesterification process, which is a chemical reaction between vegetable oils or animal fats and alcohol, generally the methanol or ethanol. In order to raise the efficiency of the reaction, the conversion is undertaken under heated temperature with catalysts, usually the sodium hydroxide and sodium methoxide. The following figure 2-30 shows the chemical function of transesterification. [AOCS, 2001].

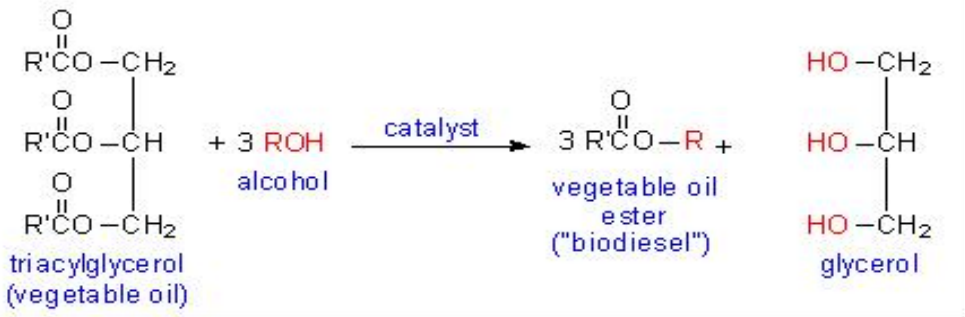


**Figure 2-30** Chemical reaction of Transesterification process.

Initially, the triglycerides contained by vegetable oils or animal fats are converted into alkyl esters, which is a form of FAME and known as biodiesel. This is due to the ester exchange during the reaction. Then later, the rest part of the triglycerides and alcohol will generate by-product call glycerol. Both the biodiesel and glycerol are produced in liquid form, therefore liquid to liquid separation method is applied so as to filter out the

biodiesel. Since the physical densities of these two products are different, therefore the filter equipment commonly used is either gravitational or centrifugal. The coalescers sometimes are applied in the filter equipment in order to accelerate the filtering.

The chemical and physical properties of biodiesels are similar to the petroleum diesel, with biodiesel having slightly higher viscosity and lower energy density or calorific value (about 5% lower than diesel). However, the biodiesel is in absence of sulfur and aromatic compounds and therefore CO, HC, PM, and $SO_2$ emissions from biodiesels are lower [globalgwa.org, 2011]. The transesterification technology is a mature and well-established method for biodiesel production. Researchers are also trying to utilize the biodiesel on gas turbines, indicating the possibility of powering generation station or aviation industry with biodiesel. For instance, the spray combustion method is under immigrating, even though previous studies have shown large difference of physical properties differs from diesel such as vapor pressure, density, surface tension, kinematic viscosity, etc. [Yasin, et al, 2012].

Despite the advantages of the biodiesel, it still has disadvantages such as relatively high viscosity and low volatility. For instance, the Khiari's research in 2015 found that biodiesel produced from Pistacia Lentiscus oil will be not possible to be directly used in direct inject diesel engine because of the problems generated from high viscosity and low volatility. [Khiari, et al, 2015]. Therefore, many biodiesels are blended with petroleum diesel in order to acquire better performance. For example, the Jatropha crude oil which contains phorbol esters, a promoter of cancer, if it is blended with diesel at mixing ratio 60%, then the phrbol ester generated will be decomposed by combustion itself and behaves lower than detection limit. [Macamo , 2014].

Hiroki Arai [2011]. investigated the performance of three types biodiesels on combustion and emission and found that the soot emission differences among biodiesel fuels are small and biodiesel can achieve low enough soot emission by its nature (Oxygen containing and aromatic components none-containing). However, the NOx emission is related to the cetane number and H/C ratio, as the high cetane number leads shorter ignition delay and reduces the premixed combustion, thus enables lower NOx emission; while the low H/C ratio can reduce the adiabatic flame temperature, and consequently

enables lower NOx emission. Therefore, biodiesel with low H/C ratio and high cetane number might be the optimum. [Arai, 2011]. In fact, low cetane number will improve the premixing, resulting less PM and soot emissions [Janssen, et al, 2010]. but increase the NOx. Therefore, systematic research should be implemented to find the key properties which lay influences on emissions, particular for $NO_X$ and PM.

Besides the bioethanol, biodiesel, HVO and GTL, there are many other forms of alternative fuels, for instance the straight vegetable oil. These fuels have different production procedures when compared to bioethanol and biodiesel. They are also intended to reduce emissions and buffering the heavy reliance on fossil derived fuels. The cooking oil (straight vegetable oil) blends with diesel in diesel engine successfully reduced emissions respectively around 50% in smoke, 33% in HC and 38% in CO. [Kanthavelkumaran and Seenikannan, 2014]. The used cooking oil applied in heavy good vehicles significantly reduced the PM emission by approximately 70% and the CO emission by 50%, with slightly reduced the HC emission. [Hadavi, et al, 2015].

Zervas [2008]. reports on the PM emissions from aliphatic fuels compared to diesel, and there doesn't tend to be much difference at low loads. Zervas [2008]. also reports on the particle size distribution and shows that there is little difference between the total particle number and the distribution of the sizes. Zervas [2008]. denotes that reduced sulphur content like in aliphatic fuels should decrease the particle number, as sulphur is key in the nucleation mode. Therefore, the control of the nucleation-mode must come from another source and Zervas [2008]. denotes this to carbon condensation.

As so far, though many studies have been done in the application of biofuel blending. The study by Petersen, et al, showed that the unburned hydrocarbon and CO emission for blended biofuels were mainly depended on the ignition quality instead of fuel vitality. [Petersen, et al, 2010] And another study leaded by Janssen found that blend 10 vol-% of rapeseed oil with EN590 diesel could successfully reduce the soot emission up to 50% compared to use diesel only. [Janssen, et al, 2010]. Also, according to the research leaded by Mittal, blending the n-butanol with diesel could improve the CO and PM emissions, however in contrast to CO and PM, the HC and NOx emission increased with the increasing blending ratio. [Mittal, et al, 2015].

# Chapter 3. Experiment and methodologies

This chapter consists of two parts: the first part presents experimental instruments, experiment procedure and data analysing of particle number measurement research. The second part provides the experiment methodology and data processing method used for blended fuel research.

## 3.1 Equipment and methods for particle number measurement research

### 3.1.1 Experiment instruments

This section presents the introduction of particle number instruments used in this research, the working principles of a burner which is used to produce exhaust sample, and the description of dilution system applied.

**Mini cast burner**

This research applied a Jing Aerosol real soot generator model 5203 type C mini-CAST. The soot particles are produced with diffusion flame during pyrolysis. As shown in figure 3-1, the exhaust gas generated from the gaseous fuel (propane) is coated by insufficient air, thus to produce soot particles. Nitrogen then used as quenching gas so as to prevent further combustion as well as stabilize the soot. After the soot particle is generated, dilution air is applied to dilute the particle stream and adjust the soot particle concentrations. [Jing LTD, 2013].

This mini-CAST is capable of produce particles with mean mobility diameter from 20 to 200 nm, and with high concentration from $10^7$ to $10^8$ particle/ $cm^3$. With suitable flow settings, it can produce exhaust gas mimicking the diesel exhaust in concentration level and particle size range. [Richard, 2014]. The Mini-CAST settings is shown in table 3-1. Because the particles produced from the mini-CAST can have different physicochemical properties based on different mini-CAST settings, for instance, the different affinities for butanol and the different light absorption per mass of elemental carbon (n), this research tested a wide range of particle concentration's exhausts from mini-CAST and attempted to achieve the most comprehensive experiment data. [Mamakos, 2013].

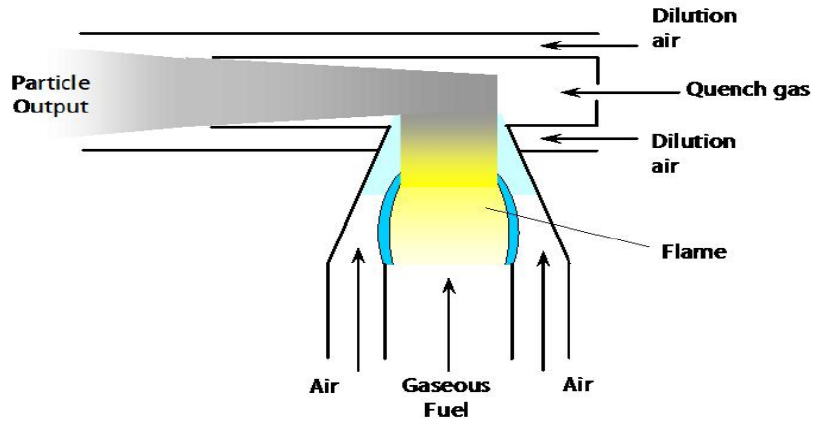


**Figure 3-1** The principle of mini-CAST soot generator.

**Table 3-1** Mini-CAST settings.

| Setting | Set point | Unit |
|---|---|---|
| Fuel Gas | 86 | ml/min |
| Mixing $N_2$ | 0.06 | l/min |
| Oxidation Air | 2.5 | l/min |
| Dilution Air | 60 | l/min |
| Quench $N_2$ | 20 | l/min |

**HORIBA SPCS**

The HORIBA MEXA 2300 SPCS is designed to measure the solid particle number concentration from raw engine exhaust in real time. In this research, two Horiba MEXA 2300 SPCS are used. The reason using two SPCSs was to find out the differences in between as they connected with different dilution system. The two SPCSs were calibrated under different methods, one was calibrated by PMP/EU method, using soot as reference; the other was calibrated by PMP method, using emery oil as reference, and which was recommended by the Horiba manufacture. [Horiba[b], 2013]. The technical specification of MEXA 2300 SPCS is shown in following table 3-2.

**Table 3-2** The specification of MEXA 2300 SPCS.

| | |
|---|---|
| **Model** | MEXA-2300SPCS |
| **Conformed standard** | • UN/ECE Regulation No.83 *[1]<br>• UN/ECE Regulation No.49 *[1]<br>• CE, FCC, KC |
| **Application** | Measurement of solid particles in engine exhaust with and without after-treatment systems (diesel, gasoline) |
| **Sampling variation** | • Dilution sampling by full flow dilution tunnel *[1,2]<br>• Dilution sampling by partial flow dilution tunnel *[1, 2, 3]<br>• Direct sampling from tail pipe *[1] |
| **Measuring components and range** | Number concentration of solid particles: (0 to 10000) up to (0 to 50000) particles/cm3 (after internal dilution) *[4] |
| | |
| **Measuring principle** | Laser scattering condensation particle counting (CPC) |
| **Data monitoring and saving** | • Monitoring on the display of control PC - Instantaneous values (CPC count, dilution factor) - Averaged values after data logging (CPC count, dilution factor)<br>• Data saving in text format (Instantaneous values, such as particle concentrations, dilution |

| | |
|---|---|
| | factors, flows, temperatures, analog inputs etc.) |
| **Inputs and outputs** | • Analog output: 0 V to 10 V (4 channels)<br>• Analog input: 0 V to 10 V (4 channels)<br>• Parallel input: 8 channels (logging start/logging stop, etc.)<br>• LAN interface: communication with a host PC (AK protocol) |
| **Interval of data updating** | Data saving: 0.1/0.2/0.5/1.0 s (selectable)<br>LAN communication: 0.1 s |
| **Configuration** | Standard system consists of following units<br>• Main unit<br>-volatile particle remover (VPR): primary diluter (PND1), evaporation tube and secondary diluter (PND2)<br>-particle number counter (PNC): condensation particle counter (CPC)<br>-particle transfer system (PTS): particle transfer tube (PTT), pre-classifier<br>- sample flow controller (SFC): pump, mass flow controller<br>- other main parts: interface unit, vacuum pump, HEPA filter, solenoid valves, temperature control unit, etc.<br>• Direct sampling unit (DSU) |

| | |
|---|---|
| | particulate sampling probe (PSP), pre-diluter<br>• Control unit<br>control PC (laptop with Windows 7)<br>Optional units<br>• Dilution factor checker (DFC)<br>• Linearity check unit (LCU)<br>• Volatile-particle generation unit (VGU) |
| **Power supply voltage and frequency** | 200/220/230/240 V AC (–10%, max. 250 V), 50/60 Hz (–1.0 Hz), single phase (to be specified when ordering) |
| **Power requirements** | Main unit (with heated sampling tube) + DSU: Max. 2.6 kVA Main unit (with heated sampling tube) + DSU + all optional units (DFC/LCU/VGU): Max. 3.5 kVA |
| **Dimensions** | Main unit: 434 (W) · 910 (D) · 637 (H) mm (Standard) (without DSU, transfer tube, control unit, optional units and excluding any projections) |
| **Mass** | Main unit: Approx. 145 kg (without DSU, transfer tube, control unit and optional units) |
| *1: The UN/ECE Regulation No.83 and the UN/ECE Regulation No.49 require dilution sampling method by connecting with full flow dilution tunnel or partial flow dilution tunnel. Direct sampling method does not conform to the UN/ECE Regulation No.83 and No.49. *2: For dilution sampling, DSU is not used. Sample flow is extracted from dilution | |

tunnel without a hatted probe or a pre-classifier. *3: MEXA-2300SPCS has a function to feed the sample flow back into the partial flow dilution system as required in the UN/ECE Regulation No.49. *4: Dilution factor of the system should be determined so that the particle concentration after dilution fits into the measuring range.

**DMS500**

One Cambustion DMS 500 MK II was used in this research to acquire the particle size distribution. It's a worldwide use particle size analyzer, and this research was trying to see the impact from different sampling frequency settings. More importantly, trying to find the lowest concentration limits for DMS 500, as accurate particle measurement in low particle concentration range is critical to the particle research. The sampling frequency tested was 1 Hz, 5 Hz and 10 Hz, for each test, the sampling time at each stable emission condition is 3 to 4 mins. The technical specification of DMS is shown in table 3-3.

**Table 3-3** The technical specification of DMS 500.

| | |
|---|---|
| **Particle size range** | 5 nm – 1 µm or 5 nm – 2.5 µm versions |
| **Spectral Elements** | 38 (1 µm) or 45 (2.5 µm) (at 16/decade, 32/decade also available) |
| **Size Classification** | Electrical Mobility |
| **Dilution Factor Range** | 1–5 (one stage) |
| | 1–3000 (optional two stage) |
| **Maximum Primary Dilution / Heated Line temperature** | 150 º C |
| **Sample Flow rate** | 8 slpm (1 µm range) / 2.5 slpm (2.5 µm range) at 0º C + 100 kPa |
| **Instrument Dimensions/ Weight** | 980h×380w×520d mm with wheels |
| | 80 kg |
| **External pump dimensions / Weight** | 443l×328w×372h mm plus wheels |

| | |
|---|---|
| | 44 kg |
| **Analogue Outputs** | 4; software configurable, 0–10V 47Ω, up to 10 Hz data rate |
| **Analogue Inputs** | 4; software configurable, ±10V |
| **Instrument Zeroing** | Automatic; internal HEPA filter |
| **Warm-up Time** | 30 minutes from switch on |
| **Number of Electrometers** | 22 |
| **Minimum resolvable gsd** | 1.05 (lognormal output) |
| **Output Data Rate** | 10/sec – 1/min |
| **Time Response** | T10–90% 200 ms (1 µm range) |
| | T10–90% 500 ms (2.5 µm range) |
| **Calibrations:** | |
| **Non-agglomerate:** | By NIST traceable PSL spheres & DMA size selected NaCl/H2SO4, comparison with standard electrometer |
| **Agglomerate (Diesel):** | DMA size selected soot, comparison with standard electrometer |
| **Calibration interval** | 12 months |
| **Warranty period** | 12 months (extendable) |
| **Max Concentration** | ≈1011 dN/dlogDp /cc (diluter on) |
| **PC Interface** | Ethernet |
| **Remote Control** | AK protocol |
| **PC Option** | Laptop or Desktop |
| **Maximum Sample Temperature** | 800 ºC |
| **Electrical Supply** | 100–115 / 220–240V 1500W |
| **Compressed air (only for engine exhaust sampling)** | Oil-free @ 3-8 bar gauge, Dewpoint 3º C or lower |
| **Extract for vacuum pump exhaust** | 12 mm internal diameter pipe |

| | |
|---|---|
| **Exhaust pipe connection to heated line** | 6 mm or 1/4-inch Swagelok |
| **Operating temperature range** | 5 – 40 ° C, subject to non-condensing humidity |

**SMPS**

One TSI 3080 SMPS was used in this research to measure the size distribution. The instrument consisted with one 3080 TSI type controller platform and one 3080L TSI Type electrostatic classifier. It could detect particles from 10 to 1000 nm in diameter, and the results were analyzed with results from two SPCSs, Cambustion DMS500, and AVL micro soot sensor. Table 3-4 provides the technical specification of SMPS. [SMPS, 2001]

**Table 3-4** The technical specification of SMPS.

| **3080 Controller Platform** | |
|---|---|
| **Mode of operation:** | Bipolar charge neutralization and differential mobility analysis (requires installation of DMA) |
| **Flow rates:** | |
| **Aerosol:** | 0 to 3 L/min, determined by external pressure or vacuum |
| **Sheath air and excess air:** | 1 to 20 L/min, manually selectable |
| **Air mover:** | 0 to 20 L/min, bypass or auxiliary flow |
| **Aerosol temperature range:** | 10 to 40°C (instrument must be within 3°C of aerosol temperature) |
| **Charger:** | Bipolar, Kr-85, 2 millicurie, half-life of 10.4 years (Model 3077 Aerosol Neutralizer* supplied with instrument) |
| **Aerosol pressure range:** | 1 ±0.2 atm |
| **Front panel display:** | Backlit, alphanumeric, 320×240-pixel LCD |
| **Calibration:** | NIST-traceable voltage and flow standards |

| | |
|---|---|
| **Dimensions (LWH):** | 45.7 cm × 41.4 cm × 40.6 cm (18 in. × 16.3 in. × 16 in.) |
| **Weight:** | 17.6 kg (38.9 lb) |
| **Power requirements:** | 85 to 260 VAC, 50/60 Hz, 200 W maximum |
| **3080L Electrostatic Classifier** | |
| **DMA included:** | Long (Model 3081) |
| **Particle type:** | Solids and nonvolatile liquids |
| **Particle size range (generation mode):** | Adjustable from 10 to 1000 nm |
| **Maximum input concentration:** | 108 particles/cm3 at 10 nm |
| **Voltage:** | 10 to 10,000 VDC |
| **Flow rate** | |
| **Sheath Air:** | 2 to 15 L/min |
| **Aerosol:** | 0.2 to 2 L/min |
| **Bypass:** | None |
| **Physical measurements** | Long DMA |
| **Height:** | 61 cm (24 in.) |
| **Outside diameter:** | 7.6 cm (3 in.) excluding ports |
| **Weight:** | 5.4 kg (11.8 lb) |
| **Complete instrument Dimensions (LWH):** | 45.7 cm × 41.4 cm × 64.3 cm (18 in. × 16.3 in. × 25.3 in.) |
| **Weight:** | 23.2 kg (51.2 lbs) |

**AVL 483**

One AVL micro soot sensor measurement unit 483 was used in this research to measure the mass concentration from soot particles. The results were analyzed against the size distribution from TSI, SMPS, and was used to estimate the particle density at different particle size (in diameter). The following table 3-5 shows the technical specification of AVL 483. [AVL[f], 2012].

**Table 3- 5** The technical specification of AVL 483.

| | |
|---|---|
| **Measured quantity** | Soot concentration ("elementary carbon") <50 mg/$m^3$ |
| **Display resolution (digital)** | 0.001 mg/$m^3$ |
| **Data rate** | Digital: max. 5 Hz Analog: 100 Hz |
| **Noise** | ≤ 0.01 mg/m3 (defined as 3 times the standard deviation of the measurement variation of the zero signal [clean, filtered air] with 1 s data smoothing) |
| **Resolution of the measurement value** | ≤ 0.01 mg/m3 (defined as 3 times the standard deviation of the measurement variation of the zero signal [clean, filtered air] with 1 s data smoothing) |
| **Drift** | ≤ 0.01 mg/m3 per hour (defined as change of the average of the zero signal [clean, filtered air] over one hour) |
| **Repeatability and reproducibility** | ≤3% (defined by the deviation to a gravimetric reference value of identical particle composition with identical sampling probe, after a successful span check) |
| **Voltage supply** | • 230 V AC version, 50/60 Hz Power consumption: 500 VA max. Fuses: 2 × 5 AT (slow blow) |

| | |
|---|---|
| | • 100/115 V AC version, 50/60 Hz<br>Power consumption: 500 VA max.<br>Fuses: 2 × 10 AT (slow blow) |
| **Ambient temperatures** | Operation: 5 … 43 °C; Storage: -5 … 70 °C (other temperature ranges on request) |
| **Humidity during operation** | corresponding to a humidity of maximum 95 % at 25 °C If this cannot be achieved, clean and dry shop air must be supplied at the relevant connector of the device. |
| **Tolerance of the exhaust input pressure** | -50 … +50 mbar |
| **Permissible exhaust temperature at the inlet** | +20 … +60 °C |
| **Humidity of the measured exhaust gas** | max. 90 % at ≤ 52 °C, non-condensing |
| **Dimensions** | Measuring unit: 19" × 5 HU × 550 mm (W × H × D) Pump unit: 19" × 4 HU × 320 mm (W × H × D) |
| **Weight Measuring unit:** | approx. 20 kg |

**Dilution system (DSU & BG3)**

Two dilution systems were used in this research in order to see the impact of sampling dilution on particle measurement. One was Direct sampling unit (DSU), which was connected to Horiba SPCS 1, dilution ratio setting was 10, the other was BG3 dilute system, which was connected to Horiba SPCS 2, dilution ratio setting was 10 and 30.

### 3.1.2 Experiment procedure

The experiment consisted of 15 stages. At each stage, the Mini-CAST burner generated exhaust gases with a certain stable particle concentration. Therefore 15 different concentrations' sampling gases were measured in this research. The concentration range acquired was from $2.99\times10^3$ (#/cm$^3$) to $1.11\times10^7$ (#/cm$^3$), and the particle size range obtained was from 65 nm to 85 nm. The different particle concentration exhaust was achieved by controlling the extracted flow from Mini-CAST burner. The relationship between particle number concentration and extracted flow from Mini-CAST is shown in figure 3-2. The concentration above $2.0\times10^6$ (#/cm$^3$) was produced by reducing the dilution air supplied to the soot rig unit. This was trying to represent the exhaust from diesel engine's upstream (before DPF), and downstream (after DPF).

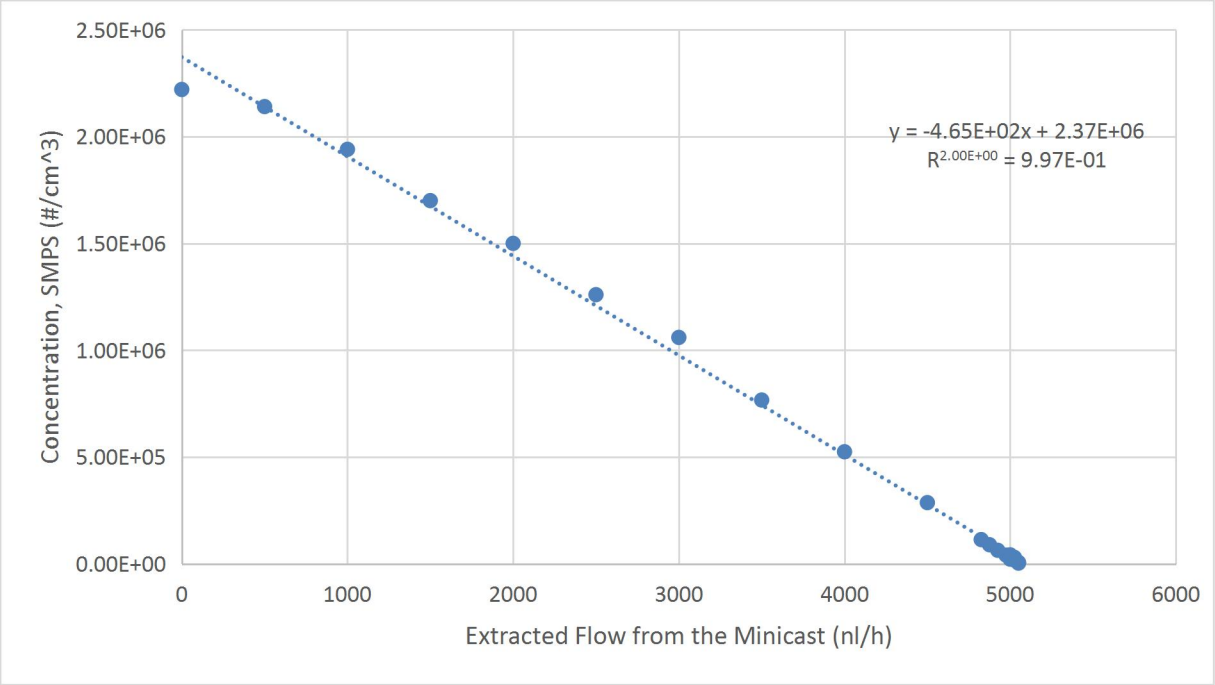


**Figure 3-2** SMPS concentration against extracted flow from the Mini-CAST.

During the experiment, five particle number and size instruments were applied simultaneously to collect experiment data. The tested particle number instrument summary is given in table 3-6. The experiment set up diagram is shown in figure 3-3. Initially, the particle soot was generated in the Mini-CAST burner, and then passed through the first diluter, oxidation catalyst, second dilutor, and residence chamber.

Then, five experiment instruments sampling at the same time with five sampling points started to measure the exhaust gas and recorded experiment data at each experiment stage. At each stage, the Horiba SPCS1's dilution settings were changed between 10 (using DSU), 10 (using BG3 diluter) and 30 (using BG3 diluter), and the AVL 483'S dilution ratio settings were changed between 2, 3, and 5. Also, the DMS 500's sampling frequency settings was changed between 1 Hz, 5 Hz, and 10 Hz. Therefore, each stage contains three groups of experiments. All the experiments were repeated for three times in order to acquire the most reliable data. The total sampling time spent was 15 (stages) × 3 (experiments) × 3 (repeated times) × 3 mins (experiment sampling duration) = 405 mins.

**Table 3-6** Summary of experiment PN instruments.

| Instrument | Manufacture | Size measurement | PN Measurement |
|---|---|---|---|
| SMPS | TSI | Yes (10¬1000nm) | Yes |
| MEXA-2300SPCS 1(Soot Cal) | HORIBA | No | Yes |
| MEXA-2300SPCS 2(Emery Oil Cal) | HORIBA | NO | YES |
| DMS500 | Cambustion | Yes (5nm¬1000nm) | Yes |
| AVL483 | AVL | No | No |

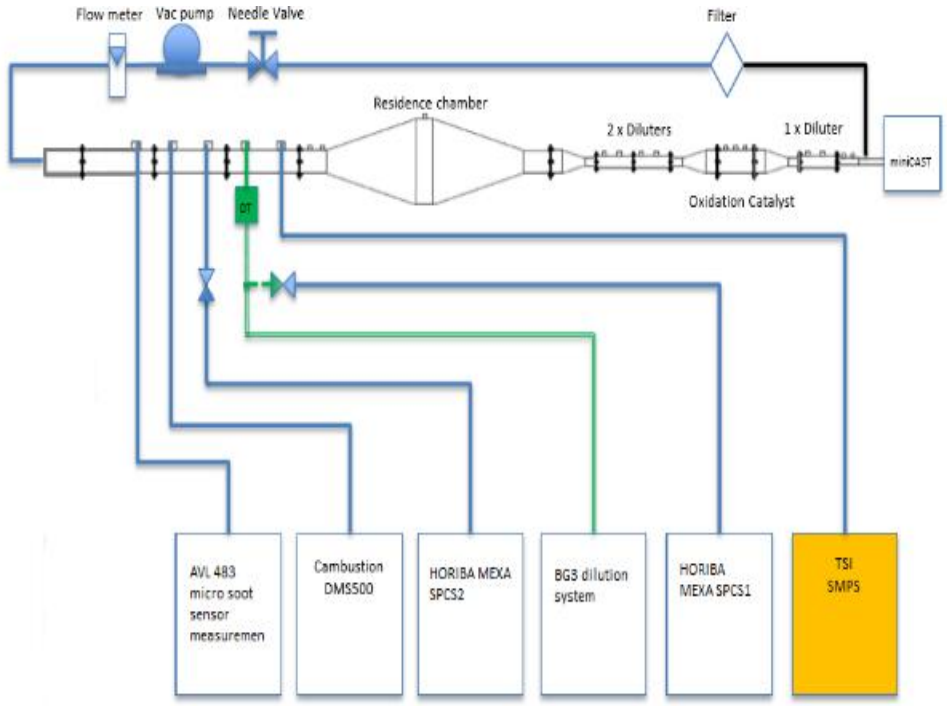


**Figure 3-3** Experiment setup diagram.

### 3.1.3 Data analysis

This section describes how raw data acquired from experiment was processed to final data presented in this thesis, and the data processed can be classified into five categories:

- The instruments comparison and correlation factors among instruments
- Particle loss analysing under the impact of different dilution ratio
- DMS 500 frequency influences on PN measurement and its measurement limits
- Particle mass concentration in relation to particle number
- Particle density estimation

### 3.1.3.1 Correlation factors among instruments

The particle number concentrations measured by SMPS, SPCS1, SPCS2, and DMS 500 were aligned with each other, and the linear relationship and correlation formulas were generated using Excel software the following figure shows an example of linear relationship between SPCS2 and SMPS. From the figure 3-4, it can be addressed that the correlation factor between SPCS2 and SMPS was 0.9636, indicating the particle number concentration measured by SPCS2 was slightly lower than from SMPS. In this way, all instruments were compared to each other, and correlation factors among them were acquired.

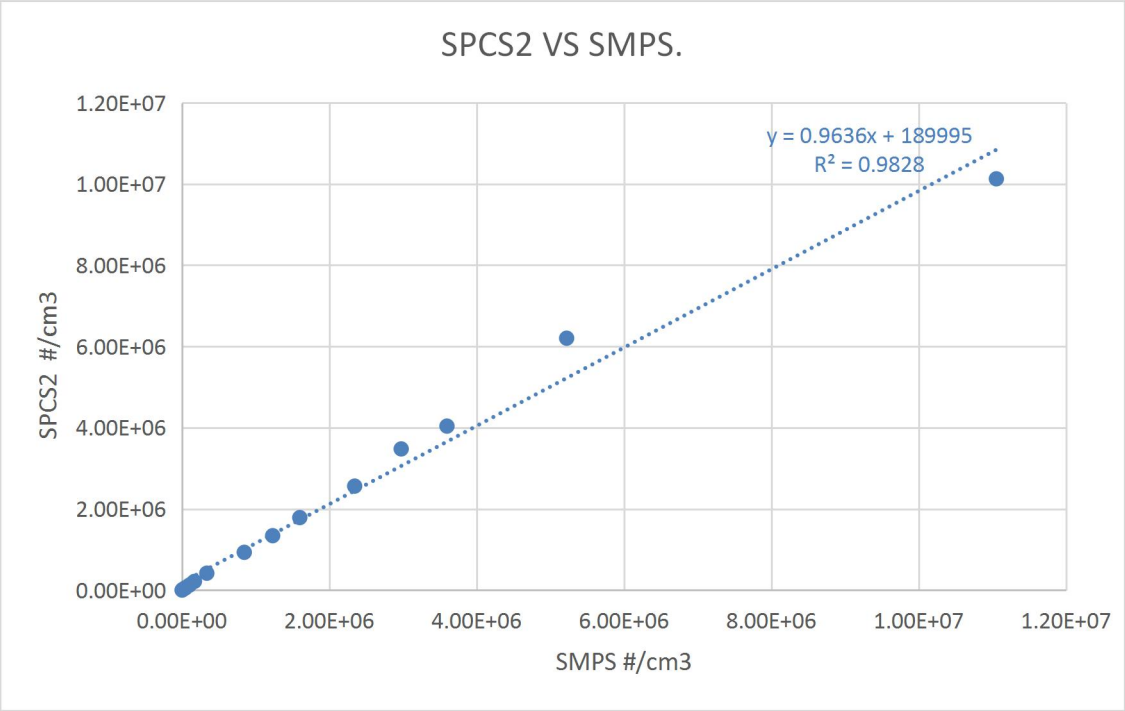


**Figure 3-4** Linear relationship between SPCS2 and SMPS.

### 3.1.3.2 Particle loss calculation

Considering the PSCS1's dilution ratios were changed from 10 to 30, the particle number losses can be calculated using the PN data measured from dilution ratio 10 and dilution ratio 30. The following table 3-7 shows an example of the losses calculated. With the PN losses calculated for all tests, the dilution ratios' impact on particle number measurement can be acquired from relationship between dilution ratio and particle losses. This will be provided in detail in chapter 4.

**Table 3-7** Particle loss calculation example.

| SPCS1 Avg. (#) Concentration with BG3.DR 10 | SPCS1 Avg. (#) Concentration with BG3.DR 30 | Particle Concentration (#) differences between BG3 DR 10& BG3 DR 30 | Particle loss.%. Between BG3 DR 10& BG3 DR 30 |
|---|---|---|---|
| 408 | 6345 | -5938 | -14.55 |
| 8140 | 29295 | -21155 | -2.60 |
| 42453 | 40767 | 1686 | 0.04 |
| 45333 | 47786 | -2453 | -0.05 |

#### 3.1.3.3 DMS 500 data analysis

The DMS 500 was tested under three different sampling frequency settings: 1 Hz, 5 Hz, and 10 Hz. The results were first averaged in each test, and then compared to each other using Excel software. For instance, at the first experiment stage, three averaged total PN values would be acquired in respectively 1 Hz, 5 Hz, and 10 Hz. Then at the second experiment stage, another three averaged PN values would be acquired. After processed all 15 experiment stages data collected from DMS 500. The linear relationship of DMS 500 using different sampling frequency can be acquired.

When comparing the PN values acquired from DMS 500 with other PN instruments' results, it was found that the linear relationship disappeared at lower PN concentration tests. In order to find out the lower detection limits of DMS 500, more systematic comparison of DMS 500's results with SPCS2 was provided in chapter six, explaining how the lower detection limits of DMS 500 was determined based on this PN research project.

#### 3.1.3.4 Particle mass concentration against particle number

The particle mass concentration data was acquired from AVL 483. Three different dilution ratio settings (2, 3 and 5) were applied for this research. First, the mass concertation values measured for each test were averaged. Then all results were compared to other particle number concentration results acquired from other PN instruments. This was trying to determine the mass concentration's relationship to number concentration.

### 3.1.3.5 Particle density estimation

With the particle mass concentration data acquired from AVL 483, particle number concentration data and particle diameter size data from SMPS, the particle density can be estimated using methods explaining below:

Considering one unit (1 $cm^3$) of sampling gas, and assuming particles were physically in sphere structure, then with the particle diameter data achieved from SMPS, the volume of particles can be calculated using formula expressed as following:

$$Volume\ of\ particle\ = \frac{4}{3} \times \pi \times (\ Particle\ diameter\ \div 2)^3,$$

Then, total particle volume can be calculated using this volume multiply the number concentration in 1 $cm^3$, and the total mass can be calculated using the mass concentration multiply 1 $cm^3$.

Therefore, the particle density can be estimated using the total particle mass in 1 $cm^3$ divided by the total volume of particles in 1 $cm^3$.

The following table 3-8 shows an example calculating particle density in Excel file using particle diameter, particle mass concentration, and particle number concentration.

**Table 3-8** Particle density calculation example.

| Experiment stages | SMPS | | AVL483 | Volume of particle $cm^3$ | Density g/cc |
|---|---|---|---|---|---|
| | Avg. Diameter nm | Avg. Conc. #/$cm^3$ | Avg. Conc. mg/$m^3$ | | |
| A | 81.73 | 8222456.522 | 0.92 | 2.86E-16 | 0.39 |
| B | 69.10 | 3304860.87 | 0.38 | 1.73E-16 | 0.66 |
| C | 68.41 | 2116378.261 | 0.23 | 1.68E-16 | 0.66 |

## 3.2 Engine instrumentation and procedures for blended fuels research

This section describes the experimental equipment used for blended fuel test on the diesel engine, the experiment methodology, and how raw data was acquired and processed.

### 3.2.1 Experiment equipment

The experiment equipment used for the engine tests can be classified into four categories: engine, engine control system, emission measuring system, and combustion performance measuring system. The following figure 3-5 explains those equipment in detail. Additional fuel property tests were carried out so as to acquire more comprehensive understanding of chemical components' effect on engine combustion and emission production. Therefore, another section will involve instruments used in the fuel property tests.

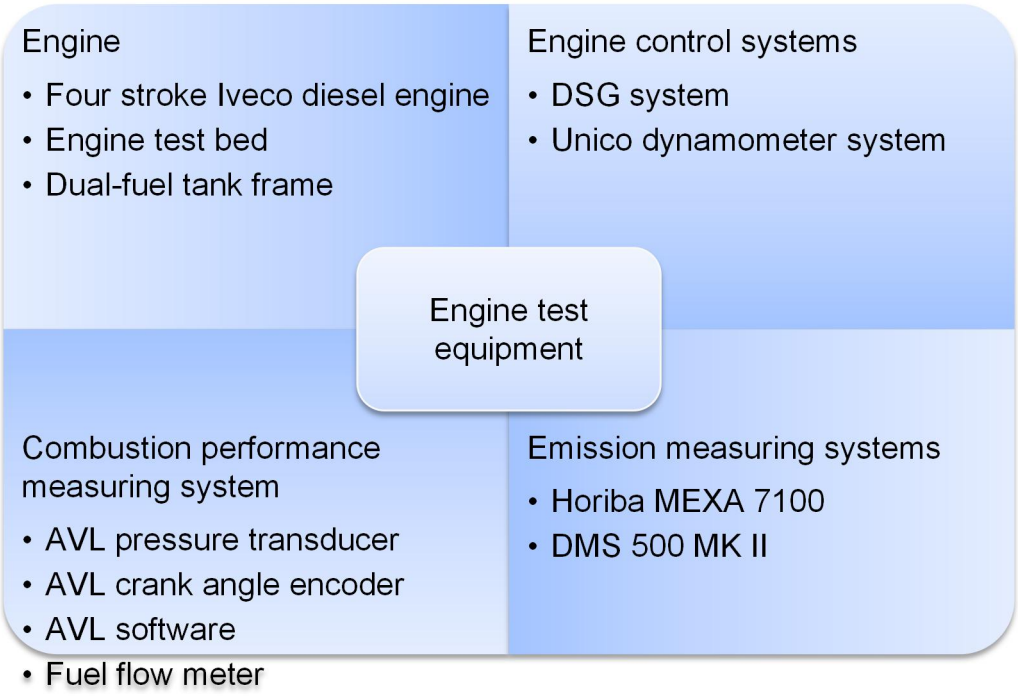


**Figure 3-5** The experimental equipment applied in blended fuel research.

#### 3.2.1.1 Engine system

The engine utilized a 3.0 L EURO 5 emission compliance IVECO diesel engine. The engine was equipped with the turbocharger, intercooler and EGR system. The engine exhaust gas after treatment system consisted a DOC (Diesel oxidation catalyst) and DPF (Diesel particulate filter). The main engine specifications are shown in table 3-9.

**Table 3-9** The specifications of the IVECO engine.

| | |
|---|---|
| **Engine type** | Iveco FICE0481F |
| **Cycle** | Diesel 4 strokes |
| **Supply** | Turbocharged with intercooler |
| **Number of cylinders** | 4 in line |
| **Total displacement** | 2998 $cm^3$ |
| **Injection type** | Direct & High pressure common rail |
| **Bore** | 104 mm |
| **Stroke** | 95.8 mm |
| **Compression ratio** | 18 |
| **Injection sequence** | 1-3-4-2 |
| **Injection pressure (maximum)** | 1600 bar |
| **Maximum torque** | 250 Nm |
| **Maximum power** | 122 KW |
| **Turbocharger air temperature** | Activates at ≥ 75 °C and deactivates at ≤ 65 °C |

The multiple fuel injection strategy of the IVECO engine used is shown in figure 3-6. Eight fuel injections can occur when the engine is working at high power condition. As it is shown in figure 3-6, the first fuel injection is designed to improve the premix of fuel and air in combustion chamber. The second fuel injection ignites the fuel, and it is followed by three main fuel injections which trying to achieve constant pressure combustion. After the main fuel injection, another small amount of fuel injection occurs and this is to oxidize the soot. Finally, the last fuel injection is to raise the temperature of

exhaust gas flow for the regeneration of DPF, thus allowing the DPF to remove the soot in exhaust gas more efficiently. This only happens when there is a DPF regeneration event.

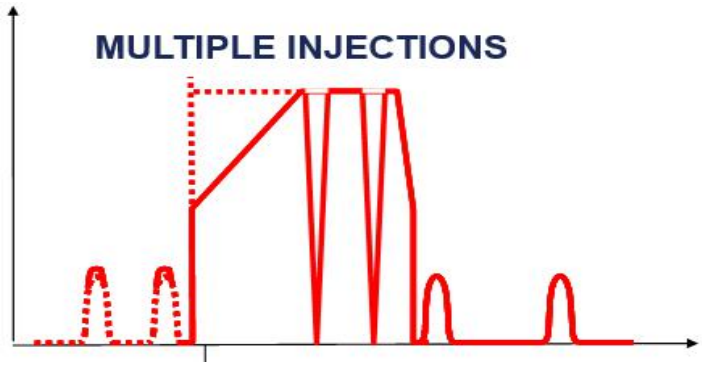


**Figure 3-6** The multiple fuel injection of IVECO engine. [Schmidt, 2014]

The engine is connected to a dynamometer allowing the engine to run at maximum torque of 238 NM. The dynamometer was controlled by the DSG software, which is also used to control the engine rpm, throttle position, and to record engine power data, emission data, and temperature data at 14 specific locations of the engine. Based on the engine and dynamometer capability, nine stable engine working conditions were selected for this research. The figure 3-7 shows the photo of the experimental engine settled on the test bed.

**Figure 3-7** The experiment engine.

In order to compare different fuels' performance in combustion and emission, two fuel tanks with capacity of 41 litres, weighted 9 Kg each, made from high-density polyethylene (HDPE), which is suitable for diesel storage, are applied in the research. Therefore, it's convenient for storage of different types of fuels during the research. In order to place the two fuel tanks, support fame was designed based on the geometric size of the two tanks and manufactured by the workshop from the University. This is shown in the following figure 3-8.

**Figure 3-8** The dual fuel tanks in the designed tank frame.

#### 3.2.1.2 Engine control system

The engine control system consists with the ignition system, DSG software and Unico Dynamometer. First, the engine is ignited by the electronic ignition system which is controlled by the electronic control system next to the engine as shown in the following figure 3-9; then the DSG software/system which is designed to control the Unico Dynamometer will motor the dynamometer and control the engine throttle, and thus engine speed is controlled by the dynamometer while the engine torque is decided by the throttle position. The throttle percentage in this research refers to the pedal percentage, which controls the amount of fuel injected. For instance, 0% throttle indicates there is no fuel injection, and 100% throttle indicated the maximum fuel injection. Both engine rpm and torque (via throttle position) can be adjusted from the DSG software interface on the DSG PC.

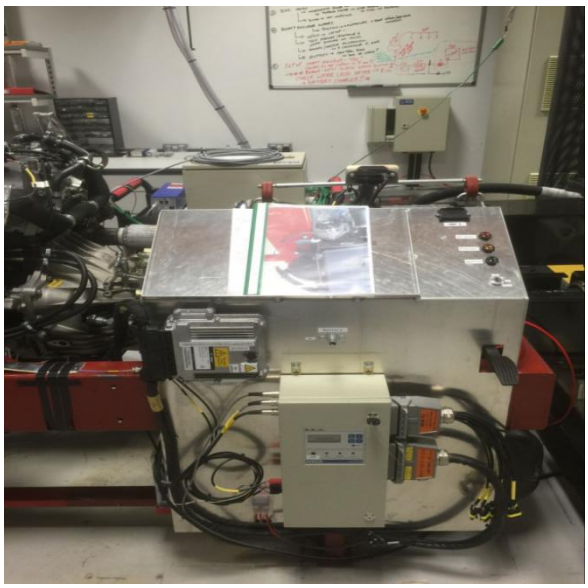

**Figure 3-9** The electronic control system of the experimental engine.

The Unico dynamometer is connected to the end of the engine as shown in the following figure 3-10. Its working rotation is in accord with the engine running direction, therefore once the dynamometer starts running, the pistons in the engine cylinders will start moving simultaneously. Via fuel injection and throttle position controlling, the engine will be able to run under desirable power.

The DSG system is the software applied to control the engine power and measuring relevant parameters, mainly the engine speed and engine torque. It controls the ignition, running of dynamometer and engine throttle position. The main operation interface is shown in figure 3-11.

The DSG system can also be connected with other channels for different data acquiring, for instance, currently, the DSG display interface also provides the emission data achieved from HORIBA emission measuring system. This is because the HORIBA data accessing channels are connected to the DSG computer.

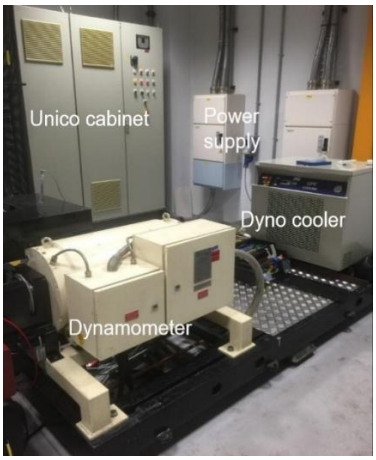


**Figure 3-10** The Unico dynamometer.

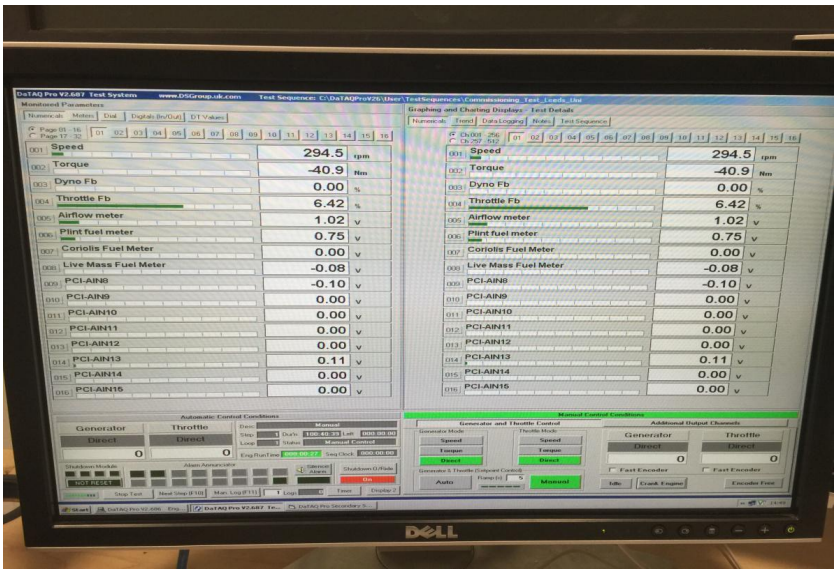


**Figure 3-11** The main operation interface of DSG system.

### 3.2.1.3 Combustion performance measuring system

The AVL system is used to acquire the pressure data of the combustion cylinder. It consisted of a pressure transducer, AVL amplifier, AVL crank angle encoder, and AVL software. A pressure transducer is installed to one cylinder of the engine on one side and inputs the signals to the amplifier as shown in figure 3-12. The AVL amplifier receives two types of signals from the experimental engine: one is the pressure signal from the cylinder; the other is the crank angle signal from the crank angle encoder. Thus, the AVL acquires both in combustion cylinder pressure and crank angle degree data.

The technical specifications of AVL pressure transducer, crank angle encoder and amplifier are provided in table 3-10 [AVL[a], 2014], table 3-11 [AVL[b], 2014]. and table 3-12 [AVL[c], 2014]. During the measurement, the amplifier receives signals from the engine and passes them to the AVL Indicom software via one Ethernet cable connected between the amplifier and computer. The software will normally record 100 combustion cycles' data (the cycle number can be modified according to requirement) and present the most recent data as shown in figure 3-13 as an example, where the average engine speed is 790 rpm.

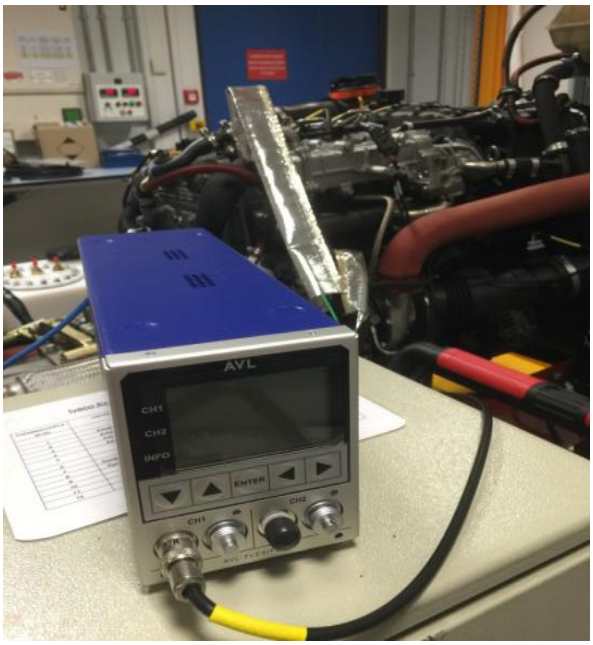


**Figure 3-12** The AVL transducer and amplifier.

**Table 3-10** The technical specification of AVL pressure transducer.

| | |
|---|---|
| **Measuring range** | 0... 250 (bar) |
| **Sensitivity** | 16 (pC/bar) nominal |
| **Linearity** | ≤ ± 0.3% FSO |
| **Thermal sensitivity change** | ≤± 2% 20… 400°C |
| | ≤0.5% 250 ±100°C |
| **Cyclic temperature drift *** | ≤ ± 0.4 bar |
| ***at 7 bar IMEP and 1300 rpm, diesel** | |

**Table 3-11** The technical specification of AVL crank encoder.

| | |
|---|---|
| **Speed range:** | 50 rpm ... 20 000 pm |
| **Vibration-resistance axial and radial (measured at the Angle Encoder cover):** | 500 x 9.81 m/s² (500 g) with peaks up to 1000 g (momentary) |
| **Permissible ambient temperature** | - 40° C … + 70° C for the electronics |
| | - 40° C … + 120° C for mechanical components and lens at standstill, during operation the permissible ambient temperature is lower by 2° C per 1000 rpm |
| **Permissible temperature at mounting face:** | - 40° C … + 100° C |
| **Service life:** | at least 10 million revolutions at 500 g vibrational load |
| **Mass load of crank shaft:** | depending on mounting position and position of flexible hose approx. 300 g when support arm horizontal approx. 350 g when support arm vertical |
| **Moment of inertia of rotating masses:** | 3.8 x 10-5 kgm² moment of inertia GD² = 1.5 x 10-3 Nm² |
| **Degree of protection:** | IP54 |

**Table 3-12** The general technical specifications of AVL amplifier.

| | |
|---|---|
| **Power supply** | Input voltage range 9.5 V ... 36 V DC |
| **Max. continuous current load of supply connector** | 8A |
| **Power consumption** | 20 W start-up power, 10 W continuous power |
| **Dimensions** | 86 x 112 x 270 mm (width x height x depth). Depth including cable connections: 350 mm |

| | |
|---|---|
| **Weight** | 1 AVL FI Piezo 2P2x = 1.6 kg |
| **Ambient temperature** | -10 °C ... +50 °C |
| **Storage temperature** | 0 °C ... +65 °C<br>Maximum relative humidity 80% for temperatures up to 31° C, with a linear decrease to 50% relative humidity at 40° C, non-condensing. |

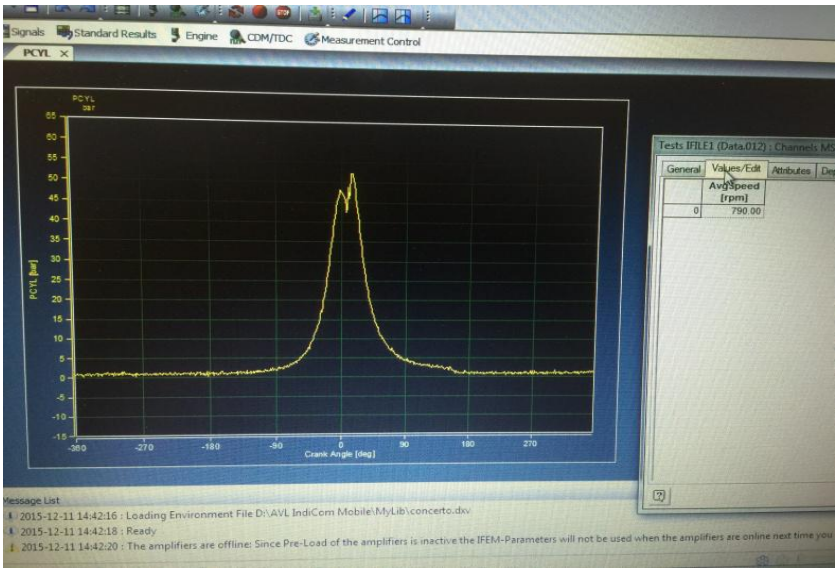


**Figure 3-13** An example of AVL pressure-crank measurement.

At the beginning of software installation, the AVL indicom software requests the engine specification to be set up in the software, therefore the AVL can automatically determine the TDC position and presents the aligned pressure-crank angle graph as shown in figure 3-8. The TDC position determined for this research is 107.1 degree with subtle error less than 0.1 degree. [AVL[d], 2014].

The data measured and recorded by the AVL Indicom software can later exported to the AVL data processing software called AVL Concerto, which enables the advanced calculation, such as heat release, customized formulas, etc. [AVL[e], 2014].

#### 3.2.1.4 Combustion performance measuring system

In order to measure the fuel consumption, one AIC-904 Veritas fuel flow meter was installed on the engine. The flow meter was capable of measuring fuel consumption of diesel engine up to 515 k, and is based on direct flow measurement principle, indicating there was no fuel return to the fuel tank and the fuel was reinjected to the fuel circulation in the fuel meter itself. The following figure 3-14 shows the fuel meter connected with the fuel flow circulation of the tested engine. [AIC, 2018]. The technical specification of the fuel meter is provided in table 3-13. [AIC, 2018].

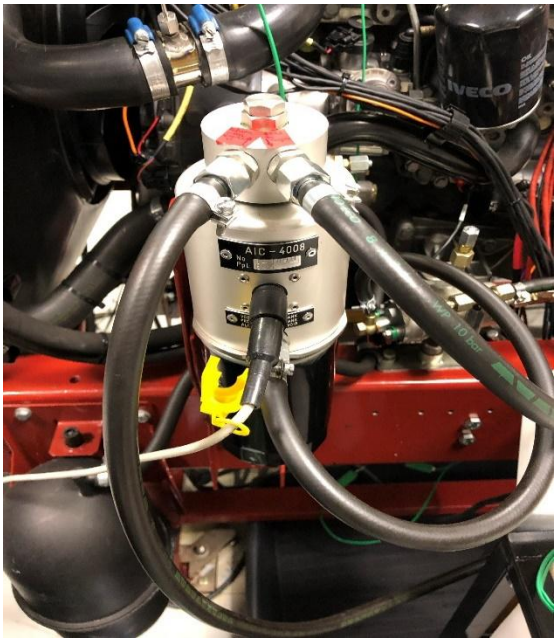


**Figure 3-14** Fuel flow meter applied on the experiment engine.

**Table 3-13** The technical specification of AIC fuel meter.

| | |
|---|---|
| **Manufacturer** | AIC SYSTEMS S.A. |
| **Dimensions (L×l×p)** | 280×100×160 mm (incl. filter) |
| **Weights** | 2.5 kg (incl. filter) |
| **Material for flow meter sensor** | Brass, aluminum |
| **Material for connectors** | Steel protection TAAC3, stainless steel, anodised aluminium |
| **Material for casting** | Anodised aluminium |

| | |
|---|---|
| **Measuring principle** | Volumetric, oscillating piston, with microprocessor-controlled pulse emitter (Pat. AIC) |
| **Measuring range** | 1 to 80 l/h |
| **Accuracy** | Better than 1% of reading |
| **Repeatability** | Better than 0.2% of reading |
| **Admissible pressure** | -1 to 10 bar |
| **Mounting position** | Indifferent |
| **Operating temperature** | -30 … 90 °C |
| **Ingress protection** | Sensor and electronic, IP 68 |
| **Power supply** | 8-28 VDC |
| **Pulse signal** | Rectangular, duty cycle 50% |
| **Pulse rate** | 200 ppl |

#### 3.2.1.5 Emission measurement system

In this research, the gaseous emission was measured using a Horiba MEXA 7100 system, and the particle number was measured using DMS 500 MK II. Multiple sampling points were installed on the engine exhaust pipe, both before and after the aftertreatment system, and thus allowing the efficiency of exhaust aftertreatment system to be measured.

The Horiba system is capable of measuring THC, NOx, O2, CO, CO2, and air to fuel ratio. The Air to fuel ratio was calculated by the data it collected and all emission levels can be directly monitored from the Horiba display screen and be logged using DSG software. The principle of the AFR calculation will be detailly explained in the data analysis section **3.2.1.3**. During the experiment, the measured data was logged using DSG system together with other temperature data, engine rpm data, engine throttle position data, and engine power data. The MAXA-7100 specifications are shown in the table 3-14.

**Table 3- 14** The specification and gas measuring principles of Horiba MAXA 7100 mode type.

| | |
|---|---|
| **Model name** | MEXA-7100 |
| **Sample line** | With a direct measurement line and an additional EGR line (EGR line is optional) |
| **System configuration** | • Main cabinet (System rack)<br>• Main control unit (MCU) mounted in the main cabinet<br>• Interface unit (IFC)<br>• Analyzer rack (ANR) for none-heated analyzers<br>• Power supply unit (PSU)<br>• Solenoid valve unit (SVS)<br>• Sample handing unit (SHS)<br>• Oven rack (OVN) for heated analyzer |
| **Type of analyzer** | • ANR type analyzer:<br>Sample gas is supplied from SHS, up to 5 sets can be installed in ANR.<br>• OVN type heated analyzer:<br>To be installed in OVN rack with heated sampling parts. |
| **Exhaust gas measuring principle** | |
| **CO and $CO_2$** | Non-Dispersive Infrared (NDIR) |
| **NO and $NO_X$** | Chemi-luminescence detector (CLD) |
| **THC** | Flame ionization detector (FID) |
| **$O_2$** | Magneto-pneumatic detection (MPD) |
| **Measuring range and sensitivity** | |
| **CO (H)** | 0 … 12.00 Vol%, sensitivity 0.01 Vol% |

| | |
|---|---|
| **$CO_2$** | 0 … 20.00 Vol%, sensitivity 0.01 Vol% |
| **CO (L)** | 0 … 5000 ppm, sensitivity 1ppm |
| **$O_2$** | 0 … 25.00 Vol%, sensitivity 0.01 Vol% |
| **THC** | 0 … 50000 ppm, sensitivity 1ppm |
| **NO and $NO_X$** | 0 … 10000 ppm, sensitivity 1ppm |
| **Environment** | • Ambient temperature: 5°c to 40°c<br>• Relative humidity: under 80% |
| **Power supply** | 240 (210 to 250) V AC, 50 Hz ± 1 Hz, single phase |
| **Power capacity** | 1.5 k VA to 2.5 K VA (standard) |
| **Dimension** | 570 (w) × 850 (D) × 1970 (H) mm |
| **Mass** | Approx. 350 kg (max.) |

The particle number distribution was measured by DMS 500 MK II. The DMS utilizes electrical mobility particle size classifier and electrical particle number counter, thus allowing particle size distribution to be measured in real time. The measured particle size range was from 4 nm to 1000 nm. The data was logged to an independent computer installed with DMS software. The technical specification of DMS was already given in previous table 3-3. The figure 3-15 shows the DMS used in this research.


**Figure 3-15** DMS 500 MKII connected to experiment engine.

#### 3.2.1.6 Fuel property test instruments

In order to acquire fuel property details of diesel fuel, GTL fuel and HVO fuel, three instruments were used in this research to determine fuel distillation characteristics (TGA), elemental composition (CHNS analyser) and chemical compositions (GC-MS)

A thermogravimetry instrument manufactured by METLLER TOLEDO was used to measure the mass change of fuels and lube oils when they were exposed to temperature from 30°C to 600°C. Pure white diesel, pure GTL fuel, pure HVO fuel, fresh engine lube oil and used engine lube oil were tested. The photo of the experimental TGA analyser in shown in figure 3-16, and the specification of instrument is provided in table 3-15. [Metller-toledo,2015].

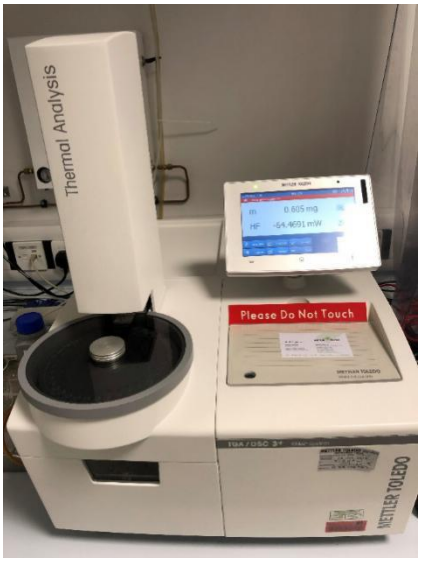


**Figure 3-16** The experiment METLLER TOLEDO thermogravimetric analysis instrument.

**Table 3-15** The specification of experiment METLLER TOLEDO thermogravimetric analysis instrument.

| **Mode of instrument** | TGA/DSC 3+ |
|---|---|
| **Temperature data** | |
| Temperature range | RT to 1100°C |
| Temperature accuracy | ± 0.25k |
| Furnace temperature resolution | 0.001 K |
| Heating time | 5 min (RT to 1100 °C) |
| Cooling time | 20 min (1100 to 100 °C) |
| Cooling time with helium | ≤10 min (1100 to 100 °C) |
| Heating rate | 250 K/min |
| Cooling rate | –20 K/min (≥150 °C) |
| **Balance data** | |
| Sample volume | ≤100 µL |
| Measurement range | ≤1 g |
| Resolution | 1.0 µg |
| Weighing accuracy | 0.005% |

| | |
|---|---|
| Repeatability | <0.001 mg |
| Typical Minimum Weight | 0.19 mg |
| Blank curve reproducibility | better than ±10 µg over the whole temperature range |
| **Calorimetric data** | |
| Sensor type | DSG 3+ |
| Surface material | ceramic |
| Number of thermocouples | 6 |
| Signal time constant at 900 °C | 14 s |
| sensitivity | 0.1 mW |
| Temperature resolution | 0.00003 K |
| Enthalpy reproducibility (standard deviation) | better than 5% |
| **Sampling rate** | maximum 10 values/second |

One Thermo Scientific FLASH 2000 HT Elemental Analyzer was used to measure the carbon, hydrogen, nitrogen, sulphur weight percentages and heat capacity of diesel fuel, GTL fuel, HVO fuel. The tests were repeated by two times and the final data in the fuel specification was the average value from two repeated tests. The elemental analyser is shown in figure 3-17 and its specification is listed in table 3-16. [Thermo Scientific, 2014].

**Table 3-16** The specifications of Thermo Scientific FLASH 2000 HT Elemental Analyzer.

| **Instrument description** | |
|---|---|
| • Base unit FLASH 2000 HT elemental analyzer (two furnaces)<br>• Eager 300 software<br>• MAS 200R autosampler for solids with 32-sample tray<br>• Standard outfit for H&O and N&C determination for approx. 1000 analyses each | |
| **Gases** | |
| Helium | 99.999% purity |

| | |
|---|---|
| Oxygen | 99.995% purity |
| **External Precision for Isotope Ratios C, N, S, O, H, (n = 10), δ-Notation** | |
| Urea or Acetanilide at Natural Abundance for C and N – IRMS. 50 µg C, N | $^{13}C/^{12}C$ 0.15‰; $^{15}N/^{14}N$ 0.15‰ |
| Urea or Acetanilide at Natural Abundance for C and N – IRMS. 5 µg C or 10 µg N | $^{13}C/^{12}C$ 0.2‰; $^{15}N/^{14}N$ 0.2‰ |
| Sulfanilamide at Natural Abundance for S. 50 µg S | $^{34}S/^{32}S$ 0.2‰ |
| Benzoic Acid at Natural Abundance for H and O – IRMS. 50 µg O, 25 µg H | $^{18}O/^{16}O$ 0.4‰; D/H 3‰ |
| Pure Water at Natural Abundance. 0.5 µL. | $^{18}O/^{16}O$ 0.2‰; D/H 2‰ |
| **External Precision for Elemental Concentration (RSD), Mass Traces** | |
| 50 µg C, N (urea) | C 1%; N 1% |
| 50 µg O, 25 µg H (benzoic acid) | 0 2%; H 2% |
| **Power supply** | 230 V, 50/60 Hz, 1400 VA |
| **Dimensions and Weight** | 590 x 580 x 500 mm (w x d x h) 67 kg (net value) |

**Figure 3-17** The experiment Thermo Scientific FLASH 2000 HT Elemental Analyzer.

To acquire the organic compound distribution of diesel fuel, GTL fuel and HVO fuel, one Shimadzu gas chromatograph-mass spectrometer was used in this research.

The GC-MS analysis consisted of two part: the GC analysis, which allowing the compounds of test sample to be separated from each other; and the MS analysis, which allowing the compounds of test sample to be identified and quantified. In the GC analysis, first the sample was diluted with n-pentane in 100 dilution ratio, meaning 10 µl of tested fuel was diluted with 990 µl of n-pentane. Then the sample prepared was injected in to the GC analyser. The inject temperature was 250 °C. After the liquid sample was vaporised in the hot inlet, the gas sample travelled through the GC column, and different compounds were separated due to their different chemical characteristics. The gas chromatography column used for the test was manufactured by Agilent technologies and the size was 25m×0.25mm×0.25µm. The column oven temperature program was set from 40°C to 320°C with 10°C/mins increasing rate. The compounds with higher carbon fractions would travel slower and had longer retention time (the time compound takes to pass through the GC column). Finally, the separated compounds were ready to be send to MS for identification and quantification. [Elscience, 2016].

In the MS analysis, first, the separated compounds were broken into ionised fragments with high energy beam. The ion source temperature and interface temperature of the mass spectrometer was respectively 200°C and 250°C. Then the fragments travelled through a tunnel exposed to magnetic field and hit the detection plate. Since each fragment had certain mass and charge, therefore the mass to charge ratio (m/z) of different compounds was different. This would affect the deflection of fragments in the magnetic field. After that, the mass to charge ratio and the amount of fragments (relative abundance) were calculated in the MS analyser based on the signal received from the detection plate. Finally, a GC software was used to calculated mass spectrum and matched for a peak with the spectra in a database library. A hit number is given when the compounds were identified. The number is generally out of 100, and the closer to 100, the better the match. Thus, the compounds were identified and quantified. The database used is called NIST 11 mass spectral database, which contained 243,893 spectra of 212,961 different chemical compounds. [NIST, 2011]. The photo of

experiment GCMS instrument is shown in figure 3-18 and its specifications is explained in table 3-17. [Shimadzu, 2018].

**Figure 3-18** Shimadzu gas chromatograph-mass spectrometer QP-2010 SE used in this research.

**Table 3-17** The specifications of Shimadzu gas chromatograph-mass spectrometer QP-2010 SE.

| | |
|---|---|
| **GC** | |
| Model | Shimadzu GC-2010 Plus |
| Oven temperature | Up to 450˚C |
| Injector port temp | Up to 450˚C |
| AFC pressure range | 0 to 970 kPa |
| **MS** | |
| Type | Direct connection with capillary column |
| Temperature | 50 to 350˚C |
| Ion source temperature | 140 to 300˚C |
| Filament | Dual (Automatic Switching) |
| Electron energy | 10 to 200 eV |
| Emission current | 5 to 250 µA |
| **Power requirement** | |
| Frequency | 50/60 Hz |

| | |
|---|---|
| GC | 1800 VA (115 VAC)/*2600 VA (230 VAC) * High-power oven |
| MS | 1000 VA (100 – 230 VAC) |
| **Environment** | |
| Temperature | Constant temperature between 18 and 28˚C |
| Humidity | 40 to 70 % (No condensation) |
| **Size and Weight** | |
| GC/MS | 74 Kg |
| Rotary pump | 10 Kg |

### 3.2.2 Experimental procedures and conditions

The experiment was designed to test the combustion and emission performance of different kinds of blended fuels on the diesel the engine. Therefore, for each type of fuel the measured parameters were: engine power, gaseous emissions, particle number concentration and size distribution, in cylinder pressure and crank angle data, various temperature data and fuel consumption. Tested fuels in this research were pure diesel, pure GTL, GTL blended with diesel at 70%, 50%, and 30% in volume, pure HVO, HVO blended with diesel at 70%, 50%, and 30% in volume. The diesel fuel experiments were taken first as the baseline. The engine was then purged with 5 liters new type of test fuel before all the measurements for the new fuel were taken. For instance, when the 70% GTL fuel was completed, and the new test intended to test 50% GTL fuel, then the engine would be running with 5 liters of 50% GTL first before any 50% GTL fuel was conducted. The figure 3-19 below shows the whole system set up for the engine, dynamometer and measurements systems.

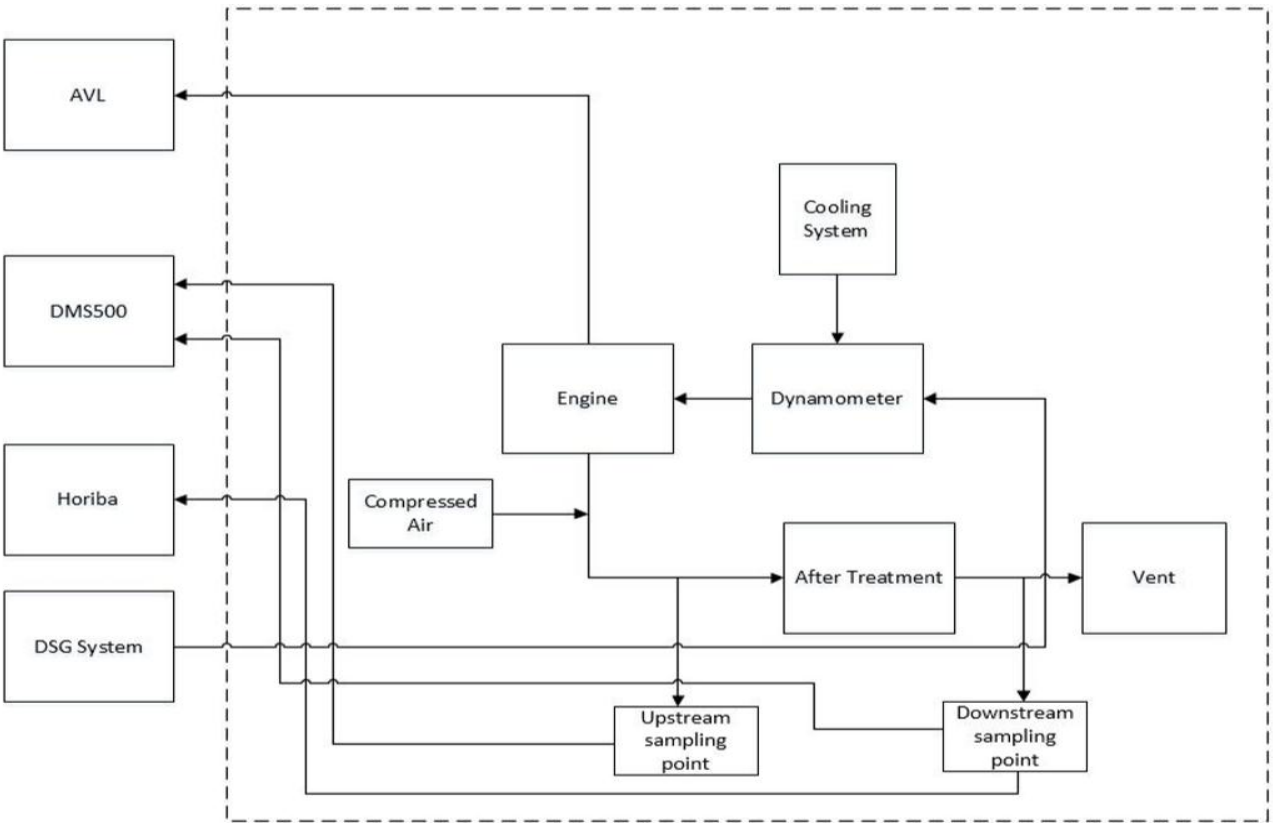


**Figure 3-19** Schematic view of engine and testing system set up.

The HORIBA MEXA7100 and DMS 500 were connected to the upstream and downstream of the engine exhaust aftertreatment system in order to find out the efficiency of the aftertreatment system. Nine engine testing conditions were selected as shown in table 3-18. Three rpm settings were chosen: 1000, 1600, and 1900. 1000 rpm represented idle speeds. 1600 and 1900 rpm were the peak torque (235Nm) conditions. The maximum torque this engine can achieve is 300 Nm, however, the dynamometer in our lab can only produce 235 Nm at maximum. The purpose of the nine testing conditions was to cover as wide as possible engine ranges within allowed capability of the lab, engine and dynamometer. The relationship between engine power, torque and nine test conditions is shown in figure 3-20.

**Table 3-18** The tested engine working conditions.

| Stage of experiment | Engine rpm | Throttle position % | Torque Nm | Power Kw |
|---|---|---|---|---|
| 1 | 1000 | 30 | 125 | 13 |
| 2 | 1000 | 40 | 183 | 19 |
| 3 | 1000 | 50 | 207 | 22 |
| 4 | 1600 | 40 | 115 | 20 |
| 5 | 1600 | 50 | 157 | 26 |
| 6 | 1600 | 60 | 214 | 36 |
| 7 | 1900 | 50 | 135 | 27 |
| 8 | 1900 | 60 | 181 | 36 |
| 9 | 1900 | 70 | 233 | 47 |

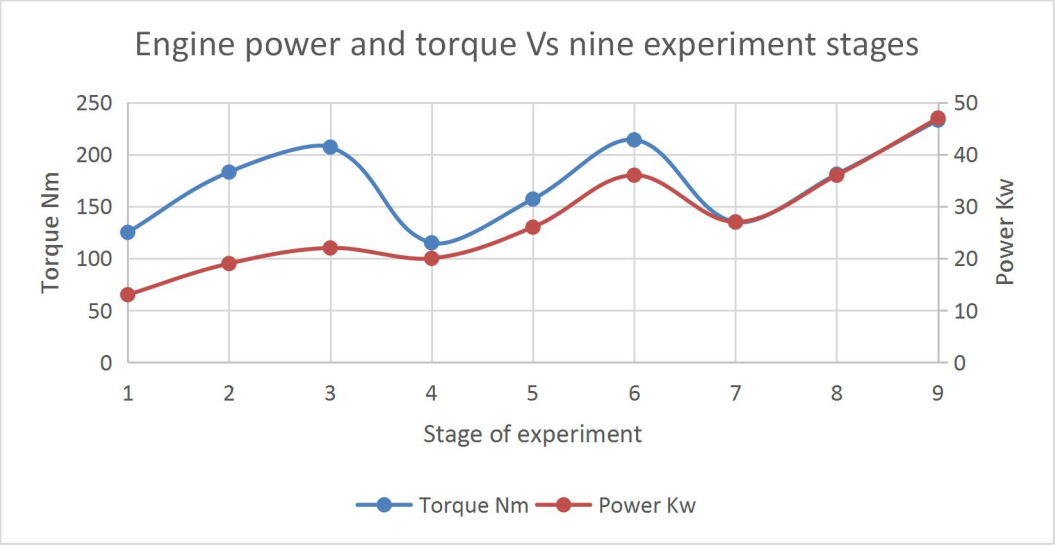


**Figure 3-20** Engine power and torque Vs nine experiment stages.

### 3.2.3 Data analysis

This section explains how the raw data was collected from the experiment and then processed. The data can be classified into four categories:

- The engine power data, including the engine rpm, engine torque, engine power etc.
- The combustion data, including the in-cylinder pressure to crank angle curve, ignition delay, IMEP, maximum combustion pressure etc.
- The gaseous emission data, including THC, CO, $CO_2$, NO, $NO_2$, $NO_X$, AFR, etc.
- The particle number data, including total particle number, particle size distribution, etc.

#### 3.2.1.1 Engine power data

The engine power data was recorded by the DSG software, and the measured parameters were: engine rpm, engine torque (Nm), engine power (Kw), exhaust- post filter temperature, exhaust-pre filter temperature, exhaust manifold temperature, air inlet temperature, oil sump temperature, engine coolant water temperature, dyno water inlet temperature, dyno water outlet temperature, air inlet manifold temperature, exhaust stack temperature, EGR temperature, fuel tank temperature, fuel flow rate, and emission data including concentrations of THC, CO, $CO_2$, NO, $NO_2$, $NO_X$, and AFR.

The engine speed in rpm and engine torque in Nm can be directly measured. The engine power in Kw was calculated using a programmed formula installed in the DSG software. The formula is shown below:

Since,

Equation 18… $Engine\ power\ (kw) = engine\ torque\ (NM) \times engine\ rpm \times 2\pi/60/1000$

Thus,

Equation 19…… $Engine\ power\ (kw) = engine\ torque\ (NM) \times engine\ rpm\ /9549.3$

The BMEP was calculated based on thermodynamics using the formula shown in below:

Since,

Equation 20…… $The\ work\ per\ thermal\ cycle = BMEP \times Total\ displacement = \frac{engine\ power \times 2}{rpm \div 60}$

Therefore,

Equation 21……$BMEP = \frac{4\pi \times engine\ torque}{total\ displacement}$

In this way, the engine power data was acquired for all the experiment tests, including engine power, speed, torque, BMEP, and temperature data.

#### 3.2.1.2 Combustion data

The combustion data refers to the in-cylinder pressure and crank angle. The pressure was measured by AVL pressure transducer and the crank angle was measured by crank angle encoder. Those data were logged using AVL Indicom software and then the logged file can be converted to Excel format using the AVL Concerto software. The engine specification was put into the software allowing the software to automatically generate P-V diagram and calculate the IMEP. The engine specification data programmed to the software is shown in table 3-19.

**Table 3-19** AVL engine specification settings.

| Cylinder specifications | Geometry (mm) |
|---|---|
| STROKE | 104 |
| CONROD | 160 |
| BORE | 95.8 |

The P-V diagrams and P-crank angle diagrams were generated using AVL Concerto software. The figure 3-21 and figure 3-22 are shown as two examples. The P-V diagram was acquired from 50% GTL fuel engine test with 1600 rpm engine speed and 50% throttle setting. The P-crank angle diagram was acquired from diesel fuel engine test with 1600 rpm engine speed and 66% throttle setting.

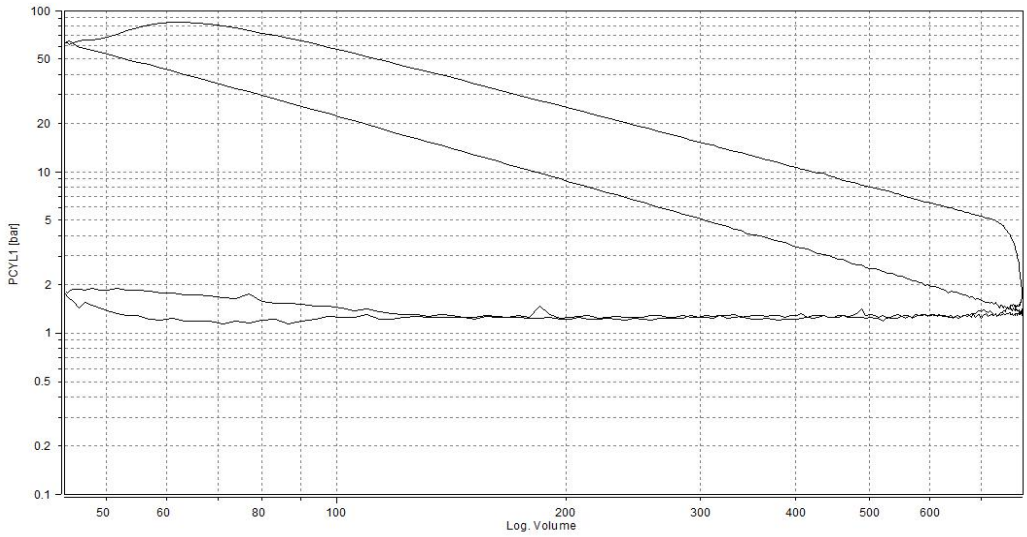


**Figure 3-21** P-V diagram example.

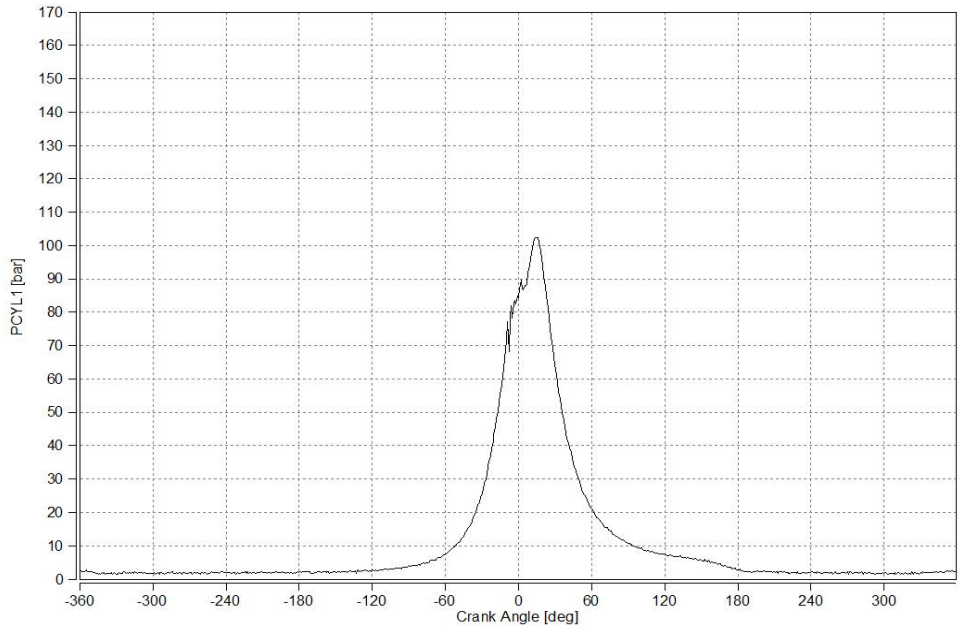


**Figure 3-22** P-crank angle diagram example.

In order to find out the pressure curve detail near top dead centre, zoomed in pressure curves were made manually with pressure and crank angle data from Excel file converted by AVL Concerto software. The figure 3-23 provides an example. The figure was acquired using data from blended GTL fuel test in comparison with diesel fuel. With the pressure data acquired from AVL, the maximum combustion pressure, average

combustion pressure can be calculated. The ignition delays were calculated based on engine rpm. Start of fuel injection and start of combustion were decided manually.

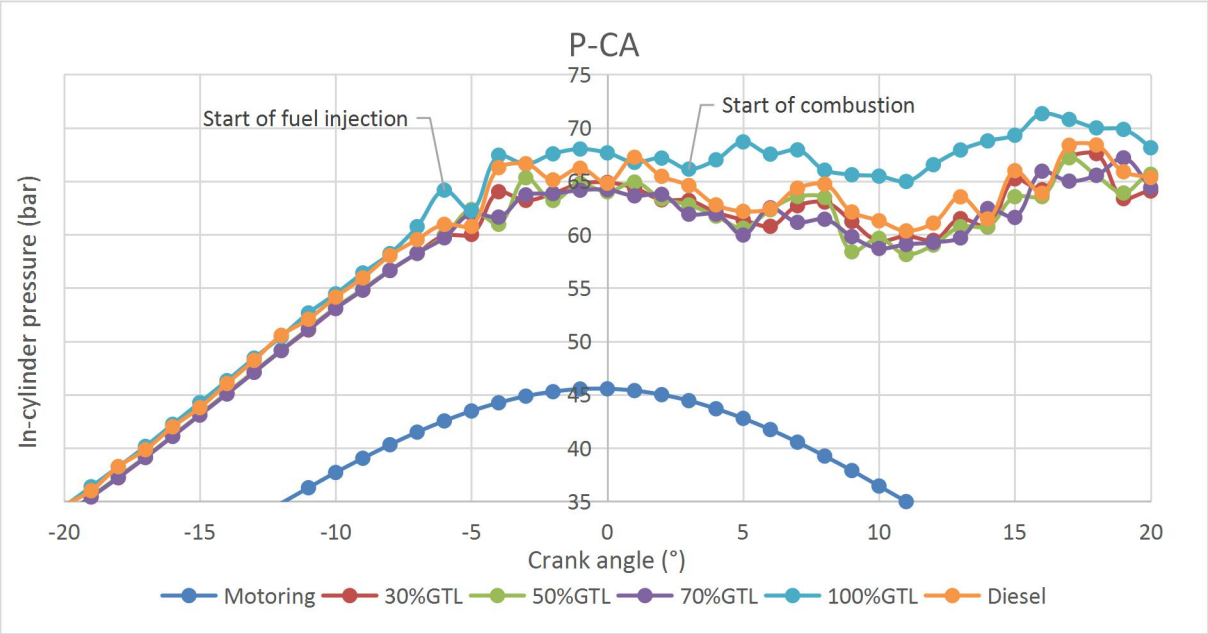


**Figure 3-23** Pressure curve near TDC example.

### 3.2.1.3 Gaseous emission data

The exhaust gas emission concentrations were measured by HORIBA MEXA 7100 and logged with DSG system. The measured data were following: $CO_2$ in percentage, CO in ppm, $O_2$ in percentage, THC in ppmc, NO and $NO_x$ in ppm (The HORIBA MEXA 7100 can either measure NO or $NO_x$, thus the tests with same engine running conditions were repeated to acquire NO and $NO_x$ emission data.), and AFR.

The raw emission data were averaged first, then errors in percentage were calculated based on the average values and standard deviation values. Later, the emissions data were further converted to emission index, and emissions mass flow in grams per second, and grams per kWh. The air to fuel ratio data were calculated by HORIBA system using The Chan's AFR calculation programmed in the system [Chan and Zhu, 1996].

The calculation formula can be expressed as following:

If the composition of the fuel used can be presented as $C_\alpha H_\beta O_\gamma$

Then,

Equation 22……$A/F_{chan} = \frac{138}{12.011\alpha+1.008\beta+15.999\gamma} \times \frac{A_1\beta-A_2+2\alpha A_3A_4-2\gamma(A_1+A_5)}{2(A_1+A_5)\times 2.0028-0.0014\times 2A_3A_4}$,

Where,

K was considered as 3.5 in this research,

Equation 23……$A_1$= [CO] $_{concentration}$+ [CO2] $_{concentration}$+ [HC] $_{concentration}$,

Equation 24……$A_2$= X×[HC] $_{concentration}$, and X = Ratio of elemental hydrogen to elemental carbon,

Equation 25……$A_3$= [CO] $_{concentration}$+2 [CO2] $_{concentration}$+ 2[O2] $_{concentration}$+ [NO] $_{concentration}$ + [NO2] $_{concentration}$,

Equation 26.....$A_4$ = 1 + [CO] $_{concentration}$ ÷ (K× [CO2] $_{concentration}$),

Equation 27.....$A_5$ = [CO] $_{concentration}$ ÷ (K× [CO2] $_{concentration}$),

With the AFR, considering the emissions' concentrations and their respectively chemical molecular weight the emission index of NOx, NO, and NO2 can be acquired using formula shown in below [Hu, L. et al, 2014]:

Equation 28.....Emission index = $(1 + AFR) \times C_i \times \left(\frac{MW_i}{MW_a}\right) \times 1000$ (g / kg of fuel),

Where, $C_i$ was the concentration of the emission component, in ppm or %. The equation should be multiplied by $10^6$ in the case of ppm or $10^{-2}$ in the case of %.

$MW_i$ was the molecular weight of the emission component,

$MW_a$ was the molecular weight of the air and was considered as 28.96.

With the emission index, the emission mass flow can be calculated using formula in below based on physics principle:

Equation 29.....Mass emission rate (g/s) = Emission index (g/kg fuel) × Fuel consumption (L/s) × Density of fuel (Kg/L)

Equation 30……Specific emission(g/kWh) = EI (g/kg of fuel) × fuel consumption (kg of fuel/h) / engine power (kW)

The volumetric fuel consumption was measured by the fuel flow meter and this was converted to mass fuel consumption using the fuel density data. The densities of blended fuels were calculated according to the blending ratios. The results are shown in table 3-21. Since the pure HVO and pure GTL shared the same density, thus their blends with the same blending ratio also shared the same density. The emission mass flow data were finally converted to gas emission in grams per kWh, when considering the engine power in 3600 seconds. The following table 3-22 presents an example of raw emission data been converted to emission index, emission mass flow, and emission in grams per kWh.

**Table 3-21** Blended fuel density calculation.

| Diesel Density (g/ml) | GTL/HVO Density (g/ml) | V% of diesel | V% of GTL/HVO | Blended fuel density (g/ml) |
|---|---|---|---|---|
| 0.83 | 0.78 | 1 | 0 | 0.83 |
| 0.83 | 0.78 | 0.7 | 0.3 | 0.815 |
| 0.83 | 0.78 | 0.5 | 0.5 | 0.805 |
| 0.83 | 0.78 | 0.3 | 0.7 | 0.795 |
| 0.83 | 0.78 | 0 | 1 | 0.78 |

**Table 3-22** Gaseous emission calculation example.

| NO ppm | AFR | EI of NO | Fuel density (g/ml) | Fuel consumption (ml/s) | NO Emission g/s | NO emission g/kwh |
|---|---|---|---|---|---|---|
| 445.13 | 23.40 | 11.27 | 0.83 | 3.33 | 0.03 | 2.77 |
| 273.57 | 23.26 | 6.89 | 0.82 | 3.33 | 0.02 | 1.87 |
| 324.10 | 23.67 | 8.30 | 0.81 | 3.33 | 0.02 | 2.24 |
| 300.75 | 23.69 | 7.71 | 0.80 | 3.33 | 0.02 | 2.06 |

#### 3.2.1.4 Particle number data and DPF efficiency

The particle numbers of different particle sizes were measured and logged by DMS 500 MKII at 1Hz. At least 300 readings were acquired. The average readings were reported. For the efficiency of the DPF on the removal of particle numbers, both the total particle number concentrations and concentrations for each size range were used. The efficiency was calculated using the equation below:

Equation 31.....$\text{DPF efficiency } \% = \frac{PN\ \ up\ stream - PN\ downstream}{PN\ downstream} \times 100\%$

#### 3.2.1.5 Experiment repeatability and error

The engine combustion and emission data was measured at nine stable engine working conditions and the measurement was taken at 1 Hz for at least five minutes after the engine was stable at each condition, i.e. at least 300 data points were acquired. All the experiments were repeated three times. In order to provide the most reliable data, the engine power and emission data was averaged at each engine working condition. The maximum value of standard deviation divided by average (STEDV/mean) for engine power and $NO_x$ is respectively 2% and 3%, which is considered to be caused by engine repeatability. The maximum value of STEDV/mean for CO and THC emission is within 5% for most of the test conditions, however, the STEDV/ mean for THC can be up to 10%~18% at exhaust downstream sometimes. This was due to that the concentration of THC measured at the downstream of aftertreatment system was too low (within 10 ppm) ,close to the detection limit of the FID instrument.

The particle number raw data measured by DMS500 was averaged. Because when the engine power changed, there was a transition period (typically 30 seconds) for the reading of particle number to be stable. Therefore, only the data acquired from stable readings was used. The STEDV/mean values for the raw particle number data can be up to 22% and the refined data had the STEDV/ mean ranging from 2% to 8%.

The STEDV/mean values of in-cylinder pressure measured by the AVL were within 1%, and hardly any differences can be found from the pressure to crank angle diagram. The

following figure shows an example of pressure to crank angle curves from three different measurement at 1600 rpm, 50% throttle.

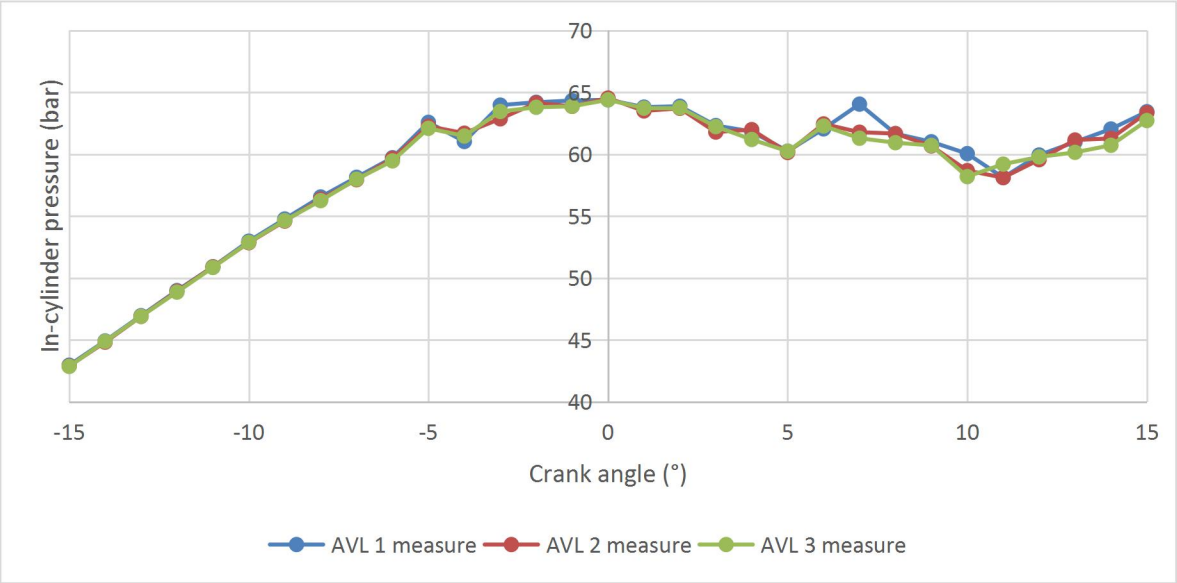


**Figure 3-24** Repeatability of pressure to crank angle diagram**.**

# Chapter 4. Investigation of particle number measurement- influence of instrument and sampling conditions, and determination of detection limit.

Combustion oriented particles are comprised of carbonaceous materials, liquid droplets and ashes. Due to its negative impacts on the ecosystem and human health, particle emissions from combustion engines have become a popular topic. Especially for those ultrafine and nanoparticles, which can cause severe health problems such as increased asthma, increased deep lung deposition. In addition, Particles' toxicity can be increased with the decreasing of their size [Kittelson, 2015].

The determination of particle number concentrations is affected by many parameters such as sampling flow rate, temperature and instrument used. Different instruments may give different readings. Particle number and size distribution measurement can be strongly affected by sampling conditions as particle nucleation and agglomeration occurs during the sampling process. According to the research from Abdul and Kittelson [1999], the dilution condition can affect the nucleation rate of diesel exhaust particles. Higher dilution ratio with higher temperature, shorter residence time, lower relative humidity would result in lower particle number in measurement. On the contrary, higher particle number measurement would be achieved in the test condition with lower dilution ratio, lower dilution temperature, longer residence time, and higher relative humidity. [Abdul-Khalek, et al,1999]. Therefore, there is no consensus on which instrument can be used a gold standard or benchmarking.

This has raised a question on the comparison of results measured by different instruments. [Wang, et al, 2016] compared the particle size distribution of diesel engine exhaust emissions between the measurement of SMPS and EEPS and have found that the greatest difference between particle size distribution was for particles with diameter smaller than 15nm.  Similar research has been taken using AVL Micro soot sensor 483, DMS 500, AVL Opacimeter 439 and Laser Induced Incandescence device sourcing from passenger car equipped with a diesel engine and revealed the Laser Induced Incandescence device showing the best sensitivity and dynamics among all other tested devices [Viskup, et al, 2011]. However, research gaps still existed in determine particle

measurement devices' performance under the impact of sampling dilution system, sampling frequency and the concentration of sampling gas. Especially the detailed study from stable emissions, which provide the opportunity to analyze the differences between particle measurement devices.

This research presents the comparison of PN (Particle Number) measurement results from 5 PN instruments with different sampling frequency and various dilution settings. The particles were generated from a miniature combustion aerosol standard (Mini-CAST) soot generator using propane as fuel which is able to provide different particle concentrations. The compared instruments include a DMS500 MK II tested with three sampling frequency settings (1Hz, 5Hz and 10Hz), two HORIBA MEXA 2300 SPCSs connected with two different dilution systems, a TSI3080 SMPS, and one AVL 483 micro soot sensor measurement unit. The tests were carried out with various dilution settings including zero dilution.  In order to bring the most reliable data for comparison, five separated sampling points were made available on the exhaust pipe of the Mini-CAST soot generator which allow all the instruments to measure simultaneously with exactly the same exhaust. The experiment setup diagram is given in figure 3-3 in chapter 3.

The aim of this research is to investigate the differences of five PN instruments and find out correlations among tested instruments. The impacts of sampling frequency and dilution ratios on PN measurements were investigated. The particle density estimation was also achieved in this research. The results obtained will provide better understanding of PN detection and support the future PN measurement instrumentation and methodology development. The results will also provide suggestions to the legislation on diesel particle numbers.

## 4.1 Comparison among instruments

4 instruments were compared for particle number concentration: DMS500 MKII, two HORRIBA MEXA SPCSs and TSI3080 SMPS. SPCS1 was calibrated using PMP/EU method 2, using soot as reference and SPCS1 was calibrated by emery oils (PMP method 1). The PN measurement frequency of DMS500 MKII in figure 4-1 was 1Hz. The dilution system applied was DSU (Direct sampling unit) and the dilution ratio was

10. The results showed good linear correlations between the instruments. DMS500 gave a slightly overestimated reading while the two SPCSs produced slightly underestimated readings compared to SMPS. All the instruments had very close readings at concentration lower than $4*10^4$ (#/cm$^3$).

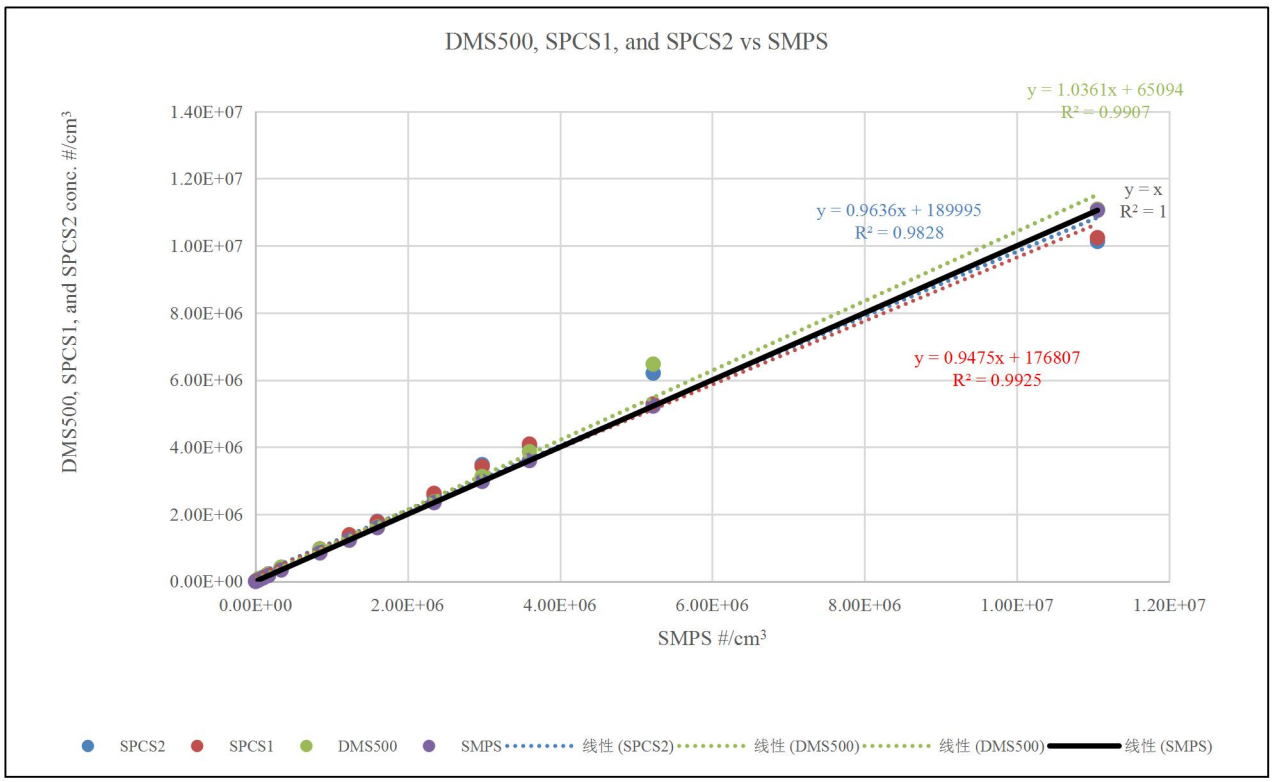


**Figure 4-1** Comparison among two SPCSs, DMS500, and SMPS.

Similar result was acquired by Price s' research [2006]. in comparison of DMS500, ELPI, CPC and PASS, in which the DMS500 was found to give the highest reading. Also, from the research by Tonegawa, Y., et al, [2007]. the DMS 500 measured the concentration 1.2 to 3.3 times higher than that from SMPS. This result showed the fact that the electricity charger counter is more effective to capture particles from sampling gas than Condensation particle counter (CPC), because the previous method is directly measurement of particle number without condensation process which can result particle loss in CPC. This can be further proved from the comparison between DSM500 and SPMS in figure 4-4.

In order to acquire the correlation factors between experiment PN instruments, the linear relationship between instruments were calculated, and provided in table 4-1. The DMS500 was tested using three different frequency settings: 1Hz, 5Hz and 10Hz. From the table it can be seen that the increasing of DMS500 measurement frequency would increase the value of PN in measurement, because higher measurement frequency allows more particles to be captured by the measurement system. The DMS500 results from using the 10 Hz test was nearly the same from using 5 Hz, indicating using 5 to 10 Hz is suitable for stable exhaust sampling PN tests.

**Table 4-1** Correlation factors between experiment PN instruments.

| Correlation factor | DMS500 1Hz | DMS500 5Hz | DMS500 10Hz | SPCS 1 | SPCS 2 | SMPS |
|---|---|---|---|---|---|---|
| DMS500 1Hz | 1.0000 | 1.0244 | 1.0231 | 0.9087 | 0.9313 | 0.9562 |
| DMS500 5Hz | 0.9762 | 1.0000 | 0.9986 | 0.8863 | 0.9076 | 0.9340 |
| DMS500 10Hz | 0.9774 | 1.0014 | 1.0000 | 0.8873 | 0.9092 | 0.9349 |
| SPCS1 | 1.1005 | 1.1283 | 1.1270 | 1.0000 | 1.0185 | 1.0475 |
| SPCS2 | 1.0738 | 1.1018 | 1.0999 | 0.9818 | 1.0000 | 1.0199 |
| SMPS | 1.0458 | 1.0707 | 1.0696 | 0.9547 | 0.9805 | 1.0000 |

The particle number measured by two HORIBA SPCS were lower than from SMPS, this was due to the absence of a particle size classifier in HORIBA SPCS. Since the particle agglomeration occurs among nanoparticles during the exhaust gas sampling process, the particle classifier could enable particles to be counted in number before they agglomerated together. Thus, the particle number measurement from SMPS was higher than from HORIBA SPCS, and it can be assumed the particle difference in particle number between SMPS and HORIBA SPCS was the number of particles undertaken agglomeration. From the comparison between SPCS2 and SMPS, 2.60 % of particles were agglomerated in the sampling procedure.

The correlation factors among DMS500 in three frequency settings, HORIBA SPCS in two calibration methods, and Tsi SMPS can be used in other research in order to have comparison among those PN analysis instruments.

## 4.2 Impact of dilution ratio and particle loss

The particle emission measurements can be affected by the sampling and dilution method in a significant way [Kittelson, 2000], so it is meaningful to study the impact of dilution ratio on particle measurements and the particle losses caused by dilution.

The particle loss analysis was based on the data from HORIBA SPCS2, which did the particle measurement of the same exhaust sample with different dilution ratio settings. HORIBA MEXA SPCS2 was tested using BG3 dilution system at two dilution ratios, 10 and 30. Particle losses in terms of particle number concentration due to higher dilution ratio were observed. From figure 4-2, it can be found that when the particle concentration is higher than $1\times10^5$ (#/cm$^3$), higher dilution ratio can cause 3% to 8% particle losses in PN measurement. The losses could not be determined accurately when the concentration was lower than $2\times10^4$ (#/cm$^3$) because at such low concentration the Mini-CAST did not generate stable exhaust, and the SPCS did not show reasonable measurement.

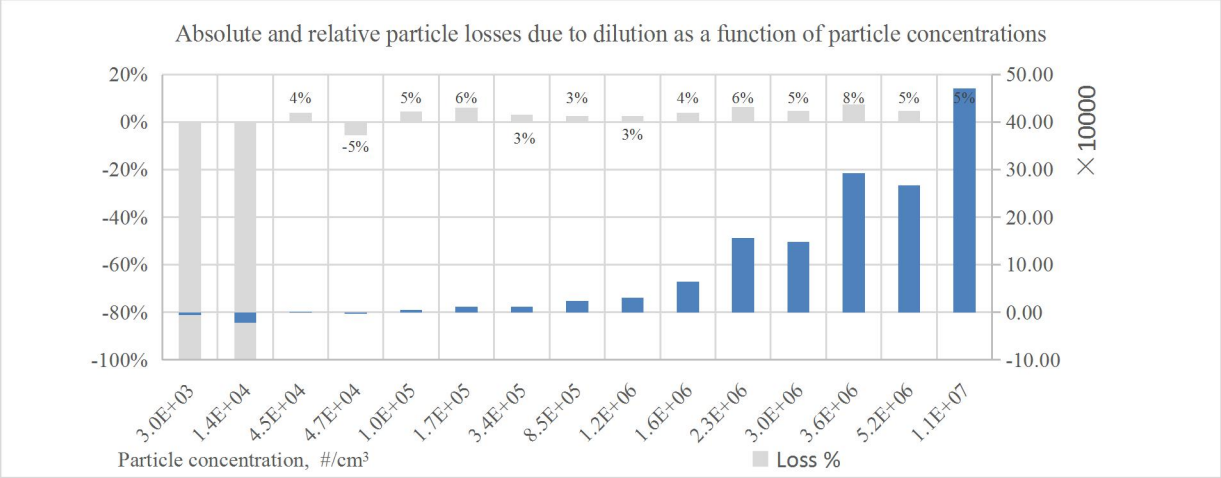


**Figure 4-2** Absolute and relative particle losses due to dilution as a function of particle concentrations.

## 4.3 DMS performance under different frequency settings and lower limits analysis

The DMS500 was used to measure particle concentration at 1 Hz, 5 Hz, and 10 Hz, and the results are very close to each other. The data measured at 5 Hz, and 10 Hz was nearly the same and was only slightly higher than at 1 Hz. This is due to the exhaust gas flow generated from the Mini-CAST burner is quite stable, therefore changing the measurement frequency will not affect the measurement obviously.

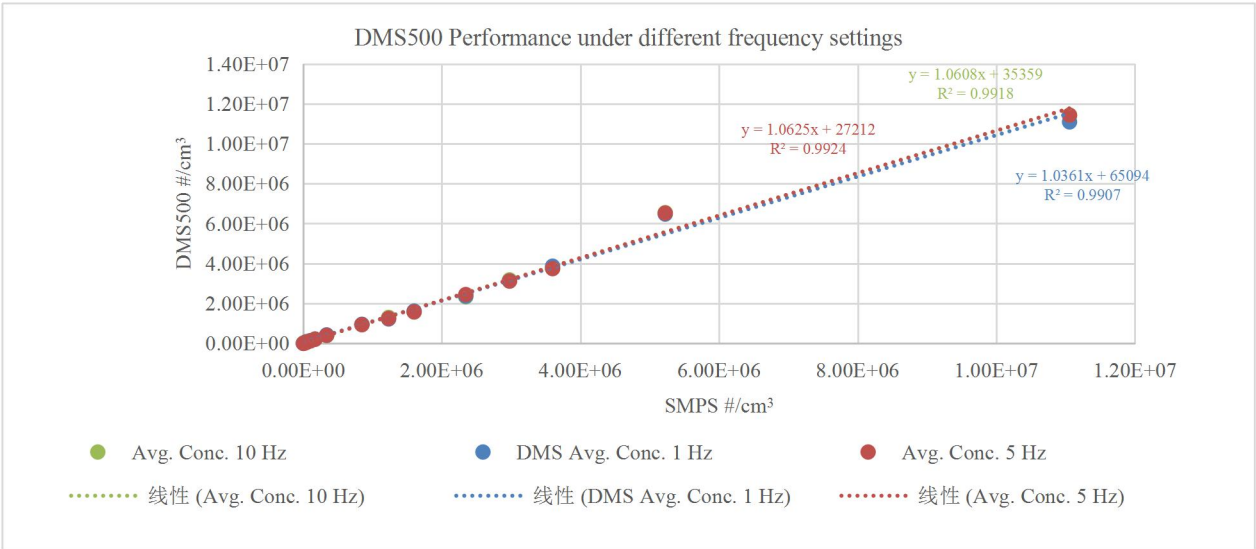


**Figure 4-3** DMS500 Performance under different frequency settings.

This result showed a reasonable relationship between DMS 500 and TSI 3080 SMPS and correlated to the study made by Cavina et al [2013], who measured the particle size distribution with DMS500 sampling from the exhaust flow from a prototype vehicle installed on chassis a dynamometer and acquired a relation level at 0.989.

However, if take a closer look at the correlation between DMS 500 and other PN measurement devices, one common scenario can be clearly notified. That is above the concentration $2.0*10^4$ (#/$cm^3$), the particle number concentration measured by DMS500 and other particle number devices were all in linear relationship, however the differences below such concentration became significant. Figure 4-4 provided the comparison between DMS 500 and SPCS2. As it can be seen, the differences between two instruments became more and more obvious below the concentration $2.0\times10^4$ (#/$cm^3$). This is due to the lower detect limit of DMS500. From the DMS 500 data collected below the concentration of $2.0\times10^4$ (#/$cm^3$), it was found that the DMS 500 would give zero reading when it reaches its lower detection limits because the signal was too weak to be captured by the device.

In order to prove this lower detection limits and try to find out the solution, additional tests were carried using DMS 500 at two dilution ratios (1 and 5). The result was shown in figure 4-5. It can be noticed, for DMS 500 under a dilution ratio 5, the drop outs start to be significantly below the threshold concentration of $2.0\times10^4$ (#/$cm^3$). However, if the dilution ratio was reduced, which can be the same if increase the concentration of sampling gas, the drop outs went back to zero. This well explained the DMS 500's lower concentration detection limits.

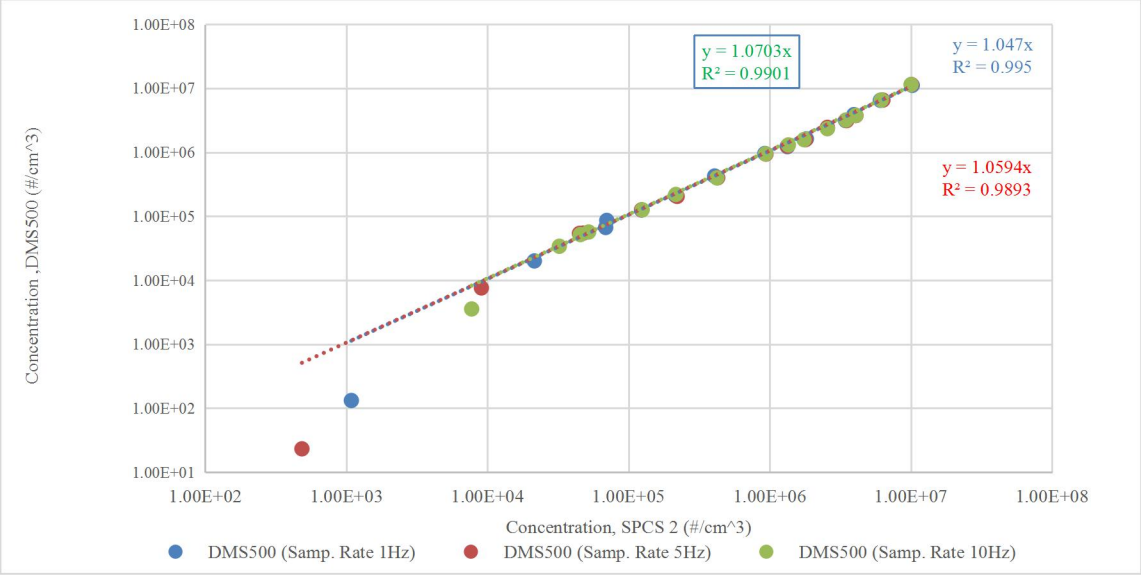


**Figure 4-4** DMS 500 against SPCS2.

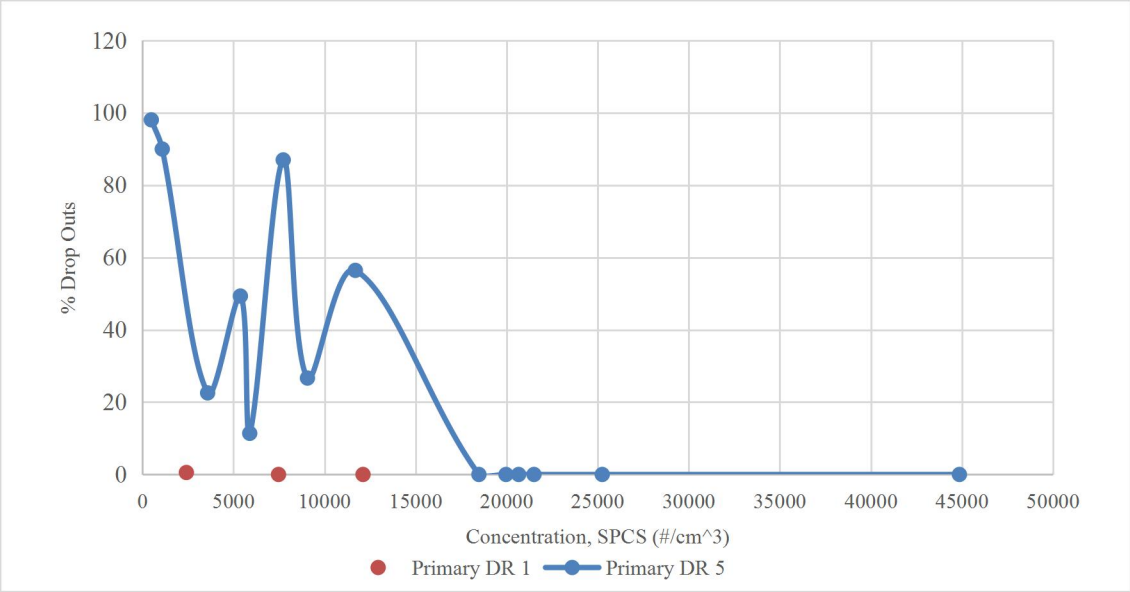


**Figure 4-5** DMS 500 drop outs percentage against SPCS concentration.

Therefore, the DMS 500 would not show too much difference if measures from stable exhaust at different frequency settings. However, the lower detect limits can affect measurement at lower particle number concentration below $2.0*10^4$ (#/cm$^3$), which is very close to ambient air condition. The solution is either to keep the sampling gas above this threshold or reduce the dilution ratio settings to achieve the detectable

concentration. Otherwise, DMS 500 is not suitable for such lower particle number concentration measurement.

### 4.4 AVL mass concentration

Different PN concentration gases were generated by removing some of the undiluted flow from the Mini-CAST, and 15 different particle number concentration gases were measured with AVL 438, which at three dilution ratios settings (2, 3 and 5). Particle mass concentration measured by AVL 483 and particle number concentration measured by SMPS were compared in figure 4-6. A good linear correlation was seen, indicating at certain concentration of sampling gas, the average density of all particles (including all the size range) was quite stable.

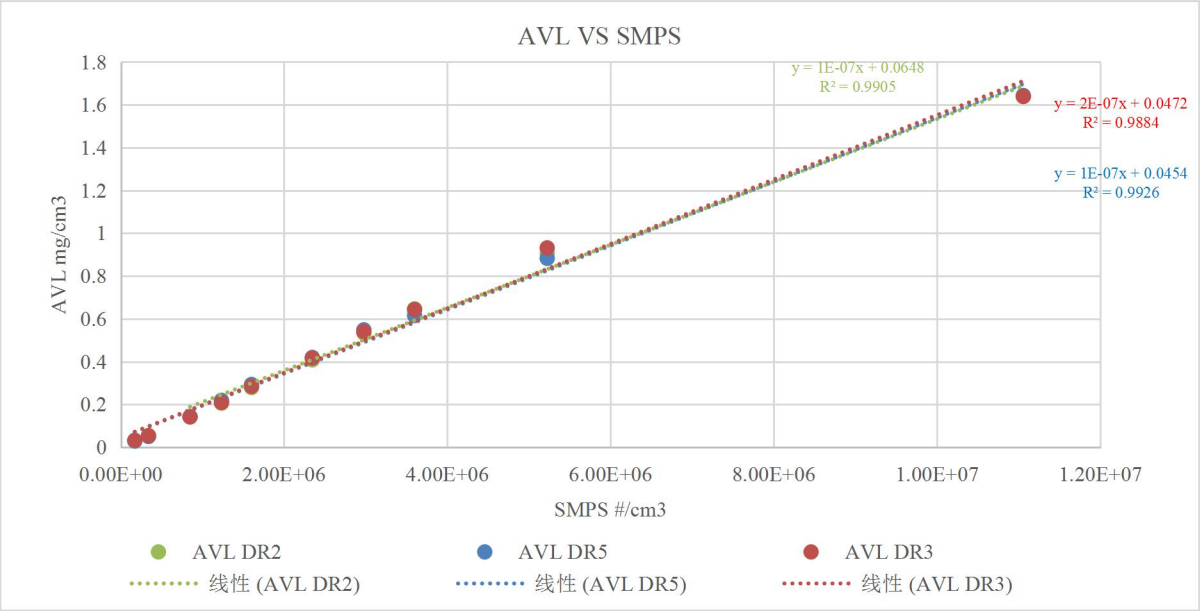


**Figure 4-6** AVL particle mass concentration against SMPS particle number concentration.

From figure 4-6, it can also be seen that the dilution ratio did not affect the correlation obviously. This is due to the stability of the sample soot generated by Mini-CAST as at each stage of the experiment, the Mini-CAST was in the stable setting condition. However, if the sample gas was sourcing from transient measurement, for instance from a diesel engine working under NEDC cycle, the differences between dilution ratios can be more obvious.

## 4.5 Density estimation

With the mass concentration measured by AVL 483, and the number concentration and average particle diameter measured by TSI SMPS, the particle density can be estimated by assuming particles were in sphere structure. First, as the average diameter was known from the SMPS data, the volume of particles can be calculated. Then, consider for certain size of particles in each $cm^3$, the total mass equals the total number of particles multiply by the mass of each particles. Since the total mass and total number were respectively achieved by AVL 438 and SMPS, the mass per particle at certain particle size can be calculated. And with the consideration for particle volume, the particle density thus can be estimated.

The calculated particle densities were lower than these reported in literature for diesel exhaust because the fuel used in this research was propane. The results show the particle density decreases with the increasing of its size, either in average diameter or in size by volume. This indicates the agglomeration of particles can be a process in which "heavier" particles attract "lighter" particles, and agglomerate into "bigger" particles, but with lower physical density. This result showed similar density distribution curve with Khalek an Premnath [2015].

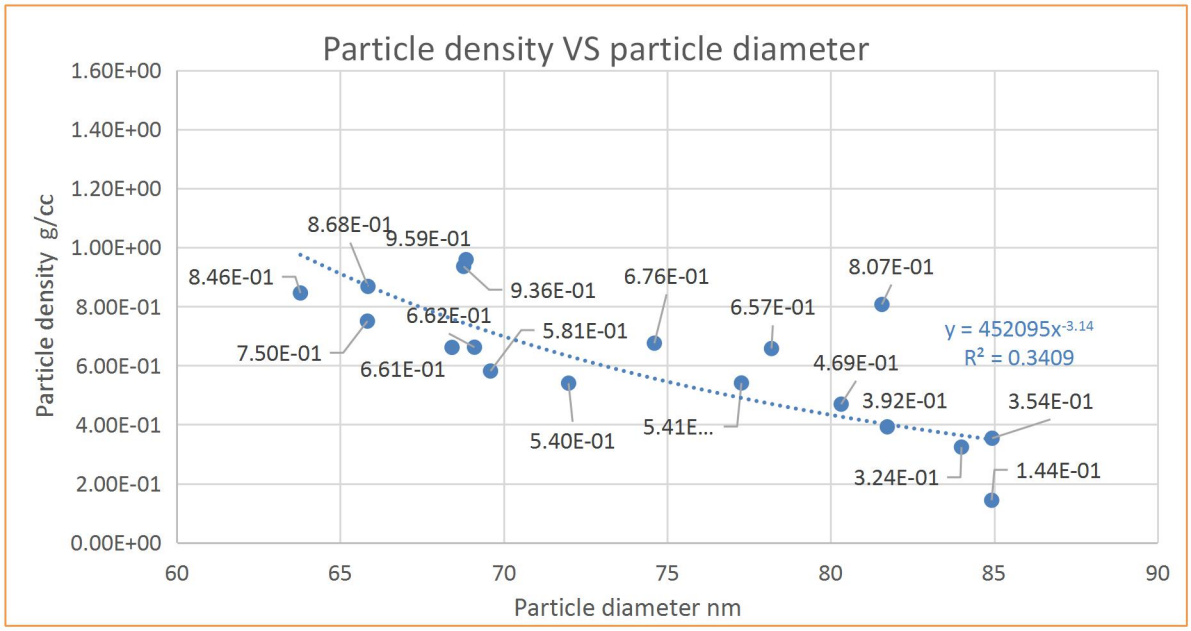


**Figure 4-7** Particle density against particle diameter.

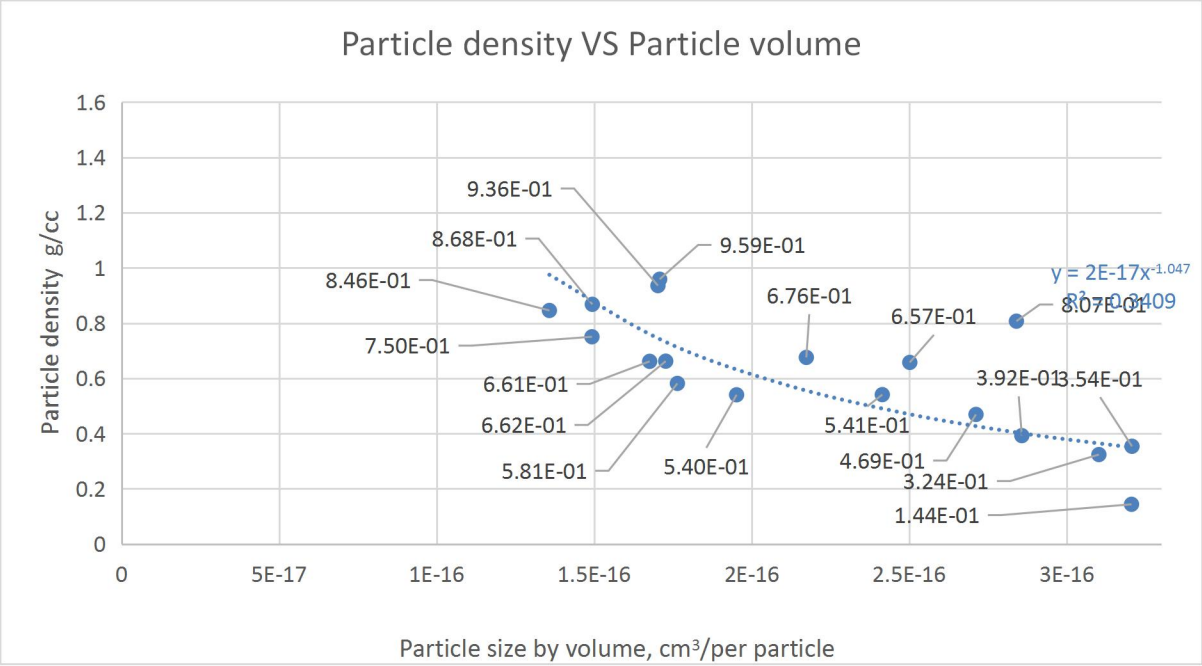


**Figure 4-8** Particle density VS Particle volume.

## 4.6 Conclusion

Based on the results of this research, the following conclusions can be achieved:

• All PN instruments tested showed close correlations among each other: the greatest difference was 12.8% and the majority of differences were within 10%. All correlation factors between instruments have been acquired and listed in table 4-1.

• The DMS 500 showed the highest PN concentration to the tests, and its sampling frequency does not affect the results significantly.

• The detection limits for particle number concentration for DMS 500 MK II is $2\times10^4$ #/$cm^3$.

• Increasing dilution ratio can cause particle losses for particle number measurements.

• Mass concentrations showed a good linear correlation with the PN concentrations.

• Particle density from aerosol decreases with the increasing of its size due to particle agglomeration process.

In summary, the PN instruments tested in this research are all capable of measuring particle number concentration in the range from $4\times10^4$ (#/cm$^3$) to $1.11\times10^7$ (#/cm$^3$). The test results were close from all tested instruments. However, differences did exist due to different principles applied in particle size classifier and particle number counter technology. The DMS 500 MK II showed the highest PN concentration readings as the electrical mobility classifier and electricity charger counter allowing it to capture particles with minimum particle lose, but when the sample particle number drops to $2\times10^4$ #/cm$^3$ and below, the DMS 500 would not be capable of capture particle due to its detection limit. Therefore, using DMS 500 to measure sample lower than $2\times10^4$ #/cm$^3$ is not recommended, for instance using DMS 500 to measure certain exhaust which already passed through some high efficiency particulate filter. Particle mass concentration correlates with particle number concentration in good linear relationship. In addition, based on the density estimation it can be found that the agglomeration process is a key factor that affects the particle density. The PN sample dilution condition can cause particle loses depending on the sample concentration and dilution ratio settings. Thus, for the future PN legislation, it is recommended to define the type of instrument to be used and the sampling conditions be deployed for the legislation and certification test.

# Chapter 5. Fuel property and combustion analysis of GTL and its blends

This chapter presents the test results of pure GTL fuel, GTL diesel blends, and pure diesel fuel. Three different blending ratios were tested 30% GTL, 50% GTL, and 70% GTL by volume. The results include the emission and combustion performances. All results were compared based on fuel types, then discussion and analysis on emission and combustion performance are presented.

## 5.1 Introduction

In order to find out how GTL fuel can improve the diesel engine combustion and emission performances, initially, the pure diesel and GTL fuels were tested. Then, the tests for the blends of GTL 30%, 50%, and 70% were carried out.

The tests were conducted using nine stable engine working conditions: 1000 rpm, 30%, 40%, and 50% throttle, 1600 rpm, 40%,50%, and 60% throttle, and 1900 rpm, 50%, 60%, and 70% throttle. The measured data were CO, $CO_2$, THC, NO, $NO_2$, NOx, PN concentration and size distribution, AFR, engine power, engine speed, engine torque, in-cylinder pressure, crank angle position, and temperatures at 14 specific points. The detail of temperature measurement locations are: exhaust- post filter temperature, exhaust-pre filter temperature, exhaust manifold temperature, air inlet temperature, oil sump temperature, engine coolant water temperature, dynamometer water inlet temperature, dyno water outlet temperature, air inlet manifold temperature, exhaust stack temperature, EGR temperature, and fuel tank temperature.

To ensure the validity of the experiment results, all experiments were repeated three times. Also, to make sure the fuel properties were exactly the same for each blend, enough blended fuels for each blending ratio was prepared in one time. For each type of blend of fuel, 40 litres were prepared because the total fuel consumption for each fuel test was nearly 30 litres, and the purging of the engine fuel loop system required another 5 litres at least.

From the results, it was found that GTL and GTL blended fuels can significantly reduce the particle number emissions both from engine exhaust out (upstream of the

aftertreatment system) and downstream of aftertreatment system. The reduction in particle number emission increased with the increasing of GTL blending ratios. The reduction of THC emissions also increased with the increasing of GTL blending ratios. The pure GTL fuel did not show significant improvement in $NO_X$ emissions when compared to diesel fuel, however, all blended fuel showed moderate $NO_X$ emission reductions. CO and $CO_2$ emission between GTL, diesel, and blended GTL fuel were quite close. The combustion of pure GTL was faster than pure diesel, and the ignition delay decreased with the GTL blending ratio increasing. All blended fuel showed very close combustion performance based on their in-cylinder pressure results.

At the end of this chapter, the conclusion of pure GTL, and blended GTL fuel tests are presented. Based on the conclusion and summary, recommendation for future application of GTL fuel in modern diesel engine is given.

## 5.2 Fuel property analysis

In order to acquire fuel property detail, three tests were used in this research. The CHNS elemental analysis test, the TGA (thermogravimetric analysis) test, and the GCMS tests (gas chromatography-mass spectrometry). The weight percentages of sulphur, hydrogen, carbon, and nitrogen of diesel and GTL fuels were measured from the CHNS elemental test. The calorific values of two kinds of fuels were also acquired from CHNS tests. The result is listed with the fuel specification data acquired from manufacturer and shown in table 5-1. [Shell, 2018].

**Table 5-1** The fuel specification and properties for diesel and GTL fuels.

| Property | Unit | Diesel | GTL |
|---|---|---|---|
| Appearance at +25 ° C | | Clear | Clear & Bright |
| Cetane number | | ⩾ 51.0 | 74…80 |
| Density at +15 ° C | $kg/m^3$ | 840 | 780 |
| Total aromatics | % (m/m) | 25 | < 1.0 |
| Polyaromatics | % (m/m) | ⩽ 8 | < 0.1 |
| Sulphur | wt % | 0 | 0 |
| Hydrogen | wt % | 11.39 | 12.58 |
| Carbon | wt % | 80.59 | 81.43 |

| | | | |
|---|---|---|---|
| Nitrogen | wt % | 0.59 (trace) | 0.60 (trace) |
| Net calorific value | MJ/Kg | 42.9 | 44.0 |
| FAME-content | % (V/V) | ⩽ 7.0 | 0 |
| Flash point | ° C | > 55 | 75.5 |
| Carbon residue on 10 % distillation | % (m/m) | ⩽ 0.30 | |
| Ash | % (m/m) | ⩽ 0.01 | ⩽ 0.01 |
| Water | mg/kg | ⩽ 200 | ⩽ 200 |
| Total contamination | mg/kg | ⩽ 24 | ⩽ 24 |
| Viscosity at +40 ° C | $mm^2/s$ | 2.00 ⋯ 4.50 ⩾ 1.20 * | 3.20 …. 3.90 |
| Distillation 95 % (v/v) | ° C | ⩽ 360 | ⩽ 360 |
| Final boiling point | ° C | < 330 | |

From table 5-1, it can be found that the main difference between diesel fuel and GTL fuel is that the GTL fuel has lower density, higher cetane number, almost aromatic free. The GTL fuel and diesel fuel has very similar sulphur, nitrogen, hydrogen, and carbon weight percentages. The massed based net calorific value of GTL fuel is only slightly higher than diesel fuel. Based on those characteristics of GTL fuel, it can be assumed that the blended fuel and pure GTL fuel should have shorter ignition delay, and reductions in THC and particle emissions mainly because the GTL fuel has higher cetane number value and chemically almost aromatic free. The engine power generated by those fuels should be very close as the calorific values are very similar. However, still many details and other aspect of comparison need to be analysed in order to bring the conclusion, for instance the combustion pressure behaviour differences between fuels, $NO_X$ emission performances, particle number size distribution etc.

The distillation characteristics of diesel fuel and GTL fuel were investigated by TGA test, along with fresh and used engine lube oils, and the result is shown in figure 5-1. From the figure, it can be seen that the GTL fuel has the same evaporating rate as the diesel fuel before 180 °C and then shows lighter fractions than the diesel after 180 °C till the end. The ending temperature of GTL fuel is 270 °C, which is 20 °C earlier than that of diesel fuel. More lighter fractions in the GTL fuel could lead to more complete fuel

combustion, and thus lower particle and total hydrocarbon emissions should be produced from the GTL fuel. The analysis of the used engine lube oil shows no obvious fuel dilutions occurred as there was no increase in fractions lighter than 290 °C in the used lube oil (compared to fresh lube oil). In addition, the used lube oil was lighter than the fresh lube oil (after 310 °C). This was not due to the fuel dilution as the fuel dilution would result in more weight losses before 290 °C rather than after 310 °C. The lower evaporation temperatures of the used lube oil after 310 °C was likely due to the breakdown of the lube oil.

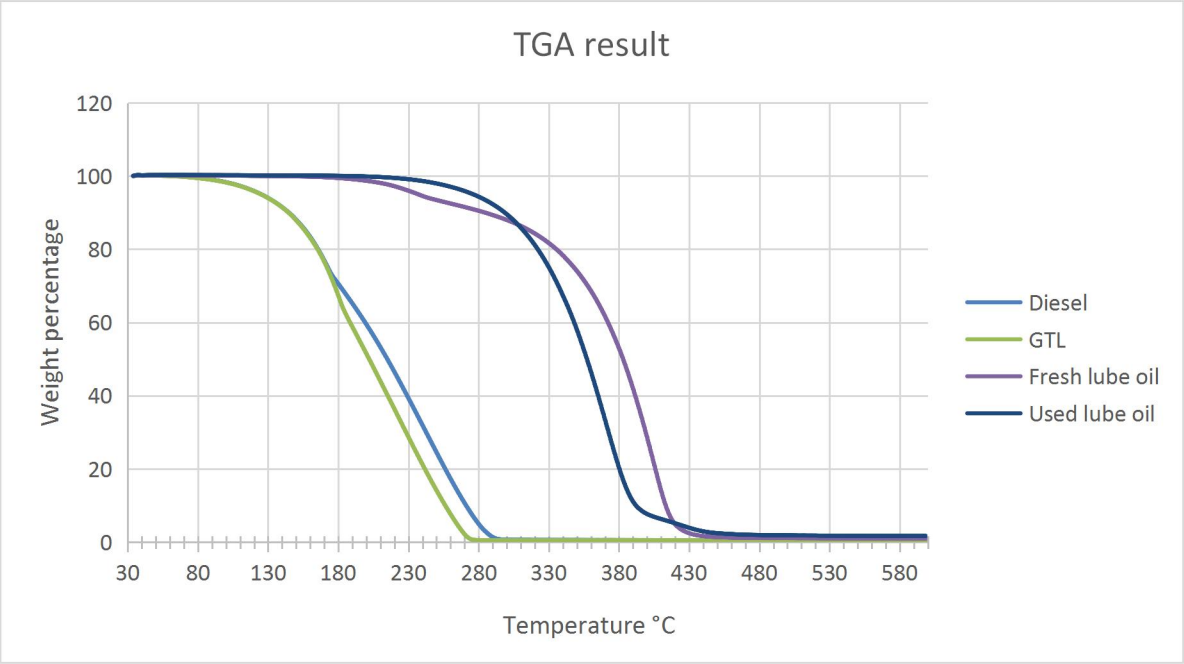


**Figure 5-1** The TGA analysis results of diesel fuel, GTL fuel, fresh engine lube oil, and used engine lube oil.

The GCMS tests were performed to measure the composition and distribution of carbon chains in diesel and GTL fuels. Their respective mass spectra are shown in figure 5-2 and figure 5-3. The detailed component names sort from highest concentration to lowest with molecular formula are presented in tables from table 5-2 to table 5-10. From the mass spectrum and component comparison, it was found the difference between GTL fuel and diesel fuel is GTL fuel consists of almost all straight chains or branched alkanes and in absence of aromatics. Also, GTL fuel contains more lighter fraction

carbon chains than diesel fuel, particularly higher $C_{10}$ and $C_{14}$ compared to diesel fuel. The highest intensity of $C_{19}$ in diesel fuel was believed to be a marker of the fuel manufacture applied so as to distinguish from their product from other fuel manufacture.

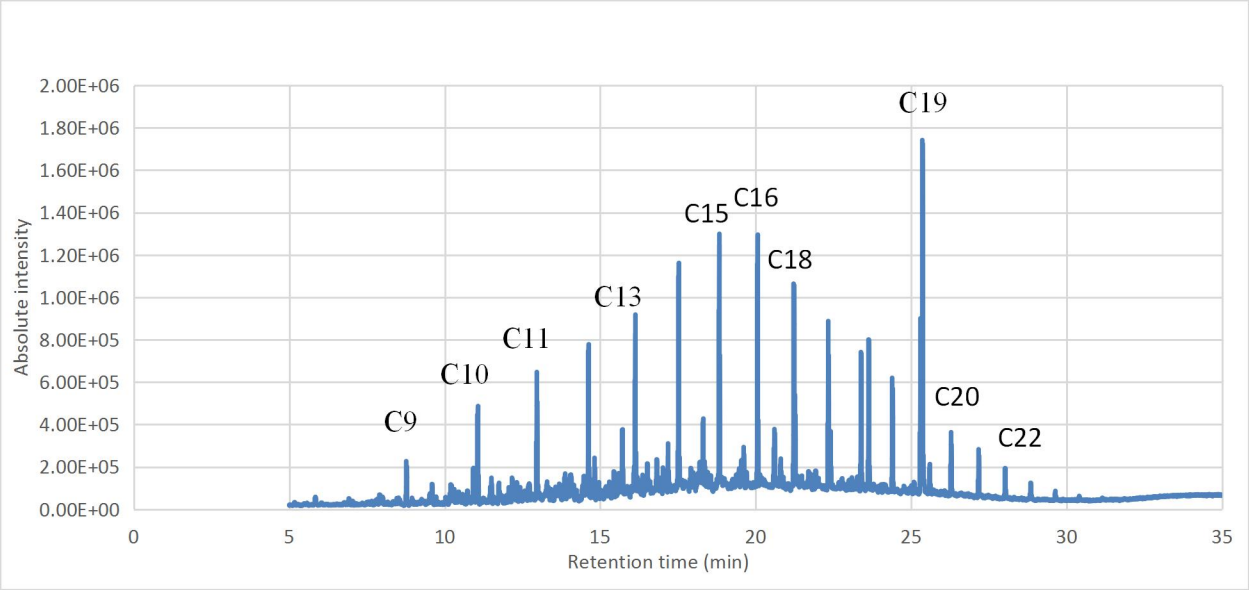


**Figure 5-2** The total ion chromatogram of diesel fuel.

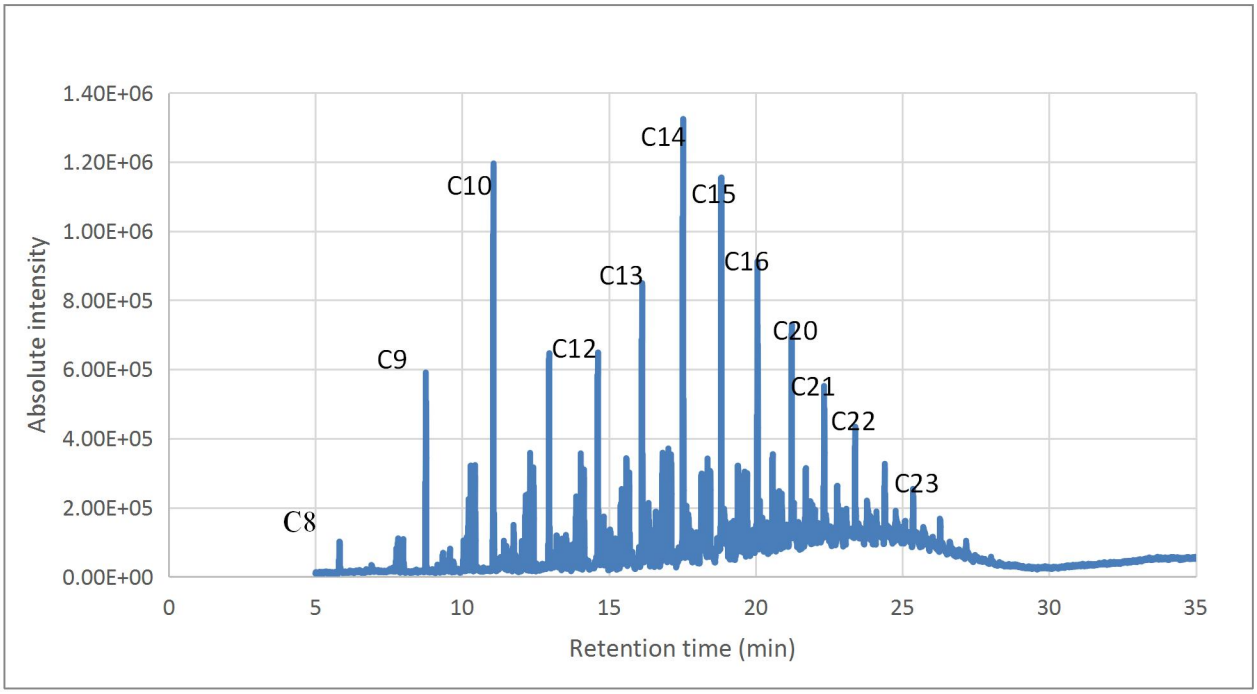


**Figure 5-3** The total ion chromatogram of GTL fuel.

**Table 5- 2** The mass spectrum peak absolute intensity table of diesel fuel part one.

| Name | Molecular formula | Conc. (%) | Cumu. Conc. (%) | Ret.Time (mins) | Area | Height |
|---|---|---|---|---|---|---|
| 9-Octadecenoic acid (Z)-, methyl ester | $C_{19}H_{32}O_2$ | 6.05 | 6.05 | 25.369 | 2760071 | 1652980 |
| Tetradecane | $C_{14}H_{30}$ | 4.52 | 10.57 | 17.529 | 2063053 | 1081736 |
| Pentadecane | $C_{15}H_{32}$ | 4.35 | 14.92 | 18.833 | 1985300 | 1197228 |
| Hexadecane | $C_{16}H_{34}$ | 3.82 | 18.74 | 20.065 | 1740319 | 1189635 |
| Octadecane | $C_{18}H_{38}$ | 3.52 | 22.26 | 21.233 | 1607122 | 966031 |
| Tridecane | $C_{13}H_{28}$ | 2.85 | 25.11 | 16.134 | 1297888 | 849129 |
| Hexadecanoic acid, methyl ester | $C_{17}H_{34}O_2$ | 2.81 | 27.92 | 23.64 | 1281821 | 716201 |
| 9,12-Octadecadienoic acid (Z,Z)-, methyl ester | $C_{19}H_{34}O_2$ | 2.81 | 30.73 | 25.305 | 1283091 | 822617 |
| Tridecane | $C_{13}H_{28}$ | 2.64 | 33.37 | 14.628 | 1205950 | 731966 |
| Octadecane | $C_{18}H_{38}$ | 2.63 | 36 | 22.339 | 1201609 | 785362 |
| Undecane | $C_{11}H_{24}$ | 2.5 | 38.5 | 12.968 | 1138550 | 608136 |
| Eicosane | $C_{20}H_{42}$ | 2.29 | 40.79 | 23.394 | 1043177 | 650216 |
| Eicosane | $C_{20}H_{42}$ | 1.83 | 42.62 | 24.401 | 835844 | 532898 |
| Pentadecane, 2,6,10,14-tetramethyl- | $C_{19}H_{40}$ | 1.76 | 44.38 | 21.264 | 804428 | 448036 |
| Decane | $C_{10}H_{22}$ | 1.65 | 46.03 | 11.07 | 750361 | 461939 |
| Dodecane, 2,6,11-trimethyl- | $C_{15}H_{32}$ | 1.64 | 47.67 | 18.314 | 749337 | 340050 |
| Dodecane, 2,6,11-trimethyl- | $C_{15}H_{32}$ | 1.57 | 49.24 | 15.717 | 717785 | 320373 |
| Heptadecane | $C_{17}H_{36}$ | 1.37 | 50.61 | 20.61 | 622547 | 275709 |
| Nonadecane | $C_{19}H_{40}$ | 1.25 | 51.86 | 22.407 | 568553 | 273124 |
| Eicosane | $C_{20}H_{42}$ | 1.1 | 52.96 | 26.288 | 501691 | 295609 |
| 1-Tetradecene | $C_{14}H_{28}$ | 0.99 | 53.95 | 18.209 | 450288 | 137134 |
| Pentadecane, 2-methyl- | $C_{16}H_{34}$ | 0.82 | 54.77 | 19.618 | 372192 | 192266 |
| Octacosane | $C_{28}H_{58}$ | 0.82 | 55.59 | 27.175 | 376026 | 223921 |
| Cyclohexane, (1-octylnonyl)- | $C_{23}H_{46}$ | 0.8 | 56.39 | 19.548 | 363394 | 132665 |
| Undecane, 2-methyl- | $C_{12}H_{26}$ | 0.79 | 57.18 | 14.054 | 361662 | 121728 |
| Dodecane, 2,6,11-trimethyl- | $C_{15}H_{32}$ | 0.79 | 57.97 | 17.188 | 362533 | 234835 |
| Naphthalene, 1,2,3,4-tetrahydro-1,4-dimethyl- | $C_{12}H_{16}$ | 0.78 | 58.75 | 16.52 | 353949 | 145111 |
| Nonane | $C_9H_{20}$ | 0.74 | 59.49 | 8.775 | 336942 | 204365 |
| Undecane, 2,6-dimethyl- | $C_{12}H_{28}$ | 0.69 | 60.18 | 14.822 | 316643 | 194850 |
| Tetradecane, 1-chloro- | $C_{14}H_{29}Cl$ | 0.67 | 60.85 | 13.874 | 305351 | 127552 |
| 4,6-Decadiyne | $C_{10}H_{14}$ | 0.66 | 61.51 | 12.171 | 298731 | 118625 |
| Benzene, 2-butenyl- | $C_{10}H_{12}$ | 0.66 | 62.17 | 12.722 | 302203 | 88405 |
| Cetene | $C_{16}H_{32}$ | 0.66 | 62.83 | 16.823 | 301819 | 146317 |
| Naphthalene, 1,8-dimethyl- | $C_{12}H_{16}$ | 0.65 | 63.48 | 17.918 | 297776 | 110712 |
| Dodecane, 2,6,10-trimethyl- | $C_{15}H_{32}$ | 0.65 | 64.13 | 18.148 | 297016 | 84065 |
| Cyclohexane, (1-hexadecylheptadecyl)- | $C_{39}H_{78}$ | 0.63 | 64.76 | 20.808 | 288060 | 136814 |
| Benzene, 1,2,3-trimethyl- | $C_9H_{12}$ | 0.6 | 65.36 | 10.923 | 273708 | 167996 |
| Octadecane, 2-methyl- | $C_{19}H_{40}$ | 0.59 | 65.95 | 18.363 | 268043 | 137052 |

**Table 5- 3** The mass spectrum peak absolute intensity table of diesel fuel part two.

| Name | Molecular formula | Conc. (%) | Cumu. Conc. (%) | Ret.Time (mins) | Area | Height |
|---|---|---|---|---|---|---|
| Methyl stearate | $C_{19}H_{38}O_2$ | 0.57 | 66.52 | 25.601 | 259268 | 139111 |
| Naphthalene, 1,2,3,4-tetrahydro-1-methyl- | $C_{11}H_{14}$ | 0.55 | 67.07 | 14.482 | 249571 | 111954 |
| Dodecane, 2-methyl- | $C_{13}H_{28}$ | 0.55 | 67.62 | 15.601 | 250307 | 115053 |
| Naphthalene, 1,2,3,4-tetrahydro-5-methyl- | $C_{11}H_{14}$ | 0.53 | 68.15 | 16.095 | 242073 | 142350 |
| Cyclohexane, butyl- | $C_{10}H_{20}$ | 0.52 | 68.67 | 11.747 | 236206 | 96960 |
| Tridecane, 2-methyl- | $C_{14}H_{30}$ | 0.51 | 69.18 | 17.03 | 234766 | 122221 |
| Octacosane | $C_{28}H_{58}$ | 0.51 | 69.69 | 28.027 | 232966 | 140765 |
| Benzene, (3-methyl-2-butenyl)- | $C_{11}H_{14}$ | 0.5 | 70.19 | 15.448 | 227215 | 124586 |
| Benzene, 1-ethyl-3-methyl- | $C_9H_{12}$ | 0.48 | 70.67 | 10.2 | 217858 | 89552 |
| Nonadecane | $C_{19}H_{40}$ | 0.48 | 71.15 | 21.704 | 218989 | 86271 |
| Decane, 2-methyl- | $C_{11}H_{24}$ | 0.47 | 71.62 | 12.322 | 214653 | 96208 |
| Naphthalene, decahydro-2-methyl- | $C_{11}H_{20}$ | 0.47 | 72.09 | 13.567 | 214570 | 67118 |
| Cyclohexane, hexyl- | $C_{12}H_{24}$ | 0.47 | 72.56 | 15.296 | 213247 | 78764 |
| Naphthalene, 2-methyl- | $C_{11}H_{10}$ | 0.46 | 73.02 | 16.205 | 210273 | 89863 |
| Naphthalene, 1,5-dimethyl- | $C_{12}H_{12}$ | 0.46 | 73.48 | 17.987 | 208388 | 89514 |
| Tridecane, 3-methyl- | $C_{14}H_{30}$ | 0.45 | 73.93 | 17.122 | 206110 | 105883 |
| Dodecane, 2,6,10-trimethyl- | $C_{15}H_{32}$ | 0.45 | 74.38 | 17.633 | 205708 | 57634 |
| Dodecane, 2-methyl- | $C_{13}H_{28}$ | 0.44 | 74.82 | 18.92 | 202881 | 57920 |
| Cyclohexane, 2-butyl-1,1,3-trimethyl- | $C_{13}H_{26}$ | 0.43 | 75.25 | 15.023 | 194509 | 42760 |
| Naphthalene, decahydro-2-methyl- | $C_{11}H_{20}$ | 0.42 | 75.67 | 13.295 | 191504 | 93713 |
| Tetradecane, 3-methyl- | $C_{15}H_{32}$ | 0.42 | 76.09 | 18.454 | 189815 | 86672 |
| Naphthalene, 1,6,7-trimethyl- | $C_{13}H_{14}$ | 0.42 | 76.51 | 19.387 | 192666 | 65513 |
| Acetic acid, 10-chlorodecyl ester | $C_{12}H_{23}ClO_2$ | 0.41 | 76.92 | 17.731 | 188685 | 51670 |
| Anthracene, 1,2,3,4,5,6,7,8-octahydro- | $C_{14}H_{18}$ | 0.41 | 77.33 | 21.6 | 188846 | 29797 |
| Octadecane | $C_{18}H_{38}$ | 0.4 | 77.73 | 19.469 | 180385 | 93494 |
| Octane, 2,6-dimethyl- | $C_{10}H_{22}$ | 0.39 | 78.12 | 9.597 | 179204 | 93713 |
| Tridecane, 3-methyl- | $C_{14}H_{30}$ | 0.39 | 78.51 | 14.152 | 179099 | 72718 |
| Dodecane, 2,6,10-trimethyl- | $C_{15}H_{32}$ | 0.39 | 78.9 | 16.366 | 178802 | 96491 |
| 1-Dodecanol, 3,7,11-trimethyl- | $C_{15}H_{32}O$ | 0.38 | 79.28 | 17.39 | 173428 | 35625 |
| Decane, 4-methyl- | $C_{11}H_{24}$ | 0.37 | 79.65 | 13.962 | 166893 | 78416 |
| 1-Decanol, 2-hexyl- | $C_{16}H_{34}O$ | 0.37 | 80.02 | 18.555 | 170728 | 69909 |
| Decane, 4-methyl- | $C_{11}H_{24}$ | 0.36 | 80.38 | 11.507 | 162852 | 113755 |
| Naphthalene, decahydro-2-methyl- | $C_{11}H_{20}$ | 0.36 | 80.74 | 14.435 | 165817 | 66386 |
| Acetic acid, trifluoro-, nonyl ester | $C_{11}H_{19}F_3O_2$ | 0.36 | 81.1 | 21.339 | 165394 | 66210 |
| Benzene, 1-methyl-3-propyl- | $C_{10}H_{14}O$ | 0.35 | 81.45 | 12.067 | 159165 | 74257 |
| 1H-Indene, 2,3-dihydro-2-methyl- | $C_{10}H_{12}$ | 0.35 | 81.8 | 13.688 | 157743 | 81089 |
| Pentadecane, 2-methyl- | $C_{16}H_{34}$ | 0.35 | 82.15 | 23.274 | 157880 | 60568 |
| Naphthalene, 1,2,3,4-tetrahydro-2-methyl- | $C_{12}H_{14}O_2$ | 0.34 | 82.49 | 14.963 | 153126 | 79382 |
| Naphthalene, 2,3,6-trimethyl- | $C_{13}H_{14}$ | 0.33 | 82.82 | 19.26 | 150109 | 45921 |

**Table 5-4** The mass spectrum peak absolute intensity table of diesel fuel part three.

| Name | Molecular formula | Conc. (%) | Cumu. Conc. (%) | Ret.Time (mins) | Area | Height |
|---|---|---|---|---|---|---|
| 1-Decanol, 2-hexyl- | $C_{16}H_{34}O$ | 0.33 | 83.15 | 21.049 | 152308 | 30830 |
| Nonadecane, 9-methyl- | C20H42 | 0.32 | 83.47 | 21.786 | 143825 | 73298 |
| Octacosane | $C_{28}H_{58}$ | 0.32 | 83.79 | 25.096 | 147908 | 56172 |
| Nonane, 5-butyl- | $C_{13}H_{28}$ | 0.31 | 84.1 | 12.432 | 142587 | 72094 |
| Naphthalene, 1,2,3,4-tetrahydro-6,7-dimethyl- | $C_{12}H_{16}$ | 0.31 | 84.41 | 16.463 | 140130 | 39040 |
| 9H-Fluorene, 9-methyl- | $C_{14}H_{12}$ | 0.31 | 84.72 | 21.483 | 141801 | 66433 |
| Heptadecane, 2-methyl- | $C_{18}H_{38}$ | 0.31 | 85.03 | 21.936 | 139836 | 82973 |
| Benzene, (1-ethyl-1-propenyl)- | $C_{11}H_{14}$ | 0.3 | 85.33 | 15.188 | 139084 | 58406 |
| 1-Decanol, 2-hexyl- | $C_{16}H_{34}O$ | 0.3 | 85.63 | 20.139 | 134700 | 56594 |
| Octacosane | $C_{28}H_{58}$ | 0.3 | 85.93 | 28.848 | 138982 | 75317 |
| Benzene, 1-ethenyl-4-ethyl- | $C_{10}H_{12}$ | 0.29 | 86.22 | 13.834 | 130999 | 77909 |
| 1-Decanol, 2-hexyl- | $C_{16}H_{34}O$ | 0.29 | 86.51 | 16.279 | 134305 | 47602 |
| Heptanoic acid, octyl ester | $C_{15}H_{30}O_2$ | 0.28 | 86.79 | 14.535 | 128433 | 34095 |
| Benzene, 1,3-dimethyl-5-(1-methylethyl)- | $C_{11}H_{16}$ | 0.28 | 87.07 | 14.77 | 126558 | 31962 |
| Heptadecane, 4-methyl- | $C_{18}H_{38}$ | 0.28 | 87.35 | 16.945 | 127554 | 66401 |
| Nonadecane | $C_{19}H_{40}$ | 0.28 | 87.63 | 22.779 | 128786 | 45614 |
| Hexane, 3-ethyl-4-methyl- | $C_9H_{20}$ | 0.27 | 87.9 | 10.23 | 121229 | 82344 |
| Cinnamaldehyde, .alpha.-pentyl- | $C_{14}H_{18}O$ | 0.27 | 88.17 | 15.87 | 123578 | 50997 |
| Benzene, 1-(1,1-dimethylethyl)-4-ethenyl- | $C_{12}H_{18}$ | 0.27 | 88.44 | 16.608 | 123577 | 57193 |
| 9-Octadecyne | $C_{18}H_{34}$ | 0.27 | 88.71 | 18.037 | 121134 | 59197 |
| [1,1'-Biphenyl]-4-methanol | $C_{13}H_{12}O$ | 0.27 | 88.98 | 20.199 | 121912 | 41083 |
| Benzene, 1,2,3-trimethyl- | $C_9H_{12}$ | 0.26 | 89.24 | 11.474 | 120569 | 64607 |
| Benzene, (1,1-dimethylpropyl)- | $C_{11}H_{16}$ | 0.26 | 89.5 | 14.237 | 120287 | 46982 |
| Naphthalene, 1,2,3,4-tetrahydro-1-methyl- | $C_{11}H_{14}$ | 0.26 | 89.76 | 15.642 | 119400 | 51374 |
| 2,5-Dimethoxythiophenol | $C_8H_{10}O_2S$ | 0.26 | 90.02 | 19.046 | 120288 | 32187 |
| Decane, 4-methyl- | $C_{11}H_{24}$ | 0.25 | 90.27 | 12.239 | 112556 | 70193 |
| Benzene, 4-ethyl-1,2-dimethyl- | $C_{10}H_{14}$ | 0.25 | 90.52 | 12.581 | 114575 | 55012 |
| Benzene, (1,1-dimethylpropyl)- | $C_{11}H_{16}$ | 0.24 | 90.76 | 13.16 | 108353 | 26586 |
| Benzene, 1,2,4,5-tetramethyl- | $C_{10}H_{14}$ | 0.24 | 91 | 13.328 | 111470 | 67666 |
| Heptadecane, 4-methyl- | $C_{18}H_{38}$ | 0.24 | 91.24 | 15.515 | 107192 | 61447 |
| Benzene, 1-(1,5-dimethyl-4-hexenyl)-4-methyl- | $C_{15}H_{22}$ | 0.24 | 91.48 | 17.237 | 108788 | 43839 |
| Cyclopentane, (4-octyldodecyl)- | $C_{25}H_{50}$ | 0.24 | 91.72 | 18.687 | 107242 | 29394 |
| Tetradecane, 1-chloro- | $C_{14}H_{29}Cl$ | 0.23 | 91.95 | 13.66 | 103447 | 66784 |
| Undecane, 2,6-dimethyl- | $C_{13}H_{28}$ | 0.23 | 92.18 | 15.41 | 103671 | 57140 |
| Octanoic acid, hexadecyl ester | $C_{24}H_{48}O_2$ | 0.23 | 92.41 | 16.005 | 104703 | 50400 |
| Naphthalene, 1-(2-propenyl)- | $C_{13}H_{12}$ | 0.23 | 92.64 | 18.762 | 102880 | 51788 |
| 1-Docosene | $C_{22}H_{44}$ | 0.23 | 92.87 | 23.485 | 103170 | 35149 |
| Benzene, 1,3-dimethyl- | $C_8H_{10}$ | 0.22 | 93.09 | 7.912 | 98353 | 46365 |

**Table 5-5** The mass spectrum peak absolute intensity table of diesel fuel part four.

| Name | Molecular formula | Conc. (%) | Cumu. Conc. (%) | Ret.Time (mins) | Area | Height |
|---|---|---|---|---|---|---|
| Benzene, propyl- | ⁋ $C_9H_{12}$ | 0.22 | 93.31 | 10.033 | 101648 | 32281 |
| Octane, 2,7-dimethyl- | ⁋ C10H22 | 0.22 | 93.53 | 10.307 | 101401 | 65946 |
| 3-Heptene, 4-propyl- | C10H20 | 0.22 | 93.75 | 10.736 | 99386 | 58165 |
| Dodecane, 2,6,11-trimethyl- | ⁋ $C_{15}H_{32}$ | 0.22 | 93.97 | 13.416 | 102197 | 57138 |
| Octane, 4,5-diethyl- | $C_{12}H_{26}$ | 0.22 | 94.19 | 16.864 | 99663 | 54477 |
| 4-Methyl-.beta.-methyl-.beta.-nitrostyrene | $C_{10}H_{11}NO_2$ | 0.22 | 94.41 | 17.065 | 100993 | 62796 |
| Cyclohexane, propyl- | ⁋ $C_9H_{18}$ | 0.21 | 94.62 | 9.525 | 97403 | 46288 |
| 4-Undecene, (Z)- | $C_{11}H_{22}$ | 0.21 | 94.83 | 11.988 | 94369 | 37194 |
| Naphthalene, decahydro-, trans- | $C_{10}H_{18}$ | 0.21 | 95.04 | 12.265 | 93906 | 58724 |
| Cyclohexane, pentyl- | ⁋ $C_{11}H_{22}$ | 0.21 | 95.25 | 13.62 | 97465 | 56084 |
| Benzene, 1-(2-butenyl)-2,3-dimethyl- | $C_{12}H_{16}$ | 0.21 | 95.46 | 15.33 | 94994 | 61979 |
| Caryophyllene oxide | $C_{15}H_{24}O$ | 0.21 | 95.67 | 17.835 | 96012 | 28021 |
| Naphthalene, 1,2,3,4-tetrahydro-2,5,8-trimethyl- | $C_{13}H_{18}$ | 0.21 | 95.88 | 18.505 | 93898 | 40356 |
| Cyclohexane, (1-octylnonyl)- | $C_{23}H_{46}$ | 0.21 | 96.09 | 23.099 | 96169 | 57045 |
| cis-7-Tetradecen-1-ol | $C_{14}H_{28}O$ | 0.2 | 96.29 | 11.589 | 93275 | 32516 |
| Benzene, 1,4-dimethyl-2-(2-methylpropyl)- | $C_{12}H_{18}$ | 0.2 | 96.49 | 15.825 | 90179 | 26757 |
| m-Menthane, (1S,3S)-(+)- | $C_{10}H_{20}$ | 0.2 | 96.69 | 16.048 | 90049 | 46976 |
| Cyclohexane, 1-methyl-2-pentyl- | $C_{12}H_{24}$ | 0.2 | 96.89 | 18.999 | 88976 | 51045 |
| Hexadecane, 2-methyl- | $C_{17}H_{36}$ | 0.2 | 97.09 | 19.707 | 90787 | 62037 |
| Hexane, 3-ethyl- | ⁋ $C_9H_{20}$ | 0.19 | 97.28 | 5.842 | 86940 | 36091 |
| Benzene, 1,2,3-trimethyl- | $C_9H_{12}$ | 0.19 | 97.47 | 10.389 | 84743 | 46013 |
| Nonane, 3-methyl- | $C_{10}H_{22}$ | 0.19 | 97.66 | 10.448 | 87417 | 51993 |
| Tetrahydrocarvone | $C_{10}H_{18}O$ | 0.19 | 97.85 | 12.82 | 86048 | 38691 |
| Undecane, 5-methyl- | $C_{12}H_{26}$ | 0.19 | 98.04 | 13.255 | 88506 | 50996 |
| Heptadecane, 2-methyl- | $C_{18}H_{38}$ | 0.19 | 98.23 | 20.892 | 88163 | 49669 |
| Spiro[4.5]decane | ⁋ $C_{10}H_{18}$ | 0.18 | 98.41 | 13.09 | 80221 | 26965 |
| Benzene, 1,3-diethyl-5-methyl- | $C_{11}H_{16}$ | 0.18 | 98.59 | 13.99 | 80640 | 55556 |
| Acetic acid, 10-chlorodecyl ester | $C_{12}H_{23}ClO_2$ | 0.18 | 98.77 | 18.96 | 81803 | 37363 |
| / | / | 0.18 | 98.95 | 21.415 | 84048 | 24094 |
| Heptadecane, 4-methyl- | $C_{15}H_{32}$ | 0.18 | 99.13 | 21.863 | 84112 | 48491 |
| Cyclohexane, 1-methyl-2-pentyl- | $C_{12}H_{24}$ | 0.18 | 99.31 | 23.71 | 80539 | 21254 |
| Benzene, 4-ethyl-1,2-dimethyl- | $C_{10}H_{14}$ | 0.17 | 99.48 | 12.531 | 79537 | 40173 |
| Pentadecane, 2-methyl- | $C_{16}H_{34}$ | 0.17 | 99.65 | 20.658 | 79762 | 43567 |
| Octadecane, 2-methyl- | $C_{19}H_{40}$ | 0.17 | 99.82 | 23.009 | 79150 | 47637 |
| n-Tridecylcyclohexane | $C_{20}H_{40}$ | 0.17 | 99.99 | 24.171 | 78956 | 32378 |

**Table 5- 6** The mass spectrum peak absolute intensity table of GTL fuel part one.

| Name | Molecular formula | Conc. (%) | Cum. Conc. (%) | Ret.Time (mins) | Area | Height |
|---|---|---|---|---|---|---|
| Tetradecane | $C_{14}H_{30}$ | 3.85 | 3.85 | 17.532 | 2072208 | 1293491 |
| Decane | $C_{10}H_{22}$ | 3.43 | 7.28 | 11.072 | 1847389 | 1169197 |
| Pentadecane | $C_{15}H_{32}$ | 3.15 | 10.43 | 18.837 | 1695766 | 1109543 |
| Tridecane | $C_{13}H_{28}$ | 2.56 | 12.99 | 16.136 | 1374859 | 817680 |
| Hexadecane | $C_{16}H_{34}$ | 2.52 | 15.51 | 20.067 | 1356317 | 841836 |
| Octadecane | $C_{28}H_{58}$ | 1.95 | 17.46 | 21.233 | 1046841 | 654859 |
| Decane | $C_{10}H_{22}$ | 1.82 | 19.28 | 12.968 | 981327 | 618668 |
| Dodecane | $C_{12}H_{26}$ | 1.76 | 21.04 | 14.63 | 949046 | 619672 |
| Nonane | $C_9H_{20}$ | 1.74 | 22.78 | 8.769 | 936887 | 571039 |
| Dodecane, 2,6,11-trimethyl- | $C_{15}H_{32}$ | 1.54 | 24.32 | 19.401 | 829275 | 269477 |
| Octadecane | $C_{28}H_{58}$ | 1.5 | 25.82 | 22.34 | 808437 | 468370 |
| Pentadecane | $C_{15}H_{32}$ | 1.24 | 27.06 | 18.163 | 666669 | 261748 |
| Tridecane, 2-methyl- | $C_{14}H_{30}$ | 1.19 | 28.25 | 17.033 | 639802 | 343180 |
| Heptadecane, 4-methyl- | $C_{18}H_{38}$ | 1.15 | 29.4 | 20.584 | 620185 | 286713 |
| Eicosane | $C_{20}H_4$ | 1.12 | 30.52 | 21.713 | 602948 | 236955 |
| Tetradecane | $C_{14}H_{30}$ | 1.1 | 31.62 | 16.833 | 592859 | 332993 |
| Tridecane, 3-methyl- | $C_{14}H_{30}$ | 1.1 | 32.72 | 17.126 | 591701 | 324896 |
| Decane, 2-methyl- | $C_{11}H_{24}$ | 1.09 | 33.81 | 12.321 | 585711 | 338439 |
| Pentadecane, 2-methyl- | $C_{16}H_{34}$ | 1.09 | 34.9 | 18.366 | 585263 | 301157 |
| Pentadecane | $C_{15}H_{32}$ | 1.01 | 35.91 | 17.638 | 542937 | 174195 |
| Tridecane | $C_{13}H_{28}$ | 0.99 | 36.9 | 23.395 | 533073 | 318594 |
| Undecane, 2-methyl- | $C_{12}H_{26}$ | 0.99 | 37.89 | 13.892 | 531643 | 214043 |
| Octadecane | $C_{28}H_{58}$ | 0.99 | 38.88 | 14.051 | 532954 | 334196 |
| Tridecane, 2-methyl- | $C_{14}H_{30}$ | 0.97 | 39.85 | 15.604 | 522927 | 318517 |
| Nonadecane, 9-methyl- | $C_{20}H_{42}$ | 0.95 | 40.8 | 22.784 | 512918 | 177145 |
| Tetradecane | $C_{14}H_{30}$ | 0.93 | 41.73 | 15.7 | 498684 | 278374 |
| Nonane, 5-butyl- | $C_{13}H_{28}$ | 0.91 | 42.64 | 12.434 | 488116 | 296613 |
| Heptadecane, 4-methyl- | $C_{18}H_{38}$ | 0.9 | 43.54 | 18.286 | 482966 | 236697 |
| Pentadecane, 2-methyl- | $C_{16}H_{34}$ | 0.9 | 44.44 | 18.457 | 483407 | 265757 |
| Octane, 2,7-dimethyl- | $C_{10}H_{22}$ | 0.88 | 45.32 | 10.306 | 472092 | 304917 |
| Undecane, 2,4-dimethyl- | $C_{13}H_{28}$ | 0.87 | 46.19 | 16.874 | 469825 | 253942 |
| Nonane, 3-methyl- | $C_{10}H_{22}$ | 0.84 | 47.03 | 10.444 | 451221 | 301984 |
| Pentadecane, 2-methyl- | $C_{16}H_{34}$ | 0.84 | 47.87 | 19.623 | 453162 | 246694 |
| Eicosane | $C_{20}H_4$ | 0.81 | 48.68 | 24.404 | 435797 | 227365 |
| Tridecane, 4-methyl- | C14H30 | 0.79 | 49.47 | 16.949 | 424041 | 245483 |
| Tridecane, 3-methyl- | $C_{14}H_{30}$ | 0.75 | 50.22 | 18.209 | 405607 | 257233 |

**Table 5-7** The mass spectrum peak absolute intensity table of GTL fuel part two.

| Name | Molecular formula | Conc. (%) | Cum. Conc. (%) | Ret.Time (mins) | Area | Height |
|---|---|---|---|---|---|---|
| Tridecane, 2-methyl- | $C_{14}H_{30}$ | 0.75 | 50.97 | 14.154 | 404337 | 279577 |
| Tetradecane | $C_{14}H_{30}$ | 0.73 | 51.7 | 16.359 | 395259 | 188760 |
| Pentadecane, 4-methyl- | $C_{16}H_{34}$ | 0.72 | 52.42 | 19.546 | 386370 | 191266 |
| Tridecane, 4-methyl- | C14H30 | 0.71 | 53.13 | 15.52 | 381712 | 209701 |
| Pentadecane, 4-methyl- | $C_{16}H_{34}$ | 0.7 | 53.83 | 19.712 | 378369 | 229299 |
| Hexadecane, 2-methyl- | $C_{17}H_{36}$ | 0.7 | 54.53 | 17.712 | 377014 | 148645 |
| Pentadecane | $C_{15}H_{32}$ | 0.69 | 55.22 | 19.47 | 369780 | 219308 |
| Heptadecane, 2-methyl- | $C_{18}H_{38}$ | 0.69 | 55.91 | 18.93 | 369307 | 151524 |
| Undecane, 2,4-dimethyl- | ↑ $C_{13}H_{28}$ | 0.67 | 56.58 | 15.443 | 362032 | 230760 |
| Heptadecane, 4-methyl- | $C_{18}H_{38}$ | 0.66 | 57.24 | 20.735 | 356343 | 164466 |
| Octadecane | ↑ $C_{28}H_{58}$ | 0.65 | 57.89 | 20.811 | 348667 | 176397 |
| Hexadecane, 2-methyl- | $C_{17}H_{36}$ | 0.65 | 58.54 | 20.149 | 349177 | 151269 |
| Decane, 4-methyl- | ↑ $C_{11}H_{24}$ | 0.64 | 59.18 | 12.237 | 345051 | 221709 |
| Decane, 5-methyl- | ↑ $C_{11}H_{24}$ | 0.62 | 59.8 | 12.168 | 335233 | 217588 |
| Eicosane | $C_{20}H_4$ | 0.62 | 60.42 | 21.302 | 334832 | 140207 |
| Hexane, 3-ethyl-4-methyl- | $C_9H_{20}$ | 0.6 | 61.02 | 10.225 | 320335 | 207092 |
| Undecane, 4-methyl- | $C_{12}H_{26}$ | 0.59 | 61.61 | 13.964 | 317241 | 207238 |
| Heptadecane, 4-methyl- | $C_{18}H_{38}$ | 0.56 | 62.17 | 22.257 | 303502 | 63093 |
| Undecane, 2,6-dimethyl- | $C_{13}H_{28}$ | 0.55 | 62.72 | 21.867 | 296934 | 139875 |
| Hexadecane, 2-methyl- | $C_{17}H_{36}$ | 0.55 | 63.27 | 19.171 | 298428 | 107261 |
| Heptadecane, 4-methyl- | $C_{18}H_{38}$ | 0.55 | 63.82 | 25.718 | 296028 | 58915 |
| Octacosane | ↑ $C_{28}H_{58}$ | 0.55 | 64.37 | 15.413 | 298070 | 191241 |
| Eicosane | $C_{20}H_4$ | 0.54 | 64.91 | 25.367 | 291545 | 161951 |
| Dodecane, 2,6,11-trimethyl- | ↑ $C_{15}H_{32}$ | 0.53 | 65.44 | 16.611 | 287242 | 163133 |
| Heptadecane, 2-methyl- | $C_{18}H_{38}$ | 0.53 | 65.97 | 20.897 | 287175 | 169733 |
| Eicosane | $C_{20}H_4$ | 0.52 | 66.49 | 21.384 | 280618 | 72653 |
| Undecane, 2,6-dimethyl- | $C_{13}H_{28}$ | 0.51 | 67 | 14.824 | 274718 | 150294 |
| Octadecane, 2-methyl- | $C_{19}H_{40}$ | 0.5 | 67.5 | 22.404 | 266400 | 96597 |
| Pentadecane, 2-methyl- | $C_{16}H_{34}$ | 0.47 | 67.97 | 20.661 | 251917 | 158892 |
| Nonane, 5-butyl- | ↑ $C_{13}H_{28}$ | 0.46 | 68.43 | 21.939 | 249044 | 128049 |
| Pentadecane | $C_{15}H_{32}$ | 0.46 | 68.89 | 14.941 | 248551 | 110221 |
| Heptadecane, 2-methyl- | $C_{18}H_{38}$ | 0.46 | 69.35 | 17.993 | 245733 | 93346 |
| Dodecane, 2-methyl- | ↑ C13H28 | 0.45 | 69.8 | 16.248 | 243261 | 105244 |
| Heptane, 3-ethyl-2-methyl- | C10H22 | 0.45 | 70.25 | 20.615 | 243435 | 175914 |
| Nonadecane, 9-methyl- | C20H42 | 0.45 | 70.7 | 23.8 | 239474 | 126116 |

**Table 5-8** The mass spectrum peak absolute intensity table of GTL fuel part three.

| Name | Molecular formula | Conc. (%) | Cum. Conc. (%) | Ret.Time (mins) | Area | Height |
|---|---|---|---|---|---|---|
| Eicosane | C20H4 | 0.44 | 71.14 | 19.937 | 238774 | 63625 |
| Eicosane | $C_{20}H_4$ | 0.44 | 71.58 | 21.175 | 235521 | 79482 |
| Hexadecane | $C_{16}H_{34}$ | 0.44 | 72.02 | 22.454 | 237212 | 64950 |
| Dodecane, 2,6,11-trimethyl- | $C_{15}H_{32}$ | 0.43 | 72.45 | 11.758 | 233770 | 129318 |
| Dodecane, 4,9-dipropyl- | C18H38 | 0.43 | 72.88 | 18.97 | 230267 | 115708 |
| Tridecane | $C_{13}H_{28}$ | 0.42 | 73.3 | 22.942 | 223597 | 104299 |
| Heptadecane, 4-methyl- | $C_{18}H_{38}$ | 0.42 | 73.72 | 17.245 | 227260 | 46750 |
| Heptadecane, 2-methyl- | $C_{18}H_{38}$ | 0.41 | 74.13 | 21.793 | 222547 | 118713 |
| Heptadecane, 3-methyl- | $C_{18}H_{38}$ | 0.41 | 74.54 | 22.025 | 217836 | 114038 |
| Tetradecane | $C_{14}H_{30}$ | 0.4 | 74.94 | 15.811 | 212546 | 49331 |
| Tridecane | $C_{13}H_{28}$ | 0.39 | 75.33 | 17.807 | 211081 | 100634 |
| Octadecane, 2-methyl- | $C_{19}H_{40}$ | 0.39 | 75.72 | 15.056 | 212065 | 115013 |
| Heptadecane, 4-methyl- | $C_{18}H_{38}$ | 0.39 | 76.11 | 14.889 | 211380 | 106009 |
| Nonane, 3-methyl- | $C_{10}H_{22}$ | 0.38 | 76.49 | 16.285 | 204145 | 109862 |
| Octadecane, 2-methyl- | $C_{19}H_{40}$ | 0.38 | 76.87 | 21.462 | 205682 | 83188 |
| Nonadecane, 9-methyl- | $C_{20}H_{42}$ | 0.37 | 77.24 | 24.777 | 201439 | 87789 |
| Tridecane | $C_{13}H_{28}$ | 0.36 | 77.6 | 16.441 | 195671 | 104361 |
| Eicosane | $C_{20}H_4$ | 0.35 | 77.95 | 22.55 | 186970 | 61607 |
| Octadecane, 2-methyl- | $C_{19}H_{40}$ | 0.34 | 78.29 | 23.098 | 181732 | 97919 |
| Nonadecane, 2-methyl- | $C_{20}H_{42}$ | 0.34 | 78.63 | 23.011 | 182160 | 80698 |
| Hexane, 3-ethyl- | $C_8H_{18}$ | 0.33 | 78.96 | 11.625 | 175173 | 52037 |
| Decane, 2-methyl- | $C_{11}H_{24}$ | 0.33 | 79.29 | 22.874 | 176596 | 87745 |
| Tridecane | $C_{13}H_{28}$ | 0.33 | 79.62 | 5.829 | 175976 | 87833 |
| Pentadecane, 4-methyl- | $C_{16}H_{34}$ | 0.33 | 79.95 | 20.229 | 176540 | 103231 |
| Tridecane | $C_{13}H_{28}$ | 0.33 | 80.28 | 13.549 | 178002 | 102162 |
| Heptadecane, 2-methyl- | $C_{18}H_{38}$ | 0.33 | 80.61 | 21.014 | 175894 | 51585 |
| Tetradecane | $C_{14}H_{30}$ | 0.32 | 80.93 | 24.122 | 172247 | 85805 |
| Heptane, 2,4-dimethyl- | $C_9H_{20}$ | 0.32 | 81.25 | 19.01 | 173480 | 95771 |
| Eicosane, 2-methyl- | $C_{21}H_{44}$ | 0.32 | 81.57 | 16.32 | 172067 | 101600 |
| Tridecane, 3-methyl- | $C_{14}H_{30}$ | 0.31 | 81.88 | 19.262 | 169218 | 112034 |
| Hexadecane | $C_{16}H_{34}$ | 0.31 | 82.19 | 24.84 | 166367 | 51626 |
| Pentadecane, 2-methyl- | $C_{16}H_{34}$ | 0.31 | 82.5 | 18.884 | 165423 | 93547 |
| Heptadecane, 3-methyl- | $C_{18}H_{38}$ | 0.31 | 82.81 | 26.62 | 169318 | 35035 |
| Octane, 3-ethyl- | $C_{10}H_{22}$ | 0.31 | 83.12 | 23.825 | 165492 | 104184 |
| Heptane, 3-ethyl-2-methyl- | $C_{10}H_{22}$ | 0.31 | 83.43 | 19.094 | 168816 | 99803 |

**Table 5-9** The mass spectrum peak absolute intensity table of GTL fuel part four.

| Name | Molecular formula | Conc. (%) | Cum. Conc. (%) | Ret.Time (mins) | Area | Height |
|---|---|---|---|---|---|---|
| Octacosane | $C_{28}H_{58}$ | 0.31 | 83.74 | 15.152 | 166248 | 87955 |
| Octane, 2-methyl- | $C_9H_{20}$ | 0.3 | 84.04 | 13.223 | 162269 | 91670 |
| Heptane, 2,5-dimethyl- | $C_9H_{20}$ | 0.3 | 84.34 | 26.291 | 159416 | 91354 |
| Decane, 2,5-dimethyl- | C12H26 | 0.3 | 84.64 | 22.132 | 162539 | 74461 |
| Tridecane | $C_{13}H_{28}$ | 0.3 | 84.94 | 7.996 | 162749 | 93749 |
| Octadecane, 2-methyl- | $C_{19}H_{40}$ | 0.3 | 85.24 | 24.039 | 158920 | 69774 |
| Heneicosane | $C_{21}H_{44}$ | 0.3 | 85.54 | 16.523 | 163384 | 110404 |
| Nonadecane, 2-methyl- | $C_{20}H_{42}$ | 0.3 | 85.84 | 7.822 | 162687 | 95013 |
| Eicosane | $C_{20}H_4$ | 0.3 | 86.14 | 15.234 | 160249 | 89222 |
| Pentane, 3-ethyl-2,4-dimethyl- | $C_9H_{20}$ | 0.29 | 86.43 | 21.75 | 154530 | 114786 |
| Undecane, 2-methyl- | $C_{12}H_{26}$ | 0.29 | 86.72 | 17.933 | 154480 | 86333 |
| Hexadecane | $C_{16}H_{34}$ | 0.29 | 87.01 | 20.023 | 157624 | 80859 |
| Pentadecane, 2-methyl- | $C_{16}H_{34}$ | 0.29 | 87.3 | 10.176 | 156450 | 98142 |
| Decane, 2,5-dimethyl- | C12H26 | 0.29 | 87.59 | 12.046 | 153791 | 86246 |
| 1-Hexene, 4-methyl- | $C_7H_{14}$ | 0.28 | 87.87 | 15.92 | 152260 | 19794 |
| Pentadecane, 2-methyl- | $C_{16}H_{34}$ | 0.28 | 88.15 | 18.774 | 152637 | 72520 |
| Nonadecane, 9-methyl- | $C_{20}H_{42}$ | 0.28 | 88.43 | 17.386 | 152401 | 56755 |
| Undecane | $C_{11}H_{24}$ | 0.27 | 88.7 | 22.83 | 147633 | 92026 |
| Tridecane, 2-methyl- | $C_{14}H_{30}$ | 0.27 | 88.97 | 23.971 | 145438 | 75211 |
| Octadecane, 2-methyl- | $C_{19}H_{40}$ | 0.27 | 89.24 | 21.06 | 142955 | 78757 |
| Octadecane | $C_{28}H_{58}$ | 0.27 | 89.51 | 17.892 | 145467 | 76553 |
| Decane, 2,5-dimethyl- | C12H26 | 0.27 | 89.78 | 16.773 | 147253 | 87933 |
| Heptadecane, 4-methyl- | $C_{18}H_{38}$ | 0.27 | 90.05 | 10.056 | 143671 | 84490 |
| Tetradecane | $C_{14}H_{30}$ | 0.26 | 90.31 | 23.901 | 141022 | 81639 |
| Octadecane, 2-methyl- | $C_{19}H_{40}$ | 0.26 | 90.57 | 16.656 | 142150 | 93749 |
| Decane, 5-methyl- | $C_{11}H_{24}$ | 0.25 | 90.82 | 11.432 | 134378 | 80895 |
| Dodecane, 2,6,11-trimethyl- | $C_{15}H_{32}$ | 0.25 | 91.07 | 13.415 | 135033 | 90418 |
| Undecane, 2-methyl- | $C_{12}H_{26}$ | 0.25 | 91.32 | 18.695 | 132758 | 69192 |
| Hexadecane | $C_{16}H_{34}$ | 0.25 | 91.57 | 13.781 | 136033 | 76072 |
| Undecane, 2-methyl- | $C_{12}H_{26}$ | 0.24 | 91.81 | 21.6 | 128194 | 47250 |
| Tridecane, 2-methyl- | $C_{14}H_{30}$ | 0.24 | 92.05 | 20.389 | 129987 | 90035 |
| Pentadecane, 8-hexyl- | $C_{21}H_{44}$ | 0.24 | 92.29 | 15.336 | 127280 | 79669 |
| Heptadecane, 3-methyl- | $C_{18}H_{38}$ | 0.24 | 92.53 | 14.772 | 131412 | 64598 |
| Pentadecane, 2-methyl- | $C_{16}H_{34}$ | 0.23 | 92.76 | 20.19 | 121129 | 67314 |
| Dodecane, 4,9-dipropyl- | C18H38 | 0.23 | 92.99 | 20.464 | 122152 | 74202 |

**Table 5-10** The mass spectrum peak absolute intensity table of GTL fuel part five.

| Name | Molecular formula | Conc. (%) | Cum. Conc. (%) | Ret.Time (mins) | Area | Height |
|---|---|---|---|---|---|---|
| Pentadecane, 4-methyl- | $C_{16}H_{34}$ | 0.23 | 93.22 | 21.095 | 121525 | 66291 |
| Heptadecane, 2-methyl- | $C_{18}H_{38}$ | 0.23 | 93.45 | 18.115 | 123861 | 75455 |
| Octadecane | ⎡ C28H58 | 0.23 | 93.68 | 20.308 | 125950 | 63177 |
| Octane, 2,6-dimethyl- | $C_{10}H_{22}$ | 0.22 | 93.9 | 22.08 | 118512 | 34882 |
| Hexadecane, 2-methyl- | $C_{17}H_{36}$ | 0.22 | 94.12 | 21.534 | 120988 | 58775 |
| 3-Ethyl-3-methylheptane | $C_{10}H_{22}$ | 0.22 | 94.34 | 9.591 | 117022 | 65499 |
| Heptane, 2,4-dimethyl- | ⎡ $C_9H_{20}$ | 0.21 | 94.55 | 23.855 | 112838 | 73999 |
| Tridecane | $C_{13}H_{28}$ | 0.21 | 94.76 | 7.765 | 115332 | 66494 |
| Tridecane | $C_{13}H_{28}$ | 0.21 | 94.97 | 25.098 | 112487 | 56910 |
| Cyclohexanone, 4-(1,1-dimethylethyl)- | C10H18O | 0.21 | 95.18 | 13.17 | 111646 | 44501 |
| Octacosane | ⎡ $C_{28}H_{58}$ | 0.21 | 95.39 | 13.682 | 110667 | 74004 |
| Tetradecane, 3-methyl- | $C_{14}H_{30}$ | 0.2 | 95.59 | 24.491 | 108486 | 41681 |
| Heptadecane, 3-methyl- | $C_{18}H_{38}$ | 0.2 | 95.79 | 17.585 | 105538 | 51335 |
| Decane, 4-methyl- | ⎡ $C_{11}H_{24}$ | 0.19 | 95.98 | 11.505 | 101303 | 68540 |
| Pentadecane, 4-methyl- | $C_{16}H_{34}$ | 0.19 | 96.17 | 18.526 | 100014 | 41677 |
| Decane, 5,6-dimethyl- | $C_{12}H_{26}$ | 0.18 | 96.35 | 13.25 | 94833 | 75121 |
| Undecane, 4-methyl- | $C_{12}H_{26}$ | 0.18 | 96.53 | 22.616 | 95251 | 31770 |
| Hexadecane, 2-methyl- | $C_{17}H_{36}$ | 0.18 | 96.71 | 23.501 | 95519 | 42544 |
| Nonadecane, 9-methyl- | $C_{20}H_{42}$ | 0.18 | 96.89 | 13.358 | 96263 | 64306 |
| Tridecane, 3-methyl- | $C_{14}H_{30}$ | 0.17 | 97.06 | 16.037 | 91249 | 62602 |
| Hexadecane | $C_{16}H_{34}$ | 0.17 | 97.23 | 20.349 | 92814 | 50176 |
| Pentadecane, 8-hexyl- | $C_{21}H_{44}$ | 0.17 | 97.4 | 13.65 | 92029 | 38540 |
| Tetradecane | $C_{14}H_{30}$ | 0.16 | 97.56 | 18.735 | 84912 | 50072 |
| Undecane, 2,6-dimethyl- | $C_{13}H_{28}$ | 0.16 | 97.72 | 24.954 | 88371 | 46323 |
| Dodecane, 2-methyl- | ⎡ $C_{13}H_{28}$ | 0.16 | 97.88 | 17.47 | 84755 | 42765 |
| Heptadecane, 4-methyl- | $C_{18}H_{38}$ | 0.16 | 98.04 | 17.767 | 84597 | 50954 |
| Hexane, 3-ethyl-4-methyl- | $C_9H_{20}$ | 0.15 | 98.19 | 27.176 | 83225 | 47700 |
| Undecane, 2-methyl- | ⎡ $C_{12}H_{26}$ | 0.15 | 98.34 | 25.825 | 82647 | 33453 |
| Nonadecane, 2-methyl- | ⎡ $C_{20}H_{42}$ | 0.15 | 98.49 | 17.44 | 78696 | 45891 |
| Hexadecane | $C_{16}H_{34}$ | 0.15 | 98.64 | 9.351 | 83315 | 52541 |
| Tricosane, 2-methyl- | $C_{24}H_{50}$ | 0.15 | 98.79 | 16.09 | 78257 | 45910 |
| Eicosane, 2-methyl- | $C_{21}H_{44}$ | 0.15 | 98.94 | 25.016 | 79117 | 41854 |
| Eicosane | $C_{20}H_4$ | 0.15 | 99.09 | 13.45 | 81282 | 56369 |
| Octane, 2,6-dimethyl- | $C_{10}H_{22}$ | 0.14 | 99.23 | 18.66 | 77697 | 30207 |

**Table 5-11** The mass spectrum peak absolute intensity table of GTL fuel part six.

| Name | Molecular formula | Conc. (%) | Cum. Conc. (%) | Ret.Time (mins) | Area | Height |
|---|---|---|---|---|---|---|
| Octane, 3-ethyl- | $C_{10}H_{22}$ | 0.14 | 99.37 | 22.688 | 74129 | 40282 |
| Tetradecane | $C_{14}H_{30}$ | 0.14 | 99.51 | 9.708 | 74953 | 30048 |
| 1-Decanol, 2-hexyl- | $C_{16}H_{34}O$ | 0.14 | 99.65 | 10.348 | 77686 | 51558 |
| Dodecane, 4,9-dipropyl- | C18H38 | 0.14 | 99.79 | 18.565 | 75529 | 40010 |
| Tricosane, 2-methyl- | $C_{24}H_{50}$ | 0.14 | 99.93 | 25.95 | 76132 | 28834 |

## 5.3 Combustion performance

In this section, the combustion performance is discussed in three topics, the engine power comparison, the in-cylinder pressure to crank angle curve comparison, and the PV diagram comparison. From table 5-1, it can be found that compared to diesel fuel, GTL fuel has higher cetane number, lower density, much lower aromatics and shares very similar calorific value. This indicates that some differences and similarities in combustion performances among diesel, GTL and blended fuel are predictable based on a literature review, and the detailed discussion is presented in this section.

### 5.3.1 Engine power

In this part, six the engine power parameters are compared, engine torque, engine power, BMEP, IMEP, maximum combustion pressure, and average combustion pressure. The engine torque and engine power data were directly measured from the engine control system, and the rest of the four was calculated based on the data of in-cylinder pressure measurement. The results of all tests are shown in nine tables from table 5-12 to table 5-20, each of them presented one specific engine working condition.

From the comparison of those tables, generally, it can be addressed that the engine power between diesel fuel, GTL fuel and GTL blended fuel were quite similar in all tested engine working conditions. This is due to the calorific value difference between diesel fuel and GTL fuel is low and the fuel consumptions of each engine working condition were the same. The diesel fuel obtains 42.9 MJ/Kg while the GTL obtains 44.0 MJ/Kg. The engine power (KW) is nearly the same for all fuels at each test condition, however, there is slight difference in torque, which is caused by the fluctuations of torque measurement. The variation of torque is ± 3 Nm. Besides, small differences can

be found from detailed pressure data, especially from IMEP values, maximum and average combustion pressure.

**Table 5-12** The engine power of GTL blended tests at 1000 rpm, 30% throttle.

| Fuel Type | Torque (Nm) | Power (Kw) | BMEP (bar) | IMEP (bar) | P max (bar) | P max location (°CA) | P average (bar) |
|---|---|---|---|---|---|---|---|
| Diesel | 125 | 13 | 5.3 | 7.3 | 61.2 | 17 | 7.2 |
| 30% GTL | 123 | 13 | 5.2 | 7.4 | 59.2 | 18 | 6.6 |
| 50% GTL | 124 | 13 | 5.2 | 7.0 | 58.4 | 18 | 6.6 |
| 70% GTL | 128 | 13 | 5.4 | 7.2 | 58.9 | 18 | 6.5 |
| 100% GTL | 128 | 13 | 5.4 | 6.6 | 65.9 | 12 | 6.4 |

**Table 5-13** The engine power of GTL blended tests at 1000 rpm, 40% throttle.

| Fuel Type | Torque (Nm) | Power (Kw) | BMEP (bar) | IMEP (bar) | P max (bar) | P max location (°CA) | P average (bar) |
|---|---|---|---|---|---|---|---|
| Diesel | 182 | 19 | 7.6 | 9.8 | 73.6 | 16 | 8.3 |
| 30% GTL | 185 | 19 | 7.7 | 10.0 | 72.9 | 17 | 7.8 |
| 50% GTL | 185 | 19 | 7.8 | 9.9 | 74.2 | 17 | 7.9 |
| 70% GTL | 186 | 19 | 7.8 | 10.2 | 75.4 | 17 | 7.9 |
| 100% GTL | 186 | 19 | 7.8 | 10.2 | 76.7 | 14 | 7.6 |

**Table 5-14** The engine power of GTL blended tests at 1000 rpm, 50% throttle.

| Fuel Type | Torque (Nm) | Power (Kw) | BMEP (bar) | IMEP (bar) | P max (bar) | P max location (°CA) | P average (bar) |
|---|---|---|---|---|---|---|---|
| Diesel | 207 | 22 | 8.7 | 11.8 | 85.0 | 16 | 8.6 |
| 30% GTL | 207 | 22 | 8.7 | 10.9 | 83.8 | 16 | 8.5 |
| 50% GTL | 206 | 22 | 8.6 | 11.1 | 85.0 | 15 | 8.5 |
| 70% GTL | 206 | 21 | 8.6 | 11.2 | 86.0 | 15 | 8.5 |
| 100% GTL | 207 | 22 | 8.7 | 11.6 | 86.9 | 13 | 8.3 |

From table 5-12 to table 5-14, the IMEP behaviour of blended fuel was quite close but was irregular with either increasing blending ratio or decreasing blending ratio. This was due to at 1000 rpm engine running condition, which is a relevantly low rpm setting for this diesel engine, thus the slightly calorific value differences impact on engine IMEP could hardly be seen. However, if comparing the maximum combustion pressure between diesel and pure GTL fuel, it can be found that the maximum combustion pressure of GTL was always higher than diesel. This is because the pure GTL fuel has a faster combustion rate than diesel, which can be evidenced by figure 5-4.

The combustion process of hydrocarbons refers to the reaction between hydrocarbons and oxygen to create carbon dioxide, water and heat. The energy required to break the chemical bonds in hydrocarbons are less than the energy released when $CO_2$ and $H_2O$, and thus the combustion process release thermal energy. [Westbrook and Dryer, 1984]. The aromatic hydrocarbon require more energy to break its chemical bond than pure alkanes, because double bonds existed in aromatics are stronger than the single bond in alkanes. Since pure GTL consisted with all alkanes and in absence of aromatics, therefore the diffusion flame can spread faster. Actually, at the flame diffusion phase, the aromatic-containing diesel fuel was decomposed with more difficulty. On the one hand, the aromatics with benzene ring structure were more difficult to be combusted because the strong chemical bound of benzene ring; on the other hand, diesel fuel had more heavy saturated hydrocarbons, which also require higher energy to completely combust off. [Kee, et al, 2005]. All other blended fuel showed lower maximum combustion pressure in 1000 rpm tests and this will be further discussed later when comparison of all tests is completed in the next paragraph.

From the results of 1600 rpm tests, table 5-15 to table 5-17, it can be found that the pure GTL acquired higher IMEP, higher maximum combustion pressure and equal or higher engine power. This result compromised with the finding in 1900 rpm tests, table 5-18 to table 5-20. However, when blend ratio increased from 30% to 70%, neither did the maximum combustion pressure nor the IMEP kept increasing or decreasing. This shared the same finding in 1000 rpm tests, thus it can be concluded the power generated by blended GTL fuel is less than from pure diesel fuel and pure GTL fuel.

The average combustion pressure and BMEP of all tests results were similar, and in the majority of tests, the GTL blended fuel showed slightly even or lower BMEP and average combustion pressure.

**Table 5-15** The engine power of GTL blended tests at 1600 rpm, 40% throttle.

| Fuel Type | Torque (Nm) | Power (Kw) | BMEP (bar) | IMEP (bar) | P max (bar) | P max location (°CA) | P average (bar) |
|---|---|---|---|---|---|---|---|
| Diesel | 119 | 20 | 5.0 | 6.9 | 60.7 | 18 | 7.2 |
| 30% GTL | 114 | 19 | 4.8 | 6.9 | 60.1 | 15 | 6.9 |
| 50% GTL | 113 | 19 | 4.7 | 6.6 | 58.5 | 16 | 6.8 |
| 70% GTL | 114 | 19 | 4.8 | 6.9 | 60.8 | 17 | 7.0 |
| 100% GTL | 116 | 20 | 4.8 | 7.2 | 68.4 | 14 | 7.4 |

**Table 5-16** The engine power of GTL blended tests at 1600 rpm, 50% throttle.

| Fuel Type | Torque (Nm) | Power (Kw) | BMEP (bar) | IMEP (bar) | P max (bar) | P max location (°CA) | P average (bar) |
|---|---|---|---|---|---|---|---|
| Diesel | 153 | 26 | 6.4 | 8.8 | 68.4 | 17 | 8.4 |
| 30% GTL | 158 | 27 | 6.6 | 8.8 | 67.6 | 18 | 8.0 |
| 50% GTL | 156 | 26 | 6.6 | 8.7 | 67.2 | 17 | 7.9 |
| 70% GTL | 153 | 26 | 6.4 | 8.6 | 67.2 | 19 | 7.9 |
| 100% GTL | 164 | 27 | 6.9 | 9.3 | 71.3 | 16 | 8.3 |

**Table 5-17** The engine power of GTL blended tests at 1600 rpm, 60% throttle.

| Fuel Type | Torque (Nm) | Power (Kw) | BMEP (bar) | IMEP (bar) | P max (bar) | P max location (°CA) | P average (bar) |
|---|---|---|---|---|---|---|---|
| Diesel | 215 | 36 | 9.0 | 11.5 | 87.4 | 17 | 10.2 |
| 30% GTL | 214 | 36 | 9.0 | 11.5 | 86.9 | 16 | 9.6 |
| 50% GTL | 214 | 36 | 9.0 | 11.5 | 86.8 | 16 | 9.7 |
| 70% GTL | 211 | 36 | 8.9 | 11.4 | 86.8 | 17 | 9.6 |
| 100% GTL | 217 | 37 | 9.1 | 12.1 | 88.4 | 16 | 9.9 |

**Table 5-18** The engine power of GTL blended tests at 1900 rpm, 50% throttle.

| Fuel Type | Torque (Nm) | Power (Kw) | BMEP (bar) | IMEP (bar) | P max (bar) | P max location (°CA) | P average (bar) |
|---|---|---|---|---|---|---|---|
| Diesel | 135 | 27 | 5.7 | 7.8 | 65.1 | 18 | 8.0 |
| 30% GTL | 135 | 27 | 5.7 | 7.7 | 65.6 | 18 | 7.7 |
| 50% GTL | 132 | 26 | 5.5 | 7.8 | 66.4 | 16 | 7.7 |
| 70% GTL | 134 | 27 | 5.6 | 7.8 | 66.9 | 17 | 7.7 |
| 100% GTL | 138 | 28 | 5.8 | 8.2 | 66.2 | 17 | 7.8 |

**Table 5-19** The engine power of GTL blended tests at 1900 rpm, 60% throttle.

| Fuel Type | Torque (Nm) | Power (Kw) | BMEP (bar) | IMEP (bar) | P max (bar) | P max location (°CA) | P average (bar) |
|---|---|---|---|---|---|---|---|
| Diesel | 183 | 36 | 7.7 | 9.8 | 78.1 | 18 | 9.7 |
| 30% GTL | 181 | 36 | 7.6 | 9.8 | 76.8 | 17 | 9.2 |
| 50% GTL | 181 | 36 | 7.6 | 9.5 | 75.1 | 17 | 9.0 |
| 70% GTL | 179 | 36 | 7.5 | 9.7 | 76.4 | 17 | 9.1 |
| 100% GTL | 183 | 37 | 7.7 | 10.4 | 77.5 | 18 | 9.3 |

**Table 5-20** The engine power of GTL blended tests at 1900 rpm, 70% throttle.

| Fuel Type | Torque (Nm) | Power (Kw) | BMEP (bar) | IMEP (bar) | P max (bar) | P max location (°CA) | P average (bar) |
|---|---|---|---|---|---|---|---|
| Diesel | 238 | 47 | 10.0 | 12.6 | 102.6 | 13 | 11.4 |
| 30% GTL | 234 | 47 | 9.8 | 12.5 | 104.6 | 16 | 11.1 |
| 50% GTL | 232 | 46 | 9.7 | 12.7 | 105.1 | 14 | 11.2 |
| 70% GTL | 231 | 46 | 9.7 | 12.4 | 102.2 | 13 | 11.1 |
| 100% GTL | 231 | 46 | 9.7 | 12.9 | 103.6 | 15 | 11.2 |

Thus, it can be summarized that in the engine power comparison part GTL and its blended fuel showed very similar engine power performance with diesel fuel because of

their similarities in calorific values. The pure GTL could generate slightly higher maximum combustion pressure while its blended fuel performed both even or lower BMEP and average combustion pressure.

### 5.3.2 In cylinder pressure curve and ignition delay

This section focuses on the in-cylinder pressure to crank angle curves near TDC for all the tests. The crank angle for the start of fuel injection and start of combustion crank angle point were decided based on the pressure curve detail and ignition delay was calculated and presented in table 5-21 to table 5-29, the pressure curves are presented from figure 5-4 to figure 5-12.

In general, from comparison of all tests results, the ignition delays from pure GTL were shorter than that from diesel due to that the GTL fuel has higher cetane number. The blended fuels performed equal ignition delays to pure diesel in most test conditions however still behaved shorter in some of the experiments.

**Table 5-21** The ignition delays of GTL blended fuels at 1000rpm, 30% throttle.

| Fuel Type | SOI CA° | SOC CA° | ID CA° | ID (ms) |
|---|---|---|---|---|
| Diesel | -2 | 7 | 9 | 1.50 |
| 30% GTL | -2 | 7 | 9 | 1.50 |
| 50% GTL | -2 | 7 | 9 | 1.50 |
| 70% GTL | -2 | 7 | 9 | 1.50 |
| 100% GTL | -2 | 1 | 3 | 0.50 |

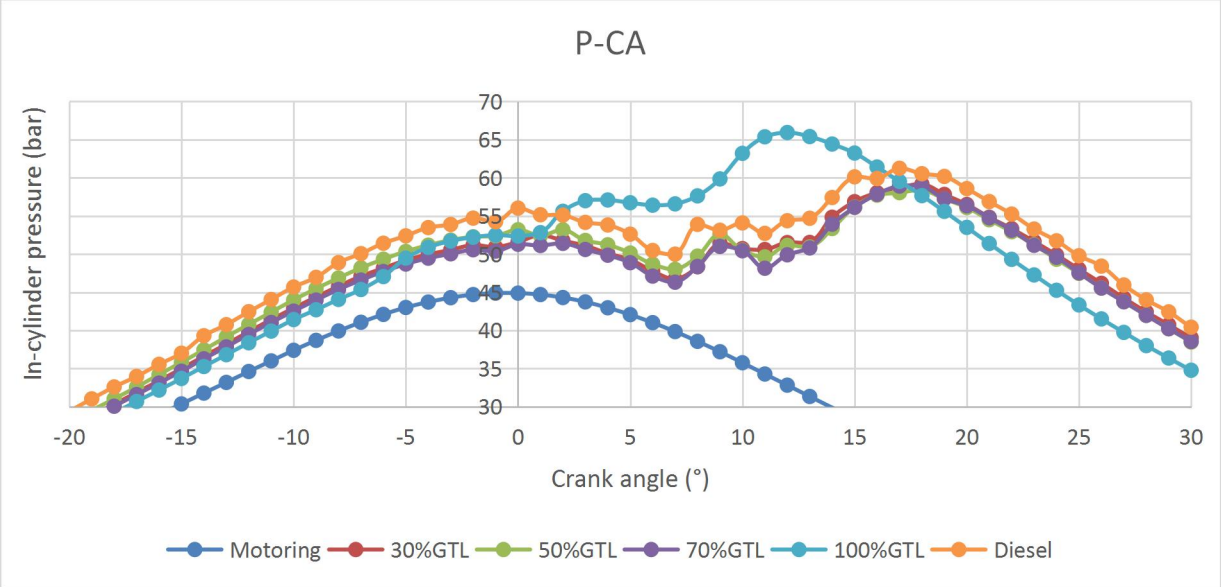


**Figure 5-4** The pressure curve near TDC of GTL blended fuels at 1000rpm, 30% throttle.

From figure 5-4, in the 1000 rpm, 30% throttle engine condition, all fuel injections started 2 degrees BTDC evidenced by the pressure drop caused by fuel injection. Unlike the rest of the fuels, the pure GTL started combustion sooner, and reached higher peak pressure. The combustion process of the pure GTL fuel also ended earlier, thus resulting the pressure behaved lower than any other fuels 20 degrees after the piston passed the TDC. The combustion pressure curves between pure GTL fuel and other fuel were obviously different in 1000 rpm, 30% throttle engine condition. The ignition delay of GTL fuel was obviously shorter than the blended fuels, and the combustion pressure was also clearly higher. This was due to the high cetane number and chemical composition-pure alkanes without aromatics. Similar research from Kidoguchi, et al [2000]. also showed that fuels with higher cetane number and lower aromatics content would have shorter ignition delay and faster combustion rate. Because the aromatics with ring structure require more energy to break (to be ignited). [Kee, et al, 2005]. This can also be supported by the work of Vandersickel et al. [2005]. The same results were found from 1000 rpm, 40% throttle tests (figure 5-5), albeit with the increase of throttle setting, the variation between pure GTL and other fuels was getting smaller.

**Table 5-22** The ignition delays of GTL blended fuels at 1000rpm, 40% throttle.

| Fuel Type | SOI CA° | SOC CA° | ID CA° | ID (ms) |
|---|---|---|---|---|
| Diesel | -2 | 5 | 7 | 1.17 |
| 30% GTL | -2 | 5 | 7 | 1.17 |
| 50% GTL | -2 | 5 | 7 | 1.17 |
| 70% GTL | -2 | 5 | 7 | 1.17 |
| 100% GTL | -2 | 1 | 3 | 0.50 |

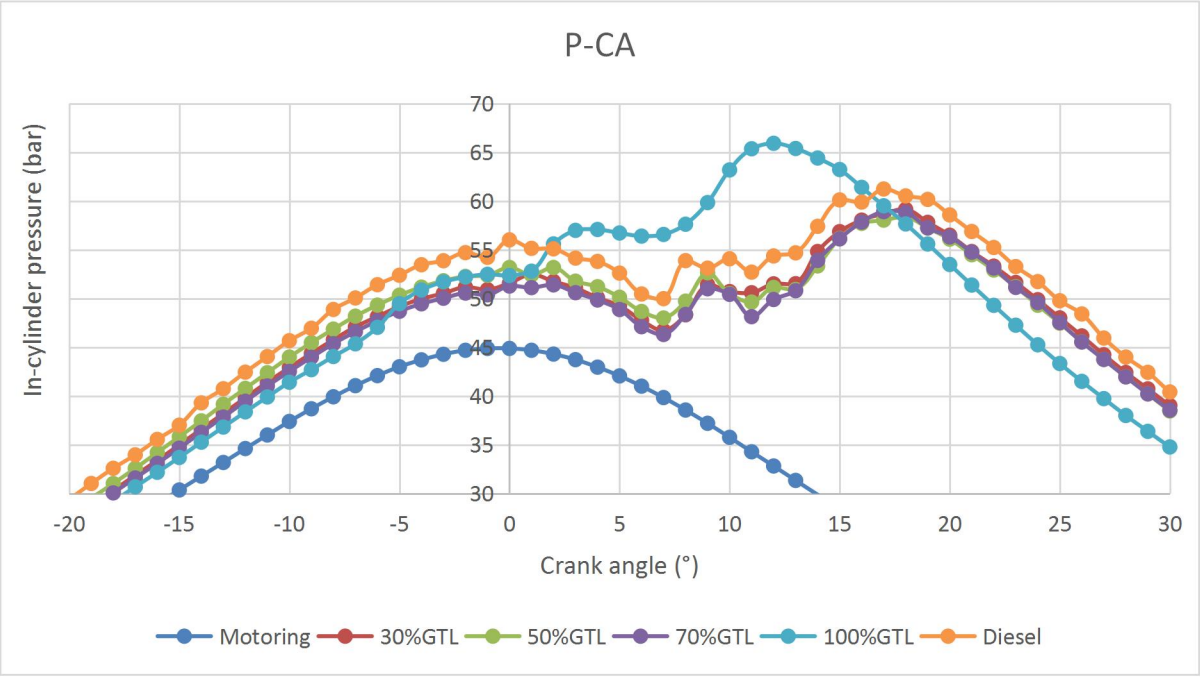


**Figure 5-5** The pressure curve near TDC of GTL blended fuels at 1000rpm, 40% throttle.

**Table 5-23** The ignition delays of GTL blended fuels at 1000rpm, 50% throttle.

| Fuel Type | SOI CA° | SOC CA° | ID CA° | ID (ms) |
|---|---|---|---|---|
| Diesel | -3 | 4 | 7 | 1.17 |
| 30% GTL | -3 | 3 | 6 | 1.00 |
| 50% GTL | -3 | 3 | 6 | 1.00 |
| 70% GTL | -3 | 3 | 6 | 1.00 |
| 100% GTL | -5 | 1 | 6 | 1.00 |

When the engine throttle was increased, the difference between pure GTL and other blended or diesel fuels was becoming even smaller. It can be found that at a specific engine rpm, the P-CA is less sensitive to throttle or torque increases between fuels, for instance, at the higher power conditions, the variation between different fuels for in-cylinder pressure is smaller. In contrast, the lower the engine power settings, the more obvious the variations can be found. With the engine power setting rise, the average and peak in-cylinder pressure rise, and combustion temperature also increases. Therefore, it can be concluded the difference in pressure curve caused by fuel properties would be abated with the engine power increases, or the engine power settings has dominant impacts on combustion pressure.

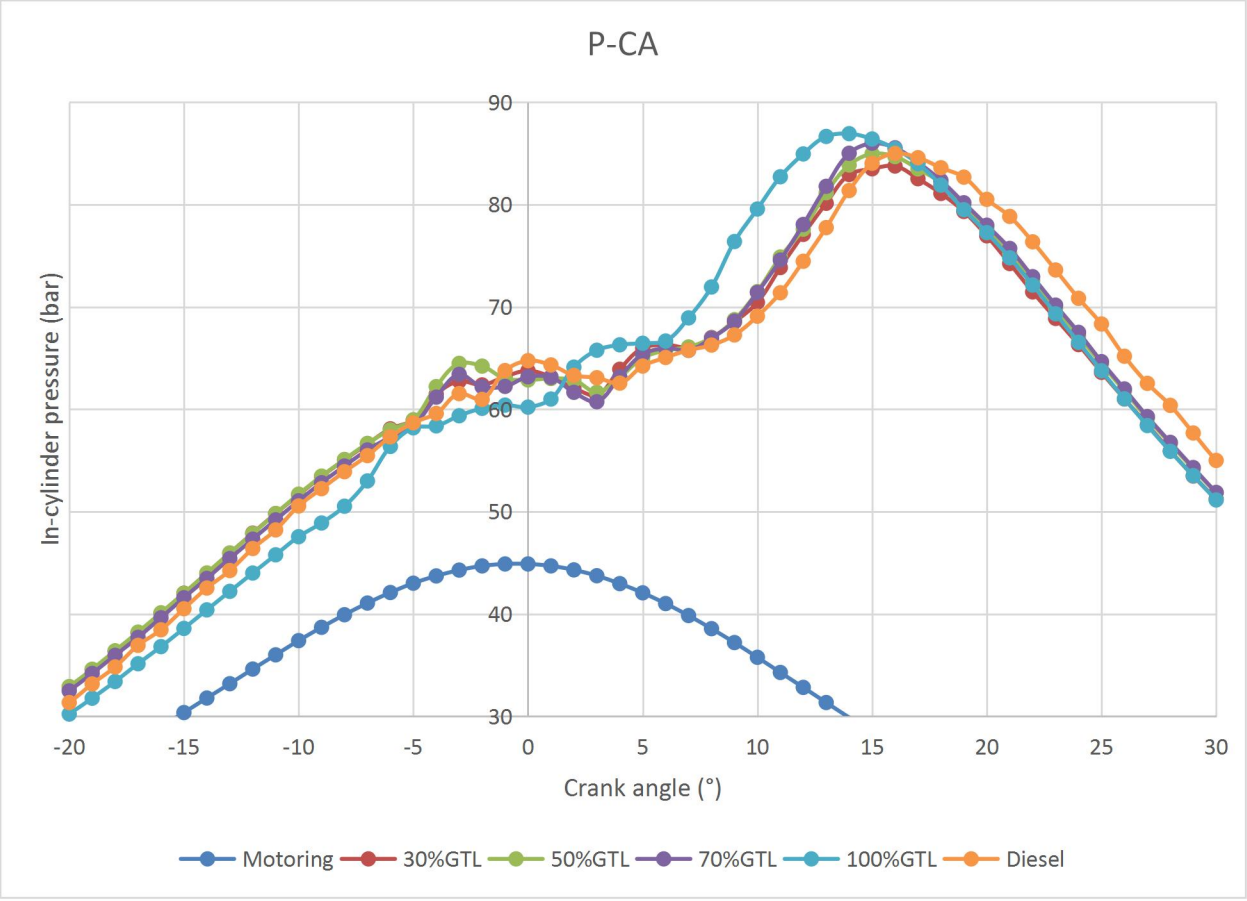


**Figure 5-6** The pressure curve near TDC of GTL blended fuels at 1000rpm, 50% throttle.

**Table 5-23** The ignition delays of GTL blended fuels at 1600rpm, 40% throttle.

| Fuel Type | SOI CA° | SOC CA° | ID CA° | ID (ms) |
|---|---|---|---|---|
| Diesel | -5 | 5 | 10 | 1.04 |
| 30% GTL | -5 | 5 | 10 | 1.04 |
| 50% GTL | -4 | 5 | 9 | 0.94 |
| 70% GTL | -4 | 5 | 9 | 0.94 |
| 100% GTL | -5 | 2 | 7 | 0.73 |

**Table 5-24** The ignition delays of GTL blended fuels at 1600rpm, 50% throttle.

| Fuel Type | SOI CA° | SOC CA° | ID CA° | ID (ms) |
|---|---|---|---|---|
| Diesel | -6 | 5 | 11 | 1.15 |
| 30% GTL | -6 | 5 | 11 | 1.15 |
| 50% GTL | -5 | 5 | 10 | 1.04 |
| 70% GTL | -5 | 5 | 10 | 1.04 |
| 100% GTL | -6 | 1 | 7 | 0.73 |

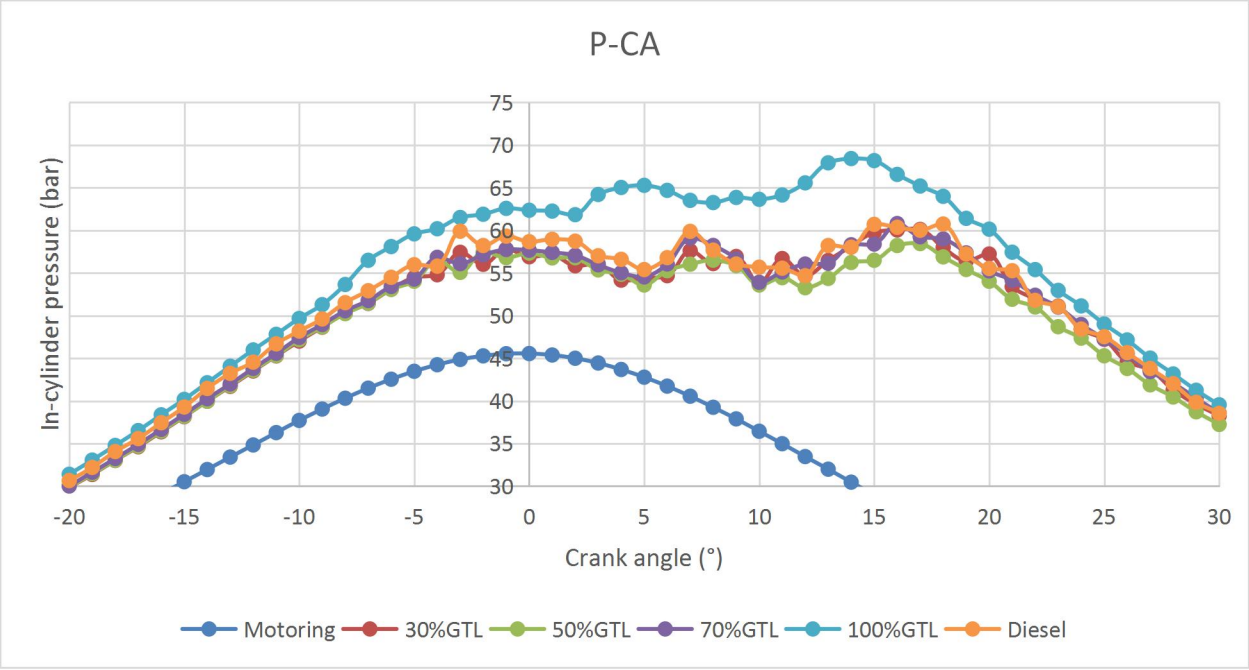


**Figure 5-7** The pressure curve near TDC of GTL blended fuels at 1600rpm, 40% throttle.

In the 1600 rpm engine tests, similar findings were obtained to the 1000 rpm tests. With the engine rpm and throttle setting both increased, the differences in ignition delay between diesel fuel, blended fuel and pure GTL were clear. From the analysis of table 5-23 and figure 5-7, the ignition delays were becoming shorter with the blending ratio increased. This was due to the average cetane number of experimental fuels were increased with the increasing of blending ratio. Also, in the 1600 rpm tests, the combustion process of all fuels was tended to become constant pressure combustion. Multiple fuel injections can be seen 5 degrees to 15 degrees after TDC, which is the method of how this IVECO diesel engine tried to acquire its constant pressure combustion and achieve higher thermal efficiency.

**Table 5-25** The ignition delays of GTL blended fuels at 1600rpm, 60% throttle.

| Fuel Type | SOI CA° | SOC CA° | ID CA° | ID (ms) |
|---|---|---|---|---|
| Diesel | -9 | 1 | 10 | 1.04 |
| 30% GTL | -9 | 1 | 10 | 1.04 |
| 50% GTL | -9 | 1 | 10 | 1.04 |
| 70% GTL | -9 | 1 | 10 | 1.04 |
| 100% GTL | -9 | 1 | 10 | 1.04 |

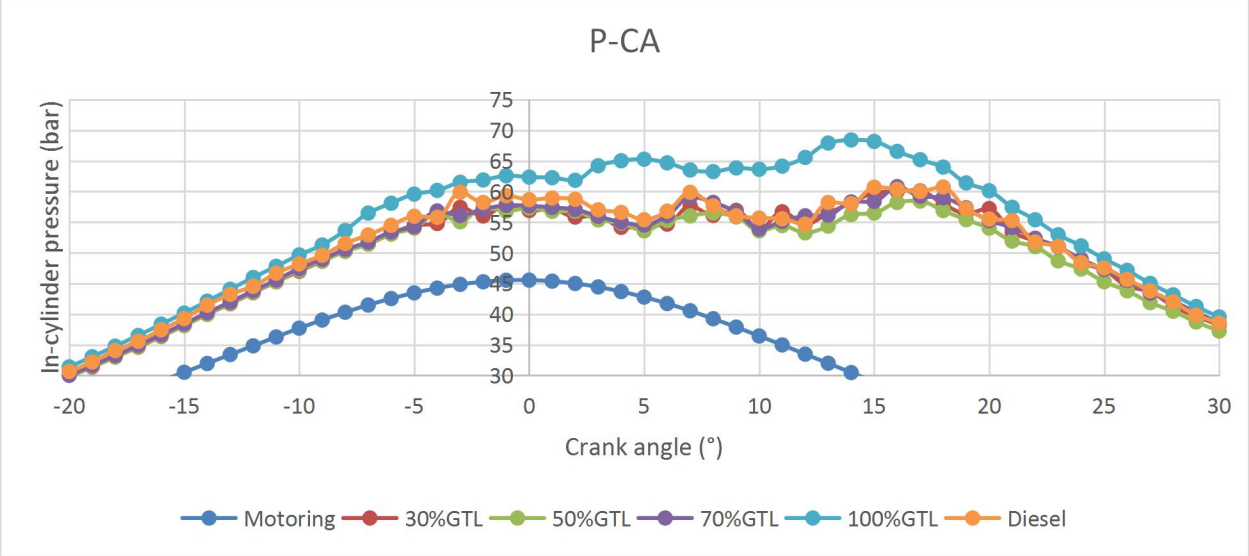


**Figure 5-8** The pressure curve near TDC of GTL blended fuels at 1600rpm, 50% throttle.

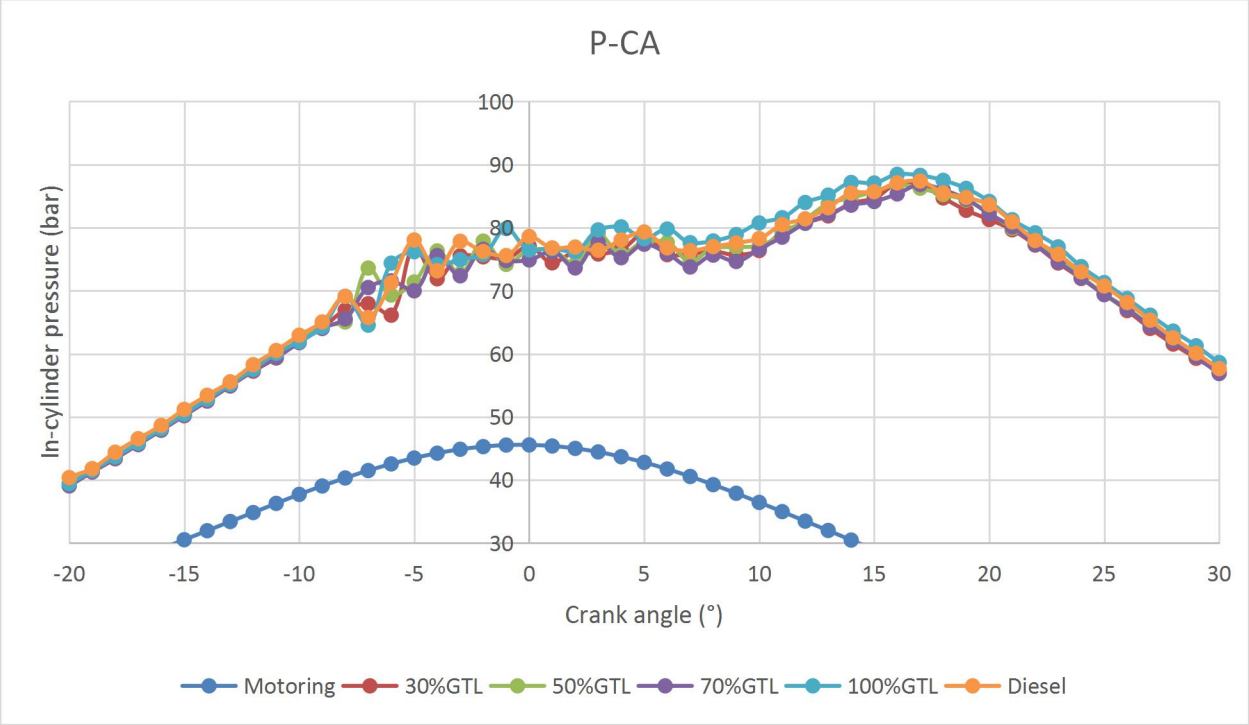


**Figure 5-9** The pressure curve near TDC of GTL blended fuels at 1600rpm, 60% throttle.

Another interesting finding from the 1600 rpm tests was the in-cylinder pressure would sometimes experience a sudden little rise before the start of fuel injection. This is obvious in figure 5-9 shown above. The pressure drops generally caused by fuel injection occurred at 8 degrees BTDC, however, all fuels experienced a pressure rise at 9 degrees BTDC from 0.5 bar to 3.9 bar. The rise is small and unlikely to be caused by pilot combustion. One explanation for this is that soon after the fuel was injected to the combustion cylinder, before the fuel started to absorb heat and lead to pressure drop, some light fractions of diesel fuel is more likely to evaporate and leading to the pressure increase. Since the evaporation of lighter fractions occurs at lower temperature than heavier fractions. [Stiver, 1984]. Once the light fractions evaporated, the liquid fuel droplet was transformed to gas, which immediately occupied the combustion cylinder and caused the in-cylinder pressure to rise. This scenario was more obvious with diesel fuel than the blended or pure GTL fuel. This can be treated as with the increasing of blend ratio, the diesel in the fuel is reducing, thus the pressure rising reaction related to diesel is becoming less obvious with the increasing of blend ratio. The carbon chain

fraction distribution of GTL fuel and diesel fuel are presented in figure 5-2 and figure 5-3 in the previous fuel property section of this chapter.

**Table 5-27** The ignition delays of GTL blended fuels at 1900rpm, 50% throttle.

| Fuel Type | SOI CA° | SOC CA° | ID CA° | ID (ms) |
|---|---|---|---|---|
| Diesel | -7 | 4 | 11 | 0.96 |
| 30% GTL | -6 | 4 | 10 | 0.88 |
| 50% GTL | -6 | 4 | 10 | 0.88 |
| 70% GTL | -6 | 4 | 10 | 0.88 |
| 100% GTL | -6 | 3 | 9 | 0.79 |

**Table 5-28** The ignition delays of GTL blended fuels at 1900rpm, 60% throttle.

| Fuel Type | SOI CA° | SOC CA° | ID CA° | ID (ms) |
|---|---|---|---|---|
| Diesel | -5 | 4 | 9 | 0.79 |
| 30% GTL | -3 | 4 | 7 | 0.61 |
| 50% GTL | -3 | 4 | 7 | 0.61 |
| 70% GTL | -3 | 4 | 7 | 0.61 |
| 100% GTL | -3 | 3 | 6 | 0.53 |

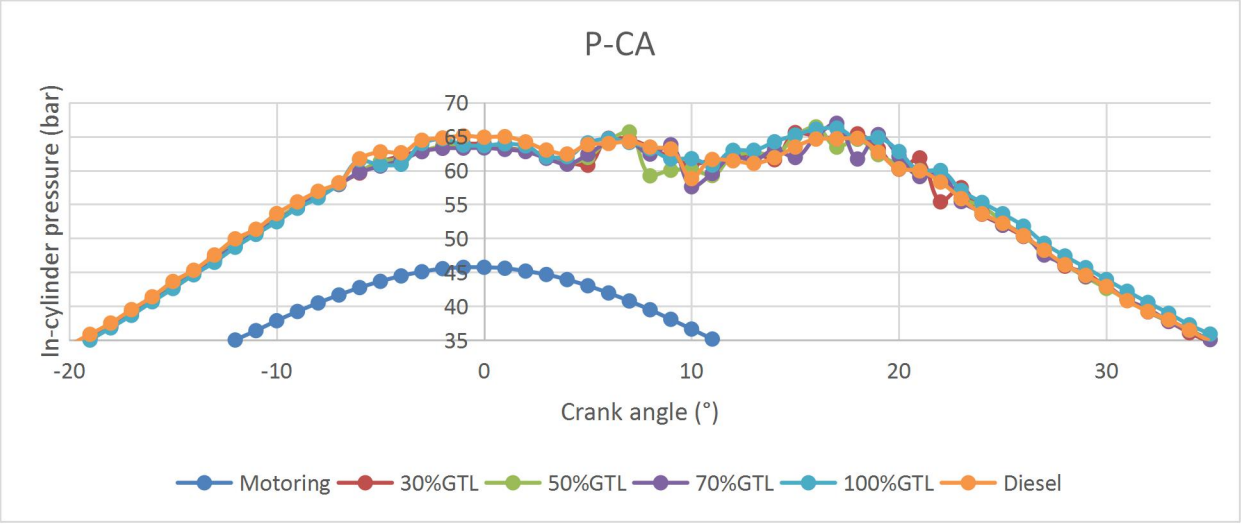


**Figure 5-10** The pressure curve near TDC of GTL blended fuels at 1900rpm, 50% throttle.

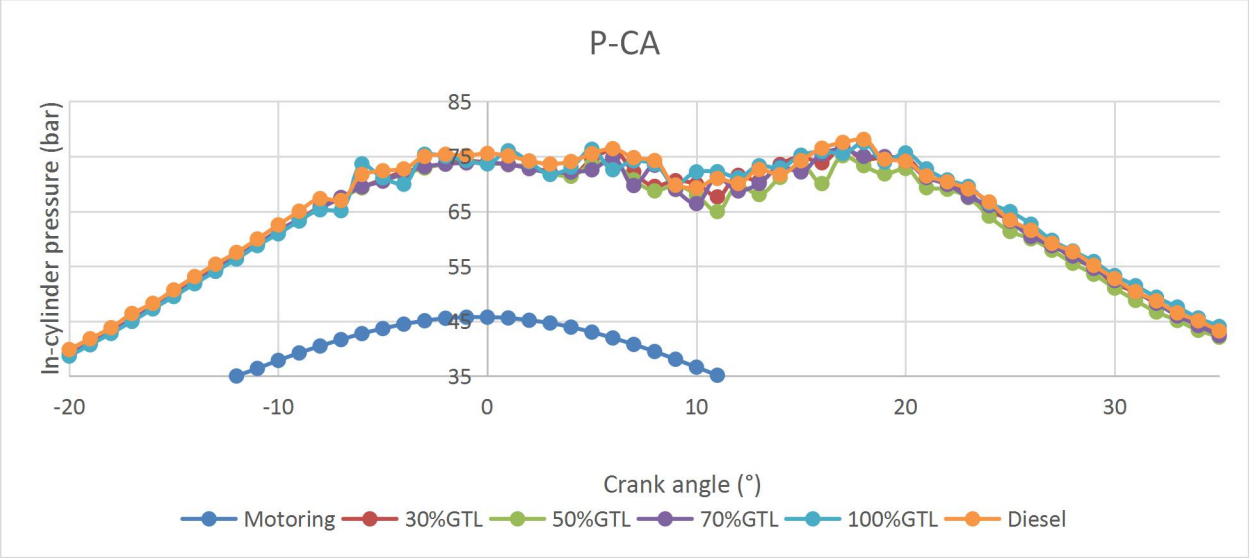


**Figure 5-11** The pressure curve near TDC of GTL blended fuels at 1900rpm, 60% throttle.

**Table 5-29** The ignition delays of GTL blended fuels at 1900rpm, 70% throttle.

| Fuel Type | SOI CA° | SOC CA° | ID CA° | ID (ms) |
|---|---|---|---|---|
| Diesel | -12 | -1 | 11 | 0.96 |
| 30% GTL | -11 | -1 | 10 | 0.88 |
| 50% GTL | -11 | -1 | 10 | 0.88 |
| 70% GTL | -11 | -1 | 10 | 0.88 |
| 100% GTL | -11 | -1 | 10 | 0.88 |

The ignition delay results from 1900 rpm tests compromised with those results in 1000 rpm and 1600 rpm tests. Compared to them, the pressure curves near TDC at 1900 rpm tests showed more evidence of multiple fuel injection strategy of the engine. At least five injections occurred near TDC, and this can be seen from several pressure drops near TDC for all the tested fuels. Figure 5-12 provides an example. Those multiple fuel injection helped the engine to acquire relevant stable and constant pressure combustion. As it can be seen from figure 5-10, figure 5-11, and figure 5-12, the fuel combustion process happened with pressure variety less than 9 bar. The constant pressure combustion performance of this engine will be discussed more in detail in next PV diagram section.

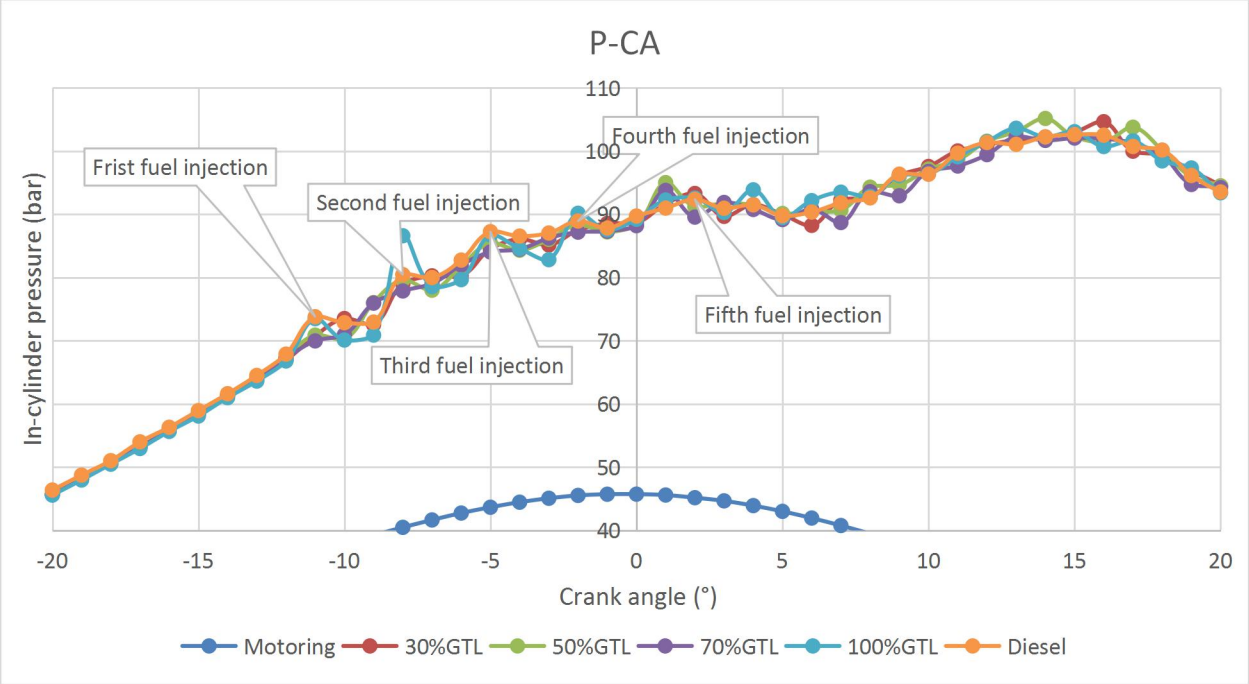


**Figure 5-12** The pressure curve near TDC of GTL blended fuels at 1900rpm, 70% throttle.

In summary, from the in-cylinder pressure analysis, the ignition delay decreased with the blending ratio increased because the cetane number in the fuel raised. The pure GTL fuel could have a higher combustion peak pressure; however, this became negligible with the engine power increased. The light fraction component in diesel fuel can cause in-cylinder pressure to rise before it causes pressure drop via absorbing heat. Multiple fuel injections have been captured of this IVECO diesel engine, and it helped the engine to maintain a relevant constant pressure combustion.

### 5.3.3 PV diagram

The PV diagrams of diesel fuel and blended fuel showed quite close behaviours among each other. This was due to the pressure curve differences showed in previous section was too little. This section provides the PV diagrams of 30% GTL fuel and pure GTL fuel as two representative fuel types. The reason to choose those two fuels types is one is blended with the lowest GTL fraction while the other is pure GTL. The large blending ratio difference can enlarge the pressure difference and allowing more clear comparison analysis to be made. The PV diagram for 30% GTL blended fuel and pure GTL fuel is

shown from figure 5-13 to figure 5-30 in bellow. The rest of the PV diagrams of other blended fuels are listed in the appendix.

The experiment engine is a four-cylinder diesel engine with total displacement of 2998 $cm^3$. Thus, the swept volume per cylinder equals to 2998÷4 = 749.5 $cm^3$. Considering the compression ratio is 18, the clearance volume for the combustion cylinder equals to 749.5÷ (18+1) = 39.4 $cm^3$. Therefore, the volume maximum value in all PV diagram is 788.9 $cm^3$ (749.5+39.4). The pressure values in all PV diagrams are absolute pressure, meaning the pressure values are zero-referenced against a perfect vacuum, and 1 bar on Y-axis indicates the ambient atmospheric pressure in experiments. It can be found in following PV diagrams that all initial air inlet pressure values are higher than ambient atmospheric pressure. This is due to the experiment engine being equipped with a turbocharger, thus the air being sucked into the combustion cylinder is compressed air.

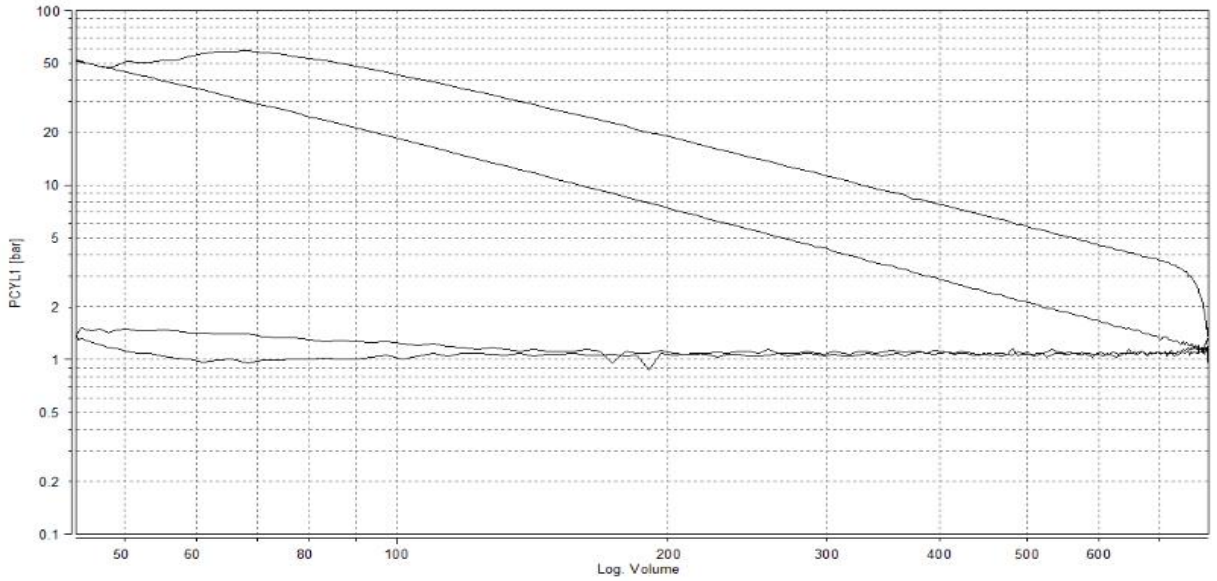


**Figure 5-13** PV diagram of 30%GTL at 1000rpm, 30% throttle.

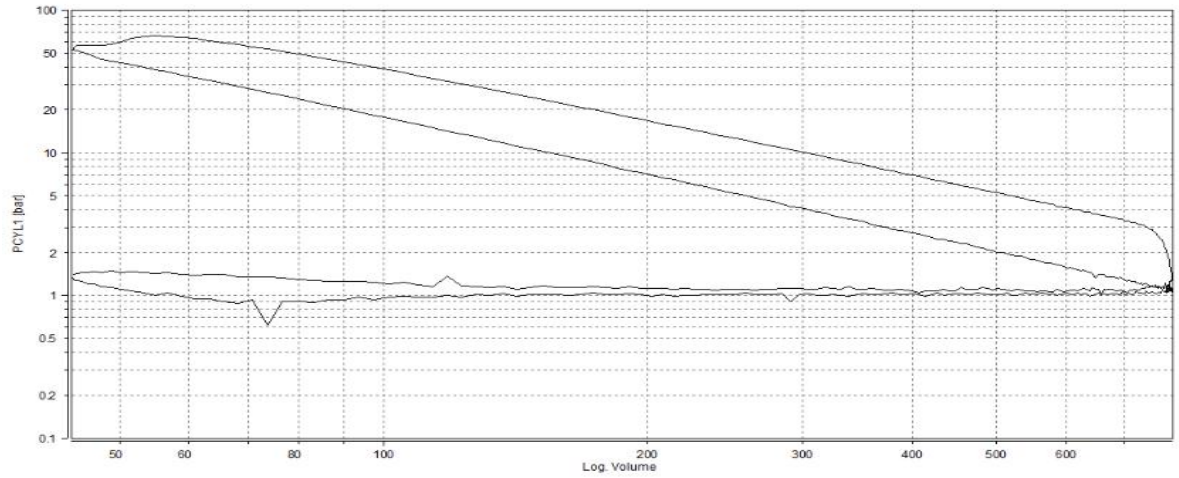


**Figure 5-14** PV diagram of 100%GTL at 1000rpm, 30% throttle.

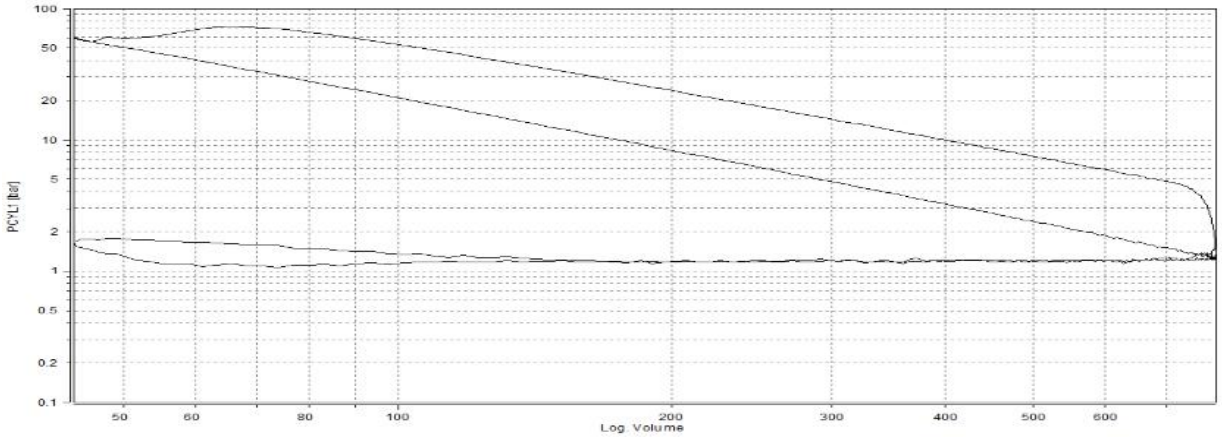


**Figure 5-15** PV diagram of 30%GTL at 1000rpm, 40% throttle.

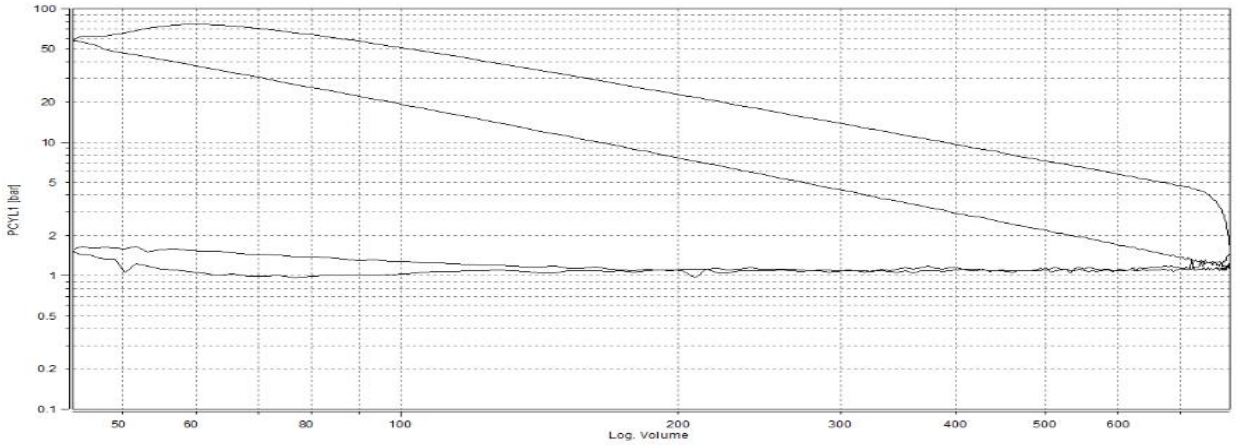


**Figure 5-16** PV diagram of 100%GTL at 1000rpm, 40% throttle.

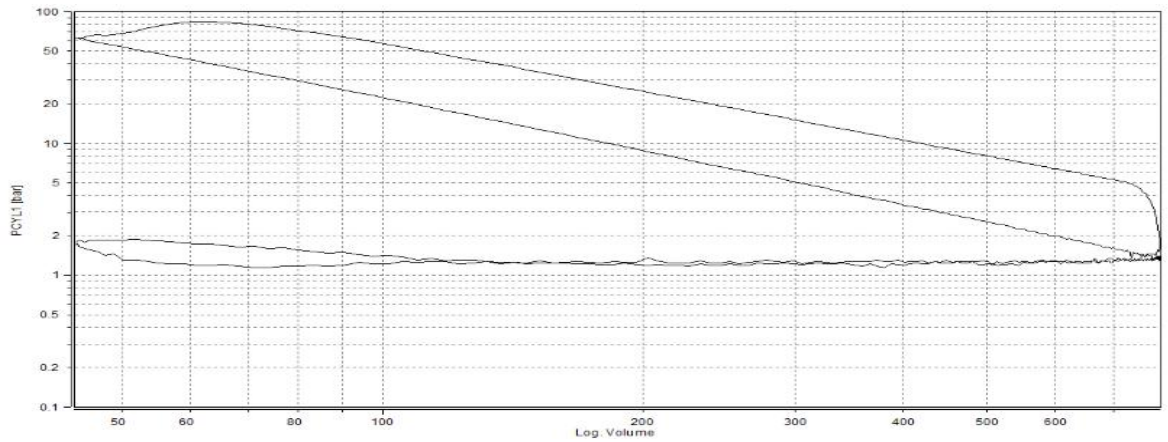


**Figure 5-17** PV diagram of 30%GTL at 1000rpm, 50% throttle.

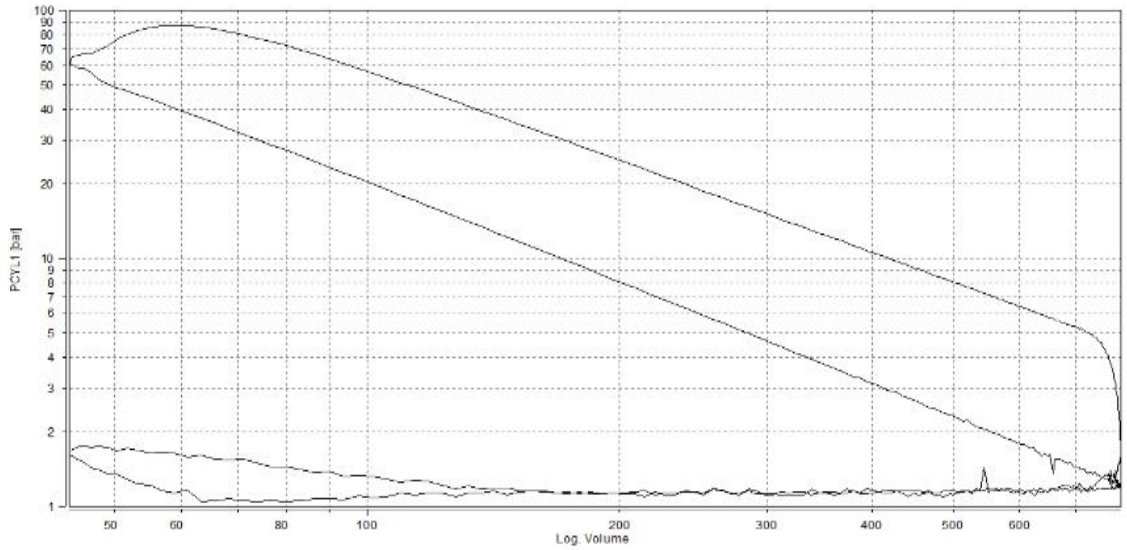


**Figure 5-18** PV diagram of 100%GTL at 1000rpm, 50% throttle.

From the comparison between 30% GTL blended fuel and pure GTL fuel, it can be found that the pure GTL combusts faster than 30% GTL fuel. In all three throttle settings, the combustion cylinder pressure for pure GTL dropped in the power stroke immediately after the cylinder volume expanded over to 60 $cm^3$, however, the 30% GTL preformed the pressure drop after the cylinder power volume expanded greater than 70 $cm^3$. And from figure 5-13 to figure 5-18, it can be seen the start of combustion for both fuel types occurred very close, around 50 $cm^3$ from the PV diagrams. Thus, it can be seen as the pure GTL combusted faster than 30% GTL. This is due to the pure GTL contains nearly all straight carbon chain and branched alkanes, as discussed in the fuel property

section with GCMS test results. Those straight carbon chains are more likely to be broken during combustion, and thus caused the GTL to be burned off faster. This phenomenon is quite obvious in 1000 rpm tests, which are relevantly low engine power working conditions. In 1000 rpm tests, hardly any difference can be found with the turbocharger as there is hardly any difference in initial air inlet pressure sending to combustion cylinder.

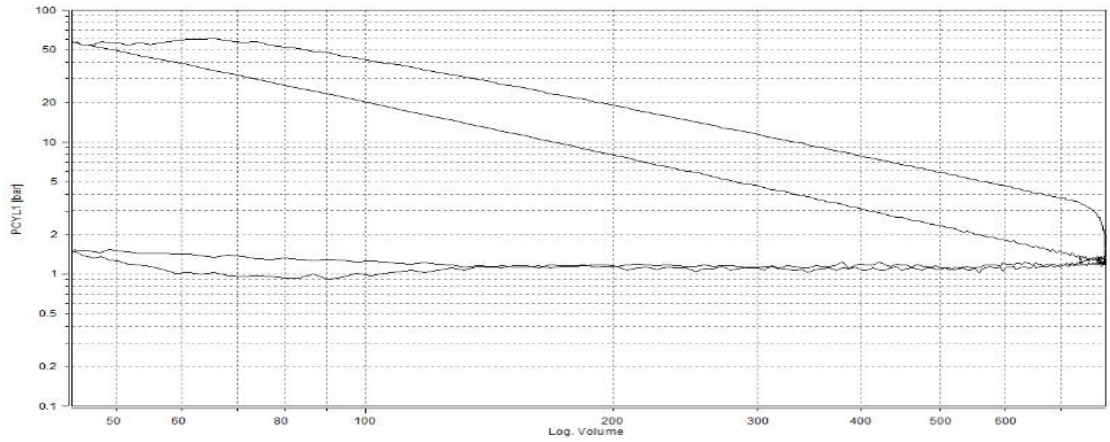


**Figure 5-19** PV diagram of 30%GTL at 1600rpm, 40% throttle.

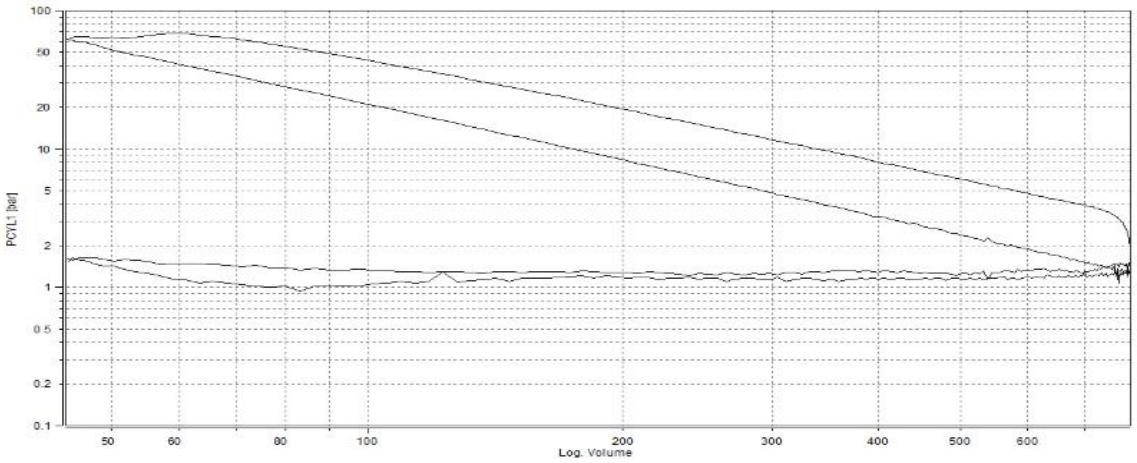


**Figure 5-20** PV diagram of 100%GTL at 1600rpm, 40% throttle.

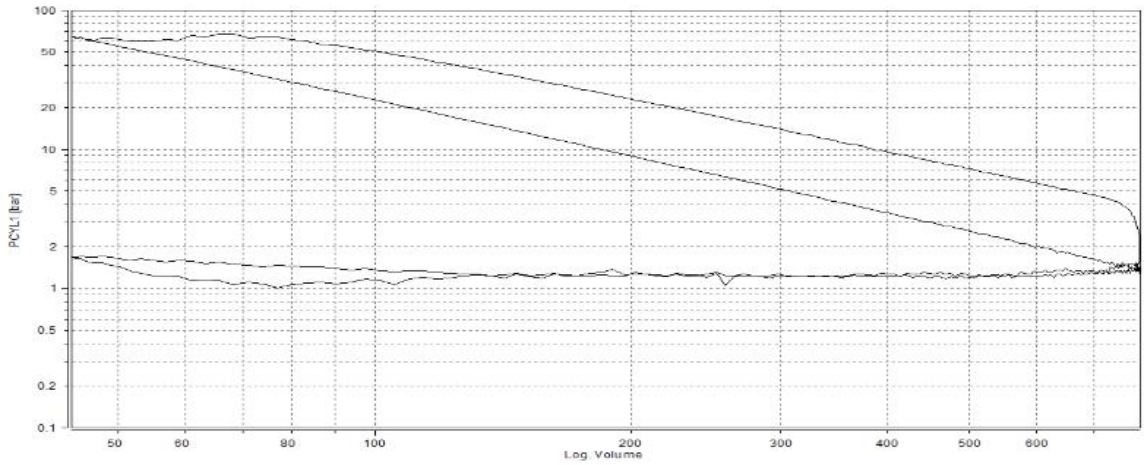


**Figure 5-21** PV diagram of 30%GTL at 1600rpm, 50% throttle.

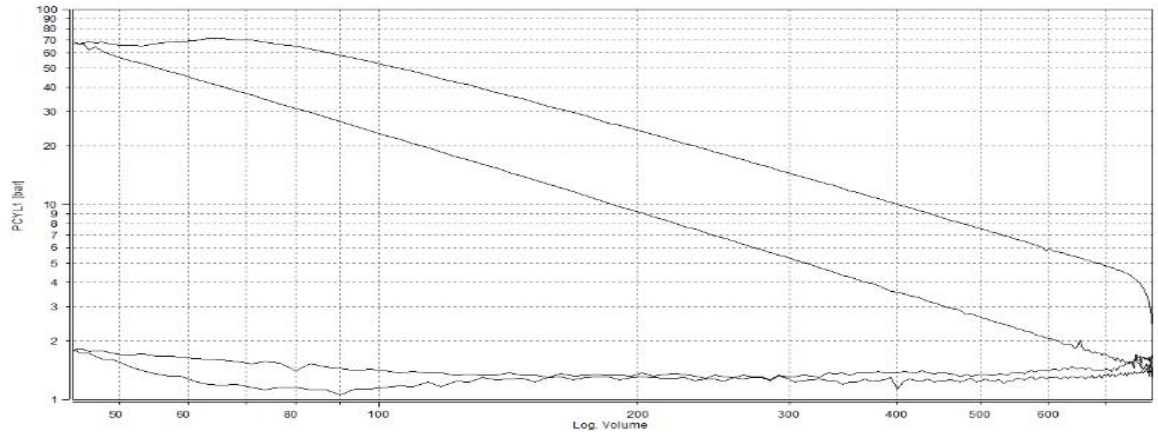


**Figure 5-22** PV diagram of 100%GTL at 1600rpm, 50% throttle.

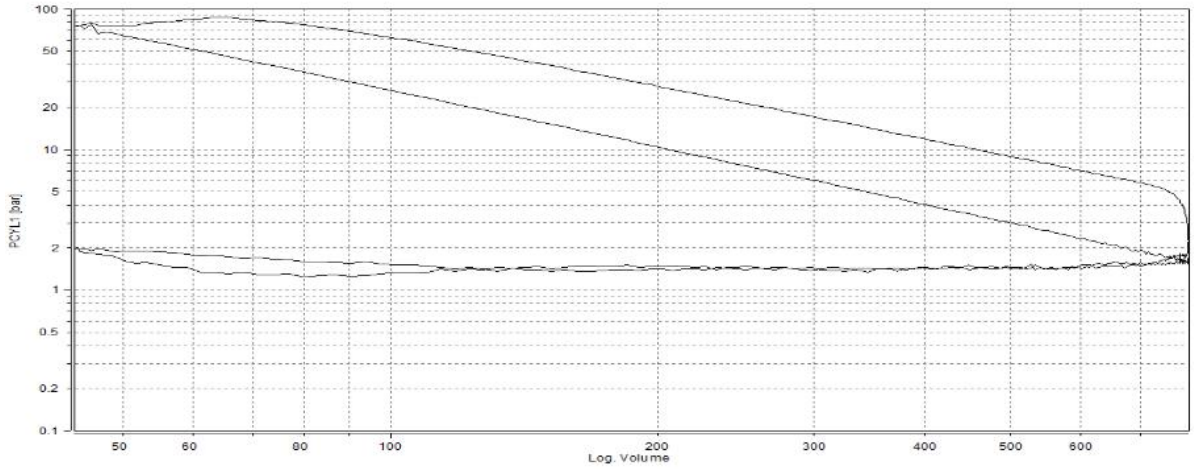


**Figure 5-23** PV diagram of 30%GTL at 1600rpm, 60% throttle.

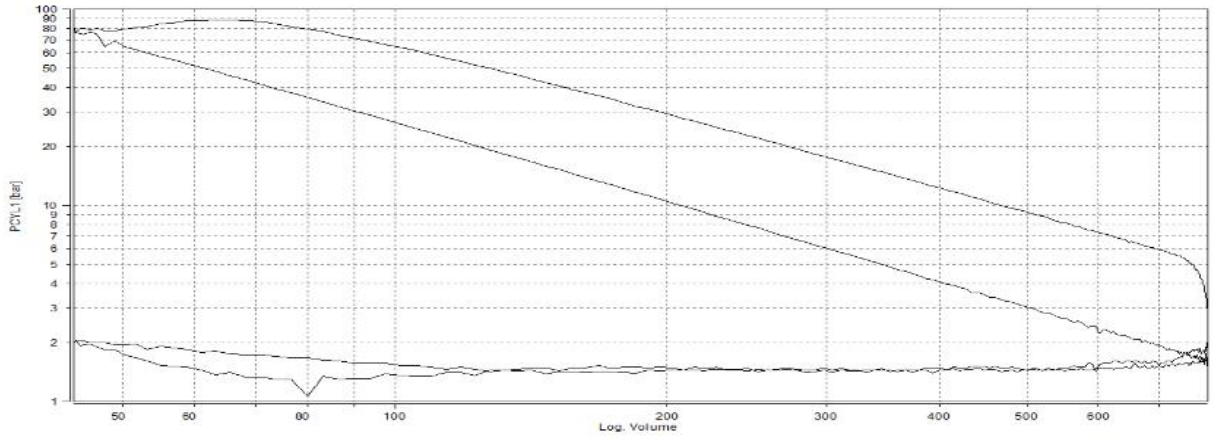


**Figure 5-24** PV diagram of 100%GTL at 1600rpm, 60% throttle.

From the 1600 rpm, 40% throttle engine set up test (figure 5-19 and 5-20), the same findings are acquired compared to the 1000 rpm's analysis. Hardly any impact on the pressure of turbocharged inlet air can be seen. And the 30% GTL fuel experienced an obvious longer combustion duration than pure GTL fuel, and the in-cylinder pressure drop from 30% GTL fuel happened 10 $cm^3$ later than the GTL fuel in the expansion stroke. However, when the throttle percentage increases to 50%, from the comparison in figure 5-21 and figure 5-22, this difference is abated. The 30% GTL fuel showed the pressure drop at approximately 68 $cm^3$, and the pure GTL fuel showed the pressure drop at about 65 $cm^3$. This difference even become neglectable when the throttle percentage increased to 60%. And this result compromise with the previous discussion in pressure to crank angle analysis. The difference in combustion pressure caused by fuel properties in GTL and GTL blended fuel would be abated with engine power set up increased. Because, when the engine rpm and throttle settings reached a certain set up, the advantage of GTL fuel would disappear since the diesel fuel can also be burned off easily at high engine power working conditions. So, it is necessary to find out this power off set, and in order to acquire this the discussion on 1900 rpm is presented.

From the analysis on 1900 rpm test, the difference in the fuel combustion duration can hardly be seen in all three throttle settings (50%, 60%, 70%). The engine power for those three throttle settings are respectively 27 KW, 36 KW and 46 KW. The engine power acquired from 1600 rpm, 40% throttle and 1600rpm, 60% throttle are respectively

27 KW and 36 KW. Since at 1600 rpm, 40% throttle result, the variation in the combustion duration was already small. Thus, this engine power threshold should be 27 KW, indicating the combustion advantage of GTL or GTL blended fuel would disappear when the engine power increased greater than 27 KW.

From the PV diagram in 1900 rpm engine test, it can be seen from figure 5-25 to figure 5-30 that both 30% GTL blended fuel and pure GTL fuel performed identical diesel engine constant pressure combustion. The fuel combustion started at around 50 $cm^3$ in the power stroke and lasted for approximately 30 $cm^3$. This indicates the pressure increased from fuel combustion nearly equals to the pressure reduction caused by the cylinder volume expansion as the piston moving down. It can also be seen from figure 5-29 and figure 5-30 that there were few pressure-drops in the end of compression stroke. This is caused by the multiple fuel injection occurred before the piston reach top dead centre. If compared to the 1900 rpm 70% throttle results (figure 5-29 and 5-30), it can also be observed that 100% GTL fuel showed more obvious fuel injections before TDC. This is due to the diesel fuel obtains higher density, thus the amount of GTL fuel injected is greater than fuel blended with diesel. This tiny difference caused the pressure drop being more obvious, however this will not cause obvious difference in engine power. And as is the same as 1000 rpm and 1600 rpm results, no differences have been found with the pressure of turbocharged air sending to combustion cylinder.

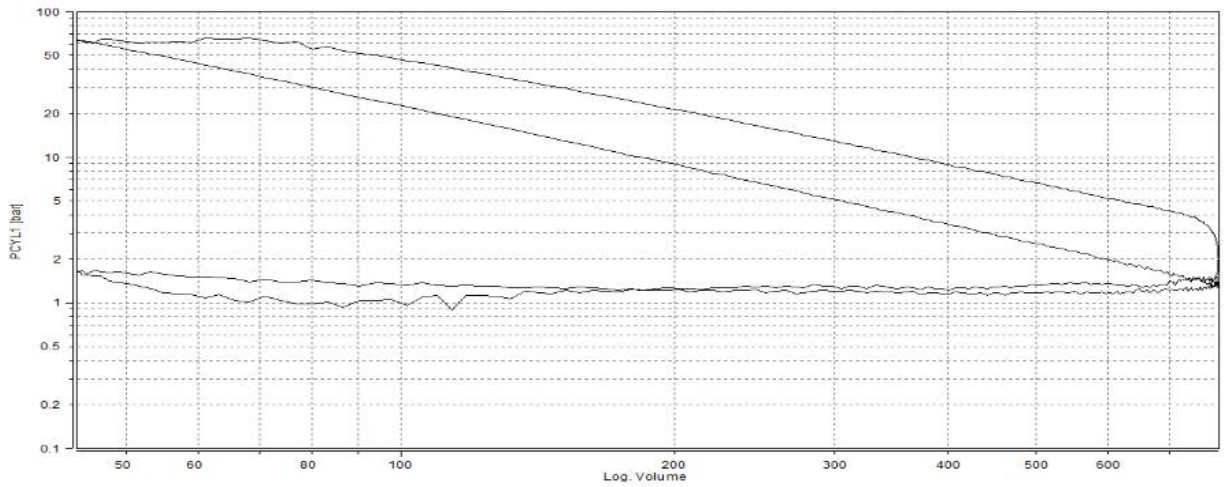


**Figure 5-25** PV diagram of 30%GTL at 1900rpm, 50% throttle.

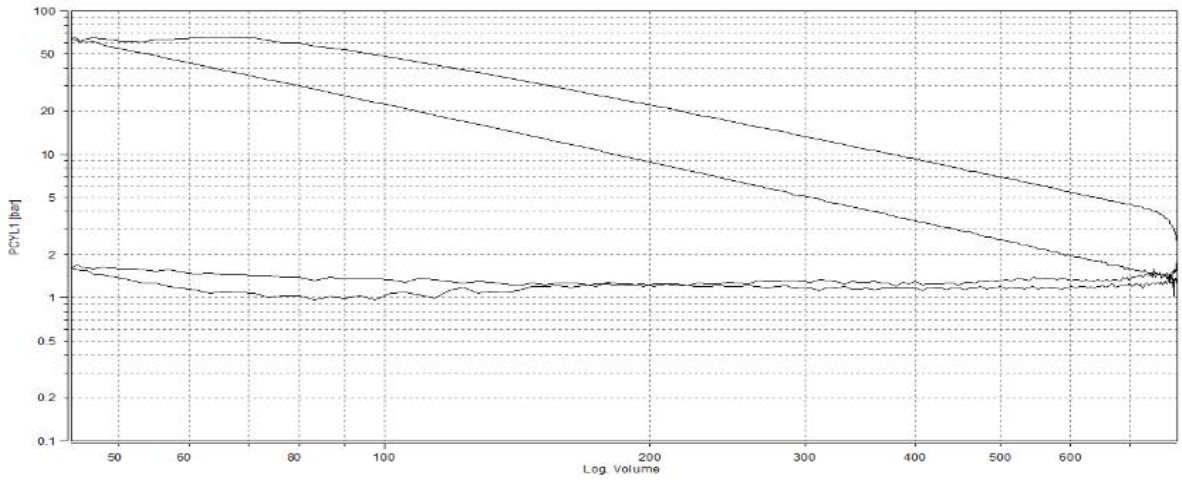


**Figure 5-26** PV diagram of 100%GTL at 1900rpm, 50% throttle.

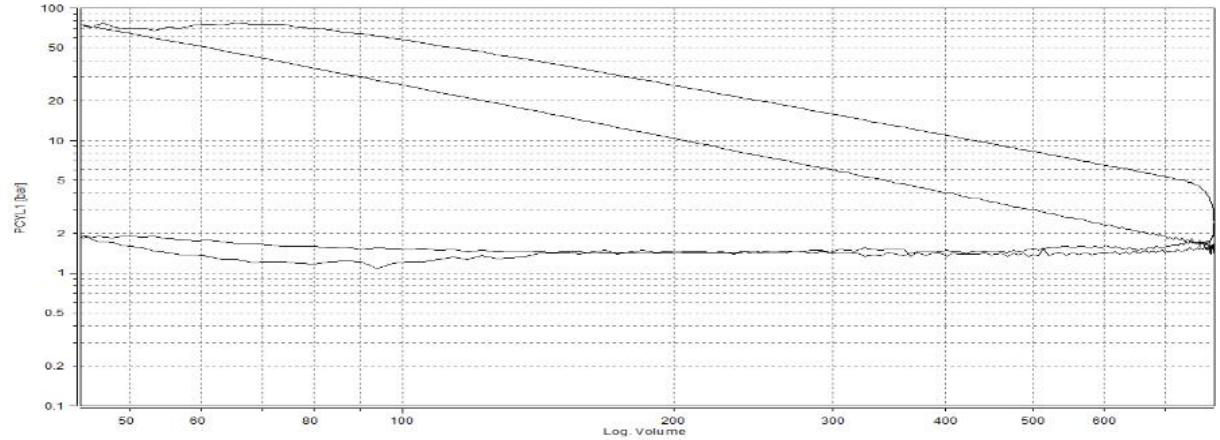


**Figure 5-27** PV diagram of 30%GTL at 1900rpm, 60% throttle.

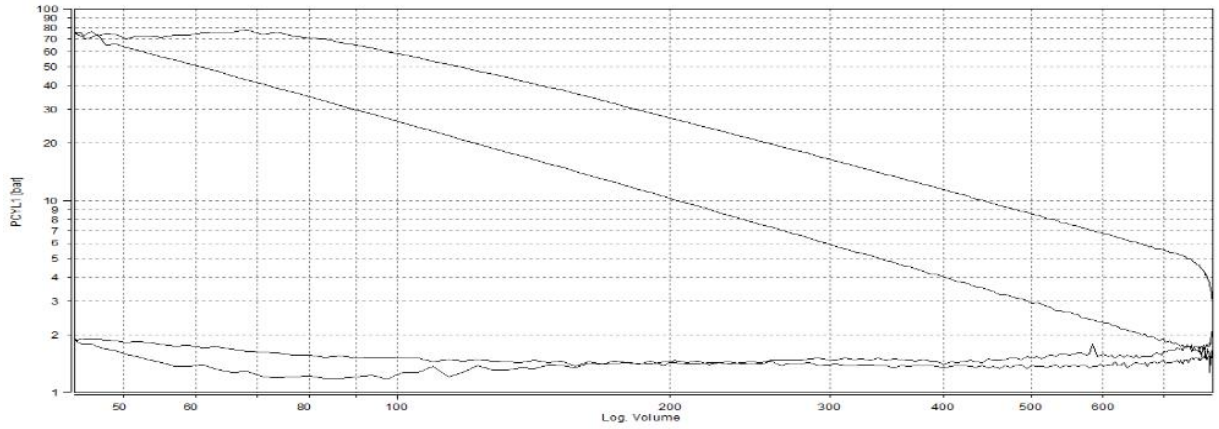


**Figure 5-28** PV diagram of 100%GTL at 1900rpm, 60% throttle.

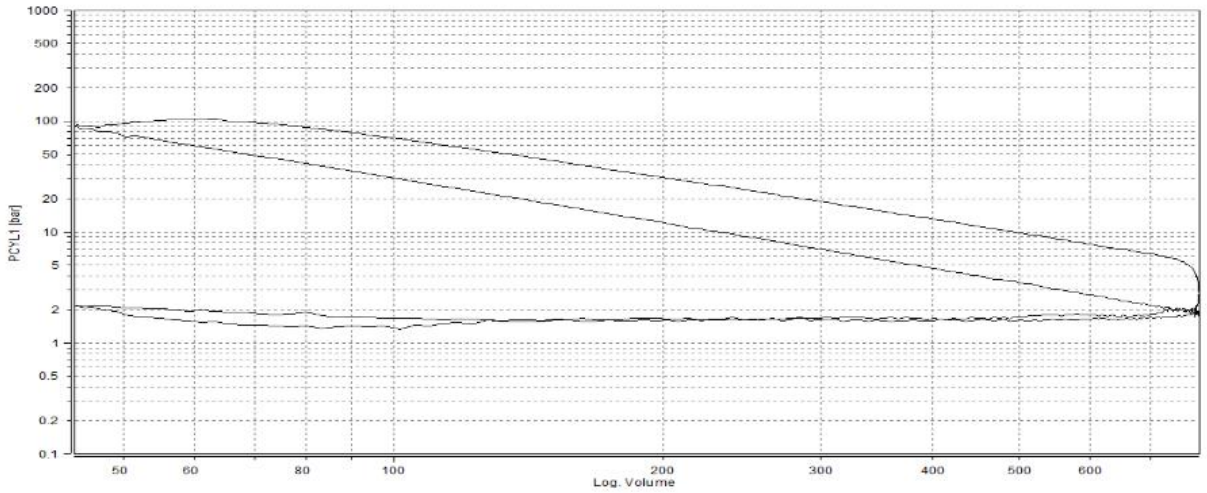


**Figure 5-29** PV diagram of 30%GTL at 1900rpm, 70% throttle.

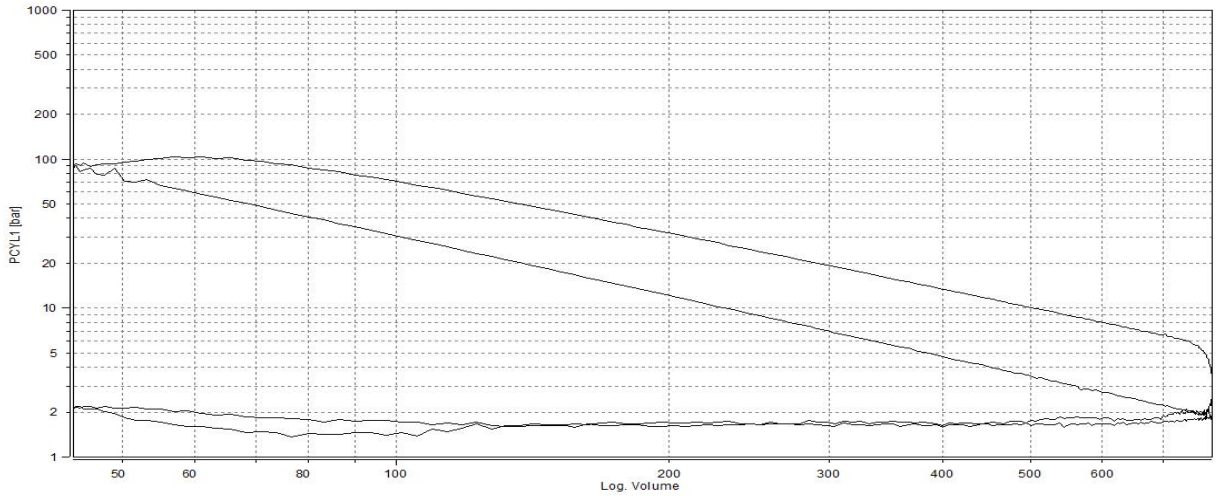


**Figure 5-30** PV diagram of 100%GTL at 1900rpm, 70% throttle.

In summary, from the PV diagram analysis, it can be seen from low engine power test that pure GTL would combust faster than blended fuel due to chemically it obtains more straight chain and branched alkanes. However, with the engine power increased to 27 kw, this difference became small because diesel fuel can also burn quickly in such engine power conditions. Therefore, increasing the blending ratio of GTL fuel will achieve most improved combustion at lower engine power conditions. The fuel blending strategy will not impact performance of turbocharger: the pressure of compressed air sending to combustion cylinder is same. Multiple fuel injections occurred before TDC

can be observed from PV diagram in high engine power working condition because the amount of fuel injected is abundant enough to trigger obvious pressure drop in PV diagram. The multiple fuel injection is more likely to be observed from PV diagram for fuels with lower density (higher blending ratio.eg. pure GTL).

## 5.4 Conclusion

Based on the analysis in fuel property and combustion performances, the following conclusions can be achieved:

- The main difference between GTL fuel and diesel fuel is that the GTL fuel consisted of straight chains, branched alkanes, and no aromatics. The carbon number distribution of GTL fuel was $C_9$ to $C_{20}$ which was similar to diesel. The GTL fuel has more light fractions than diesel, particularly $C_{10}$ and $C_{14}$. Compared to diesel, the GTL fuel has lower density and slightly higher calorific value.
- The average combustion pressure, peak combustion pressure, IMEP, BEMP, and engine power generated from blended fuels, pure GTL fuel, and pure diesel fuel were similar, except occasionally the pure GTL could have slightly higher peak combustion pressure.
- The ignition delays were reduced when the blend ratio was increased at each engine operating condition, because the pure GTL fuel had higher cetane number than diesel.
- The engine demonstrated multiple fuel injection strategy to achieve consistent pressure combustion, and this was observed from all the fuels' tests.
- GTL fuel and its blends had shorter combustion duration than diesel. However, this advantage became insignificant when the engine power reached 27 KW. This is because at the higher engine power and thus higher temperature and pressure, the diesel fuel could also be easily burned off despite its combustibility is not as good as GTL fuel.

# Chapter 6. Emission analysis of GTL fuel and its blends

## 6.1 $NO_X$, NO and $NO_2$ emissions

$NO_X$ emissions from diesel engine are always a critical topic in diesel engine research. Therefore, it's important to have detailed analysis in $NO_X$ emissions. In this research, $NO_X$ emissions were measured as total $NO_X$ and NO in ppm in experiments. $NO_2$ emissions were calculated from their differences. $NO_x$ emissions were also sampled both at upstream and downstream of the aftertreatment system, thus allowing the analysis of aftertreatment impact on $NO_X$ emission to be conducted. All measured raw data was converted to an emission index (g/kgfuel) and specific emissions (g/kWh).

The formation of $NO_X$ in diesel engines as explained in the literature review chapter is mainly due to nitrogen and oxygen being exposed to high temperature and called as thermal $NO_x$. Thus, it's an inevitable product from diesel engine. The lean combustion characteristics indicates there is an abundant amount of air containing nitrogen entering the engine combustion and also temperature is high as a result of compressed ignition. Therefore, $NO_X$ production from the diesel engine is decided by the combustion temperature and the amount of air joined in the combustion. From the combustion pressure analysis presented in the previous section, the average combustion pressure and peak combustion pressure behaved similarly, indicating the overall combustion temperatures for all tested fuels at each specific engine working condition are similar. All tested fuels showed nearly the same air to fuel ratios, indicating the amount of nitrogen and oxygen joined in the combustion is similar as well. In addition, the CHNS elemental analysis also showed similar nitrogen weight percentages for diesel and pure GTL: from table 5-1 it can be seen there is 0.59% nitrogen in diesel and 0.60% in GTL. In other words, there is hardly any difference in fuel bond nitrogen $NO_x$ production between GTL fuel, diesel fuel and GTL blended fuel. Thus, the differences in $NO_x$ production cannot be explained as blended fuels or pure GTL fuel would either change the combustion temperature or change the amount of nitrogen, oxygen joined in the $NO_x$ production. Instead, the various behaviours of $NO_X$ emissions should be contributed by something in microscope which pure GTL and blended fuel impacted.

This analysis will be presented after the summarizing of findings from all tested results later in this section.

Figure 6-1 and figure 6-2 presented the $NO_X$ specific emissions and emission index results of 5 test fuels at 1000rpm, 30% throttle condition. In general, at the engine out (upstream of the aftertreatment system), 82% to 99% of $NO_x$ is consisted of NO. The GTL and GTL blended fuel showed lower NO, $NO_2$ and total $NO_x$ emissions when compared to diesel fuel. At the downstream of aftertreatment system, the proportion of NO in total $NO_x$ reduces to 20% to 28%. The blended GTL fuel and pure GTL performed lower $NO_x$ emissions than diesel as well. The main difference in $NO_x$ emission between upstream and downstream is the NO or $NO_2$ proportion. The downstream contains less NO and more $NO_2$ because oxidation reaction occurred when exhaust gas passed through the DOC.  Around 70% of NO was oxidized to $NO_2$ at this engine working condition.

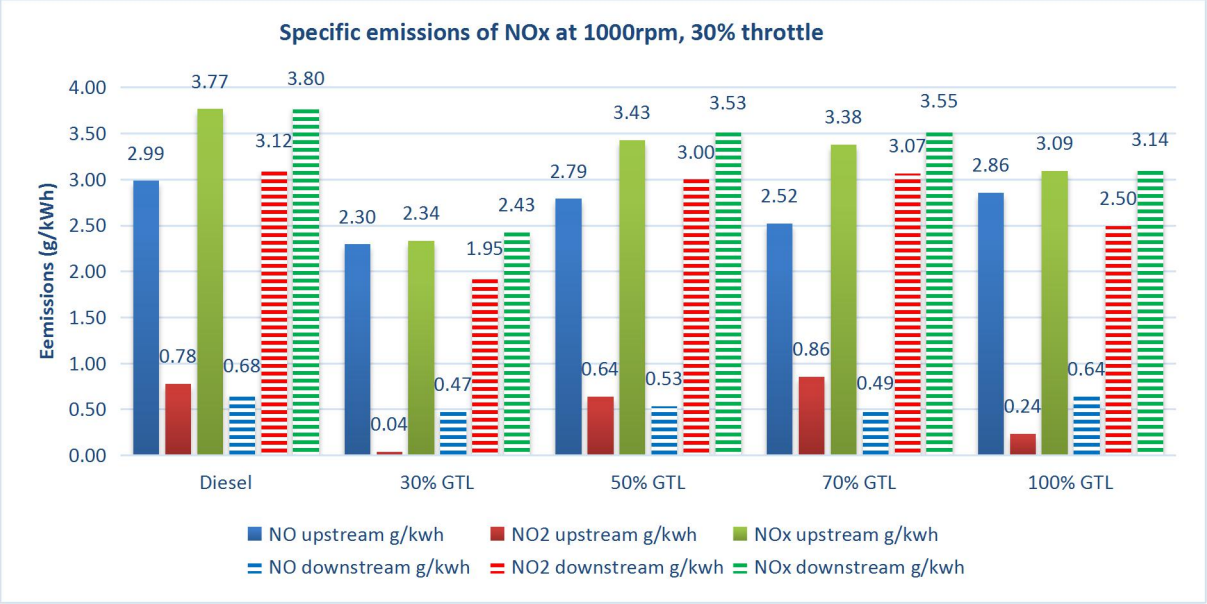


**Figure 6-1** NOx specific emissions at 1000rpm, 30% throttle.

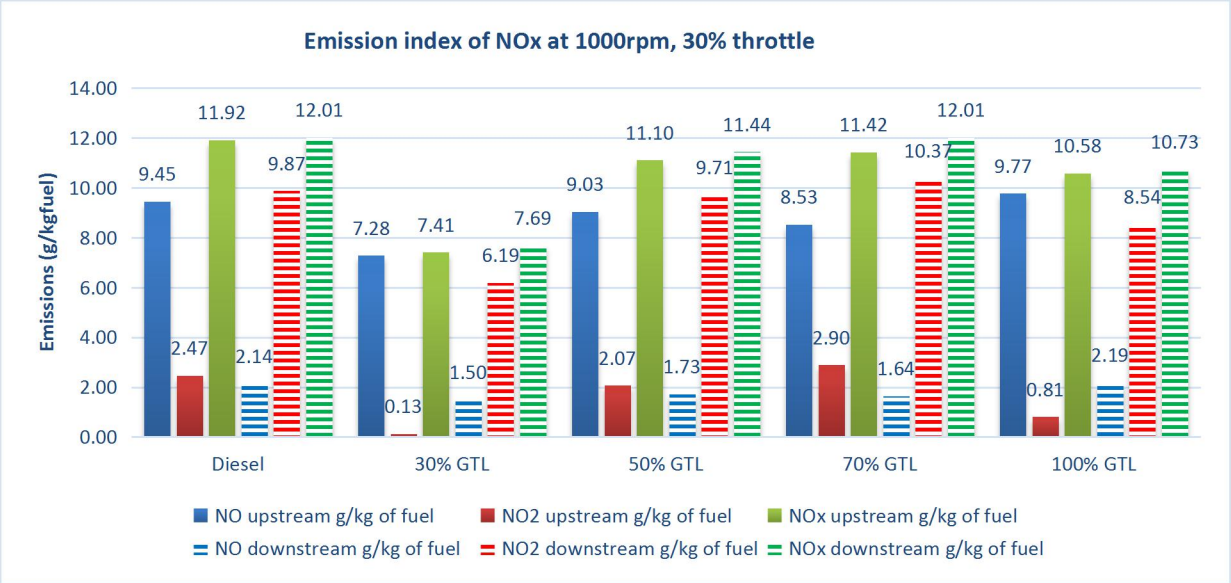


**Figure 6-2** NOx emission index at 1000rpm, 30% throttle.

In detail, it can be found that at 1000 rpm, 30% throttle engine working condition, the 30% GTL fuel produced lowest $NO_x$ emissions, and it reduced the specific $NO_x$ emission by up to 36% at downstream of aftertreatment system. The main reason is 30% GTL fuel produced hardly any $NO_2$ from combustion. The $NO_x$ emission from downstream is in difference between 0.8% to 5.1% from upstream, and this can be caused by variation in engine emission testing repeatability.

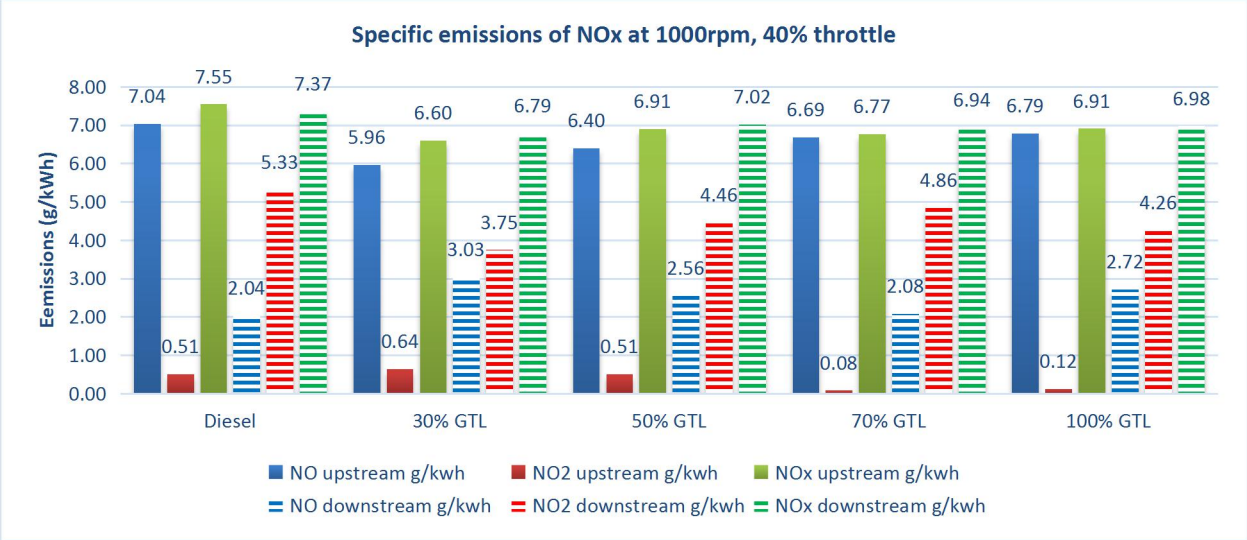


**Figure 6-3** NOx specific emissions at 1000rpm, 40% throttle.

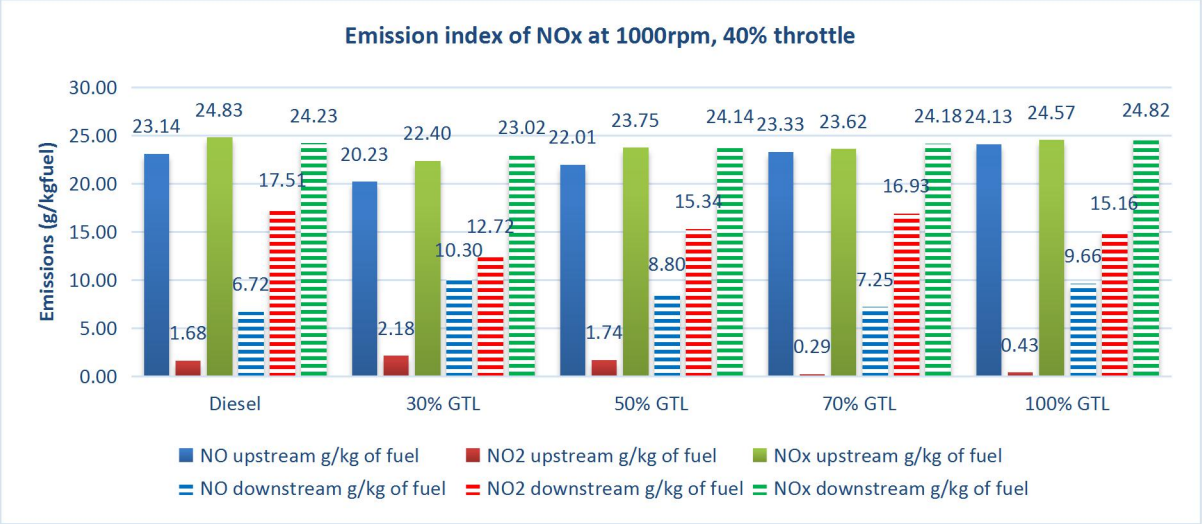


**Figure 6-4** NOx emission index at 1000rpm, 40% throttle

When the throttle percentage increased to 40%, similar findings were acquired from figure 6-3 and figure 6-4. The GTL and blended fuel could improve the specific $NO_X$ emission by 5% to 8% at the catalyst out emissions. The most effective reduction was observed from 30% blended GTL fuel, and the least effective one was from pure GTL fuel. The emissions from downstream can be 1.0% to 2.8% different from upstream. The NO to $NO_x$ rates at 1000rpm, 40% is ranging from 93% to 99% at exhaust upstream and from 37% to 55% at exhaust downstream, and the aftertreatment could oxidize up to 58% NO to $NO_2$. This is lower than from 30% throttle's 70% oxidation rate.

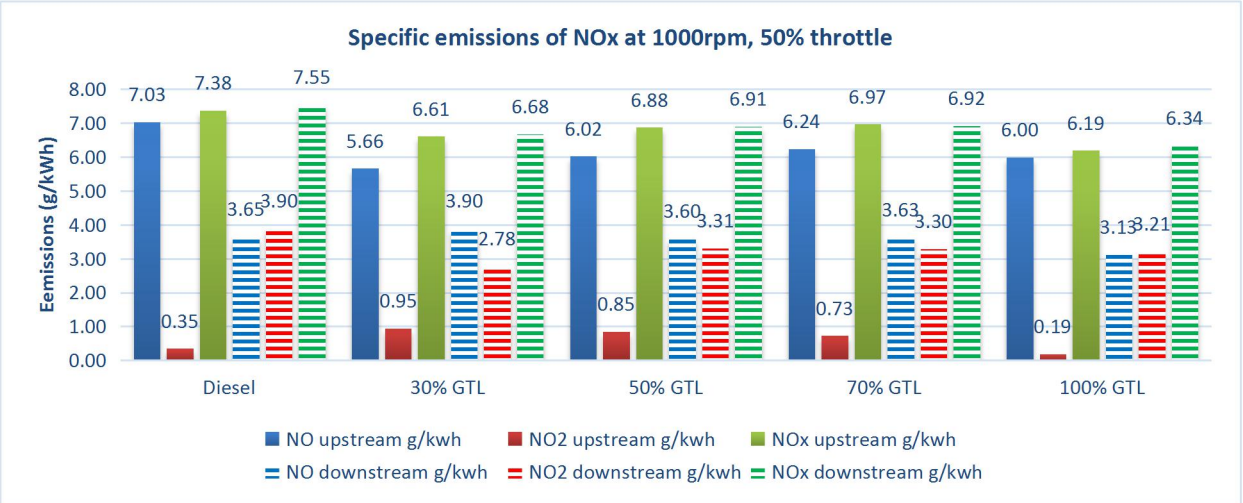


**Figure 6-5** NOx specific emissions at 1000rpm, 50% throttle.

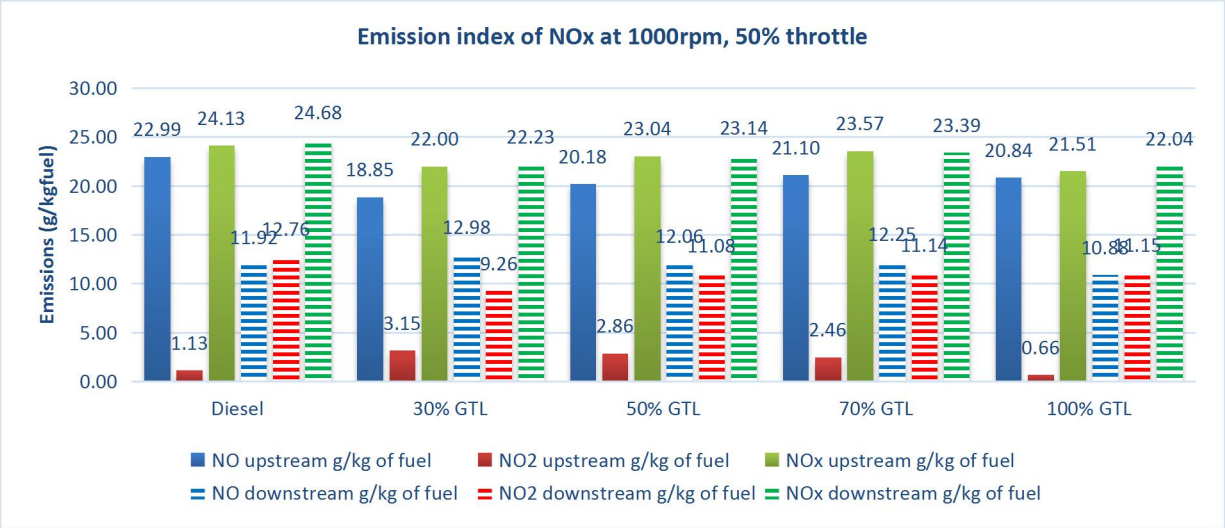


**Figure 6-6** NOx emission index at 1000rpm, 50% throttle.

When the throttle setting was further increased to 50% at 1000 rpm (figure 6-5 and figure 6-6), the 30% GTL blended fuel still performed most effective $NO_x$ improvement with a reduction of 12% in specific emissions compared to diesel performance. The least effective performance was observed from 70% GTL, with 8%. The NO oxidization rate at this working condition is 40%, and the $NO_X$ measured from exhaust downstream can be 0.7% to 2.5% different from exhaust upstream.

In summary of the 1000 rpm test result, it can be concluded that the pure GTL and GTL blended fuels can all improve the total $NO_x$ emissions from 5% to 31% depending on the blending ratio. The 30% GTL blended fuel behaved most effectively in $NO_X$ reductions, while 70% GTL blended fuel behaved the poorest. The NO oxidation rate reduced from 70%, 58% and 40% as throttle settings increased from 30% to 40%, and 50% respectively. This phenomenon can be attributed to two reasons. The DOC was designed to remove CO and THC, thus the capacity for NO oxidation can be limited. As the engine total NO emissions go up at higher engine power, the conversion of NO in terms of ratio will be reduced, i.e. still same amount of NO can be converted to $NO_2$, resulting in the NO oxidation rate being reduced. The $NO_x$ measured at exhaust downstream can be around 2.1% different than at exhaust upstream, and since there should not be extra thermal $NO_x$ generated while the exhaust passed through the

exhaust aftertreatment system, therefore, this difference is believed to be caused by the variation in engine testing repeatability.

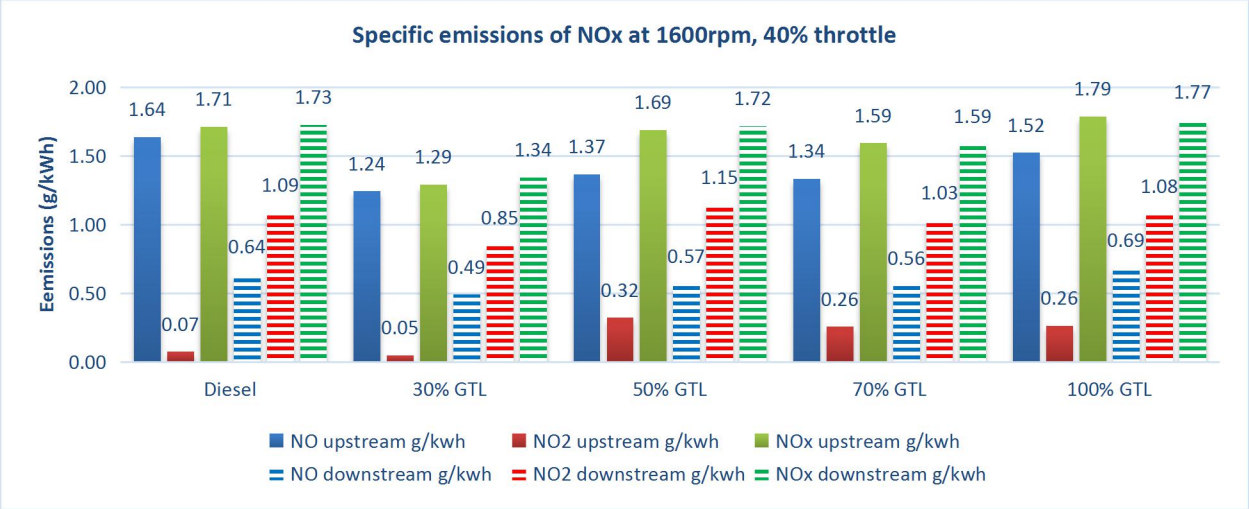


**Figure 6-7** NOx specific emissions at 1600rpm, 40% throttle.

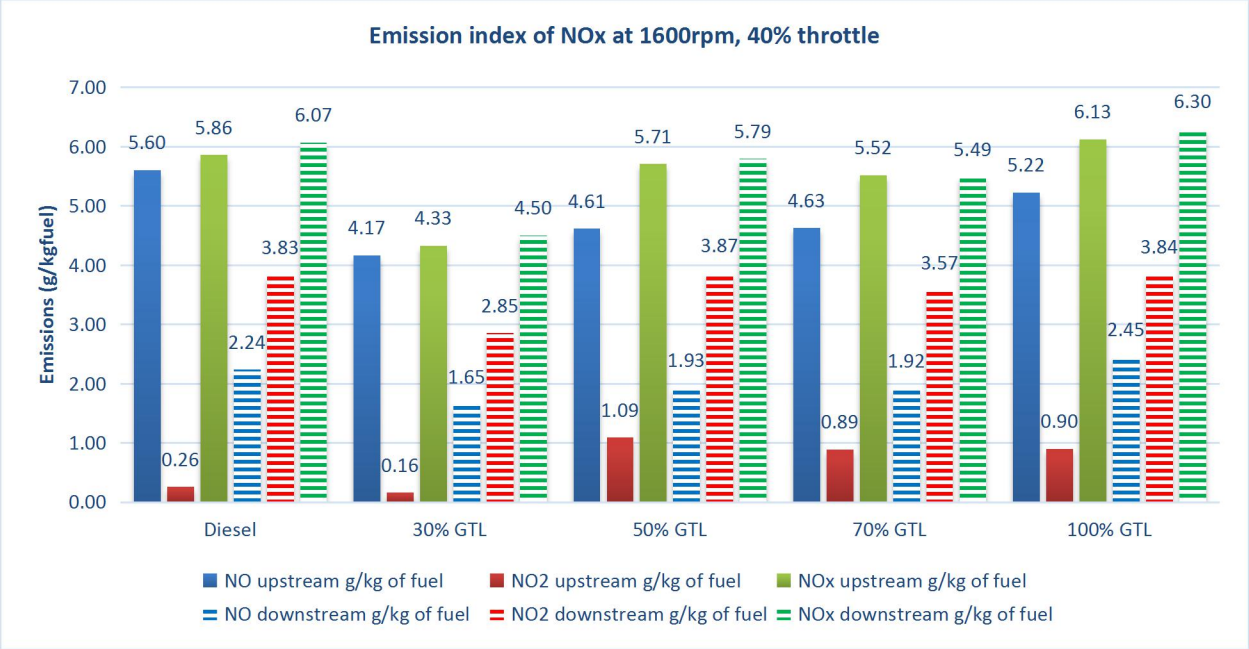


**Figure 6-8** NOx emission index at 1600rpm, 40% throttle.

$NO_x$ emissions performances at 1600 rpm tests are presented in figure 6-7 to figure 6-12. It can be found from figure 6-7 and figure 6-8, that at 40% throttle condition, all blended GTL fuels showed reductions in downstream $NO_x$. The 30% GTL blended fuel

improved the emission most effectively with a reduction of 25% in g/kWh and behaved as the lowest $NO_X$ at engine out emissions. The 50% GTL and 70% GTL shared similar reductions with respectively 11% and 7%. The emission index and specific emissions of total $NO_X$ at this operating condition from pure GTL fuel behaved 5% slightly higher than diesel fuel. This is due to the raw $NO_x$ emission measured in ppm of pure GTL fuel was indeed slightly higher than diesel, and from the pressure to crank angle analysis on this status (in figure 5-7). The pure GTL obtained higher combustion pressure while the duration for the combustion period was similar to diesel, so it is believed that the more thermal $NO_x$ was formed at this status from pure GTL than diesel. The emission measured at this condition from exhaust downstream was 0.5% to 4.0% different from upstream. The oxidation rate of NO to $NO_2$ is from 43% to 50%.

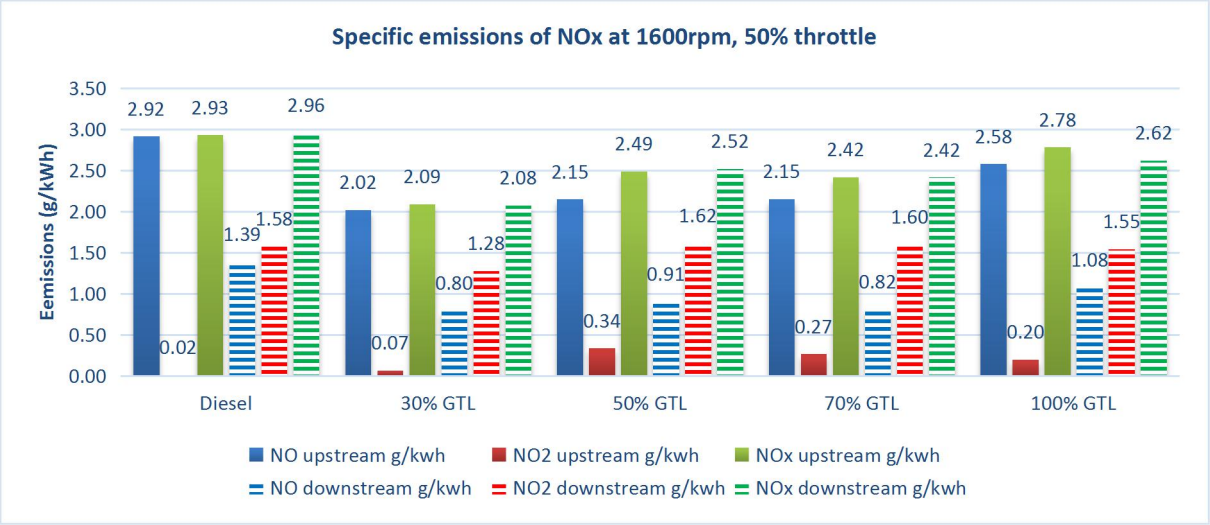


**Figure 6-9** NOx specific emissions at 1600rpm, 50% throttle.

When the throttle increased to 50%, it can be clearly addressed from figure 6-9 and figure 6-10 that 30% GTL fuel was still the most effective fuel for $NO_X$ control. It improved the emissions by 29% at exhaust upstream and by 30% at exhaust downstream. 50%, 70% and 100% GTL fuel also showed $NO_X$ improvement compared to diesel fuel. The pure GTL's $NO_X$ emission index was higher than all blended fuel, however the specific emissions of $NO_X$ was still lower. This was due to the pure GTL fuel obtained lower density, thus less fuel in weight was required by GTL fuel than diesel fuel to acquire the same engine power. Therefore, even the emission index for

GTL was higher, still the specific emissions can be lower as less fuel was required. The difference in total $NO_X$ between upstream and downstream is less than 5%, and the NO oxidation rate ranges around 44% at this engine operating conditions.

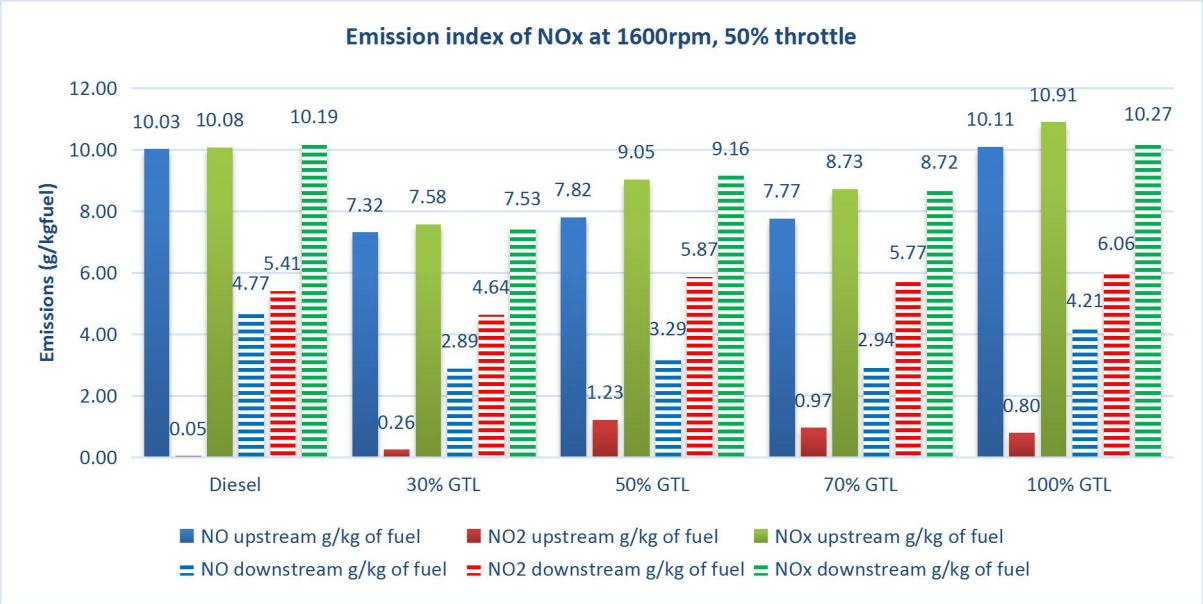


**Figure 6-10** NOx emission index at 1600rpm, 50% throttle.

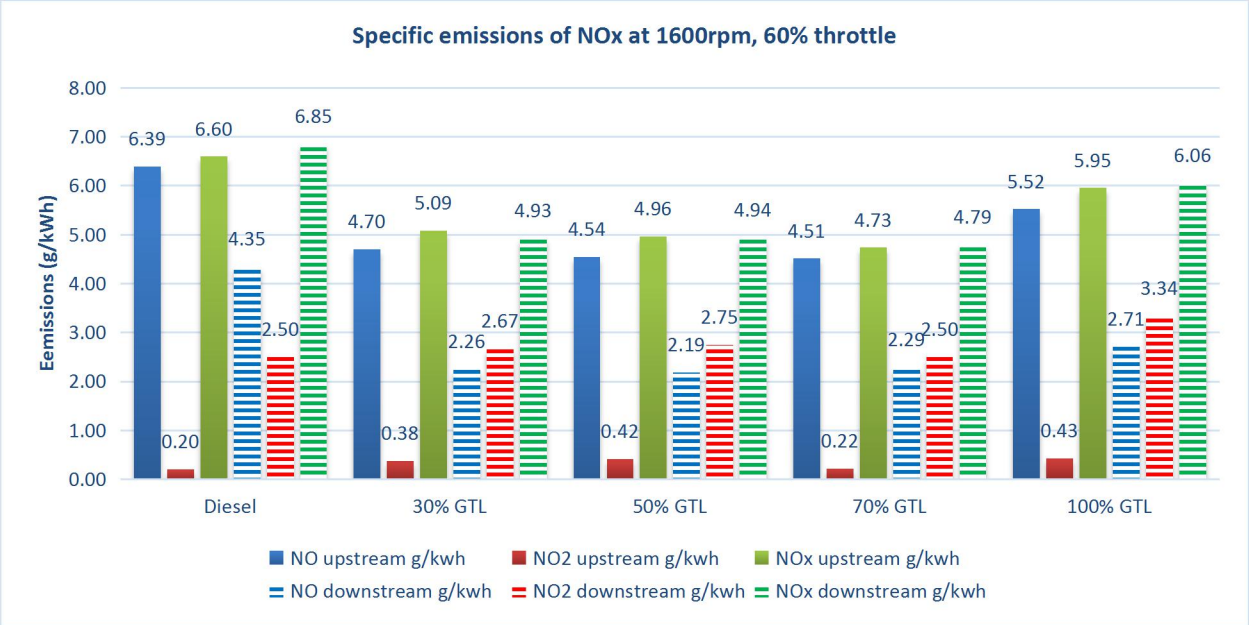


**Figure 6-11** NOx specific emissions at 1600rpm, 60% throttle.

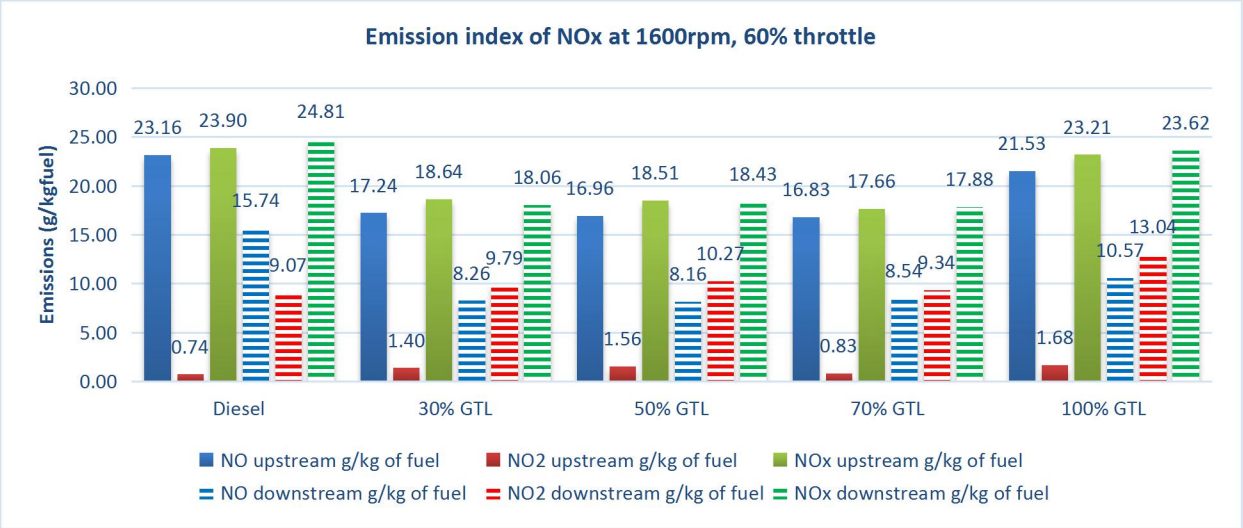


**Figure 6-12** NOx emission index at 1600rpm, 60% throttle.

With the throttle setting increased to 60% (figure 6-11 and figure 6-12), the most effective $NO_X$ emission reduction increases from 30% to 70%, with 28% $NO_X$ reduction being acquired. However, the $NO_X$ emission measured from both at the exhaust upstream and downstream were quite close between the results of 30%, 50% and 70% of GTL blended fuels. The 100% pure GTL was also capable of bringing lower $NO_X$ than diesel, however, it was not as effective as blended fuels, only 12% of reduction was achieved. The NO oxidation rate slightly reduced at this operating condition, and ranged from 25% to 40%, and the total $NO_X$ emission difference between exhaust upstream and downstream was within 3.8%.

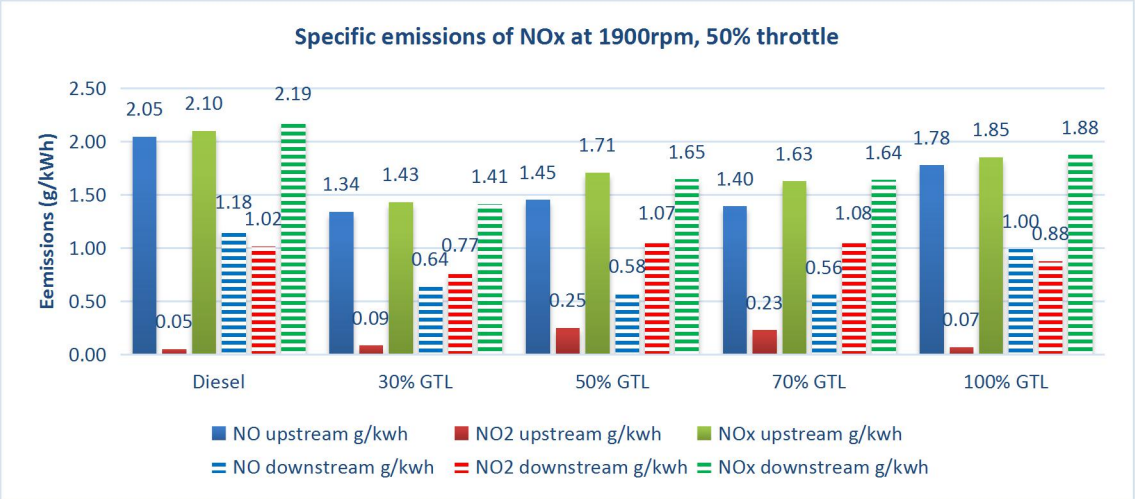

**Figure 6-13** NOx specific emissions at 1900rpm, 50% throttle.

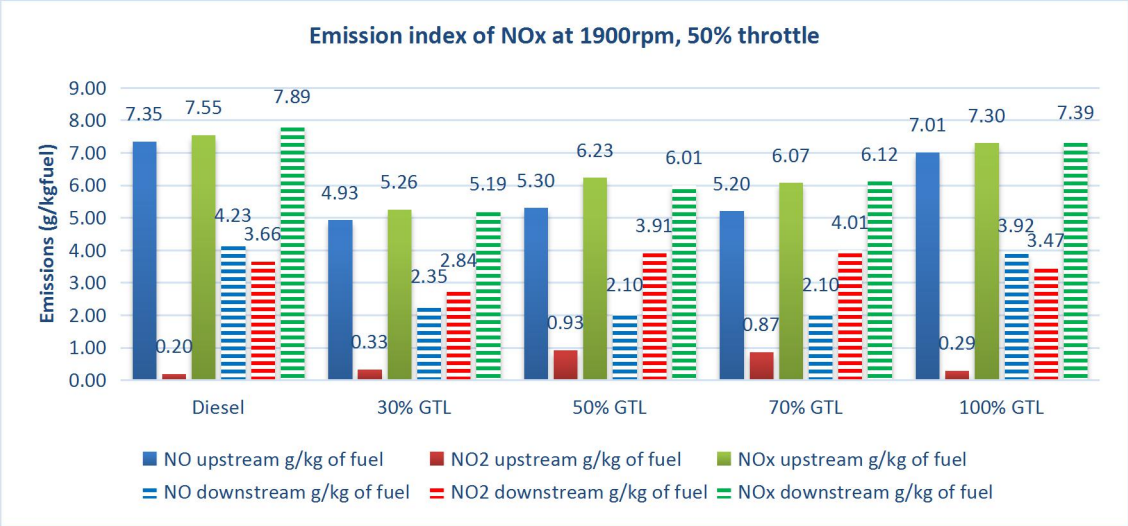


**Figure 6-14** NOx emission index at 1900rpm, 50% throttle.

The findings from 1900 rpm tests were compared with the findings at 1600 rpm. The most effective reduction of $NO_X$ was found from GTL blended fuel, and all three blended fuels showed very close $NO_X$ emissions at both exhaust upstream and downstream. Pure GTL fuel is also capable of reducing $NO_X$ emission, however, its performances were not as significant as its blended fuel with diesel. At 50% throttle setting, 30% GTL fuel improved the $NO_X$ emission by 36%, while 50%, 70% and 100% GTL fuel achieved reduction respectively 25%, 25%, and 14%. At 60% throttle setting, GTL blended fuel improved the $NO_X$ emission by 30% to 33% while the pure GTL fuel only improved by 12%. At 70% throttle setting, the 30% GTL reduced the $NO_X$ production by 40%, while 50% and 70% improved the emission by 40% and 41%. The pure GTL only improved the $NO_X$ emission by 17% at 1900 rpm, 70% throttle engine working condition. The NO oxidation rates at 1900 rpm also moderately reduced as the throttle setting was increased. At 50% throttle, 35% to 44% NO would be oxidised to $NO_2$, while 60% and 70% showed NO oxidation rate ranges respectively from 31% to 40% and 28% to 38%. However, no relationship between blending ratio and NO oxidation rate has been found. The total $NO_X$ emission difference between exhaust upstream and downstream is within 5.0% in 1900 rpm's tests.

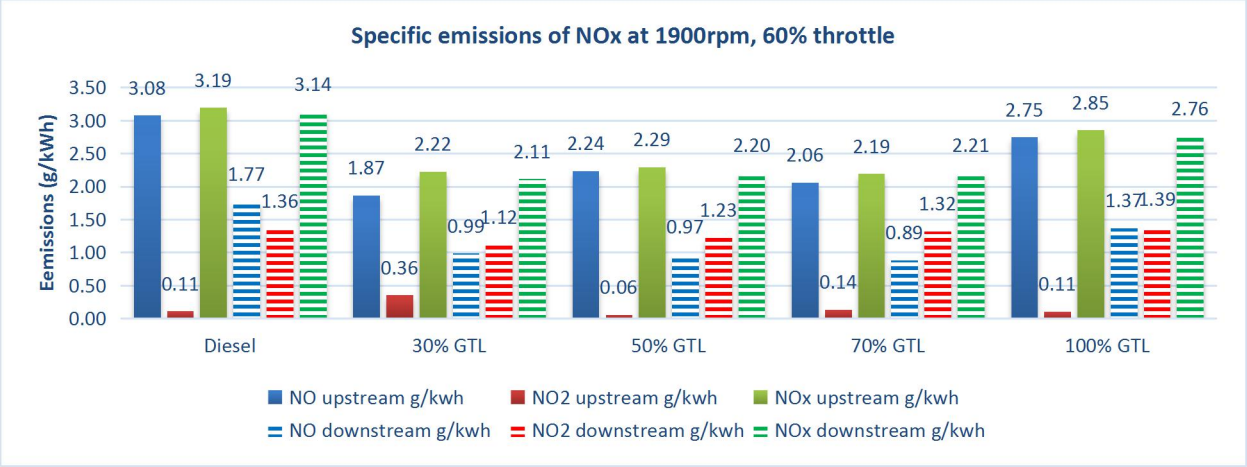


**Figure 6-15** NOx specific emissions at 1900rpm, 60% throttle.

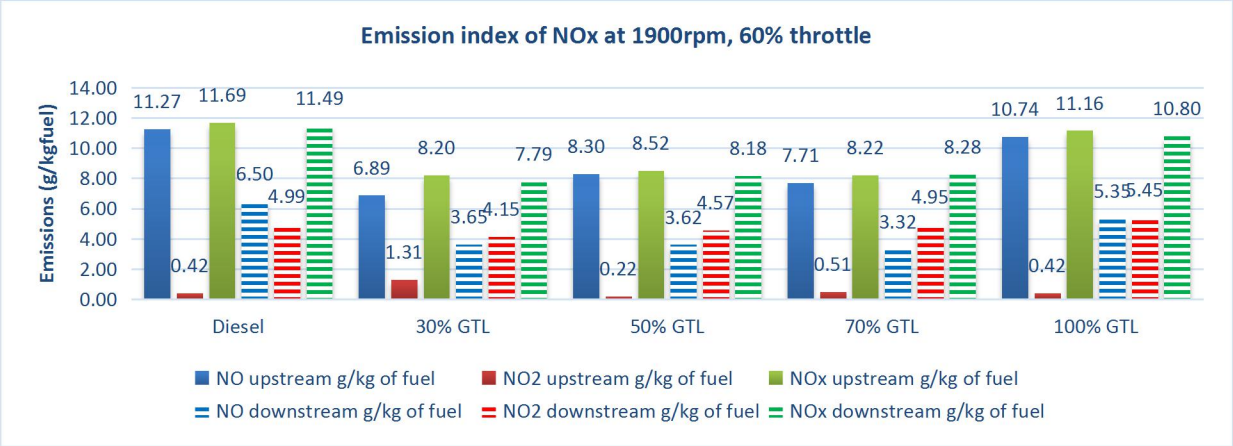


**Figure 6-16** NOx emission index at 1900rpm, 60% throttle.

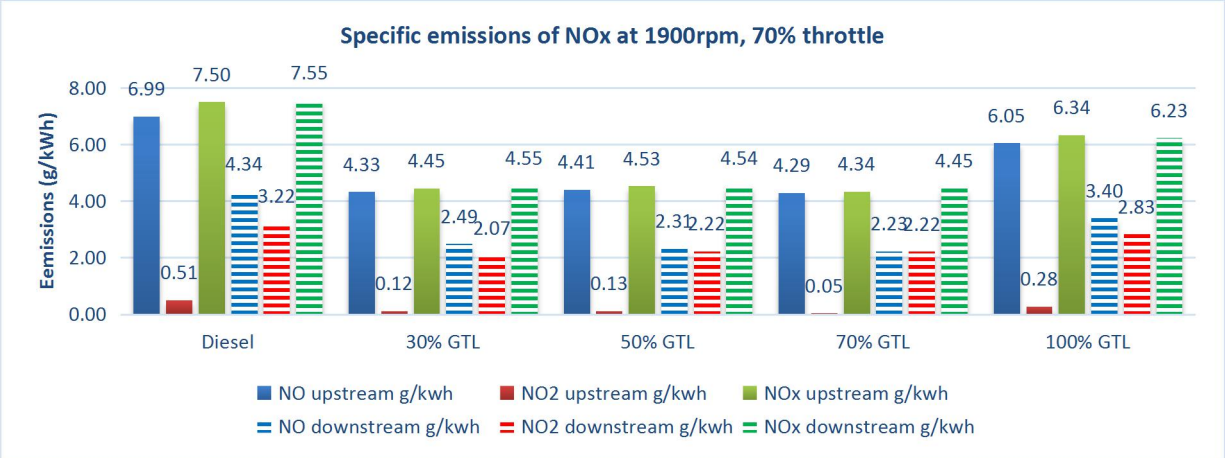


**Figure 6-17** NOx specific emissions at 1900rpm, 70% throttle.

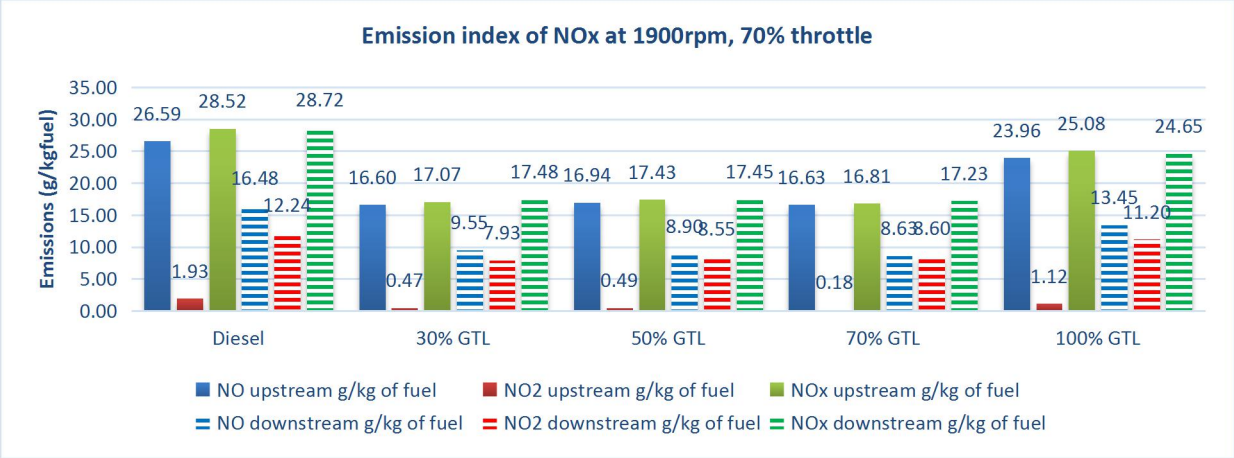


**Figure 6-18** NOx emission index at 1900rpm, 70% throttle.

Therefore, the findings from $NO_X$ emission behaviour against fuel blending can be summarised as:

- 100% pure GTL fuel can reduce $NO_X$ emission in most of the tested engine working conditions but could be 2.3% higher than diesel in only one test condition (1600rpm, 40% throttle).
- With 30% GTL fuel blended into diesel, the $NO_x$ emission can be reduced from 8% to 40% based on engine operating condition and maintained at approximate 25% to 35% at the majority of tested conditions (6 of total 9).
- 30%, 50%, and 70% GTL blended fuel is very effective in $NO_X$ emission control. However, the reduction of $NO_X$ emission didn't show any regular relationship either with blending ratio increasing or decreasing.
- The $NO_X$ reduction by percentages from 30%, 50% and 70% GTL blended fuels are close, and almost equal when the engine power reached 36 kw and beyond.
- The NO generated directly from fuel combustion would be oxidised to $NO_2$ when the exhaust gas passed through the DOC, and the oxidation ratio decreases with the throttle percentage increasing at each specific engine rpm.
- The differences in total NOx emissions between exhaust upstream and downstream ranges from 2% to 3%, and occasionally can reach 5%. This is believed to be caused by the differences in engine test repeatability.

As discussed at the beginning of this section, the pure GTL fuel and GTL blended fuels did not bring down the combustion temperature and did not bring down the air joined in fuel combustion. Thus, the reason contributing to the improvement in $NO_X$ emissions from GTL blended fuels should be something in local scale mixing and chemical compositions. Therefore, it's important to recall the discussion from the fuel property section provided at the beginning of this chapter. The main difference between GTL fuel and diesel fuel is that GTL fuel consisted of almost all straight chains and branched alkanes, indicating the GTL fuel is more easily to be burned off. This is due to the aromatics in diesel fuel are unsaturated chain, which provide low hydrogen and high carbon content. In contrast to aromatics, the straight chains and branched alkanes in GTL fuel has lower carbon content. [Garner, 2009]. Therefore, the GTL is more easily to be combusted completely when compared to diesel. The TGA results in figure 5-1 proved that the GTL fuel is lighter than diesel fuel, i.e. have more lighter fractions. This explains why the pure GTL fuel had slightly lower $NO_X$ emissions than diesel fuel because the ignition delay and combustion duration is shorter. Since the shorter ignition delay stands for the less time required by the fuel to air mix before auto-ignition [Wang, 2005] and combustion duration required by lighter fraction is shorter [Kitano, et al, 2005], therefore, leaving less time allowed for the formation of thermal $NO_X$. This can be proved from the analysis of pressure curves near TDC between GTL fuel and diesel fuel in Chapter 5. With fast and easy combustion characteristics, the pure GTL did have slightly higher combustion pressure than diesel. But the impact from slightly higher temperature is little and the faster combustion characteristics still dominates the $NO_X$ formation in most engine operating conditions. Though it can be concluded that pure GTL showed lower $NO_X$ emissions, there is the possibility that at specific engine operating conditions, the $NO_X$ emissions from pure GTL could be slightly higher than diesel fuel. This is the case for 1600 rpm, 40% throttle tests. This was due to the fuel-air mixing at specific engine operating condition that in-cylinder pressure rise from pure GTL fuel was higher than diesel and combustion duration was close to diesel. This scenario could bring the total $NO_X$ slightly higher as the combustion temperature of pure GTL is slightly higher. The correspond combustion detail can be found in its pressure to crank angle curve in figure 5-7.

The GTL blends with diesel all showed significant $NO_X$ emission reduction. The reduction effectiveness showed no certain relationship with blending ratio. This indicated that the factor contributed to $NO_X$ emissions should not be anything in linear relationship, for instance, fuel density, fuel droplet size, fuel viscosity, aromatics ratio, straight chain ratio etc. Because those quantitative factors are all in linear relationship with blend ratio change and would not be able to explain why the reduction from different blending ratio obtained has no trend and even being very similar at especially high engine power condition. Thus, it is something that the blended fuels differ from pure diesel that contribute to the $NO_X$ emission reduction. As it can be found, the only factor that significantly changed between pure diesel fuel and blended fuels is the aromatic content. From the literature review it's found that aromatics can act as antioxidant in fuel combustion in direct injection diesel engine because it acts as inhibitors for the formation of hydrocarbon free radicals. [Varatharajan, and Cheralathan, 2013]. However, the concentration of aromatics is the highest in diesel fuel and the diesel fuel produced the highest $NO_X$ emissions. So, the explanation is that aromatics would only behaves as antioxidants at a specific concentration range. In pure diesel fuel the aromatics concentration is too high and they wouldn't make effective antioxidant actions, and thus $NO_X$ emissions would be only impacted by the combustion performances and fuel consumption. The pure GTL fuel is aromatics free, thus, its $NO_X$ formation is determined by the temperature. Since the fuel consumption of GTL is equal to diesel fuel, indicating the same energy feed and similar combustion temperature while the combustion period is shorter albeit peak combustion pressure can be slightly higher. Therefore, $NO_X$ from pure GTL can be close but slighter lower than diesel because of shorter combustion duration. The aromatics in blended fuels did act as antioxidants because its concentrations were reduced as aromatic-free GTL fuel been blended into. From this research, it can be found that, with 30% GTL blend ratio, the aromatics would already start to act as antioxidants. With more GTL fuel being added, the $NO_X$ reduction won't be further improved and even at higher power engine test conditions. Since the diesel fuel contains 25% of aromatics and pure GTL fuel contains none, thus the 30% and 70% GTL contained 17.5% to 7.5% of aromatics. This seems to be an optimised aromatics concentration range to act as antioxidants for $NO_x$ reductions.

The detail of the threshold that aromatics can act as antioxidant need more blended tests to be carried out at a blend ratio range between 0% to 30%.

The reason that NO oxidization rate dropped with the increased engine power at each specific rpm is that the DOC aftertreatment system was designed to remove THC and CO instead of removing NO and was limited in NO to $NO_2$ conversion. Therefore, the increase in the power would increase the total NO sent to the DOC, and with limited conversion capacity, the more NO generated from engine, the lower oxidation rate would be achieved.

The total $NO_x$ emissions between exhaust upstream and downstream ranged from 0% to 5%, with 2% to 3% in most of tested conditions. This is believed to be caused by the engine emission repeatability. This showed agreement with other researchers' finding that the coefficient variation of $NO_x$ emission can be 3.1% according their different engine repeatability tests. [Jaworski, et al, 2018].

### 6.2 Particle size distribution, number concentration and DPF efficiency

This section presents the results of particle number emissions from diesel fuel, blended GTL fuel and pure GTL fuel. The particle number emissions from the engine were sampled from exhaust upstream and exhaust downstream, thus allowing the impact of a diesel particulate filter (DPF) to be analysed. The particle number emissions were measured as total particle number and particle number distribution against particle size.

In this section, the analysis on total particle number emission was first conducted in order to find the impact of blending ratio on particle productions. Then, the efficiencies of DPF were calculated using the total particle number acquired before and after the exhaust gas passed through the DPF. After that, the detail of particle size distribution analysis is presented to find out how GTL and GTL blended fuel can improve the particle number generations at different particle size. This is to determine the GTL fuel's impact on nucleation mode and accumulation mode particle generation at different engine operating conditions. Finally, the summary of PN emissions from GTL and GTL blended fuel will be made.

### 6.2.1 Total particle number results analysis

The total particle number emissions measured from exhaust upstream and downstream are presented in figure 6-19 and figure 6-20. It can be seen that the GTL blended fuels and pure GTL fuel can improve the PN emissions significantly both at exhaust upstream and exhaust downstream. The pure GTL fuel can improve the total PN productions at engine out by 27% to 53% based on different engine operating conditions. At the downstream of the aftertreatment system, the blended fuels and pure GTL fuel showed PN emissions lower than the DMS 500 MK II's detection limit ($2.0\times10^4$, which was discussed in chapter four) in most of test conditions. Except the 30% GTL blended fuel showed some results higher than $2.0\times10^4$ (number/cc), but it still improved the total PN emission by at least 26%.

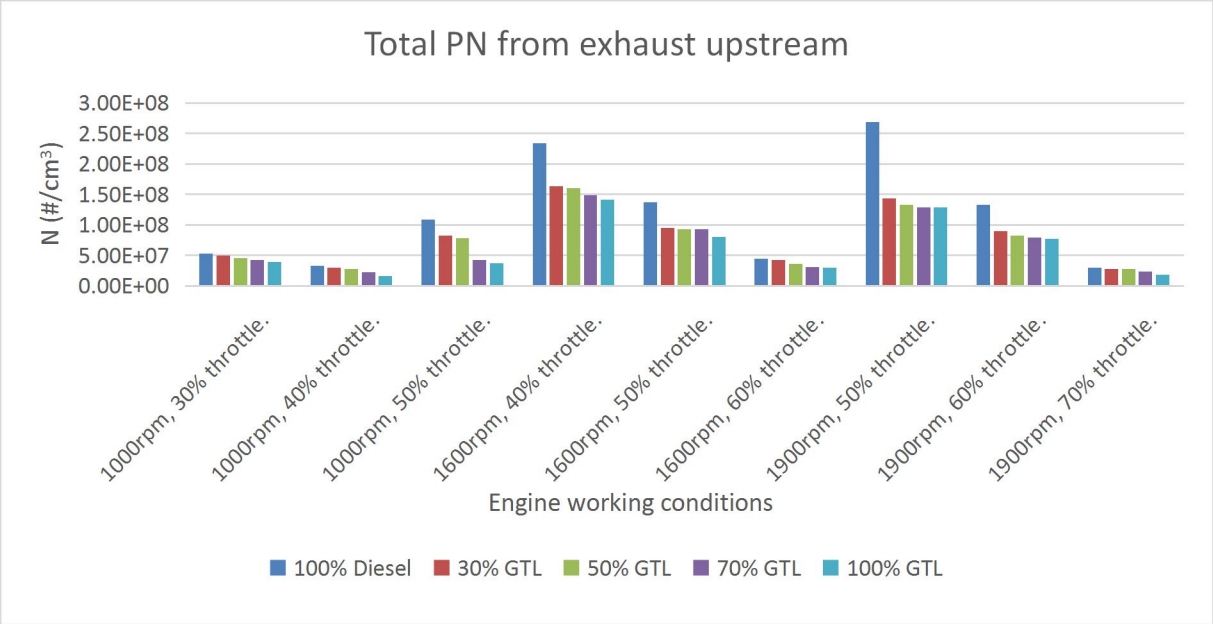


**Figure 6-19** Total PN from exhaust upstream of GTL blended tests.

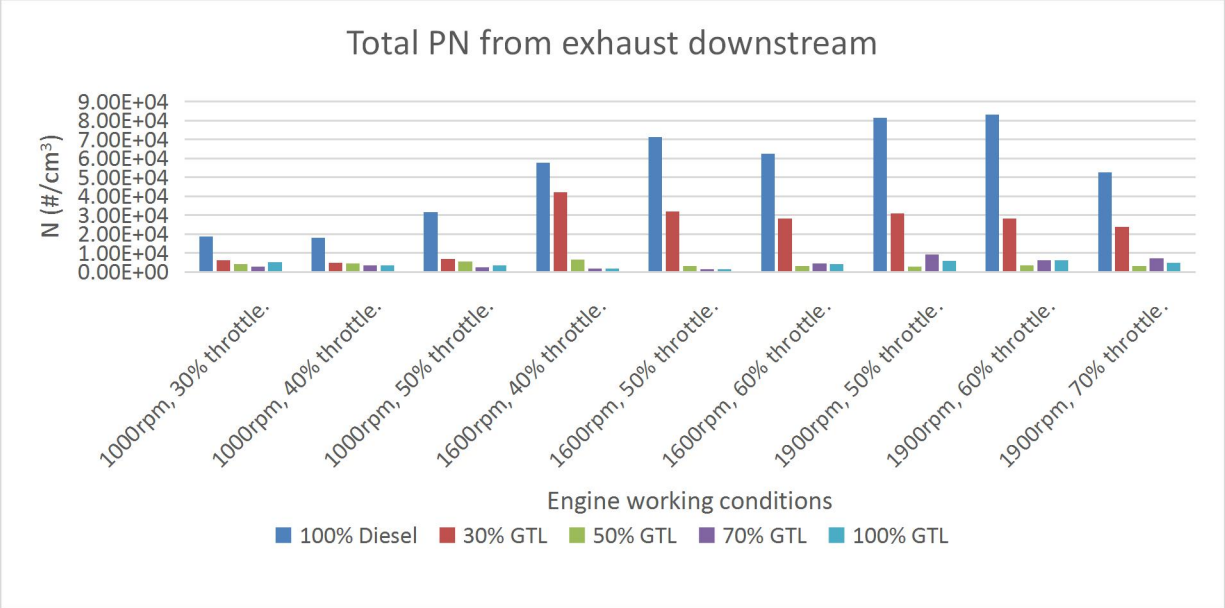


**Figure 6-20** Total PN from exhaust downstream of GTL blended tests.

The reason that pure GTL fuel and it blends can improve the PN production effectively is due to the chemical property of the GTL fuel. The GTL fuel, as discussed in the fuel property section of this chapter, consisted of all straight chains and branched alkanes, which allowing it to be burned off more rapidly, more easily, and more completely. Since the particle number emission is mainly sourced from unburnt and partially burnt fuels, therefore, the aromatics free GTL can be burned more completely and consequently the GTL fuel dose have the ability to reduce PN emission.

If comparing the PN production against the blend ratio, it can be found that the total PN emission gradually reduces with the increasing of blending ratio as each specific engine operating status. This is more obvious from exhaust upstream PN measurement than exhaust downstream, because at the exhaust downstream, the highly effective DPF removed most of the particles and left particles hardly can be accurate measured by the device. If comparing the PN emission at each specific engine rpm, it can be addressed from the figure 6-18 that the total PN reduces with the throttle percentage increases, except for the 1000 rpm 40% throttle test condition. This was due to increasing the throttle settings would improve the air to fuel mixing and increase the average combustion pressure and temperature, thus allowing less particles to be generated. The

1000 rpm 40% throttle was a test condition that showed poor fuel to air mixing performances as discussed earlier in CO emission section of this chapter, therefore the PN emission behaved a little bounce up at this operating status for all tested fuels. From the downstream result, it can be found from figure 6-19, that the 30% blended fuel showed similar findings as upstream to the 1600 rpm and 1900 rpm test, and the diesel fuel showed same findings as upstream only at 1000 rpm. The rest of the tested fuels showed undetectable PN measurement due to the low PN production at exhaust upstream and the highly effective DPF. The reason that diesel fuel didn't present similar results at 1600 rpm and 1900 rpm is believed to be the DPF filtering limitation. Once the engine reaches 27 KW power condition (started from 1600rpm, 50% throttle), the diesel fuel combustion would start to generate accumulation mode particles and exceed the large particle filtration limit of the DPF, and consequently bring the DPF efficiency. This can be proved in following section's discussion.

In summary, GTL fuel and it blends can significantly improve the PN emission by 27% to 53% at exhaust upstream, and at least 26% at exhaust downstream. The more GTL fuel blended into diesel fuel, the more effective reduction of particle number production can be achieved.

### 6.2.2 DPF efficiency analysis

Based on the total particle number results, the DPF efficiency was acquired by calculations explained in chapter three's data processing section. The result is shown in table 6-1 below.

It can be seen that for all tests, the DPF achieved very high efficiencies with all above 99%. Because the total particle number measured at engine out was in the scale of $10^7$ to $10^8$ while the all particle number measured at exhaust downstream was in the scale of $10^4$, thus the particle number measured from exhaust downstream is at least 1000 times lower than that from exhaust upstream. However, if take a close look at diesel's DPF data, it can be found that when the engine power setting reached 1600 rpm, 50% and beyond, the DPF efficiencies of diesel fuel were all slightly lower than pure GTL fuel

and GTL blended fuels. This indicates that when the engine power reached 27 kw and beyond, the diesel fuel would produce more accumulation mode particles which failed to be filtered out by the DPF because the DPF reached its filtration limit. This explains why the total particle number emissions from diesel fuel at exhaust downstream didn't reduce with throttle increasing at each engine power. More details will be provided in the PN distribution section to prove the increased accumulation particles generated from diesel when engine power reached 27 KW and beyond.

**Table 6-1** DPF efficiency of GTL blended fuel tests.

| Engine working condition | | DPF efficiency | | | | |
|---|---|---|---|---|---|---|
| engine rpm | throttle% | 100% Diesel | 30% GTL | 50% GTL | 70% GTL | 100% GTL |
| 1000 | 30 | 99.9647% | 99.9875% | 99.9910% | 99.9932% | 99.9866% |
| | 40 | 99.9450% | 99.9832% | 99.9846% | 99.9842% | 99.9771% |
| | 50 | 99.9710% | 99.9918% | 99.9929% | 99.9940% | 99.9342% |
| 1600 | 40 | 99.9753% | 99.9742% | 99.9959% | 99.9987% | 99.9988% |
| | 50 | 99.9478% | 99.9666% | 99.9966% | 99.9983% | 99.9909% |
| | 60 | 99.8591% | 99.9331% | 99.9917% | 99.9850% | 99.9315% |
| 1900 | 50 | 99.9697% | 99.9783% | 99.9978% | 99.9929% | 99.9866% |
| | 60 | 99.9377% | 99.9682% | 99.9958% | 99.9921% | 99.9762% |
| | 70 | 99.8233% | 99.9148% | 99.9887% | 99.9702% | 99.9183% |

### 6.2.3Particle number size distribution analysis

This section presents the results and discussion of particle size distribution curves. The measurements were taken both from the exhaust upstream and downstream, thus allowing for the analysis of DPF efficiencies. The measured particle diameter range is from 4.87 nm to 1000 nm, with total 38 different sizes of particles being measured in number concentrations (#/cm$^3$). The results are presented in figure 6-21 to figure 6-38 in below.

The majority of particle number emissions from diesel engine ranged from 10 nm to 200 nm. Therefore, the particle number distribution measured at the upstream of DPF clearly shows the particles generated directly from engine combustion. Generally, the

magnitude is $10^{7\sim8}$ (#/cm$^3$), which is the same to the results reported by Hawker, et al. [1998]. The peak model size measured at the upstream of DPF ranged from 100 to 150 nm. The particle size range at the downstream of DPF is still the same as at the upstream, however the quantity of particles was dramatically reduced to $10^{4\sim5}$ (#/cm$^3$) and the peak model size ranged from 20 to 40 nm, which is the same to the results reported by Caroca, et al. [2010]. This is due to the high efficiency of DPF. The particle agglomerations can occur when the exhaust gas passed through the aftertreatment system, indicating more large particles can be formed. [Ho, et al, 2002]. However, due to the high efficiency of DPF, all the particles are greatly reduced at the downstream of DPF, leaving the particle agglomeration impossible to be detected.

From the 1000 rpm results, it can be observed from figure 6-21, figure 6-23 and figure 6-25 that some blended GTL fuels can have higher peak values of accumulation mode particles at lower power settings, but this phenomenon would disappear when the throttle settings increased to 50%. This can be caused by the relevantly low combustion temperature and poor air to fuel mixing at 30% and 40% throttle settings. The peak values of nucleation mode particles from GTL and its blends are lower than from diesel in general despite 100%, 70%, 50% GTL fuel and diesel fuel shared similar nucleation particle distribution curve at 1000 rpm, 30% throttle tests.

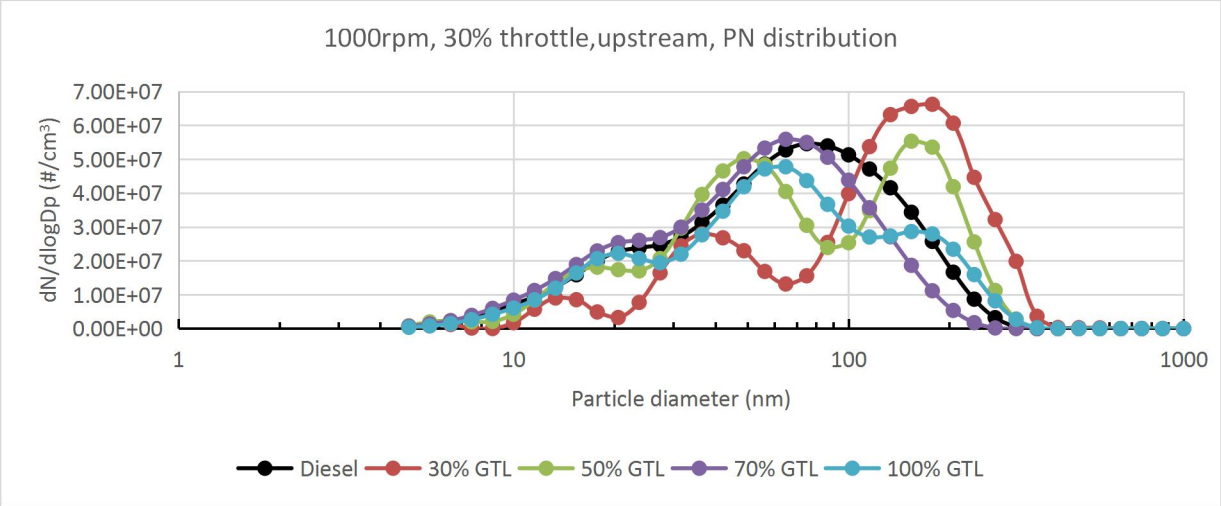


**Figure 6-21** Particle size distribution from exhaust upstream at 1000 rpm, 30% throttle.

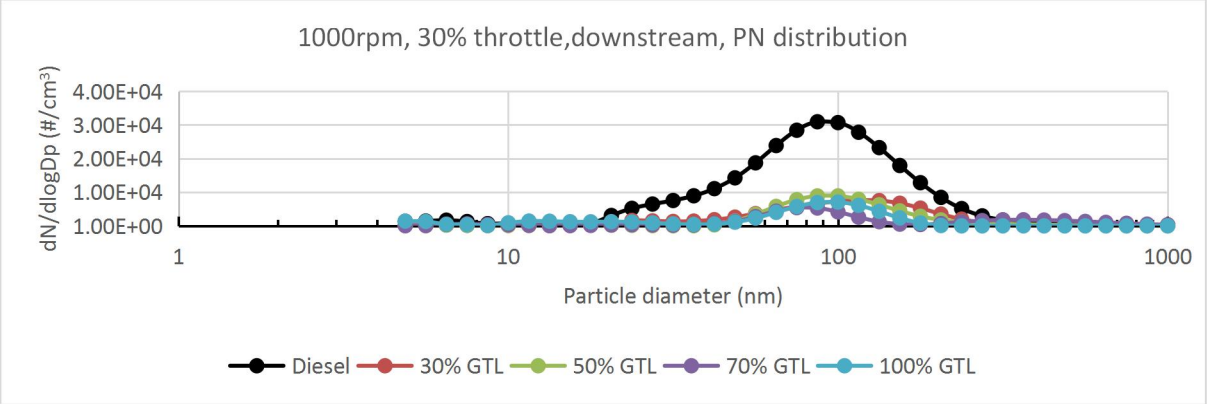


**Figure 6-22** Particle size distribution from exhaust downstream at 1000 rpm, 30% throttle.

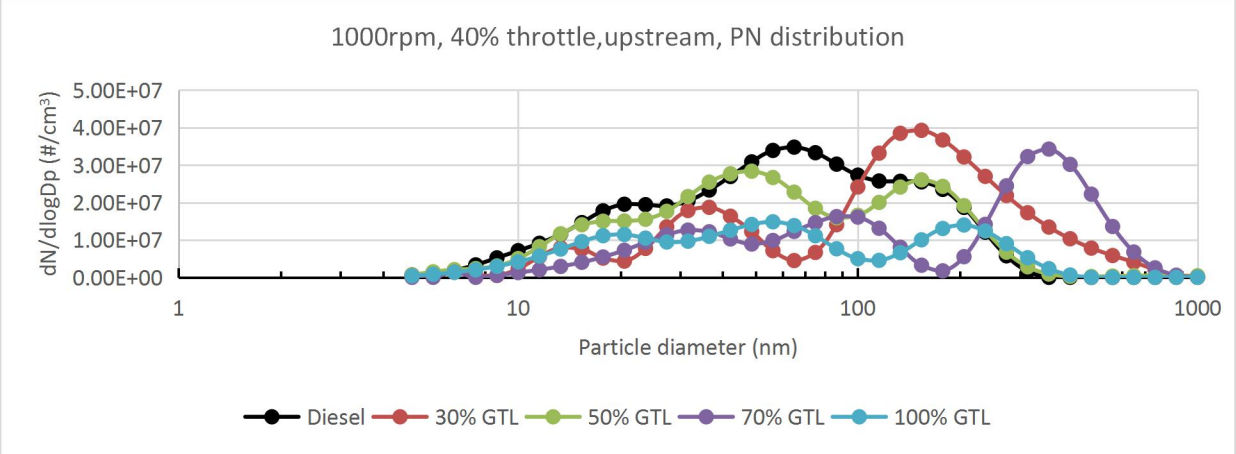


**Figure 6-23** Particle size distribution from exhaust upstream at 1000 rpm, 40% throttle.

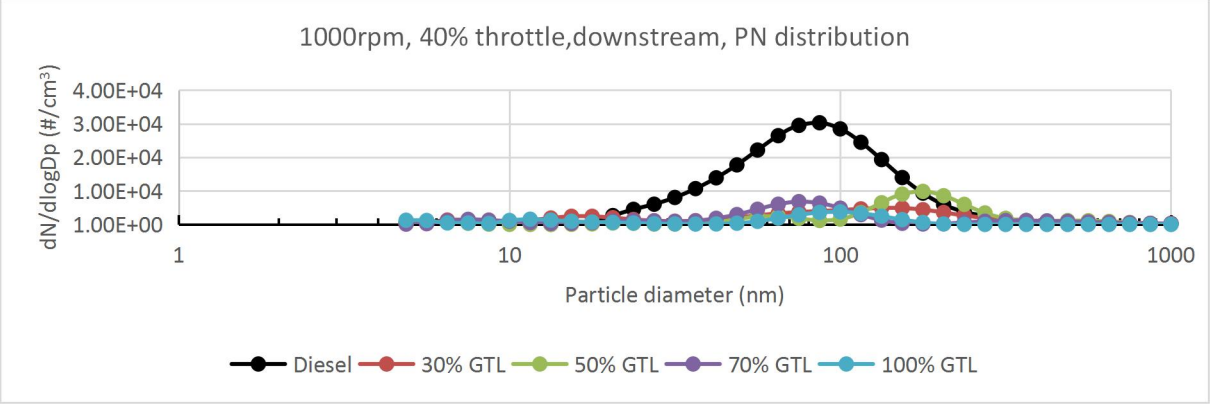


**Figure 6-24** Particle size distribution from exhaust downstream at 1000 rpm, 40% throttle.

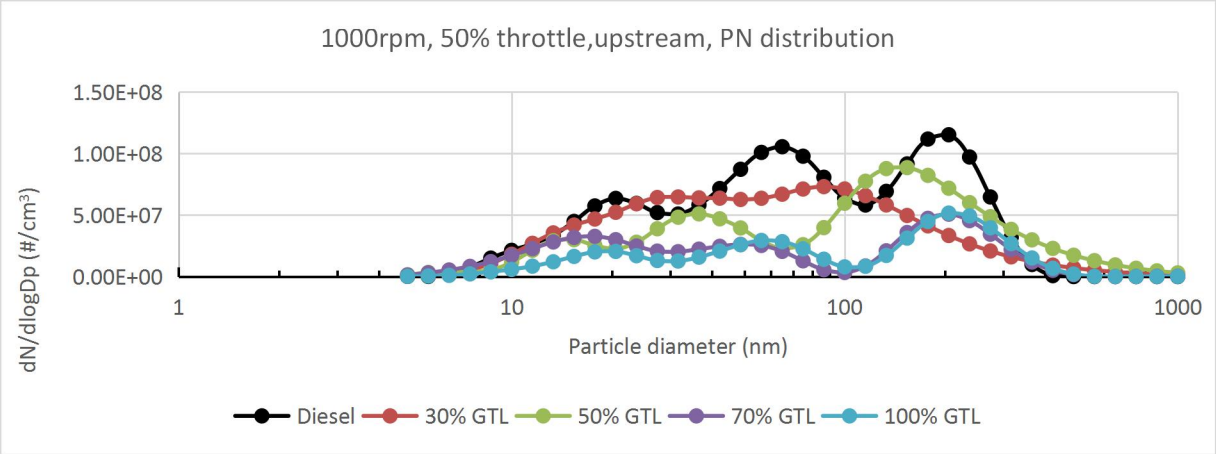


**Figure 6-25** Particle size distribution from exhaust upstream at 1000 rpm, 50% throttle.

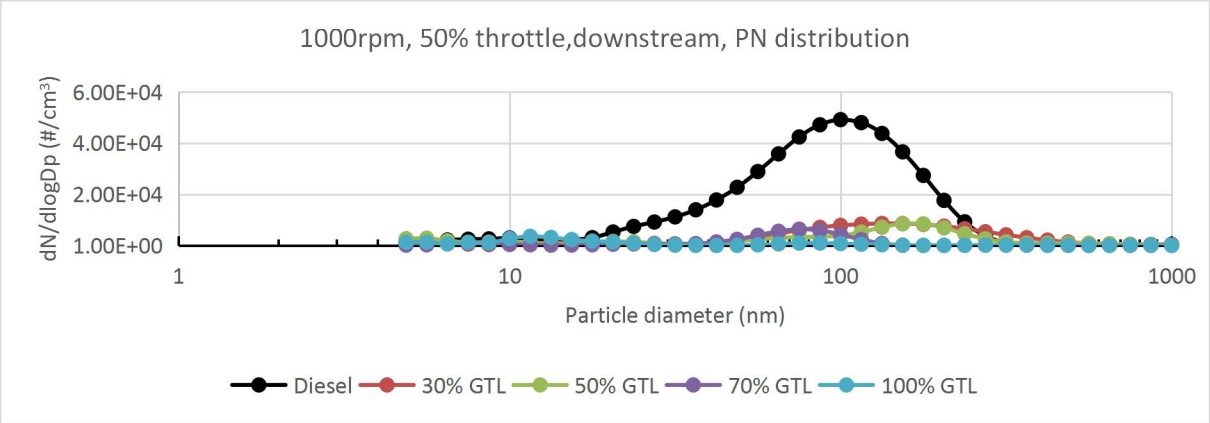


**Figure 6-26** Particle size distribution from exhaust downstream at 1000 rpm, 50% throttle.

From exhaust upstream PN size distribution, the nucleation mode particles' peak values of all tested fuels ranged from 11nm to 21 nm, and the accumulation mode particles' peak values ranged from 86 nm to 365 nm. This indicates that the productions of accumulation mode particles were more sensitive to blending ratio than the nucleation mode particles, and similar findings were reported by Du's research team, that accumulation mode particles especially in diameter range around 100 nm are more sensitive to GTL blending ratios than nucleation mode particles. [Du, et al., 2014]. In 1000 rpm tests, GTL and its blends showed particle number reduction in nucleation mode particles, despite some blended fuels showed higher number emissions for accumulation particle. The total PN emissions for all tested alternative fuels were still

lower than diesel fuel because the GTL and it blends significantly reduced the particle production with diameter smaller than 100 nm. From the exhaust downstream, it can be found that all blended GTL fuels and pure GTL fuel showed much lower particle emissions than diesel, and those particle number concentrations measured in were all lower than $2\times10^4$ (#/cm$^3$), which is the lower detect limits of the DMS 500.

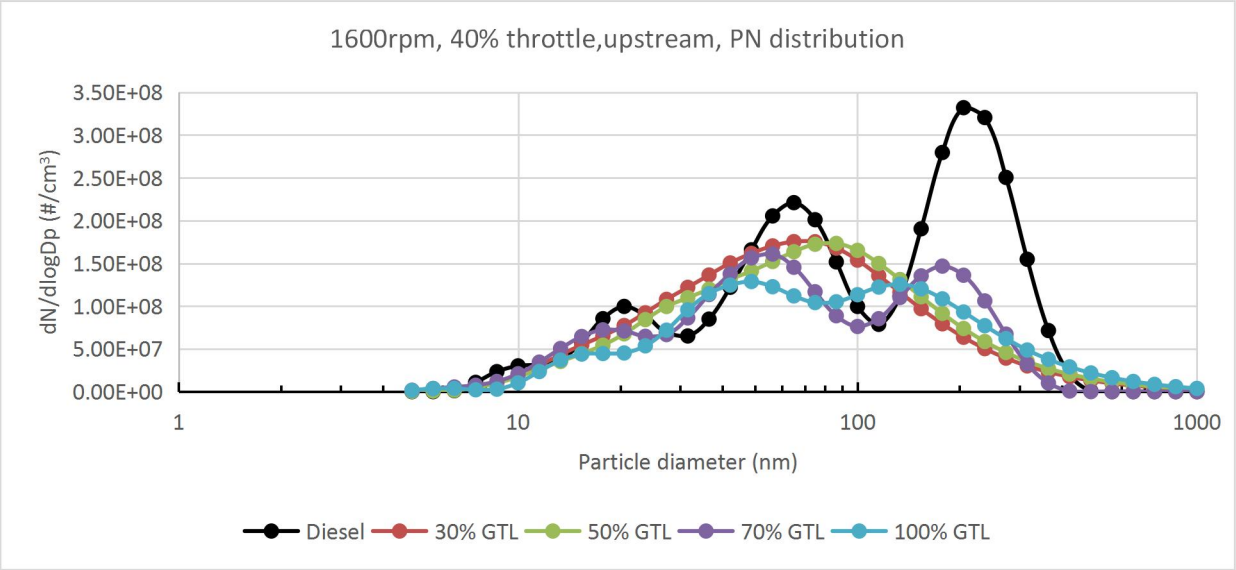


**Figure 6-27** Particle size distribution from exhaust upstream at 1600 rpm, 40% throttle.

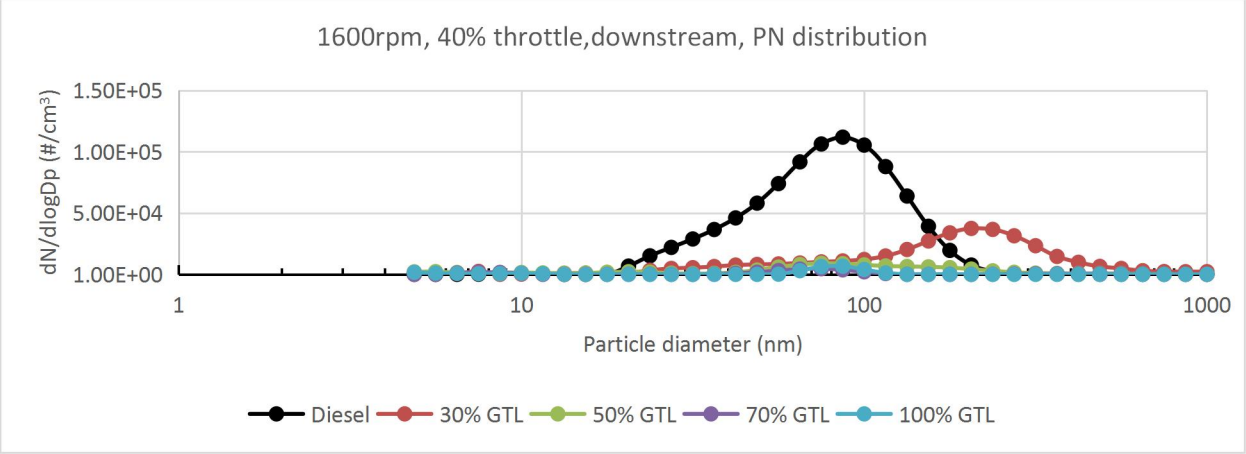


**Figure 6-28** Particle size distribution from exhaust downstream at 1600 rpm, 40% throttle.

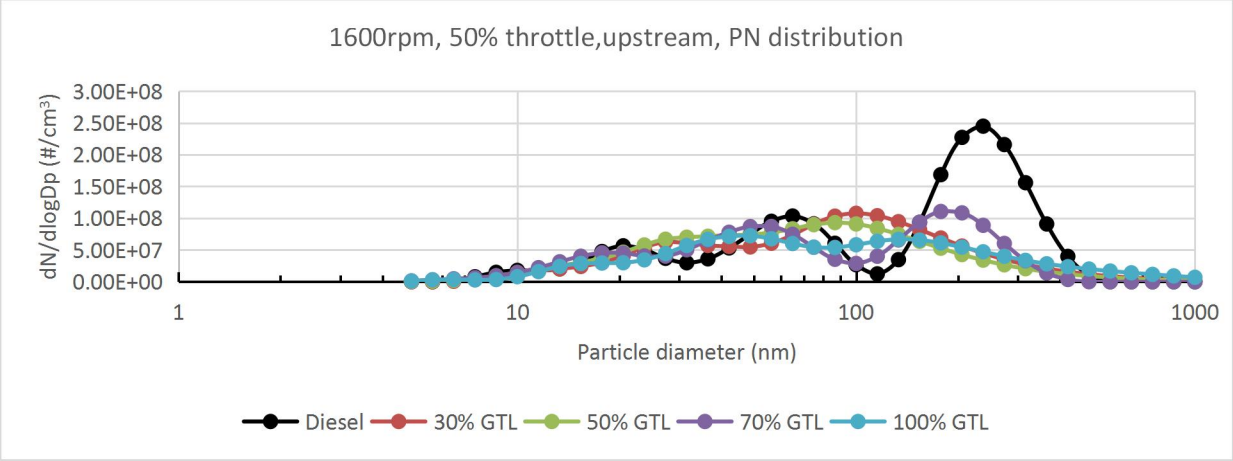


**Figure 6-29** Particle size distribution from exhaust upstream at 1600 rpm, 50% throttle.

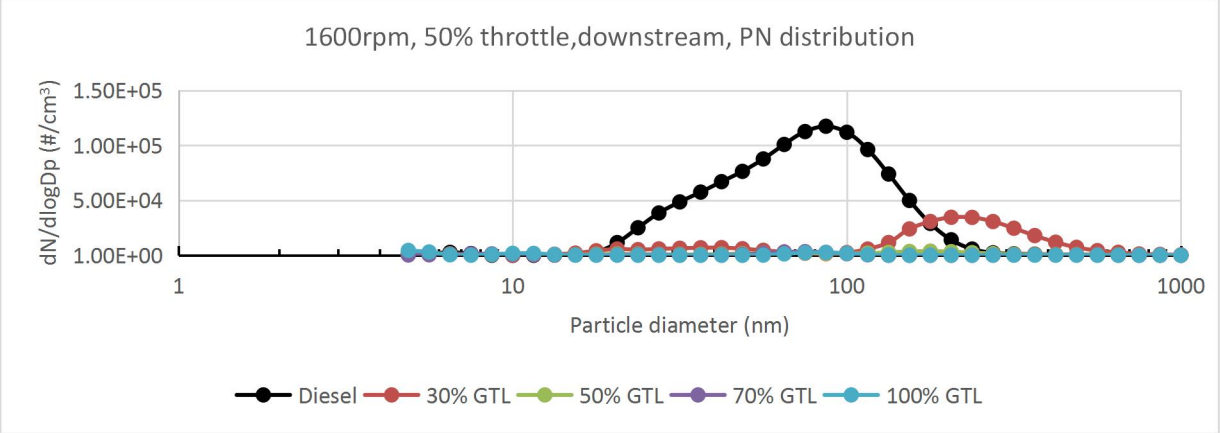


**Figure 6-30** Particle size distribution from exhaust downstream at 1600 rpm, 50% throttle.

When the engine rpm was increased to 1600 rpm, it can be observed from figure 6-27, figure 6-29 and figure 6-31 that GTL and it blends can significantly reduce the particle numbers with diameter larger than 154 nm. The mode size for accumulation mode particles from 70% and 100% GTL fuel is between 154 nm to 205 nm, while the 30% and 50% GTL fuel had their accumulation peaks around 100 nm. It can be seen from figure 6-31, the mode size of accumulation mode particles increases with the blending ratio increase and this corresponds to the similar findings in figure 6-25, which presented the PN distribution of the 1000 rpm, 50% throttle test condition. The GTL and its blends reduced particle numbers in nucleation mode when the throttle was 40% and

50%, however with 60% throttle, the nucleation particle distributions between fuels are similar. Thus, the significant particle number reduction at 154 nm and beyond caused the PN emission reduction from GTL and its blended fuels.

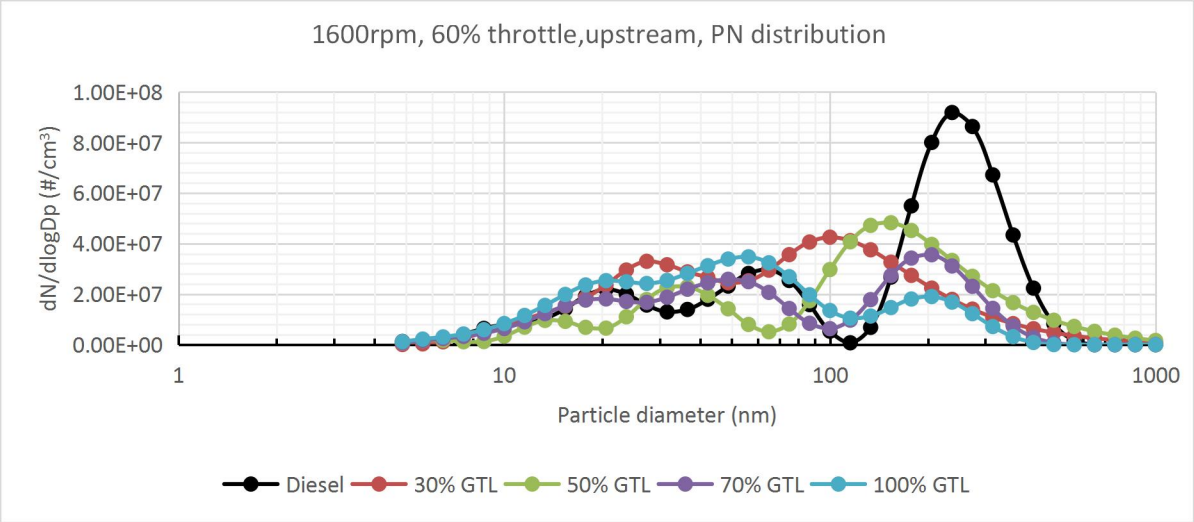


**Figure 6-31** Particle size distribution from exhaust upstream at 1600 rpm, 60% throttle.

From the exhaust downstream results at 1600 rpm, the GTL and blended fuels showed almost undetectable particles, except for the 30% blended GTL fuel, which was observed to have peak values of accumulation mode particles between 205 nm to 240 nm. When looking back the 30% GTL blended fuel performance at exhaust upstream, it was found the 30% GTL fuel obtained the highest particle number production in diameter around 100 nm. Therefore, one possible explanation is that those particles with approximately 100 nm diameter generated from 30% GTL fuels were more likely to agglomerate with other nano-particles during the exhaust gas passed through the engine exhaust aftertreatment system, and finally formed as accumulation particles with peak diameter range from 205 nm to 240 nm.

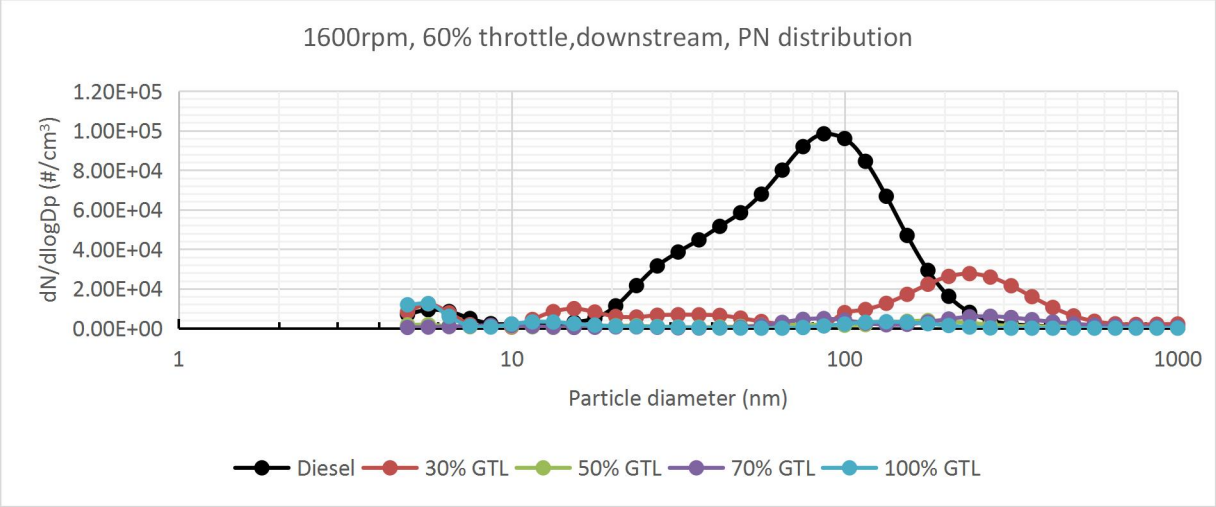


**Figure 6-32** Particle size distribution from exhaust downstream at 1600 rpm, 60% throttle.

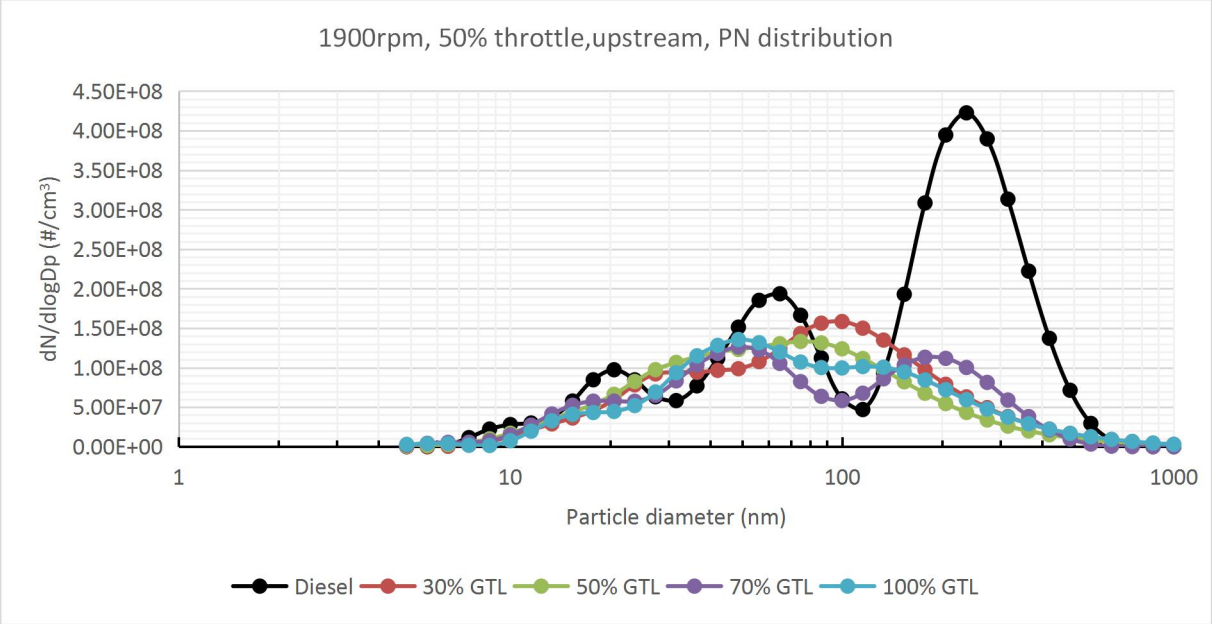


**Figure 6-33** Particle size distribution from exhaust upstream at 1900 rpm, 50% throttle.

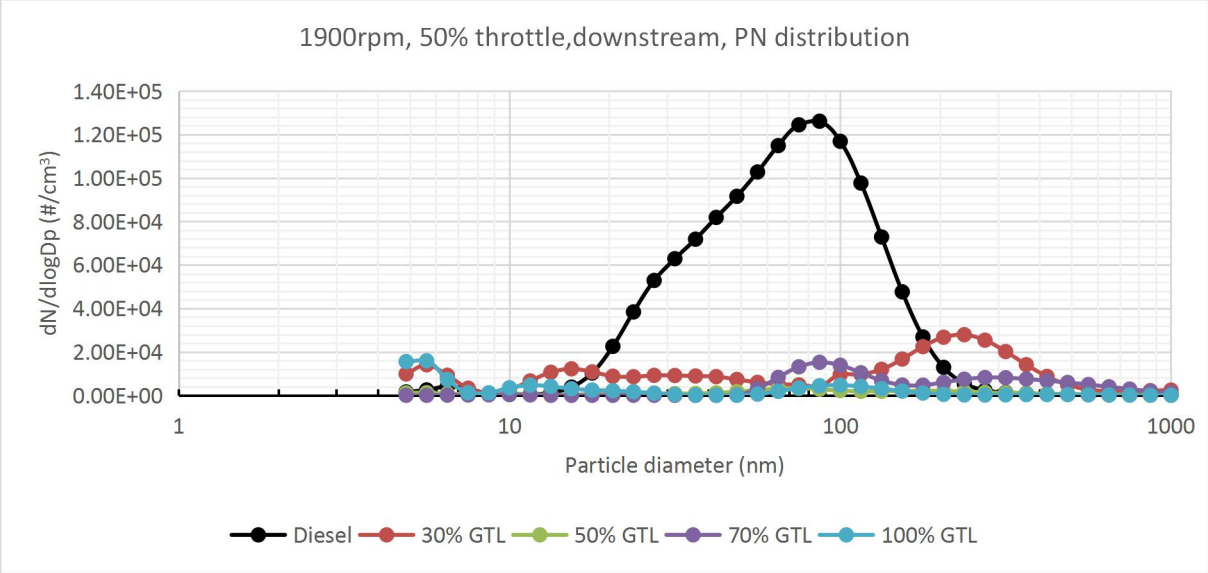


**Figure 6-34** Particle size distribution from exhaust downstream at 1900 rpm, 50% throttle.

When the engine rpm increased to 1900, it can be seen from figure 6-33, figure 6-35 and figure 6-37 that the peak values for accumulation particles decreased as the blending ratio increased, and this is most obvious in figure 6-37 which is the highest engine power test status. Particles with diameter greater than 154 nm were significantly reduced from all GTL and GTL blended fuel as in previous tests. The 30% and 50% GTL blended fuels still tended to have smaller size than 70% and 100% GTL fuel. The nucleation particle number distribution of blended fuels and pure GTL fuel are close to each other and with most of nucleation particles in diameter region from 10 nm to 31 nm. From the exhaust downstream, same findings can be observed for 30% GTL.

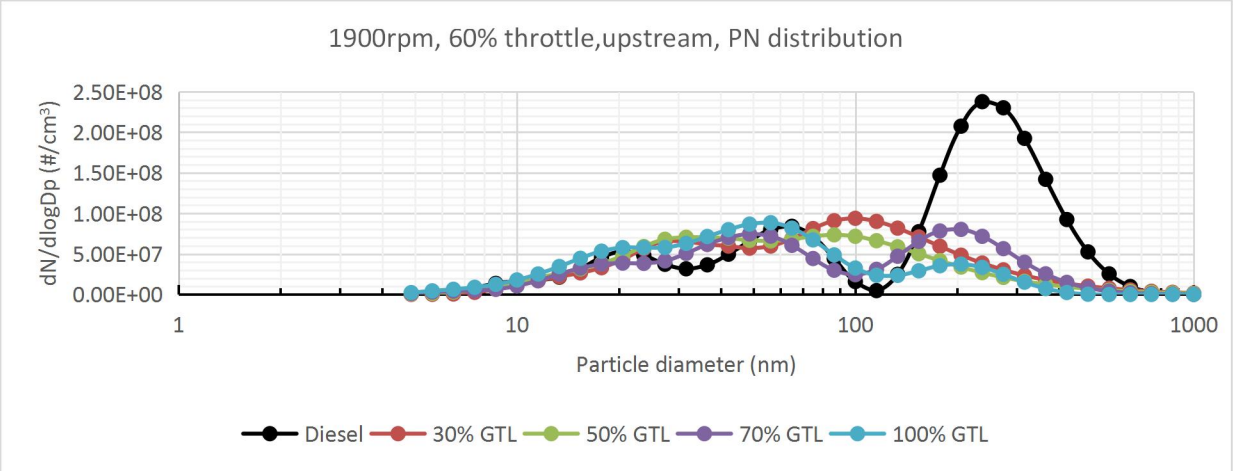


**Figure 6-35** Particle size distribution from exhaust upstream at 1900 rpm, 60% throttle.

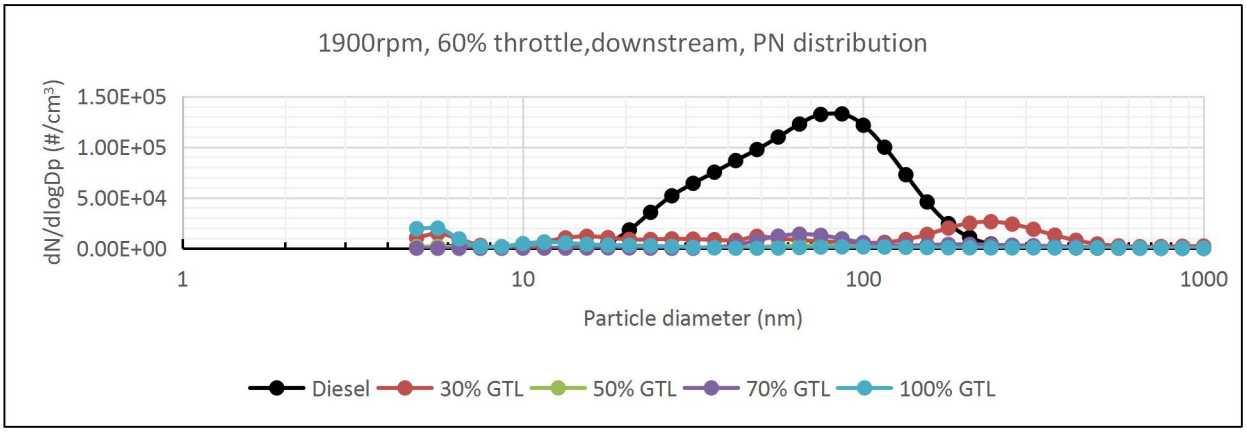


**Figure 6-36** Particle size distribution from exhaust upstream at 1900 rpm, 60% throttle.

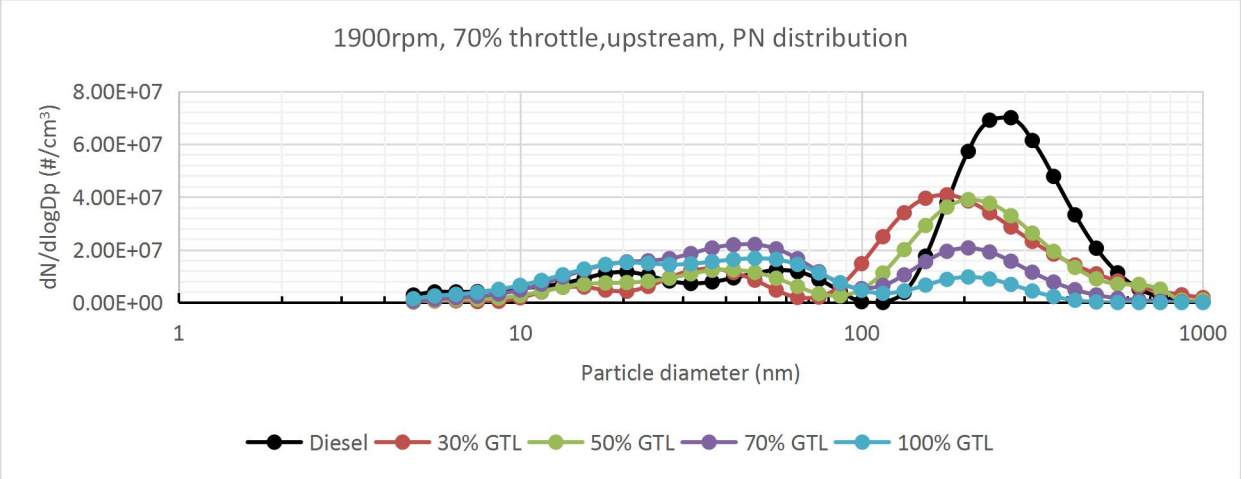


**Figure 6-37** Particle size distribution from exhaust upstream at 1900 rpm, 70% throttle.

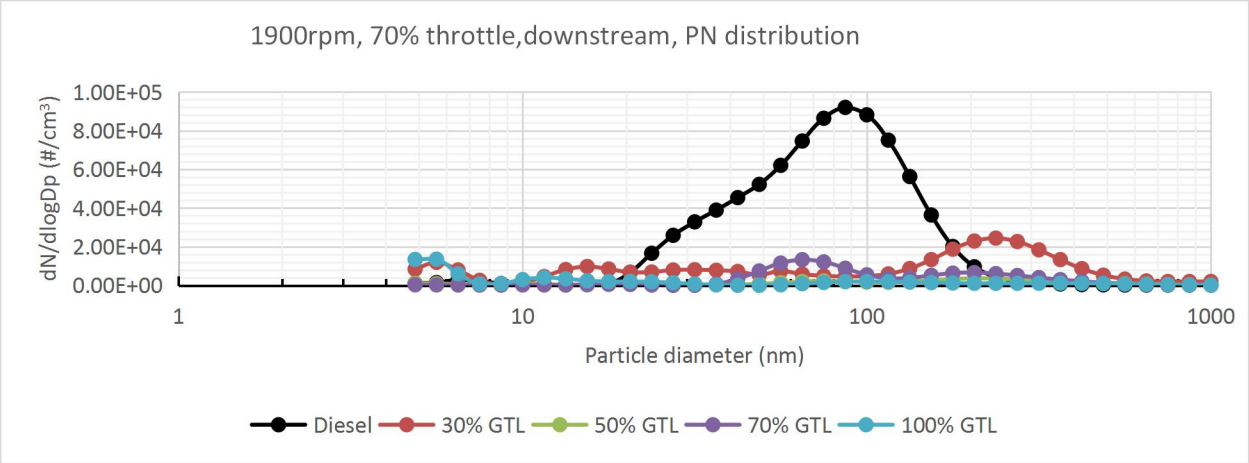


**Figure 6-38** Particle size distribution from exhaust upstream at 1900 rpm, 70% throttle.

In summary, the GTL and its blended fuels can significantly reduce the particle number emissions by producing much fewer accumulation mode particles with diameter greater than 154 nm. In general, the peak values for accumulation mode particles reduces with the increasing of blending ratio, indicating the more GTL fuel blended into with diesel, the smaller the accumulation particles will be produced. The GTL and its blends also reduce the nucleation particles. However, when the engine power increased, the nucleation particle number distribution between tested fuels can be similar. From the downstream of DPF, its hardly to provide any detectable particle numbers from GTL and its blends due to the high efficiency of DPF and the DMS 500 detection limitation.

## 6.3 THC emissions

This section provides the results and analysis of THC emissions from all test fuels. The THC emissions were measured from sampling points both located before and after the exhaust after treatment system, which consisted of DOC and DPF. The measured raw data was converted to emission index and emission in grams per kwh. DOC efficiencies were calculated using the differences between upstream and downstream divided by THC emission from upstream.

The source of hydrocarbon emissions from diesel engine is mainly from two aspects: the volume of fuel in the sac and the fuel premixing. [Greeves, et al, 1977]. The former is decided by the size of fuel injection nozzle and the latter can be decided by the fuel

property. For this research, the fuel injectors were remained the same, therefore, the changing of fuel types could result differences in fuel premixing and thus caused the variation in THC emissions. Compared to diesel fuel, the GTL fuel should have better premix performances because straight chains and branched alkanes consisted in GTL fuel are more easily to be burned. From the TGA analysis result in figure 5-1 at the beginning fuel property section of this chapter. It can be found that pure GTL fuel evaporates faster than diesel fuel, indicating that the pure GTL fuel is able to achieve better premixing than pure diesel fuel. This can also be proved from the differences in ignition delays, as GTL and GTL blended fuels obtained shorter ignition delays, which meaning the premix process of GTL and GTL blended fuel is more easily to occur than pure diesel. The GTL fuel also has smaller fuel droplet size than diesel, [Li, et al, 2010]. which could also help GTL fuel to improve its fuel premix performances.

The exhaust gas temperature measured of all test conditions is given in table 6-2. Since all the tests for different kind of fuels were carried out in same power set up sequence, which stated from 1000 rpm with 30% throttle and ended at 1900 rpm with 70% throttle. Hence, the exhaust gas temperature was the same at specific engine test condition regardless of the fuel type. It can be seen from table 6-2 that the exhaust gas temperature values were all above 400 °C; a temperature DOC was fully operational. [Wittrock, et al, 2017]. The THC emission results from all tests are presented in following tables from table 6-3 to table 6-11, and the respective THC emission relation against blending ratio are shown in figures from figure 6-39 to figure 6-47.

**Table 6-2** The exhaust gas temperature of all test conditions.

| Engine rpm | Throttle percentage (%) | Exhaust gas temp at exhaust manifold(°C) |
|---|---|---|
| 1000 | 30 | 400 |
| 1000 | 40 | 480 |
| 1000 | 50 | 544 |
| 1600 | 40 | 430 |
| 1600 | 50 | 490 |
| 1600 | 60 | 550 |
| 1900 | 50 | 485 |
| 1900 | 60 | 520 |
| 1900 | 70 | 550 |

**Table 6-3** THC emissions of GTL blended fuels from exhaust upstream and downstream, with DOC efficiency, at 1000rpm 30% throttle.

| Fuel Type | THC Upstream | | | | THC Downstream | | | | DOC efficiency |
|---|---|---|---|---|---|---|---|---|---|
| | ppm | EI g/kgfuel | g/kWh | STDEVA/mean | ppm | EI g/kgfuel | g/kWh | STDEVA/mean | |
| Diesel | 108 | 1.66 | 0.52 | 9.93% | 2 | 0.03 | 0.01 | 0.00% | 98.15% |
| 30% GTL | 86 | 1.15 | 0.36 | 4.35% | 2 | 0.02 | 0.01 | 18.20% | 98.12% |
| 50% GTL | 59 | 0.81 | 0.25 | 3.78% | 3 | 0.05 | 0.01 | 3.01% | 94.20% |
| 70% GTL | 55 | 0.73 | 0.22 | 3.80% | 4 | 0.05 | 0.02 | 3.47% | 92.74% |
| 100% GTL | 50 | 0.69 | 0.20 | 1.71% | 3 | 0.05 | 0.02 | 9.70% | 94.02% |

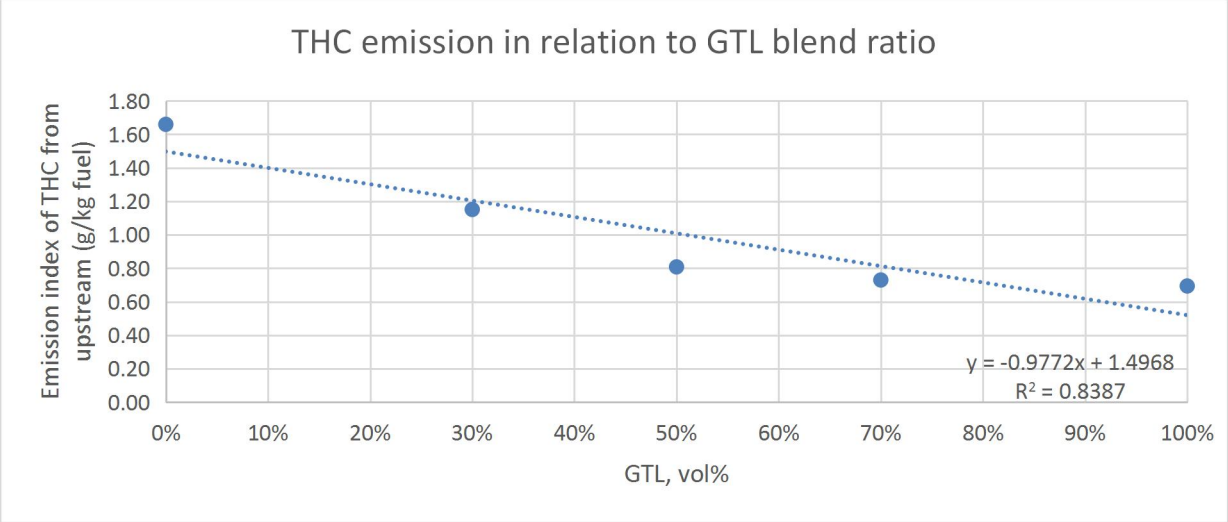


**Figure 6-39** THC emission in relation to GTL blend ratio based on THC emission from upstream at 1000rpm, 30% throttle.

**Table 6-4** THC emissions of GTL blended fuels from exhaust upstream and downstream, with DOC efficiency, at 1000rpm, 40% throttle.

| Fuel Type | THC Upstream | | | | THC Downstream | | | | DOC efficiency |
|---|---|---|---|---|---|---|---|---|---|
| | ppm | EI g/kgfuel | g/kWh | STDEVA/mean | ppm | EI g/kgfuel | g/kWh | STDEVA/mean | |
| Diesel | 77 | 0.98 | 0.30 | 8.29% | 2 | 0.03 | 0.01 | 0.00% | 97.39% |
| 30% GTL | 66 | 0.78 | 0.23 | 5.97% | 2 | 0.02 | 0.01 | 3.90% | 97.14% |
| 50% GTL | 61 | 0.74 | 0.22 | 2.03% | 4 | 0.05 | 0.02 | 2.97% | 92.87% |
| 70% GTL | 59 | 0.71 | 0.21 | 3.99% | 5 | 0.06 | 0.02 | 2.96% | 91.53% |
| 100% GTL | 52 | 0.63 | 0.18 | 2.22% | 5 | 0.06 | 0.02 | 0.00% | 90.32% |

From the comparison of the 1000 rpm test, it can be found that the TCH emissions sampled before the aftertreatment system showed gradual reductions with the increasing of blending ratio. And from figure 6-39 to figure 6-41, it can be found that those THC emission reduction was almost behaved as linear relationship with the blending ratio. The THC measured after the exhaust gas aftertreatment system didn't show reasonable trend, and it believed the THC concentration from exhaust downstream was too low to be measured as valid data. According to the specification of MEXA 7100, the equipment's measurement range for THC is from 0 to 50000 ppm, indicating that 0.01% error should be 5 ppm. Thus, the THC measured at 5 ppm and lower, should be considered as below the detection limit of the instrument.

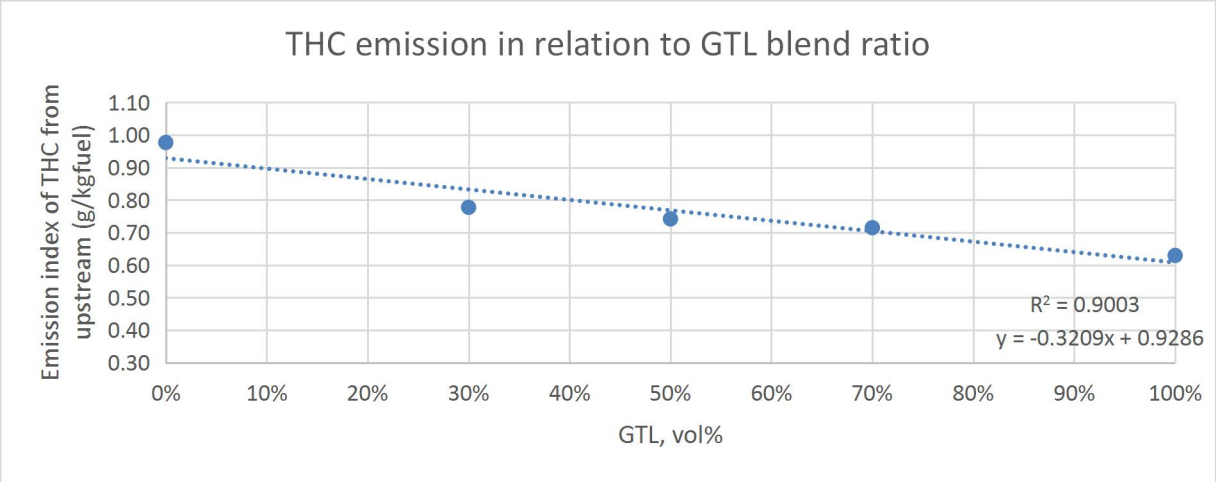


**Figure 6-40** THC emission in relation to GTL blend ratio based on THC emission from upstream at 1000rpm, 40% throttle.

**Table 6-5** THC emissions of GTL blended fuels from exhaust upstream and downstream, with DOC efficiency, at 1000rpm 50% throttle.

| Fuel Type | THC Upstream | | | | THC Downstream | | | | DOC efficiency |
|---|---|---|---|---|---|---|---|---|---|
| | ppm | EI g/kgfuel | g/kWh | STDEVA/mean | ppm | EI g/kgfuel | g/kWh | STDEVA/mean | |
| Diesel | 66 | 0.74 | 0.23 | 3.61% | 2 | 0.02 | 0.01 | 0.00% | 96.95% |
| 30% GTL | 55 | 0.61 | 0.16 | 6.80% | 2 | 0.02 | 0.01 | 1.95% | 96.01% |
| 50% GTL | 51 | 0.56 | 0.17 | 2.90% | 5 | 0.06 | 0.02 | 2.00% | 90.23% |
| 70% GTL | 49 | 0.55 | 0.16 | 2.78% | 5 | 0.06 | 0.02 | 0.75% | 89.83% |
| 100% GTL | 42 | 0.47 | 0.13 | 2.58% | 5 | 0.06 | 0.02 | 0.00% | 88.18% |

From the 1000 rpm tests, it can also be found that the magnitude of THC reduction reduced with the throttle percentage being increased. At 1000 rpm, 30% throttle, the pure GTL fuel showed 58 ppm reduction of THC, while at the 40% an 50%, the reduction of THC reduced to respectively 25 ppm and 24 ppm. Similar findings were acquired from 1600 rpm and 1900 rpm test. Because when the throttle parentage increases at each specific rpm, the average in-cylinder pressure increased and thus provided a better environment for fuel premixing. The relevant high-pressure combustion environment would benefit all kinds of fuel's premixing, therefore, the advantages of burning GTL fuel would become less significant. This phenomenon can also be seen from the linear relationships between THC emission and blending ratio. The slope factors for 1000 rpm 30%, 40% and 50% throttle settings acquired from figure 6-39 to figure 6-41 are respectively -0.98, -0.32 and -0.23.

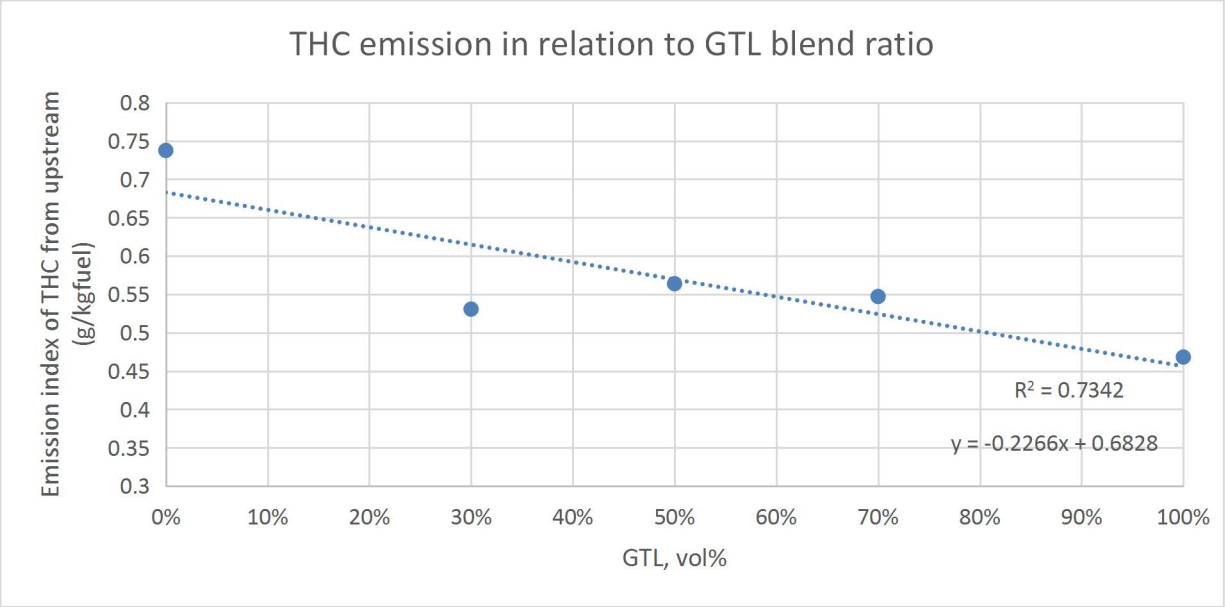


**Figure 6-41** THC emission in relation to GTL blend ratio based on THC emission from upstream at 1000rpm, 50% throttle.

**Table 6-6** THC emissions of GTL blended fuels from exhaust upstream and downstream, with DOC efficiency, at 1600rpm 40% throttle.

| Fuel Type | THC Upstream | | | | THC Downstream | | | | DOC efficiency |
|---|---|---|---|---|---|---|---|---|---|
| | ppm | EI g/kgfuel | g/kWh | STDEVA/mean | ppm | EI g/kgfuel | g/kWh | STDEVA/mean | |
| Diesel | 83 | 1.19 | 0.35 | 3.55% | 8 | 0.11 | 0.03 | 9.66% | 90.56% |
| 30% GTL | 77 | 1.08 | 0.32 | 4.27% | 7 | 0.10 | 0.03 | 12.95% | 90.41% |
| 50% GTL | 69 | 1.01 | 0.30 | 3.13% | 5 | 0.07 | 0.02 | 2.08% | 92.92% |
| 70% GTL | 62 | 0.90 | 0.26 | 3.30% | 5 | 0.07 | 0.02 | 0.87% | 91.95% |
| 100% GTL | 54 | 0.80 | 0.22 | 2.26% | 4 | 0.06 | 0.02 | 0.00% | 92.61% |

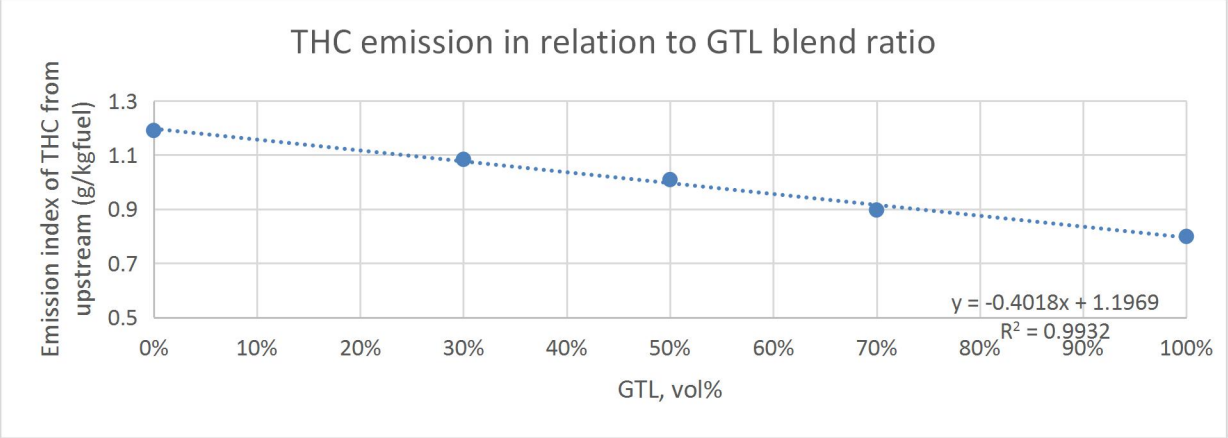


**Figure 6-42** THC emission in relation to GTL blend ratio based on THC emission from upstream at 1600rpm, 40% throttle.

**Table 6-7** THC emissions of GTL blended fuels from exhaust upstream and downstream, with DOC efficiency, at 1600rpm 50% throttle.

| Fuel Type | THC Upstream | | | | THC Downstream | | | | DOC efficiency |
|---|---|---|---|---|---|---|---|---|---|
| | ppm | EI g/kgfuel | g/kWh | STDEVA/mean | ppm | EI g/kgfuel | g/kWh | STDEVA/mean | |
| Diesel | 71 | 0.96 | 0.28 | 1.74% | 7 | 0.10 | 0.03 | 5.40% | 89.85% |
| 30% GTL | 69 | 0.92 | 0.26 | 3.21% | 4 | 0.06 | 0.02 | 7.69% | 93.54% |
| 50% GTL | 58 | 0.79 | 0.22 | 1.87% | 4 | 0.06 | 0.02 | 1.70% | 92.60% |
| 70% GTL | 58 | 0.79 | 0.22 | 1.87% | 4 | 0.06 | 0.02 | 1.24% | 93.10% |
| 100% GTL | 49 | 0.67 | 0.17 | 2.09% | 4 | 0.06 | 0.01 | 0.00% | 91.78% |

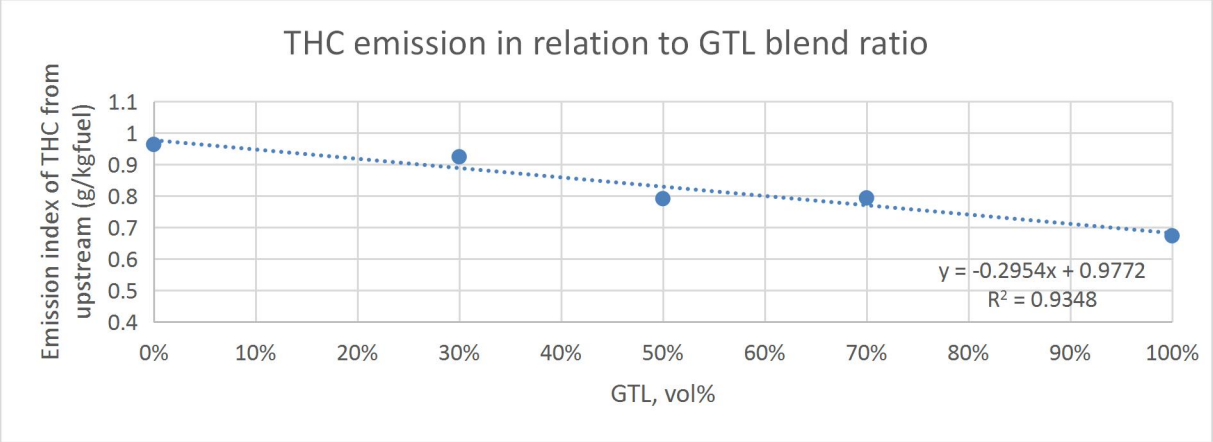


**Figure 6-43** THC emission in relation to GTL blend ratio based on THC emission from upstream at 1600rpm, 50% throttle.

**Table 6-8** THC emissions of GTL blended fuels from exhaust upstream and downstream, with DOC efficiency, at 1600rpm 60% throttle.

| Fuel Type | THC Upstream | | | | THC Downstream | | | | DOC efficiency |
|---|---|---|---|---|---|---|---|---|---|
| | ppm | EI g/kgfuel | g/kWh | STDEVA/mean | ppm | EI g/kgfuel | g/kWh | STDEVA/mean | |
| Diesel | 62 | 0.81 | 0.22 | 2.33% | 7 | 0.09 | 0.03 | 14.03% | 88.71% |
| 30% GTL | 60 | 0.78 | 0.21 | 4.16% | 4 | 0.05 | 0.01 | 1.34% | 93.14% |
| 50% GTL | 50 | 0.67 | 0.18 | 1.99% | 5 | 0.06 | 0.02 | 3.19% | 90.60% |
| 70% GTL | 53 | 0.70 | 0.19 | 2.77% | 5 | 0.06 | 0.02 | 2.55% | 90.57% |
| 100% GTL | 47 | 0.63 | 0.16 | 2.14% | 4 | 0.06 | 0.01 | 10.67% | 90.93% |

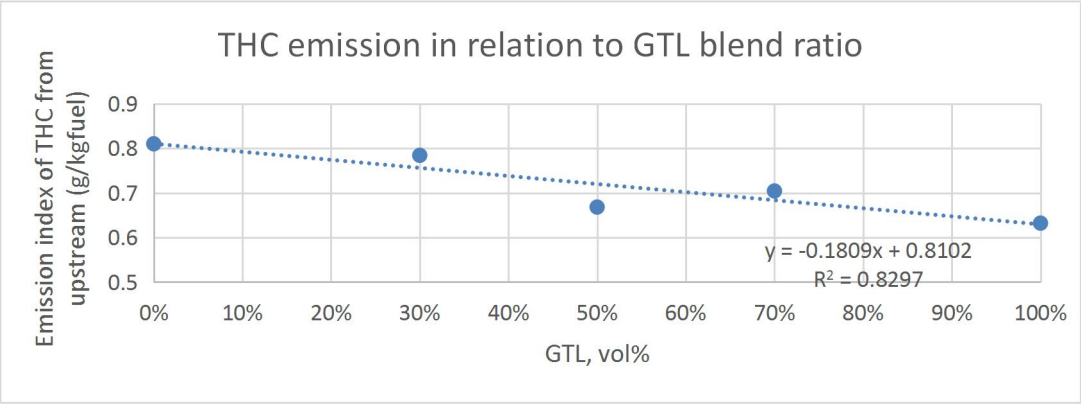


**Figure 6-44** THC emission in relation to GTL blend ratio based on THC emission from upstream at 1600rpm, 60% throttle.

In general, the 1600 rpm tests showed similar trends to 1000 rpm. However, the DOC efficiencies were no longer related to THC concentrations. All DOC THC conversion efficiencies from 1600 rpm tests stayed at approximately 90%. It can be seen from the data sampled at exhaust upstream in table 6-6 to table 6-8, the THC emission reduction increases with the increase of blending ratio. The THC reduction relationships against blending ratio were most significant in 1600 rpm, 40% throttle, and became less significant with the throttle setting increased. If considering the THC measured from exhaust downstream with value equal and lower than 5 ppm as none-detectable, then blending 30% of GTL would already be enough to improve the THC emissions at exhaust downstream. Because all blended fuels and pure GTL fuel had THC emissions lower than the equipment's' accurate detect range and only table 6-6 showed one valid value 7 ppm for 30% GTL blended fuel, which is still lower than diesel's 8 ppm.

From the results in figure 6-43 and figure 6-44, it can also be seen that the THC emissions from 50% and 70% GTL blended fuels were quite close. The same outcome can be observed from 1900 rpm test according to figure 6-45 to figure 6-47. One common characteristics of these five working conditions is that the engine powers all exceeded 27 KW. This compromises with the analysis from PV diagram discussion previously that the combustion advantage of GTL fuel at 27 kw engine power and over can be little, indicating the fuel premixing performances can be very similar. Thus, the result is very similar for the THC emission measured.

**Table 6-9** THC emissions of GTL blended fuels from exhaust upstream and downstream, with DOC efficiency, at 1900rpm 50% throttle.

| Fuel Type | THC Upstream | | | | THC Downstream | | | | DOC efficiency |
|---|---|---|---|---|---|---|---|---|---|
| | ppm | EI g/kgfuel | g/kWh | STDEVA/mean | ppm | EI g/kgfuel | g/kWh | STDEVA/mean | |
| Diesel | 75 | 1.05 | 0.29 | 2.11% | 7 | 0.10 | 0.03 | 7.79% | 90.67% |
| 30% GTL | 71 | 1.00 | 0.27 | 2.54% | 4 | 0.05 | 0.01 | 2.78% | 94.63% |
| 50% GTL | 66 | 0.95 | 0.26 | 1.69% | 5 | 0.07 | 0.02 | 2.12% | 92.13% |
| 70% GTL | 66 | 0.95 | 0.26 | 1.32% | 5 | 0.07 | 0.02 | 0.63% | 92.33% |
| 100% GTL | 57 | 0.81 | 0.21 | 1.24% | 4 | 0.06 | 0.01 | 0.00% | 92.93% |

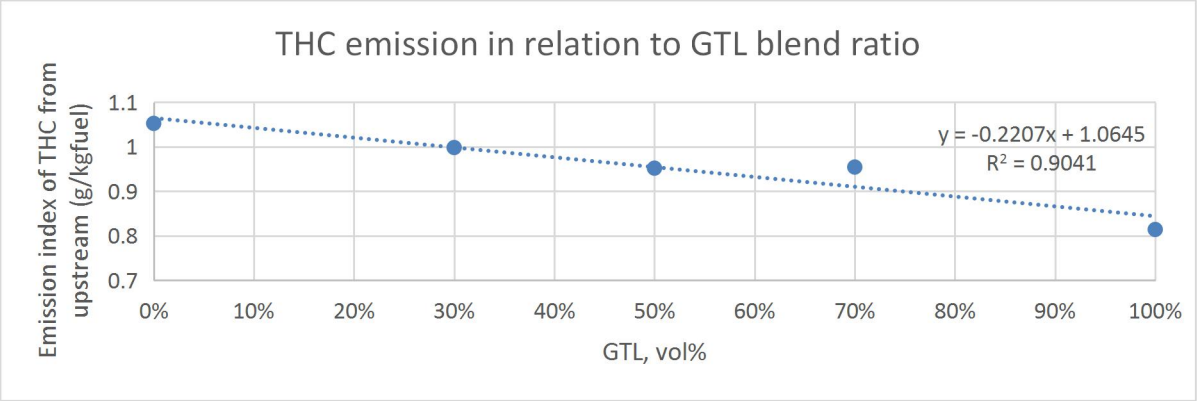


**Figure 6-45** THC emission in relation to GTL blend ratio based on THC emission from upstream at 1900rpm, 50% throttle.

**Table 6-10** THC emissions of GTL blended fuels from exhaust upstream and downstream, with DOC efficiency, at 1900rpm 60% throttle.

| Fuel Type | THC Upstream | | | | THC Downstream | | | | DOC efficiency |
|---|---|---|---|---|---|---|---|---|---|
| | ppm | EI g/kgfuel | g/kWh | STDEVA/mean | ppm | EI g/kgfuel | g/kWh | STDEVA/mean | |
| Diesel | 74 | 1.00 | 0.27 | 1.52% | 9 | 0.12 | 0.03 | 11.72% | 87.93% |
| 30% GTL | 67 | 0.90 | 0.24 | 2.53% | 3 | 0.04 | 0.01 | 3.05% | 95.58% |
| 50% GTL | 59 | 0.81 | 0.22 | 2.25% | 5 | 0.06 | 0.02 | 2.13% | 92.07% |
| 70% GTL | 61 | 0.84 | 0.22 | 1.66% | 5 | 0.06 | 0.02 | 1.25% | 92.28% |
| 100% GTL | 56 | 0.78 | 0.20 | 1.91% | 4 | 0.06 | 0.01 | 0.00% | 92.90% |

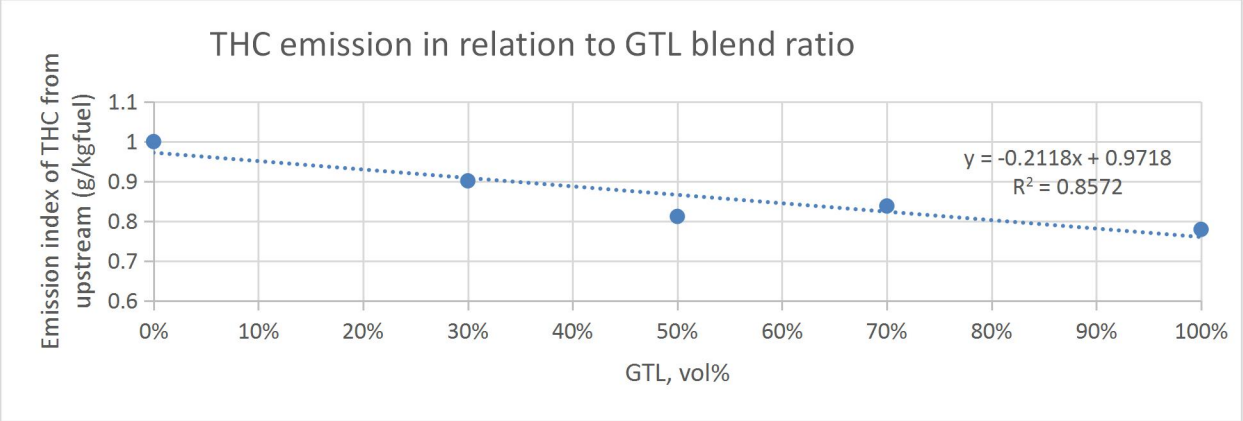


**Figure 6-46** THC emission in relation to GTL blend ratio based on THC emission from upstream at 1900rpm, 60% throttle.

**Table 6-11** THC emissions of GTL blended fuels from exhaust upstream and downstream, with DOC efficiency, at 1900rpm 70% throttle.

| Fuel Type | THC Upstream | | | | THC Downstream | | | | DOC efficiency |
|---|---|---|---|---|---|---|---|---|---|
| | ppm | EI g/kgfuel | g/kWh | STDEVA/mean | ppm | EI g/kgfuel | g/kWh | STDEVA/mean | |
| Diesel | 68 | 0.94 | 0.25 | 1.76% | 7 | 0.10 | 0.03 | 14.35% | 89.03% |
| 30% GTL | 61 | 0.83 | 0.22 | 2.94% | 3 | 0.04 | 0.01 | 1.82% | 95.01% |
| 50% GTL | 60 | 0.83 | 0.22 | 1.75% | 5 | 0.07 | 0.02 | 3.15% | 91.49% |
| 70% GTL | 57 | 0.79 | 0.20 | 1.85% | 5 | 0.07 | 0.02 | 1.55% | 91.26% |
| 100% GTL | 53 | 0.77 | 0.19 | 2.71% | 5 | 0.07 | 0.02 | 0.00% | 90.61% |

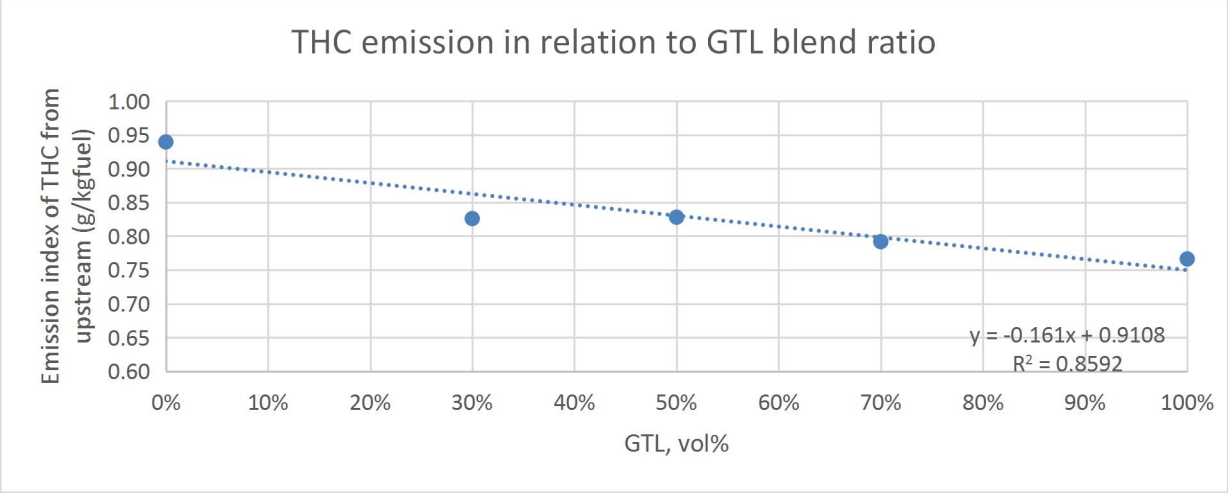


**Figure 6-47** THC emission in relation to GTL blend ratio based on THC emission from upstream at 1900rpm, 70% throttle.

The 1900 pm test also showed the same trend as the1600 rpm tests. The more the GTL fuel blended, the more the THC emissions reduced. The reduction gradient in THC emissions was reduced at the higher power. So besides comparing the result at each specific rpm, it's also important to investigate the THC emissions at different rpm setting with same throttle settings. From the results of 50% throttle settings at 1000, 1600, and 1900 rpm (in table 6-5, table 6-7 and table 6-9), it can be seen that the THC emissions gradually increased for all fuel types with the increasing of engine rpm. This is due to the fact that the engine power was increased so as the fuel consumption, thus all

emissions were elevated. The same findings were observed when comparing 40% throttle at 1000 and 1600 rpm and comparing 60% throttle at 1600 and 1900 rpm.

In summary, the GTL blended fuels and pure GTL fuel can significantly reduce the THC emissions by up to 54% (1000 rpm, 30% throttle, comparing pure GTL with pure diesel). The more GTL blended into diesel, the more THC emission would be reduced. However, this trend behaved less significant when the engine power increased. The THC emissions were almost in linear relationships with blending ratios at all tested engine conditions. When the engine power increased to 27 KW and beyond, and the blending ratio of GTL fuel increased to 50%, the reductions in THC emissions by GTL became insignificant. THC emissions measured at downstream of aftertreatment system (DOC and DPF) were very low for all the fuels, approaching the detection limit of the MEXA 7100 THC analyser. The DOC efficiencies in THC conversion was quite high and ranged from 87% to 97%.

### 6.4 CO emissions

This section provides the CO emission result analysis from all GTL blended tests. The CO emissions were measured both from exhaust upstream (before the aftertreatment system) and exhaust downstream (after the aftertreatment system). The raw data measured was in ppm and being converted to emission index and emission in grams per kwh. The CO emission results are listed in tables from 6-11 to table 6-19 based on engine working condition settings.

Diesel engine inherently has low CO emissions due to its principle of lean combustion. In lean combustion process, the abundant oxygen in combustion should be able to oxidise carbon element to carbon dioxide and left hardy any carbon monoxide. In addition, this engine is equipped with a DOC and DPF, which can effectively oxidise exhaust gases. Therefore, the CO emissions at downstream of aftertreatment system should be very low. From the HORIBA MEXA 7100 specification presented in Chapter 3, the CO emission measurement range is from 0 to 5000 ppm. Thus 0.04 % error would be 2 ppm, indicating measurement for CO concentration lower than 2 ppm could not be considered as valid and accurate.

**Table 6-11** CO emissions of GTL blended fuel at 1000rpm, 30% throttle.

| Fuel Type | CO Upstream | | | | CO Downstream | | | |
|---|---|---|---|---|---|---|---|---|
| | ppm | EI g/kgfuel | g/kWh | STDEVA/mean | ppm | EI g/kgfuel | g/kWh | STEDEVA/mean |
| Diesel | 157 | 4.22 | 1.33 | 4.14% | 0 | 0.00 | 0.00 | 0.00% |
| 30% GTL | 130 | 3.06 | 0.96 | 4.88% | 0 | 0.00 | 0.00 | 0.00% |
| 50% GTL | 139 | 3.33 | 1.03 | 4.26% | 0 | 0.00 | 0.00 | 0.00% |
| 70% GTL | 131 | 3.04 | 0.90 | 2.33% | 0 | 0.00 | 0.00 | 0.00% |
| 100% GTL | 140 | 3.40 | 0.99 | 4.47% | 2 | 0.05 | 0.01 | 0.00% |

**Table 6-12** CO emissions of GTL blended fuel at 1000rpm, 40% throttle.

| Fuel Type | CO Upstream | | | | CO Downstream | | | |
|---|---|---|---|---|---|---|---|---|
| | ppm | EI g/kgfuel | g/kWh | STDEVA/mean | ppm | EI g/kgfuel | g/kWh | STEDEVA/mean |
| Diesel | 161 | 3.59 | 1.090664 | 8.53% | 0 | 0.00 | 0.00 | 0.00% |
| 30% GTL | 175 | 5.07 | 1.493815 | 10.62% | 0 | 0.00 | 0.00 | 0.00% |
| 50% GTL | 164 | 4.19 | 1.21831 | 8.84% | 0 | 0.00 | 0.00 | 0.00% |
| 70% GTL | 161 | 2.83 | 0.81249 | 6.52% | 0 | 0.00 | 0.00 | 0.00% |
| 100% GTL | 176 | 3.76 | 1.056776 | 7.92% | 2 | 0.04 | 0.01 | 13.29% |

From the 1000 rpm CO emission result, it can be found that in general, when the throttle percentage setting increases the CO emission would increase at 1000 rpm. This indicates that at 1000 rpm, the mixing between fuel and air is getting worse with the throttle percentage increases. Thus, the poor mixing hindered the ideal lean combustion to occur, and carbon elements in the fuel mixture were failed to be oxidised to carbon dioxide during the combustion. Especially when the engine is running at 1000 rpm, 50% throttle, the CO emission was over six times than 30% and 40% results, indicating it's the poorest fuel mixing. The fuel injected into the combustion chamber with 50% throttle opened could not be well mixed with air at 1000 rpm, due to the engine speed was too low to create powerful enough turbulence required by ideal fuel-air mixing. This aligned with the PN result that the PN emissions suddenly increased at 1000 rpm, 50% throttle condition. The correlation between throttle settings and CO emissions indicate that the higher fuel injection rate at higher throttle setting condition worsened the fuel mixing and

consequently generated more CO emissions. The GTL blending ratio presented irregular impact on CO emissions, and the CO emissions measured from exhaust downstream is zero or close to zero, indicating the after-treatment system oxidised all CO from engine out exhaust. The 2 ppm and 1 ppm measured from 100% GTL tests is believed to be approaching the instrument's detection limit.

**Table 6-13** CO emissions of GTL blended fuel at 1000rpm, 50% throttle.

| Fuel Type | CO Upstream | | | | CO Downstream | | | |
|---|---|---|---|---|---|---|---|---|
| | ppm | EI g/kgfuel | g/kWh | STDEVA/mean | ppm | EI g/kgfuel | g/kWh | STEDEVA/mean |
| Diesel | 1405 | 27.64 | 8.46 | 3.47% | 0 | 0.00 | 0.00 | 0.00% |
| 30% GTL | 1466 | 28.15 | 8.45 | 6.87% | 0 | 0.00 | 0.00 | 0.00% |
| 50% GTL | 1446 | 28.20 | 8.42 | 4.15% | 0 | 0.00 | 0.00 | 0.00% |
| 70% GTL | 1246 | 24.27 | 7.18 | 4.65% | 0 | 0.00 | 0.00 | 0.00% |
| 100% GTL | 1610 | 31.20 | 8.98 | 4.04% | 1 | 0.02 | 0.01 | 0.00% |

With the increasing of rpm setting to 1600, it can be addressed from table 6-14 to table 6-16 that at when the throttle setting increases from 40% to 60%, the overall CO emission would reduce. The air to fuel ratio measured in for 40%, 50% and 60% at 1600 rpm was respectively 25, 24 and 23 indicating the amount of air joined in the lean combustion at those three working statuses is similar. And considering the fuel consumption increases with throttle percentage increases, the only reason brought down the CO emission is fuel to air mixing. Even the air was slightly less and even the fuel injected was slightly more, the higher throttle setting at 1600 rpm still improved the air-fuel mixing and producing less CO exhausts. This indicates that after the engine reaches 1600 rpm, the working of engine is closer to ideal lean combustion operating condition. Pure GTL and blended GTL fuel showed the slight lower CO emissions in most test conditions, however with the blending ratio increases the behaviour of CO was irregular. Hardly any detectable CO can be found from exhaust downstream.

**Table 6-14** CO emissions of GTL blended fuel at 1600rpm, 40% throttle.

| Fuel Type | CO Upstream | | | | CO Downstream | | | |
|---|---|---|---|---|---|---|---|---|
| | ppm | EI g/kgfuel | g/kWh | STDEVA/mean | ppm | EI g/kgfuel | g/kWh | STEDEVA/mean |
| Diesel | 182 | 4.57 | 1.34 | 1.67% | 0 | 0.00 | 0.00 | 0.00% |
| 30% GTL | 185 | 4.58 | 1.37 | 3.05% | 0 | 0.00 | 0.00 | 0.00% |
| 50% GTL | 169 | 4.32 | 1.28 | 2.46% | 0 | 0.00 | 0.00 | 0.00% |
| 70% GTL | 167 | 4.22 | 1.22 | 4.41% | 0 | 0.00 | 0.00 | 0.00% |
| 100% GTL | 165 | 4.26 | 1.18 | 3.15% | 1 | 0.02 | 0.01 | 26.71% |

**Table 6-15** CO emissions of GTL blended fuel at 1600rpm, 50% throttle.

| Fuel Type | CO Upstream | | | | CO Downstream | | | |
|---|---|---|---|---|---|---|---|---|
| | ppm | EI g/kgfuel | g/kWh | STDEVA/mean | ppm | EI g/kgfuel | g/kWh | STEDEVA/mean |
| Diesel | 117 | 2.80 | 0.81 | 2.41% | 0 | 0.00 | 0.00 | 0.00% |
| 30% GTL | 116 | 2.72 | 0.75 | 2.60% | 0 | 0.00 | 0.00 | 0.00% |
| 50% GTL | 115 | 2.74 | 0.75 | 2.34% | 0 | 0.00 | 0.00 | 0.00% |
| 70% GTL | 113 | 2.70 | 0.75 | 3.97% | 0 | 0.00 | 0.00 | 0.00% |
| 100% GTL | 114 | 2.75 | 0.70 | 3.49% | 1 | 0.02 | 0.01 | 0.00% |

**Table 6-16** CO emissions of GTL blended fuel at 1600rpm, 60% throttle.

| Fuel Type | CO Upstream | | | | CO Downstream | | | |
|---|---|---|---|---|---|---|---|---|
| | ppm | EI g/kgfuel | g/kWh | STDEVA/mean | ppm | EI g/kgfuel | g/kWh | STEDEVA/mean |
| Diesel | 97 | 2.23 | 0.62 | 4.54% | 2 | 0.05 | 0.01 | 28.57% |
| 30% GTL | 88 | 2.01 | 0.55 | 3.83% | 0 | 0.00 | 0.00 | 0.00% |
| 50% GTL | 78 | 1.82 | 0.49 | 4.27% | 0 | 0.00 | 0.00 | 0.00% |
| 70% GTL | 80 | 1.87 | 0.50 | 5.38% | 0 | 0.00 | 0.00 | 0.00% |
| 100% GTL | 91 | 2.13 | 0.55 | 4.16% | 2 | 0.05 | 0.01 | 13.99% |

The 1900 rpm tests showed similar findings to 1600 rpm tests. The CO emissions from all kinds of fuel gradually reduced with the throttle percentage setting increases, and the CO emission behaved irregularly in relation to the blending ratio. Admittedly, the pure GTL performed slight lower CO emissions, however the 30% and 50% GTL fuels

performed higher CO emissions than diesel, and 70% GTL showed CO emissions in the middle between 50% and 100% blending ratio. This is probably due to the ideal lean combustion of blended fuel was irregular and capricious with either engine power settings being increased or decreased. Therefore, the more detailed study of how CO emissions generated from blended fuels is necessary in the future work. The after-treatment system could oxidize all CO from raw exhausts and left hardly detectable CO can be found at engine exhaust downstream.

**Table 6-17** CO emissions of GTL blended fuel at 1900rpm, 50% throttle.

| Fuel Type | CO Upstream | | | | CO Downstream | | | |
|---|---|---|---|---|---|---|---|---|
| | ppm | EI g/kgfuel | g/kWh | STDEVA/mean | ppm | EI g/kgfuel | g/kWh | STEDEVA/mean |
| Diesel | 153 | 3.77 | 1.05 | 1.96% | 2 | 0.05 | 0.01 | 0.00% |
| 30% GTL | 159 | 3.92 | 1.07 | 1.18% | 0 | 0.00 | 0.00 | 0.00% |
| 50% GTL | 159 | 4.03 | 1.10 | 1.49% | 0 | 0.00 | 0.00 | 0.00% |
| 70% GTL | 151 | 3.81 | 1.02 | 1.10% | 0 | 0.00 | 0.00 | 0.00% |
| 100% GTL | 150 | 3.78 | 0.96 | 2.67% | 1 | 0.03 | 0.01 | 0.00% |

**Table 6-18** CO emissions of GTL blended fuel at 1900rpm, 60% throttle.

| Fuel Type | CO Upstream | | | | CO Downstream | | | |
|---|---|---|---|---|---|---|---|---|
| | ppm | EI g/kgfuel | g/kWh | STDEVA/mean | ppm | EI g/kgfuel | g/kWh | STEDEVA/mean |
| Diesel | 98 | 2.31 | 0.63 | 2.54% | 2 | 0.05 | 0.01 | 0.00% |
| 30% GTL | 109 | 2.56 | 0.69 | 1.76% | 0 | 0.00 | 0.00 | 0.00% |
| 50% GTL | 105 | 2.51 | 0.68 | 2.25% | 0 | 0.00 | 0.00 | 0.00% |
| 70% GTL | 97 | 2.33 | 0.62 | 1.66% | 0 | 0.00 | 0.00 | 0.00% |
| 100% GTL | 92 | 2.23 | 0.57 | 2.96% | 1 | 0.02 | 0.01 | 0.00% |

**Table 6-19** CO emissions of GTL blended fuel at 1900rpm, 70% throttle.

| Fuel Type | CO Upstream | | | | CO Downstream | | | |
|---|---|---|---|---|---|---|---|---|
| | ppm | EI g/kgfuel | g/kWh | STDEVA/mean | ppm | EI g/kgfuel | g/kWh | STEDEVA/mean |
| Diesel | 55 | 1.34 | 0.35 | 3.92% | 3 | 0.08 | 0.02 | 19.23% |
| 30% GTL | 71 | 1.69 | 0.44 | 4.53% | 0 | 0.00 | 0.00 | 0.00% |
| 50% GTL | 62 | 1.51 | 0.39 | 2.98% | 0 | 0.00 | 0.00 | 0.00% |
| 70% GTL | 57 | 1.39 | 0.36 | 3.28% | 0 | 0.00 | 0.00 | 0.00% |
| 100% GTL | 54 | 1.37 | 0.35 | 3.68% | 3 | 0.07 | 0.02 | 15.04% |

In summary of the CO performance, at 1000 rpm (relevant low engine rpm operating conditions), increasing throttle settings would worsen the air-fuel mixing and producing high CO emissions. And when the engine reaches 1600 rpm and 1900 rpm, the pure GTL could slight improve the CO emissions, and the CO emissions were improved with the throttle settings being increased at each rpm setting. However, the CO emissions' behaviour in relation to blending ratio were still irregular. Therefore, it's necessary to conduct a future study involving more detailed research on how CO emissions would behave in relation to different blending ratios and how these blending ratios could lay impact on their corresponsive ideal lean combustion requirements. The exhaust aftertreatment system could remove all the CO residues in the raw exhausts via oxidation and left undetectable CO at engine exhaust downstream.

## 6.5 Conclusions

This section presented the emission performances of GTL fuel and its blended fuels in comparison with diesel. According to all the results, discussions and analysis presented above, the following conclusions can be reached:

- The pure GTL fuel could help to reduce the total $NO_X$ emissions by up to 17% but can be 2.3% higher than diesel fuel very occasionally. The blended GTL fuels were more effective in $NO_x$ reductions, even with just 30% GTL blended into diesel, 25% to 35% of $NO_x$ reduction was observed in the majority of test conditions. The 50%, 70% GTL blended fuels showed similar reduction

efficiencies. However, the reduction didn't show particular relationship with blending ratio. It's believed that a certain amount of aromatics in a fuel could act as anti-oxidants that helps to control $NO_x$ emissions. The concentration of aromatics is estimated to be in a range from 7.5% to 17.5%.

- The engine out NO could be converted to $NO_2$ by DOC. The conversion rate was found to be 25% to 70%. The NO oxidation rate reduced with the throttle setting increased at each engine rpm, and this is due to the conversion limitation of the DOC.
- The GTL and GTL blended fuel can reduce the particle number emissions both in nucleation and accumulation mode particles. The reduction in nucleation mode particles were obvious in lower engine power conditions (up to 65%), while the reduction in particles with diameter greater than 154 nm was significant in high engine power conditions (up to 75%). And the total particle number reduction increased with the blending ratio increased, which is shown in figure 6-19. The accumulation mode particles are more sensitive to blending ratios than the nucleation mode particles. In general, the mode size of accumulation mode particles reduced with the blending ratio increased and ranged from 86 nm to 205 nm. The nucleation mode particle distribution between fuels are similar and most of the nucleation mode particles are in diameter region of 10 to 20 nm.
- The DPF showed efficiencies of higher than 99% in all test conditions and left hardly any detectable particles at the downstream of the DPF.
- The GTL fuel and its blends can reduce the THC emissions by up to 54%, and the reduction increased when the blend ratio was increased. However, the reduction became insignificant when the engine power increased, because fuel premixing was improved with increased engine power settings. The DOC efficiency ranged from 87% to 97% and left hardly any THC at downstream of the DOC.
- The CO emissions from diesel fuel, pure GTL fuel and GTL blended fuels were similar at each specific engine operating condition and showed no particular trend with blending ratios.

In summary, the pure GTL fuel can significantly reduce the particle number and THC emissions from the diesel engine while it did not show obvious reduction in $NO_X$ and CO emissions. The GTL blended fuels, in addition to show significant reduction in PN and THC emissions, they also showed effective $NO_X$ emission reduction. The combustion performances between all tested fuels were similar, and the most obvious improvement was that the ignition delays reduced with the increasing of blending ratio. Therefore, the application of GTL blending strategy can benefit both the PN and $NO_X$ emissions, which are two major pollutants emissions from diesel engine. The PN reduction reduces with the blend ratio increase, while the $NO_x$ emission can be reduced by the anti-oxidant effects of aromatics in certain concentration range. The estimated optimised concentration range of aromatics is from 17.5% to 7.5%, however, it's still necessary for the future research to investigate if the upper concentration can be increased. Because this relates to the minimum blending ratio that can improve $NO_x$ emissions and the minimum fuel production cost.

# Chapter 7. Fuel property and combustion analysis of HVO and its blends

This chapter presents the emission and combustion results from the hydrotreated vegetable oil (HVO) and its blended fuels. The discussion started with the fuel property analysis of the HVO fuel, from which the main chemical and physical differences between HVO fuel and diesel fuel are addressed. Then the combustion performance was discussed in three topics: the engine power generation performances; pressure to crank angle performance; and PV diagrams. Based on those discussion and analysis, the emissions were discussed in four categories: the THC emissions, the CO emissions, the $NO_X$ emissions (include the NO, $NO_2$ and $NO_x$), and the particle number distribution behaviour. All these emissions were sampled both from upstream and downstream of the aftertreatment system, thus allowing the efficiencies and impact of aftertreatment system to be understood. This chapter ends with the conclusions achieved from combustion and emission analysis of HVO fuel and its blends, and the suggestions for future research and future HVO fuel application will be provided as well.

## 7.1 Introduction of the tests

The particle and $NO_x$ emissions are always of concerned to the public when talking about diesel engine applications. These two kinds of emissions could lay negative impacts on the environment and human health in a variety of ways. More importantly, these two kinds of emissions would have trade-off relationship to each other, because lower particle generation always require higher combustion temperature which could boost the $NO_X$ production; and lower $NO_X$ emissions always occur under lower combustion temperature which could contribute to more particle generation. Thus, finding out the solution to control these two kinds of emission in the optimum way can be a critical research topic. Based on the findings from GTL fuel and its blends, it was observed that fuels with more straight chains and branched carbon chain paraffins are more easily to be burned off completely, and thus can reduce the particle emission significantly. Also, by blending aromatic free fuels into diesel fuel, the aromatic concentration can be reduced and a certain amount of aromatics in a fuel could behave as anti-oxidants which could reduce the $NO_X$ emissions effectively. The HVO fuel is

similar to the GTL fuel, as chemically it is aromatic free and consisted of straight chains and saturated paraffins. However, the carbon chain distributions are different between the HVO and GTL fuels. Therefore, followed by the GTL blended fuel work, this research selected HVO fuel as another alternative fuel, and same engine operating test conditions were applied so as to verify some conclusions based on the same theory and to understand their differences based on different fuel properties. Same as the GTL blended fuel tests, all results were compared against to diesel fuel, and the blending ratios with diesel fuel applied were respectively 30%, 50%, 70% and 100% HVO. The engine, engine combustion and emission measurement devices were all the same as used in the previous GTL blended fuel research.

## 7.2 Fuel property analysis

Before the understanding of fuel combustion and emission production, it's important to find out the fuel property characteristics of the tested fuels. Table 7-1 presents the fuel specification of the HVO fuel compared to experiment diesel fuel. The carbon, hydrogen, nitrogen, sulphur weight percentages and calorific values were acquired from CHNS elemental analysis, and the rest of the data was acquired from the manufacture. [Neste, 2014] It can be seen from the fuel property that HVO fuel contained 7% more nitrogen element in weight percentages by measurement, but the nitrogen measured was believed to be below the CHNS detection sensitivity. The mass based calorific value of the HVO fuel is also 7.1% higher than diesel fuel. However, when converting to volume based calorific value, the two fuels have very similar values due to lower density of HVO fuel. ($5.56\times10^6$ Kcal/$m^3$ for diesel, $5.52\times10^6$ Kcal/$m^3$ for HVO) The HVO fuel contained no FAME content and aromatics because instead of having transesterification process like biodiesel, vegetable oils were hydrotreated in the isomerization process, and all triglycerides were breached into fully saturated paraffins. The cetane number of HVO is higher than diesel fuel, implying the HVO fuel can have shorter ignition delay. The density of HVO fuel is slightly lower than diesel fuel and the viscosity is similar.

**Table 7-1** The fuel specification and properties for diesel and HVO fuels.

| Property | Unit | Diesel | HVO |
|---|---|---|---|
| Appearance at +25 ° C | | | Clear & Bright |
| Cetane number | | ⩾ 51.0 | > 70.0 |
| Density at +15 ° C | kg/m$^3$ | 840 | 780 |
| Total aromatics | % (m/m) | 25 | < 1.0 |
| Polyaromatics | % (m/m) | ⩽ 8 | < 0.1 |
| Sulphur | wt % | 0 | 0 |
| Hydrogen | wt % | 11.39 | 11.93 |
| Carbon | wt % | 80.59 | 86.30 |
| Nitrogen | wt % | 0.59 (trace) | 0.66 (trace) |
| Net calorific value | MJ/Kg | 42.9 | 44.1 |
| FAME-content | % (V/V) | ⩽ 7.0 | 0 |
| Flash point | ° C | > 55 | > 61 |
| Carbon residue on 10 % distillation | % (m/m) | ⩽ 0.30 | < 0.10 |
| Ash | % (m/m) | ⩽ 0.01 | < 0.001 |
| Water | mg/kg | ⩽ 200 | < 200 |
| Total contamination | mg/kg | ⩽ 24 | < 10 |
| Viscosity at +40 ° C | mm$^2$/s | 2.00 ⋯ 4.50 ⩾ 1.20 * | 2.00 ⋯ 4.00 |
| Distillation 95 % (v/v) | ° C | ⩽ 360 | < 320 |
| Final boiling point | ° C | < 330 | |

The distillation characteristics of HVO fuel was acquired from TGA test and the results are shown in figure 7-1. From the result, it can be found that the HVO fuel evaporated faster than diesel fuel below temperature 176 °C and above temperature 242 °C, while showed slower distillation rate between 176 °C and 242 °C. This indicates that the HVO fuel contains two groups of hydrocarbons. The first group has lighter than diesel fractions-represented by a fast mass loss up to 157 °C. The second group of hydrocarbons had their weight loss roughly from 210 °C to 260 °C where the gradient of the curve started to increase at approximately 210 °C followed by a sharper than diesel fall in gradient till the end. The weight loss curve of the diesel fuel showed a steady

gradient from 150 °C to 290 °C, indicating an evenly distributed light to heavy hydrocarbon chains. The starting temperature of both fuels is the same but the ending temperature of the HVO fuel is about 30 °C earlier than the diesel fuel, demonstrating that the HVO fuel contains fewer heavy fractions. This is proved by the GC-MS results in figure 7-2 and 7-3. The lube oil didn't show obvious fuel dilution had occurred. The used lube oil evaporates quicker than fresh lube oil since the temperature reached 310 °C, and it's likely to be caused by the breakdown of lube oil.

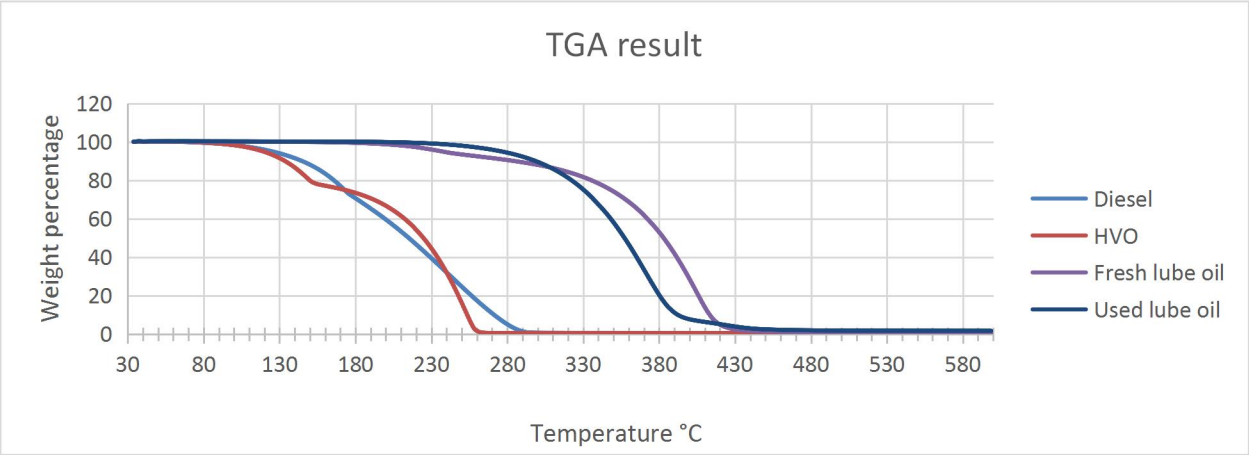


**Figure 7-1** The TGA analysis results of diesel fuel, HVO fuel, fresh engine lube oil, and used engine lube oil.

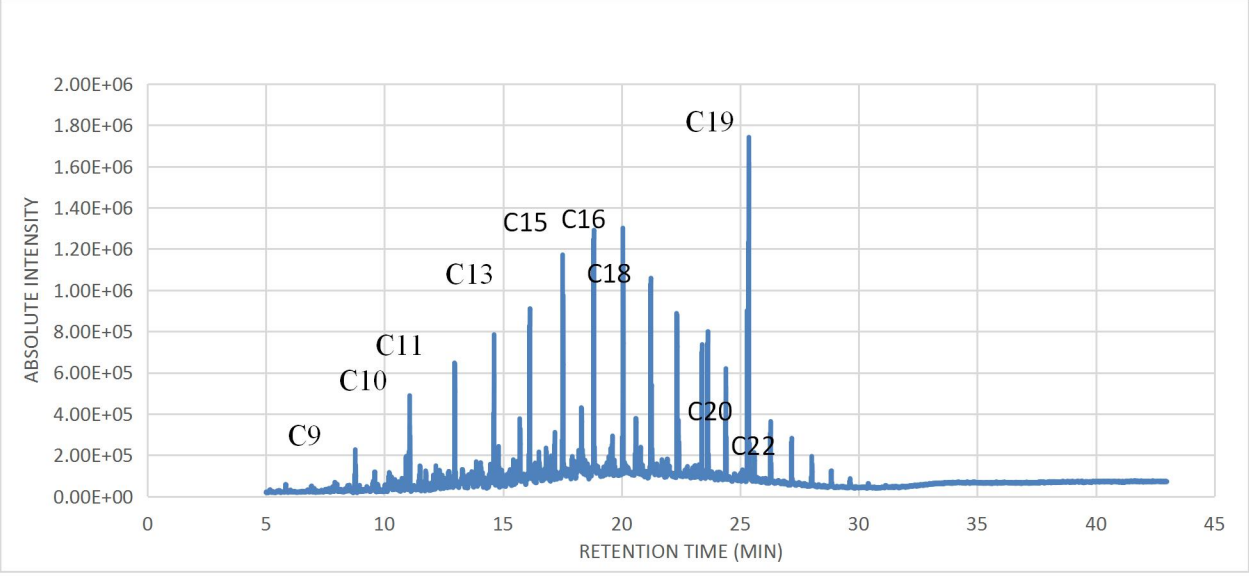


**Figure 7-2** The total ion chromatogram of diesel fuel.

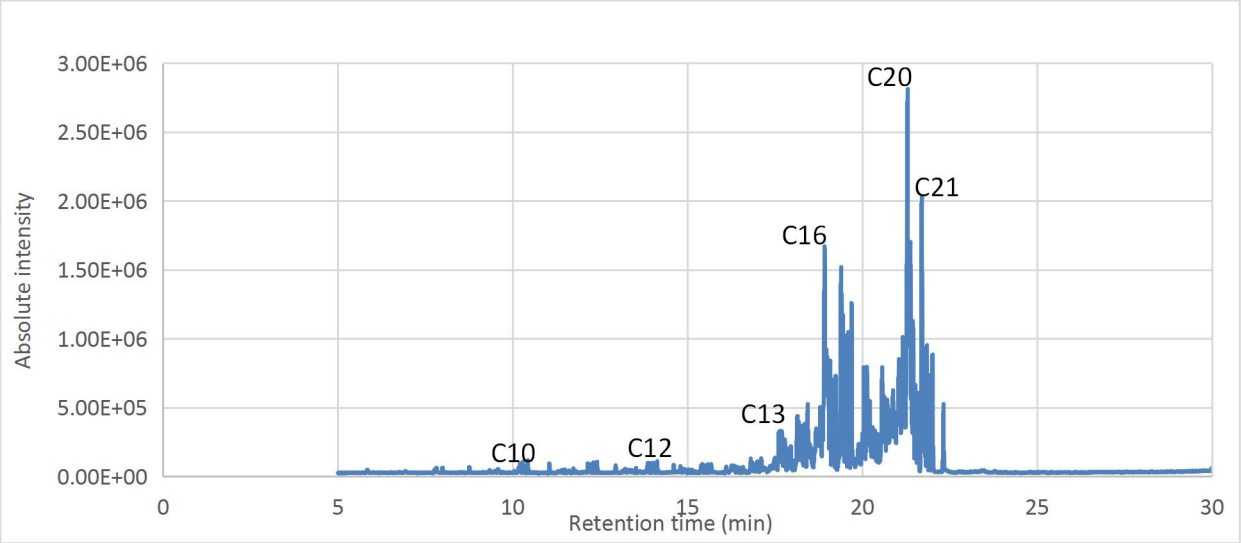


**Figure 7-3** The total ion chromatogram of HVO fuel.

The carbon number distribution was acquired from GCMS test, and the results for diesel fuel and HVO fuel are shown in figure 7-2 and figure 7-3. From the comparison, it can be observed that the HVO fuel mainly consisted of hydrocarbon chains ranged from $C_{13}$ to $C_{21}$ and this showed the agreement with the manufacturer that the carbon distribution for straight chains are typically between $C_{12}$ to $C_{20}$. This is decided by the feed stock type [Neste, 2018], which was waste cooking oils and animal fats and generally had carbon chains of $C_{13}$-$C_{20}$. Those shorter chains can be formed in the decarboxylation process occurred simultaneously and contributing to the light fraction composition shown from the previous TGA result in figure 7-1. Since the straight chains and saturated paraffins dominate the composition of HVO fuel, the majority of carbon chains distribution in figure 7-3 are ranged from $C_{13}$ to $C_{21}$. The absolute intensity of carbon chains ranged from $C_{16}$ to $C_{21}$ was clearly higher than diesel fuel. The detail of molecular formula and corresponded concentration, retention time is of HVO fuel acquired from the GCMS test is listed in following tables from table 7-2 to table 7-4. From those tables, it can be seen that HVO fuel contained no aromatics and consisted of only straight carbon chains and saturated paraffinic hydrocarbon chains ($C_nH_{2n+2}$).

**Table 7-2** The mass spectrum peak absolute intensity table of HVO fuel part one.

| Name | Molecular formula | Conc. (%) | cum. Conc. (%) | Ret.Time (mins) | Area | Height |
|---|---|---|---|---|---|---|
| Eicosane | $C_{20}H_{42}$ | 7.4 | 7.4 | 21.299 | 7188006 | 2771619 |
| Nonadecane | $C_{19}H_{40}$ | 5.62 | 13.02 | 21.703 | 5458486 | 1990002 |
| Pentadecane, 8-hexyl- | ↱ $C_{21}H_{44}$ | 4.9 | 17.92 | 21.375 | 4754672 | 1661231 |
| Hexadecane | ↱ $C_{16}H_{34}$ | 4.27 | 22.19 | 19.395 | 4146598 | 1477266 |
| Hexadecane | ↱ $C_{16}H_{34}$ | 4.1 | 26.29 | 18.927 | 3978627 | 1625892 |
| Octadecane | $C_{18}H_{38}$ | 3.04 | 29.33 | 21.162 | 2949617 | 969000 |
| Octane, 4,5-diethyl- | $C_{12}H_{26}$ | 2.24 | 31.57 | 19.001 | 2177461 | 830863 |
| Pentadecane, 8-hexyl- | $C_{21}H_{44}$ | 2.24 | 33.81 | 21.456 | 2176398 | 1081732 |
| Tridecane, 6-methyl- | $C_{14}H_{30}$ | 2.23 | 36.04 | 21.34 | 2162726 | 1361525 |
| Hexadecane, 2-methyl- | ↱ $C_{17}H_{36}$ | 2.04 | 38.08 | 19.7 | 1982545 | 1211207 |
| Tridecane, 6-methyl- | ↱ $C_{14}H_{30}$ | 1.99 | 40.07 | 18.972 | 1928978 | 881056 |
| Nonane, 5-butyl- | ↱ $C_{13}H_{28}$ | 1.99 | 42.06 | 20.571 | 1931191 | 749558 |
| Heptadecane, 2-methyl- | ↱ $C_{18}H_{38}$ | 1.95 | 44.01 | 20.883 | 1897458 | 585559 |
| Eicosane | $C_{20}H_{42}$ | 1.85 | 45.86 | 20.133 | 1797198 | 755633 |
| Pentadecane, 4-methyl- | $C_{14}H_{34}$ | 1.8 | 47.66 | 19.534 | 1749582 | 972854 |
| Pentadecane | $C_{15}H_{32}$ | 1.8 | 49.46 | 21.05 | 1748166 | 811962 |
| Heptadecane, 2-methyl- | ↱ $C_{18}H_{38}$ | 1.76 | 51.22 | 19.459 | 1705455 | 1123048 |
| Octadecane | $C_{18}H_{38}$ | 1.74 | 52.96 | 21.216 | 1687822 | 771533 |
| Pentadecane, 2-methyl- | ↱ $C_{16}H_{34}$ | 1.73 | 54.69 | 19.611 | 1681600 | 1007291 |
| Pentadecane, 2-methyl- | ↱ $C_{16}H_{34}$ | 1.54 | 56.23 | 19.161 | 1491963 | 658829 |
| Hexadecane | ↱ $C_{16}H_{34}$ | 1.48 | 57.71 | 20.052 | 1436318 | 752935 |
| Heptadecane, 4-methyl- | ↱ $C_{18}H_{38}$ | 1.44 | 59.15 | 21.855 | 1400761 | 908842 |
| Heptadecane, 4-methyl- | ↱ $C_{18}H_{38}$ | 1.41 | 60.56 | 20.72 | 1368062 | 518233 |
| Octadecane | $C_{18}H_{38}$ | 1.41 | 61.97 | 21.08 | 1371547 | 678197 |
| Hexadecane, 2-methyl- | ↱ $C_{18}H_{38}$ | 1.41 | 63.38 | 21.785 | 1372049 | 861960 |
| Pentadecane, 2-methyl- | $C_{16}H_{34}$ | 1.4 | 64.78 | 19.083 | 1362583 | 799315 |
| Heptadecane, 4-methyl- | $C_{14}H_{34}$ | 1.37 | 66.15 | 21.528 | 1326946 | 624699 |
| Pentadecane | $C_{15}H_{32}$ | 1.32 | 67.47 | 18.804 | 1285291 | 462313 |
| Heptadecane, 2-methyl- | $C_{18}H_{38}$ | 1.32 | 68.79 | 21.928 | 1280042 | 693882 |
| Heptadecane, 3-methyl- | ↱ $C_{18}H_{38}$ | 1.31 | 70.1 | 22.012 | 1270367 | 846039 |
| Nonadecane | $C_{19}H_{40}$ | 1.21 | 71.31 | 20.929 | 1173434 | 416217 |
| Heptadecane, 3-methyl- | ↱ $C_{18}H_{38}$ | 1.19 | 72.5 | 21.604 | 1152846 | 566683 |
| Pentadecane | $C_{15}H_{32}$ | 1.15 | 73.65 | 18.148 | 1114483 | 398124 |
| Heptadecane, 2-methyl- | $C_{18}H_{38}$ | 1.14 | 74.79 | 20.797 | 1105990 | 430470 |
| Pentadecane, 2-methyl- | $C_{16}H_{34}$ | 1.12 | 75.91 | 20.65 | 1083285 | 533882 |
| Heptadecane | $C_{17}H_{36}$ | 1.12 | 77.03 | 21.003 | 1088661 | 432922 |
| Octadecane | $C_{18}H_{38}$ | 1.11 | 78.14 | 18.682 | 1082579 | 307329 |

**Table 7-3** The mass spectrum peak absolute intensity table of HVO fuel part two.

| Name | Molecular formula | Conc. (%) | cum. Conc. (%) | Ret.Time (mins) | Area | Height |
|---|---|---|---|---|---|---|
| Hexadecane, 2-methyl- | $C_{18}H_{38}$ | 1.11 | 79.25 | 19.247 | 1076031 | 689813 |
| Pentadecane, 2-methyl- | $C_{16}H_{34}$ | 1.06 | 80.31 | 18.441 | 1028903 | 481834 |
| Decane, 5-methyl- | $C_{11}H_{24}$ | 1.05 | 81.36 | 18.745 | 1017559 | 285656 |
| Pentadecane, 2-methyl- | $C_{16}H_{34}$ | 0.95 | 82.31 | 20.217 | 926802 | 509021 |
| Octane, 2,3-dimethyl- | $C_{10}H_{22}$ | 0.89 | 83.2 | 20.603 | 862327 | 546240 |
| Heptadecane, 4-methyl- | $C_{14}H_{34}$ | 0.83 | 84.03 | 18.269 | 809047 | 325525 |
| Octadecane | $C_{18}H_{38}$ | 0.74 | 84.77 | 22.325 | 717479 | 482625 |
| Pentadecane, 2-methyl- | $C_{16}H_{34}$ | 0.73 | 85.5 | 18.35 | 706311 | 340815 |
| Undecane, 2,6-dimethyl- | $C_{13}H_{28}$ | 0.69 | 86.19 | 17.649 | 674763 | 289157 |
| Heptadecane | $C_{17}H_{36}$ | 0.69 | 86.88 | 20.176 | 673523 | 382724 |
| Hexadecane, 2-methyl- | $C_{18}H_{38}$ | 0.66 | 87.54 | 20.375 | 641080 | 293477 |
| Eicosane | $C_{20}H_{42}$ | 0.62 | 88.16 | 20.005 | 604082 | 272279 |
| Heptadecane, 4-methyl- | $C_{14}H_{34}$ | 0.62 | 88.78 | 20.295 | 601043 | 317764 |
| Tetradecane | $C_{14}H_{30}$ | 0.61 | 89.39 | 18.866 | 595145 | 323108 |
| Tridecane, 2-methyl- | $C_{14}H_{30}$ | 0.58 | 89.97 | 18.192 | 558793 | 356185 |
| Heptadecane, 2-methyl- | $C_{18}H_{38}$ | 0.58 | 90.55 | 20.451 | 563202 | 268242 |
| Dodecane, 2,6,11-trimethyl- | $C_{15}H_{32}$ | 0.55 | 91.1 | 17.702 | 536323 | 288541 |
| Octadecane | $C_{18}H_{38}$ | 0.53 | 91.63 | 17.619 | 518620 | 282540 |
| Dodecane, 2,6,10-trimethyl- | $C_{15}H_{32}$ | 0.5 | 92.13 | 18.503 | 483751 | 195475 |
| Heptadecane, 3-methyl- | $C_{18}H_{38}$ | 0.41 | 92.54 | 19.334 | 396828 | 228802 |
| Pentadecane, 4-methyl- | $C_{16}H_{34}$ | 0.4 | 92.94 | 19.935 | 385386 | 171653 |
| Octadecane, 2-methyl- | $C_{19}H_{40}$ | 0.39 | 93.33 | 17.79 | 374407 | 227731 |
| Pentadecane, 2-methyl- | $C_{16}H_{34}$ | 0.38 | 93.71 | 19.892 | 369769 | 195743 |
| Pentadecane, 2-methyl- | $C_{16}H_{34}$ | 0.36 | 94.07 | 17.961 | 347053 | 178331 |
| Tetradecane | $C_{14}H_{30}$ | 0.35 | 94.42 | 18.541 | 341614 | 169890 |
| Tridecane | $C_{13}H_{28}$ | 0.34 | 94.76 | 17.514 | 331435 | 95959 |
| Dodecane, 4,6-dimethyl- | $C_{14}H_{30}$ | 0.33 | 95.09 | 20.76 | 324045 | 223948 |
| Dodecane, 2,6,11-trimethyl- | $C_{15}H_{32}$ | 0.29 | 95.38 | 17.874 | 285541 | 161415 |
| Decane, 2,5-dimethyl- | $C_{12}H_{26}$ | 0.28 | 95.66 | 20.254 | 267133 | 178746 |
| Tetradecane | $C_{14}H_{30}$ | 0.27 | 95.93 | 19.854 | 261351 | 97665 |
| Tridecane, 3-methyl- | $C_{14}H_{30}$ | 0.22 | 96.15 | 17.11 | 212582 | 93318 |
| Heptadecane, 8-methyl- | $C_{18}H_{38}$ | 0.21 | 96.36 | 20.334 | 207768 | 126106 |
| Octadecane | $C_{18}H_{38}$ | 0.2 | 96.56 | 19.76 | 198957 | 83227 |
| Undecane, 2,6-dimethyl- | $C_{13}H_{28}$ | 0.19 | 96.75 | 17.751 | 184531 | 111783 |
| Undecane, 2-methyl- | $C_{12}H_{26}$ | 0.16 | 96.91 | 13.874 | 153346 | 68920 |
| Tetradecane | $C_{14}H_{30}$ | 0.16 | 97.07 | 16.814 | 158536 | 100044 |
| Heptadecane, 2-methyl- | $C_{18}H_{38}$ | 0.15 | 97.22 | 16.856 | 143012 | 71177 |

**Table 7-4** The mass spectrum peak absolute intensity table of HVO fuel part three.

| Name | Molecular formula | Conc. (%) | cum. Conc. (%) | Ret.Time (mins) | Area | Height |
|---|---|---|---|---|---|---|
| Tridecane, 2-methyl- | $C_{14}H_{30}$ | 0.15 | 97.37 | 17.012 | 146621 | 77393 |
| Octane, 2,6-dimethyl- | ↱ $C_{10}H_{22}$ | 0.14 | 97.51 | 10.435 | 139011 | 90738 |
| Decane, 2-methyl- | $C_{11}H_{24}$ | 0.13 | 97.64 | 12.304 | 124537 | 75530 |
| Nonane, 5-butyl- | $C_{13}H_{28}$ | 0.13 | 97.77 | 12.418 | 129371 | 80062 |
| Undecane, 2-methyl- | $C_{12}H_{26}$ | 0.13 | 97.9 | 14.032 | 122189 | 73060 |
| Tridecane, 3-methyl- | $C_{14}H_{30}$ | 0.13 | 98.03 | 14.135 | 123610 | 83144 |
| Pentadecane | $C_{15}H_{32}$ | 0.13 | 98.16 | 16.335 | 127018 | 44941 |
| Tetradecane, 3-methyl- | ↱ $C_{15}H_{32}$ | 0.13 | 98.29 | 18.051 | 123170 | 73019 |
| Octane, 2,7-dimethyl- | $C_{10}H_{22}$ | 0.12 | 98.41 | 10.296 | 118899 | 76982 |
| Hexane, 3-ethyl-4-methyl- | ↱ $C_9H_{20}$ | 0.11 | 98.52 | 10.216 | 109139 | 67378 |
| Decane | $C_{10}H_{22}$ | 0.11 | 98.63 | 11.054 | 108304 | 68677 |
| Undecane, 4-methyl- | $C_{12}H_{26}$ | 0.11 | 98.74 | 13.946 | 106201 | 70991 |
| Tetradecane | $C_{14}H_{30}$ | 0.11 | 98.85 | 15.681 | 103156 | 61165 |
| Decane, 5-methyl- | ↱ $C_{11}H_{24}$ | 0.1 | 98.95 | 12.153 | 95981 | 65304 |
| Decane, 4-methyl- | $C_{11}H_{24}$ | 0.1 | 99.05 | 12.222 | 96623 | 61486 |
| Undecane, 2-methyl- | $C_{12}H_{26}$ | 0.1 | 99.15 | 15.425 | 99318 | 63434 |
| Dodecane, 2-methyl- | $C_{13}H_{28}$ | 0.1 | 99.25 | 15.584 | 98592 | 60894 |
| Tridecane, 2-methyl- | $C_{14}H_{30}$ | 0.1 | 99.35 | 16.93 | 98584 | 61235 |
| Hexadecane | $C_{16}H_{34}$ | 0.1 | 99.45 | 17.915 | 93865 | 62103 |
| Tridecane | $C_{13}H_{28}$ | 0.09 | 99.54 | 14.61 | 83245 | 54138 |
| Dodecane, 4-methyl- | ↱ $C_{13}H_{28}$ | 0.09 | 99.63 | 15.501 | 83993 | 54149 |
| Pentadecane, 2-methyl- | $C_{16}H_{34}$ | 0.09 | 99.72 | 17.36 | 85123 | 33956 |
| Undecane | $C_{11}H_{24}$ | 0.08 | 99.8 | 12.95 | 78176 | 53152 |
| Undecane, 2,6-dimethyl- | $C_{13}H_{28}$ | 0.08 | 99.88 | 15.395 | 73071 | 50745 |
| Decane, 2,5-dimethyl- | C12H26 | 0.07 | 99.95 | 13.21 | 71376 | 24846 |
| Pentadecane | $C_{15}H_{32}$ | 0.07 | 100.02 | 17.45 | 72447 | 40831 |

In summary, the HVO is aromatic free and consisted of only straight carbon chains and fully saturated paraffinic hydrocarbons. This indicates the HVO should be burned off more completely than diesel fuel and thus produce less particle emissions. This is very similar to GTL fuel. The HVO fuel also has higher cetane number and lower density when compared to diesel fuel.

## 7.3 Combustion performance

This part discusses the fuel combustion performances in three topics: the engine power generation, the pressure to crank angle curves near top dead centre, and the PV diagram analysis. The aim is to figure out how the blending ratio using HVO fuels can lay impacts on those measured parameters, and the blended fuel's combustion performances with experimental engine.

### 7.3.1 Engine power

This section presents the results of engine power, engine torque, IMEP, BMEP, maximum combustion pressure and average combustion pressure using diesel fuel, HVO blended fuel and pure HVO fuel. The results are shown in following tables from table 7-5 to table 7-13. From the results, it can be found that in general, the HVO blended fuel and pure HVO fuel showed almost the same value in engine power output at each specific engine operating condition. The biggest difference in engine power is 5%, when the engine was running at 20 KW (1000 rpm, 40% throttle and 1600 rpm, 405 throttle). The difference in engine torque, IMEP, and BMEP is low as well between all tested fuels. The error bar of torque measurement was ±3 Nm. This indicates that despite the mass based calorific value of pure HVO fuel is 7.1% higher than diesel fuel, hardly any difference in engine power output can be achieved using either pure HVO fuel or HVO blended fuel when the engine was running at same rpm and throttle settings. However, a relevantly more obvious difference in maximum combustion pressure and average combustion pressure was observed from this research.

**Table 7-5** The engine power of HVO blended tests at 1000 rpm, 30% throttle.

| Fuel Type | Torque (Nm) | Power (Kw) | BMEP (bar) | IMEP (bar) | P max (bar) | STDEVA/ mean for P max | P max location (°CA) | P average (bar) |
|---|---|---|---|---|---|---|---|---|
| Diesel | 125 | 13 | 5.3 | 7.3 | 61.2 | 0.78% | 17 | 7.2 |
| 30% HVO | 125 | 13 | 5.2 | 7.4 | 58.6 | 0.69% | 16 | 6.6 |
| 50% HVO | 126 | 13 | 5.3 | 7.2 | 58.2 | 0.74% | 16 | 6.6 |
| 70% HVO | 125 | 13 | 5.2 | 7.2 | 57.0 | 0.75% | 17 | 6.5 |
| 100% HVO | 125 | 13 | 5.2 | 7.2 | 59.2 | 0.58% | 17 | 6.8 |

**Table 7-6** The engine power of HVO blended tests at 1000 rpm, 40% throttle.

| Fuel Type | Torque (Nm) | Power (Kw) | BMEP (bar) | IMEP (bar) | P max (bar) | STDEVA/ mean for P max | P max location (°CA) | P average (bar) |
|---|---|---|---|---|---|---|---|---|
| Diesel | 182 | 19 | 7.6 | 9.8 | 73.6 | 0.56% | 16 | 8.3 |
| 30% HVO | 186 | 20 | 7.8 | 10.0 | 72.1 | 0.66% | 16 | 7.8 |
| 50% HVO | 189 | 20 | 7.9 | 9.9 | 73.8 | 0.64% | 16 | 7.9 |
| 70% HVO | 185 | 19 | 7.8 | 9.9 | 73.0 | 0.57% | 17 | 7.9 |
| 100% HVO | 186 | 19 | 7.8 | 9.9 | 74.7 | 0.52% | 17 | 8.2 |

**Table 7-7** The engine power of HVO blended tests at 1000 rpm, 50% throttle.

| Fuel Type | Torque (Nm) | Power (Kw) | BMEP (bar) | IMEP (bar) | P max (bar) | STDEVA/ mean for P max | P max location (°CA) | P average (bar) |
|---|---|---|---|---|---|---|---|---|
| Diesel | 207 | 22 | 8.7 | 11.8 | 85.0 | 0.63% | 16 | 8.6 |
| 30% HVO | 208 | 22 | 8.7 | 11.1 | 84.1 | 0.50% | 15 | 8.5 |
| 50% HVO | 207 | 22 | 8.7 | 11.1 | 84.2 | 0.52% | 15 | 8.5 |
| 70% HVO | 206 | 22 | 8.6 | 11.1 | 84.2 | 0.58% | 15 | 8.5 |
| 100% HVO | 207 | 22 | 8.7 | 11.0 | 85.0 | 0.50% | 16 | 8.8 |

**Table 7-8** The engine power of HVO blended tests at 1600 rpm, 40% throttle.

| Fuel Type | Torque (Nm) | Power (Kw) | BMEP (bar) | IMEP (bar) | P max (bar) | STDEVA/ mean for P max | P max location (°CA) | P average (bar) |
|---|---|---|---|---|---|---|---|---|
| Diesel | 119 | 20 | 5.0 | 6.9 | 60.7 | 0.76% | 18 | 7.2 |
| 30% HVO | 114 | 19 | 4.8 | 6.7 | 60.2 | 0.84% | 16 | 6.8 |
| 50% HVO | 114 | 19 | 4.8 | 6.8 | 60.2 | 0.88% | 16 | 6.9 |
| 70% HVO | 115 | 19 | 4.8 | 6.8 | 60.1 | 0.88% | 16 | 6.8 |
| 100% HVO | 116 | 19 | 4.8 | 6.7 | 60.2 | 0.81% | 16 | 7.1 |

**Table 7-9** The engine power of HVO blended tests at 1600 rpm, 50% throttle.

| Fuel Type | Torque (Nm) | Power (Kw) | BMEP (bar) | IMEP (bar) | P max (bar) | STDEVA/ mean for P max | P max location (°CA) | P average (bar) |
|---|---|---|---|---|---|---|---|---|
| Diesel | 153 | 26 | 6.4 | 8.8 | 68.4 | 0.83% | 17 | 8.4 |
| 30% HVO | 157 | 27 | 6.6 | 8.7 | 66.9 | 0.82% | 17 | 8.0 |
| 50% HVO | 160 | 27 | 6.7 | 8.9 | 67.6 | 0.72% | 17 | 8.0 |
| 70% HVO | 158 | 27 | 6.6 | 8.8 | 66.9 | 0.89% | 17 | 7.9 |
| 100% HVO | 158 | 26 | 6.6 | 8.9 | 68.4 | 0.93% | 18 | 8.3 |

**Table 7-10** The engine power of HVO blended tests at 1600 rpm, 60% throttle.

| Fuel Type | Torque (Nm) | Power (Kw) | BMEP (bar) | IMEP (bar) | P max (bar) | STDEVA/ mean for P max | P max location (°CA) | P average (bar) |
|---|---|---|---|---|---|---|---|---|
| Diesel | 215 | 36 | 9.0 | 11.5 | 87.4 | 0.68% | 17 | 10.2 |
| 30% HVO | 216 | 36 | 9.0 | 11.6 | 88.4 | 0.65% | 16 | 9.8 |
| 50% HVO | 213 | 36 | 8.9 | 11.3 | 85.7 | 0.77% | 16 | 9.6 |
| 70% HVO | 212 | 36 | 8.9 | 11.5 | 86.4 | 0.72% | 16 | 9.6 |
| 100% HVO | 219 | 37 | 9.2 | 11.6 | 88.9 | 0.73% | 16 | 10.1 |

From table 7-5 to table 7-7, it can be found that the maximum and average in-cylinder pressure values between HVO fuel and are hardly differentiable. However, all HVO blended fuels showed slightly lower maximum combustion and average in-cylinder pressure values in all the 1000 rpm tests. The same finding was obtained from the 1600 rpm tests and the1900 rpm tests. Despite in the1600 rpm, 40% throttle test condition the difference in maximum in-cylinder pressure was little, however, the average in-cylinder pressure values from blended fuels were all lower than pure diesel fuel and pure HVO fuel. The average in-cylinder pressure from blended fuels can be 6% lower than from diesel and pure HVO fuel when the engine was running at 1000 rpm and 1600 rpm; and can be up to 7% lower when the engine was running at 1900 rpm. This phenomenon will be explained in the next section after the analysis of pressure change. Besides, this

phenomenon means that the average in-cylinder temperatures using blended HVO fuels can be slightly lower than using pure diesel fuel or pure HVO fuel, indicating the thermal $NO_X$ formation from HVO blended fuels can be less.

**Table 7-11** The engine power of HVO blended tests at 1900 rpm, 50% throttle.

| Fuel Type | Torque (Nm) | Power (Kw) | BMEP (bar) | IMEP (bar) | P max (bar) | P max location (°CA) | P average (bar) |
|---|---|---|---|---|---|---|---|
| Diesel | 135 | 27 | 5.7 | 7.8 | 65.1 | 18 | 8.0 |
| 30% HVO | 131 | 26 | 5.5 | 7.8 | 65.4 | 16 | 7.7 |
| 50% HVO | 134 | 27 | 5.6 | 7.9 | 65.4 | 18 | 7.8 |
| 70% HVO | 134 | 27 | 5.6 | 8.0 | 65.8 | 17 | 7.7 |
| 100% HVO | 138 | 27 | 5.8 | 7.8 | 66.6 | 17 | 8.0 |

**Table 7-12** The engine power of HVO blended tests at 1900 rpm, 60% throttle.

| Fuel Type | Torque (Nm) | Power (Kw) | BMEP (bar) | IMEP (bar) | P max (bar) | P max location (°CA) | P average (bar) |
|---|---|---|---|---|---|---|---|
| Diesel | 183 | 36 | 7.7 | 9.8 | 78.1 | 18 | 9.7 |
| 30% HVO | 179 | 36 | 7.5 | 9.9 | 76.4 | 18 | 9.1 |
| 50% HVO | 184 | 37 | 7.7 | 10.1 | 76.0 | 17 | 9.2 |
| 70% HVO | 181 | 36 | 7.6 | 9.9 | 74.5 | 17 | 9.0 |
| 100% HVO | 182 | 36 | 7.6 | 9.8 | 77.6 | 17 | 9.5 |

**Table 7-13** The engine power of HVO blended tests at 1900 rpm, 70% throttle.

| Fuel Type | Torque (Nm) | Power (Kw) | BMEP (bar) | IMEP (bar) | P max (bar) | P max location (°CA) | P average (bar) |
|---|---|---|---|---|---|---|---|
| Diesel | 238 | 47 | 10.0 | 12.6 | 102.6 | 15 | 11.4 |
| 30% HVO | 235 | 47 | 9.8 | 12.6 | 102.2 | 16 | 11.2 |
| 50% HVO | 238 | 48 | 10.0 | 12.7 | 105.6 | 16 | 11.3 |
| 70% HVO | 235 | 47 | 9.9 | 12.7 | 103.2 | 15 | 11.0 |
| 100% HVO | 237 | 47 | 10.0 | 12.6 | 103.2 | 15 | 11.5 |

In summary, the engine power generation from diesel fuel, HVO blended fuel and pure HVO fuel is almost the same. The pure HVO and pure diesel fuel also shared nearly the same peak and average in-cylinder pressure, however, the blended HVO fuels obtained lower peak combustion pressure and lower average in-cylinder pressure when compared to those two pure fuel types.

### 7.3.2 In-cylinder pressure curve and ignition delay

In order to figure out the in-cylinder pressure behaviour at the end of compression stroke and how the pressure changes during fuel injection and combustion. The pressure to crank angle curves near TDC are presented in this section. The ignition delay analysis is provided because it presents the performance of fuel droplet atomization, vaporization and the fuel to air mixing [Lakshminarayanan, and Aghav, 2010], and therefore can be important for emission production, for instance hydrocarbon and Nano-particles. Based on nine different engine test conditions, the result of ignition delay detail and pressure curves are provided in the following tables and figures.

**Table 7-14** The ignition delays of HVO blended fuels at 1000rpm, 30% throttle.

| Fuel Type | SOI CA° | SOC CA° | ID CA° | ID (ms) |
|---|---|---|---|---|
| Diesel | -2 | 7 | 9 | 1.50 |
| 30% HVO | -2 | 7 | 9 | 1.50 |
| 50% HVO | -2 | 7 | 9 | 1.50 |
| 70% HVO | -2 | 7 | 9 | 1.50 |
| 100% HVO | -2 | 7 | 9 | 1.50 |

**Table 7-15** The ignition delays of HVO blended fuels at 1000rpm, 40% throttle.

| Fuel Type | SOI CA° | SOC CA° | ID CA° | ID (ms) |
|---|---|---|---|---|
| Diesel | -4 | 5 | 8 | 1.50 |
| 30% HVO | -4 | 5 | 8 | 1.50 |
| 50% HVO | -4 | 5 | 8 | 1.50 |
| 70% HVO | -4 | 5 | 8 | 1.50 |
| 100% HVO | -4 | 5 | 8 | 1.50 |

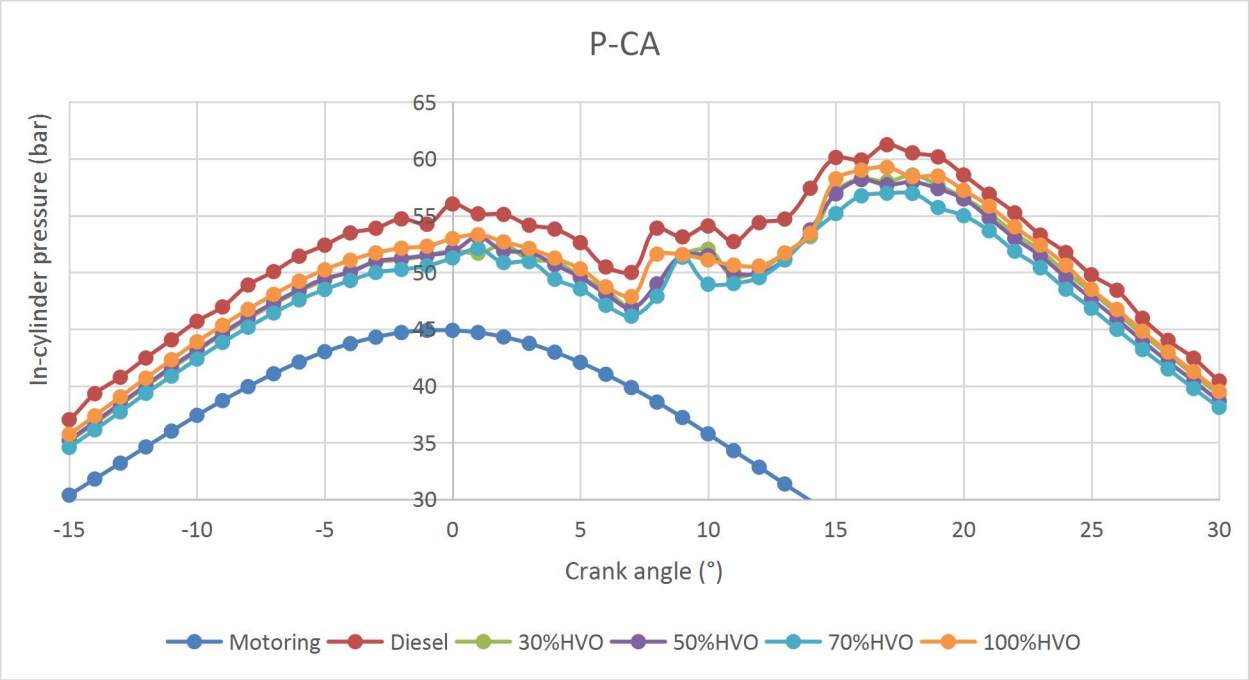


**Figure 7-4** The pressure curve near TDC of HVO blended fuels at 1000rpm, 30% throttle.

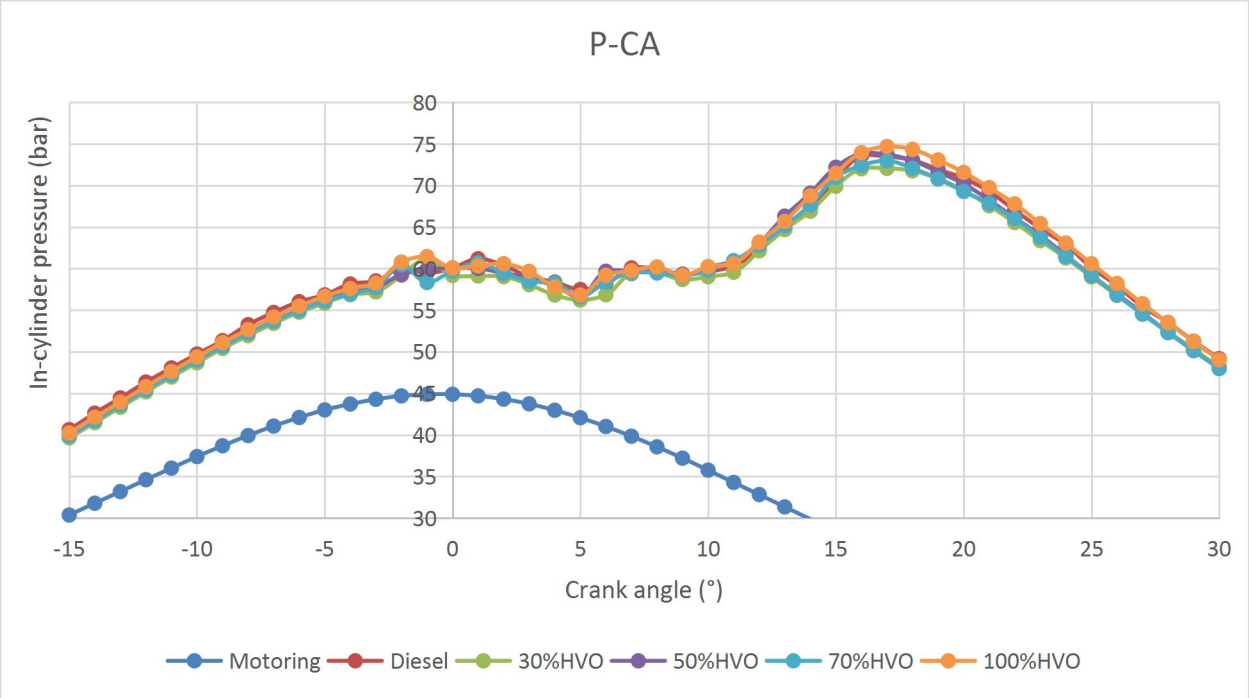


**Figure 7-5** The pressure curve near TDC of HVO blended fuels at 1000rpm, 40% throttle.

**Table 7-16** The ignition delays of HVO blended fuels at 1000rpm, 50% throttle.

| Fuel Type | SOI CA° | SOC CA° | ID CA° | ID (ms) |
|---|---|---|---|---|
| Diesel | -3 | 4 | 7 | 1.17 |
| 30% HVO | -3 | 3 | 6 | 1.00 |
| 50% HVO | -3 | 3 | 6 | 1.00 |
| 70% HVO | -3 | 3 | 6 | 1.00 |
| 100% HVO | -2 | 3 | 6 | 1.00 |

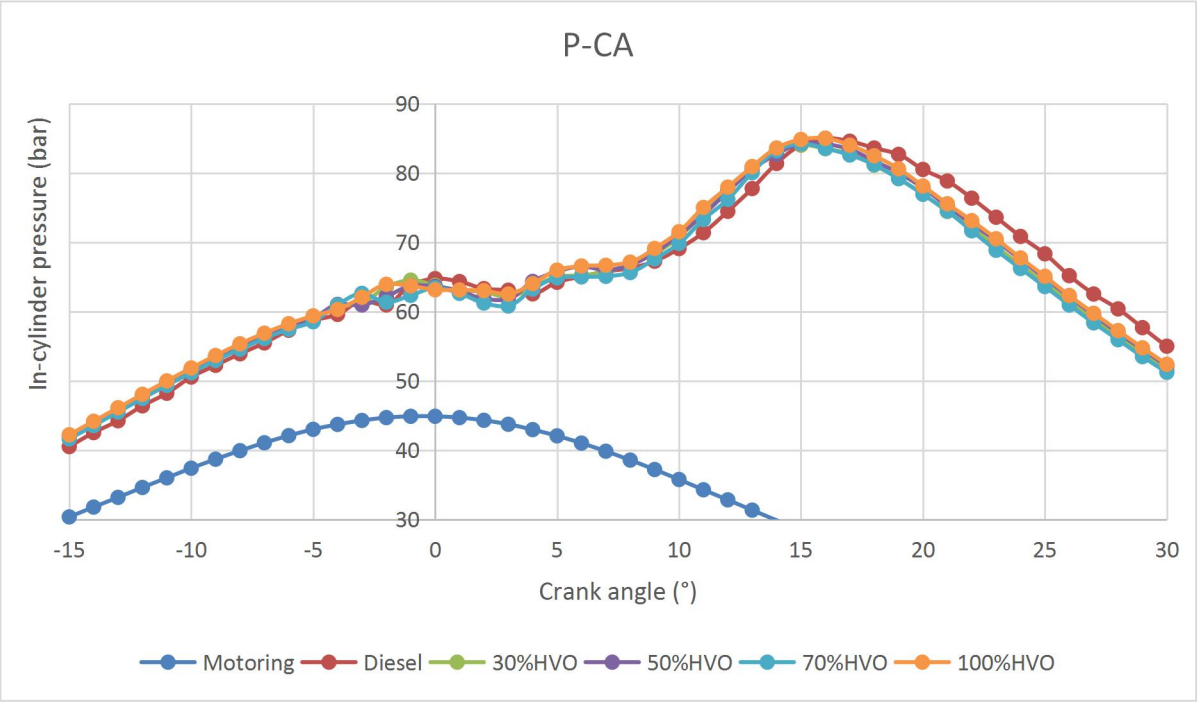


**Figure 7-6** The pressure curve near TDC of HVO blended fuels at 1000rpm, 50% throttle.

At the first stage of 1000 rpm test, the engine was running with 30% throttle opened, and from the results in table 7-14 and figure 7-4, it can be found that the differences between pure diesel fuel, pure HVO fuel and HVO blended fuel is still detectable. The diesel fuel obtained the highest combustion pressure curve followed by the pure HVO fuel, the blended fuels all showed lower combustion pressure and the differences among them is little. Because, the pure HVO fuel is more likely to be burned, thus the pure HVO fuel generated higher in-cylinder pressure. This can also be proved as in

figure 7-4, all HVO blended fuels and HVO fuel showed in cylinder pressure lower than diesel fuel since 15 degrees before the piston arrives TDC. Besides, the relevantly higher calorific value obtained by pure HVO fuel can also contribute to its high-pressure performance in fuel combustion. All blended fuels showed lower combustion pressure than pure HVO fuel and diesel fuel. The start of fuel injection point and fuel start of combustion point are the same at this engine operating condition, therefore all tested fuels demonstrated the same ignition delay time. When the engine throttle increased to 40% and 50%, it can be seen from figure 7-5 and figure 7-6 that all tested fuels presented very similar pressure changes and no obvious difference in ignition delay can be seen. This could be due to at 30%, 40% and 50% throttle settings, the engine rpm was too low to achieve the ideal fuel to air mixing. The fuel to air mixing relied on mostly the turbulence generated by piston moving, which was decided by the engine rpm setting.  Thus, the advantage of HVO fuel (high cetane number) could not be realized at these operating conditions.

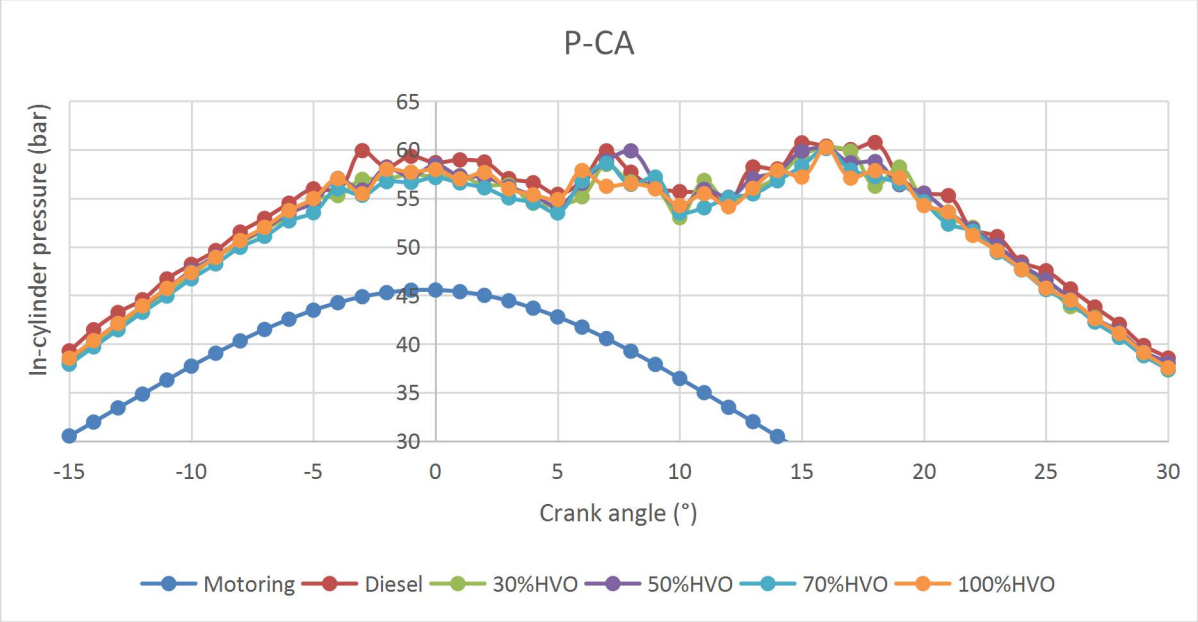


**Figure 7-7** The pressure curve near TDC of HVO blended fuels at 1600rpm, 40% throttle.

**Table 7-17** The ignition delays of HVO blended fuels at 1600rpm, 40% throttle.

| Fuel Type | SOI CA° | SOC CA° | ID CA° | ID (ms) |
|---|---|---|---|---|
| Diesel | -5 | 5 | 10 | 1.04 |
| 30% HVO | -4 | 5 | 9 | 0.94 |
| 50% HVO | -4 | 5 | 9 | 0.94 |
| 70% HVO | -4 | 5 | 9 | 0.94 |
| 100% HVO | -4 | 5 | 9 | 0.94 |

**Table 7-18** The ignition delays of HVO blended fuels at 1600rpm, 50% throttle.

| Fuel Type | SOI CA° | SOC CA° | ID CA° | ID (ms) |
|---|---|---|---|---|
| Diesel | -6 | 5 | 11 | 1.15 |
| 30% HVO | -6 | 5 | 11 | 1.15 |
| 50% HVO | -4 | 5 | 9 | 0.94 |
| 70% HVO | -4 | 5 | 9 | 0.94 |
| 100% HVO | -6 | 5 | 11 | 1.15 |

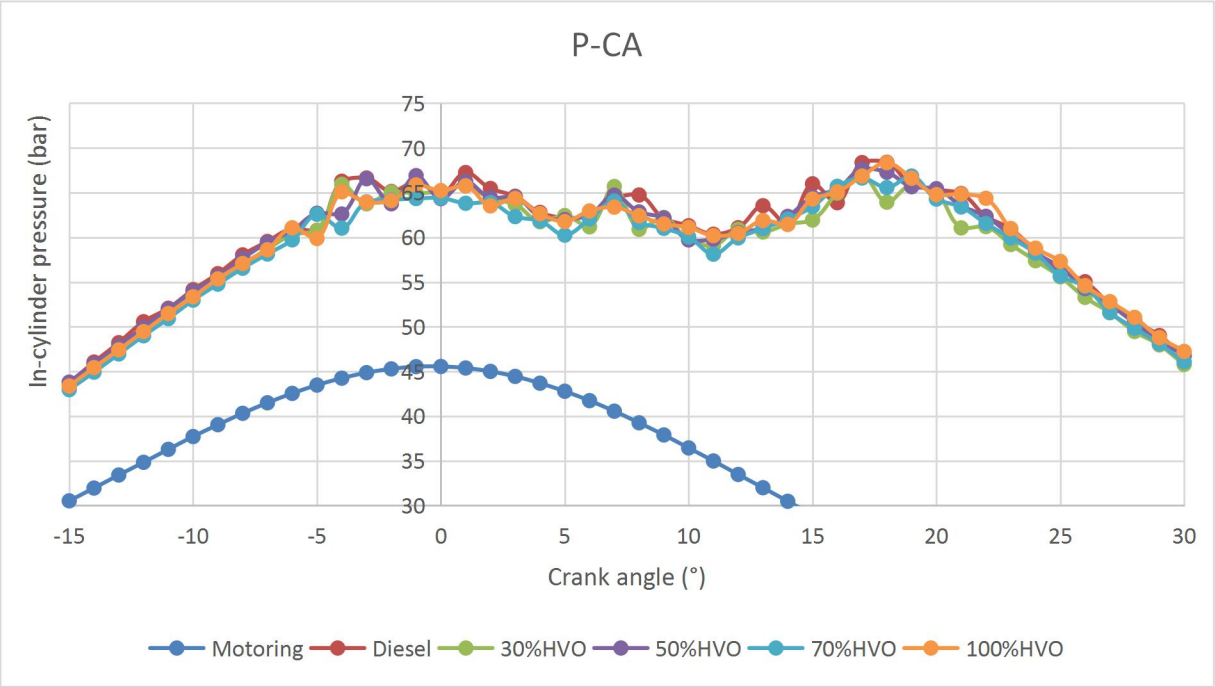


**Figure 7-8** The pressure curve near TDC of HVO blended fuels at 1600rpm, 50% throttle.

**Table 7-19** The ignition delays of HVO blended fuels at 1600rpm, 60% throttle.

| Fuel Type | SOI CA° | SOC CA° | ID CA° | ID (ms) |
|---|---|---|---|---|
| Diesel | -9 | 2 | 11 | 1.15 |
| 30% HVO | -8 | 1 | 9 | 0.94 |
| 50% HVO | -8 | 1 | 9 | 0.94 |
| 70% HVO | -9 | 1 | 10 | 1.04 |
| 100% HVO | -9 | 1 | 10 | 1.04 |

When the engine rpm increased to 1600 rpm, it can be seen from figure 7-7, the combustion pressure behaviour between tested fuels started to become very close. Comparing figure 7-7 with figure 7-8 and figure 7-9, it can be observed that at all test conditions in 1600 rpm, the in-cylinder pressure from all tested fuels are very close. This indicates that the HVO fuel can be blended with diesel at any desirable blending ratio and the blending ratio wouldn't affect the combustion performance negatively, for instance, bring down the engine power output. Unlike the scenario in 1000 rpm, 30% throttle test, in the 1600 rpm tests, the pressure curves were very close for all the tested fuels from 15 degrees BTDC, indicating the heat absorbed by different fuels was very similar as abundant heat was generated at 1600 rpm engine speed. However, all HVO blended fuels showed slightly lower combustion pressure, particular peak pressure. From the results, it can also be found that the diesel fuel obtained longer ignition delay as its cetane number is lower. The in-cylinder pressure behaviours from pure HVO fuel was in general similar to diesel fuel. However, it can be slightly higher than diesel sometimes. This can be proved in figure 7-9, that during the fuel combustion process the pure HVO fuel achieved the highest pressure.

Multiple fuel injections were observed from the 1600 rpm result as the multiple pressure drops near TDC were identified caused by different fuel injections. Each time when there was a fuel injection event, in-cylinder pressure would drop as the fuel injected into combustion chamber will absorb heat during vaporisation and atomization and create pressure decline. As discussed in the experimental chapter, the IVECO engine manufacture designed the multiple fuel injection strategy to improve the engine combustion and emission performance. It can be addressed from figure 7-9, that the

first pressured drop near 9 degrees BTDC ignited the fuel. The fuel injection designed to improve the fuel air premix was not captured in figure 7-9, because there was no visible changes in pressure curves. The pilot fuel injection was followed by 3 to 4 main fuel injection at respectively 5 degrees BTDC, 3 degrees BTDC, 0 degrees BTDC and 5 degrees ATDC. The fuel injection designed to oxidize soot and regenerate DPF was not captured in pressure curves, because no DPF regeneration event was captured during the experiment.

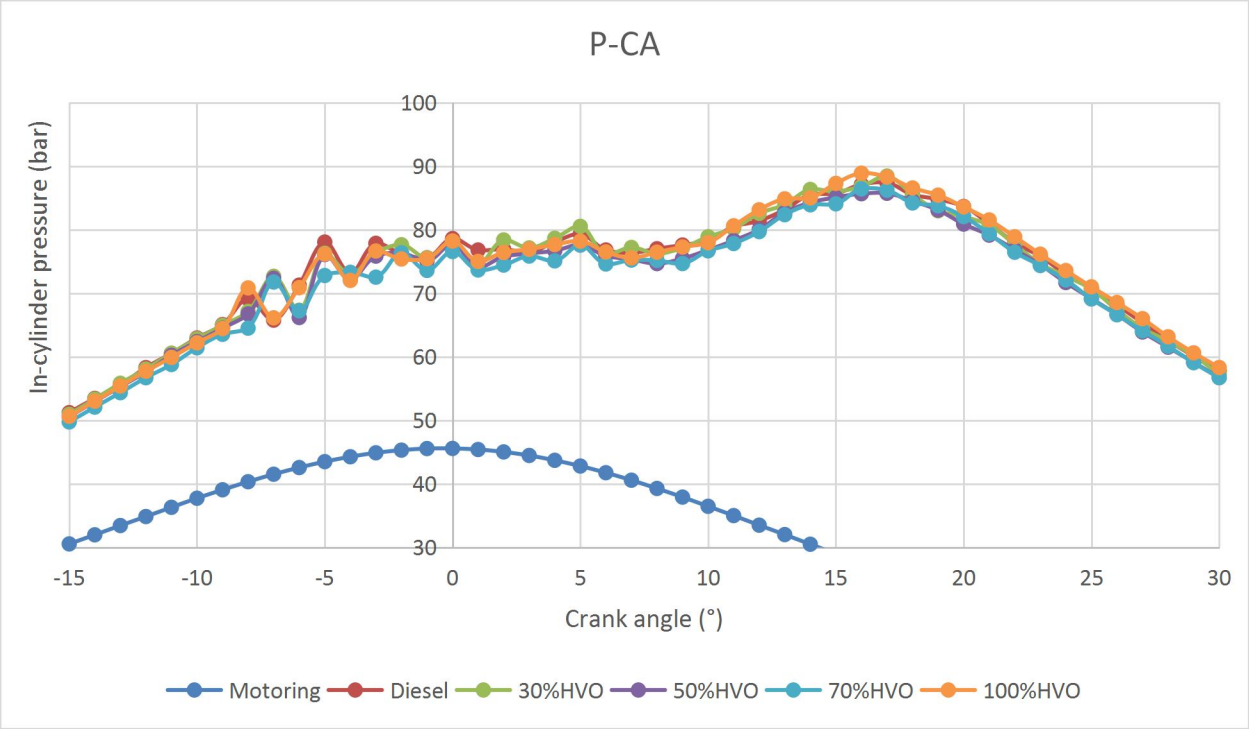


**Figure 7-9** The pressure curve near TDC of HVO blended fuels at 1600rpm, 60% throttle.

**Table 7-20** The ignition delays of HVO blended fuels at 1900rpm, 50% throttle.

| Fuel Type | SOI CA° | SOC CA° | ID CA° | ID (ms) |
|---|---|---|---|---|
| Diesel | -6 | 4 | 10 | 0.88 |
| 30% HVO | -6 | 4 | 10 | 0.88 |
| 50% HVO | -6 | 4 | 10 | 0.88 |
| 70% HVO | -6 | 4 | 10 | 0.88 |
| 100% HVO | -5 | 4 | 9 | 0.79 |

**Table 7-21** The ignition delays of HVO blended fuels at 1900rpm, 60% throttle.

| Fuel Type | SOI CA° | SOC CA° | ID CA° | ID (ms) |
|---|---|---|---|---|
| Diesel | -6 | 3 | 9 | 0.79 |
| 30% HVO | -6 | 3 | 8 | 0.79 |
| 50% HVO | -6 | 3 | 8 | 0.79 |
| 70% HVO | -6 | 3 | 8 | 0.79 |
| 100% HVO | -5 | 3 | 8 | 0.70 |

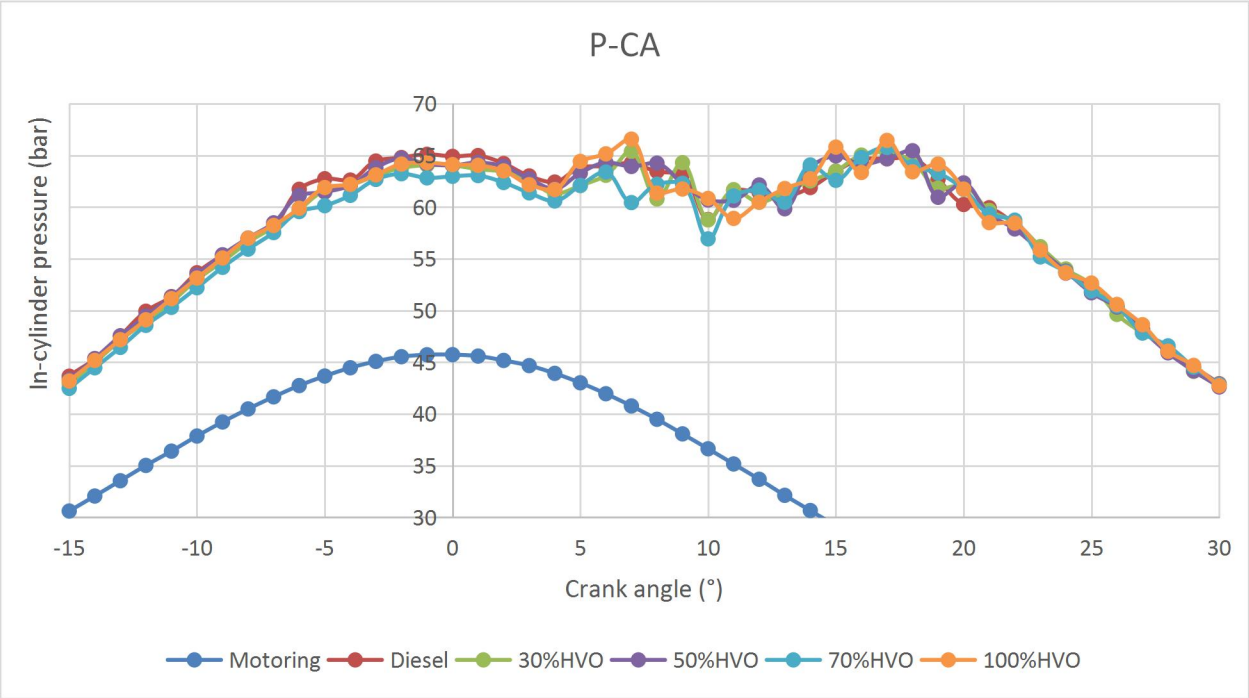


**Figure 7-10** The pressure curve near TDC of HVO blended fuels at 1900rpm, 50% throttle.

**Table 7-22** The ignition delays of HVO blended fuels at 1900rpm, 70% throttle.

| Fuel Type | SOI CA° | SOC CA° | ID CA° | ID (ms) |
|---|---|---|---|---|
| Diesel | -11 | -1 | 10 | 0.88 |
| 30% HVO | -11 | -1 | 10 | 0.88 |
| 50% HVO | -11 | -1 | 10 | 0.88 |
| 70% HVO | -11 | -1 | 10 | 0.88 |
| 100% HVO | -10 | -1 | 9 | 0.79 |

When the engine speed was raised to 1900 rpm, similar findings were obtained. The pressure-curves between tested fuels are very close in general. In detail, the pure HVO fuel can occasionally achieve higher combustion pressure than diesel and all blended HVO fuels had slightly lower combustion pressure as it can be seen from figure 7-10 and figure 7-11. In 1900rpm, 70% test, all fuel showed almost the same pressure behaviours as shown in figure 7-12. This is due to the engine power setup is high enough that the influences caused by fuel property differences can be ignored. That's the reason why in the 1900 rpm, 70% throttle test, all fuels had the same ignition delay time, except for pure HVO. Though diesel fuel had relatively lower cetane number, diesel fuel can be well mixed with air and easily ignite as high cetane number HVO fuel. From 50% and 60% throttle settings results, only the HVO fuel showed improvement in ignition delay. Multiple fuel injections were observed at this engine speed as well.

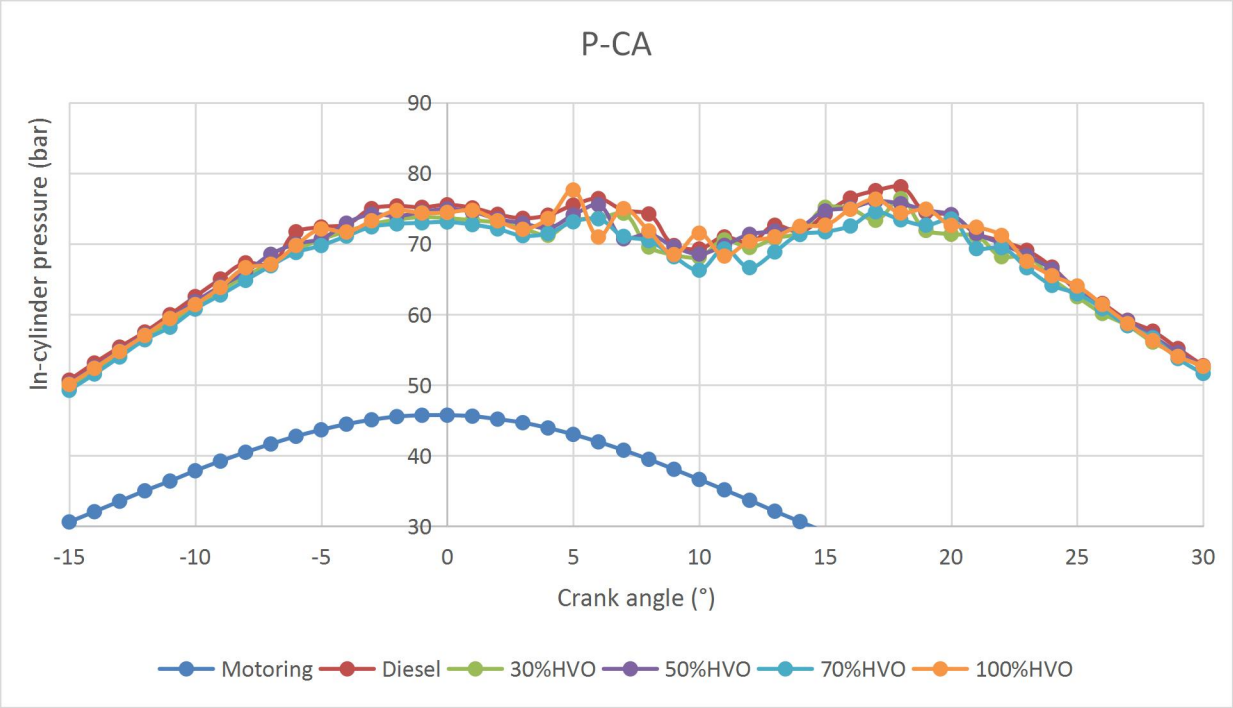


**Figure 7-11** The pressure curve near TDC of HVO blended fuels at 1900rpm, 60% throttle.

In summary, the in -cylinder pressure behaviour between diesel fuel, HVO fuel and its blends were similar in general. The combustion pressure from pure HVO can be slightly higher than diesel sometimes since it's more likely to be burned; while the combustion

pressure from HVO blended fuels were always slightly lower than that from pure tested fuels. The reason contribute to this phenomenon is that once HVO fuel was being blended with diesel fuel, the blends would contain with both unsaturated chains and saturated chains. And since those saturated paraffinic chains are long carbon chains as analysed in fuel property section, or in other words heavy fractions. Therefore, in order to achieve complete combustion, the blends must absorb more heat than diesel during atomization and vaporisation, and thus the overall combustion pressure be slightly lower. The reason why pure HVO fuel would had higher combustion pressure than its blends is that it is in absence of unsaturated chains, thus once any fractions being ignited, the flame can easily bring complete combustion to the fuel. In other words, the heat required for trigger complete combustion of pure HVO fuel is less than that of its blends.

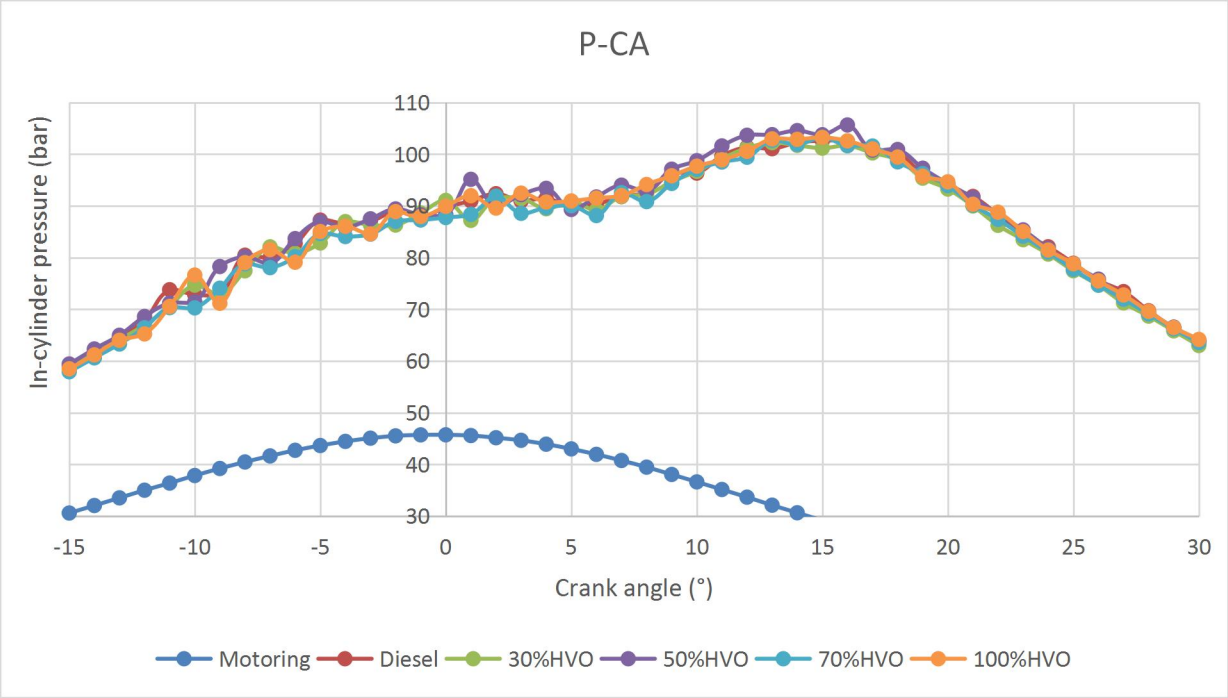


**Figure 7-12** The pressure curve near TDC of HVO blended fuels at 1900rpm, 70% throttle.

### 7.3.3 PV diagram

As shown and discussed in previous section, it can be addressed that the pressure to crank angle differences among diesel fuel, HVO fuel, and blended HVO fuels were very little. The PV diagrams were generated by AVL data processing software using

pressure values, crank angle degrees, and other fixed engine parameters for instance, bore size, stroke length, total displacement etc. Therefore, the PV diagrams generated from HVO blended tests at each specific engine power set up among different fuel types were very similar. In this section, 50% HVO blended fuel was selected as representative fuel type, and all nine tested engine conditions' PV performances are shown. The rest of other blending ratio's PV diagram results are listed in appendix.

The PV diagrams are in log scale for volume, meaning the 1.0 on X- axis represents the displacement of single combustion cylinder and is 749.5 $cm^3$, the clearance volume is 39.4 $cm^3$ as the compression ratio is 18 for this engine. The Y-axis represents absolute pressure in bar, thus the first 1.0 bar indicates the experiment ambient pressure. In the 1000 rpm tests, it can be found from figure 7-13 to figure 7-15 that with the throttle increased from 30% to 50%, the start of fuel combustion occurred sooner. The combustion at 30% throttle occurred when the piston moved to around 8% of total volume after TDC, while the 40% and 50% throttle occurred respective at around 7.5% and 7%. The turbocharger added about 0.2 bar pressure to gas sending to combustion at 30% throttle and increased to 0.8 bar and 1.0 bar respectively in 40% and 50% throttle test condition.

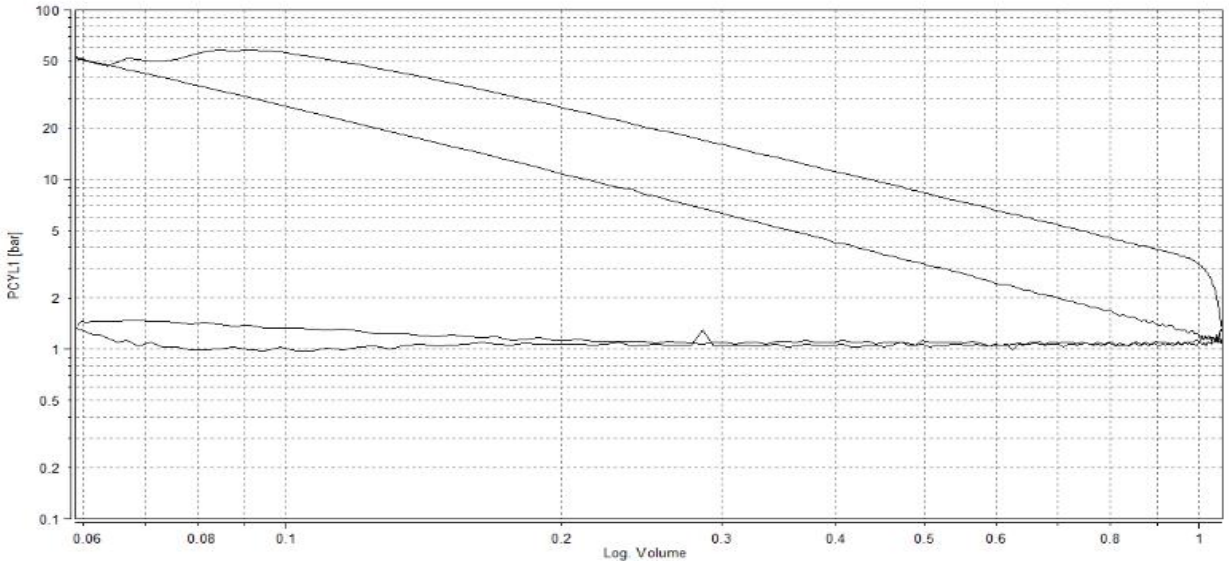


**Figure 7-13** PV diagram of 50%HVO at 1000rpm, 30% throttle.

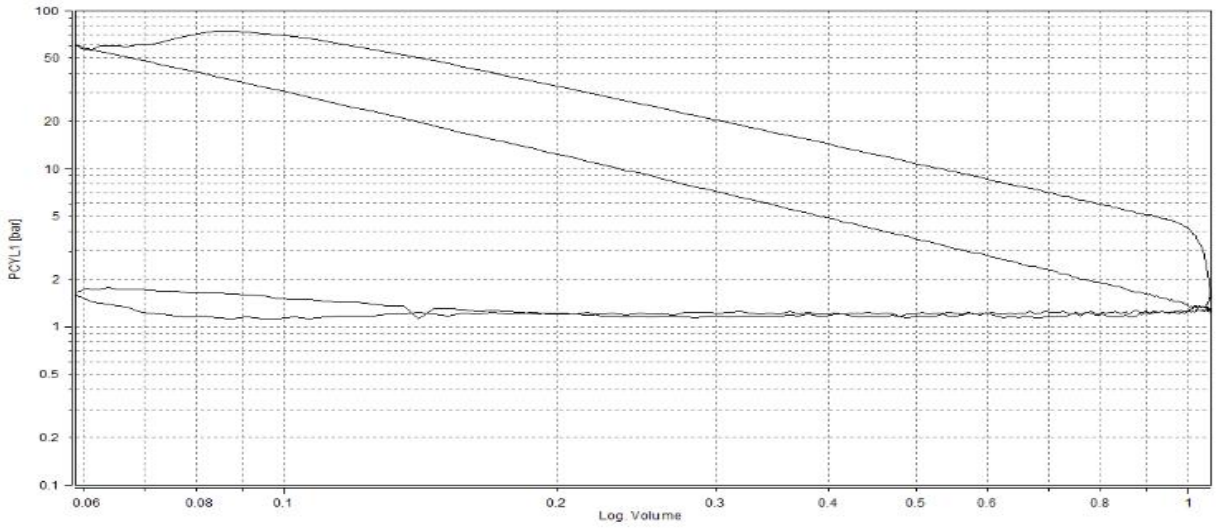


**Figure 7-14** PV diagram of 50%HVO at 1000rpm, 40% throttle.

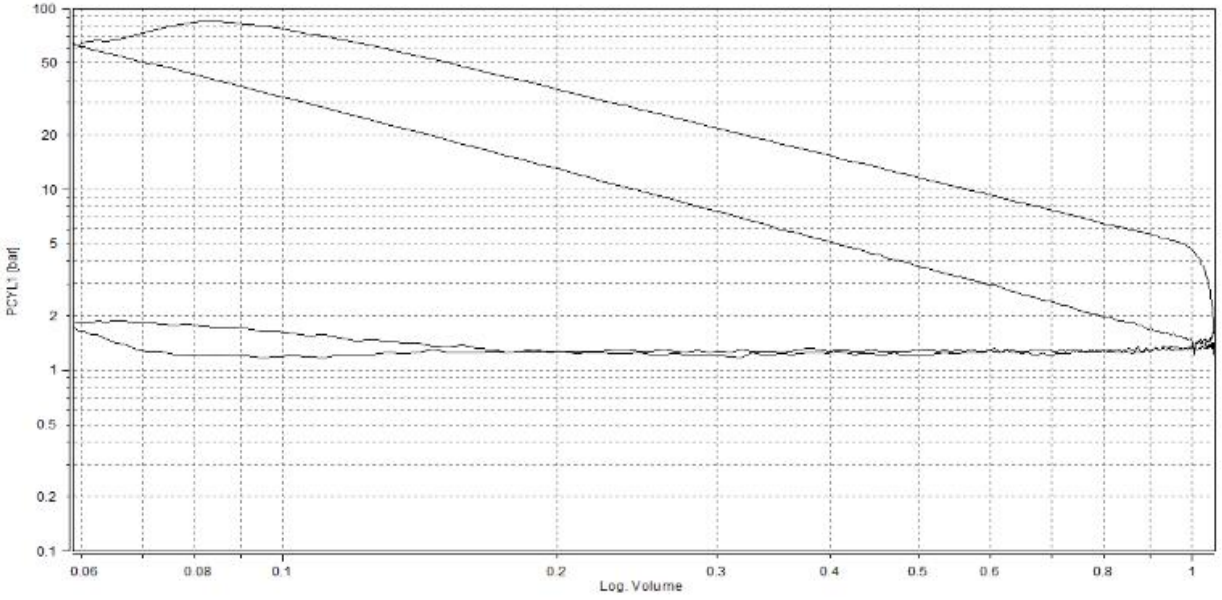


**Figure 7-15** PV diagram of 50%HVO at 1000rpm, 50% throttle.

When the engine rpm increased to 1600 rpm, it can be addressed from figure 7-16 to figure 7-18 that the start of combustion also happened earlier when the throttle increased to 60%. The start of combustion between 40% and 50% are similar. Multiple fuel injections after the piston passed TDC can be seen from 40% and 50% throttle setting test condition, and in the 60% throttle settings test, multiple fuel injections were also be found and the end of compression stroke.

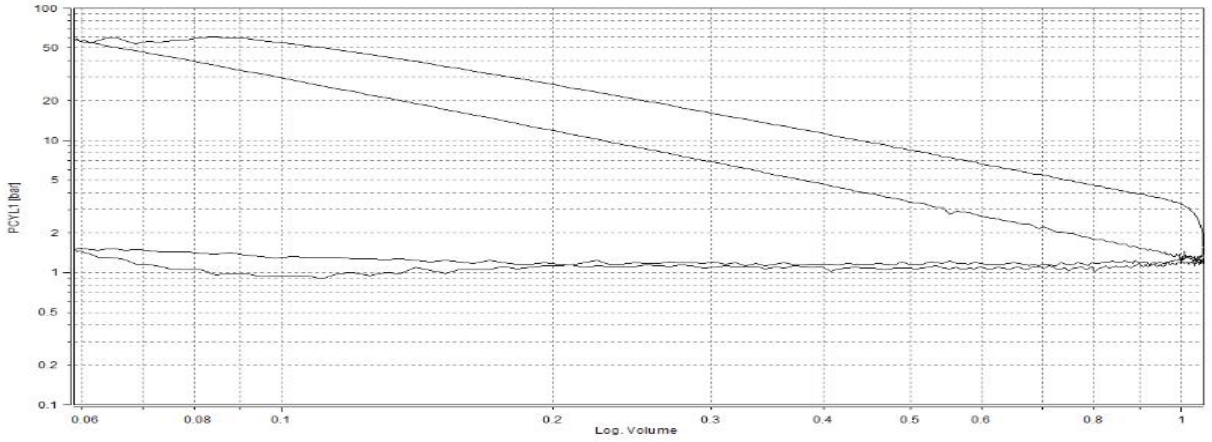


**Figure 7-16** PV diagram of 50%HVO at 1600rpm, 40% throttle.

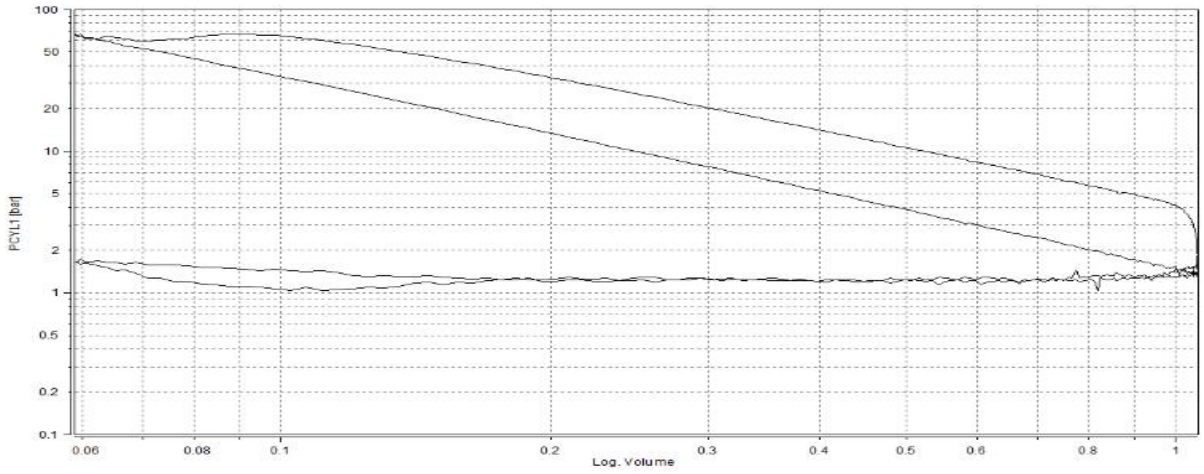


**Figure 7-17** PV diagram of 50%HVO at 1600rpm, 50% throttle.

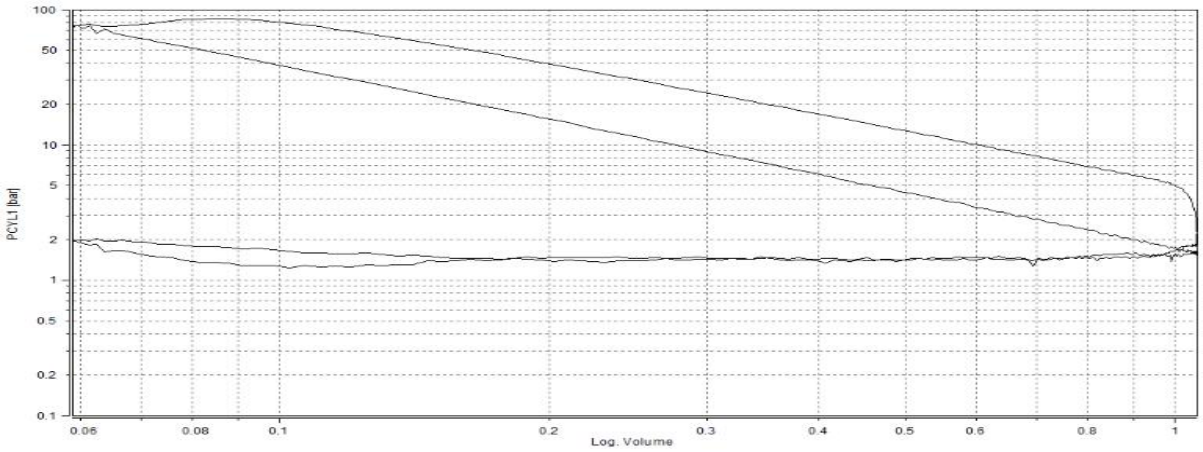


**Figure 7-18** PV diagram of 50%HVO at 1600rpm, 60% throttle.

When the engine speed up to 1900 rpm, the more obvious constant volume combustion can be achieved. This is obvious when comparing the 1900 rpm to 1600 rpm and 1000 rpm. With multiple fuel injection strategy, the experiment engine could maintain nearly constant combustion covering about 3% of total displacement, which is equivalent to 22.5 $cm^3$ volume change. The turbocharger could pressurize the inlet air by up to around 1.0 bar at this specific rpm operating condition.

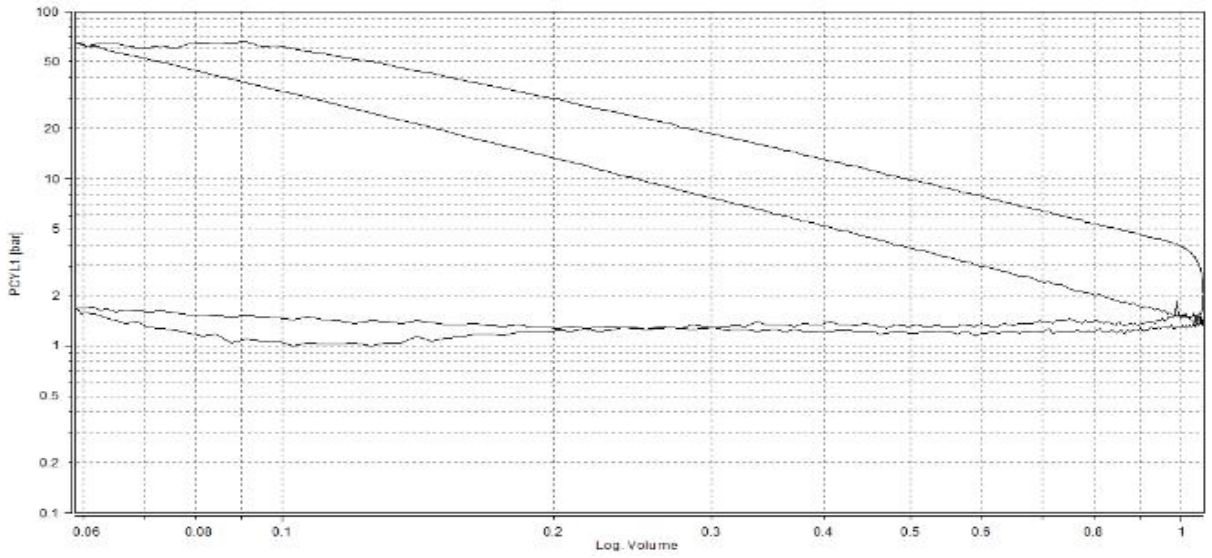


**Figure 7-19** PV diagram of 50%HVO at 1900rpm, 50% throttle.

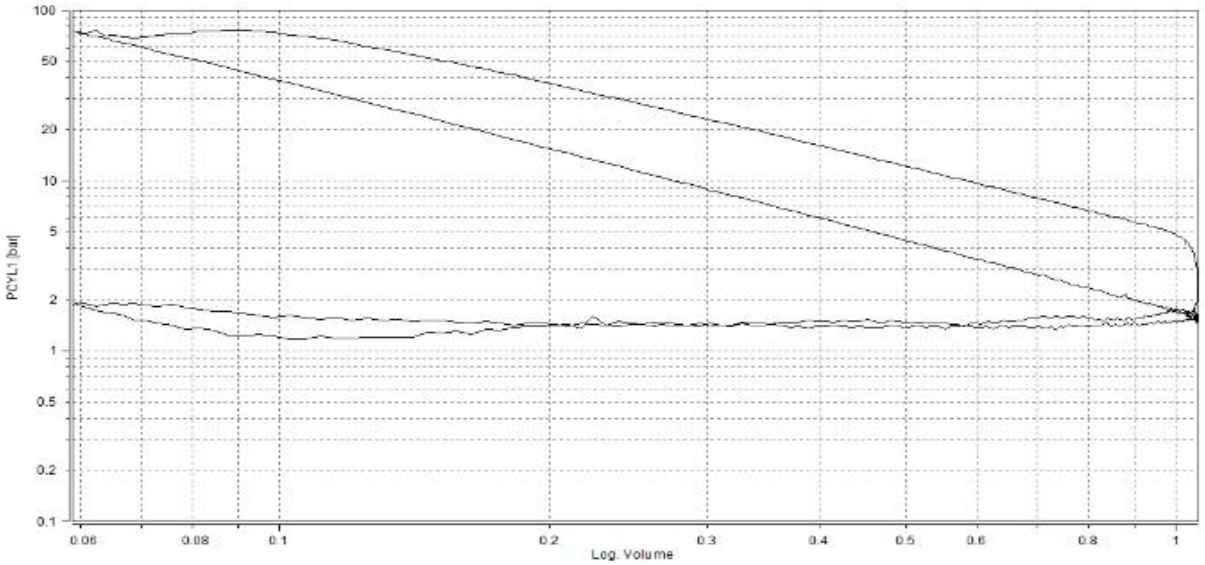


**Figure 7-20** PV diagram of 50%HVO at 1900rpm, 60% throttle.

In summary, the PV illustration of 50% HVO represented the PV performances of all HVO blended fuel tests. From the results, it can be suggested that constant pressure can be acquired by multiple fuel injection strategy when the engine power reaches 27 Kw (started from 1600 rpm, 50% throttle). Multiple fuel injections can be observed from PV diagram both before and after the TDC. The experiment turbocharger was capable of pressurize approximately 1.0 bar to gas sending to combustion cylinder.

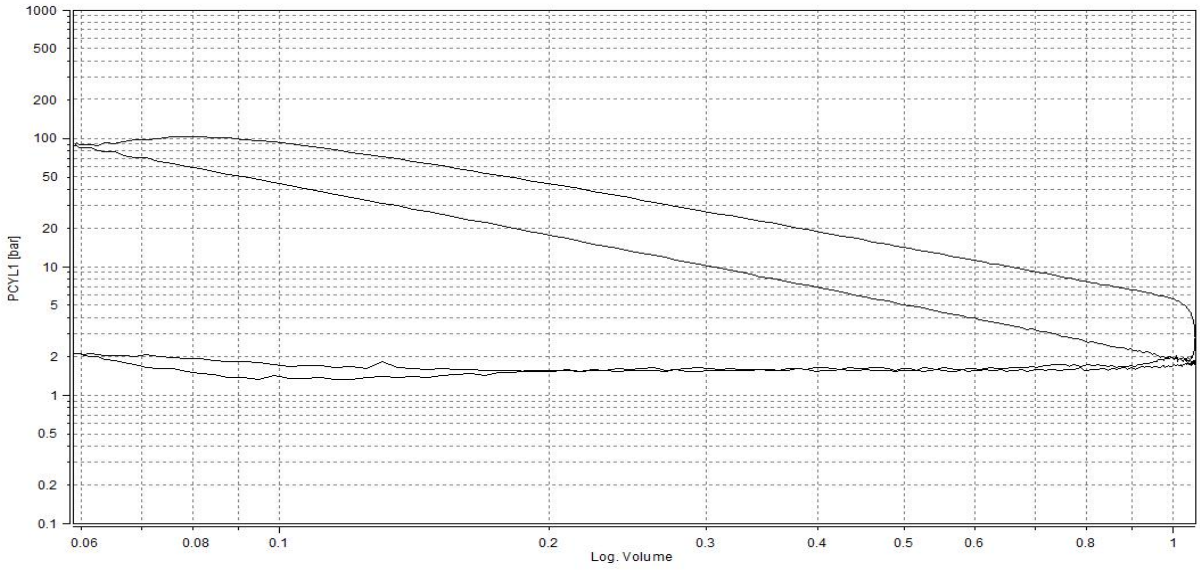


**Figure 7-21** PV diagram of 50%HVO at 1900rpm, 70% throttle.

## 7.4 Conclusion

According to the fuel property and combustion characteristics analysis of HVO and its blends the following conclusions can be obtained:

- The main difference between HVO fuel and diesel fuel is that the HVO fuel consisted of straight chains, saturated paraffins, and no aromatics. The carbon number distribution of HVO fuel from $C_{10}$ to $C_{13}$ was lighter than diesel. But the HVO fuel is heavier than diesel from $C_{16}$ and $C_{21}$. Compared to diesel, the HVO fuel has lower density and slightly higher mass based calorific value.
- The peak combustion pressure, IMEP, BEMP, and engine power generated from blended fuels, pure HVO fuel, and pure diesel fuel were similar in general. Only

occasionally the pure HVO could have slightly higher peak combustion pressure. However, all HVO blends have lower average in-cylinder pressure than pure diesel and HVO fuels.

- The ignition delays were reduced when the blend ratio increased at each engine operating condition, because the pure HVO fuel had higher cetane number.
- The engine demonstrated multiple fuel injection strategy to achieve consistent pressure combustion, and this was observed from all kinds of fuels' tests when engine power reached 27 KW.

Therefore, the most important difference between HVO blends and pure diesel and HVO fuels is that the HVO blended fuels performed a lower average in-cylinder pressure. This indicates that the average combustion temperature from HVO blends is lower, which is beneficial to reduce the thermal $NO_x$ formation.

# Chapter 8. Emission analysis of HVO and its blends

This chapter involves the emission results and discussion of HVO and its blends. The emission included the NO, $NO_2$, $NO_X$, total particle number, particle number distribution, THC, and CO.

## 8.1 $NO_X$, NO and $NO_2$ emissions

This section discusses the result of $NO_X$ emissions from HVO and its blends. The $NO_x$ emissions from diesel engine are source from three forms: thermal $NO_x$, prompt $NO_x$, and fuel bounded $NO_x$. Before the discussion, it's important to recall the discussion in fuel property and fuel combustion provided earlier in this chapter. The HVO fuel had similar calorific value and contained with 7% more nitrogen element in weight percentage. (The nitrogen element measured by CHNS was trace, however it can't confirm if the HVO contained more nitrogen. Based on the data measured from experiment, it's likely to be that the HVO contains more nitrogen.) The average combustion pressure values of blended HVO fuels were slightly lower than both pure diesel and pure HVO fuel. These results will be used in this section to explain the $NO_x$ formation from this research. The $NO_x$ emission discussed included with NO, $NO_2$, and total $NO_X$ emissions, and the results are presented in following figures.

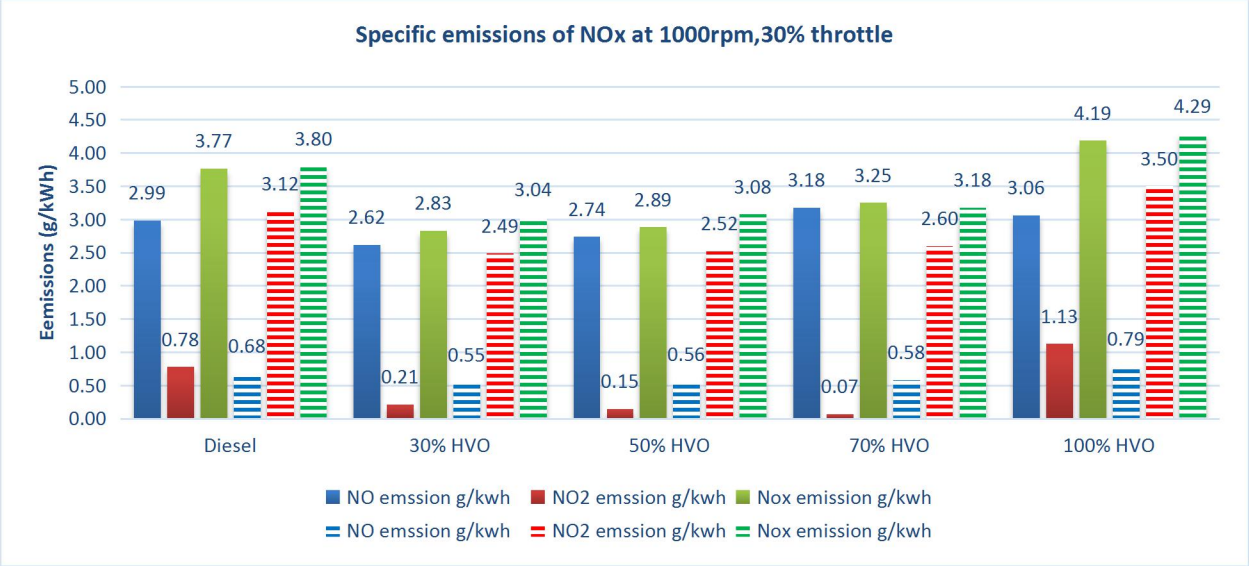


**Figure 8-1** NOx specific emissions at 1000rpm, 30% throttle.

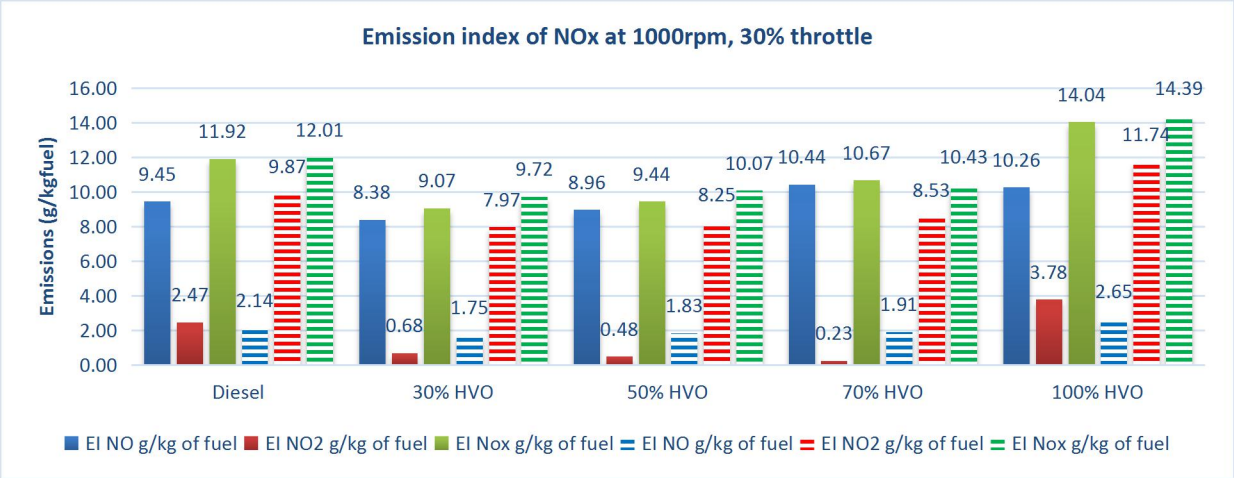


**Figure 8-2** NOx emission index at 1000rpm, 30% throttle.

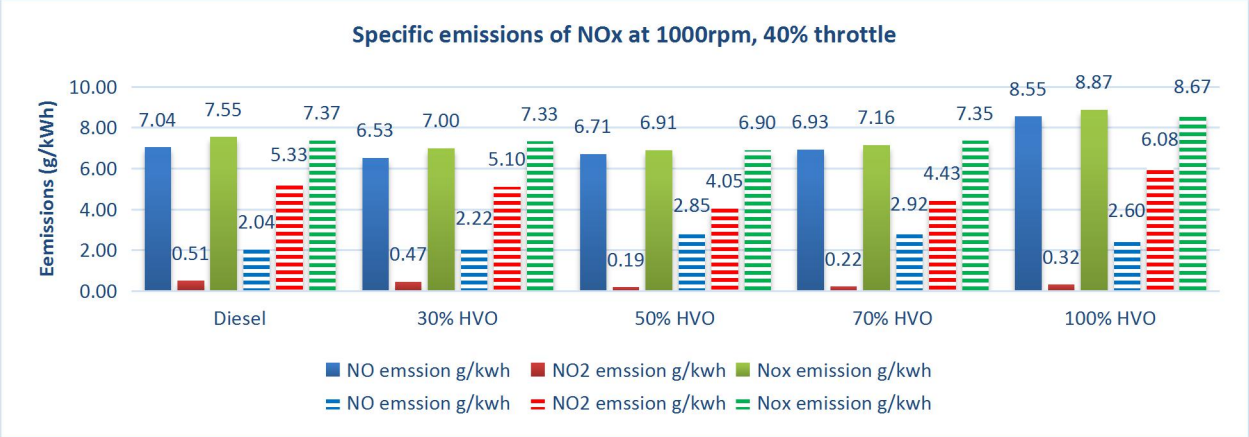


**Figure 8-3** NOx specific emissions at 1000rpm, 40% throttle.

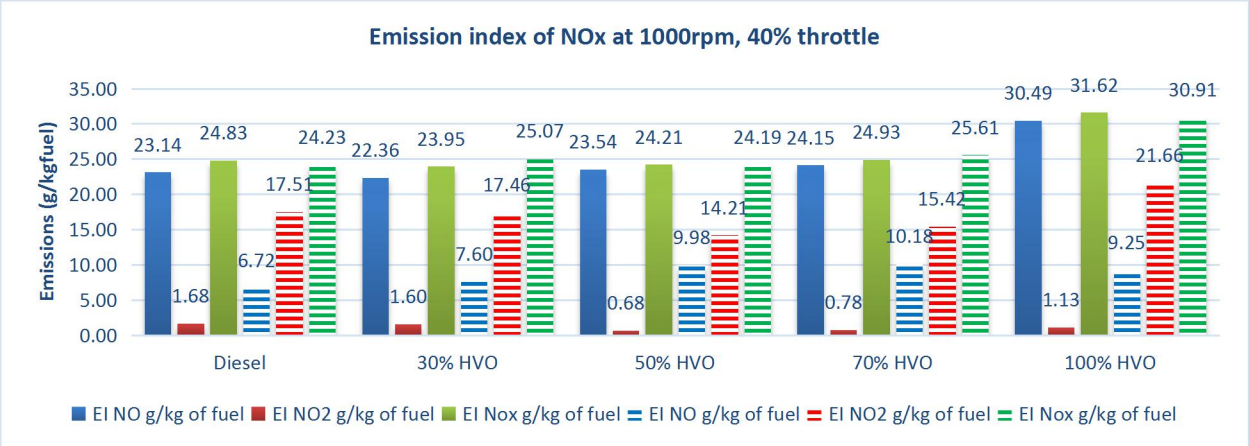


**Figure 8-4** NOx emission index at 1000rpm, 40% throttle.

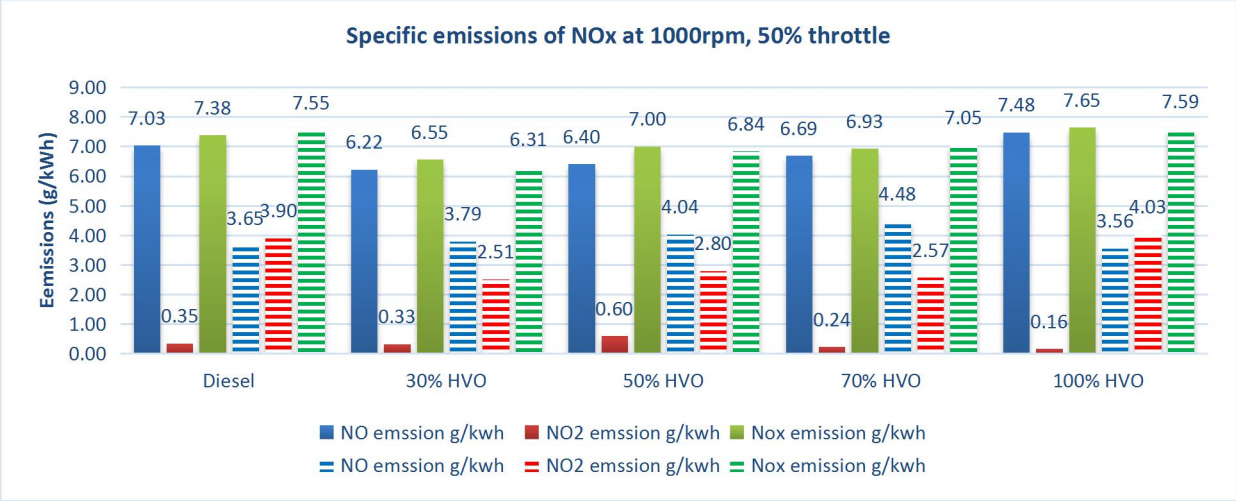


**Figure 8-5** NOx specific emissions at 1000rpm, 50% throttle.

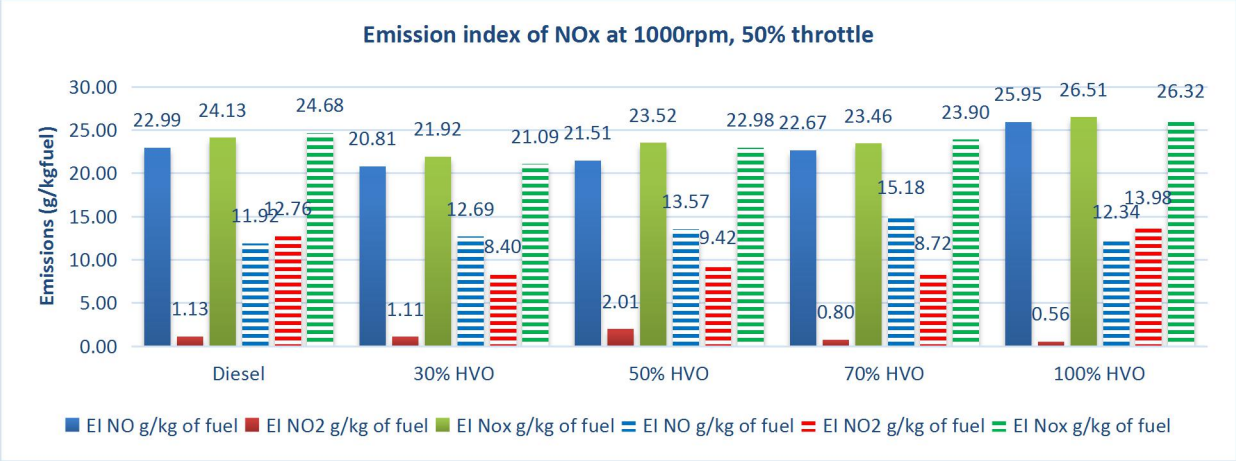


**Figure 8-6** NOx emission index at 1000rpm, 50% throttle.

The $NO_x$ emission performances from exhaust upstream and downstream at 1000 rpm engine operating condition tests are presented from figure 8-1 to figure 8-5. In general, it can be addressed that the pure HVO can produce slightly more total $NO_x$ emissions than diesel fuel. At 30% and 40% throttle settings, the HVO increased the specific $NO_x$ emission by respectively 13%, 15%. When the throttle increased to 50%, the HVO showed very close total $NO_x$ emission with diesel fuel, and only 0.5% higher than diesel fuel. From the combustion analysis at 1000 rpm provided in previous pressure curve analysis section, it was found the average combustion pressure at 30% and 40% throttle settings for diesel fuel is slightly higher than pure HVO, while the pressure was

even slightly lower than HVO at 50% throttle condition. This indicates the extra $NO_x$ produced from pure HVO shouldn't be thermal $NO_x$, instead it should be the fuel bounded $NO_x$ from pure HVO fuel. This could be contributing to that pure HVO contained with more nitrogen element. Another general trend can be addressed from 1000 rpm tests is that all HVO blended fuel showed obviously total $NO_x$ improvement. At 30% throttle settings, the 30% HVO blended fuel improved the total $NO_x$ by 26% while 50%, and 70% HVO blended fuel behaved slightly less effective in $NO_x$ reduction. At 40% throttle condition, the 30% and 50% HVO blended fuel reduced approximately 7% of total $NO_x$. And at 50% throttle settings, the total $NO_x$ could be reduced up to 16% with the effort of 30% HVO blended into diesel.

From the comparison between exhaust upstream and exhaust downstream, the $NO_2$ increased significantly at exhaust downstream because of the oxidation reaction occurred in DOC would convert NO to $NO_2$. At 30%, 40% and 50% throttle settings, the DOC could convert respectively about 60%, 40%, and 30% NO to $NO_2$. The total $NO_x$ emission between upstream and downstream is little and it's within 5%. The total $NO_x$ also increased as the throttle setting increased. This s due to the increasing of throttle percentages would increasing the fuel injection and bring up the average combustion temperature, and consequently more thermal $NO_x$ would be formed.

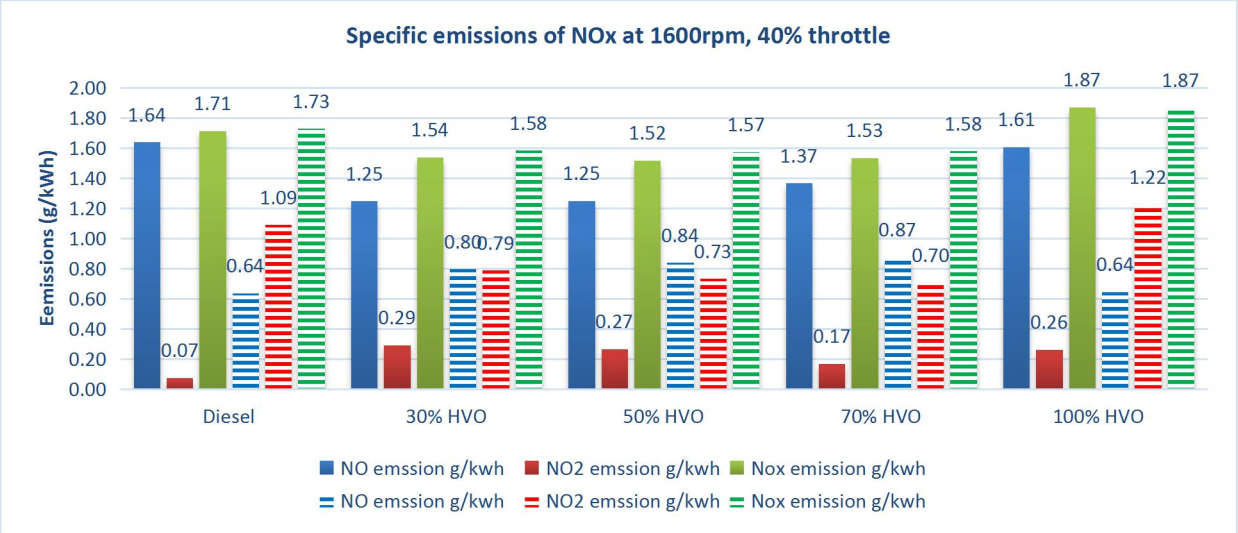


**Figure 8-7** NOx specific emissions at 1600rpm, 40% throttle.

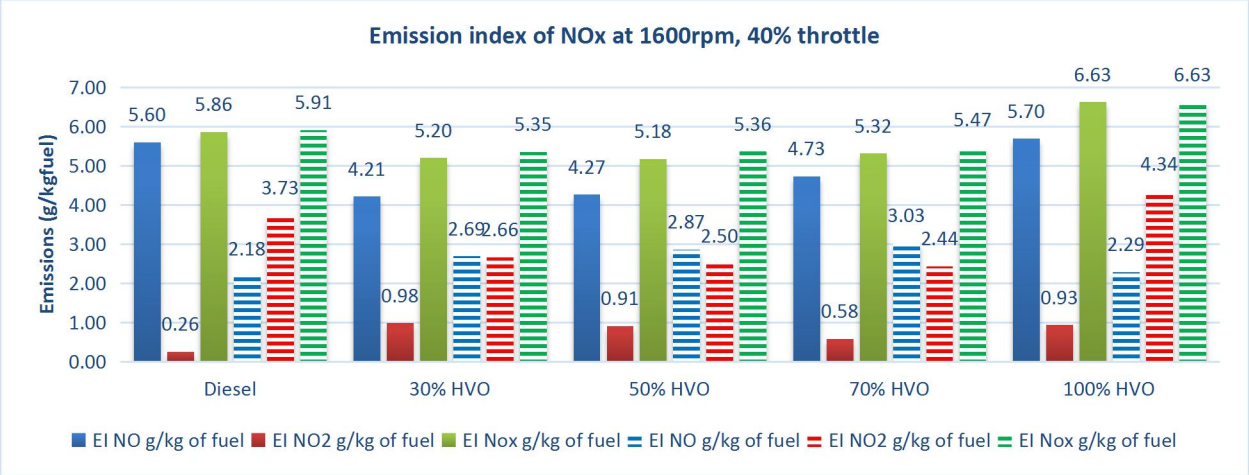


**Figure 8-8** NOx emission index at 1600rpm, 40% throttle.

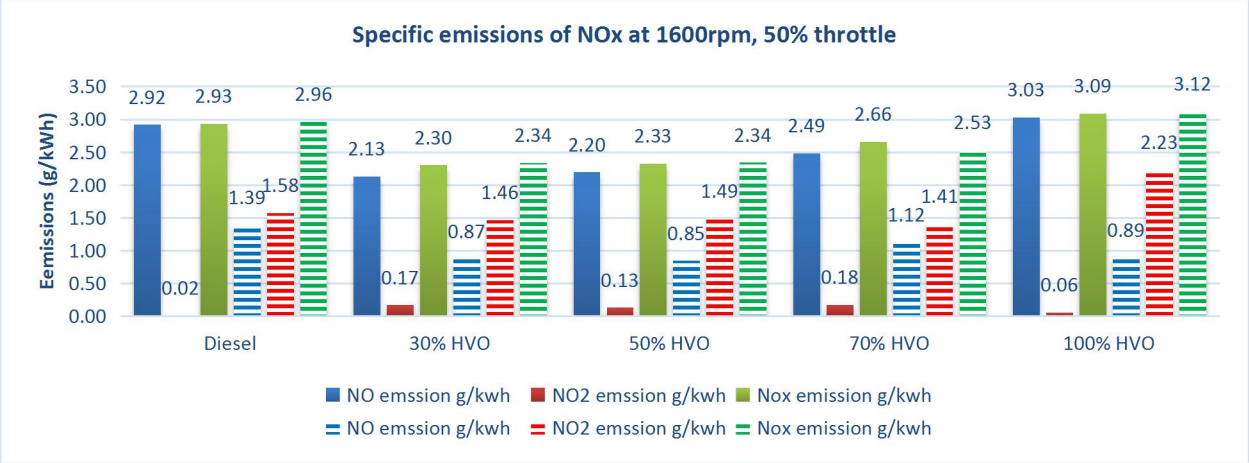


**Figure 8-9** NOx specific emissions at 1600rpm, 50% throttle.

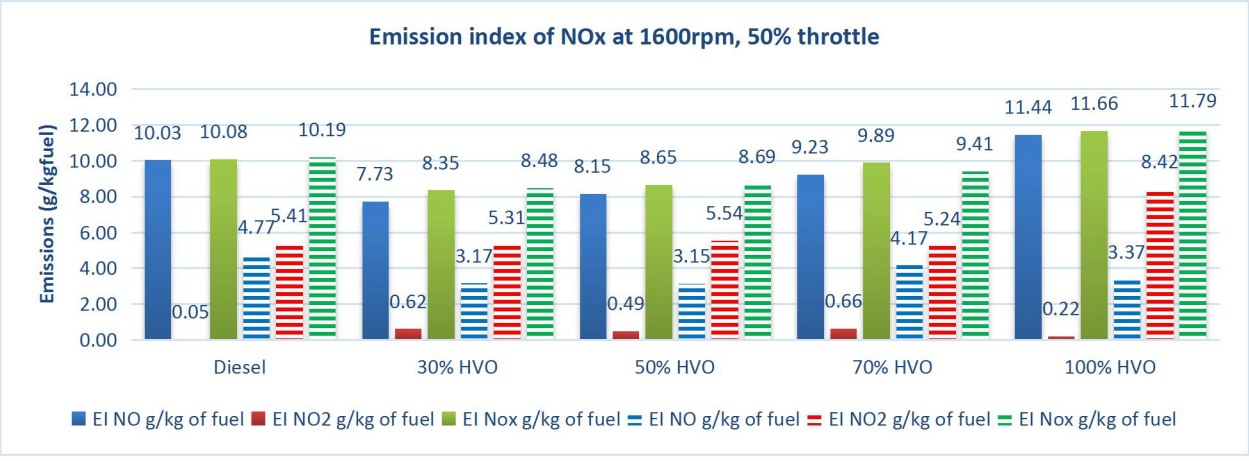


**Figure 8-10** NOx emission index at 1600rpm, 50% throttle.

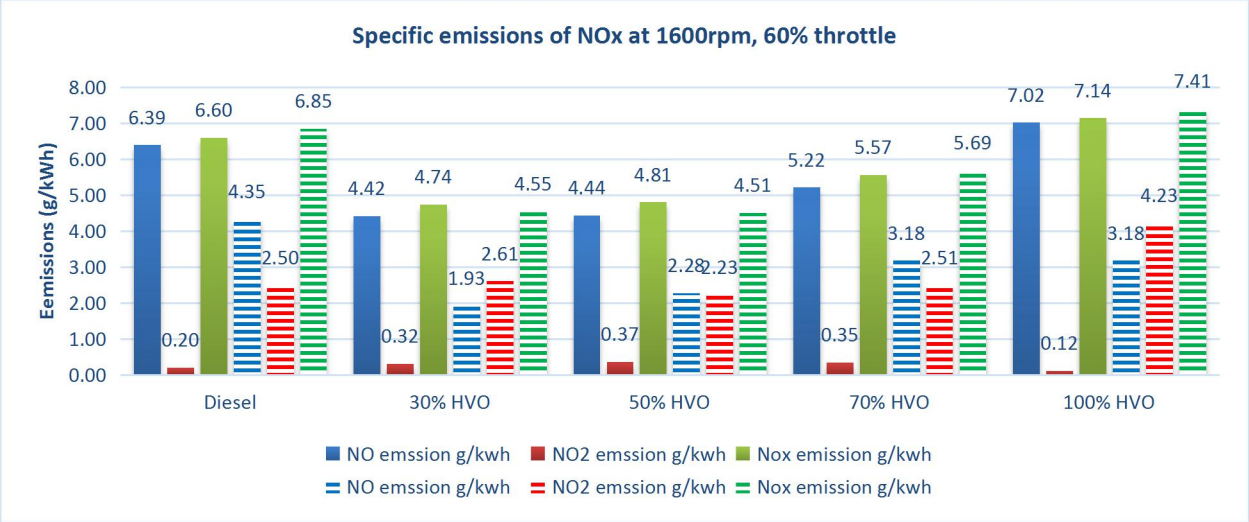


**Figure 8-11** NOx specific emissions at 1600rpm, 60% throttle.

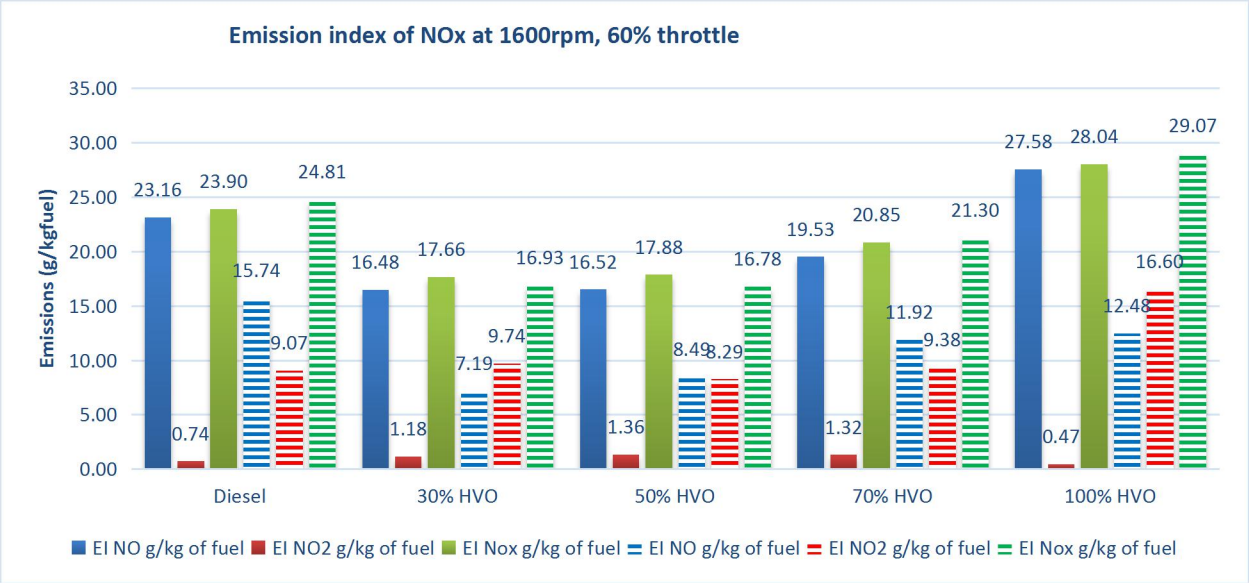


**Figure 8-12** NOx emission index at 1600rpm, 60% throttle.

When the engine rpm increased to 1600 rpm, similar finding can be obtained as from 1000 rpm's tests. The total specific $NO_x$ produced from pure HVO fuel is 9%, 5% and 8% higher than that of diesel in respectively 40%, 50% and 60% throttle settings. As its discussed in the fuel combustion section, the pressure differences between pure HVO and pure diesel is little, thus the additional $NO_x$ produced from pure HVO were likely to be fuel bounded $NO_x$ production. All the blended fuels showed obvious $NO_x$ reduction at 1600 rpm tests with 30% HVO blended fuel performed as the more effective one in most

conditions. It acquired the total $NO_x$ reduction at downstream of aftertreatment system by 10%, 21% and 34% at respectively 40%, 50%, and 60% throttle settings. The 50% and 70% HVO blended fuel showed very similar reduction efficiencies as 30% HVO blends. This corresponded to the findings with GTL blended fuels, so it's believed that once pure HVO being blended into diesel fuel, the aromatics can be diluted and started to be act as anti-oxidant, which buffered the formation of $NO_x$. Besides, the fuel combustion pressure behaviour analysed in previous sections showed that blended HVO fuels always acquired slightly lower average in-cylinder pressure, implying the overall temperature in combustion cylinder should be lower. The lower temperature environment would also benefit the reduction in $NO_x$ generation.

The DOC oxidation rate for NO can ranged from 25% to 55% at this engine speed and behaved as irregular either with blending ratio or engine power settings. The total $NO_x$ production from all fuels would increase with the engine throttle settings being increased, and the difference between exhaust upstream and downstream in total $NO_x$ can be less than 4%. This difference can be caused by the engine repeatability as the $NO_x$ measurement at exhaust upstream and downstream were conducted separately.

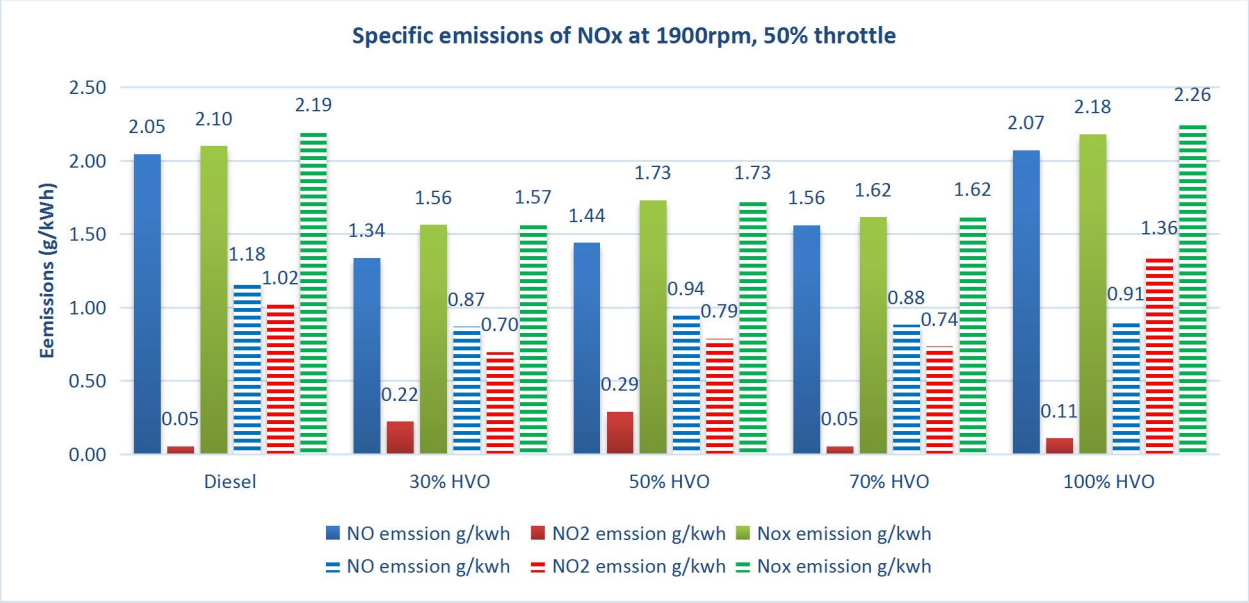


**Figure 8-13** NOx specific emissions at 1900rpm, 50% throttle.

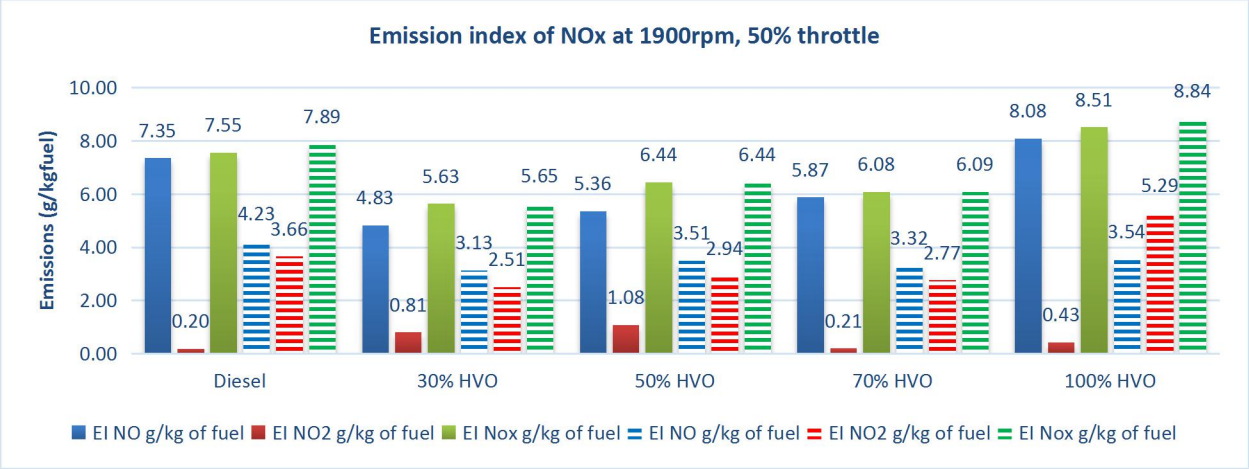


**Figure 8-14** NOx emission index at 1900rpm, 50% throttle.

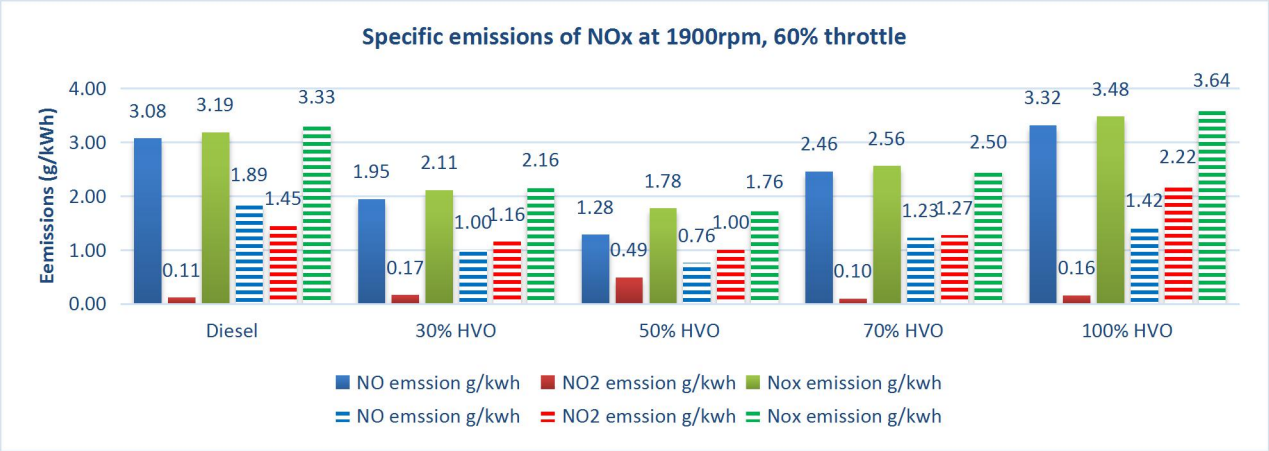


**Figure 8-15** NOx specific emissions at 1900rpm, 60% throttle.

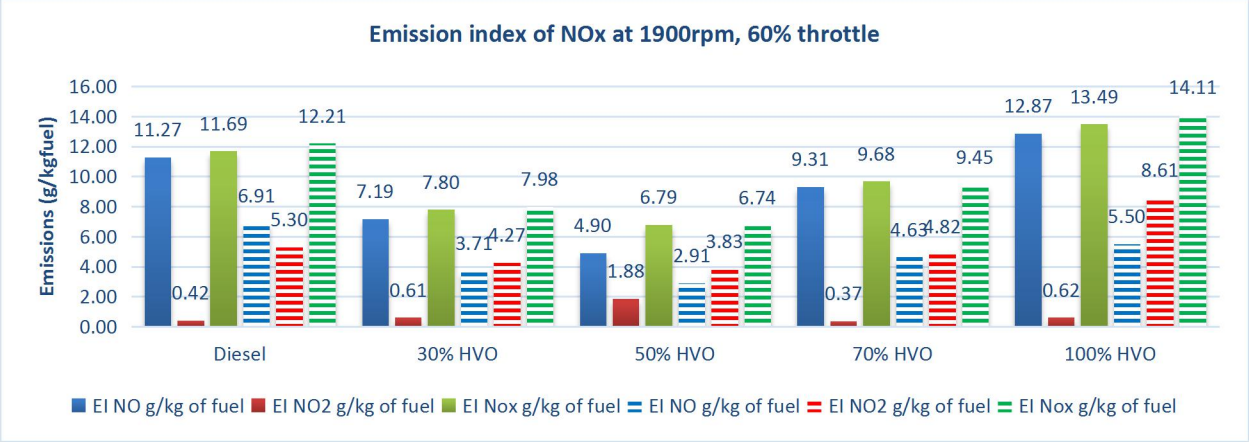


**Figure 8-16** NOx emission index at 1900rpm, 60% throttle.

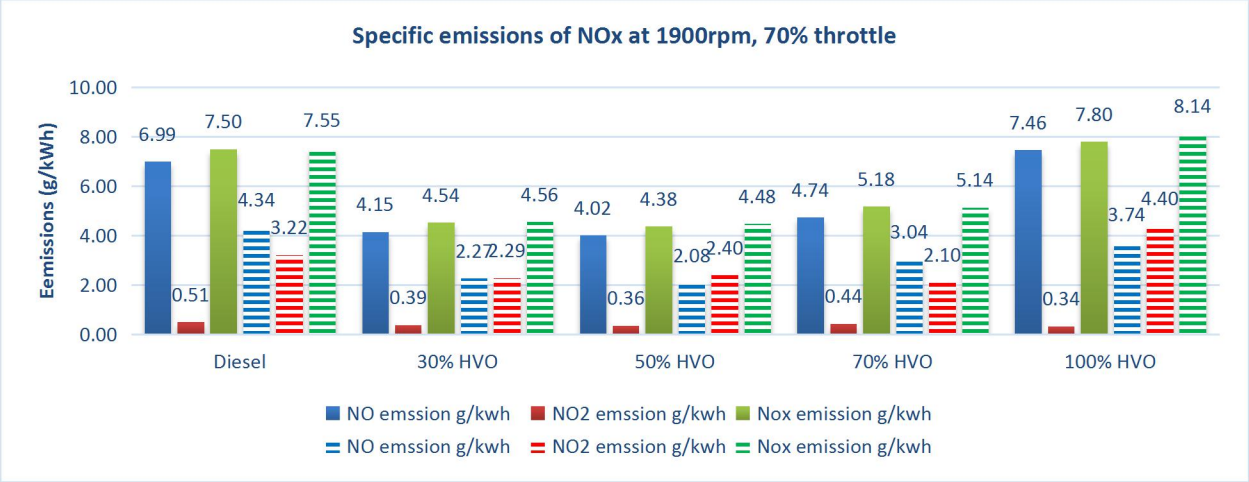


**Figure 8-17** NOx specific emissions at 1900rpm, 70% throttle.

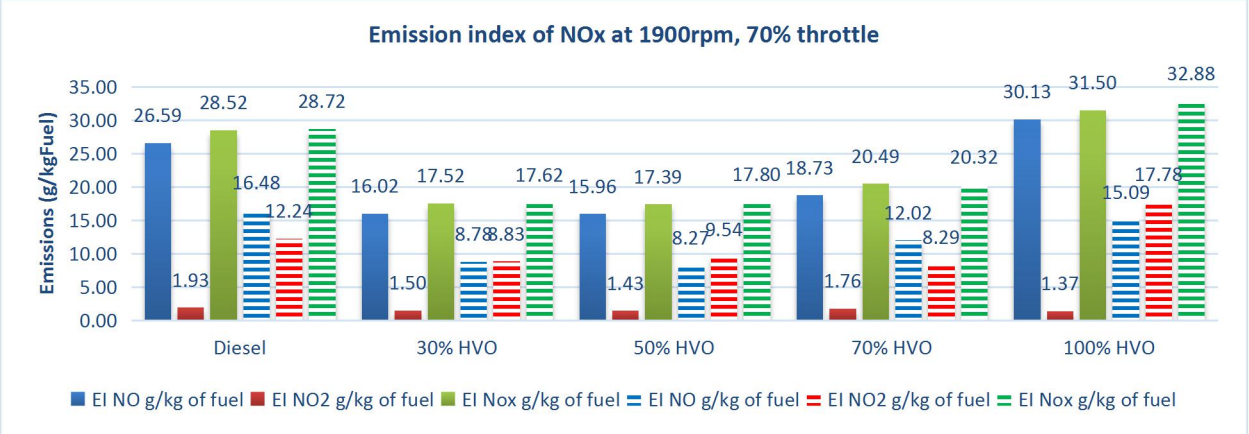


**Figure 8-18** NOx emission index at 1900rpm, 70% throttle.

With the engine rpm increased to 1900 rpm, the similar findings can still be acquired. The pure HVO still failed to improve the total $NO_X$ while the blended fuels showed significant specific $NO_X$ reduction by 28% 47% 40% at respectively 50%, 60% and 70% throttle condition. The $NO_X$ reduction rate between three blended fuels are similar in general. In detail, the most effective reduction at 50% throttle settings was observed from 30% HVO blends and it shift to 50% blended fuel in the rest of tests. The NO oxidation ratio at this engine operating speed ranged from 25% to 38% and doesn't present any relationship with either blend ratio or throttle settings.

In summary, the findings from HVO fuel showed agreement of the findings in GTL fuel, that the blended fuels can significantly reduce the total $NO_X$ emission from 10% to 47%. The only difference is that the pure HVO fuel couldn't improve the $NO_X$ emission even slightly, instead, it behaved slightly higher than diesel fuel in all tested conditions. This was likely due to the fuel composition of HVO fuel contained more nitrogen element than diesel fuel, so the fuel bounded $NO_X$ contributed to the additional $NO_X$ generation.

The reasons that HVO fuel could reduce $NO_x$ emissions effectively can be two. First is that at all test conditions, the combustion temperature of HVO blends was slightly lower than pure diesel and pure HVO fuels. This can be proved by the analysis in previous combustion section. Therefore, the production of thermal $NO_x$ was reduced. Second, it the anti-oxidant effect from aromatics. This reason is the main reason that why HVO blends had lower $NO_X$ emissions, because in most of the tests, in-cylinder pressure measured was similar and thus the combustion temperature should be similar as well, indicating the significant reduction of $NO_X$ emissions cannot be attributed to combustion temperature. Besides, the HVO blends demonstrated very similar reduction efficiencies as GTL blends, which no evidence showed GTL blends had lower combustion temperature.

As previously discussed in GTL chapter, the aromatics with certain concentration would be act as anti-oxidants in fuel combustion. Because aromatics can supress the formation of free radicals which determines the oxidation rate. [Varatharajan, and Cheralathan, 2013]. In addition, its reported that with the increasing of antioxidants concentration, sharp increases in activity would be observed at first, then followed by smaller increases. [Dunn, 2005]. This indicates that effectiveness of antioxidants is related to its concentration. This make sense that via blending straight chains and saturated paraffins into diesel could allow the aromatics in diesel to enable its anti-oxidant activity Comprehensively speaking, the $NO_X$ reduction from blended HVO fuels became more significantly with the engine power set up increased, which is also similar to GTL blended fuels' performances. Therefore, it's also believed that with the fuel combustion pressure and temperature increased, the anti-oxidant ability of aromatics can also be improved. Its's estimated that the optimised aromatics concentration is from

7.5% to 17.5%. In the future research it is necessary not only to find out the concentration behaviours for aromatic acting as anti-oxidant, but also necessary to find its anti-oxidant behaviours against chemical reaction pressure and temperature.

## 8.2 Particle size distribution, number concentration and DPF efficiency

This section provides the results and discussion on particle number emission. The total particle number concentration and particle size distribution from engine exhaust upstream and downstream are involved.

### 8.2.1 Total particle number results analysis

The total particle number concentration performance of HVO and HVO blends are shown in Figure 8-19 and figure 8-20. At exhaust upstream, it can be found that HVO and HVO blends could improve the total particle number significantly and the reduction in total particle number increases with the blending ratio increases. Since the particle number concentration at exhaust downstream was lower than the detect limits of DMS500, thus, the differences between HVO and its blends can hardly be distinguished.

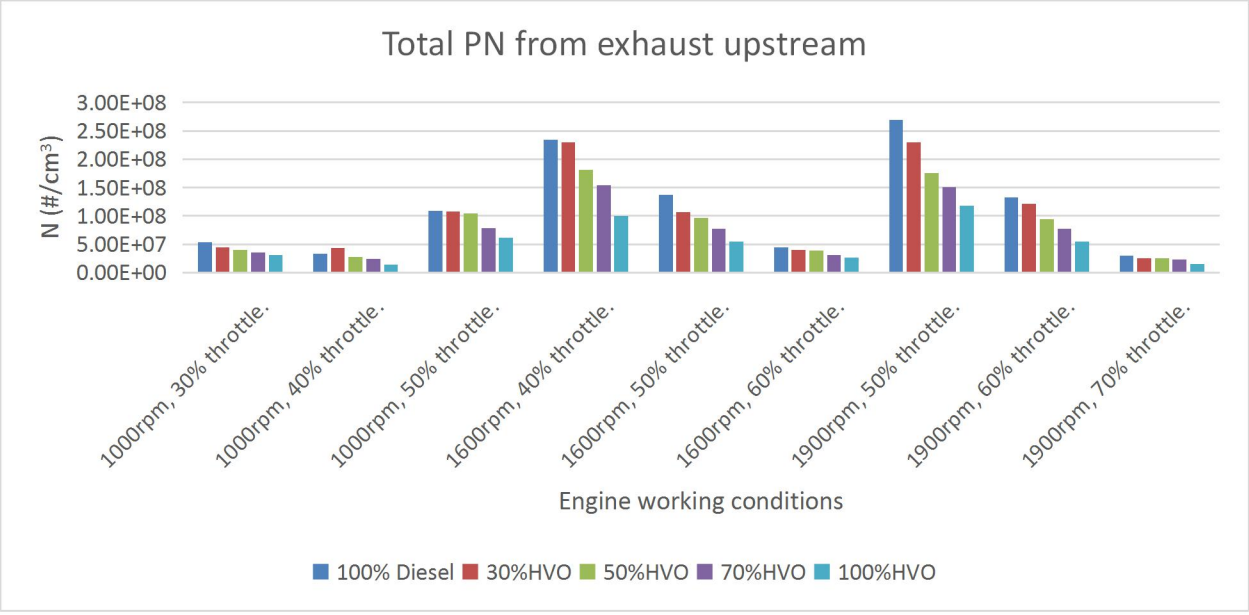


**Figure 8-19** Total PN from exhaust upstream of HVO blended tests.

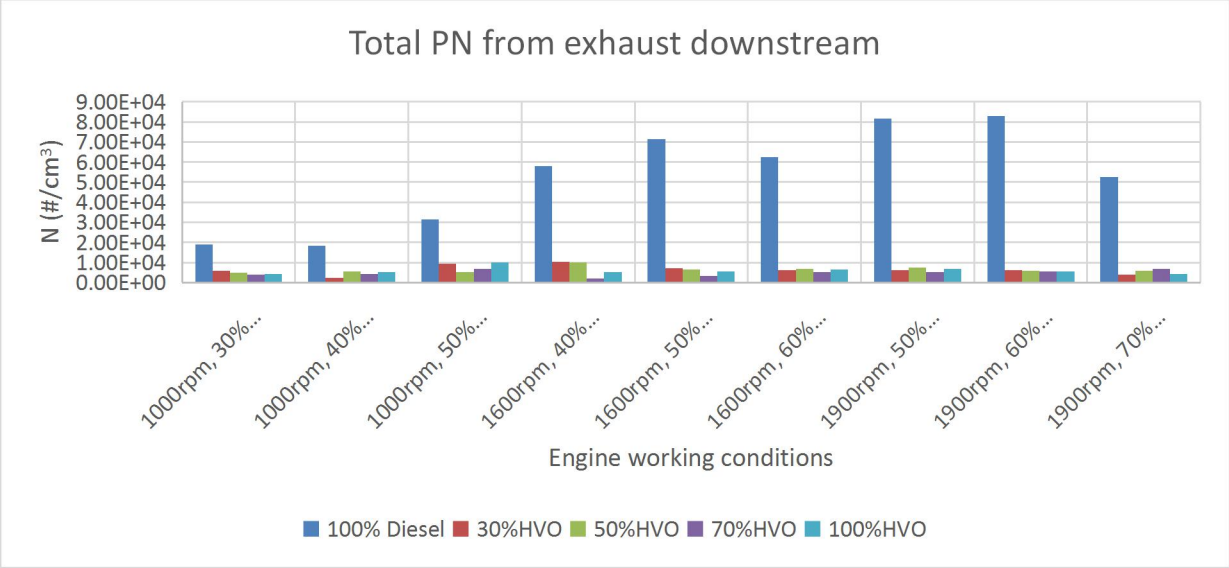


**Figure 8-20** Total PN from exhaust downstream of HVO blended tests.

At the exhaust upstream, the pure HVO could improve the total particle number emission by up to 59% (when the engine was running at 1900 rpm with 60% throttle opened) while HVO blends acquired lower reduction. The 30% HVO blended fuel performed very close PN emission to diesel fuel and even 32% higher than diesel fuel when the engine was running at 1000 rpm with 40% throttle opened. This is due to the poor fuel-air mixing performances achieved at 1000 rpm resulted incomplete combustion of the fuels. This can be further proved as when the engine was working at 1000 rpm with 50% throttle settings, the total PN emissions from all fuels increased dramatically. In the 1600 rpm and 1900 rpm tests, the fuel-air mixing performances were improved as the engine rpm increased, therefore, increasing the throttle percentage at these specific engine speed would be increasing the temperature and pressure in the combustion chamber, and consequently more completely fuel combustion would be achieved. The more completely the fuel combusted, the less PN would be generated, and this explains why the total PN emission at 1600 rpm and 1900 rpm decreases with the throttle settings being increased. The PN measured at exhaust downstream is generally below the DMS500 lower detect limits ($2\times10^4$), therefore the differences between fuels in total PN can hardly be figured out. However, it still can be acquired that all blended fuel and pure HVO fuel could significantly improve the total PN at exhaust downstream as well.

### 8.2.2 DPF efficiency analysis

From the comparison of total particle number production sampled before and after the DPF, it can be found that the total PN emission at DPF catalyst out was much lower than from engine exhaust out. The total PN emission measured from engine out was in scale of $10^7$ to $10^8$ while it's $10^4$ from downstream of DPF. This means the total particle numbers measured after filtration were more than 1000 times lower than before. And this explained the high efficiency of DPF being achieved in this research. The calculated DPF efficiencies are provided in the table 8-1.

**Table 8-1** The DPF efficiency of HVO blended tests.

| Engine working condition | | DPF efficiency | | | | |
|---|---|---|---|---|---|---|
| Engine rpm | Throttle% | 100% Diesel | 30% HVO | 50% HVO | 70% HVO | 100% HVO |
| 1000 | 30 | 99.9647% | 99.9872% | 99.9879% | 99.9886% | 99.9886% |
| | 40 | 99.9450% | 99.9945% | 99.9800% | 99.9823% | 99.9702% |
| | 50 | 99.9710% | 99.9913% | 99.9951% | 99.9912% | 99.9620% |
| 1600 | 40 | 99.9753% | 99.9955% | 99.9945% | 99.9986% | 99.9883% |
| | 50 | 99.9478% | 99.9933% | 99.9932% | 99.9957% | 99.9847% |
| | 60 | 99.8591% | 99.9843% | 99.9822% | 99.9831% | 99.9803% |
| 1900 | 50 | 99.9697% | 99.9973% | 99.9958% | 99.9965% | 99.9935% |
| | 60 | 99.9377% | 99.9949% | 99.9937% | 99.9930% | 99.9885% |
| | 70 | 99.8233% | 99.9838% | 99.9768% | 99.9714% | 99.9782% |

### 8.2.3 Particle number size distribution

In order to see how HVO and its blends can impact the particle production, the particle size distribution measurement and analysis is presented in this section. The particle diameter size range measured was from 4.87 nm to 1000 nm 38, and totally 38 different size of particles were measured within this range.

The PN distributions at 1000 rpm engine speed with 30% throttle are shown in figure 8-21 and figure 8-22. From the upstream of DPF, it can be seen that the peak values for accumulation mode particles gradually reduced with the increasing of blending ratio,

and the mode size was generally from particles with diameter of 65 nm. However, it can be seen that for 30% and 50% HVO blends, it tended to have more particles in diameter from 153 nm to 200 nm. This can be caused by the poor fuel-air mixing at 1000 rpm. The mode size of nucleation mode particle for all fuels were located at about 20 nm diameter. The PN distribution curves acquired from DPF downstream shows the diesel fuel obtained the highest emission and followed by 30% HVO blends. The rest of HVO blends and pure HVO performed very close distributions to each other. The DPF removed nearly all the particles in nucleation mode, and the mode size of accumulation mode located at about 100 nm diameter.

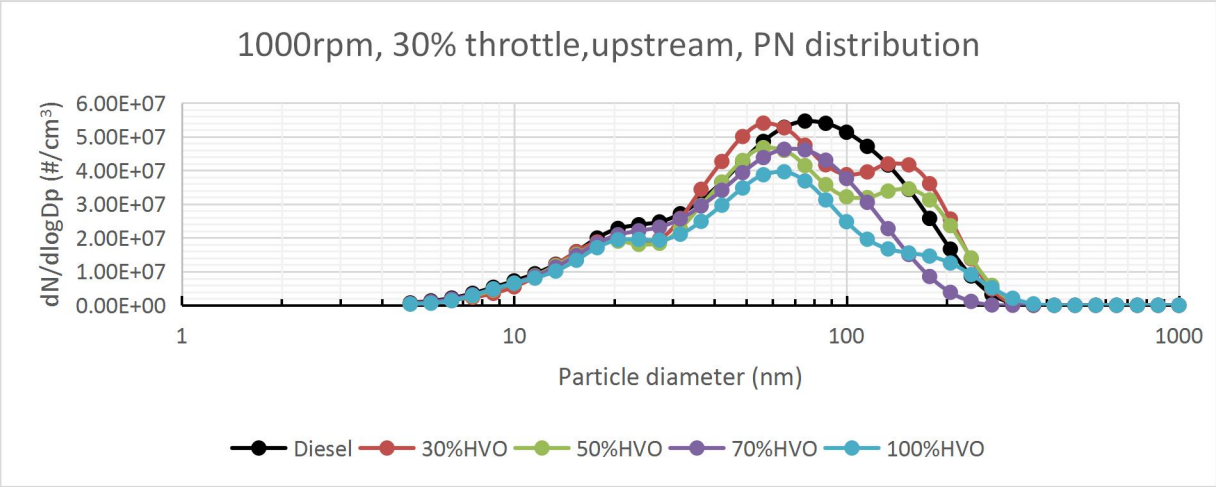


**Figure 8-21** Particle size distribution from exhaust upstream at 1000rpm, 30% throttle.

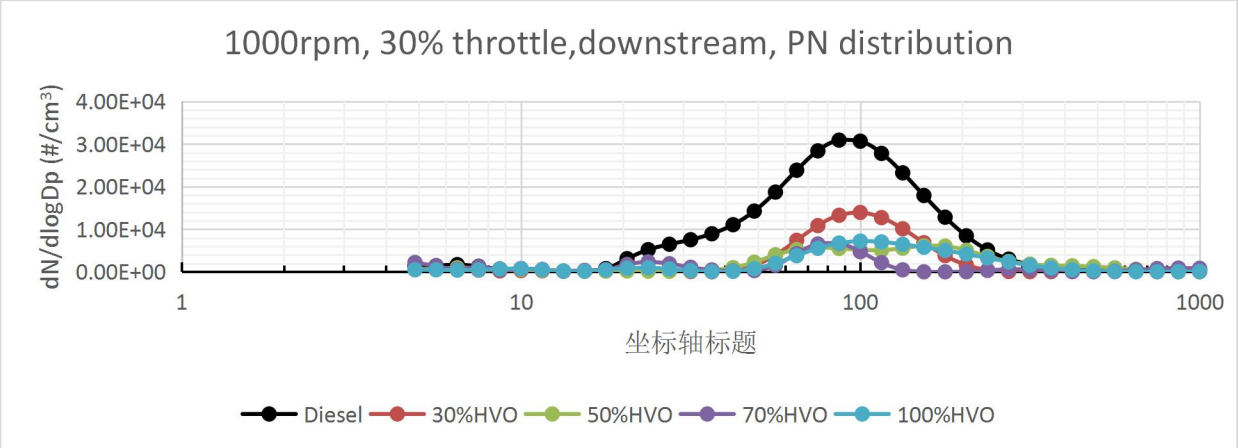


**Figure 8-22** Particle size distribution from exhaust downstream at 1000rpm, 30% throttle.

When the throttle settings increased to 40% and 50%, the HVO blends with lower blending ratio produced more particles in accumulation mode with diameter from 153 nm to 486 nm. The 30% HVO blended fuel showed dramatically high production of accumulation mode particles in 40% and 50% throttle tests, and 50% HVO blends behaved similar distribution pattern to 30% HVO blends at 50% throttle settings. This indicates the HVO blends with low blending ratio could generate more accumulation particles at low engine power setup due to the failure to acquired appropriate fuel mixing. The poor fuel-air mixing at 1000 rpm can further be proved in later section of CO emission. The peak values for accumulation mode particles still gradually reduced with the increasing of blending ratio in general. The peak values for nucleation mode particles located at about 20nm diameter and all HVO blends and pure HVO showed lower nucleation particle production than diesel fuel. The PN distribution from DPF downstream consisted mainly with accumulation mode particles failed to be filtered out by DPF, and since the concentration was too low to be accurately detected, the relationship between fuels can hardly be address.

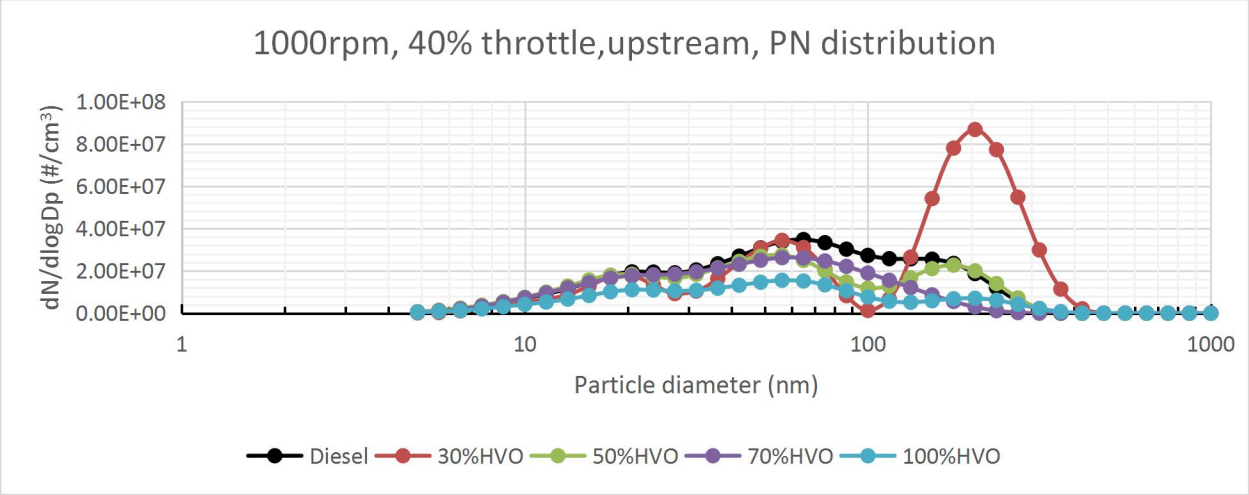


**Figure 8-23** Particle size distribution from exhaust upstream at 1000rpm, 40% throttle.

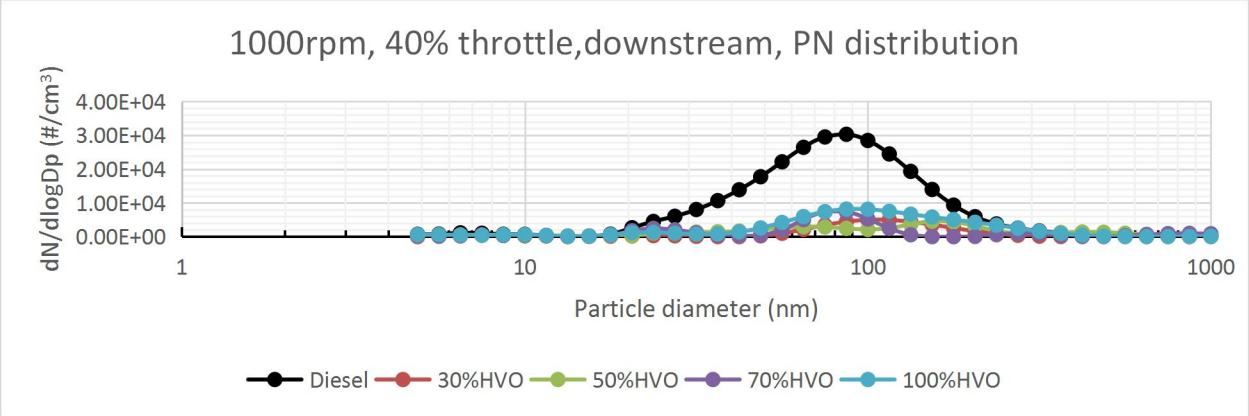


**Figure 8-24** Particle size distribution from exhaust downstream at 1000rpm, 40% throttle.

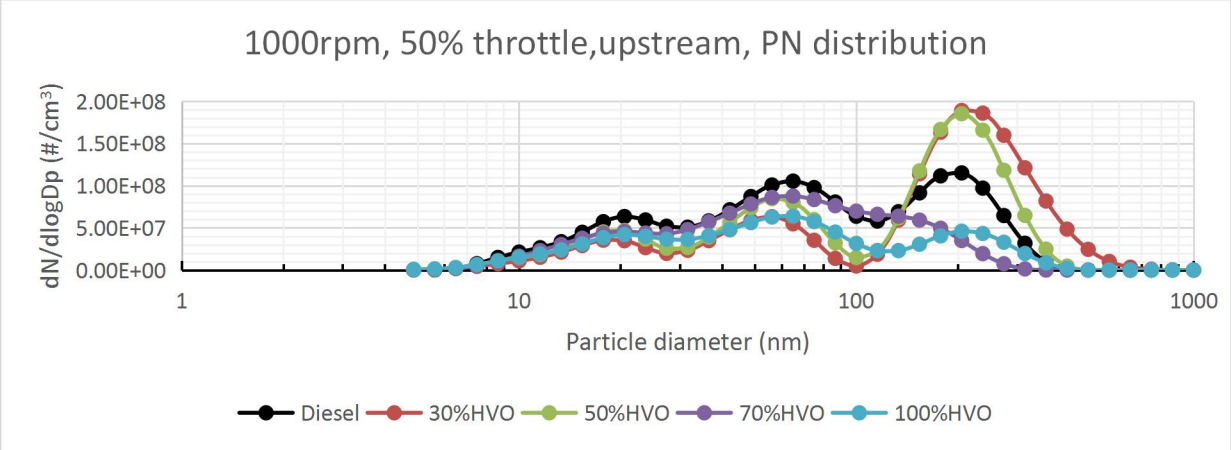


**Figure 8-25** Particle size distribution from exhaust upstream at 1000rpm, 50% throttle.

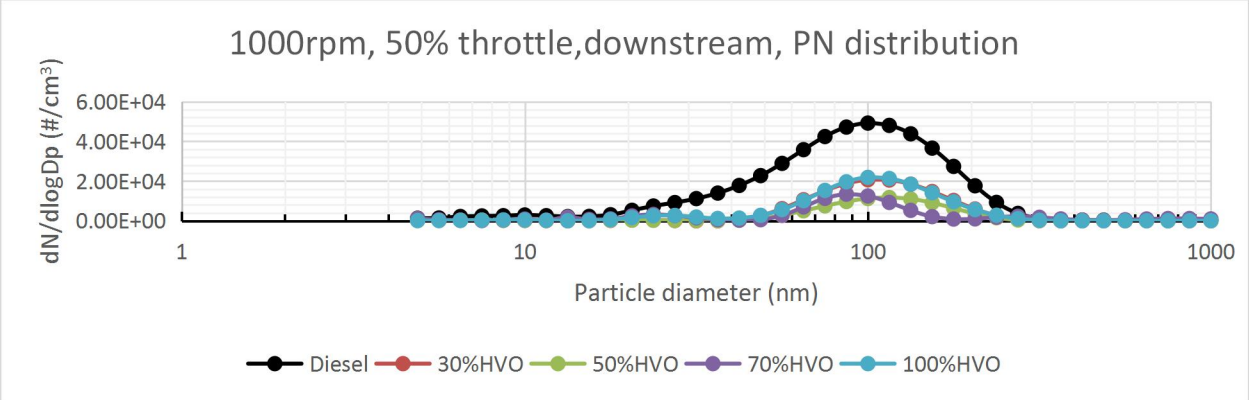


**Figure 8-26** Particle size distribution from exhaust downstream at 1000rpm, 50% throttle.

The distribution before exhausts passed the DPF at 1600 rpm showed the peak values for accumulation particles at around 237 nm diameter for all tested fuels. And in general, the peak value reduced with the increasing of blending ratio. However, 30% and 50% HVO blends showed relevantly similar peak values. The nucleation mode particle peaks between tested fuels were located at about 20 nm diameter. The diesel fuel still performed the highest PN emission at exhaust downstream, and nearly no detectable particles can be found from HVO fuel and it blends.

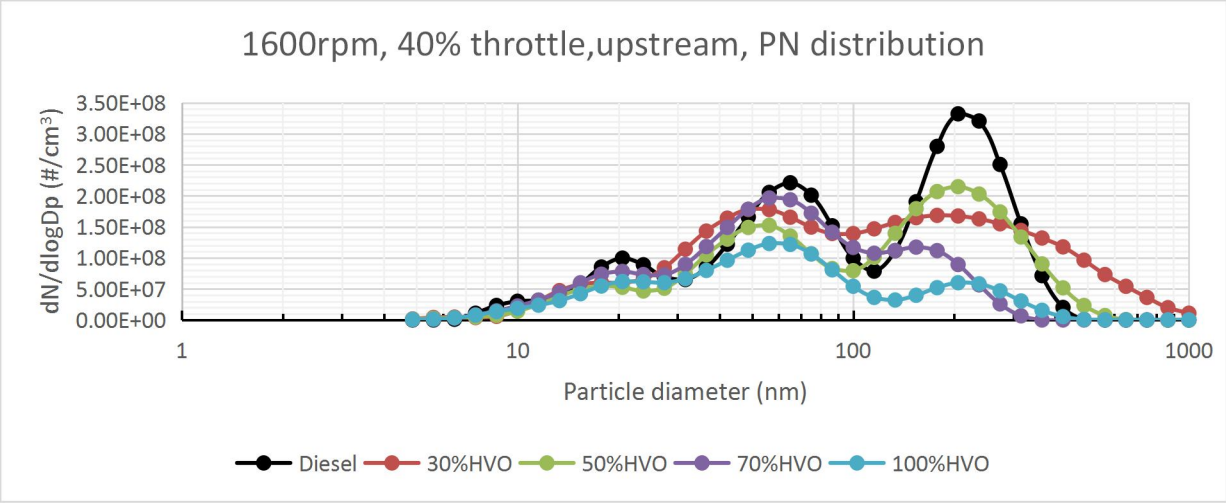


**Figure 8-27** Particle size distribution from exhaust upstream at 1600rpm, 40% throttle.

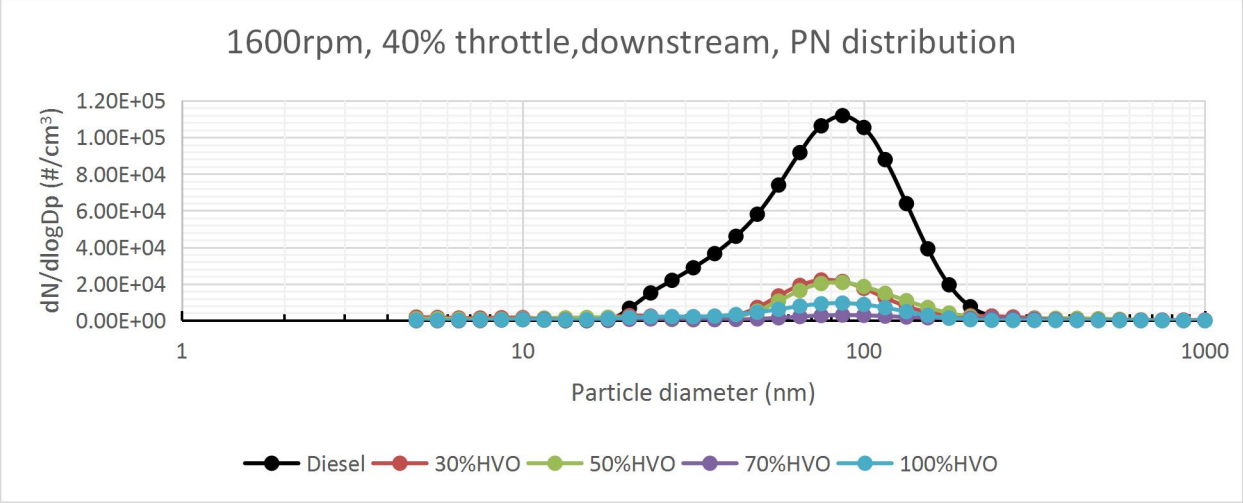


**Figure 8-28** Particle size distribution from exhaust downstream at 1600rpm, 40% throttle.

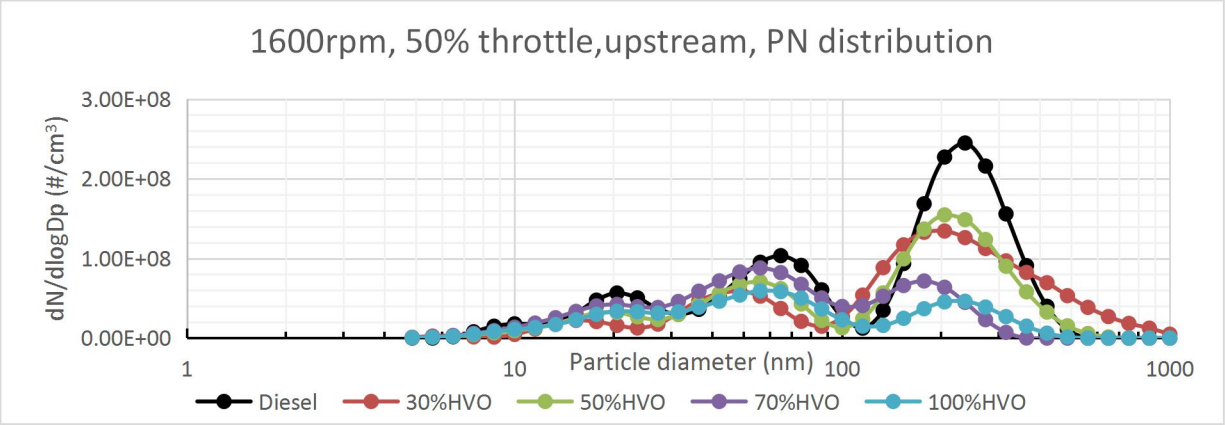


**Figure 8-29** Particle size distribution from exhaust upstream at 1600rpm, 50% throttle.

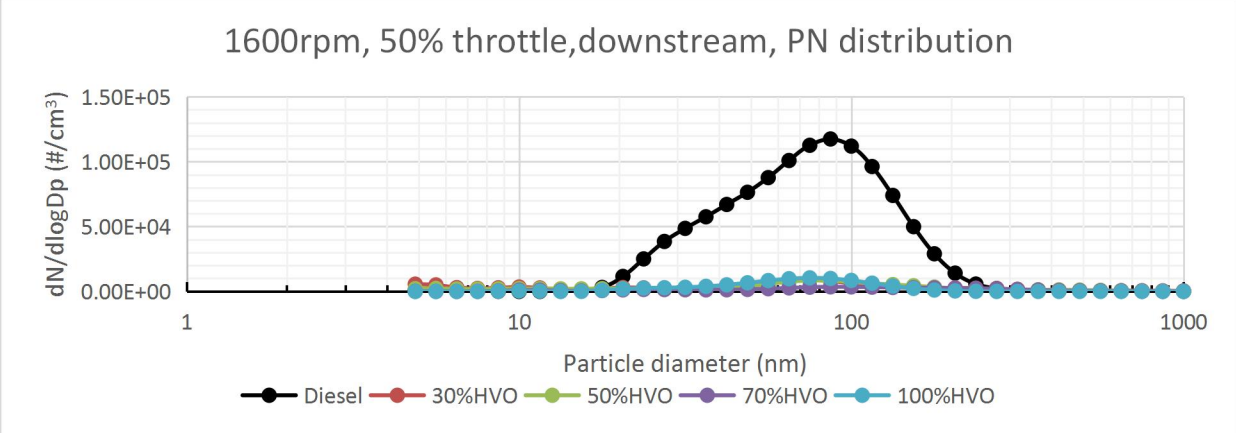


**Figure 8-30** Particle size distribution from exhaust downstream at 1600rpm, 50% throttle.

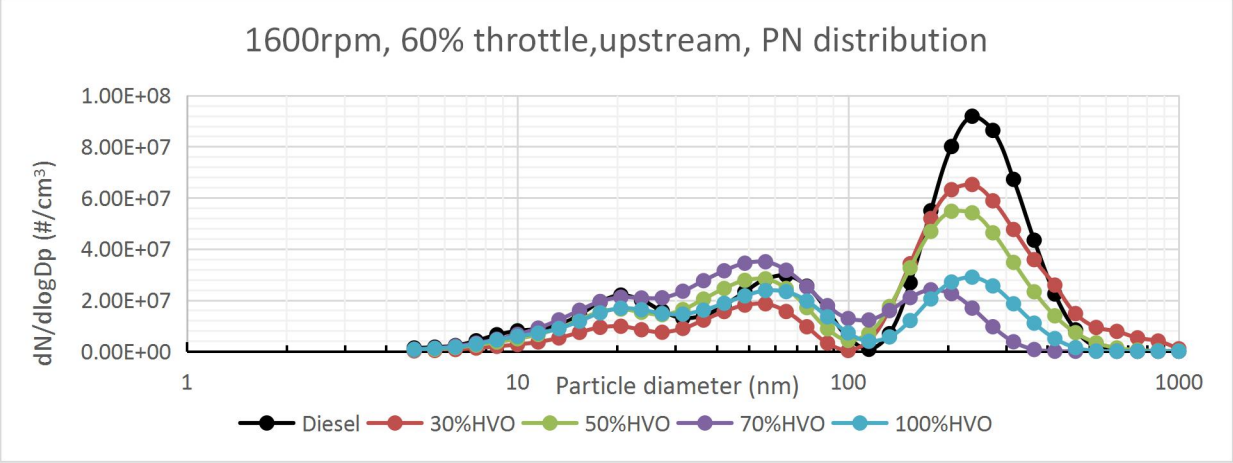


**Figure 8-31** Particle size distribution from exhaust upstream at 1600rpm, 60% throttle.

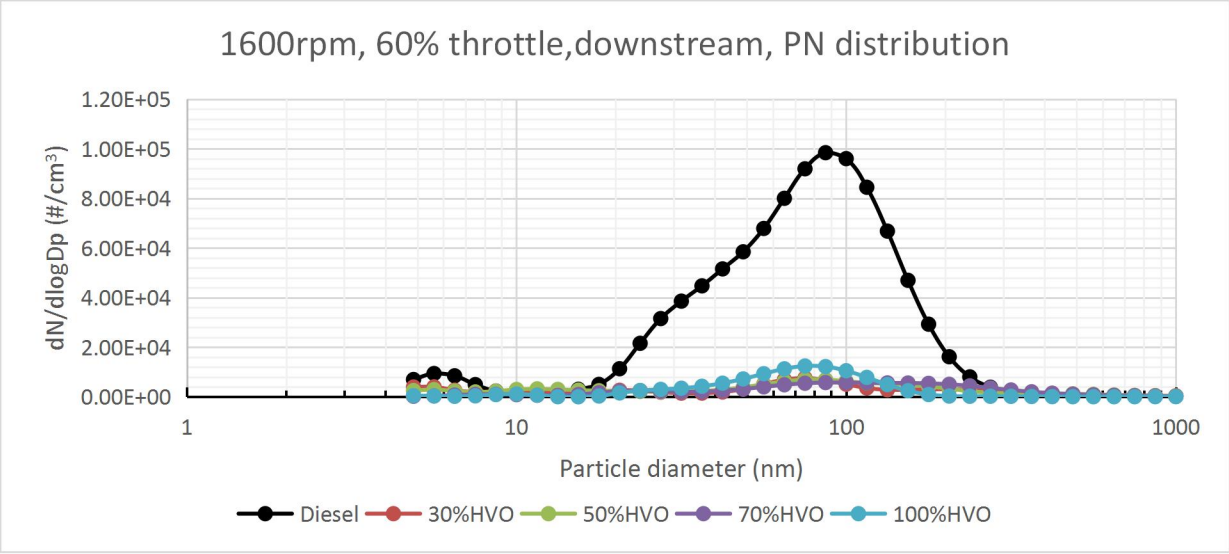


**Figure 8-32** Particle size distribution from exhaust downstream at 1600rpm, 60% throttle.

The 1900 rpm tests showed similar finding to 1600 rpm. 30% and 50% HVO showed higher peak values in accumulation mode particles than 70% and 100% HVO fuel. But all HVO blended fuel and pure HVO fuel showed significantly reduction in accumulation mode particle production. Reductions in nucleation particles were also observed from HVO and it blends, but they behaved not as significant as in accumulation mode particles.

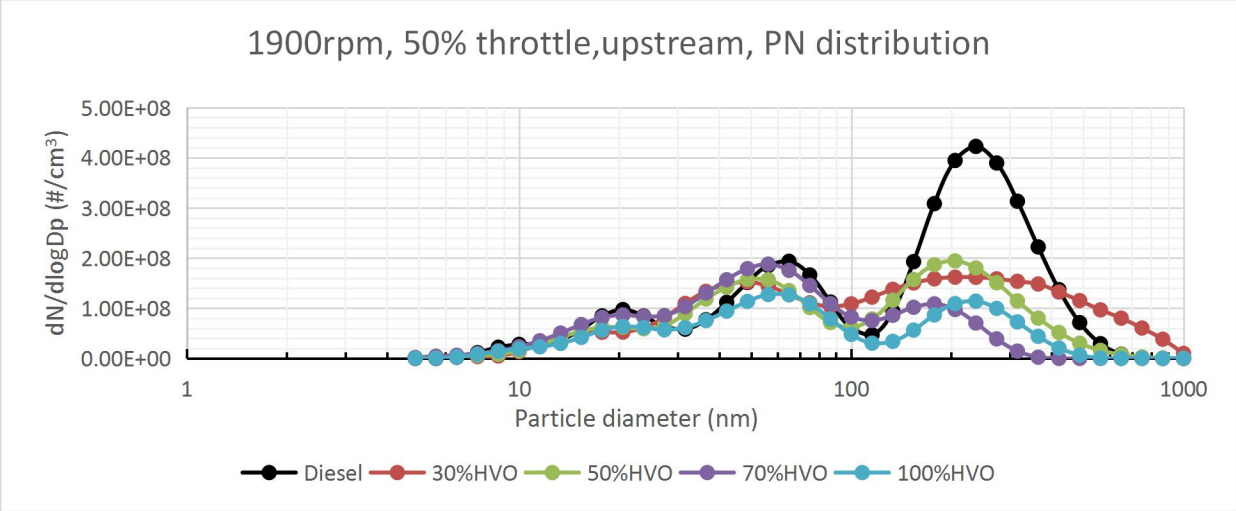


**Figure 8-33** Particle size distribution from exhaust upstream at 1900rpm, 50% throttle.

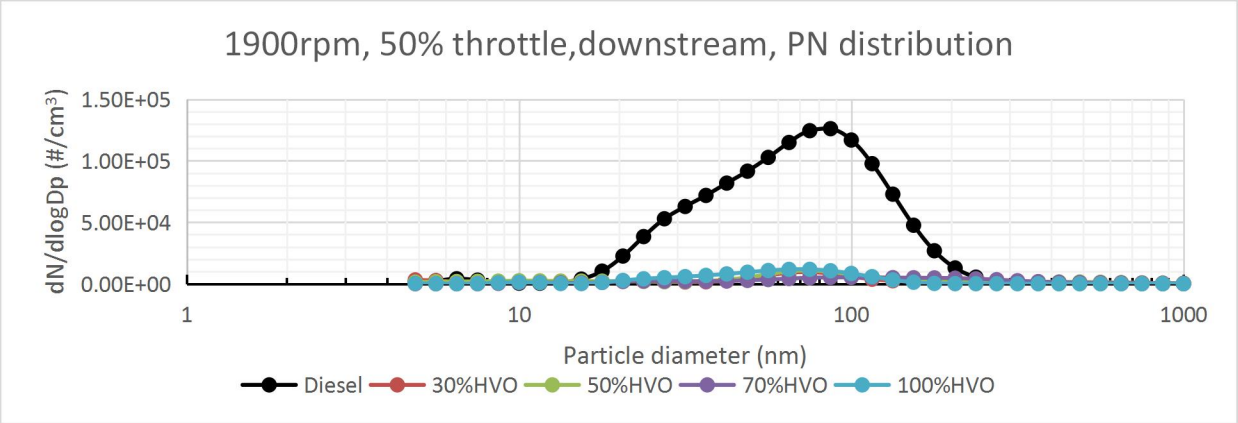


**Figure 8-34** Particle size distribution from exhaust downstream at 1900rpm, 50% throttle.

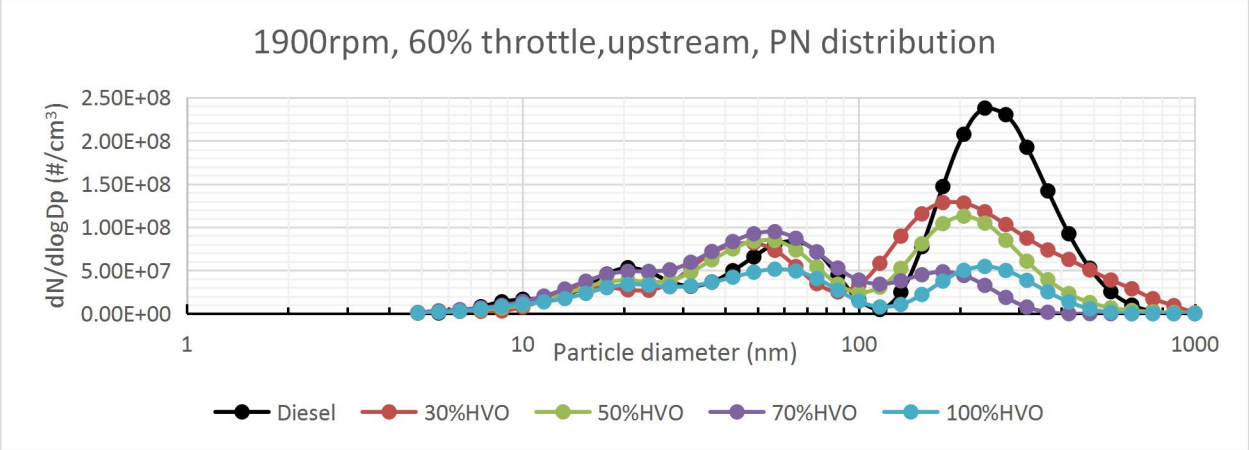


**Figure 8-35** Particle size distribution from exhaust upstream at 1900rpm, 60% throttle.

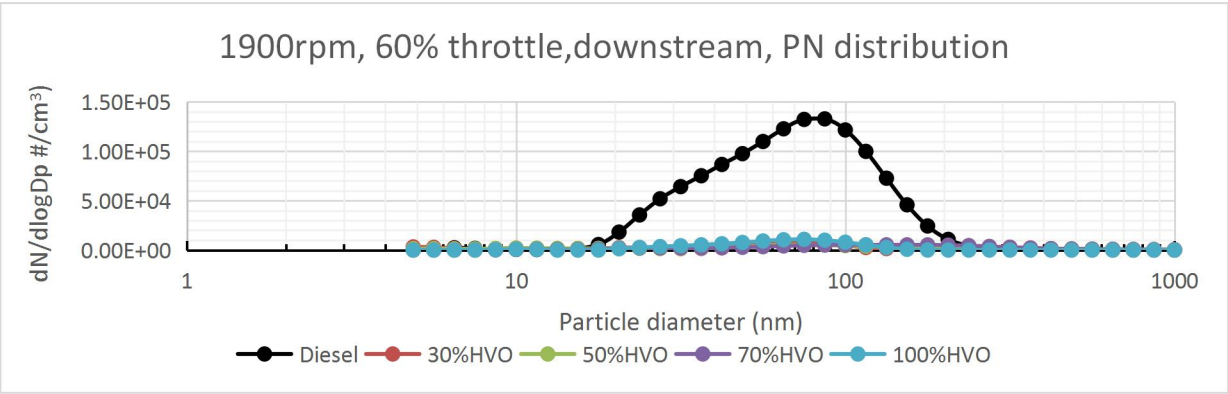


**Figure 8-36** Particle size distribution from exhaust downstream at 1900rpm, 60% throttle.

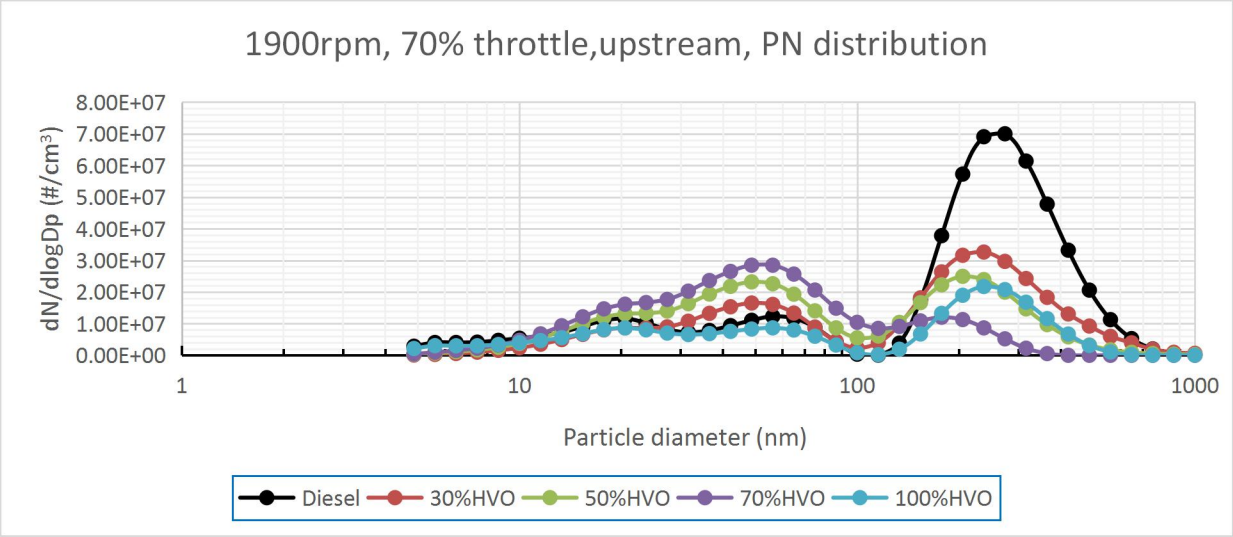


**Figure 8-37** Particle size distribution from exhaust upstream at 1900rpm, 70% throttle.

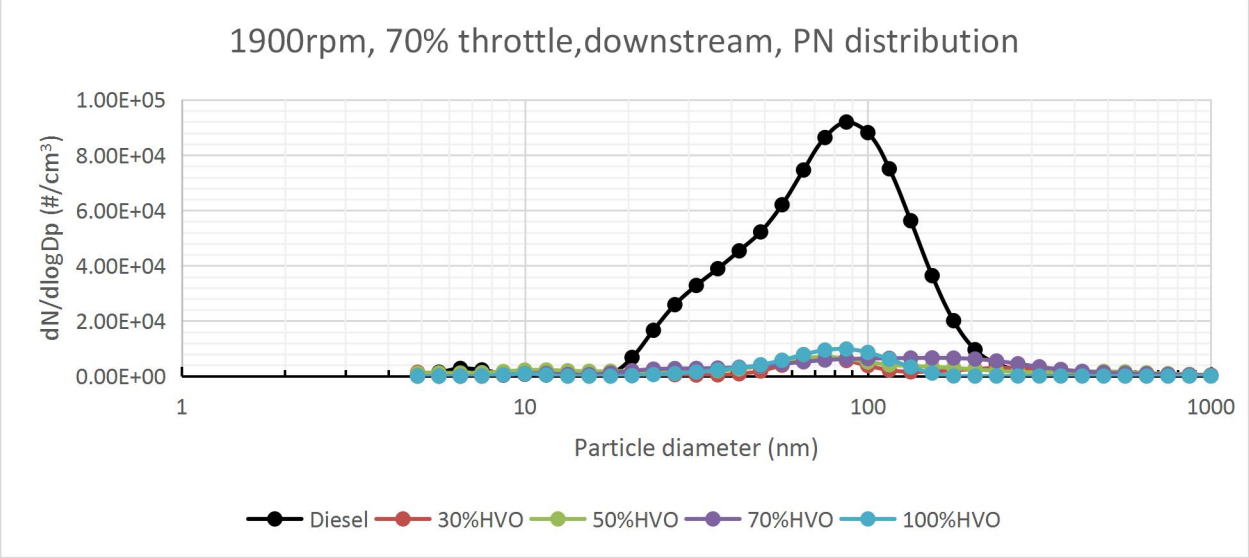


**Figure 8-38** Particle size distribution from exhaust downstream at 1900rpm, 70% throttle.

In summary, HVO and it blends can significantly improve the particle number emissions by reducing the production of accumulation mode particles ranged from 115 nm to 486 nm. The production of nucleation mode particles was also reduced by HVO and its blends albeit not as significantly as accumulation mode particles. The peak values for accumulation mode particles in general would reduce with the increasing of blending ratio but can have very similar distribution adjacent blending ratios, for instance 30%

and 50% HVO blends. The mode sizes of accumulation and nucleation mode particles located respectively at region from 237 nm to 316 nm and around 20 nm. This was due to the HVO fuel consisted of straight chains and saturated carbon paraffins, thus it's achieved more completely combustion and consequently less particles were produced. From the fuel combustion analysis provided previously, it can also be seen that pure HVO fuel had shorter ignition delays as it had higher cetane number. This indicated that pure HVO fuel also had better fuel-air mixing performance, which contributed to lower particle number emissions as well. The reduction of particle numbers was most effective from pure HVO and reduced with the reducing of blending ratio. The PN distribution curves measured at downstream of DPF were below the DMS500 lower detect limit and thus the differences between HVO and it blends can hardly be addressed. But from the downstream distribution, it can also be seen all HVO blends and pure HVO could significantly improve the PN emissions as well.

### 8.3 THC emissions

This section includes the total hydrocarbon emission performances of HVO and its blends. The THC emission was measured by HORIBA MEXA7100 and the raw data measured in ppm was converted to emission index. The THC measuring range of HORIBA MEXA7100 is from 0 to 50000 ppm, thus 0.01% error can be 5 ppm. Since only few ppm of THC was measured from the exhaust downstream, therefore it's believed that the THC measured at exhaust downstream with concentration lower than 5 ppm is nearly to zero. The THC from diesel engine is mainly formed as incomplete fuel combustion. The HVO fuel consisted of all straight chains and fully saturated paraffins, therefore it should be more easily to be burned off and produce less THC emissions.

The THC emission performances in 1000 rpm engine tests are shown from table 8-2 to table 8-4, and the relationships between THC emission and blending ratio are provided in figure 8-39 to figure 8-41. From table 8-2 to table 8-4, it can be seen that the total hydrocarbon production decreases with the increasing of blending ratio, because the more straight-chains being added to diesel fuel, the more complete fuel combustion

would be achieved and consequently less THC can be formed. Pure HVO reduced the THC emission at exhaust upstream by 59%, 31% and 42% when the throttle setting was respectively 30%, 40% and 50%. The THC reduction showed linear relationship with blending ratio, and with the engine throttle increases, the THC reduction rate decreases. The DOC could effectively remove at least 85% of THC and left only few ppm of THC being measured at exhaust downstream.

**Table 8-2** THC emissions of HVO blended fuels from exhaust upstream and downstream, with DOC efficiency, at 1000rpm 30% throttle.

| Fuel Type | THC Upstream | | | | THC Downstream | | | | DOC efficiency |
|---|---|---|---|---|---|---|---|---|---|
| | ppm | EI g/kgfuel | g/kWh | STDEVA/mean | ppm | EI g/kgfuel | g/kWh | STDEVA/mean | |
| Diesel | 108 | 1.66 | 0.52 | 9.93% | 2 | 0.03 | 0.01 | 0.00% | 98.15% |
| 30% HVO | 76 | 1.21 | 0.38 | 1.85% | 6 | 0.10 | 0.03 | 0.00% | 92.14% |
| 50% HVO | 74 | 1.21 | 0.37 | 2.62% | 3 | 0.05 | 0.02 | 0.00% | 95.92% |
| 70% HVO | 57 | 0.97 | 0.29 | 8.09% | 4 | 0.07 | 0.02 | 0.00% | 92.97% |
| 100% HVO | 44 | 0.77 | 0.23 | 6.83% | 6 | 0.11 | 0.03 | 0.00% | 86.28% |

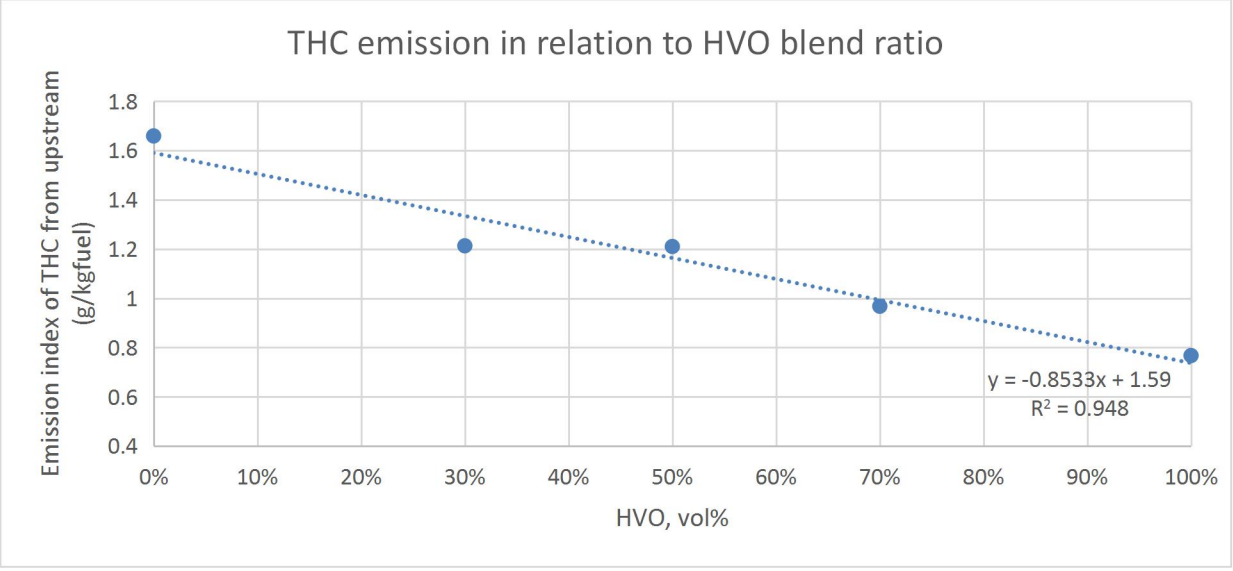


**Figure 8-39** THC emission in relation to HVO blendi ratio based on THC emission from upstream at 1000rpm, 30% throttle.

**Table 8-3** THC emissions of HVO blended fuels from exhaust upstream and downstream, with DOC efficiency, at 1000rpm 40% throttle.

| Fuel Type | THC Upstream | | | | THC Downstream | | | | DOC efficiency |
|---|---|---|---|---|---|---|---|---|---|
| | ppm | EI g/kgfuel | g/kWh | STDEVA/mean | ppm | EI g/kgfuel | g/kWh | STDEVA/mean | |
| Diesel | 77 | 0.98 | 0.30 | 8.29% | 2 | 0.03 | 0.01 | 0.00% | 97.39% |
| 30% HVO | 69 | 0.92 | 0.27 | 2.78% | 7 | 0.09 | 0.03 | 0.00% | 89.85% |
| 50% HVO | 65 | 0.90 | 0.26 | 1.91% | 3 | 0.04 | 0.01 | 0.00% | 95.39% |
| 70% HVO | 55 | 0.79 | 0.23 | 8.40% | 3 | 0.04 | 0.01 | 0.00% | 94.55% |
| 100% HVO | 53 | 0.79 | 0.22 | 3.56% | 5 | 0.07 | 0.02 | 0.00% | 90.55% |

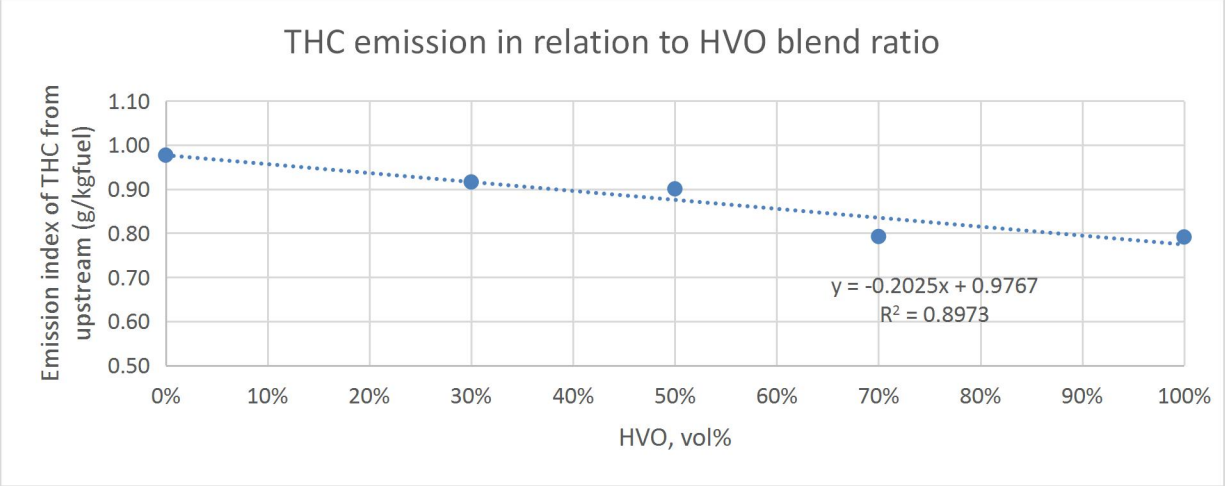


**Figure 8-40** THC emission in relation to HVO blend ratio based on THC emission from upstream at 1000rpm, 40% throttle.

**Table 8-4** THC emissions of HVO blended fuels from exhaust upstream and downstream, with DOC efficiency, at 1000rpm 50% throttle.

| Fuel Type | THC Upstream | | | | THC Downstream | | | | DOC efficiency |
|---|---|---|---|---|---|---|---|---|---|
| | ppm | EI g/kgfuel | g/kWh | STDEVA/mean | ppm | EI g/kgfuel | g/kWh | STDEVA/mean | |
| Diesel | 66 | 0.74 | 0.23 | 3.61% | 2 | 0.02 | 0.01 | 0.00% | 96.95% |
| 30% HVO | 56 | 0.66 | 0.20 | 1.99% | 2 | 0.02 | 0.01 | 4.72% | 96.42% |
| 50% HVO | 46 | 0.57 | 0.17 | 3.84% | 3 | 0.04 | 0.01 | 0.00% | 93.54% |
| 70% HVO | 38 | 0.49 | 0.15 | 2.54% | 4 | 0.05 | 0.02 | 0.00% | 89.57% |
| 100% HVO | 38 | 0.51 | 0.15 | 2.17% | 6 | 0.08 | 0.02 | 6.11% | 84.53% |

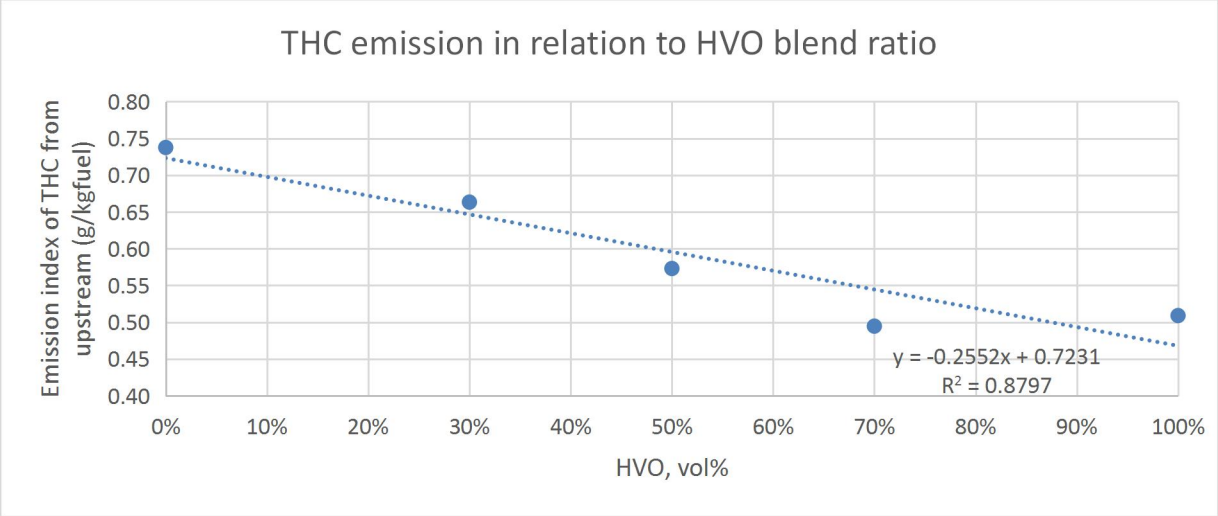


**Figure 8-41** THC emission in relation to HVO blend ratio based on THC emission from upstream at 1000rpm, 50% throttle.

**Table 8-5** THC emissions of HVO blended fuels from exhaust upstream and downstream, with DOC efficiency, at 1600rpm 40% throttle.

| Fuel Type | THC Upstream | | | | THC Downstream | | | | DOC efficiency |
|---|---|---|---|---|---|---|---|---|---|
| | ppm | EI g/kgfuel | g/kWh | STDEVA/mean | ppm | EI g/kgfuel | g/kWh | STDEVA/mean | |
| Diesel | 83 | 1.19 | 0.35 | 3.55% | 8 | 0.11 | 0.03 | 9.66% | 90.56% |
| 30% HVO | 75 | 1.12 | 0.33 | 1.71% | 6 | 0.09 | 0.03 | 0.00% | 92.04% |
| 50% HVO | 72 | 1.12 | 0.33 | 1.80% | 3 | 0.05 | 0.01 | 0.00% | 95.86% |
| 70% HVO | 54 | 0.87 | 0.25 | 1.68% | 3 | 0.05 | 0.01 | 0.00% | 94.46% |
| 100% HVO | 51 | 0.85 | 0.24 | 2.58% | 5 | 0.07 | 0.02 | 0.00% | 90.22% |

**Table 8-6** THC emissions of HVO blended fuels from exhaust upstream and downstream, with DOC efficiency, at 1600rpm 50% throttle.

| Fuel Type | THC Upstream | | | | THC Downstream | | | | DOC efficiency |
|---|---|---|---|---|---|---|---|---|---|
| | ppm | EI g/kgfuel | g/kWh | STDEVA/mean | ppm | EI g/kgfuel | g/kWh | STDEVA/mean | |
| Diesel | 71 | 0.96 | 0.28 | 1.74% | 7 | 0.10 | 0.03 | 5.40% | 89.85% |
| 30% HVO | 63 | 0.89 | 0.25 | 1.75% | 5 | 0.07 | 0.02 | 0.00% | 92.04% |
| 50% HVO | 60 | 0.89 | 0.24 | 1.51% | 3 | 0.04 | 0.01 | 0.00% | 95.01% |
| 70% HVO | 47 | 0.72 | 0.19 | 1.56% | 3 | 0.05 | 0.01 | 0.00% | 93.61% |
| 100% HVO | 44 | 0.70 | 0.19 | 1.57% | 4 | 0.06 | 0.02 | 0.00% | 91.00% |

**Table 8-7** THC emissions of HVO blended fuels from exhaust upstream and downstream, with DOC efficiency, at 1600rpm 60% throttle.

| Fuel Type | THC Upstream | | | | THC Downstream | | | | DOC efficiency |
|---|---|---|---|---|---|---|---|---|---|
| | ppm | EI g/kgfuel | g/kWh | STDEVA/mean | ppm | EI g/kgfuel | g/kWh | STDEVA/mean | |
| Diesel | 62 | 0.81 | 0.22 | 2.33% | 7 | 0.09 | 0.03 | 14.03% | 88.66% |
| 30% HVO | 53 | 0.73 | 0.20 | 1.78% | 5 | 0.07 | 0.02 | 0.00% | 90.60% |
| 50% HVO | 52 | 0.74 | 0.20 | 1.69% | 3 | 0.04 | 0.01 | 0.00% | 94.23% |
| 70% HVO | 46 | 0.67 | 0.18 | 1.95% | 4 | 0.06 | 0.02 | 0.00% | 91.23% |
| 100% HVO | 44 | 0.67 | 0.17 | 2.67% | 4 | 0.06 | 0.02 | 0.00% | 90.87% |

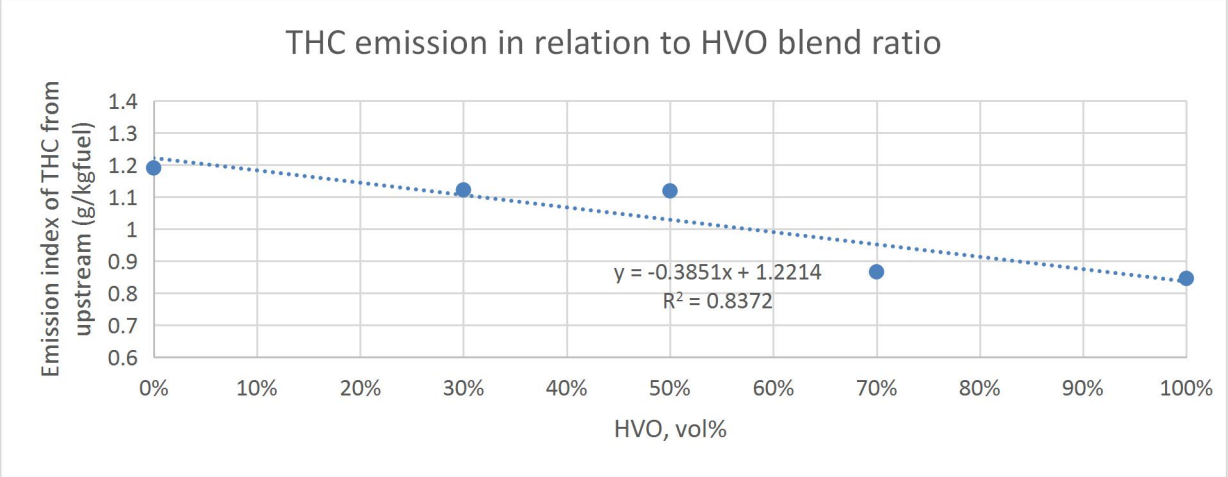


**Figure 8-42** THC emission in relation to HVO blend ratio based on THC emission from upstream at 1600rpm, 40% throttle.

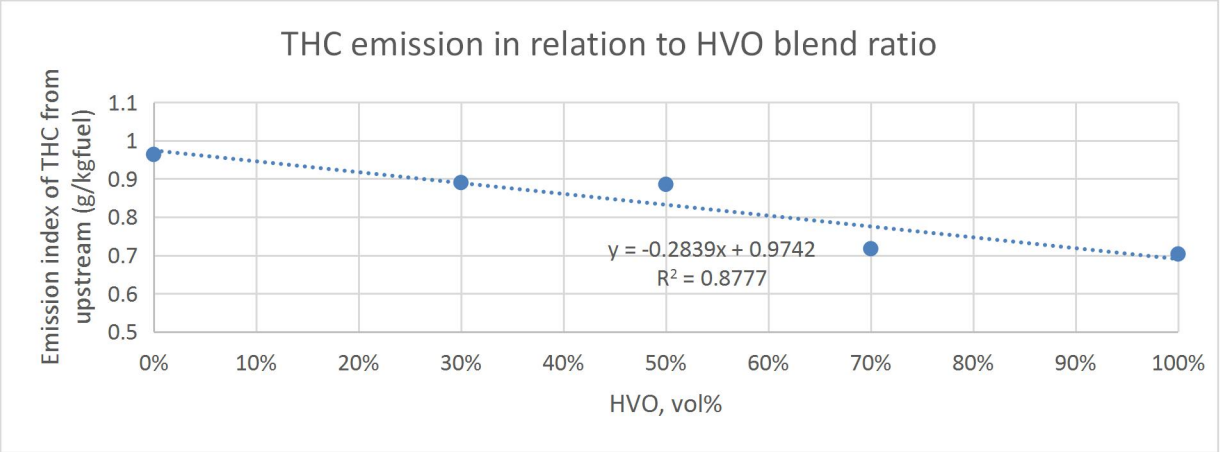


**Figure 8-43** THC emission in relation to HVO blend ratio based on THC emission from upstream at 1600rpm, 50% throttle.

From table 8-5 to table 8-7, same findings be obtained from 1600 rpm's tests as from 1000 rpm's tests: the THC emission reduces with the increasing of blending ratio. The DOC efficiencies are quite similar between different types of fuels at each specific engine operating condition at this engine speed. If compare the THC reduction performance from figure 8-42 to figure 8-44, it can be found that the gradient of THC reduction reduces from -0.39 to -0.28 and -0.14 at the respective 40%, 50% and 60% throttle settings. This was due to with the throttle percentage increased, the fuel atomization, evaporation and to air mixing performance all can be improved as the average combustion temperature being increased. Therefore, the advantage of fuel properties would become less significant. This can also be proved as the THC reduction by pure HVO fuel at 1600 rpm reduced from 39% to 38% and 29% with the throttle increased from 40% to 50% and 60%.

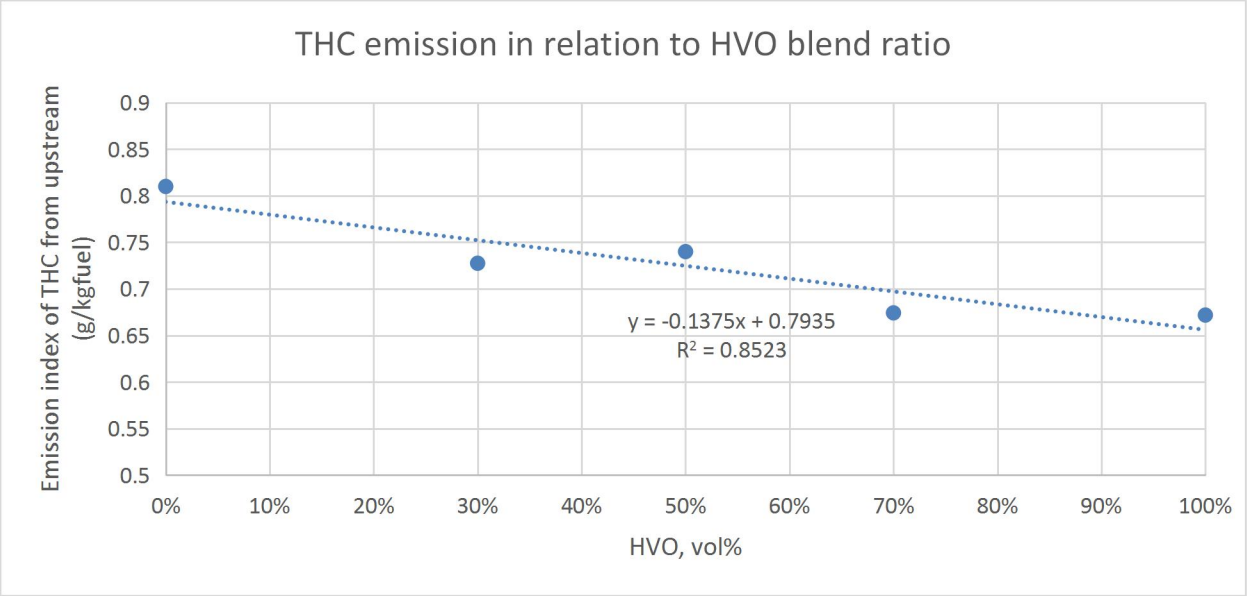


**Figure 8-44** THC emission in relation to HVO blend ratio based on THC emission from upstream at 1600rpm, 60% throttle.

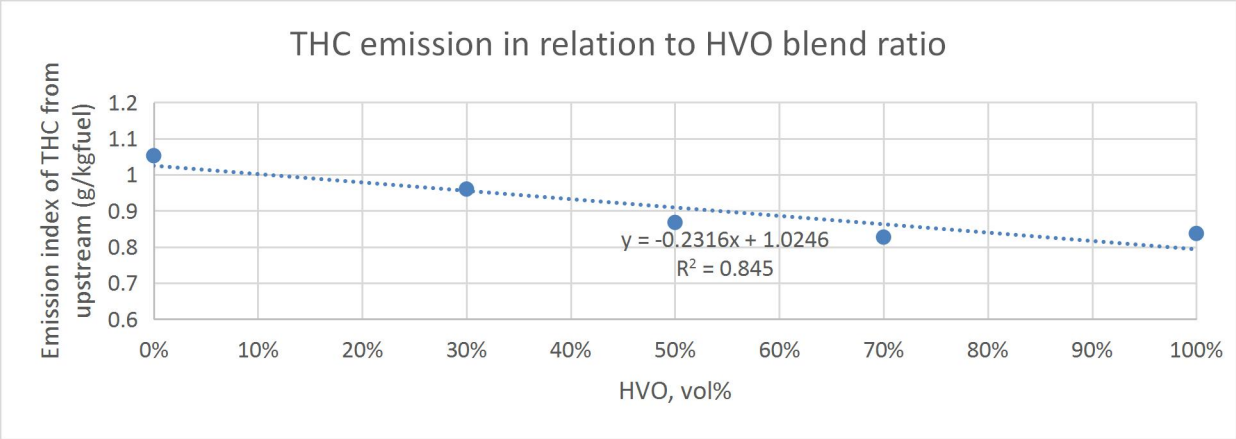


**Figure 8-45** THC emission in relation to HVO blend ratio based on THC emission from upstream at 1900rpm, 50% throttle.

**Table 8-8** THC emissions of HVO blended fuels from exhaust upstream and downstream, with DOC efficiency, at 1900rpm 50% throttle.

| Fuel Type | THC Upstream | | | | THC Downstream | | | | DOC efficiency |
|---|---|---|---|---|---|---|---|---|---|
| | ppm | EI g/kgfuel | g/kWh | STDEVA/mean | ppm | EI g/kgfuel | g/kWh | STDEVA/mean | |
| Diesel | 75 | 1.05 | 0.29 | 2.11% | 7 | 0.10 | 0.03 | 7.79% | 90.65% |
| 30% HVO | 67 | 0.96 | 0.27 | 2.00% | 5 | 0.07 | 0.02 | 0.00% | 92.50% |
| 50% HVO | 57 | 0.87 | 0.23 | 1.65% | 2 | 0.03 | 0.01 | 0.00% | 96.50% |
| 70% HVO | 53 | 0.83 | 0.22 | 1.22% | 4 | 0.06 | 0.02 | 0.00% | 92.39% |
| 100% HVO | 51 | 0.84 | 0.21 | 1.64% | 4 | 0.07 | 0.02 | 0.00% | 92.22% |

**Table 8-9** THC emissions of HVO blended fuels from exhaust upstream and downstream, with DOC efficiency, at 1900rpm 60% throttle.

| Fuel Type | THC Upstream | | | | THC Downstream | | | | DOC efficiency |
|---|---|---|---|---|---|---|---|---|---|
| | ppm | EI g/kgfuel | g/kWh | STDEVA/mean | ppm | EI g/kgfuel | g/kWh | STDEVA/mean | |
| Diesel | 74 | 1.00 | 0.27 | 1.52% | 9 | 0.12 | 0.03 | 11.72% | 87.93% |
| 30% HVO | 62 | 0.88 | 0.24 | 1.38% | 4 | 0.06 | 0.02 | 0.00% | 93.58% |
| 50% HVO | 61 | 0.89 | 0.23 | 1.68% | 3 | 0.04 | 0.01 | 0.00% | 95.05% |
| 70% HVO | 48 | 0.73 | 0.19 | 1.55% | 3 | 0.05 | 0.01 | 0.00% | 93.77% |
| 100% HVO | 46 | 0.73 | 0.19 | 1.49% | 3 | 0.05 | 0.01 | 0.00% | 93.54% |

**Table 8-10** THC emissions of HVO blended fuels from exhaust upstream and downstream, with DOC efficiency, at 1900rpm 70% throttle.

| Fuel Type | THC Upstream | | | | THC Downstream | | | | DOC efficiency |
|---|---|---|---|---|---|---|---|---|---|
| | ppm | EI g/kgfuel | g/kWh | STDEVA/mean | ppm | EI g/kgfuel | g/kWh | STDEVA/mean | |
| Diesel | 68 | 0.94 | 0.25 | 1.76% | 7 | 0.10 | 0.03 | 14.35% | 89.03% |
| 30% HVO | 56 | 0.80 | 0.21 | 2.03% | 5 | 0.07 | 0.02 | 0.00% | 91.07% |
| 50% HVO | 53 | 0.79 | 0.20 | 9.76% | 3 | 0.04 | 0.01 | 0.00% | 94.35% |
| 70% HVO | 48 | 0.74 | 0.19 | 1.75% | 4 | 0.06 | 0.02 | 0.00% | 91.70% |
| 100% HVO | 47 | 0.76 | 0.19 | 1.44% | 4 | 0.06 | 0.02 | 0.00% | 91.54% |

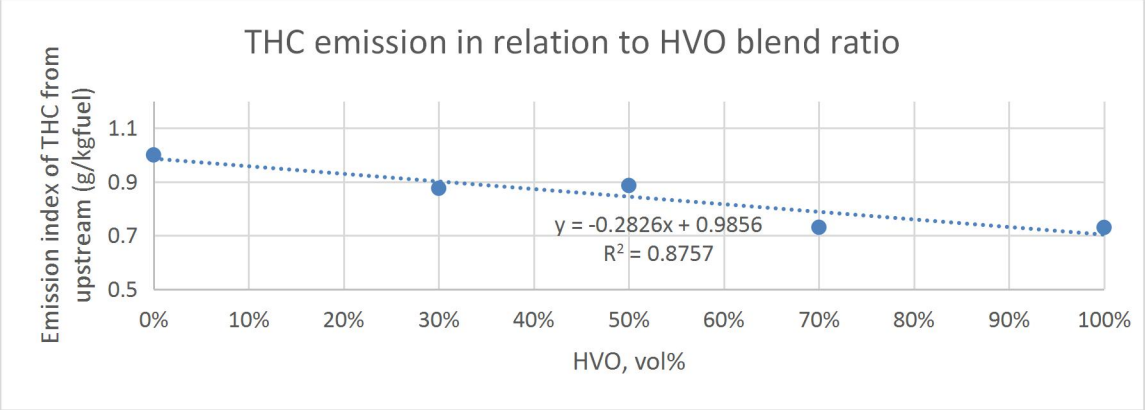


**Figure 8-46** THC emission in relation to HVO blend ratio based on THC emission from upstream at 1900rpm, 60% throttle.

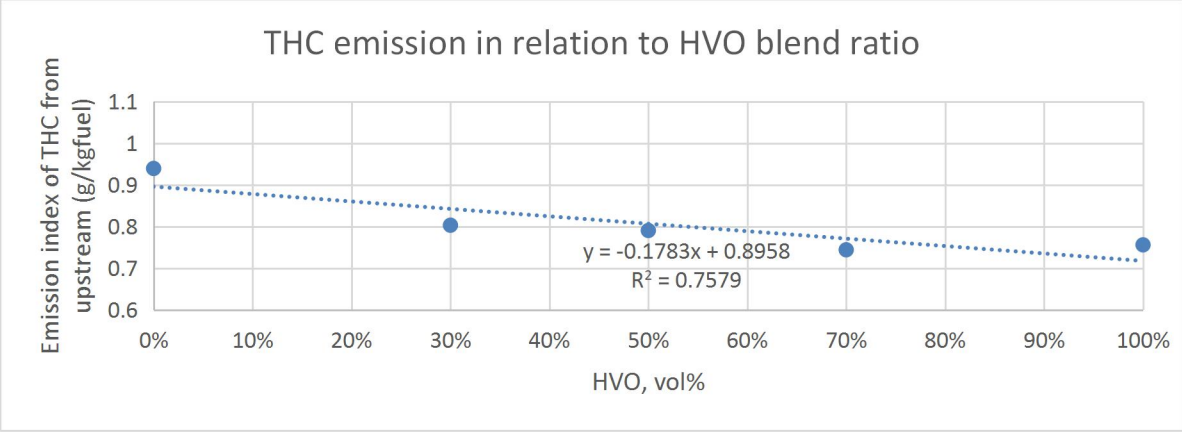


**Figure 8-47** THC emission in relation to HVO blend ratio based on THC emission from upstream at 1900rpm, 70% throttle.

When the engine rpm increased to 1900 rpm, the THC reduction by pure HVO fuel behaved similar: at 50%, 60% and 70% throttle settings, respectively 32%, 38% and 30% reductions were acquired. This is because the engine is operating at relevantly high-power condition, and when the engine power is high enough, all tested fuels can share similar fuel mixing performances regardless of either increasing or decreasing the throttle settings. Therefore, the THC reductions were between fuels are close. The DOC efficiency ranged from 87% to 97% at this engine speed.

In summary, the pure HVO fuel can significantly improve the THC production by 30% to 59% at exhaust upstream because it's more easily to be burned completely. And consequently, with the HVO blending ratio increases, the THC reduction would become more effective. The THC production and blending ratio are generally in linear relationship. The DOC aftertreatment system was able to remove at least 85% of THC from exhaust upstream and left only few ppm's THC existed at exhaust downstream.

### 8.4 CO emissions

This section presents the results and discussion of CO emissions from HVO blended fuels. The CO emission can be a critical indicator for the fuel-air mixing performances because the CO is formed as the failure to acquire 100% ideal lean combustion. The equipment used for CO measurement was HORIBA MEXA7100, with measuring range from 0 to 5000 ppm. The maximum CO concentration measured from exhaust downstream was 4 ppm, with 0 ppm in most of tests and 2 to 3 ppm very occasionally. Thus, it's believed that there was hardly any CO existed at downstream of DOC, because just 0.05% of 5000 ppm equals 2.5 ppm, and the few ppm measured at exhaust downstream can be lower than the detection lower limits. The CO emission index results are shown in following tables from 8-11 to table 8-19, and the standard deviation divided by average value is provided as well so as to indicate the stability of CO production.

From table 8-11 to table 8-19, it can be seen that only the pure HVO fuel could help to improve the CO production in all three tested conditions at 1000 rpm engine speed, while all blended fuel can either produce more or less CO than diesel. The CO production from blended fuels can be up to 22% lower or 19% higher than diesel fuel.

And with the throttle increased from 30% to 50%, the CO production from all tested fuels increased. Except for the pure HVO, CO production slightly reduced while throttle increased from 30% to 40%. This can be attribute to the CO production stability as if considering the STEDEV/mean, the CO produced from pure HVO fuel at 40% throttle could be higher than at 30% throttle. The reason all fuels demonstrated increasingly CO production with throttle percentage being raised is that 1000 rpm speed is too low to achieve satisfied fuel-air mixing required by lean combustion. And increasing the throttle would increase the fuel injection while the turbulence generated by piston moving was remained. Therefore, the fuel-air mixing was worsened at such conditions, and consequently increased the CO emission. This can be proved from table 8-13, that at 50% throttle, the CO emission was over 6 times than in previous tests, indicating the poorest fuel-air mixing occurred at this condition. This result aligned with GTL and its blends, and the PN emission also increased dramatically at this engine operating condition.

**Table 8-11** CO emissions of HVO blended fuel at 1000rpm, 30% throttle.

| Fuel Type | CO Upstream | | | | CO Downstream | | | |
|---|---|---|---|---|---|---|---|---|
| | ppm | EI g/kgfuel | g/kWh | STDEVA/mean | ppm | EI g/kgfuel | g/kWh | STDEVA/mean |
| Diesel | 157 | 4.22 | 1.33 | 4.14% | 0 | 0.00 | 0.00 | 0.00% |
| 30% HVO | 121 | 3.36 | 1.05 | 6.23% | 0 | 0.00 | 0.00 | 0.00% |
| 50% HVO | 116 | 3.35 | 1.02 | 6.98% | 0 | 0.00 | 0.00 | 0.00% |
| 70% HVO | 125 | 3.71 | 1.13 | 9.14% | 0 | 0.00 | 0.00 | 0.00% |
| 100% HVO | 104 | 3.19 | 0.95 | 7.09% | 0 | 0.00 | 0.00 | 0.00% |

**Table 8-12** CO emissions of HVO blended fuel at 1000rpm, 40% throttle.

| Fuel Type | CO Upstream | | | | CO Downstream | | | |
|---|---|---|---|---|---|---|---|---|
| | ppm | EI g/kgfuel | g/kWh | STDEVA/mean | ppm | EI g/kgfuel | g/kWh | STDEVA/mean |
| Diesel | 161 | 3.59 | 1.09 | 8.53% | 0 | 0.00 | 0.00 | 0.00% |
| 30% HVO | 191 | 4.45 | 1.30 | 6.06% | 0 | 0.00 | 0.00 | 0.00% |
| 50% HVO | 198 | 4.80 | 1.37 | 7.44% | 0 | 0.00 | 0.00 | 0.00% |
| 70% HVO | 185 | 4.67 | 1.34 | 6.00% | 0 | 0.00 | 0.00 | 0.00% |
| 100% HVO | 99 | 2.60 | 0.73 | 7.70% | 0 | 0.00 | 0.00 | 0.00% |

**Table 8-13** CO emissions of HVO blended fuel at 1000rpm, 50% throttle.

| Fuel Type | CO Upstream | | | | CO Downstream | | | |
|---|---|---|---|---|---|---|---|---|
| | ppm | EI g/kgfuel | g/kWh | STDEVA/mean | ppm | EI g/kgfuel | g/kWh | STDEVA/mean |
| Diesel | 1405 | 27.64 | 8.46 | 3.47% | 0 | 0.00 | 0.00 | 0.00% |
| 30% HVO | 1160 | 23.95 | 7.16 | 6.10% | 0 | 0.00 | 0.00 | 0.00% |
| 50% HVO | 1187 | 25.64 | 7.63 | 4.38% | 2 | 0.04 | 0.01 | 0.00% |
| 70% HVO | 1218 | 27.50 | 8.12 | 3.29% | 2 | 0.05 | 0.01 | 0.00% |
| 100% HVO | 1173 | 27.61 | 7.96 | 3.16% | 0 | 0.00 | 0.00 | 0.00% |

When the engine entered 1600 rpm tests condition, the CO production from all fuels gradually reduced with the throttle setting being increased. This indicates that when the engine reached this speed, the fuel-air mixing would be improved with the throttle increased. Because with throttle opening percentage increased, the more fuel would be injected into combustion cylinder and consequently can bring the engine higher in-cylinder temperature which is beneficial to the fuel mixing. The CO production at engine out between diesel and HVO blends was close, and still only pure HVO fuel could acquire obvious CO reduction. It improved the CO emission by 10%, 15% and 19% at respectively 40%, 50%, and 60% throttle settings. Considering the HVO fuel consisted of more vulnerable carbon chains, and the fuel-air mixing at 1600 rpm was improved with throttle increased, therefore, more significant fuel mixing can be achieved by pure HVO, and consequently the more effective CO reduction can be acquired.

**Table 8-14** CO emissions of HVO blended fuel at 1600rpm, 40% throttle.

| Fuel Type | CO Upstream | | | | CO Downstream | | | |
|---|---|---|---|---|---|---|---|---|
| | ppm | EI g/kgfuel | g/kWh | STDEVA/mean | ppm | EI g/kgfuel | g/kWh | STDEVA/mean |
| Diesel | 182 | 4.57 | 1.34 | 1.67% | 0 | 0.00 | 0.00 | 0.00% |
| 30% HVO | 189 | 4.93 | 1.46 | 1.56% | 0 | 0.00 | 0.00 | 0.00% |
| 50% HVO | 183 | 4.93 | 1.45 | 1.49% | 0 | 0.00 | 0.00 | 0.00% |
| 70% HVO | 173 | 4.85 | 1.40 | 2.98% | 0 | 0.00 | 0.00 | 0.00% |
| 100% HVO | 163 | 4.73 | 1.34 | 3.09% | 0 | 0.00 | 0.00 | 0.00% |

**Table 8-15** CO emissions of HVO blended fuel at 1600rpm, 50% throttle.

| Fuel Type | CO Upstream | | | | CO Downstream | | | |
|---|---|---|---|---|---|---|---|---|
| | ppm | EI g/kgfuel | g/kWh | STDEVA/mean | ppm | EI g/kgfuel | g/kWh | STDEVA/mean |
| Diesel | 117 | 2.80 | 0.81 | 2.41% | 0 | 0.00 | 0.00 | 0.00% |
| 30% HVO | 120 | 2.98 | 0.82 | 2.53% | 0 | 0.00 | 0.00 | 0.00% |
| 50% HVO | 121 | 3.11 | 0.84 | 2.29% | 0 | 0.00 | 0.00 | 0.00% |
| 70% HVO | 112 | 3.00 | 0.81 | 2.95% | 0 | 0.00 | 0.00 | 0.00% |
| 100% HVO | 99 | 2.76 | 0.73 | 2.80% | 0 | 0.00 | 0.00 | 0.00% |

**Table 8-16** CO emissions of HVO blended fuel at 1600rpm, 60% throttle.

| Fuel Type | CO Upstream | | | | CO Downstream | | | |
|---|---|---|---|---|---|---|---|---|
| | ppm | EI g/kgfuel | g/kWh | STDEVA/mean | ppm | EI g/kgfuel | g/kWh | STDEVA/mean |
| Diesel | 97 | 2.23 | 0.62 | 4.54% | 2 | 0.05 | 0.01 | 28.57% |
| 30% HVO | 91 | 2.17 | 0.58 | 5.07% | 1 | 0.02 | 0.01 | 0.00% |
| 50% HVO | 86 | 2.14 | 0.58 | 3.63% | 0 | 0.00 | 0.00 | 0.00% |
| 70% HVO | 78 | 2.03 | 0.54 | 6.41% | 0 | 0.00 | 0.00 | 0.00% |
| 100% HVO | 79 | 2.11 | 0.54 | 5.38% | 0 | 0.00 | 0.00 | 0.00% |

**Table 8-17** CO emissions of HVO blended fuel at 1900rpm, 50% throttle.

| Fuel Type | CO Upstream | | | | CO Downstream | | | |
|---|---|---|---|---|---|---|---|---|
| | ppm | EI g/kgfuel | g/kWh | STDEVA/mean | ppm | EI g/kgfuel | g/kWh | STDEVA/mean |
| Diesel | 153 | 3.77 | 1.05 | 1.96% | 2 | 0.05 | 0.01 | 0.00% |
| 30% HVO | 143 | 3.60 | 1.00 | 3.84% | 0 | 0.00 | 0.00 | 0.00% |
| 50% HVO | 114 | 3.03 | 0.82 | 1.81% | 0 | 0.00 | 0.00 | 0.00% |
| 70% HVO | 160 | 4.40 | 1.17 | 1.21% | 0 | 0.00 | 0.00 | 0.00% |
| 100% HVO | 143 | 4.08 | 1.05 | 2.33% | 0 | 0.00 | 0.00 | 0.00% |

The 1900 rpm's CO results are shown in following tables from table 8-17 to table 8-19. From the comparison, similar finding can be acquired as from previous 1600 rpm tests that only pure HVO fuel showed obvious CO improvement while blended fuels showed

CO emission either 10% higher or 15% lower than diesel fuel. The pure HVO fuel performed slightly higher CO emission than diesel at 1900 rpm, 70% throttle. This can be explained as the fuel injection of HVO was slightly higher than diesel fuel because the HVO fuel obtained lower density. At this test condition, the engine power is high enough to ignite all fuels, thus the advantages of straight carbon chains of HVO fuel can be insignificant. Thus, the extra fuel injection from HVO fuel could result less satisfied fuel-air mixing and consequently bring slightly higher CO production. The CO emission from blended fuels showed no certain relationship with blending ratio, indicated that HVO blends can have poor stability in fuel-air mixing before the fuel combustion started. The CO emission measured at downstream of DOC was almost zero, indicating all CO generated from exhaust upstream was oxidised to $CO_2$ when exhaust passed through the DOC system.

**Table 8-18** CO emissions of HVO blended fuel at 1900rpm, 60% throttle.

| Fuel Type | CO Upstream | | | | CO Downstream | | | |
|---|---|---|---|---|---|---|---|---|
| | ppm | EI g/kgfuel | g/kWh | STDEVA/mean | ppm | EI g/kgfuel | g/kWh | STDEVA/mean |
| Diesel | 98 | 2.31 | 0.63 | 2.54% | 2 | 0.05 | 0.01 | 0.00% |
| 30% HVO | 99 | 2.44 | 0.66 | 2.03% | 0 | 0.00 | 0.00 | 0.00% |
| 50% HVO | 99 | 2.54 | 0.67 | 2.00% | 0 | 0.00 | 0.00 | 0.00% |
| 70% HVO | 99 | 2.63 | 0.70 | 2.03% | 1 | 0.03 | 0.01 | 0.00% |
| 100% HVO | 92 | 2.54 | 0.65 | 2.97% | 0 | 0.00 | 0.00 | 0.00% |

**Table 8-19** CO emissions of HVO blended fuel at 1900rpm, 70% throttle.

| Fuel Type | CO Upstream | | | | CO Downstream | | | |
|---|---|---|---|---|---|---|---|---|
| | ppm | EI g/kgfuel | g/kWh | STDEVA/mean | ppm | EI g/kgfuel | g/kWh | STDEVA/mean |
| Diesel | 55 | 1.34 | 0.35 | 3.92% | 3 | 0.08 | 0.02 | 19.23% |
| 30% HVO | 66 | 1.66 | 0.43 | 3.96% | 0 | 0.00 | 0.00 | 0.00% |
| 50% HVO | 69 | 1.80 | 0.45 | 9.80% | 1 | 0.03 | 0.01 | 0.00% |
| 70% HVO | 62 | 1.68 | 0.43 | 3.39% | 4 | 0.11 | 0.03 | 0.00% |
| 100% HVO | 59 | 1.64 | 0.41 | 5.34% | 0 | 0.00 | 0.00 | 0.00% |

In summary, at engine exhaust upstream, the pure HVO fuel can improve the CO emission by up to 38%, while the HVO blended fuels showed CO emission up to 22% different from diesel. Because HVO consisted with all straight carbon chains as thus can achieve be ignited easier. The fuel to air mixing performances acquired in 1000 rpm were not satisfied and consequently the CO emission from all tested fuels increased with the throttle setting increased. When the engine speed reached 1600 rpm and 1900 rpm, the CO production would decrease with the throttle setting increases because the pressure and temperature in combustion cylinder raised high enough to achieve stoichiometric fuel-air mixing. At engine downstream of DOC, hardly any detectable CO was found because the DOC successfully oxidised the nearly all CO generated from upstream, and also the CO measurement device had its lower detect limit in around 3 ppm.

## 8.5 Conclusions

Based on the discussion and analysis of emissions from HVO and its blends, the following conclusions can be obtained:

- The pure HVO fuel didn't show reduction of $NO_x$ emission in all test conditions. Actually, the pure HVO could have slightly higher $NO_X$ emission from 1% to 15%.
- The blended HVO fuels were effective in $NO_x$ reductions, with just 30% HVO blended into diesel, 26% to 47% of $NO_x$ reduction was observed in the majority of test conditions. The 50%, 70% HVO blended fuels showed similar reduction efficiencies. However, the reduction didn't show particular relationship with blending ratio. It's believed that certain concentration of aromatics in a fuel could act as anti-oxidants that helps to control $NO_x$ emissions. The concentration of aromatics is estimated to be in a range from 7.5% to 17.5%.
- The engine out NO could be converted to $NO_2$ by DOC. The conversion rate was found to be 25% to 50%.
- The HVO and its blends were capable of reducing the particle number emissions both in nucleation and accumulation mode particles. The reduction in nucleation

mode particles (7-50 nm) were obvious in lower engine power conditions (up to 38%), while the reduction in particles with diameter greater than 100 nm was significant at high engine power conditions (up to 80%). Similar to the results of GTL and its blends, the total particle number reduction increased when the blending ratio was increased. The accumulation mode particles are more sensitive to blending ratios than the nucleation mode particles. In general, the peak values of accumulation mode particles reduced when the blend ratio was increased and ranged between 237 nm to 316 nm. The nucleation mode particle distribution between fuels are similar and most of the nucleation mode particles are in diameter region of 10 to 20 nm.

- The DPF showed efficiencies of higher than 99% in all test conditions, because the scale of particle number measure at upstream of DPF was over 1000 times greater than at downstream of DPF, and thus left hardly any detectable particles at the downstream of DPF.
- The pure HVO fuel and its blends can reduce the THC emissions by up to 59%, and the reduction increased when the blend ratio was increased. However, the reduction became insignificant when the engine power increased, because fuel premixing was improved with increased engine power settings. The DOC was capable of removing at least 85% of THC and left hardly any detectable THC at the downstream of DOC.
- The pure HVO fuel can help to reduce the CO emission at the engine out by up to 38%. However, the HVO blended fuels showed similar CO production with diesel fuel at each specific engine operating condition and showed no particular trend with blend ratios.

Therefore, comparing the emission results of HVO, GTL and their blends, it can be found that both these two aromatics free fuels could reduce the particle number and THC emissions significantly. And the reduction in PN and THC increased with the blend ratio increased. This is due to the aromatic free fuel which consisted of straight chains is burned more completely. The $NO_x$ emission was also reduced using their blends albeit the pure HVO and GTL fuels didn't show clear $NO_X$ emission reduction. This is due to the aromatic concentrations being changed in blended fuels and enable aromatics to be

as anti-oxidants, for instance, 30% was the most effective blend ratio in $NO_x$ reduction for both GTL and HVO fuels.

# Chapter 9. Conclusion and future work

The research of this PhD project can be summarized into two categories: the particle number measurement research and the alternative fuel research. The particle number measurement research involves the comparison of instruments and is trying to provide the optimum way for particle number measurement. The study of alternative fuels (GTL, HVO and their blended fuels) on diesel engine provides systematic research on engine combustion and emission, especially the $NO_X$ emissions. This chapter summarizes the core findings achieved from chapter 4 to chapter 8 (the detailed conclusions of is provided in the last section of each chapter). Based on these core findings, the recommendations for future research are given.

## 9.1 Conclusions

The main findings from the particle number measurement can be summarized below:

- All tested instruments were all capable of measuring particle number concentration in the range from $4\times10^4$ (#/cm$^3$) to $1.11\times10^7$ (#/cm$^3$). The difference among them can be around 10% caused by the different particle size classifier and number counter technology they used.
- The DMS 500 presented the highest PN concentration readings as the electrical mobility classifier and electricity charger counter allowing it to capture particles with minimum particle lose, but when the sample particle number drops to $2\times10^4$ #/cm$^3$ and below, the DMS 500 would not the capable of capture particle dur to its detection limit.
- Particles generated from aerosol combustion with higher mass weight are more likely to agglomerate with particles with lighter mass weight, and thus agglomeration mode particles obtain higher density than nuclei mode particles. Consequently, the particle density increases with particle size decreases.

In summary, the particle number measurement accuracy can be affected by measurement devices, sampling conditions, therefore, for future PN legislation, it's necessary to define the type of instrument to be used and the sampling conditions to be deployed for the legislation and certification tests. Also, the consideration for the instrument's detection limit is necessary when choosing a PN measurement device.

The GTL, HVO and their blends shared many core findings which were similar because chemically pure GTL and HVO fuel are both have an absence of aromatics and have the same density. Therefore, the core findings acquired from chapter 5 to chapter 8 are summarized together below:

- The main difference between pure GTL, pure HVO and diesel fuel is that GTL and HVO fuels consisted of all straight chains and no aromatics. This contributed to the reduction in THC and PN emissions. And the reduction increased with the increasing of blending ratio.
- The cetane number values of GTL and HVO fuels are higher than diesel fuel and this is the reason why with the increasing of blending ratio the ignition delay became shorter.
- The difference between HVO fuel and GTL fuel is that the HVO consists of some fractions heavier than diesel fuel, however the GTL fuel is lighter than diesel. This is proved by the TGA and GC-MS test results.
- When the engine power reached 27 KW, GTL, HVO and their blends showed similar in-cylinder pressure performance (P-CA and P-V diagrams). Because at enough high engine power condition, all the fuels can be ignited and combusted easily despite the pure GTL and HVO fuels had better combustibility.
- The GTL blends and HVO blends can both reduce $NO_X$ emissions by 25% to 35% in the majority of test conditions. The most significant $NO_X$ emission reduction was found with the 30% blend ratio for both GTL and HVO fuels. The 50% and 70% blends showed similar $NO_x$ reduction. However, the reduction didn't show particular relationship with blending ratio. It's believed that a certain concentration of aromatics in a fuel could act as anti-oxidants that helps to

control $NO_x$ emissions. The optimum concentration of aromatics is estimated to be in the range from 7.5% to 17.5%.

- The pure GTL fuel can reduce the $NO_X$ by up to 17%. However, the pure HVO showed approximately 10% higher $NO_x$ emission than diesel.
- Pure GTL, HVO and their blends are all capable of reducing particle number emissions significantly. From the engine out emission analysis, the reduction in accumulation mode particles is more obvious than in nucleation mode particles, and the peak value of accumulation mode particles reduces with the blending ratio increase. Therefore, the accumulation mode particles are more sensitive to blending ratio. From the downstream of the DPF, the particle number concentration measured was lower than the DMS 500's lower detection limit. Since the PN concentration measured at upstream of the DPF was more than 1000 times greater than that at downstream, the DPF efficiencies calculated based on PN was all higher than 99%.
- CO emissions from GTL, HVO and their blended fuels were similar and showed no particular relationship with blending ratio. The pure HVO fuel showed CO emissions reduction by up to 38% in all tested conditions.

In summary, blending GTL or HVO to diesel fuel can significantly reduce the particle number and $NO_X$ emissions, which are two major concerned pollutants from diesel engine. It's concluded from this research that 30% blend ratio can reduce $NO_x$ emission significantly, and with the blending ratio kept increasing, no further improvement on $NO_X$ reduction was observed. Thus, GTL or HVO blending can be a suitable solution to reduce the emissions and provide alternative fuels to conventional diesel fuel.

## 9.2 Future work

With the findings from this research, some research gaps are found. The recommendations for future work thus are provided below:

- Finding out the lower detection limit of other PN measurement instruments and conduct more systematic research in low concentration (less than $4\times10^4$ #/$cm^3$) accurate PN measurement.

- Conducting more experiments with blend ratio lower than 30% for GTL and HVO blended fuel and finding if there is a lower blending ratio threshold that aromatics could start to act as an antioxidant in emission prevention.
- Conduct detailed chemical studies so as to figure out which kind(s) of aromatics would act as antioxidant in fuel combustion and their concentration range. Since the anti-oxidant ability of aromatics can be significantly affected by fuel combustion temperature and pressure. Therefore, it's also necessary to find the anti-oxidation behaviour against combustion pressure and temperature.
- One of the key reasons to use GTL or HVO blends is to reduce emission. However, it is important to consider economic feasibility and cost. Another way to reduce $NO_X$ emission in diesel engine is to install SCR and DPF together to the aftertreatment system. So, it's necessary to have a systematic comparison between using fuel blending strategy and SCR+DPF aftertreatment system in terms of economics including maintenance cost. Both strategies can be used together to achieve maximum emissions reductions.

## Reference


1. 3M. 2013. *How does car work?* [Online] [Accessed on 3 June 2015] Available from: http://www.3m.co.uk/intl/uk/3Mworldly-wise/car-how-cars-wk-four-stroke-engine.htm
2. Aatola H, Larmi M, Sarjovaara T, Mikkonen S, 2008. Hydeotreated vegetable oil (HVO) as a renewable diesel fuel: Trade-off between NOx, particulate emission, and fuel consumption of a heavy-duty engine. SAE International Journal of Engines, **1**(2008)1, pp. 1251-1262
3. Abdul-Khalek, I., Kittelson, D., and Brear, F., "The Influence of Dilution Conditions on Diesel Exhaust Particle Size Distribution Measurements," SAE Technical Paper 1999-01-1142, 1999, https://doi.org/10.4271/1999-01-1142
4. Abu-Jrai, A., J. Rodríguez-Fernández, A. Tsolakis, A. Megaritis, K. Theinnoi, R. F. Cracknell, and R. H. Clark. "Performance, combustion and emissions of a diesel engine operated with reformed EGR. Comparison of diesel and GTL fuelling." Fuel 88, no. 6 (2009): 1031-1041.
5. AIC, 2014. *Fuel flow meter AIC-904/908 Veritas.* [Online] [Accessed on 5 December 2018] Available from: http://reicon.us/TIcurrent/900/TI%20900_e_07.08.pdf
6. Alam, M.S., Zeraati-Rezaei, S., Stark, C.P., Liang, Z., Xu, H. and Harrison, R.M., 2016. The characterisation of diesel exhaust particles–composition, size distribution and partitioning. Faraday discussions, 189, pp.69-84.
7. Allison, 2019. Straight chain-alkanes. [Online] [Accessed on 25 June 2019]. Available from: https://chem.libretexts.org/Courses/University_of_Kentucky/UK%3A_CHE_103_-_Chemistry_for_Allied_Health_(Soult)/Chapters/Chapter_3%3A_Compounds/3.2%3A_Straight-Chain_Alkanes
8. Andrews, G.E., 2015. Diesel engine processes that influence particulate formation. Lecture notes distributed in short course: Diesel particulates and NOx emissions, May, 2015, University of Leeds.

9. Andrews, G.E.,2015.NOx formation and control in diesel engines. Lecture notes distributed in short course: Diesel particulates and NOx emissions, May, 2015, University of Leeds.
10. Andrews, G.E.,2015.NOx formation and control in diesel engines. Lecture notes distributed in short course: Diesel particulates and NOx emissions, May, 2015, University of Leeds.
11. AOCS. 2001. Historical perspectives on vegetable oil-based diesel fuels. *Inform*, Volume 12, pp. 103-1107
12. Arai H, 2011. Effect of fuel properties of biodiesel on its combustion and emission characteristics. SAE technical paper 2011-01-1939
13. Austen, A.E.W. and Lyn, W.T., 1960. Relation between fuel injection and heat release in a direct-injection engine and the nature of the combustion processes. Proceedings of the Institution of Mechanical Engineers: Automobile Division, 14(1), pp.47-62.
14. AVL[a], 2014. Quotation 0097925/01 from 04/01/2014. [Instruction manual].
15. AVL[b], 2014. AVL ANGLE ENCODER 365 C / 365 X. [Instruction manual].
16. AVL[c], 2014. AVL FI PIEZO AMPLIFIER 2P2E/F/G/H. [Instruction manual].
17. AVL[d], 2014. AVL Indicom mobile 2015 for Indimicro and Fexifem Indi. AVL user's guide, AT3414E, Rev. 06. [Instruction manual]
18. AVL[e], 2014. AVL CONCERTO™ 2015. AVL user's guide, AT2634E, Rev. 08. [Instruction manual]
19. AVL[f], 2012. AVL micro soot sensor AVL exhaust conditioning unit operating manual. [Instruction manual]
20. B. Chehroudi, 2015. *Diesel Engine Emissions: Hydrocarbons (HC).* [Online] [Accessed on 26 November 2016] Available from: http://advtechconsultants.com/EngineTutorial/Diesel%20Engine%20Emissions_Hydrocarbons%20(HC)___.pdf
21. Balat M. et al, 2008. Progress in bioethanol processing. *Progress in energy and combustion science.* Volume 34(5), pp. 551-57
22. BBC, 2014. *Useful products from air and seawater.* [Online] [Accessed on 6 May 2016] Available from:

http://www.bbc.co.uk/schools/gcsebitesize/science/edexcel_pre_2011/oneearth/usefulproductsrev1.shtml

23. Black, F. and High, L. 1977. Automotive Hydrocarbon Emission Patterns in the Measurement of Nonmethane Hydrocarbon Emission Rates. SAE Technical Paper 770144
24. Brandt, E.P., Wang, Y. and Grizzle, J.W., 2000. Dynamic modelling of a three-way catalyst for SI engine exhaust emission control. IEEE Transactions on control systems technology, 8(5), pp.767-776.
25. Cambustion, 2015. Fast Aerosol Mobility Size Spectrometer. [Online] [Accessed on 10 December 2015] Available from: http://www.cambustion.com/sites/default/files/instruments/DMS500/DMS500aerosol.pdf
26. Cambustion, 2015. Fast Aerosol Mobility Size Spectrometer. [Online] [Accessed on 10 December 2015] Available from: http://www.cambustion.com/sites/default/files/instruments/DMS500/DMS500aerosol.pdf
27. Caroca, J.C., Millo, F., Vezza, D., Vlachos, T., De Filippo, A., Bensaid, S., Russo, N. and Fino, D., 2010. Detailed investigation on soot particle size distribution during DPF regeneration, using standard and bio-diesel fuels. Industrial & Engineering Chemistry Research, 50(5), pp.2650-2658.
28. Cavina, N., Poggio, L., Bedogni, F., Rossi, V. et al., "Benchmark Comparison of Commercially Available Systems for Particle Number Measurement," SAE Technical Paper 2013-24-0182, 2013, https://doi.org/10.4271/2013-24-0182.
29. Cheng, Y.-S, 2011. Condensation Particle Counters, in Aerosol Measurement: Principles, Techniques, and Applications, Third Edition (eds P. Kulkarni, P. A. Baron and K. Willeke), John Wiley & Sons, Inc., Hoboken, NJ, USA. doi: 10.1002/9781118001684.ch17
30. Chistensen, M. and Johansson, B., Homogeneous charge compression ignition with water injection. SAE (1999-01-0182)
31. Cleanairtrust, 1999. *Carbon Monoxide*. [Online] [Accessed on 24 June 2015] Available from: http://www.cleanairtrust.org/carbonmonoxide.html

32. Costello J. 1979. Morbidity and Mortality Study of Shale Oil Workers in the United States. *Environmental Health Perspectives*. **30**, pp. 205-208.
33. Dekati, 2017. ELPI®+. [Online] [Accessed on 15 December 2017]. Available from: https://www.dekati.com/products/Fine%20Particle%20Measurement/ELPI%C2%AE%2B
34. Dernotte, J., Hespel, C., Foucher, F., Houille, S. and Mounaim-Rousselle, C., 2011, September. Experimental study of the influence of fuel physical properties on the diesel injection process in non-vaporizing conditions. In 24th European Conference on Liquid Atomization and Spray Systems, Estoril, Portugal. ILASS Europe.
35. Dickey, P.A., 1959. The first oil well. Journal of Petroleum Technology, 11(01), pp.14-26.
36. Dizayi, B., Li, H., Tomlin, A.S. and Cunliffe, A., 2014. Evaluation of the effect of fuel properties on the fuel spray and jet characteristics in a HGV DI diesel engine operated by used cooking oils. In Applied Mechanics and Materials (Vol. 694, pp. 3-12). Trans Tech Publications.
37. Du, J., Sun, W., Wang, X., Li, G., Tan, M. and Fan, L., 2014. Experimental study on combustion and particle size distribution of a common rail diesel engine fueled with GTL/diesel blends. Applied Thermal Engineering, 70(1), pp.430-440.
38. Dunn, R.O., 2005. Effect of antioxidants on the oxidative stability of methyl soyate (biodiesel). Fuel Processing Technology, 86(10), pp.1071-1085.
39. EEA 2018. *Transport emissions of air pollutants (TERM 003) - Assessment published Nov 2018*. [Online] [Accessed on 2 June 2019] Available from: https://www.eea.europa.eu/data-and-maps/indicators/transport-emissions-of-air-pollutants-8/transport-emissions-of-air-pollutants-6
40. EL-science, 2016. The tobacco products directive. [Online] [Accessed on 25 June 2019]. Available from: https://elscience.co.uk/documents/view-our-brochure/
41. EPA[b], 2014. *Particulate Matter (PM).* [Online] [Accessed on 24 June 2015] Available from: http://www.epa.gov/airquality/particulatematter/health.html

42. Europa[a], 2011. Regulation (EC) No 715/2007 of the European Parliament and of the Council of 20 June 2007 on type approval of motor vehicles with respect to emissions from light passenger and commercial vehicles (Euro 5 and Euro 6) and on access to vehicle repair and maintenance information (Text with EEA relevance).
43. Europa[b], 2011. Regulation (EU) No 540/2014 of the European Parliament and of the Council of 16 April 2014 on the sound level of motor vehicles and of replacement silencing systems and amending Directive 2007/46/EC and repealing Directive 70/157/EEC Text with EEA relevance.
44. Extraordinaryroadtrip.org. 2015. Health and Environmental Impacts of NOx. [Online] [Accessed on 24 June 2015] Available from: http://www.extraordinaryroadtrip.org/research-library/air-pollution/understanding-air-pollution/nitrogen-dioxide/health.asp
45. Garner, S., Sivaramakrishnan, R. and Brezinsky, K., 2009. The high-pressure pyrolysis of saturated and unsaturated C7 hydrocarbons. Proceedings of the Combustion Institute, 32(1), pp.461-467.
46. Global natural gas storage (underground, above ground, and floating) market - trends & forecasts to 2019. (2014). PR Newswire Europe Including UK Disclose, Retrieved from https://go.openathens.net/redirector/leeds.ac.uk?url=/docview/1565541708?accountid=14664
47. globalgwa.org. 2011. *Biodiesel VS Petroleum diesel*. [Online] [Accessed on 16 February 2014] Available from: http://www.globalgwa.org/biodiesel-vs-petroleum-diesel.html
48. Greeves, G., Khan, I.M., Wang, C.H.T. and Fenne, I., 1977. Origins of hydrocarbon emissions from diesel engines. SAE Transactions, pp.1235-1251.
49. Hadavi S, Dizayi B, Li H, and Tomlin A, 2015. Emissions from a HGV using used cooking oil as a fuel under real world driving conditions. SAE technical paper 2015-01-0905
50. Hawker, P., Hüthwohl, G., Henn, J., Koch, W., Lüders, H., Lüers, B. and Stommel, P., 1998. Effect of a continuously regenerating diesel particulate filter

on non-regulated emissions and particle size distribution. SAE transactions, pp.374-380.

51. Hensman, John Richard. "Fischer-tropsch process." U.S. Patent 6,914,083, issued July 5, 2005.
52. Heywood, J.B., 1988, Internal Combustion Engine Fundamentals, McGraw-Hill, New York.
53. Ho, C.A. and Sommerfeld, M., 2002. Modelling of micro-particle agglomeration in turbulent flows. Chemical Engineering Science, 57(15), pp.3073-3084.
54. Horiba[b], 2013. Solid Particle Counting System MEXA-2300SPCS. [Instruction manual]. 2010 - 2013 HORIBA, Ltd.
55. Iaccsea, 2015. *$NO_X$*. [Online] [Accessed on 6 May 2016] Available from: http://www.iaccsea.com/nox/
56. Imad Khalek & Vinay Premnath. 2015. Comparison Among DMS 500, EEPS SMPS, MSS, EC/OC, CPMA, Using Laboratory “Soot” Particles. July 3. Cambridge Particle Meeting.
57. Infineum, 2016. Viscosity modifier. [Online] [Accessed on 15 January 2016] Available from: http://www.infineum.com/en/products/viscosity-modifiers/
58. Innospec, 2015. Multifunctional Diesel Formulations. [Online] [Accessed on 15 December 2015] Available from: http://www.innospecinc.com/our-markets/fuel-specialties/performance-fuel-specialties/multifunctional-diesel-formulations
59. Janssen A, Muether M, Kolbeck A, Lamping M, and Pischinger S, 2010. The impact of different biofuel components in diesel blends on engine efficiency and emission performance. SAE technical paper 2010—01-2119
60. Janssen, A., Muether, M., Kolbeck, A., Lamping, M. et al, 2010. The Impact of Different Biofuel Components in Diesel Blends on Engine Efficiency and Emission Performance. SAE Technical Paper 2010-01-2119, 2010.
61. Jaworski, A., Kuszewski, H., Ustrzycki, A., Balawender, K., Lejda, K. and Woś, P., 2018. Analysis of the repeatability of the exhaust pollutants emission research results for cold and hot starts under controlled driving cycle conditions. Environmental Science and Pollution Research, 25(18), pp.17862-17877.

62. Jing LTD, 2013. Real soot generator model 5203 type C mini-CAST. [Instruction manual]. Jing AG, Switzerland.
63. Kanthavelkumaran, N, Seenikannan, P, 2014. Advanced Materials Research, **v** (984-985), pp. 839-844
64. Kee, S.S., Mohammadi, A., Kidoguchi, Y. and Miwa, K., 2005. Effects of aromatic hydrocarbons on fuel decomposition and oxidation processes in diesel combustion. SAE transactions, pp.765-772.
65. Khiari K , Tarabet L, Awad S, Loubar K, Mahmoud R, and Tazerout M, 2015. Combustion characteristics of Pistacia Lentiscus biodiesel in DI diesel engine. SAE technical paper 2015-24-2481
66. Kidoguchi, Y., Yang, C., Kato, R. and Miwa, K., 2000. Effects of fuel cetane number and aromatics on combustion process and emissions of a direct-injection diesel engine. JSAE review, 21(4), pp.469-475.
67. Kitano, K., Sakata, I., and Clark, R., "Effects of GTL Fuel Properties on DI Diesel Combustion," SAE Technical Paper 2005-01-3763, 2005.
68. Kittelson D.B. 2000. Measurement of Engine Exhaust Particle Size. 17 February. University of California, Davis.
69. Kittelson, D.B. 1998. Engines and Nanoparticles: A Review. *Journal of Aerosol Science*. **29**(5/6), pp.575-588.
70. Kittelson, D.B. 1998. Engines and Nanoparticles: A Review. *Journal of Aerosol Science*. **29**(5/6), pp.575-588.
71. Knecht, Walter. "Diesel engine development in view of reduced emission standards." Energy 33, no. 2 (2008): 264-271.
72. Knothe, G., Matheaus, A.C. and Ryan III, T.W., 2003. Cetane numbers of branched and straight-chain fatty esters determined in an ignition quality tester. Fuel, 82(8), pp.971-975.
73. Knothe, Gerhard. "History of vegetable oil-based diesel fuels." In the Biodiesel Handbook (Second Edition), pp. 5-19. 2010.
74. Kuronen et al, 2007. Hydrotreated vegetable oil as fuel for heavy duty diesel engines. SAE technical paper 2007-01-4031.

75. Lakshminarayanan, P.A. and Aghav, Y.V., 2010. Modelling diesel combustion. Springer Science & Business Media.
76. Lapuerta M, 2008. Emissions from a diesel–bioethanol blend in an automotive diesel engine. Fuel. **87** (1), pp. 25-31
77. Laurent, A and Hauschild, MZ. 2014. Impacts of NMVOC emissions on human health in European countries for 2000-2010: Use of sector-specific substance profiles. *Atmospheric Environment*. **85**, Pp. 247-255.
78. Li, H., Lea-Langton, A., Biller, P., Andrews, G.E., Hadavi, S., Charlton, A. and Richards, P., 2010. Effect of Multifunctional Fuel Additive Package on fuel injector deposit, combustion and emissions using pure rape seed oil for a DI diesel. SAE International Journal of Fuels and Lubricants, 2(2), pp.54-65.
79. Li, Xinling, Zhen Huang, Jiasong Wang, and Wugao Zhang. "Particle size distribution from a GTL engine." Science of the total environment 382, no. 2-3 (2007): 295-303.
80. Li, Y., Tian, G., Zhang, J. and Xu, H., 2010. Comparative experimental study on microscopic spray characteristics of RME, GTL and diesel (No. 2010-01-2284). SAE Technical Paper.
81. Liu, Z. Et al. 2003. Diesel Particulate Filters: Trends and Implications of Particle Size Distribution Measurement. SAE Technical Paper 2003-01-0046.
82. Liu, Z. Et al. 2003. Diesel Particulate Filters: Trends and Implications of Particle Size Distribution Measurement. SAE Technical Paper 2003-01-0046.
83. Long, R.Q. and Yang, R.T., 2002. Reaction mechanism of selective catalytic reduction of NO with NH3 over Fe-ZSM-5 catalyst. Journal of catalysis, 207(2), pp.224-231.World Coal Association, 2015. Coal and Electricity. [Online]. Available: http://www.worldcoal.org/coal/uses-of-coal/coal-electricity/
84. Macamo A, 2014. Exhaust emission characteristics of diesel engine using jatropha crude oil blends.
85. Maly, Rudolf R. "Effect of GTL Diesel Fuels on Emissions and Engine Performance." In presentation at 10th Diesel Engine Emissions Reduction Conference, Coronado, Calif. 2004.

86. Mamakos, A., Khalek, I., Giannelli, R. and Spears, M., 2013. Characterization of combustion aerosol produced by a Mini-CAST and treated in a catalytic stripper. Aerosol Science and Technology, 47(8), pp.927-936.
87. Meinschein, W.G., 1969. Hydrocarbons—saturated, unsaturated and aromatic. In Organic geochemistry (pp. 330-356). Springer, Berlin, Heidelberg.
88. Mellor, A.M., Mello, J.P., Duffy, K.P., Easley, W.L. and Faulkner, J.C., 1998. Skeletal Mechanism for NO x Chemistry in Diesel Engines. SAE transactions, pp.786-801.
89. Metller-toledo, 2015. Thermal analysis premium. [Instruction manual].
90. Mittal, N., Patanwal, P., Sithananthan, M., Subramanian, M. et al., 2015. Experimental Investigation of n-Butanol Diesel Fuel Blends on a Passenger Car. SAE Technical Paper 2015-01-0903, 2015.
91. Moore, R.H., Ziemba, L.D., Dutcher, D., Beyersdorf, A.J., Chan, K., Crumeyrolle, S., Raymond, T.M., Thornhill, K.L., Winstead, E.L. and Anderson, B.E., 2014. Mapping the operation of the miniature combustion aerosol standard (Mini-CAST) soot generator. *Aerosol Science and Technology*, *48*(5), pp.467-479.
92. Murtagh,M, 2015. Diesel Particulate Filters (DPF). Lecture notes distributed in short course: Diesel particulates and NOx emissions, May, 2015, University of Leeds.
93. Myburgh, Ian, Mark Schnell, Koji Oyama, Hideaki Sugano, Hisashi Yokota, and Shigeki Tahara. The emission performance of a gtl diesel fuel-a japanese market study. No. 2003-01-1946. SAE Technical Paper, 2003.
94. Myers, P. 1975. The Diesel Engine for Truck Application. SAE Technical Paper 750128.
95. NASA, 2010. New Map Offers a Global View of Health-Sapping Air Pollution. [Online] [Accessed on 5 December 2017]. Available from: https://www.nasa.gov/topics/earth/features/health-sapping.html
96. Neste, 2014. Hydrotreated vegetable oil. [Online] [Accessed on 15 December 2015] Available from: https://www.neste.com/sites/default/files/attachments/hvo_handbook_original_2014.pdf

97. Neste, 2018. Neste renewable diesel handbook. [Online] [Accessed on 15 February 2019] Available from: https://www.neste.com/sites/default/files/attachments/neste_renewable_diesel_handbook.pdf
98. NIST, 2011. NIST/EPA/NIH Mass Spectral Database (NIST 11) and NIST Mass Spectral Search Program (Version 2.0g). [Online] [Accessed on 25 June 2019]. Available from: https://www.nist.gov/sites/default/files/documents/srd/NIST1a11Ver2-0Man.pdf
99. Oguma, Mitsuharu, Shinichi Goto, Kazuya Oyama, Kouseki Sugiyama, and Makihiko Mori. The possibility of gas to liquid (GTL) as a fuel of direct injection diesel engine. No. 2002-01-1706. SAE Technical Paper, 2002.
100. Petersen, B., Ekoto, I., and Miles, P., 2010. An Investigation into the Effects of Fuel Properties and Engine Load on UHC and CO Emissions from a Light-Duty Optical Diesel Engine Operating in a Partially Premixed Combustion Regime. SAE Int. J. Engines 3(2):38-55, 2010.
101. Pflaum H, Hofmann P, Geringer B, and Weissel W, 2010. Potential of hydrogenated vegetable oil (HVO) in a modern diesel engine.
102. Planchet E and Kaiser* W, 2006. Nitric oxide (NO) detection by DAF fluorescence and chemi-luminescence: a comparison using abiotic and biotic NO sources. *Journal of experimental botany*. **57** (12) pp. 3043-3055
103. Price, P., Stone, R., Collier, T., Davies, M. et al., "Dynamic Particulate Measurements from a DISI Vehicle: A Comparison of DMS500, ELPI, CPC and PASS," SAE Technical Paper 2006-01-1077, 2006, https://doi.org/10.4271/2006-01-1077.
104. Pulkrabek.W, 1997. *Engine fundamentals of the internal combustion engine.* New Jersey: Prentice-Hall, Inc.
105. R. Nave. 2014. *The diesel engine.* [Online] [Accessed on 5 May 2015]. Available from: http://hyperphysics.phy-astr.gsu.edu/hbase/thermo/diesel.html
106. Ricky, Y. 2015. Turbocharging for low emission heavy duty vehicles. Lecture notes distributed in short course: Diesel particulates and NOx emissions, May, 2015, University of Leeds.

107. Sajjad, H., H. H. Masjuki, M. Varman, M. A. Kalam, M. I. Arbab, S. Imtenan, and SM Ashrafur Rahman. "Engine combustion, performance and emission characteristics of gas to liquid (GTL) fuels and its blends with diesel and bio-diesel." Renewable and Sustainable Energy Reviews 30 (2014): 961-986.
108. Schaberg, Paul, Johan Botha, Mark Schnell, Hans-Otto Hermann, Norbert Pelz, and Rudolf Maly. Emissions performance of GTL diesel fuel and blends with optimized engine calibrations. No. 2005-01-2187. SAE Technical Paper, 2005.
109. Schanke, Dag, Edvard Bergene, and Anders Holmen. "Fischer-tropsch synthesis." U.S. Patent 6,211,255, issued April 3, 2001.
110. Schmidt, K,D., 2014. Technology of HD Euro VI truck engines and future trends towards improved fuel economy. Lecture notes distributed in short course: Diesel particulate and $NO_X$ emissions. May, 2016, University of Leeds.
111. Seaton, A., Godden, D., MacNee, W. and Donaldson, K., 1995. Particulate air pollution and acute health effects. The lancet, 345(8943), pp.176-178.
112. Shell company. Shell GTL fuel knowledge guide version 2.0. 2018.
113. Shimadzu, 2018. Specification Sheet GCMS-QP2010. [Instruction manual].
114. Sims, R. 2008 et al. *From 1st to 2nd generation of biofuel technologies.* [Online] [Accessed on 27 November 2015] Available from: https://www.iea.org/publications/freepublications/publication/2nd_Biofuel_Gen.pdf
115. SMPS, 2001. Model 3080-Series Electrostatic Classifiers. [Instruction manual]
116. Soltic, Patrik, Daniel Edenhauser, Thomas Thurnheer, Daniel Schreiber, and Arne Sankowski. "Experimental investigation of mineral diesel fuel, GTL fuel, RME and neat soybean and rapeseed oil combustion in a heavy duty on-road engine with exhaust gas aftertreatment." Fuel 88, no. 1 (2009): 1-8.
117. Spirometryworks, 2011. Different Type of oxygen Sensor. [Online] [Accessed on 16 November 2015] Available from: https://spirometryworks.wordpress.com/2011/03/28/different-type-of-oxygen-sensor/
118. Stiver, W. and Mackay, D., 1984. Evaporation rate of spills of hydrocarbons and petroleum mixtures. Environmental science & technology, 18(11), pp.834-840.

119.Stone, R., 1999. Introduction to internal combustion engines (Vol. 3). London: Macmillan.

120.Tao, T, et al. 2004. *Diesel SCR NOx Reduction and Performance on Washcoated SCR Catalysts.* SAE Technical Paper 2004-01-1293.

121.Thermo Scientific, 2014. Thermo Scientific FLASH 2000 HT Elemental Analyzer for Isotope Ratio MS. [Instruction manual].

122.Tonegawa, Y., Nakajima, T., Yanagisawa, N., Hosoya, M., Shoji, T., Iwakiri, Y., Yamashita, T., Ikeda, T., Tanaka, S., Takahashi, K. and Suzuki, T., 2007. JCAPII cross check tests of fast electrical mobility spectrometers for evaluation of accuracy (No. 2007-01-4081). SAE Technical Paper.

123.Tsi, 2015. Scanning Mobility Particle Sizer™ Spectrometer (smps) Model 3936. [Online] [Accessed on 10 December 2015] Available from: http://www.tsi.com/uploadedFiles/_Site_Root/Products/Literature/Spec_Sheets/SMPS3936-3034.pdf

124.Tutorvista, 2013. *Effects of air pollution*. [Online] [Accessed on 24 June 2015] Available from: http://www.tutorvista.com/content/biology/biology-iv/environmental-pollution/air-pollution-effects.php#carbon-monoxide-(co)

125.Ucsusa, 2015. *Diesel Engines and Public He*alth. [Online] [Accessed on 6 May 2016] Available from: http://www.ucsusa.org/clean_vehicles/why-clean-cars/air-pollution-and-health/trucks-buses-and-other-commercial-vehicles/diesel-engines-and-public.html#.VUmIivRfelg

126.Vandersickel, A., Hartmann, M., Vogel, K., Wright, Y.M., Fikri, M., Starke, R., Schulz, C. and Boulouchos, K., 2012. The autoignition of practical fuels at HCCI conditions: High-pressure shock tube experiments and phenomenological modeling. Fuel, 93, pp.492-501.

127.Varatharajan, K. and Cheralathan, M., 2013. Effect of aromatic amine antioxidants on NOx emissions from a soybean biodiesel powered DI diesel engine. Fuel processing technology, 106, pp.526-532.

128.Viskup, R., Alberer, D., Oppenauer, K. and del Re, L., 2011. Measurement of transient PM emissions in diesel engine (No. 2011-24-0197). SAE Technical Paper.

129.W. Majewski, 2012. *What Are Diesel Emissions*. [Online] [Accessed on 6 May 2016] Available from: https://www.dieselnet.com/tech/emi_intro.php

130.Walker, A and Görsmann, C, 2015. Diesel Oxidation Catalysts – 1. Lecture notes distributed in short course: Diesel particulates and NOx emissions, May 2015, University of Leeds.

131.Walker, A and Görsmann, C, 2015. Integrated Emission Control Systems. Lecture notes distributed in short course: Diesel particulates and NOx emissions, May 2015, University of Leeds.

132.Wang, F., Liu, J.B., Sinibaldi, J., Brophy, C., Kuthi, A., Jiang, C., Ronney, P. and Gundersen, M.A., 2005. Transient plasma ignition of quiescent and flowing air/fuel mixtures. IEEE Transactions on Plasma Science, 33(2), pp.844-849.

133.Wang, Hewu, Han Hao, Xihao Li, Ke Zhang, and Minggao Ouyang. "Performance of Euro III common rail heavy duty diesel engine fueled with Gas to Liquid." Applied Energy 86, no. 10 (2009): 2257-2261.

134.Wang, X., Grose, M.A., Caldow, R., Osmondson, B.L., Swanson, J.J., Chow, J.C., Watson, J.G., Kittelson, D.B., Li, Y., Xue, J. and Jung, H., 2016. Improvement of Engine Exhaust Particle Sizer (EEPS) size distribution measurement–II. Engine exhaust particles. Journal of Aerosol Science, 92, pp.83-94.

135.Wei, Y., Liu, J., Zhao, Z., Chen, Y., Xu, C., Duan, A., Jiang, G. and He, H., 2011. Highly active catalysts of gold nanoparticles supported on three‐dimensionally ordered macroporous LaFeO3 for soot oxidation. Angewandte Chemie, 123(10), pp.2374-2377.

136.Westbrook, C.K. and Dryer, F.L., 1984. Chemical kinetic modeling of hydrocarbon combustion. Progress in Energy and Combustion Science, 10(1), pp.1-57.

137.Wittrock, M., Klein, U. and Leyh, G., Deutz AG, 2017. Internal combustion engine. U.S. Patent 9,656,210.

138.Woltermann, G.M., Magee, J.S. and Griffith, S.D., 1993. Commercial preparation and characterization of FCC catalysts. In Studies in Surface Science and Catalysis (Vol. 76, pp. 105-144). Elsevier.

139.World health organization, 2016. Exposure to ambient air pollution. [Online] [Accessed on 5 December 2017]. Available from: http://gamapserver.who.int/mapLibrary/Files/Maps/Global_pm10_cities.png?ua=1

140.Wu, C.W., Chen, R.H., Pu, J.Y. and Lin, T.H., 2004. The influence of air–fuel ratio on engine performance and pollutant emission of an SI engine using ethanol–gasoline-blended fuels. Atmospheric Environment, 38(40), pp.7093-7100.

141.Y Wu, 2014. *Evaluation of emissions from Heavy Goods Vehicles (HGVs) using waste cooking oil derived fuels.* Leeds: University of Leeds.

142.Yanfeng Wang; Res. Inst. of Electron., Shizuoka Univ., Hamamatsu, Japan; Nakayama, M.; Yagi, M. ; Nishikawa, M. 2005. The NDIR CO2 monitor with smart interface for global networking. *Instrumentation and Measurement*. **54**(4), PP. 1634-1639

143.Yasin M, Cant S, Chong C, and Hochgreb S, 2012. Effects of the biodiesel fuel properties on the swirl stabilized spray combustion characteristics. SAE technical paper 2012-01-1724

144.Zervas, E., Montagne, X. and Lahaye, J., 2001. Emission of specific pollutants from a compression ignition engine. Influence of fuel hydrotreatment and fuel/air equivalence ratio. Atmospheric Environment, 35(7), pp.1301-1306.

# Appendix

**The PV diagrams of blended GTL fuel and HVO fuel.**

PV diagram of 50%GTL at 1000rpm, 30% throttle.

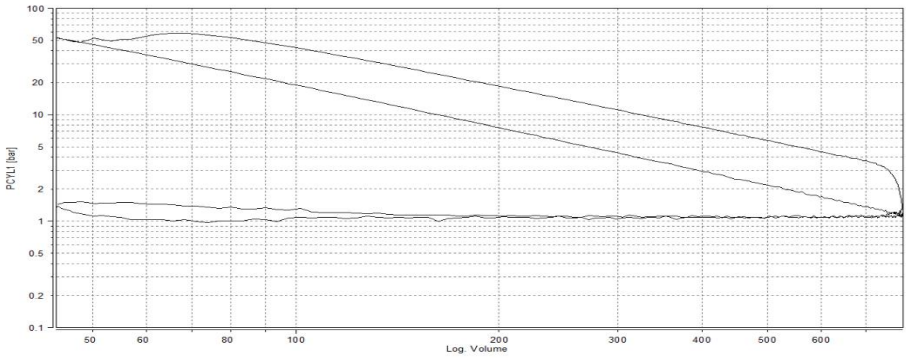


PV diagram of 50%GTL at 1000rpm, 40% throttle.

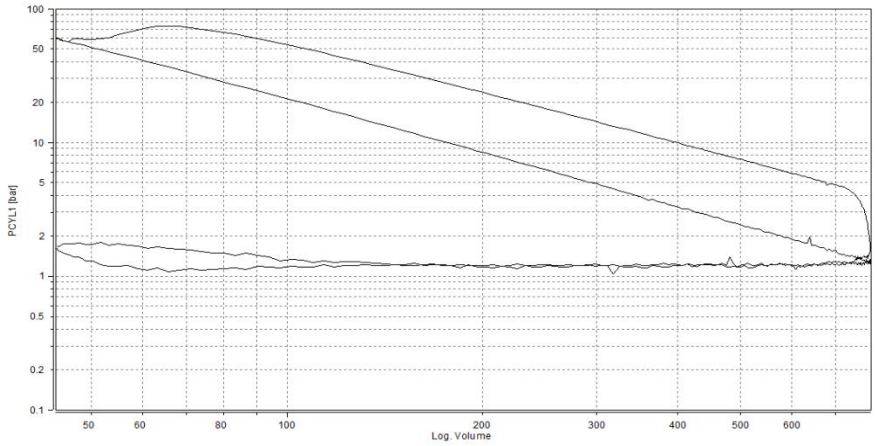


PV diagram of 50%GTL at 1000rpm, 50% throttle.

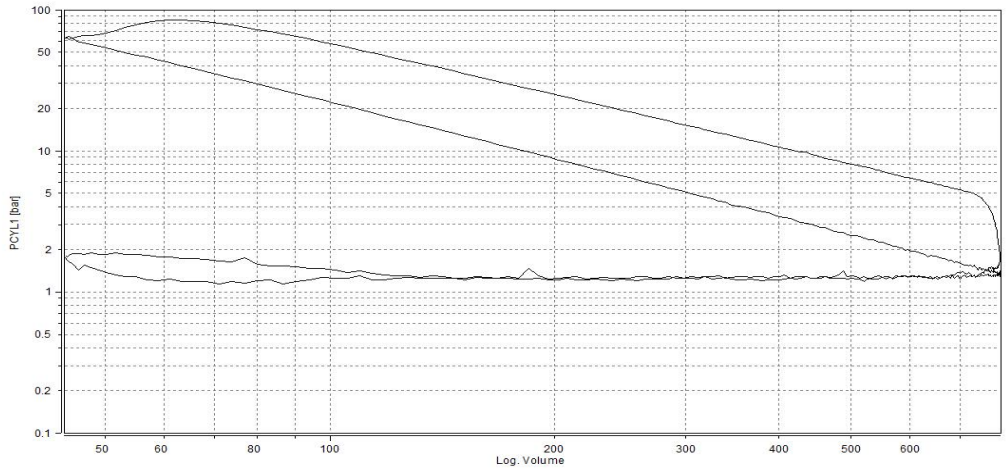

PV diagram of 50%GTL at 1600rpm, 40% throttle.

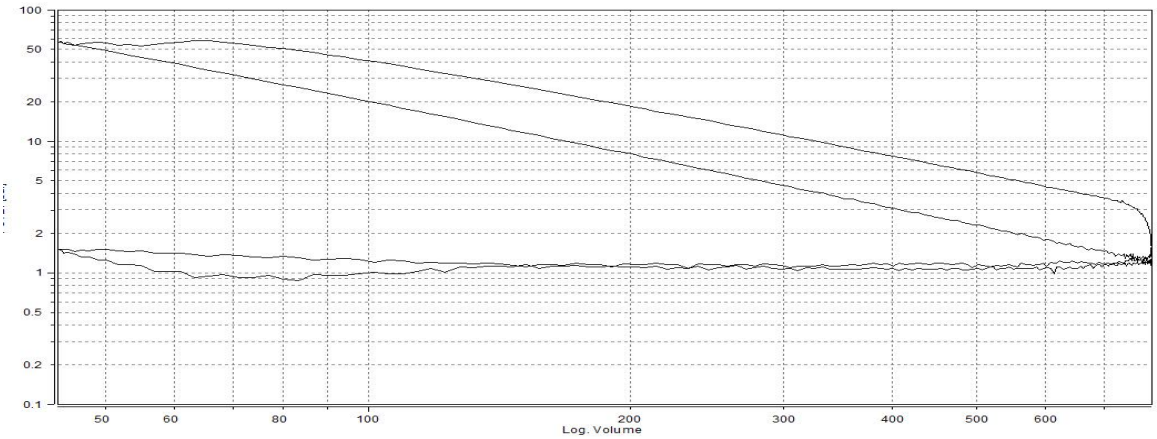


PV diagram of 50%GTL at 1600rpm, 50% throttle.

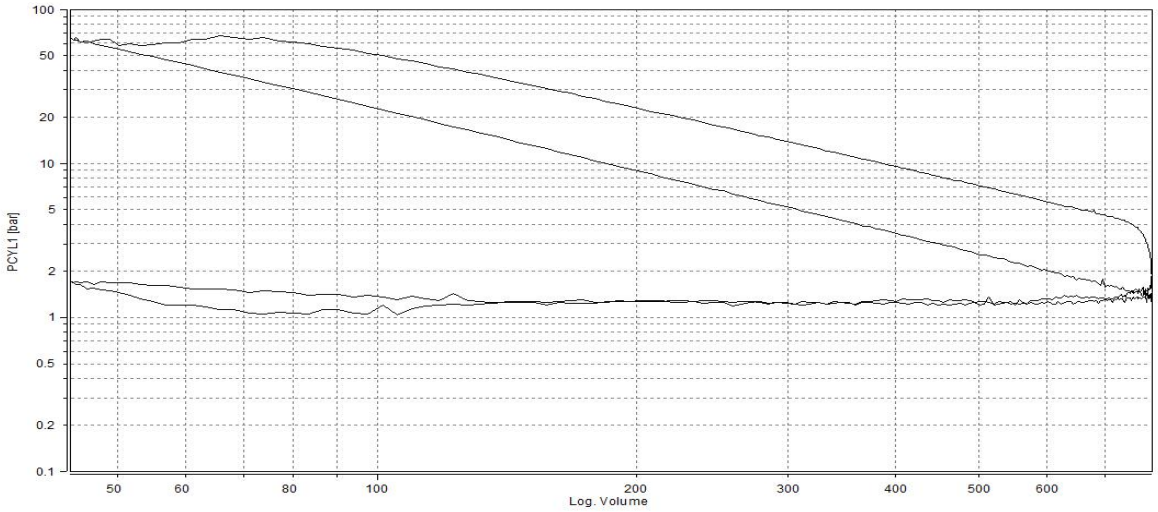


PV diagram of 50%GTL at 1600rpm, 60% throttle.

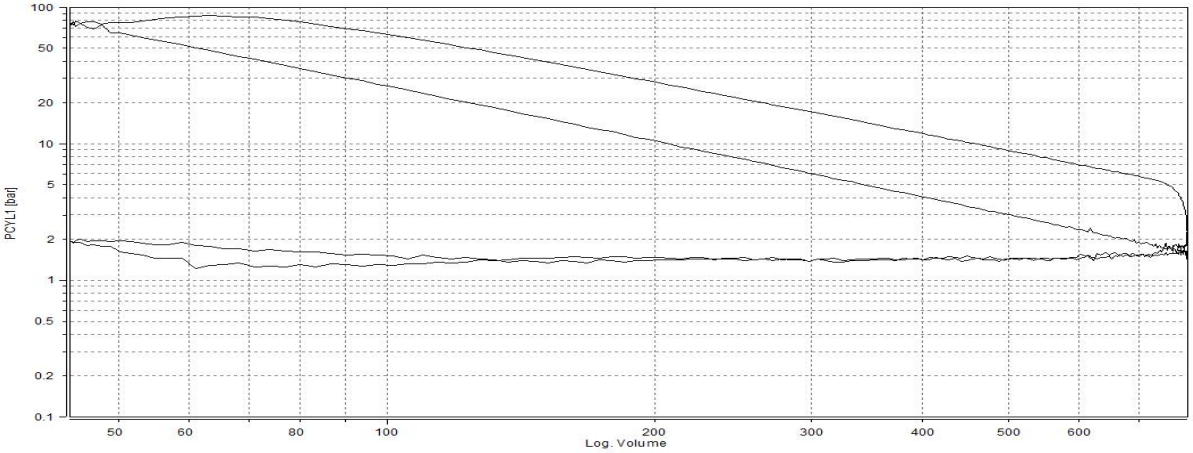

PV diagram of 50%GTL at 1900rpm, 50% throttle.

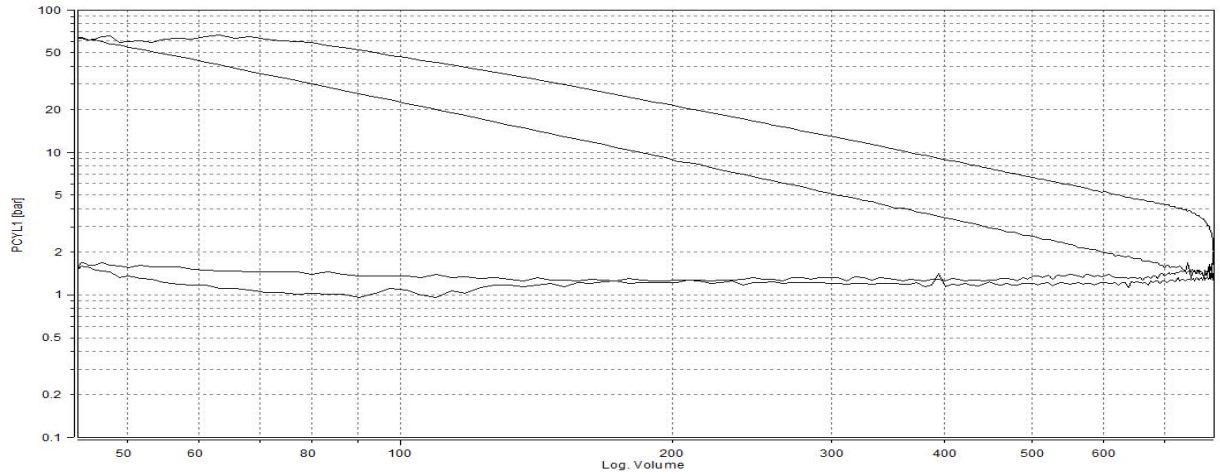


PV diagram of 50%GTL at 1900rpm, 60% throttle.

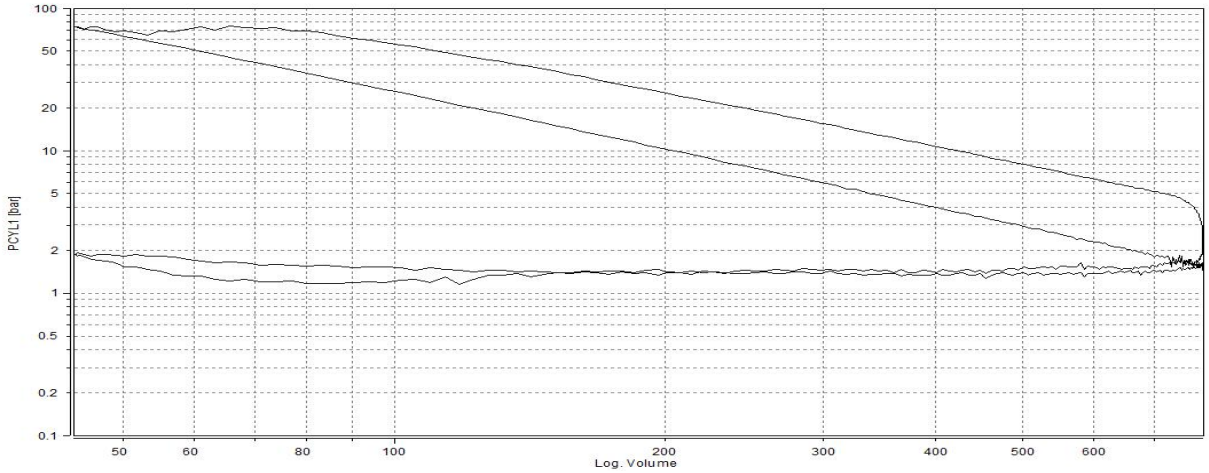


PV diagram of 50%GTL at 1900rpm, 70% throttle.

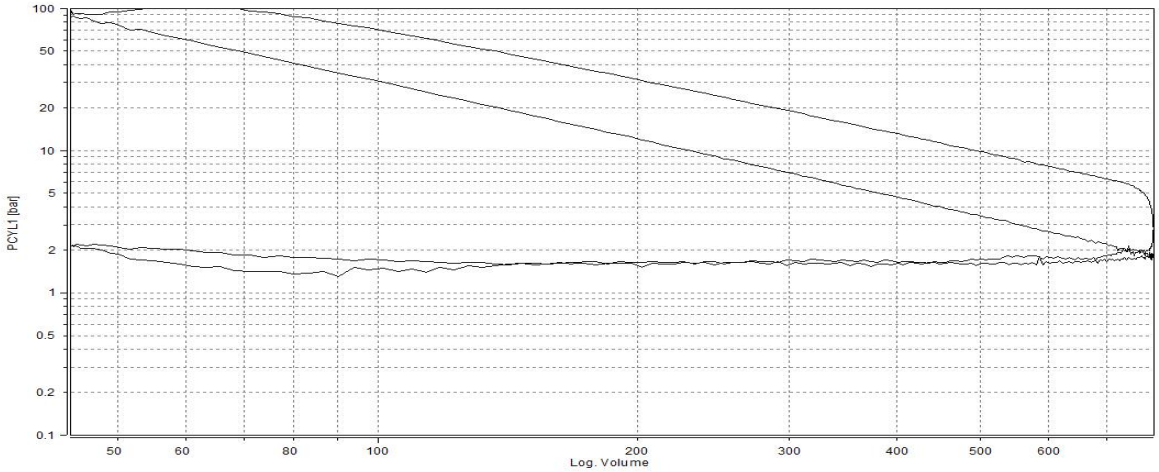

PV diagram of 70%GTL at 1000rpm, 30% throttle.

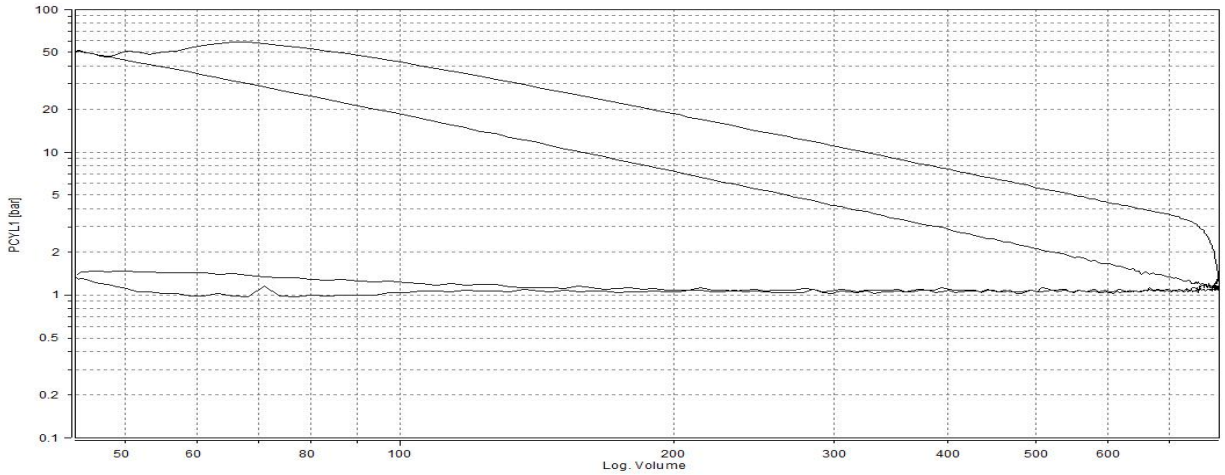


PV diagram of 70%GTL at 1000rpm, 40% throttle.

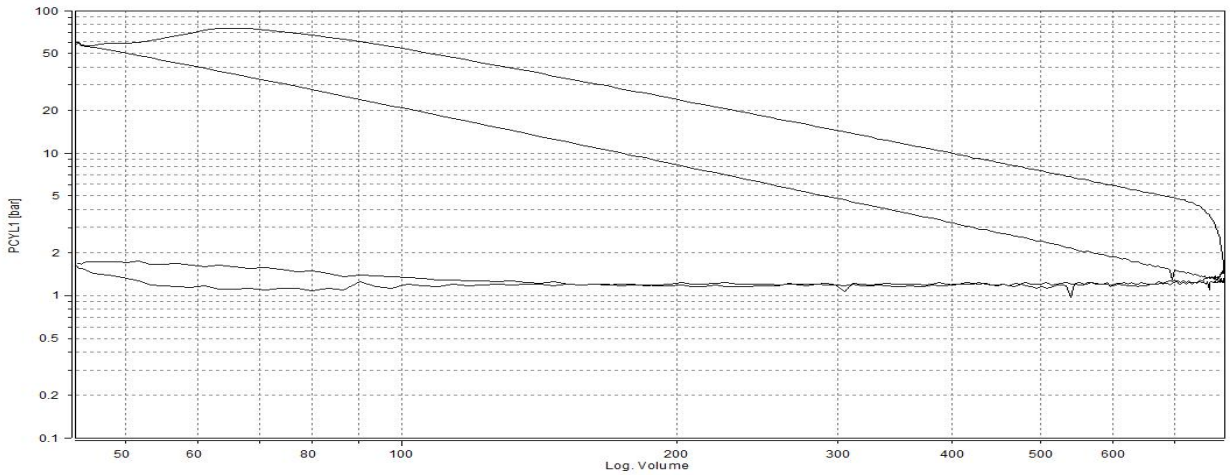


PV diagram of 70%GTL at 1000rpm, 50% throttle.

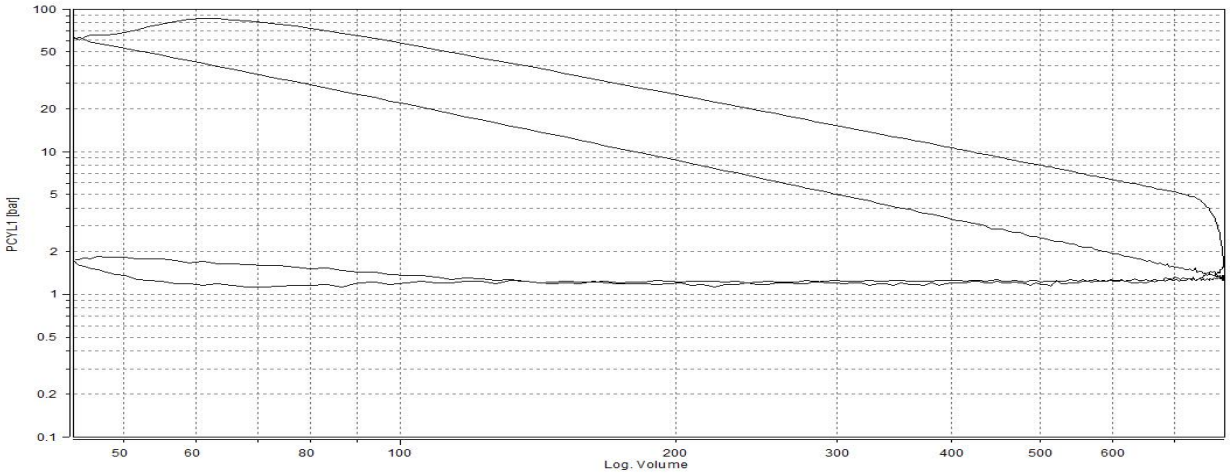

PV diagram of 70%GTL at 1600rpm, 40% throttle.

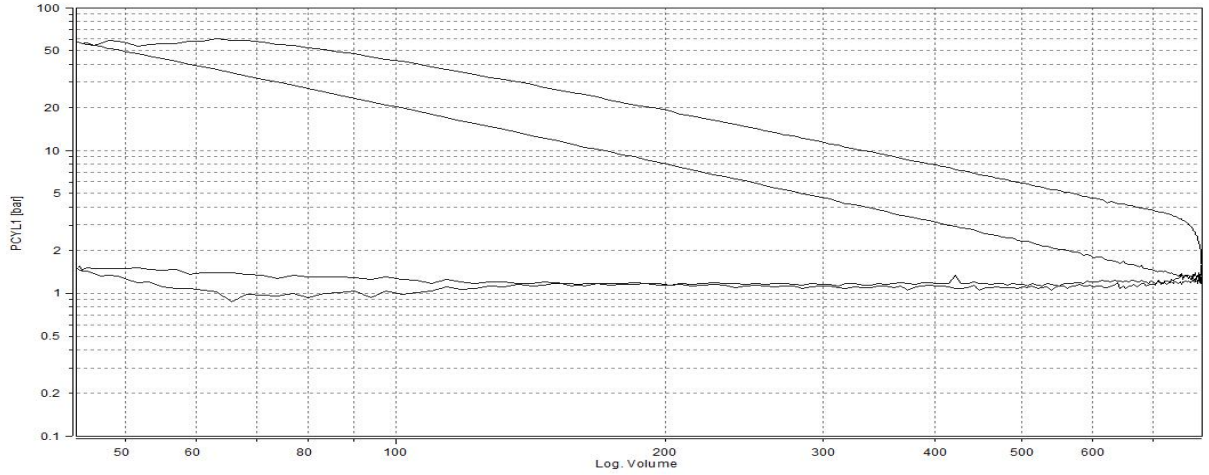


PV diagram of 70%GTL at 1600rpm, 50% throttle.

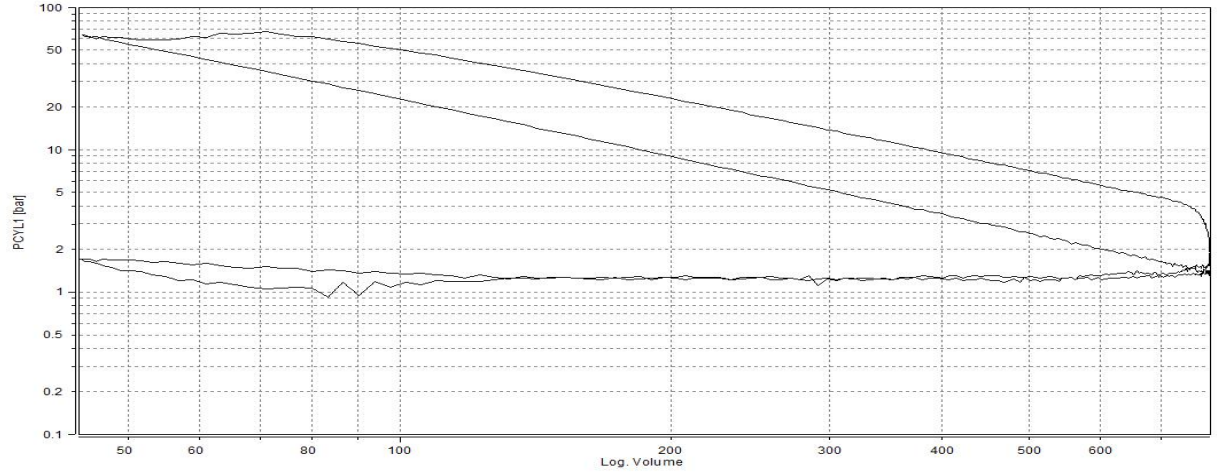


PV diagram of 70%GTL at 1600rpm, 60% throttle.

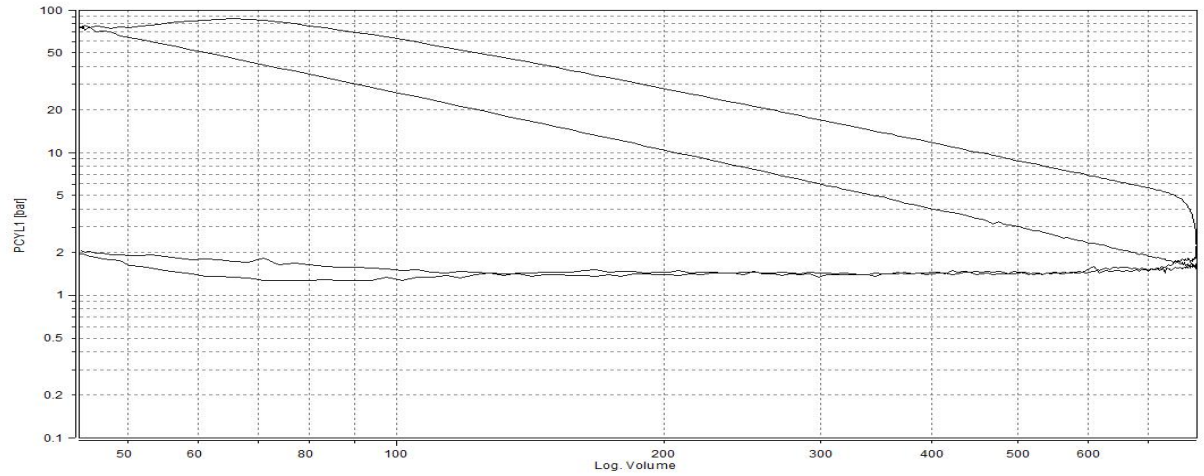

PV diagram of 70%GTL at 1900rpm, 50% throttle.

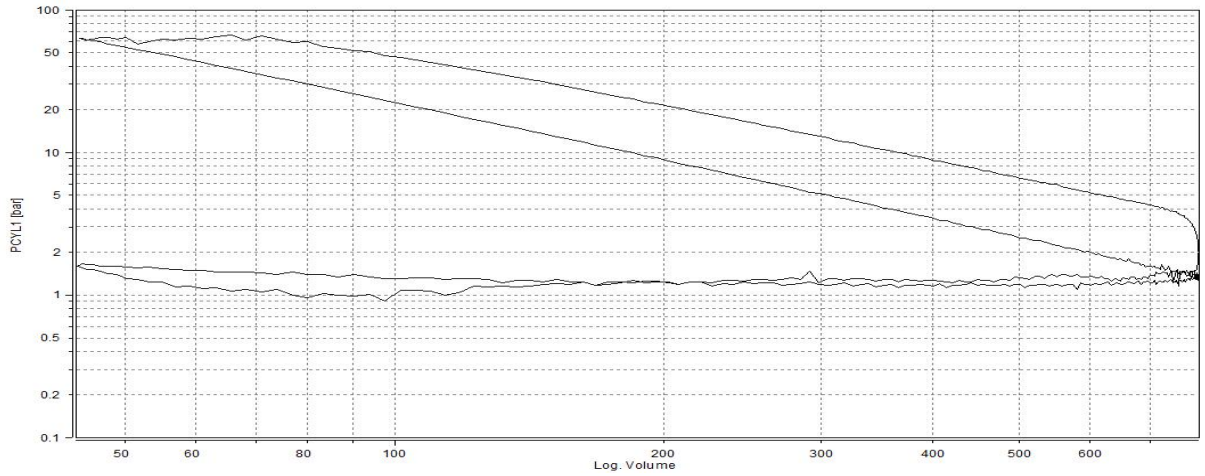


PV diagram of 70%GTL at 1900rpm, 60% throttle.

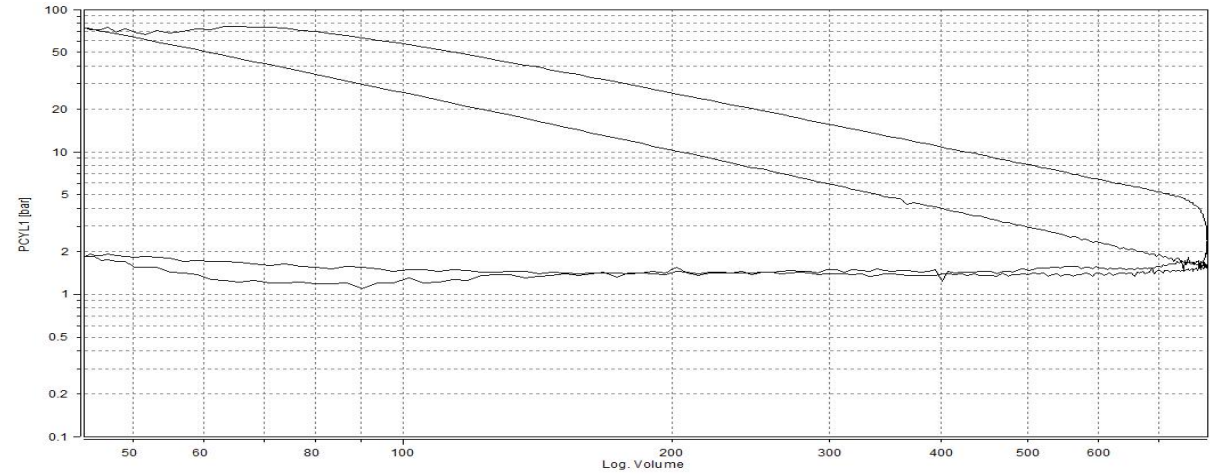


PV diagram of 70%GTL at 1900rpm, 70% throttle.

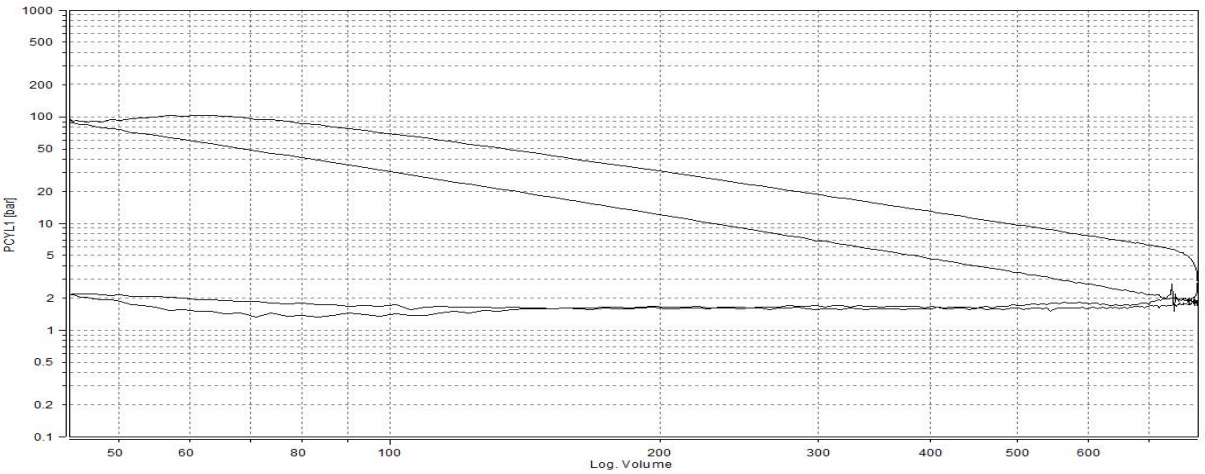

PV diagram of 30%HVO at 1000rpm, 30% throttle.

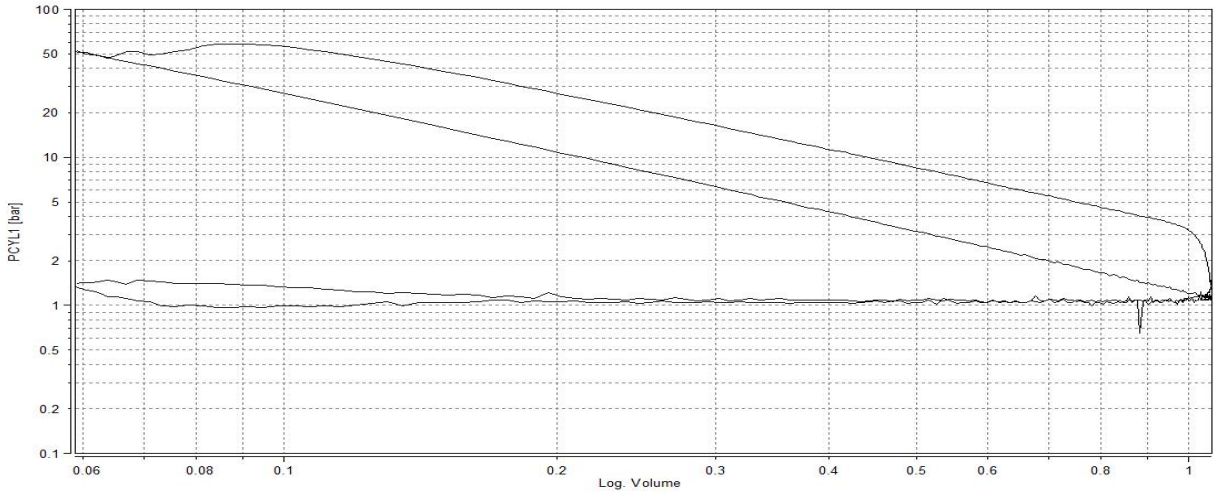


PV diagram of 30%HVO at 1000rpm, 40% throttle.

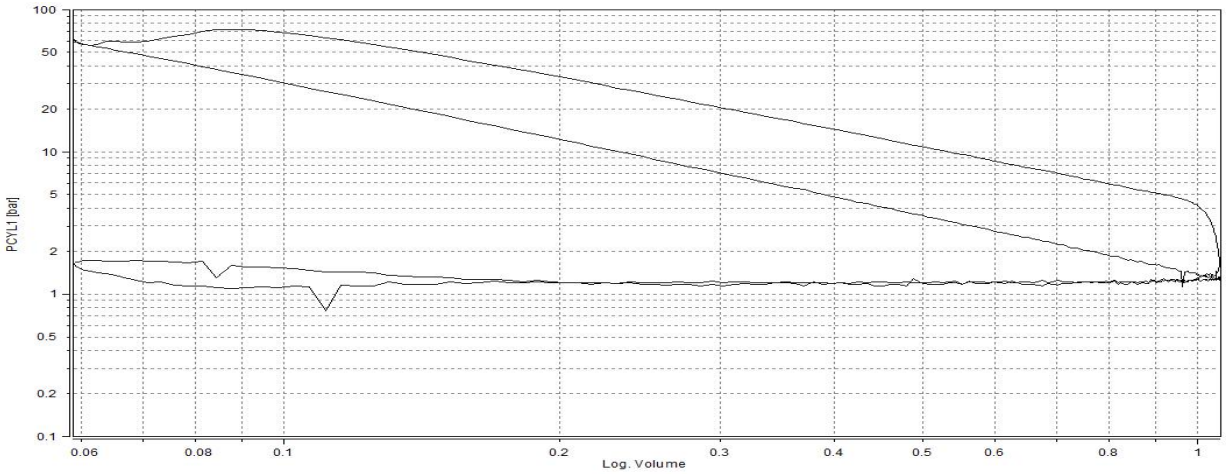


PV diagram of 30%HVO at 1000rpm, 50% throttle.

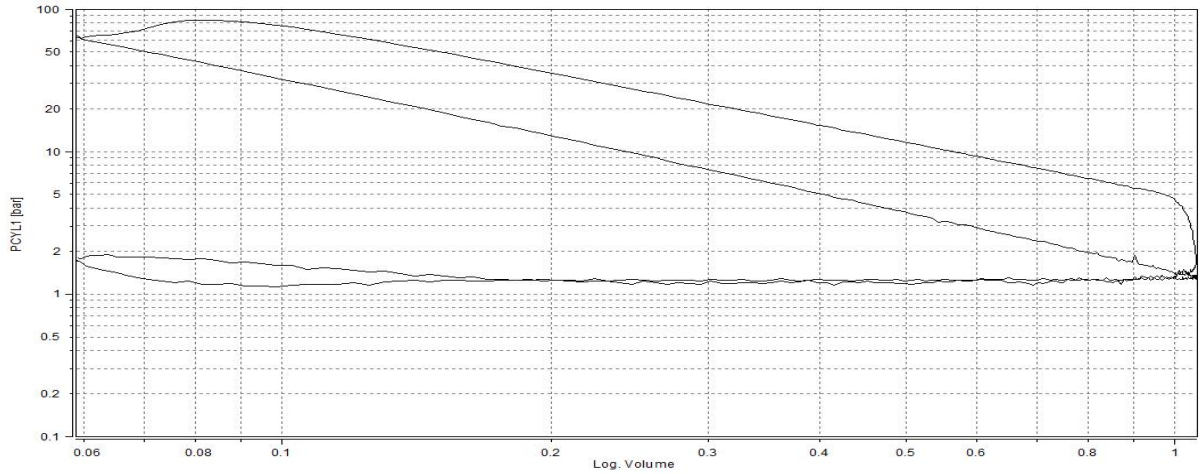

PV diagram of 30%HVO at 1600rpm, 40% throttle.

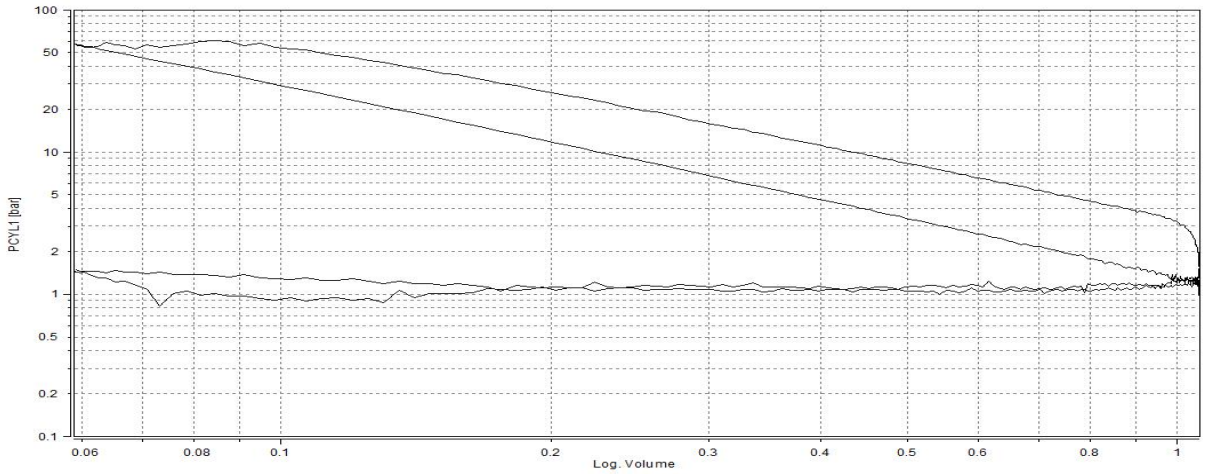


PV diagram of 30%HVO at 1600rpm, 50% throttle.

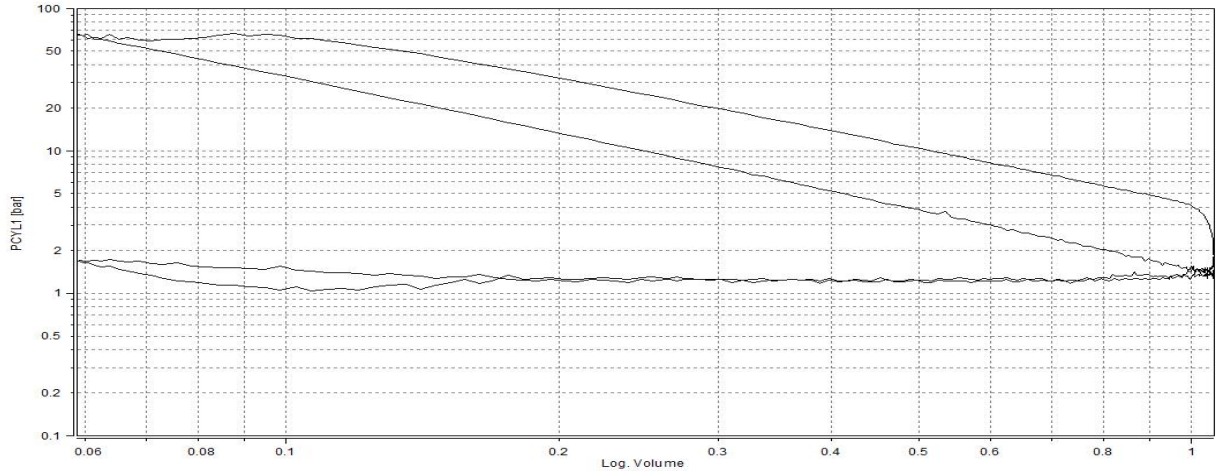


PV diagram of 30%HVO at 1600rpm, 60% throttle.

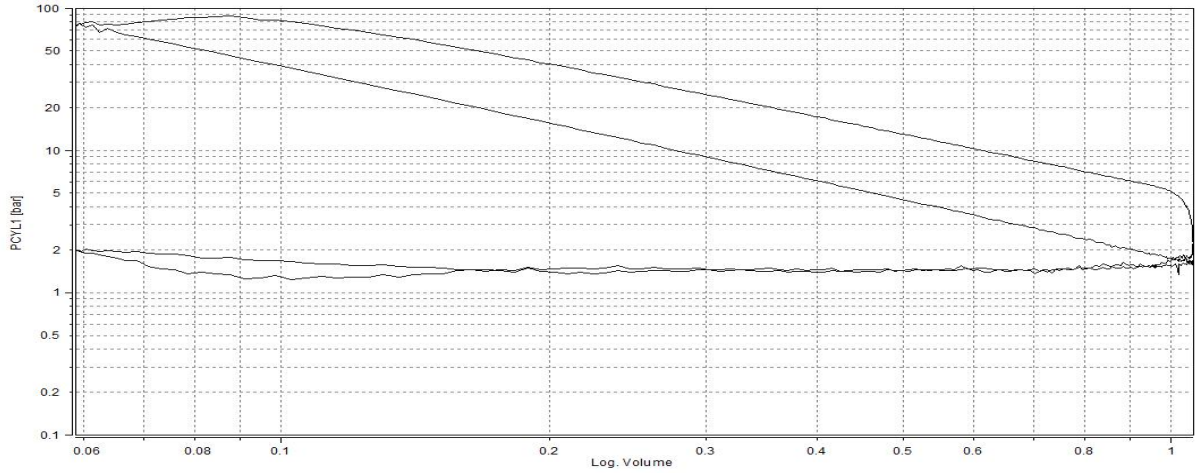

PV diagram of 30%HVO at 1900rpm, 50% throttle.

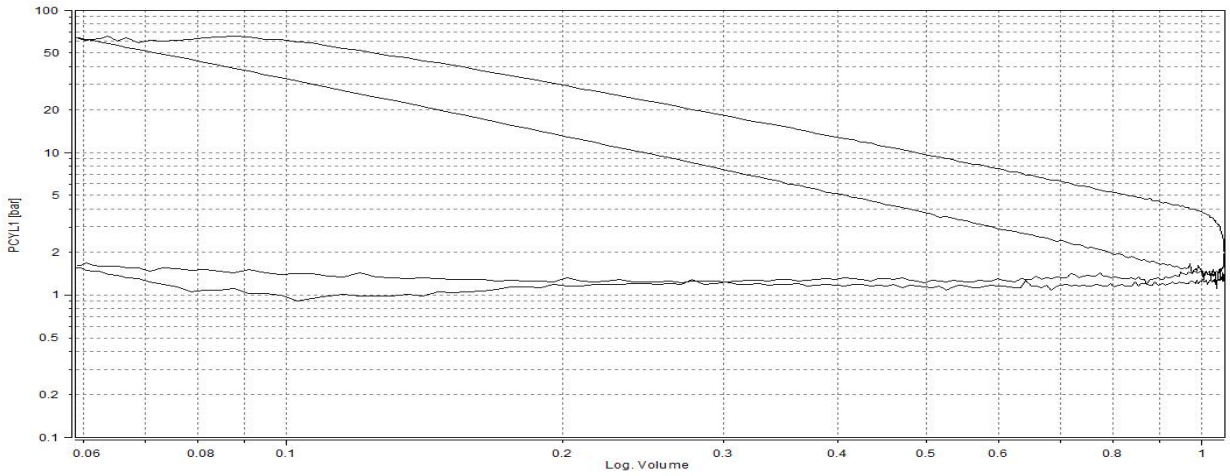


PV diagram of 30%HVO at 1900rpm, 60% throttle.

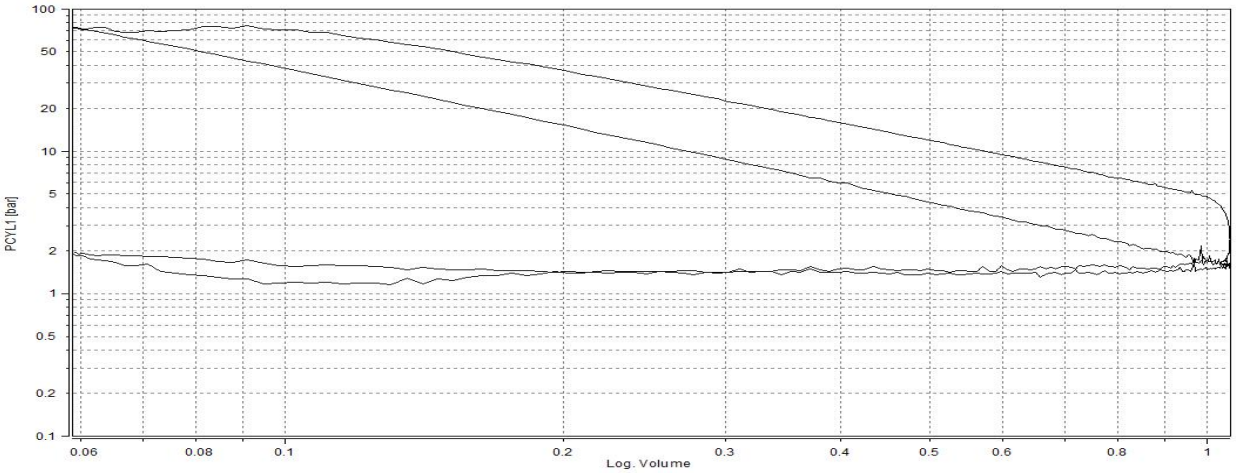


PV diagram of 30%HVO at 1900rpm, 70% throttle.

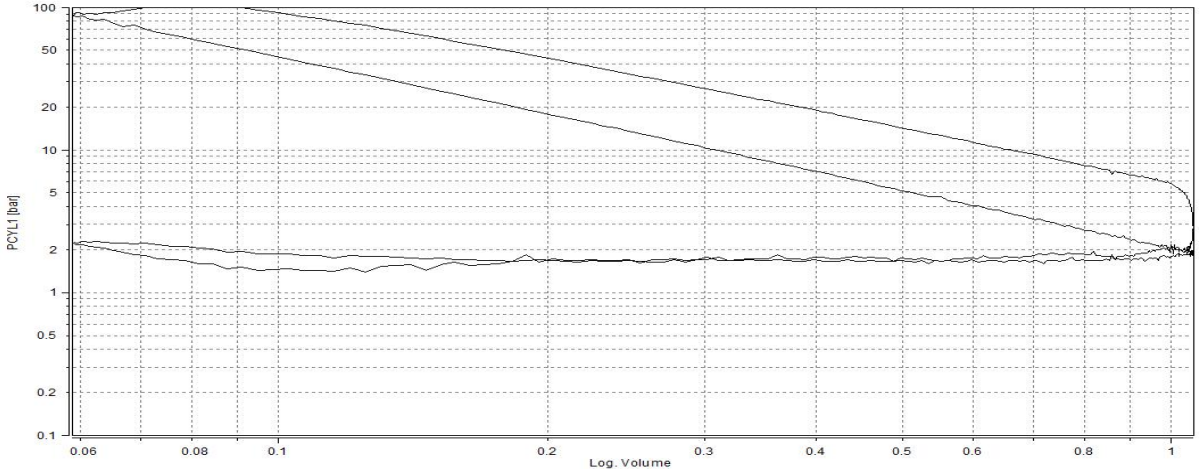

PV diagram of 70%HVO at 1000rpm, 30% throttle.

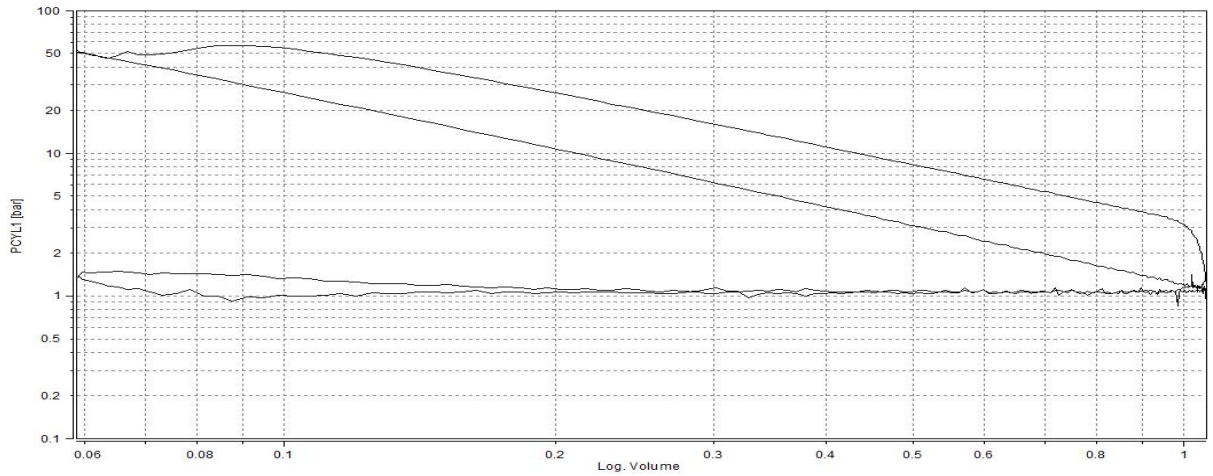


PV diagram of 70%HVO at 1000rpm, 40% throttle.

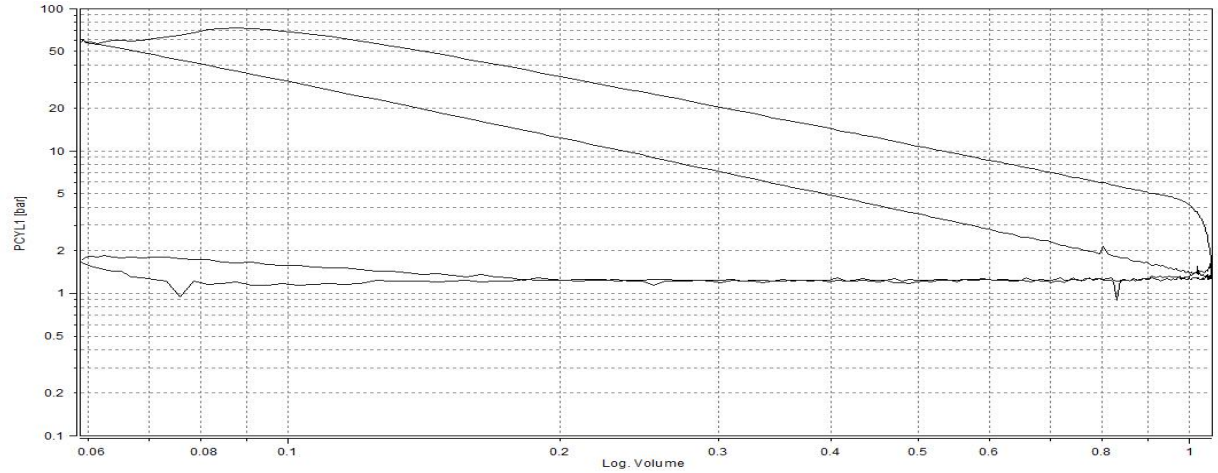


PV diagram of 70%HVO at 1000rpm, 50% throttle.

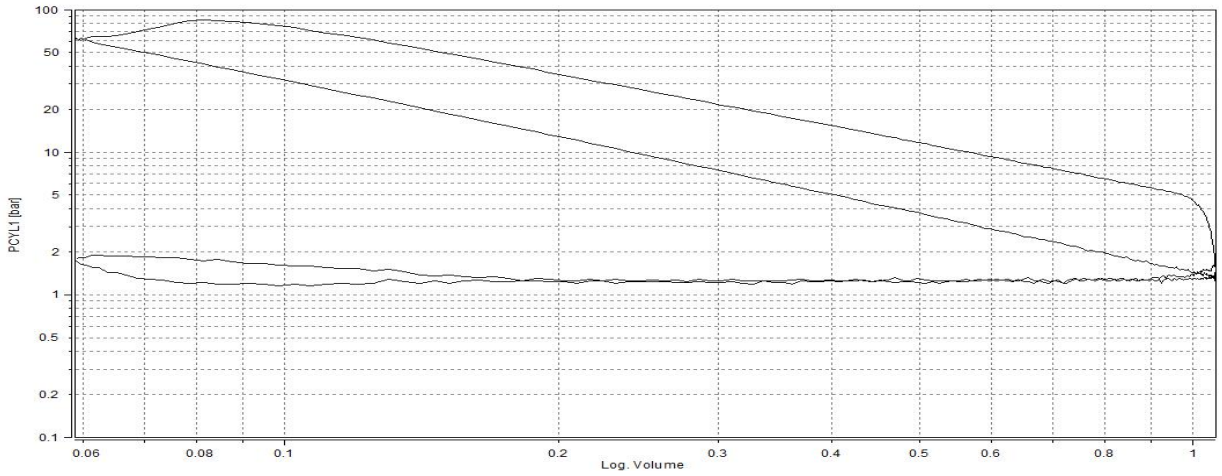

PV diagram of 70%HVO at 1600rpm, 40% throttle.

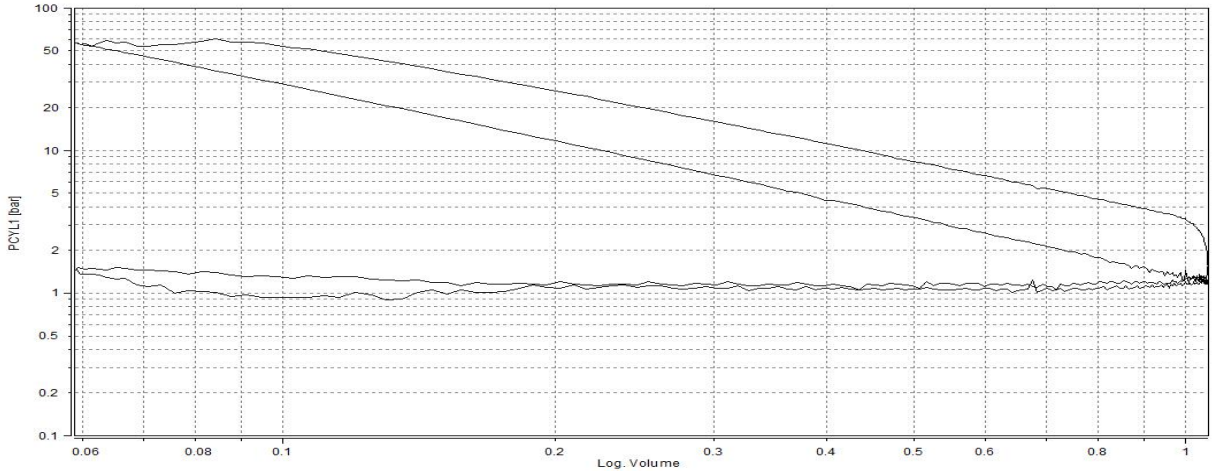


PV diagram of 70%HVO at 1600rpm, 50% throttle.

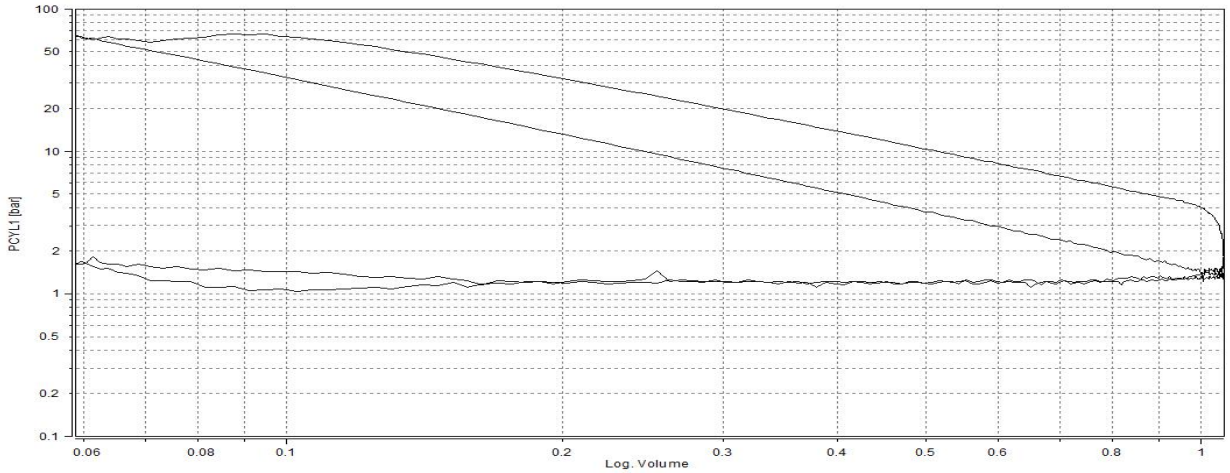


PV diagram of 70%HVO at 1600rpm, 60% throttle.

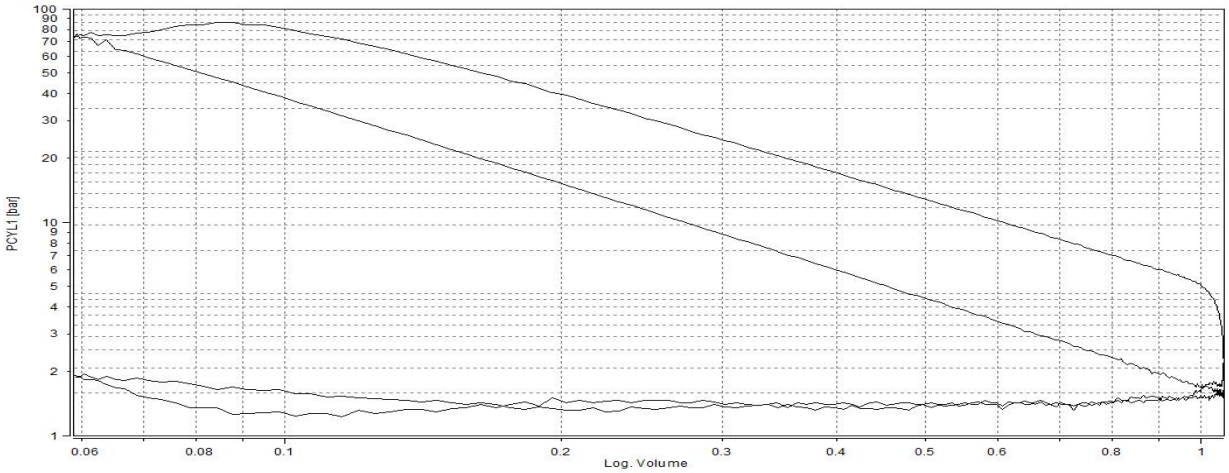

PV diagram of 70%HVO at 1900rpm, 50% throttle.

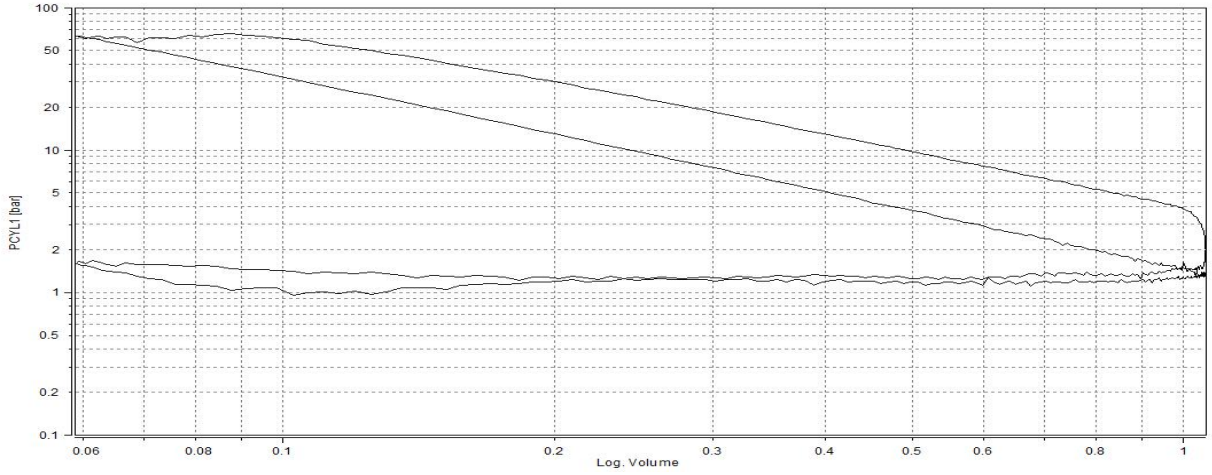


PV diagram of 70%HVO at 1900rpm, 60% throttle.

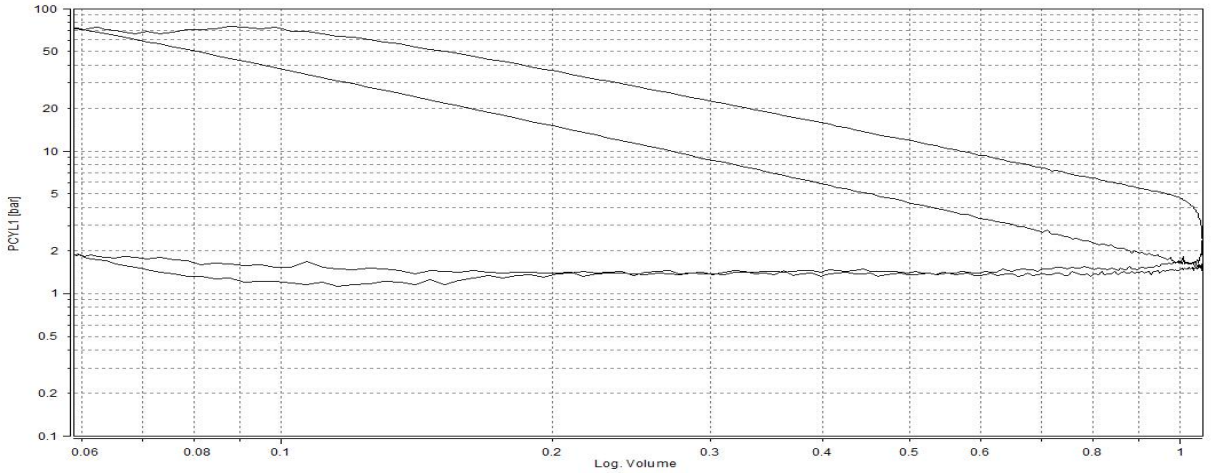


PV diagram of 70%HVO at 1900rpm, 70% throttle.